8-2013

Isolation as a Seismic Design Strategy for Bridges in the New Madrid Seismic Zone

Timothy E. Huff
thuff7@utk.edu

To the Graduate Council:

I am submitting herewith a dissertation written by Timothy E. Huff entitled "Isolation as a Seismic Design Strategy for Bridges in the New Madrid Seismic Zone." I have examined the final electronic copy of this dissertation for form and content and recommend that it be accepted in partial fulfillment of the requirements for the degree of Doctor of Philosophy, with a major in Civil Engineering.

James A. Mason, Major Professor

We have read this dissertation and recommend its acceptance:

Edwin G. Burdette, Chris Cox, J. Stanley Rabun

Accepted for the Council:
Dixie L. Thompson

Vice Provost and Dean of the Graduate School

(Original signatures are on file with official student records.)

ISOLATION

AS A

SEISMIC DESIGN STRATEGY

FOR

BRIDGES IN THE NEW MADRID SEISMIC ZONE

A Dissertation Presented for the

Doctor of Philosophy

Degree

The University of Tennessee, Knoxville

Timothy E. Huff

August 2013

DEDICATION

Printis Huff and Austie Rains Huff

Homer Coe Story and Opal Sells Story

Bill and Sue Huff

Troy

Holli

ACKNOWLEDGEMENTS

Dr. James A. Mason, Dr. Chris Cox and Dr. Stan Rabun have been supportive of this research from the day I first proposed it. Dr. Mason has provided much valuable guidance on the best way to present my findings and I can only hope to have adequately incorporated a small fraction. I am humbled and grateful for this. Thanks go to Dr. Zhenming Wang of the Kentucky Geological Survey for ground motion records form the 2008 M7.9 Wenchuan, China earthquake, and to Dr. Kim B. Olsen of San Diego State University for providing a set of 3-dimensional New Madrid Seismic Zone synthetic records. Even though I was unable to incorporate Dr. Olsen's data in my research, I have a newfound appreciation for those like him who gladly share the results of their work. Finally, thanks to Dr. Edwin G. Burdette for his support as a Committee Member and his example as a teacher.

Abstract

The seismic hazard in the New Madrid Seismic Zone (NMSZ) is primarily from the New Madrid Fault System (NMFS), which produced a series of large earthquakes in 1811-1812. Estimates of the magnitude of these earthquakes and the event magnitude appropriate for structural design in the New Madrid Seismic Zone vary greatly and have been the subject of much debate.

Current bridge design practice in the region relies primarily upon controlled damage by plastic hinging in columns/piles at piers to prevent collapse. Abutments are typically modeled with linear springs to represent piles and backfill stiffness. The usefulness, after a major seismic event, of structures designed by this method lies in doubt due to the potential for high residual displacements.

Isolation has been selected as a viable design alternative for major structures since the 1970's at least. The application of isolation to bridges in the New Madrid Seismic Zone has been limited, with the most notable example Interstate 40 over the Mississippi River (the Hernando Desoto Bridge). This was a retrofit project incorporating both Lead-Rubber Bearings (LRB) and Friction Pendulum System (FPS) bearings as isolators.

The feasibility of isolation as a design strategy for bridges in the New Madrid Seismic Zone is evaluated using non-linear response history analysis. Acceleration time histories from actual events are selected, modified, and used for the analysis. Synthetic motions are generated for target design spectra and used for analysis as well. Various options for target spectra are discussed. Currently implemented simplified procedures are evaluated. Alternative, direct displacement based design procedures are explored. Various bridge types commonly to the region are discussed. Bridge types selected for study include four pile bent bridges as well as 2 and 3-span grade crossings with multi-post, reinforced concrete bents supported on friction pile caps.

Isolation is proposed as an alternative which should be considered taking into account all factors, including economy. The proposition is made that isolation may be both effective and economical for certain bridges in the New Madrid Seismic Zone. To this end, the economic benefits which could potentially offset the cost of isolation bearings are explored.

TABLE OF CONTENTS

LIST OF TABLES

LIST OF FIGURES

LIST OF SYMBOLS

A_S: zero period design spectral acceleration for a particular site class

ATR: Active tectonic region

B_L: response modification factor for effective viscous damping

CAV: cumulative absolute velocity, in/sec

CMRS: conditional mean response spectrum

D: the diameter of a steel pipe pile; the diameter of a reinforced concrete column; the cross-sectional depth of a rectangular column, inches

D_{DEM}: seismic displacement demand on a particular element from a linear response spectrum analysis, R_d x D_{RSA}, inches

D_{ISO}: the portion of the total horizontal displacement of the center of mass relative to the fixed base which occurs within an isolation bearing along one of the principal modeled horizontal axes at a substructure, inches

D_{RES}: residual displacement remaining in a system after strong shaking and when the system has come to rest, inches

D_{RSA}: displacement demand from a linear response spectrum analysis

D_{SUB}: the portion of the total horizontal displacement of the superstructure center of mass relative to the fixed base which occurs within the substructure at a substructure, inches

D_{TOT}: the total horizontal displacement of the superstructure center of mass with respect to the fixed base of a substructure, inches; $D_{TOT} = D_{SUB} + D_{ISO}$

D_{VERT}: the vertical displacement of an isolator; typically most significant with friction-pendulum devices, inches

D_{YISO}: the yield displacement of a bi-linear isolator, inches

DBE: design basis earthquake

FPS: friction pendulum system isolation device

GMPM: Ground motion prediction model

I_{xx}: Second moment of area about the transverse axis of a bridge superstructure, ft^4

I_{yy}: Second moment of area about a vertical axis of a bridge superstructure, ft^4

K_{COMP}: the composite stiffness of an isolator in series with a sub-structure element, kips/inch

K_d: post-yield isolator stiffness, kips/inch

K_{EFF}: effective (secant) stiffness of an isolator, kips/inch

K_i: the initial stiffness of an isolation system, kips/inch

K_{SUB}: the stiffness of a sub-structure element, kips/inch

K_{SYS}: the total effective (secant) stiffness of an entire bridge system treated as a single-degree-of-freedom oscillator

L_C: clear height of a column or pile, feet

LRB: lead-rubber-bearing isolation device

M_n: nominal moment capacity, ft-kips or inch-kips

MCE: maximum considered (or credible) earthquake

ME: Mississippi Embayment

MSE: mean-square-error

M_W: moment magnitude

PE: probability of exceedance

PGA: generally, peak ground acceleration, g; also the mapped peak ground acceleration for a B/C boundary site class locale

PGD: peak ground displacement, inches

PGV: peak ground velocity, in/s

PSHA: Probabilistic seismic hazard analysis

Q_d: characteristic strength of an isolator, kips

R: radius of curvature of the concave sliding surface of an FPS isolator, inches

R_d: displacement demand amplifier for short period structures

RHA: response history analysis

RSA: response spectrum analysis

RTRS: risk-targeted response spectrum

S_1: mapped spectral acceleration at a period of 1 second for a B/C boundary site class locale

S_S: mapped spectral acceleration at a period of 0.2 seconds for a B/C boundary site class locale

S_{D1}: design spectral acceleration at a period of 1 second for a particular site class

S_{DS}: design spectral acceleration at a period of 0.2 seconds for a particular site class

SA: spectral acceleration, g

SCR: Stable continental region

SD: spectral displacement, inches

SV: spectral velocity, in/s

T*: characteristic period of a site, $T^* = S_{D1}/S_{DS}$

T_d: natural period of an isolation system based on post-yield (tangent) stiffness, K_d, seconds

T_{EFF}: natural period based on effective (secant) stiffness, K_{EFF}, seconds

T_O,T_S: periods defining the constant acceleration region of a design response spectrum, seconds

THA: Time history analysis

UHRS: uniform hazard response spectrum

w_{ss}: Weight per linear foot of a bridge superstructure, klf

α: post-yield stiffness ratio, $\alpha = K_d/K_i$

Δ_{TAR}: target displacement, inches

λ: slenderness parameter

μ_{dyn}: the dynamic coefficient of friction for a friction pendulum isolation bearing

μ_i or μ_D; the displacement ductility demand on a substructure element during seismic loading

ϕ: curvature, in^{-1}

ξ_{COMP}: effective viscous damping of an isolation system in series with a substructure unit used to model nonlinear hysteretic behavior in a linear response spectrum analysis

ξ_{EFF}: effective viscous damping of an isolation system used to model nonlinear hysteretic behavior in a linear response spectrum analysis

ξ_{SYS}: effective viscous damping of an entire bridge system used to model nonlinear hysteretic behavior in a linear response spectrum analysis

CHAPTER 1 - EARTHQUAKES AND BRIDGES IN THE NMSZ: AN OVERVIEW

1.1 Purpose of the Research

While it is impossible to predict the precise date or magnitude of an earthquake in a specific region, there are events which have been proposed to be viewed as possible precursors to seismic activity. Certain cloud shapes, strange behavior of animals, bubbling wells, a glowing sky, and muddy ponds – these have all been suggested as indicative of an impending earthquake (Villaverde, 2009). There are, however, more scientific means upon which to rely in estimating the potential seismic hazard to a region. And even these scientific ideas produce great variation in estimates of the hazard at sites where little data is available. We simply don't know whether the best engineering choice for the design basis event in the New Madrid Seismic Zone (NMSZ) should be magnitude 7.7 or magnitude 7.0 or even magnitude 6.5 earthquakes. The focus upon seismic hazard in the NMSZ has increased over the past decade, so it is wise to look for ways to efficiently and economically design bridges in the NMSZ.

The purpose of this research is to explore the feasibility of isolation as a seismic design strategy for ordinary bridges in the NMSZ. To accomplish this objective, six bridges and two sites have been selected for study. Seismic hazard at the two sites, bridge types selected for study, and analytical methods for structural design to earthquake loading are discussed later in CHAPTER 1. Essentials of seismic isolation theory as it applies to bridge structures are covered in CHAPTER 2. The process used to select and modify ground motions for detailed analysis of the isolated bridges is the subject of CHAPTER 3. A detailed study of differences in response of simple bi-linear oscillators to the ground motions developed for the two sites in the NMSZ

compared to other tectonic environments is presented in CHAPTER 4. To establish a baseline design for each non-isolated structure, response spectrum analyses are performed and the results reported in CHAPTER 5. Preliminary designs of isolators for the bridges are carried out in CHAPTER 6 using simplified analysis procedures currently used for isolation design in AASHTO codes requirements. Detailed response history analyses of the isolated bridges are presented in CHAPTER 7. Conclusions are drawn and recommendations made in CHAPTER 8.

Primary figures are included in the body of the paper, supporting figures placed in the appropriate Appendix. Figures in Appendices are linked to sections in the body of the paper through the figure number. For example, Appendix G1 consists of figures supporting the material in Chapter 1 and Figure G1.2-2 supports material found in Section 1.2 of the paper.

To introduce the work reported in this dissertation, a discussion of some basic, yet important features of the Mississippi Embayment (ME) of the NMSZ is required.

1.2 The ME of the NMSZ

Seismic hazard in the ME is primarily from the New Madrid Fault System (NMFS) and the Wabash Valley Fault System. Most earthquakes are inter-plate events at the boundaries between tectonic plates. The NMFS is an intra-plate system, a fault system on a stable continental region (SCR). We know far less about intra-plate systems than we do about their inter-plate counterparts - fault systems at the boundaries of tectonic plates. Data from large magnitude intra-plate events is sparse compared to that available from comparable magnitude events in California, and Japan and other plate boundary locations. Large earthquakes are known

to have occurred in the New Madrid Seismic Zone (NMSZ). Some notable intra-plate events have been (Gangopadhyay & Talwani, November/December 2003)

- 1811-1812 New Madrid Seismic Zone - estimated M7.0-M8.0
- 1886 Charleston, South Carolina - estimated M7.3
- 1940 Olympia, Washington - M7.1
- 1965 Seattle-Tacoma, M6.5
- 1976 Tangshan, China - M7.8
- 1982 Miramichi, Canada - M5.7
- 1988 Tennant Creek, Australia - M6.7
- 1988 Saguenay, Canada - M5.9
- 1990 Sudan - M7.2
- 2001 Nisqually, Washington - M6.8
- 2008 Wenchuan, China - M7.9
- 2010 Darfield, New Zealand - M7.10

In truth, we know relatively little about the intra-plate NMFS. No person living can recall a strong event in the area, and we have no ground motion records from an earthquake comparable to the high-magnitude historic events. The duration of strong ground shaking is one of the many unknowns for seismic hazard in the area, but intra-plate events are thought to be of shorter significant duration and are thought by some to possess stronger high frequency content compared to similar magnitude inter-plate events (Jankulovski, et al., 1996).

For purposes of seismic design, construction sites are typically assigned a site classification. In AASHTO, the site classifications are A (very hard rock), B (rock), C (soft rock and dense soil), D (soil), E (very soft soil), and F (other). Site classification is determined from either average shear wave velocity measurements in the upper 30 meters of subsurface profile or blow count correlations to shear wave velocity. So two sites, one with a 30 meter deep soil profile to bedrock and another with a 1 km soil profile to bedrock, but with identical shear wave velocity profile sin the upper 30 meters, would have identical site classifications. The subsurface profile in the ME varies from a few meters of soil at the periphery to over 1 km near the Mississippi River (see Figure 1.2-1).

So, two features make the ME unique: the intraplate tectonic setting and the deep soil deposits present.

With regard to the fault system itself, Macpherson conducted finite fault, finite difference simulations to predict surface ground motions based on a fault geometry composed of three major sections: (1) Cottonwood Grove strike slip fault, (2) Reelfoot thrust fault, and (3) New Madrid North fault (Macpherson, 2009). Table 1.2-1 summarizes features of the various faults assumed by Macpherson and Figure 1.2-2 shows the location and extent of the three faults.

Before conducting a detailed definition of the seismic hazard at the study sites, some discussion of bridge design practice will be beneficial.

Table 1.2-1. New Madrid Fault Geometry (after Macpherson, 2009)

Parameter	Fault Segment		
	Cottonwood Grove Strike-slip	Reelfoot Thrust	New Madrid North Strike-slip
Primary Scenarios			
Magnitude	M_W7.16	M_W7.08	M_W7.18
Strike	52.305^o	338.449^o	37.376^o
Dip	90^o	39.5^o	90^o
Rake	180^o	90^o	180^o
Fault length	86.549 km	75.631 km	91.084 km
Fault width	15.000 km	15.000 km	15.000 km
Hypocenter depth	9 km	9 km	9 km
Max. slip	6.681 meters	6.145 meters	6.969 meters
Avg. slip	1.318 meters	1.215 meters	1.380 meters
Alternate Scenarios			
Magnitude	M_W7.31	M_W7.14	M_W7.07
Strike	45.408^o	332.736^o	33.072^o
Dip	90^o	39.5^o	90^o
Rake	180^o	90^o	180^o
Fault length	116.236 km	57.933 km	59.511 km
Fault width	16.000 km	22.814 km	18.000 km
Hypocenter depth	9 km	9 km	9 km
Max. slip	9.270 meters	6.662 meters	5.938 meters
Avg. slip	1.830 meters	1.336 meters	1.175 meters

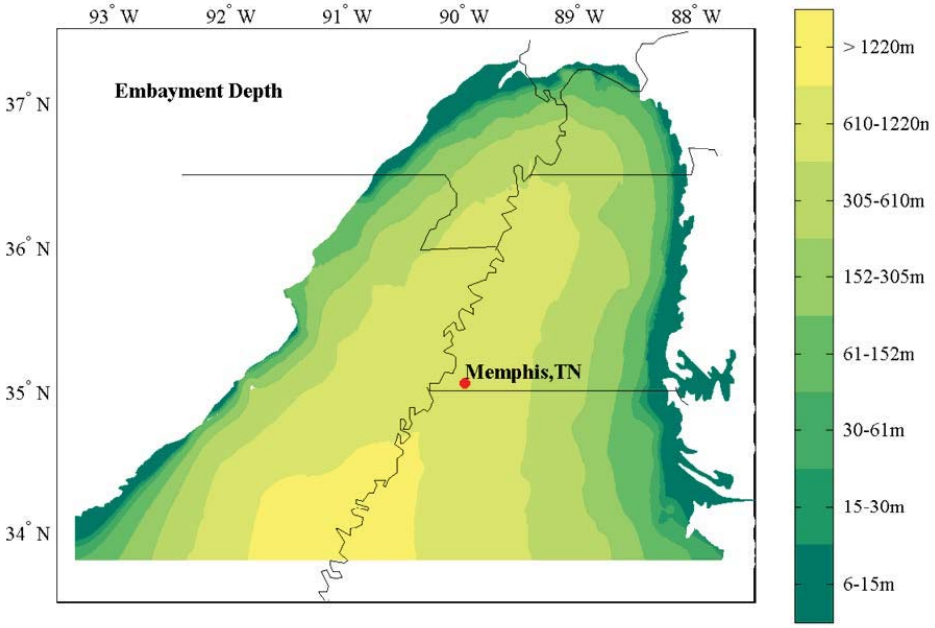

Figure 1.2-1. Mississippi Embayment Depth (From Fernandez, 2007)

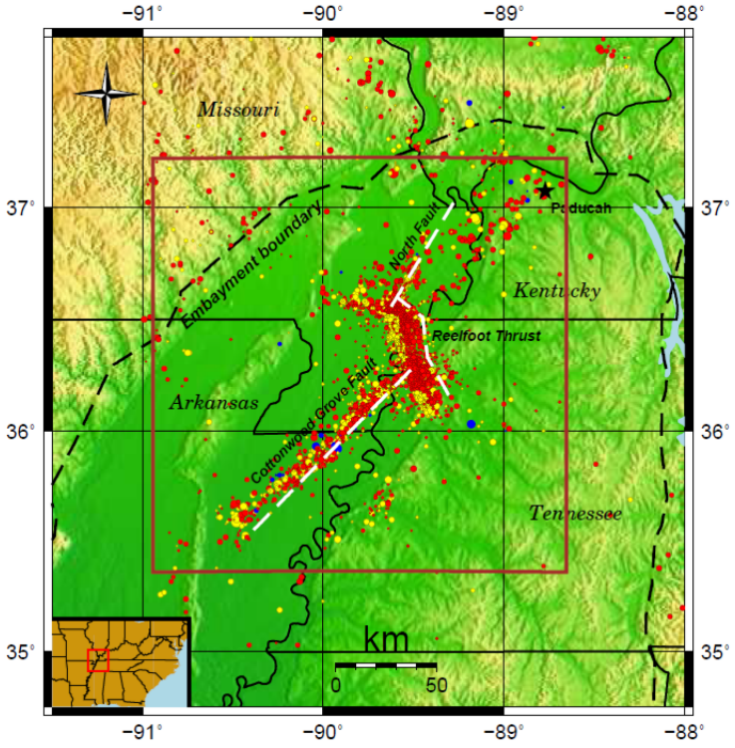

Figure 1.2-2. New Madrid Fault System (From Macpherson, 2009)

1.3 Seismic Design of Bridges in West Tennessee

Bridges in Tennessee are currently designed for controlled damage to prevent collapse when subjected to a ground motion having 7% probability of exceedance in 75 years - the Design Basis Event (DBE). There are generally three strategies available to the engineer regarding the location of the controlled damage (AASHTO, 2009) :

1. Ductile substructures with an essentially elastic superstructure
2. A ductile superstructure with an essentially elastic substructure
3. Essentially elastic substructures and superstructure with a fusing mechanism between the two

Most of the current, new design in Tennessee is classified as Type 1 construction. The superstructure is designed to remain elastic, and plastic hinges are provided for at column sections of maximum moment through either confinement reinforcing (for reinforced concrete) or thick-walled tubing (for structural steel substructures). Elements above the top of the column and elements below the bottom of the column are capacity protected, i.e., they are designed to remain elastic at some loading larger than that which causes hinging in the columns. Integral abutments are used on concrete bridges less than about 244 meters (800 feet) long and steel bridges less than about 137 meters (450 feet) long. With integral abutments, a portion of the earthquake load may be designed to be carried by passive pressure development behind the abutments. This is one area in which an isolated bridge may be advantageous - the superstructure is isolated, not only from the pier substructures, but from the abutment backfill as well.

For Type 1 bridges, the question remains as to how much useful life of the structure might be left after a strong earthquake. Of prime concern is the issue of residual displacement. Even though the bridge does not collapse, repair procedures after ground shaking could require anything from simple patching of the spalled concrete in plastic hinge zones to a complete replacement of the bridge if the residual displacement is too high. It has been suggested that residual displacements are directly proportional to the duration of strong earthquake motion (Towhata, 2008). The large magnitude NMSZ ground motions are long duration motions.

ATC-58 (Applied Technology Council, May, 2011) specifies residual displacements for buildings according to the following rules:

$$\Delta_r = 0, if\ \Delta \leq \Delta_y \quad \text{(Eq. 1-1)}$$

$$\Delta_r = 0.3(\Delta - \Delta_y), if\ \Delta_y < \Delta < 4\Delta_y \quad \text{(Eq. 1-2)}$$

$$\Delta_r = \Delta - 3\Delta_y, if\ \Delta \geq 4\Delta_y \quad \text{(Eq. 1-3)}$$

Clearly, as long as the yield displacement is not exceeded during strong ground shaking, there is no residual displacement, as indicated by equation 1-1. For ductility values less than 4, equation 1-2 specifies a residual displacement as high as 90% of the yield displacement. And for displacement ductility values larger than 4, residual displacements may be very high. For example, a structure designed for a displacement ductility of 6 - the maximum permitted by AASHTO - could have a residual displacement equal to 3 times the yield displacement according to equation 1-3.

Type 2 constructions generally would consist of ductile end diaphragms to both limit the load transferrable to the substructures and accommodate the displacements expected during strong ground shaking.

Type 3 design - specifically the seismic isolation aspect of Type 3 design - is the subject of this study. It would seem that, in certain cases, isolation should be at least considered as a design choice for bridges in the NMSZ. The study seeks to identify some of those cases and to evaluate various preliminary design procedures amenable to solution in an engineering office with regard to their ability to predict non-linear behavior of isolators. Toward this end, non-linear time history analyses are performed here and the results used as a benchmark against which simplified procedures are measured.

For isolated bridges, the isolation system is typically located between the bottom of the girders and the top of the pier caps. Shear keys may be constructed at each substructure to limit the possible movements of the isolators, thus preventing unseating of the superstructure from the supports.

1.4 Bridge Types Selected for Study

A vast majority of the bridge construction in the NMSZ consists of pre-stressed concrete beam superstructures. Structural steel girders are used when spans greater than about 46 meters (150 feet) are required. Substructures in West Tennessee are usually founded on displacement-type friction piles, either pre-stressed concrete piles or steel pipe piles. The substructures may be in the form of concrete columns and footings supported on the friction piles or, more commonly, pile bents. A pile bent is a bridge substructure consisting of piles driven to the required level of

bearing and left protruding from the ground. A reinforced concrete cap beam is cast around the piles - above ground and water - and the substructure is complete, thus eliminating the need to form footings at column bases inside an excavation of cofferdam. The method, however, is somewhat limited in the fact that it may be difficult to obtain the required bearing on spans longer than 36 meters (120 feet) or so. This limitation is solely a function of typical driving loads historically used in the NMSZ deposits - there is nothing to prevent the specification of larger driving loads to increase this reported span limit. Regardless, many bridges fall within the span limitation and are candidates for pile bent sub-structures. This type of construction is used frequently over creeks, wetlands, or otherwise environmentally sensitive areas.

It would appear that the pile bent bridge would be an ideal candidate for seismic isolation for the following reasons:

1. Displacement ductility demands larger than about 4 in pre-stressed concrete piles force the designer to opt for steel pipe piles. (AASHTO, 2009)
2. The required D/t ratio for steel pipe piles loaded beyond the elastic range is about ½ of that required for elastically responding steel pipe piles (the thickness of the pipe pile wall required for inelastic behavior, for a given pile diameter, is about twice that required when the pile remains elastic). (AASHTO, 2009)

$$\left(\frac{D}{t}\right)_{DUCTILE} \approx \frac{1}{2}\left(\frac{D}{t}\right)_{ELASTIC}$$

So, if the inelastic behavior can be limited to isolation bearings, a good deal of savings in piling cost may well offset the cost of the isolators. Driving stresses need to be considered as well, however, noting that the incorporation of large driving loads may require thicker-walled

piles. The savings in piling cost may result from either the use of concrete piling (where steel pipe piles would have been required for Type 1 construction) or the use of lighter steel pipe piles (when inelastic pile behavior is not required).

In fact, the impetus for this research has been the design of an actual pile bent bridge with severe potential scour conditions warranting the use of larger diameter pipe piles to meet slenderness requirements in the scoured condition, even though smaller diameter piles would have worked in the non-scoured condition. Now, some method of making the large diameter pipe piles work under earthquake loading in the non-scoured condition is a bit of a challenge. It is these and similar examples which require the engineer to begin thinking about non-traditional designs, isolation included.

Another frequently adopted configuration in the NMSZ consists of a 2 or 3 span pre-stressed concrete superstructure supported on multi-post cast-in-place column substructures with footings and friction piles, either pre-stressed concrete or steel pipe. This type of construction is common for interstate bridges over a county road (3-span), for example, and on state routes over interstates (2-span). Isolation could conceivably reduce the loading into the multi-post bents, resulting in less reinforcement congestion, smaller loads into the footings, fewer piles, smaller driving loads for piles, and the minimization of damage to piling, which cannot be inspected after an earthquake.

Two sites in West Tennessee are selected for this study: one in highly populated Shelby County and a second in Lake County, a sparsely populated area but one of the most severe in the nation in terms of seismic hazard.

One important factor in determining the dynamic response of bridge structures is the span-to-width ratio. A very wide bridge displaces laterally as a rigid block, with a longitudinal axis remaining virtually a straight line. Conversely, the initially straight longitudinal axis of a bridge with long, narrow spans may become a curved shape in the displaced state. The span-to-width ratio can vary from about 1.0 to about 4.0 for typical pile bent bridges. To further study the feasibility of isolation applied to pile bent bridges, the first 4 structures considered are variations on pile bent structures. Finally, to more closely investigate the possible benefits of isolation applied to multi-column bent bridges, two additional structures are selected for detailed analysis. Therefore, a total of six bridges are selected for analysis.

1. A 5-span, 15.24 meter (50') wide pile-bent structure is chosen for the low end of the span-to-width ratio range. 15.24 meter (50') span lengths make the ratio 1.0 and a symmetrical arrangement of bent heights is selected, i.e., this is a balanced bent stiffness structure. The clear height of the pipe piles from bottom of cap to point of fixity in the ground is 4.57 meters (15 feet).
2. The same 5-span, 15.24 meter (50') wide superstructure is placed on pile bents with varying heights to examine the effects of large eccentricity between mass and stiffness centers upon dynamic response. Pier height is 4.57 meters (15 feet) for Pier Nos. 1 and 3, and 10.67 meters (35 feet) for Pier Nos. 3 and 4.
3. An 8-span, 7.92 meter (26') wide bridge is analyzed to investigate the response of a structure with high span-to-deck-width ratio. Span lengths of 31.70 meters (104') make the ratio 4.0 and a symmetrical arrangement of pile bent heights is selected. Each Pier height is 4.57 meters (15 feet) from bottom of cap to point of fixity in the ground.

4. The same 8-span, 7.92 meter (26’) wide superstructure is placed on pile bents with varying heights to examine the effects of unequal, but symmetric pier heights upon dynamic response. Pier heights are 4.57 meters (15 feet) for Pier Nos. 1, 2, 6, and 7. Pier Nos. 3 and 5 are 7.62 meters (25 feet) high. Pier No. 4 is 10.67 meters (35 feet) high.
5. A 3-span superstructure with 2-column, friction pile supported bents representative of an Interstate over a county road is selected. Span lengths of 19.81m-36.57m-19.81m (65’-120’-65’) are adopted for the 13.18 meter (43’3”) wide bridge.
6. A 2-span superstructure with 2-column, friction pile supported bents representative of a state route over an Interstate is selected. Span lengths of 45.72m-45.72m (150’-150’) are selected for this 16.23 meter (53’3”) wide bridge.

Each of these 6 structures is based on an actual bridge in West Tennessee subject to the seismic hazard of the NMSZ. They are not merely hypothetical, academic subjects. Properties of the various structures are summarized in Table 1.4-1. Figures G1.4-1 through G1.4-10 depict general details of the bridges. The concept of isolation as a design alternative for routine bridges subjected to high magnitude design events is not a new one (Liao, et al., 2000) but research identifying the benefits and shortcomings of such a strategy in the ME of the NMSZ are needed.

Table 1.4-1. Bridge Properties

Property	Bridge No. 1	Bridge No. 2	Bridge No. 3	Bridge No. 4	Bridge No. 5	Bridge No. 6
w_{ss}, klf	9.38	9.38	7.53	7.53	11.26	14.57
e_{ss}, ft	5.50	5.50	6.59	6.59	7.75	8.17
I_{yy}, ft^4	5,671	5,671	1,635	1,635	6,873	14,101
I_{xx}, ft^4	50	50	90	90	170	325
A, ft^2	34.3	34.3	27.9	27.9	40.8	58.1
E_{ss}, ksi	5,148	5,148	5,148	5,148	5,460	5,460
J, ft^4	7.63	7.63	4.22	4.22	5.56	7.27

- w_{SS}: superstructure weight per linear foot
- e_{SS}: distance between the center of mass of the superstructure and the centroid of the substructure cap
- I_{yy}: second moment of area of the superstructure about a vertical axis
- I_{xx}: second moment of area of the superstructure about a horizontal axis
- A: total area of elements comprising the superstructure
- E_{SS}: Young's modulus for the superstructure
- J: torsional constant for the superstructure

1.5 Seismic Hazard at the Study Sites

Seismic hazard at the study sites is defined herein in terms of design spectral accelerations at bedrock (AASHTO B/C boundary), site classification from standard penetration test blow count correlation to average shear wave velocity in the upper 30 meters - V_{S30}, code-based site-amplification factors, and hazard deaggregation.

Design spectral accelerations at bedrock are based on 2008 USGS data available online (United States Geological Survey, 2011). These are based on probabilistic seismic hazard analysis - PSHA (Petersen, et al., 2008) and, for the NMSZ, include seven different ground motion prediction models:

1. Atkinson and Boore (2006)
2. Campbell (2003)
3. Frankel, et al., (1996)
4. Silva, et al., (2003)
5. Somerville, et al., (2001)
6. Tavakoli and Pezeshk (2005)
7. Toro, et al., (1997)

The purpose of this research is not to provide a detailed analysis of these 7 sources making up the PSHA for the sites, but a brief discussion explains decisions made in this paper regarding the nature of PSHA response spectra. Campbell (Campbell, 2003) used a hybrid empirical approach and explicitly stated that the developed ground motion model corresponds to the geometric mean of two horizontal components. Toro (Toro, et al., 1997) used the stochastic ground motion

method to develop a model for spectral acceleration and compared results to Eastern North America (ENA) ground motion data from previous work (Electric Power Research Institute, 1993). The EPRI report used the geometric mean of spectral ordinates for 66 horizontal recordings from earthquakes. While the other five referenced works are not explicit in identifying the geometric mean as the basis of the ground motion model, the basis of the USGS data is taken to be the geometric mean of two horizontal components as opposed to an arbitrary component or a maximum horizontal component. The contention that 2002 and 2008 USGS spectra are geometric mean spectra is consistent with previous work by others on relationships between various measures of ground motion intensity (Watson-Lamprey & Boore, October 2007).

Code-based site amplification is based solely on the AASHTO Site Classification. The shear wave velocity in the upper 30 meters of subsurface profile - V_{S30} - determines the Site Classification. As previously mentioned, total depth to bedrock is not considered in code-based site amplification, and the absence of profile depth in subsequent spectra poses a problem for sites in the ME of the NMSZ.

A deaggregation of the seismic hazard is needed to identify candidate events in terms of characteristic magnitude, distance (M_W,R) combinations. Deaggregation reveals the underlying (M_W,R) combinations which make up the total seismic hazard at a site. The 2008 USGS Interactive Deaggregations (Beta) online tool (United States Geological Survey, 2011) is used for this purpose. Peak ground acceleration and spectral accelerations at 0.2, 1.0, and 2.0 second periods (the longest period available from the USGS in the NMSZ is 2 seconds) are included in the deaggregation. For the NMSZ these deaggregations are for rock sites (AASHTO Site Class

B/C boundary) only and no site-effects are included. The modal event - the one most likely to produce ground motion exceeding the design value - is important in selecting records for nonlinear analysis (Bazzurro & Cornell, April, 1999).

Various metrics are used for “R” (distance) in modern ground motion databases. Some of these include: (a) distance from the site to the epicenter, (b) distance from the site to the hypocenter, (c) closest distance to the fault and (d) Joyner-Boore distance (Harmsen, USGS). For the purpose of ground motion selection at these bridge sites, no distinction is made among these. A ground motion with an epicentral distance of 60 kilometers from one database is given as much credence as a potential candidate as a record with a Joyner-Boore distance of 60 kilometers from another database.

The selection of a target response spectrum for modification of ground motion records is not a trivial step in the development of nonlinear time history analyses for isolated structures in the New Madrid Seismic Zone. Several options are available and the choice of the appropriate target spectra is vital as the effect upon results can be quite large among these options. The options discussed here include:

- Code-based uniform hazard spectra
- Hybrid empirical spectra developed specifically for the Central and Eastern United States
- Conditional mean spectra
- Risk-targeted spectra
- NMSZ-Specific spectra

1.5.1 Code-based Uniform Hazard Response Spectra

Current bridge design for seismic loading is primarily conducted using linear response spectrum analyses. A probabilistic seismic hazard analysis (PSHA) is required to define key points on the design spectrum and various rules are implemented to enable calculation of spectral values at any other point. Structural effects related to duration (low-cycle fatigue) and residual displacements are lost in this type of analysis. It is accepted for now as a reasonable design approach given the complexity of non-linear response history analysis combined with the lack of ground motion records in many areas, including the NMSZ. So development of a code-based design response spectrum is one of the first steps in the seismic design of a bridge. Crucial to the design response spectrum definition is the identification of a proper site classification for the project. The site classification determines the amplification factors to be applied to the mapped, bedrock spectrum, accounting for the effects of the subsurface profile. The primary determining factor for site classification is currently V_{S30} - the average shear wave velocity in the upper 30 meters of the subsurface profile.

OpenSHA software (Field, et al., 2003) is used to infer shear wave velocities (V_{S30}) in the upper 30 meters for both sites. The latitude, longitude, “stable continent”, and “Global Vs30 from Topographic Slope” options are specified and the results are:

- Site No. 1 - V_{S30} = 205 meters per second
- Site No. 2 - V_{S30} = 240 meters per second

Two borings at Site No. 1 indicate average blow counts in the upper 30 meters equal to 11.3 and 11.0 blows per foot, calculated in accordance with AASHTO (AASHTO, 2009). The AASHTO

breakpoint between Site Class “D” and Site Class “E” is defined either in terms of shear wave velocity (V_{S30} = 180 meters/sec) or in terms of average blow count (N = 15 blows per foot). While V_{S30} is the more accurate means of classifying sites, since the value obtained here is inferred from global data and not obtained from geotechnical testing, and since the blow count data indicate Site Class “E” conditions, Site No. 1 is conservatively place in Class “E” site conditions for soil amplification effects.

Two borings at Site No. 2 each indicate average blow counts of 23. Both blow count data and inferred V_{S30} from topographic slope (again using OpenSHA) indicate conditions well above the “D/E” break-point. Site No. 2 is a class “D” site for soil amplification effects.

USGS 2008 data are used to define the code-based design response spectra for each of the selected bridges. These spectra will represent the geometric mean of two horizontal components. Ground shaking with a 7% probability of exceedance in 75 years corresponds to a return period of approximately 1,000 years. This is the Design Basis Earthquake (DBE) in current bridge practice. Ground shaking with a 3% probability of exceedance in 75 years corresponds to a return period of about 2,500 years – often referred to as the Maximum Credible (or Considered) Earthquake (MCE). Both levels of ground motion will be included in this study. The data required for development of the various acceleration response spectra are summarized in Table 1.5.1-1. Response spectra are generated from the three control points as follows (AASHTO, 2009):

$$T_S = \frac{S_{D1}}{S_{DS}} \qquad \text{(Eq. 1-4)}$$

$$T_O = 0.2T_S \quad \text{(Eq. 1-5)}$$

For periods less than T_O, the spectral acceleration in g's is given by:

$$SA(T) = A_S + \frac{T}{T_o}(S_{DS} - A_S) \quad \text{(Eq. 1-6)}$$

For period between T_O and T_S, the spectral acceleration is constant and equal to S_{DS}. Finally, for periods greater than T_S, the spectrum is assumed to lie in a region of constant spectral velocity so that equation 1-7 is valid. Performing the indicated operations generates the design response spectra (See Figure 1.5.1-1).

$$SA(T) = \frac{S_{D1}}{T} \quad \text{(Eq. 1-7)}$$

Hazard deaggregations at each site for PGA, S_1, and S_S are obtained from an online application at the USGS web site (United States Geological Survey, 2011). Table 1.5.1-2 lists the mean and modal M, R (Magnitude, Source-to-Site-distance) combinations for each spectral acceleration and both hazard levels. Hazard deaggregation (also known as disaggregation) provides a detailed accounting of the various earthquake M, R combinations which went into the hazard analysis for a particular site. Deaggregation also provides information regarding the uncertainty in earthquake ground motions in the form of epsilon, ε. Epsilon is a normalized measure of the difference between a given spectral acceleration level and the median spectral acceleration predicted by each of the sources making up the hazard analysis. In Section 1.5.3, the conditional mean spectrum (CMS) is introduced. In areas of large uncertainty, like the NMSZ, negative epsilon values can make the CMS actually higher than the UHRS (Burks, 2010). This can make the CMS inappropriate for a target spectrum in the NMSZ.

Table 1.5.1-1 UHRS Control Points - Study Sites

Parameter	Site No. 1 - Shelby Co.		Site No. 2 - Lake Co.	
	35°19'26"N		36°23'11"N	
	89°45'25"W		89°28'03"W	
	DBE	MCE	DBE	MCE
	Mapped Accelerations		Mapped Accelerations	
PGA, g	0.330	0.591	1.086	1.809
S_1, g	0.168	0.324	0.546	1.079
S_S, g	0.629	1.136	1.963	3.409
	Site Factors (Class "E")		Site Factors (Class "D")	
F_{PGA}	1.109	0.900	1.000	1.000
F_v	3.295	2.703	1.500	1.500
F_a	1.443	0.900	1.000	1.000
	Design Accelerations		Design Accelerations	
A_S, g	0.366	0.532	1.086	1.809
S_{D1}, g	0.555	0.877	0.818	1.618
S_{DS}, g	0.907	1.023	1.963	3.409
	Periods		Periods	
T_S, sec	0.612	0.857	0.417	0.475
T_o, sec	0.122	0.172	0.083	0.095
T*, sec	0.765	1.072	0.521	0.593

Table 1.5.1-2 Hazard Deaggregation M, R Pairs - Study Sites

Parameter	Site No. 1 - Shelby Co.		Site No. 2 - Lake Co.	
	35°19'26"N		36°23'11"N	
	89°45'25"W		89°28'03"W	
	DBE	MCE	DBE	MCE
	Mean M,R		Mean M,R	
PGA, g	M_W7.14, 46.4 km	M_W7.19, 43.1 km	M_W7.58, 13.1 km	M_W7.62, 12.7 km
S_1, g	M_W7.51, 56.5 km	M_W7.58, 52.7 km	M_W7.65, 13.5 km	M_W7.68, 12.8 km
S_S, g	M_W7.29, 49.5 km	M_W7.39, 47.4 km	M_W7.61, 13.2 km	M_W7.65, 12.8 km
	Modal M,R		Modal M,R	
PGA, g	M_W7.70, 59.5 km	M_W7.70, 59.5 km	M_W7.70, 11.8 km	M_W7.70, 11.8 km
S_1, g	M_W7.70, 59.5 km	M_W7.70, 59.5 km	M_W7.70, 11.8 km	M_W7.70, 11.8 km
S_S, g	M_W7.70, 59.5 km	M_W7.70, 59.5 km	M_W7.70, 11.8 km	M_W7.70, 11.8 km

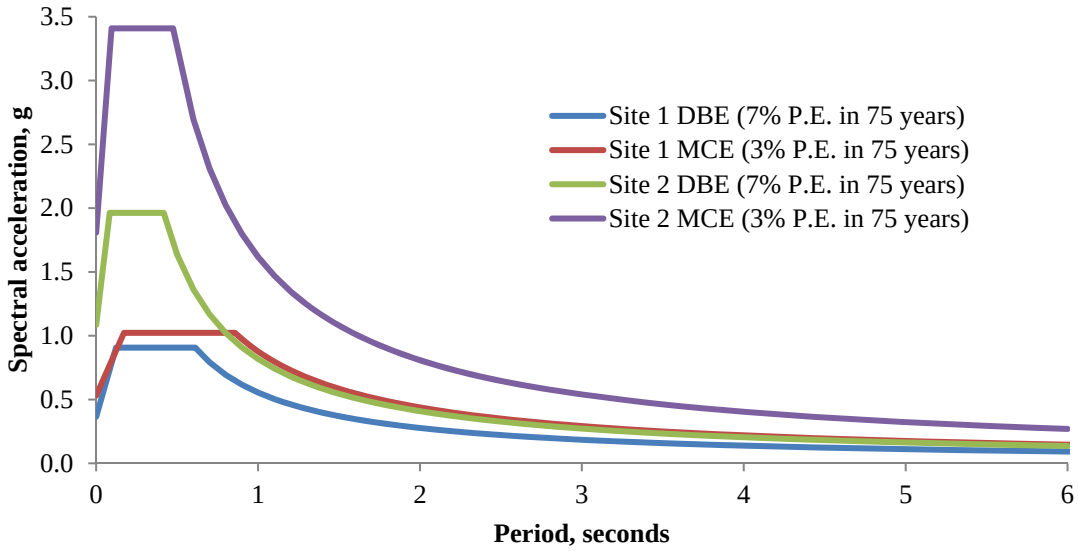

Figure 1.5.1-1. Uniform Hazard Response Spectra

1.5.2 Empirical Response Spectra

With virtually no high magnitude, strong motion data in the Central and Eastern United States (CEUS), PSHA relies upon seismological models and stochastic methods to a high degree. Recent work at the University of Memphis suggests the possibility that the current USGS uniform hazard response spectra may be overly conservative at low periods and somewhat un-conservative at medium-to-long periods under certain conditions. Methods have been developed whereby hybrid empirical spectra may be generated at bedrock (Pezeshk, et al., August, 2011). Empirical-stochastic prediction equations for eastern North America have been developed as well (Tavakoli & Pezeshk, 2005). And a stochastic finite-fault model procedure has been used to produce ground motion prediction models for eastern North America (Atkinson & Boore, 2006). Campbell (Campbell, 2003) also used a hybrid-empirical approach to estimate ground motions for eastern North America.

The current (2008) USGS hazard analysis uses the following weights on the models previously discussed for sites in the NMSZ (Petersen, 2008):

- Frankel and others (1996): single-corner point-source model - weight = 0.1
- Somerville and others (2001): full waveform simulation - weight = 0.2
- Campbell (2003): hybrid empirical - weight = 0.1
- Toro and others (1997): single corner finite fault model - weight = 0.2
- Atkinson and Boore (2006): dynamic corner frequency with 200 bar stress drop - weight = 0.1
- Atkinson and Boore (2006): dynamic corner frequency with 140 bar stress drop - weight = 0.1
- Tavakoli and Pezeshk (2005): hybrid empirical - weight = 0.1
- Silva and others (2002): single corner finite fault model - weight = 0.1

1.5.3 Conditional Mean Response Spectra

A detailed discussion of conditional mean spectra (CMS) will not be presented here. The interested reader is encouraged to investigate the work by Baker (Baker, 2011) on the theoretical background to conditional mean spectra. Essentially, a conditioning period is set and the spectral accelerations at all other period are determined based on the condition that the spectral acceleration at the conditioning period be exactly equal to the target vale. So a UHRS curve could be viewed as an envelope of several CMS curves. It may be argued that the conditional mean spectrum for a given site is a more appropriate choice than is the uniform hazard code-based spectrum when ground motion selection and scaling is concerned. Conditional mean spectra provide information on the mean response at a particular period of interest. Uniform

hazard spectra provide spectral amplitudes caused by differing earthquake events. So, while a scenario event for selecting ground motions may be an earthquake of magnitude 7.7 at 60 kilometers, the uniform hazard, code-based spectra is an envelope containing acceleration data from many other magnitude-distance combinations. The USGS has online application for generating interactive disaggregation may also be used to generate conditional mean spectra (United States Geological Survey, 2011).

1.5.4 Risk-Targeted Response Spectra

Some codes and specifications have adopted the so-called "risk-targeted" response spectra. Risk-targeted ground motions are typically smaller than uniform hazard based ground motions in the New Madrid Seismic Zone (Luco, et al., 2007). A basic idea behind the concept of a risk-targeted response spectrum is that the shape of hazard curves - intensity measure vs. probability of exceedance - varies geographically. In order to provide for a uniform probability of failure for designed structures, factors are applied to uniform hazard spectra. The logic of designing for uniform risk as opposed to uniform hazard is sound and perhaps will someday be considered for adoption by AASHTO for bridge design.

The USGS has provided an online application for generating risk-targeted spectra (United States Geological Survey, 2011). These risk-targeted spectra are maximum horizontal component spectra while uniform hazard curves and conditional mean spectra are both the geometric mean of two horizontal components. The method used to convert geometric mean spectra to maximum component spectra is to multiply the short-period (0.2 second) geometric mean ordinate by 1.1 and to multiply the 1-second period geometric mean ordinate by 1.3. For purposes of this study, geometric mean spectra will be used for all scenarios. Therefore, risk-targeted spectra generated

from the USGS application should be modified using division by the above factors prior to comparisons with uniform hazard and conditional mean spectra.

The various spectra options for both design levels at both sites are depicted in Figures 1.5.4-1 through 1.5.4-4. Conditional mean spectra shown in the figures are based on a conditional period of 1 second. Different spectra shapes would be obtained were a different conditional period to be used. The UHRS and CMS for Site No. 1 are virtually indistinguishable and this is not uncommon for areas with relatively high uncertainty due to the lack of recorded, historical strong motion data (such as the NMSZ).

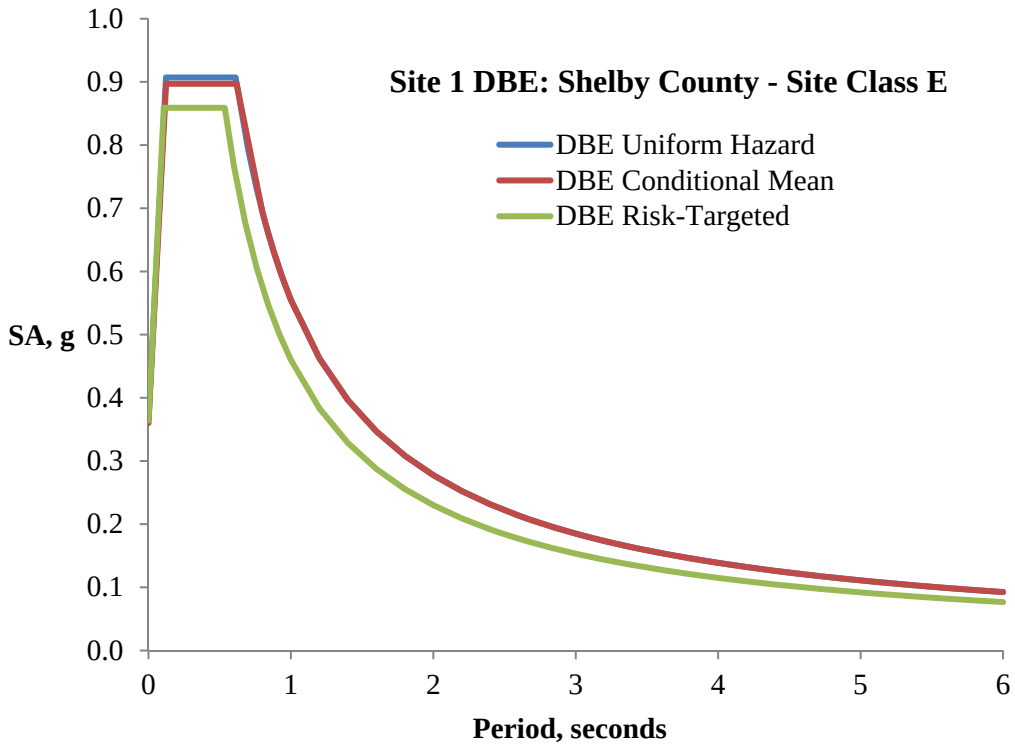

Figure 1.5.4-1. Site 1 DBE Spectra

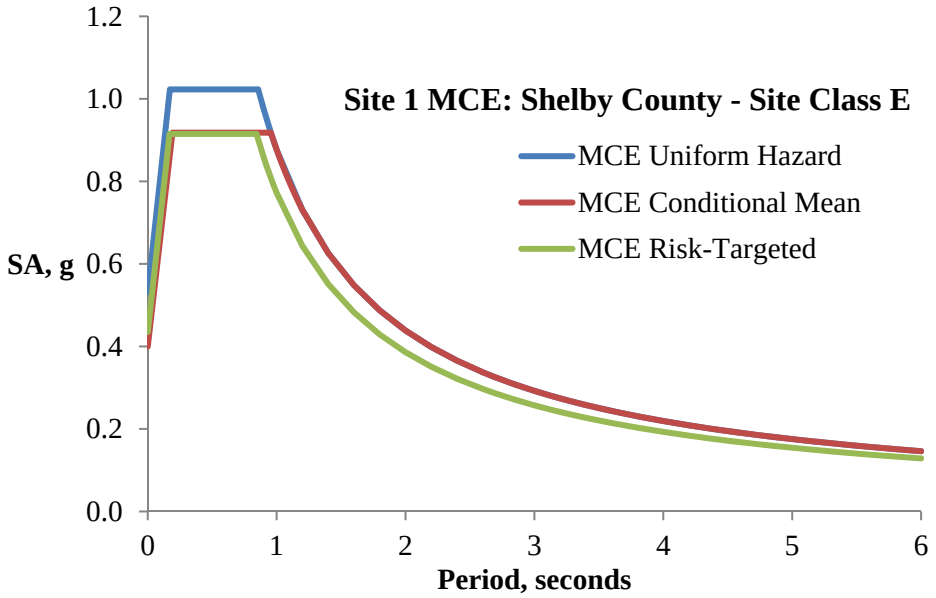

Figure 1.5.4-2. Site 1 MCE Spectra

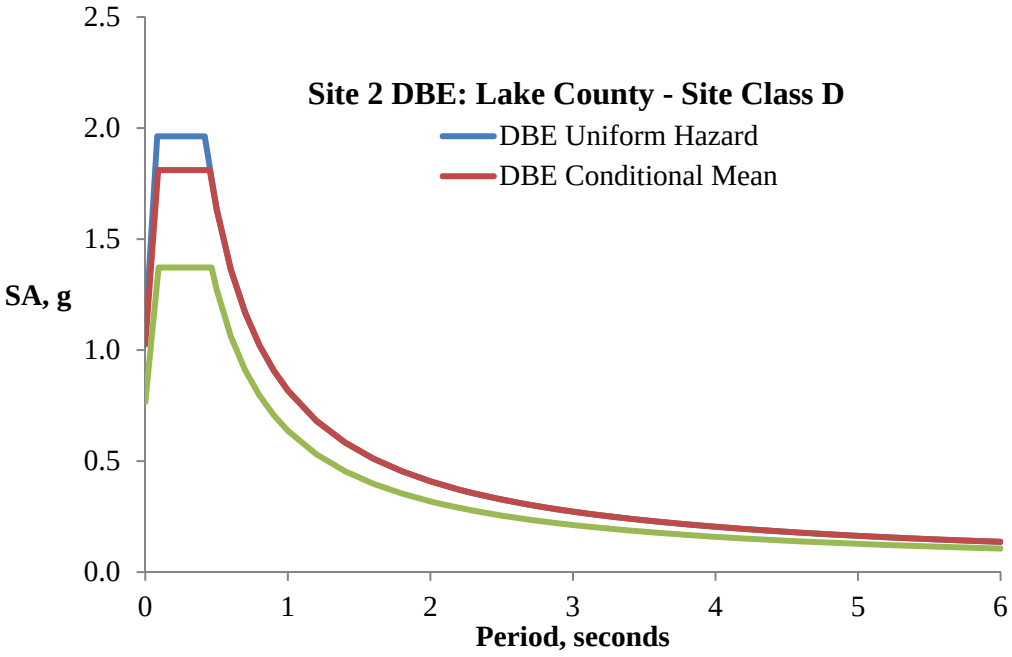

Figure 1.5.4-3. Site 2 DBE Spectra

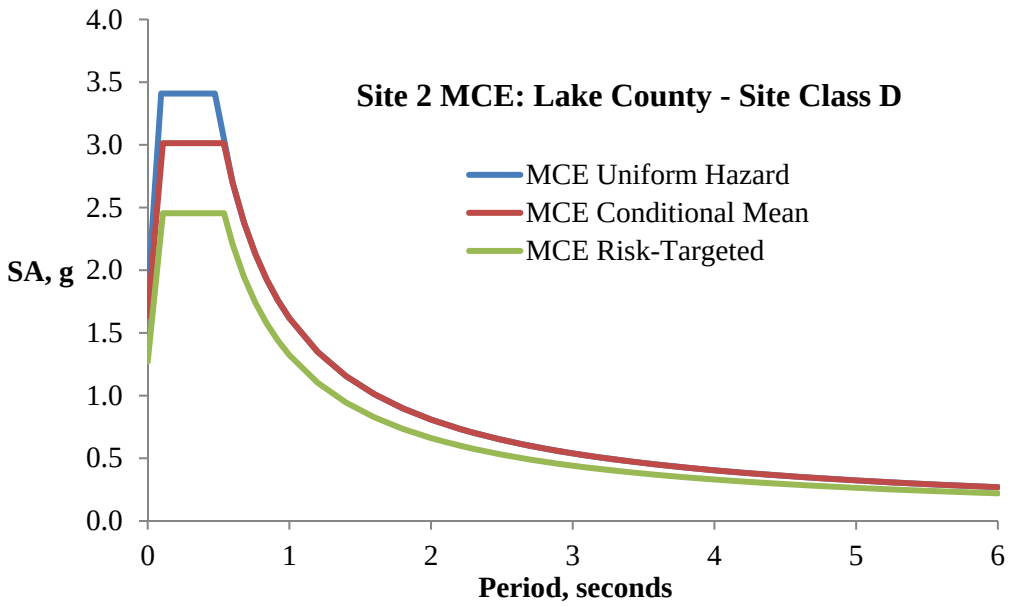

Figure 1.5.4-4. Site 2 MCE Spectra

1.5.5 NMSZ-Specific Response Spectra

There has been lots of interest in attenuation of ground motion considering site effects in the Mississippi Embayment (ME) of the NMSZ in recent years. The soil column in the ME ranges from less than 30 meters at the periphery of the embayment to more than 1000 meters at the Mississippi River. Hashash and Park (Hashash & Park, 2001) developed a one-dimensional site response model for the ME and generated response spectra for various depths of the soil column. Amplification effects commonly assumed in codes were found to be un-conservative at periods beyond 0.7 seconds. Park and Hashash (Park & Hashash, 2004) performed a full probabilistic seismic hazard analysis and concluded that 30 meter thick soil profiles produced soil amplification generally in agreement with code-based assumptions, while thicker profiles were apt to have larger amplification at longer periods. Fernandez and Rix (Fernandez & Rix, 2006) also conducted a site-specific hazard analyses in the NMSZ for various soil profile depths.

Attenuation relationships were derived similar to GMPM's typically used to generate USGS data. The general form of the relationship is defined through the independent variables R - epicentral distance in kilometers, and M - moment magnitude.

$$ln(y) = c_1 + c_2 \cdot M + c_3 \cdot (M-6)^2 + c_4 \cdot ln(R_M) + c_5 \cdot max\left[ln\frac{R}{70}, 0\right] + c_6 \cdot R_M \quad \text{(Eq. 1-8)}$$

$$R_M = R + c_7 \cdot exp(c_8 \cdot M) \quad \text{(Eq. 1-9)}$$

$$\sigma_{lny} = c_9 \cdot M + c_{10} \quad \text{(Eq. 1-10)}$$

The dependent variable - *y* - takes on the values for peak ground displacement in centimeters, peak ground velocity in cm/s, and spectral acceleration in g's at 5% damping. Correlation coefficients are obtained for 7 embayment depth ranges, three stress drop values, three source models, two soil profiles - upland and lowlands, and one set of nonlinear soil properties developed by EPRI (Electric Power Research Institute, 1993). The source models included those of Atkinson and Boore (Atkinson & Boore, 1995), Frankel (Frankel, et al., 1996), and Silva (Silva, et al., 2003). Stress drops corresponding to medium, high and low values as well as magnitudes ranging from 4.0 to 7.5 were studied. Soil profile depth ranges included:

- 6 meters - 15 meters
- 15 meters - 30 meters
- 30 meters - 61 meters
- 61 meters - 152 meters
- 152 meters - 305 meters
- 305 meters - 610 meters
- 610 meters - 1220 meters

The so-called Lowlands profile is characterized by Holocene deposits on the alluvial flood plains in the embayment while Uplands profile consists of Pleistocene deposits. Site No. 1 - east of Memphis - would correspond to an Upland profile while Site No. 2 near Reelfoot Lake would more likely be considered a Lowlands profile. The Lowlands profile is characterized by lower shear wave velocities in the upper 80 meters of soil. Hashash (Hashash, et al., 2008) reports V_{S30} values of 314 m/s for the Uplands profile and 249 m/s for the Lowlands profile. The two profiles have very similar shear wave velocity profiles once the 80 meter depth has been reached.

The coefficients were obtained and a series of spectra generated for an epicentral distance of 35 kilometers and a moment magnitude of 7.7 - slightly higher than the maximum magnitude studied in the reference work. The purpose is to examine the effect of soil profile depth upon spectral shape. Figures G1.5.5-1 through G1.5.5-9 are spectra plots for the high stress drop option. Other stress drop spectral shapes are similar.

In general, the Atkinson and Boore source model produced much lower long period response compared to the Frankel source model with Silva in between the two. Spectral peaks shift towards longer periods as the embayment depth increases for all source models. The most dramatic jumps generally occur in transitioning from the 61-152 meter bin to the 152-305 meter bin. For these thicker deposits the spectral shape in longer period regions can be observed to be more severe than code spectral shapes.

Wu (Wu & Wen, 1999) has also developed uniform hazard ground motions for various mid-America cities, including Memphis. For this study, a so-called “representative” profile was used for Memphis. The profile is summarized in Table 1.5.5-1. Atkinson (Atkinson & Beresnev,

2002) used this same profile in addition to a profile representative of St. Louis, Missouri, given in Table 1.5.5-2. Fernandez (Fernández, 2007) studied ground motions expected at 8 locations in the Mississippi Embayment. Soil column depths were assigned for each site as shown in Table 1.5.5-3. Park (Park & Hashash, 2005) selected eight sites and also assigned soil column depth to each site, as listed in Table 1.5.5-4. Recommended site response analysis parameters were derived and compared to values used by previous researchers. The two sets of values are listed in Table 1.5.5-5.

Table 1.5.5-1. Representative Soil Profile - Memphis

Layer	Material	Thickness, m	V_S, m/s	ρ, g/cm^3
1	Alluvium	7.2	360	1.92
2	Alluviun	4.8	360	2.00
3	Alluvium	14.9	360	2.08
4	Loess	9.0	360	2.16
5	Fluvial Deposits	7.9	360	1.98
6	Jackson Formation	47.3	520	2.08
7	Memphis Sand	245.6	667	2.30
8	Wilex Group	83.3	733	2.40
9	Midway Group	580	820	2.50
10	Paleozoic Rock	500	3280	2.50
11	Paleozoic Rock	8000	3600	2.80
12	Paleozoic Rock	10000	3700	2.90
13	Paleozoic Rock	20000	4200	3.00

Table 1.5.5-2. Representative Soil Profile - St. Louis

Layer	Material	Thickness, m	V_S, m/s	ρ, g/cm^3
1	Loess	6	185	1.9
2	Glacio-fluvial	10	310	2.1
3	Mississippi Limestone	984	2900	2.6
4	Paleozoic Rock	500	3280	2.5
5	Paleozoic Rock	8000	3600	2.7
6	Paleozoic Rock	10000	3700	2.9
7	Paleozoic Rock	20000	4200	3.0

Table 1.5.5-3. Soil Column Depth Variation - Fernandez

City	Latitude	Longitude	Soil Profile	Depth, m
Memphis, TN	35.050	-90.000	Lowlands	900
Memphis, TN	35.050	-90.000	Uplands	900
Jonesboro, AR	35.833	-90.700	Uplands	600
Jackson, TN	35.600	-88.917	Uplands	350
Blytheville, AR	35.950	-89.950	Lowlands	850
Paducah, KY	37.067	-88.767	Uplands	120
Cape Girardeau, MO	37.233	-89.583	Lowlands	10
Little Rock, AR	34.733	-92.233	Uplands	10

Table 1.5.5-4. Soil Column Depth Variation - Park

Station	Latitude	Longitude	Soil Profile	Depth, m	R_{EPI}, km
GLAT	36.27	-89.29	Uplands	610	291
HICK	36.54	-89.23	Uplands	500	307
HALT	35.91	-89.34	Uplands	660	274
GNAR	35.96	-90.02	Lowlands	700	217
HBAR	35.56	-90.66	Lowlands	660	149
PEBM	36.11	-89.75	Lowlands	720	237
PENM	36.45	-89.63	Lowlands	500	272
PARM	36.67	-89.75	Lowlands	250	276

Table 1.5.5-5. Site Response Parameters - Park

Parameter	EPRI-Matched	NMSZ-Derived
β	0.7	1.4
s	0.8	0.8
σ_{ref}	0.18 MPa	0.18 MPa
a	0.05	0.163
b	0.4	0.63
c	-	1.5
d	-	0.3
Bedrock V_S	-	3 km/s

These parameters are explained in detail by Hashash (Hashash, 2011) and are used to define modified hyperbolic model stress-strain and damping properties in a nonlinear one-dimensional site response analysis.

$$\tau = \frac{G_{mo}\gamma}{1+\beta\left(\frac{G_{mo}}{\tau_{mo}}\gamma\right)^{s}} = \frac{G_{mo}\gamma}{1+\beta\left(\frac{\gamma}{\gamma_r}\right)^{s}} \quad \text{(Eq. 1-11)}$$

$$G_{mo} = \rho V_s^2 \quad \text{(Eq. 1-12)}$$

$$\gamma_r = a\left(\frac{\sigma_v'}{\sigma_{ref}}\right)^{b} \quad \text{(Eq. 1-13)}$$

$$\xi = small\ strain\ damping = \frac{c}{(\sigma_v')^{d}} \quad \text{(Eq. 1-14)}$$

Values of the constants *c* and *d*, which define the pressure dependency of the damping model, are those recommended by Hashash (Hashash & Park, 2001).

As an aid in comparing sites to those studied by Fernandez, hazard deaggregations and inferred shear wave velocity estimates (from OpenSHA) are computed and summarized in Tables 1.5.5-6 through 1.5.5-13. This will be important in deciding which (if any) records from the work of Fernandez would be appropriate for a given site. Study Site No. 2 in Lake County, TN is similar to Blytheville. Obviously, study Site No. 1, a short distance from Memphis, is similar to Memphis.

As previously mentioned, Figures G1.5.5-1 through 1.5.5-9 help visualize the effect of embayment depth upon spectral shape. The figures have been generated from the Georgia Tech (Fernandez & Rix, 2006) study results for a high stress drop at an uplands profile site for each of the source models:

- Atkinson-Boore
- Frankel
- Silva

The figures show spectral acceleration, velocity, and displacement. A constant velocity region of the design response spectrum is implied by code spectral shapes at periods beyond:

$$T_S = S_{D1} / S_{DS}$$

This period, T_S, is typically about 0.7 +/- 0.3 seconds. The deviation from a constant velocity region near a period of 1 second at deep soil sites is evident in the figures, indicating that code-based spectral shapes may not be appropriate for seismic design in the ME of the NMSZ.

While not explicitly a part of design spectrum development, the site period is an important factor in earthquake engineering and may be estimated using the expression for a uniform profile with constant properties (Rahnama & Krawinkler, 1993). With an average shear wave velocity of 713 m/s and depth to bedrock of 1000 meters from Table 1.5.5-1, the estimated period for Site 1 is:

$$T_n = \frac{1}{2n-1} \cdot \frac{4H}{V_S} \rightarrow T_1 = \frac{4 \cdot 1000}{713} = 5.61\ seconds \qquad \text{(Eq. 1-15)}$$

Analysis of the profile using DEEPSOIL (Hashash, 2011) with the detailed properties from Table 1.5.5-1 produces a site period from a more rigorous approach of T_1 = 5.70 seconds. So the approximate expression of equation 1-15 works very well in this case. This could be significant for near-fault sites (source-to-site-distance less than about 12 kilometers) subjected to pulse-type

loading. Were the pulse period close to the site period of 5.6 seconds, large amplifications of the ground motion would be possible.

For the average shear wave velocity calculation, the method used in AASHTO (and most, if not all, design specifications) has been used. Rather than summing the product of layer thickness and layer V_S and dividing by the sum of all layer thickness values, the average shear wave velocity is calculated by summing the layer depth divided by the layer thickness for all layers and dividing by the sum of layer depths. Equation 1-16 is the intuitive, yet incorrect, averaging method and equation 1-17 is the method recommended by design specifications. Incorrect averaging at Site 1 gives a shear wave velocity of 226 m/s while the appropriate averaging gives a value of 217 m/s.

$$\bar{V}_S = \frac{\sum h_i \cdot V_{Si}}{\sum h_i} \qquad \text{(Eq. 1-16)}$$

$$\bar{V}_S = \frac{\sum h_i}{\sum \frac{h_i}{V_{Si}}} \qquad \text{(Eq. 1-17)}$$

Table 1.5.5-6. UHRS Control Points - Jonesboro and Jackson

Parameter	Jonesboro, AR		Jackson, TN	
	V_{S30} = 386 m/s		V_{S30} = 327 m/s	
	35.833°N		35.600°N	
	90.700°W		88.917°W	
	DBE	MCE	DBE	MCE
	Mapped Accelerations		Mapped Accelerations	
PGA, g	0.502	0.900	0.233	0.404
S_1, g	0.246	0.488	0.131	0.235
S_S, g	0.920	1.688	0.460	0.796
	Site Factors (Class ”C”)		Site Factors (Class “D”)	
F_{PGA}	1.000	1.000	1.333	1.096
F_v	1.554	1.312	2.276	1.930
F_a	1.032	1.000	1.432	1.182
	Design Accelerations		Design Accelerations	
A_S, g	0.502	0.900	0.311	0.443
S_{D1}, g	0.383	0.640	0.298	0.454
S_{DS}, g	0.950	1.688	0.658	0.941
	Periods		Periods	
T_S, sec	0.403	0.379	0.453	0.482
T_o, sec	0.081	0.076	0.091	0.096
T*, sec	0.504	0.474	0.566	0.603

Table 1.5.5-7. Hazard Deaggregation M, R Pairs - Jonesboro and Jackson

Parameter	Jonesboro, AR		Jackson, TN	
	35.833°N		35.600°N	
	90.700°W		88.917°W	
	DBE	MCE	DBE	MCE
	Mean M,R		Mean M,R	
PGA, g	M_W7.36, 32.5 km	M_W7.44, 30.4 km	M_W7.08, 67.8 km	M_W7.09, 63.4 km
S_1, g	M_W7.58, 36.6 km	M_W7.64, 34.1 km	M_W7.47, 84.7 km	M_W7.55, 80.1 km
S_S, g	M_W7.45, 33.9 km	M_W7.55, 32.2 km	M_W7.23, 72.9 km	M_W7.31, 70.4 km
	Modal M,R		Modal M,R	
PGA, g	M_W7.70, 37.9 km	M_W7.70, 37.9 km	M_W7.70, 86.5 km	M_W7.70, 86.5 km
S_1, g	M_W7.70, 37.9 km	M_W7.70, 37.9 km	M_W7.70, 86.5 km	M_W7.70, 86.5 km
S_S, g	M_W7.70, 37.9 km	M_W7.70, 37.9 km	M_W7.70, 86.5 km	M_W7.70, 86.5 km

Table 1.5.5-8. UHRS Control Points - Blytheville and Paducah

Parameter	Blytheville, AR		Paducah, KY	
	V_{S30} = 205 m/s		V_{S30} = 270 m/s	
	35.950°N		37.067°N	
	89.950°W		88.767°W	
	DBE	MCE	DBE	MCE
	Mapped Accelerations		Mapped Accelerations	
PGA, g	1.117	1.834	0.639	1.109
S_1, g	0.569	1.151	0.304	0.591
S_S, g	2.021	3.490	1.149	2.047
	Site Factors (Class "E")		Site Factors (Class "D")	
F_{PGA}	0.900	0.900	1.000	1.000
F_v	2.400	2.400	1.792	1.500
F_a	0.900	0.900	1.040	1.000
	Design Accelerations		Design Accelerations	
A_S, g	1.005	1.651	0.639	1.109
S_{D1}, g	1.366	2.762	0.545	0.877
S_{DS}, g	1.819	3.141	1.195	2.047
	Periods		Periods	
T_S, sec	0.751	0.879	0.456	0.433
T_o, sec	0.150	0.176	0.091	0.087
T*, sec	0.938	1.099	0.570	0.541

Table 1.5.5-9. Hazard Deaggregation M, R Pairs - Blytheville and Paducah

Parameter	Blytheville, AR		Paducah, KY	
	35.950°N		37.067°N	
	89.950°W		88.767°W	
	DBE	MCE	DBE	MCE
	Mean M,R		Mean M,R	
PGA, g	M_W7.58, 12.2 km	M_W7.62, 11.8 km	M_W7.41, 26.7 km	M_W7.50, 25.9 km
S_1, g	M_W7.65, 12.4 km	M_W7.68, 11.7 km	M_W7.59, 29.3 km	M_W7.65, 28.0 km
S_S, g	M_W7.61, 12.3 km	M_W7.64, 11.8 km	M_W7.50, 27.6 km	M_W7.59, 27.0 km
	Modal M,R		Modal M,R	
PGA, g	M_W7.70, 11.5 km	M_W7.70, 11.4 km	M_W7.70, 28.6 km	M_W7.70, 28.2 km
S_1, g	M_W7.70, 11.5 km	M_W7.70, 11.4 km	M_W7.70, 28.6 km	M_W7.70, 29.4 km
S_S, g	M_W7.70, 11.5 km	M_W7.70, 11.3 km	M_W7.70, 28.6 km	M_W7.70, 28.2 km

Table 1.5.5-10. UHRS Control Points - Cape Girardeau and Little Rock

Parameter	Cape Girardeau, MO		Little Rock, AR	
	V_{S30} = 218 m/s		V_{S30} = 298 m/s	
	37.233°N		34.733°N	
	89.583°W		92.233°W	
	DBE	MCE	DBE	MCE
	Mapped Accelerations		Mapped Accelerations	
PGA, g	0.455	0.808	0.121	0.212
S_1, g	0.227	0.445	0.082	0.149
S_S, g	0.841	1.533	0.256	0.446
	Site Factors (Class ”D”)		Site Factors (Class “D”)	
F_{PGA}	1.045	1.000	1.558	1.376
F_v	1.946	1.555	2.400	2.204
F_a	1.164	1.000	1.595	1.443
	Design Accelerations		Design Accelerations	
A_S, g	0.475	0.808	0.189	0.292
S_{D1}, g	0.442	0.692	0.197	0.328
S_{DS}, g	0.979	1.533	0.408	0.644
	Periods		Periods	
T_S, sec	0.451	0.451	0.482	0.510
T_o, sec	0.090	0.090	0.096	0.102
T*, sec	0.564	0.564	0.602	0.638

Table 1.5.5-11. Hazard Deaggregation M, R Pairs - Cape Girardeau and Little Rock

Parameter	Cape Girardeau, MO		Little Rock, AR	
	37.233°N		34.733°N	
	89.583°W		92.233°W	
	DBE	MCE	DBE	MCE
	Mean M,R		Mean M,R	
PGA, g	M_W7.36, 36.1 km	M_W7.44, 33.8 km	M_W7.09, 129.7 km	M_W7.02, 117.6 km
S_1, g	M_W7.57, 41.1 km	M_W7.64, 38.0 km	M_W7.48, 161.7 km	M_W7.55, 154.8 km
S_S, g	M_W7.45, 37.6 km	M_W7.55, 35.7 km	M_W7.22, 138.2 km	M_W7.25, 131.6 km
	Modal M,R		Modal M,R	
PGA, g	M_W7.70, 40.2 km	M_W7.70, 39.6 km	M_W7.70, 167.6 km	M_W7.70, 167.6 km
S_1, g	M_W7.70, 40.2 km	M_W7.70, 40.0 km	M_W7.70, 167.7 km	M_W7.70, 167.6 km
S_S, g	M_W7.70, 40.3 km	M_W7.70, 39.8 km	M_W7.70, 167.6 km	M_W7.70, 167.6 km

Table 1.5.5-12. UHRS Control Points - Memphis

Parameter	Memphis, TN	
	V_{S30} = 295 m/s	
	35.050°N	
	90.000°W	
	DBE	MCE
	Mapped Accelerations	
PGA, g	0.286	0.495
S_1, g	0.161	0.292
S_S, g	0.555	0.980
	Site Factors (Class "D")	
F_{PGA}	1.228	1.005
F_v	2.156	1.816
F_a	1.356	1.108
	Design Accelerations	
A_S, g	0.351	0.497
S_{D1}, g	0.347	0.530
S_{DS}, g	0.753	1.086
	Periods	
T_S, sec	0.461	0.488
T_o, sec	0.092	0.098
T*, sec	0.577	0.610

Table 1.5.5-13. Hazard Deaggregation M, R Pairs - Memphis

Parameter	Memphis, TN	
	35.050°N	
	90.000°W	
	DBE	MCE
	Mean M,R	
PGA, g	M_W7.17, 56.7 km	M_W7.23, 53.8 km
S_1, g	M_W7.53, 68.3 km	M_W7.59, 64.5 km
S_S, g	M_W7.31, 60.5 km	M_W7.41, 58.6 km
	Modal M,R	
PGA, g	M_W7.70, 69.0 km	M_W7.70, 68.7 km
S_1, g	M_W7.70, 69.2 km	M_W7.70, 68.9 km
S_S, g	M_W7.70, 69.1 km	M_W7.70, 68.8 km

1.6 Analysis Methods

The analytical methods used to assess a structure's response, once the earthquake loading has been defined in terms of either a design response spectrum or a set of strong ground motion records, are numerous. Since these tools will be used to evaluate both non-isolated and isolated bridges in this research, a brief discussion of some of these tools is necessary. With regard to the dynamic response of a bridge to earthquake ground motion, there are at least 4 methods one may adopt for the analysis:

1. response spectrum analysis using the elastic response spectrum with elastic damping and initial stiffness properties;
2. response spectrum analysis using the elastic response spectrum with effective damping and effective stiffness properties;
3. response spectrum analysis using inelastic spectra with initial stiffness properties;
4. non-linear response history analysis using elastic damping and non-linear stiffness properties.

In an ideal world, all four would produce and identical result, the true response. We know this is not the case. The merits and shortcomings of the four methods are discussed below.

1.6.1 Equivalent Linear Response Spectrum Analysis – Initial Properties

Given the complexity of performing non-linear dynamics time history analysis and the difficulty in interpreting the results, it is certainly desirable to have a simplified, yet accurate, method of estimating the response of structures. Response Spectrum techniques are the method of choice in current engineering offices. This is not likely to change soon.

Non-linear behavior results in energy dissipation which may be conveniently treated as added equivalent viscous damping. The stiffness is not constant during loading for non-linear systems. The question is then – which values for effective damping and effective stiffness, when used in a response spectrum analysis, will produce similar results to those obtained in a non-linear response history analysis.

Engineers may choose the initial stiffness and elastic, initial-stiffness-based viscous damping in a linear response spectrum analysis to estimate non-linear response to dynamic earthquake loading. Using the assumption that a yielding structure will experience the same displacement as a non-yielding structure for a given initial stiffness and a given ground motion, the structural damping with the initial stiffness is adopted for analysis. The so-called "equal displacement" assumption has been applied as a rule-of-thumb for decades. However, we now know that, particularly for short-period structures, the assumption is not valid. So, amplification may be applied to displacements obtained from a linear response spectrum analysis to estimate nonlinear response. AASHTO applies the following rules for displacement amplification when initial stiffness analysis is chosen. The response spectrum displacements should be magnified by R_d when T*/T is greater than 1.0.

$$T^* = 1.25T_S = 1.25\frac{S_{D1}}{S_{DS}} \qquad \text{(Eq. 1-18)}$$

$$R_d = \left(1 - \frac{1}{\mu_D}\right)\frac{T^*}{T} + \frac{1}{\mu_D} \qquad \text{(Eq. 1-19)}$$

So that, given the response spectrum displacement, D_{RSA}, one may determine the displacement demand, D_{DEM}, as follows:

$$D_{DEM} = R_d D_{RSA} \qquad \text{(Eq. 1-20)}$$

Note, however, that R_d is a function of the displacement ductility demand, μ_D, which is in turn, a function of total displacement, D_{DEM}. So, either an iterative solution is required or a little algebra may be used to arrive at a quadratic equation solution.

$$D_{DEM} = \mu_D D_y = D_{RSA}\left[\left(1 - \frac{1}{\mu_D}\right)\frac{T^*}{T} + \frac{1}{\mu_D}\right]$$

$$\mu_D^2 D_y = D_{RSA}\left(\mu_D \frac{T^*}{T} - \frac{T^*}{T} + 1\right)$$

$$\mu_D^2 D_y - \mu_D\left(D_{RSA}\frac{T^*}{T}\right) + D_{RSA}\left(\frac{T^*}{T} - 1\right) = 0$$

$$\mu_D = \frac{\left(D_{RSA}\frac{T^*}{T}\right) \pm \sqrt{\left(D_{RSA}\frac{T^*}{T}\right)^2 - 4D_{RSA}\left(\frac{T^*}{T} - 1\right)D_y}}{2D_y} \qquad \text{(Eq. 1-21)}$$

1.6.2 Equivalent Linear Response Spectrum Analysis – Effective Properties

Alternatively, effective damping and stiffness properties may be adopted for a response spectrum analysis. This is the method first proposed by Gulkan and Sozen (Gulkan & Sozen, December, 1974) and further developed by Priestley and others (Priestley, et al., 2007).

Effective stiffness is taken equal to the secant stiffness, labeled as K_{eff} in Figure 1.6.2-1. Effective viscous damping is imparted to the system through hysteretic behavior of yielding elements.

There are many proposed rules for establishing effective damping properties. For the most part, these rules are all based upon equivalent viscous damping, the method most likely to

be used for response spectrum analyses in any design office today. Some of the proposed rules are summarized in Table 1.6.2-1. Details on development of the rules may be found in the literature (Suarez, 2008), (Priestley, et al., 2007), (Buckle, et al., 2006), (Pietra, et al., 2008), (Applied Technology Council, June, 2005).

For the bi-linear isolator with post-yield stiffness ratio equal to α, it can be shown (APPENDIX C) that the maximum possible effective damping is given by the following expression.

$$\left(\xi_{eff}\right)_{max} = \frac{2(1-\alpha)}{\pi\left(1+\sqrt{\alpha}\right)^2} \qquad \text{(Eq. 1-22)}$$

This maximum possible damping occurs when the displacement ductility demand on the isolator ($\mu_D = D_{ISO} / D_y$) is equal to:

$$\mu_D = 1 + \frac{1}{\sqrt{\alpha}} \qquad \text{(Eq. 1-23)}$$

Typical LRB isolators employ $\alpha = 0.10$ giving rise to a maximum possible effective damping of 33.07%. For the FPS isolator α is essentially equal to zero. With $\alpha = 0$, the maximum possible effective damping is 63.66%. For a given combination of structure and loading, it may thus be possible to obtain generally higher damping ratios with the FPS isolator compared to the LRB isolator. Conversely, LRB isolators have the potential advantage of operating at higher pre-yield periods compared to corresponding FPS isolators.

In the equations for effective damping, μ is the displacement ductility demand on the structure, defined as the ratio of the maximum displacement to the yield displacement. A little algebra will show that the equation for a “Bilinear Isolation System (General)” and the equation for “Any Bilinear System” are identical when the elastic damping, ξ_o, is zero.

The tabulated rule for reinforced concrete bridge columns is based on a stiffness-degrading thin Takeda hysteresis model (Priestley, et al., 2007). Note that for bilinear isolation systems there is generally no degradation of stiffness throughout the inelastic response history. This degrading of stiffness upon unloading may, somewhat ironically, have a beneficial effect upon residual displacements (Ruiz-Garcia & Miranda, August 2005).

It is important to distinguish between effective damping in the isolator itself and effective damping in the structural system as a whole. For a single degree of freedom isolator on an infinitely rigid sub-structure, the terms above are both the isolator effective damping and the system effective damping. For multiple, flexible sub-structures connected by an elastic super-structure, the situation is more complex. Part of the total displacement at each sub-structure is due to flexure in the sub-structure and part is due to movement of the isolator, as depicted in Figure 1.6.2-2.

A rational approach to estimating first, the effective damping at each sub-structure/isolator unit, and then, the effective system damping must be adopted in order to apply approximate analytical methods. The approaches proposed by Priestley for effective, combined pier/isolator damping as well as for equivalent system damping will be adopted here (Priestley, et al., 2007).

$$\xi_{EFF} = \frac{\xi_{PIER}\Delta_{PIER} + \xi_{ISO}\Delta_{ISO}}{\Delta_{PIER} + \Delta_{ISO}} \qquad \text{(Eq. 1-24)}$$

$$\xi_{SYS} = \frac{\sum V_i \xi_{EFF}}{\sum V_i} \qquad \text{(Eq. 1-25)}$$

V_i is the base shear at a particular sub-structure.

Table 1.6.2-1. Effective Viscous Damping Equations for Hysteretic Behavior

Structure Type	Expression for Equivalent Damping (% of critical)
Reinforced Concrete Bridge Columns	$\xi_{eff} = 5 + 44.4\frac{\mu - 1}{\pi\mu}$
Steel Frame Buildings	$\xi_{eff} = 5 + 57.7\frac{\mu - 1}{\pi\mu}$
Bilinear Isolation Systems (post-yield Stiffness ratio = 0.20)	$\xi_{eff} = 5 + 51.9\frac{\mu - 1}{\pi\mu}$
Bilinear Isolation Systems (General)	$\xi_{eff} = \frac{2Q_d(D - D_y)}{\pi K_{eff} D^2}$
Any Bilinear System (α = post-yield stiffness ratio)	$\xi_{eff} = \xi_o + \frac{2(\mu - 1)(1 - \alpha)}{\pi\mu(1 + \alpha\mu - \alpha)}$
Elastic-Perfectly-Plastic (EPP)	$\xi_{eff} = 5 + 67.0\frac{\mu - 1}{\pi\mu}$
Concrete Frames	$\xi_{eff} = 5 + \frac{120}{\pi}\left(1 - \frac{1}{\sqrt{\mu}}\right)$
FPS with μ_{dyn} and Radius of concave plate = R	$\xi_{eff} = \frac{2\mu_{dyn}R}{\pi(\mu_{dyn}R + D_{ISO})}$

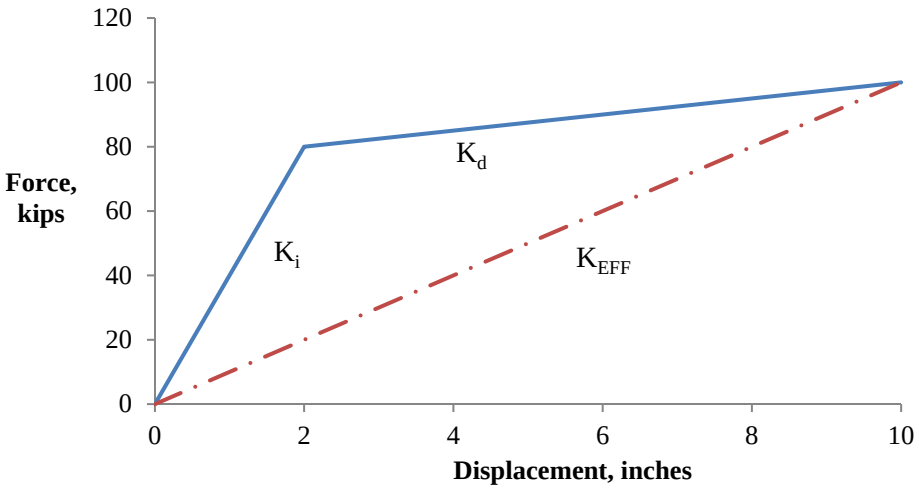

Figure 1.6.2-1 Effective Stiffness

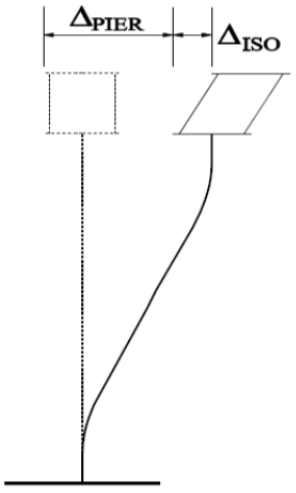

Figure 1.6.2-2. Isolated Structure Displacements

1.6.3 Equivalent Linear Inelastic Response Spectrum Analysis – Initial Properties

Another approach to the problem of matching response spectrum results to nonlinear time history results relies upon the direct development of inelastic spectra rather than treating the nonlinear, hysteretic behavior as equivalent viscous damping.

Various proposals have been developed for reducing the 5% damped elastic acceleration response spectrum to account for inelastic behavior. One method (Chopra, 2005) advocates a divisor, R_y, on the design elastic spectrum given by:

$$R_y = 1 \; for \; T < 0.03 \; seconds$$

$$R_y = \sqrt{2\mu - 1} \; for \; 0.13 < T < T_c, \qquad \text{(Eq. 1-26)}$$

$$R_y = \mu \; for \; T > 0.66$$

Another study (Ruiz-Garcia & Miranda, August 2005) concluded that, for soft soil sites and for natural periods greater than 1.5 times the predominant period of the ground motion, inelastic displacements are approximately equal to the elastic estimates.

1.6.4 Non-linear Response History Analysis

This analysis is the most time-consuming and complicated of the three. It can be the most difficult in terms of interpreting results. A ground motion acceleration history is required – this is the first problem when one is designing an actual structure as opposed to performing research. What is the appropriate ground motion for the bridge design?

There are multiple means of performing nonlinear dynamic time history analysis. These methods may be broadly grouped into two:

1. Nonlinear direct integration response history analysis

2. Nonlinear modal response history analysis

Problems in which the nonlinear behavior is limited to inelastic link-type elements between nodes are ideally suited for nonlinear modal time history analysis. Since the objective of this study is to examine the feasibility of using isolators to prevent nonlinear behavior in the substructures of bridges, and since the most attractive means of modeling isolators is by the use of bi-linear link-type elements, the second procedure will be used for the dynamic time history analyses. The procedure is extremely efficient and accurate for such a problem. SAP2000 (Computers and Structures, Inc., 2011) will be used for the analysis of the bridges. Nonlinear link elements in the SAP2000 library include biaxial hysteretic elements with coupled plasticity for the two shear deformations. It is important that coupled plasticity be included in the formulation of elements used to model the behavior of isolators.

The problem of estimating isolator displacement response - which is inherently highly nonlinear - can be best illustrated by a simple example. Consider two ground motions, each modified to match a target response spectrum. The two motions for this example are the fault-parallel components of NGA records 1176 (from the Kocaeli, Turkey earthquake discussed later in Chapter 3) and 1536 (from the Chi-Chi, Taiwan earthquake, also discussed later in Chapter 3). Spectrum matching has been used to match the records to the Site 1 DBE acceleration response spectrum. The target and matched spectra are shown in Figure 1.6.4-1. The process has produced a very close match as seen from the spectra, and one might expect very similar responses of a structure to the two records. This is not the case however. Notice from Figures 1.6.4-2 and 1.6.4-3 the very different responses of a sample isolator to the records. The sample isolator is Model Isolator No. 1 (see CHAPTER 4) - the important point for now is that the exact same structure

may respond very differently to two ground motion records which would appear to be nearly identical - as determined from examination of acceleration spectra only - when nonlinearities occur in the response. Note, in particular, that the maximum displacement for the Chi-Chi loading is about 8” while that for the Kocaeli loading is about 18”. The isolator responds in a symmetric manner to the Chi-Chi record and in a highly non-symmetric manner to the Kocaeli record.

Table 1.6.4-1 summarizes the various ground motion parameters for the two records as well as the response of Test Isolator No. 1 (CHAPTER 4) to the two records. Interestingly, the simplified response spectrum analysis introduced in Section 1.6.2 and discussed in detail in CHAPTER 6 would predict an isolator displacement demand of 36.6 cm (14.4 inches) for the DBE spectrum for Site 1. From the table it would appear that, at least for this particular case, perhaps specific energy density and significant duration are key parameters in the response of isolators to strong ground shaking.

It is instructive to examine displacement histories of the two records as well. Figures 1.6.4-4 and 1.6.4-5 reveal differences. Even though two records have almost identical acceleration response spectra within the range of interest, they may have vastly different inelastic displacement response. This is due to the fact that inelastic displacement spectra cannot accurately be generated from elastic acceleration spectra using current rules at high levels of ductility, and isolators operate at extremely high ductility levels. This is an observation from personal experience and will be further demonstrated through the generation of inelastic displacement spectra for record sets used in the study in CHAPTER 3.

Table 1.6.4-1. Example Matched Ground Motion Parameters

	1176FP	1536FP	Mean
Max Acceleration (g)	0.5083	0.3664	0.4373
Max Velocity (in/sec)	26.5061	26.2603	26.3832
Max Displacement (in)	55.0145	15.3904	35.2025
Vmax/Amax (sec)	0.1350	0.1856	0.1603
Acceleration RMS (g)	0.0577	0.0459	0.0518
Velocity RMS (in/sec)	9.3930	4.6084	7.0007
Displacement RMS (in)	21.7483	4.7338	13.2411
Arias Intensity (in/sec)	1.7949	2.9184	2.3566
Characteristic Intensity	0.0820	0.0932	0.0876
Specific Energy Density (in2/sec)	3086.6869	1911.0723	2498.8796
Cum. Abs. Velocity (in/sec)	450.4201	897.3832	673.9016
Acc Spectrum Intensity (g*sec)	0.3613	0.3546	0.3580
Vel Spectrum Intensity (in)	71.8799	76.3426	74.1112
Housner Intensity (in)	75.0960	74.4415	74.7687
Sustained Max.Acceleration (g)	0.3016	0.2566	0.2791
Sustained Max.Velocity (in/sec)	23.5213	15.3591	19.4402
Effective Design Acceleration (g)	0.4808	0.3279	0.4043
A95 parameter (g)	0.5045	0.3599	0.4322
Predominant Period (sec)	0.3200	0.3000	0.3100
Significant Duration (sec)	14.1000	35.1500	24.6250
Isolator No. 1 Maximum D_{ISO}, inches	18.7682	7.3262	13.0472
Isolator No. 1 Minimum D_{ISO}, inches	-11.6152	-7.2781	-9.4467
Isolator No. 1 Residual D_{ISO}, inches	1.1078	-0.6291	0.2393

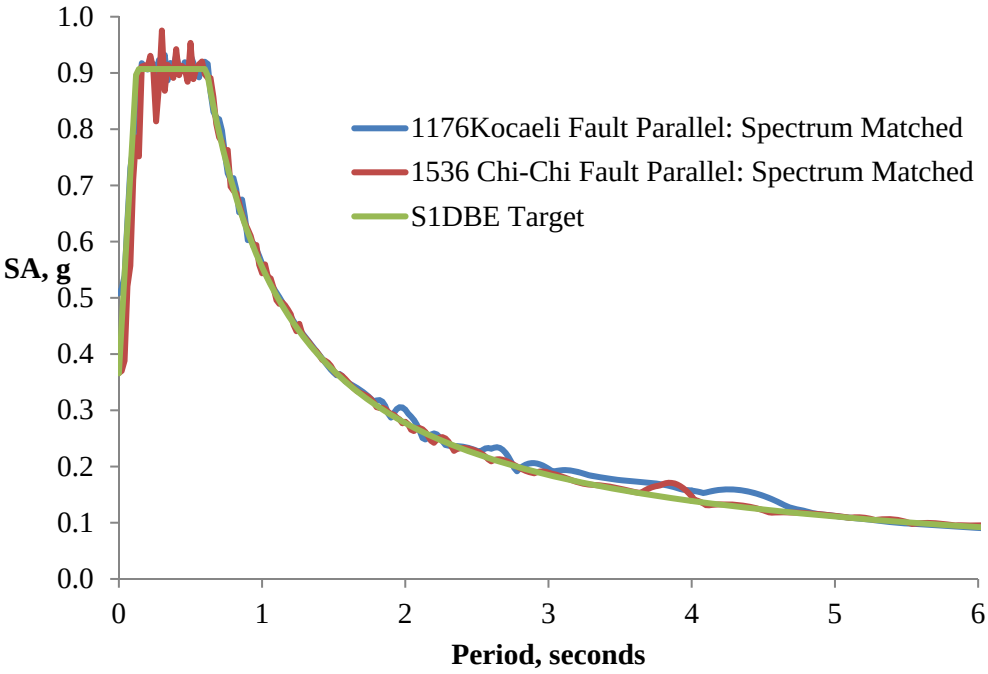

Figure 1.6.4-1. Example Matched and Target Spectra

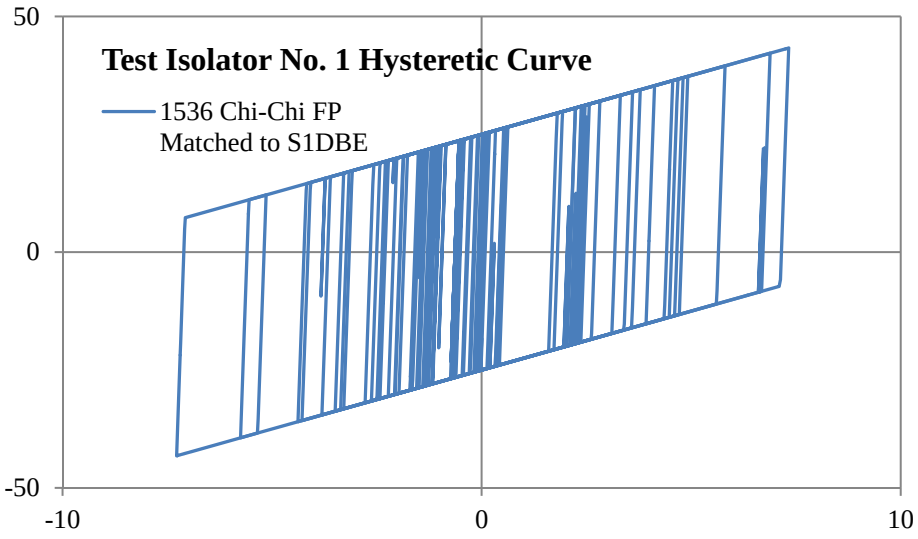

Figure 1.6.4-2. Hysteretic Response to Chi-Chi Matched Record

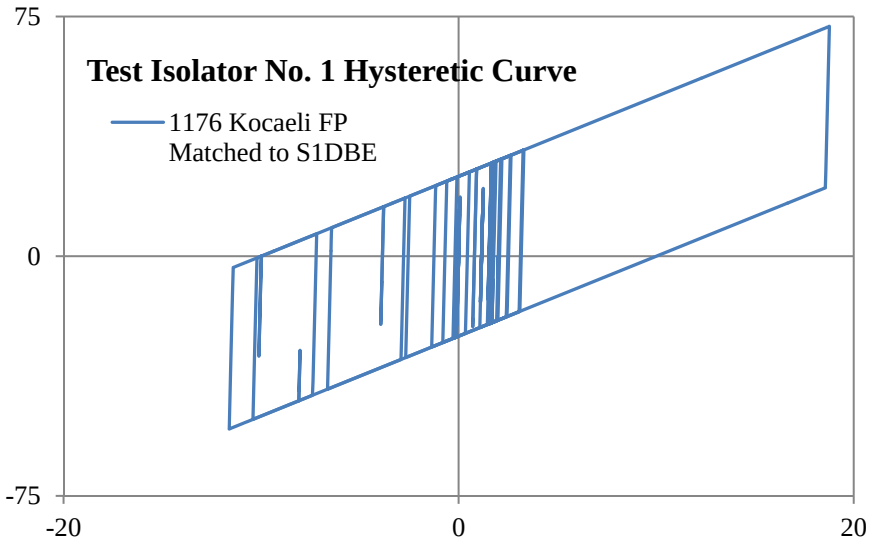

Figure 1.6.4-3. Hysteretic Response to Kocaeli Matched Record

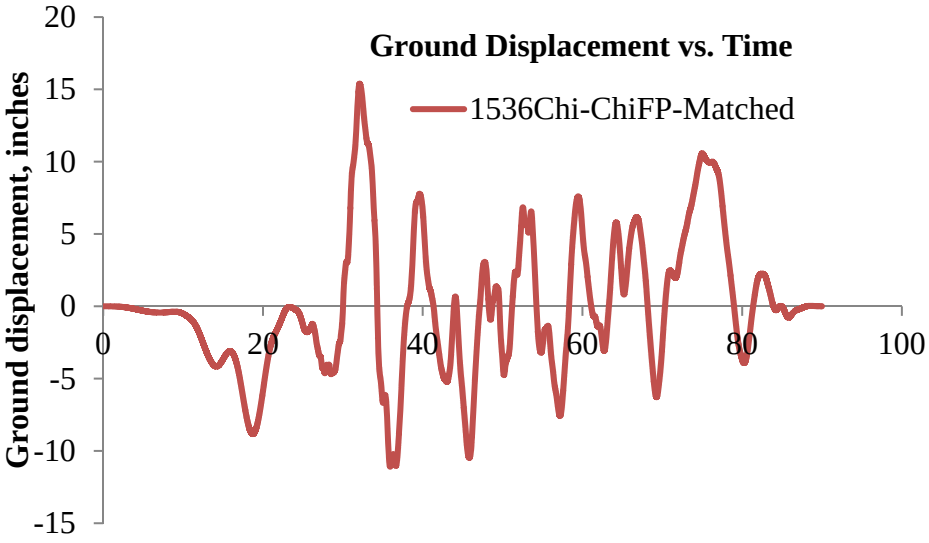

Figure 1.6.4-4. Chi-Chi Displacement History (NGA 1536FP Modified)

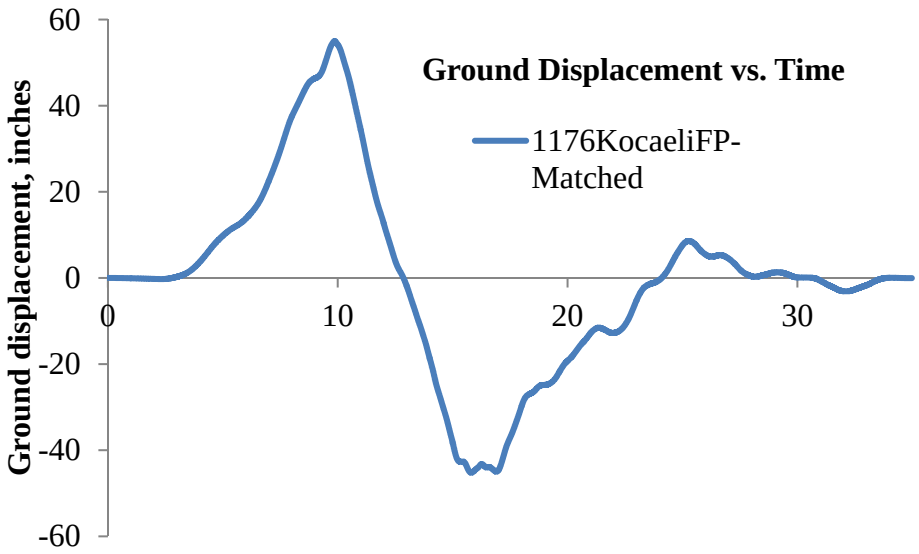

Figure 1.6.4-5. Kocaeli Displacement History (NGA 1176FP Modified)

1.6.5 Conversion of Acceleration Spectra to Displacement Spectra

With the current trend towards a displacement-based, rather than a force-based, seismic design process, the seismic loading needs to be defined as a displacement spectrum. It is easy enough to convert an acceleration spectrum to a displacement spectrum (for the elastic case only) using the traditional method based on harmonic approximation to the system response:

$$SD = SA \cdot g \cdot \left(\frac{T}{2\pi}\right)^2 \qquad \text{(Eq. 1-27)}$$

Where SD is the spectral displacement at period T, SA is the spectral acceleration at period T, and g is the acceleration of gravity.

The isolated period of a bridge is most likely greater than T_S (see Section 1.5.1) so it is possible to substitute the expression for SA within this range into the above equation to obtain:

$$SD = \frac{S_{D1}}{T} \cdot g \cdot \left(\frac{T}{2\pi}\right)^2 = \frac{S_{D1} \cdot g}{4\pi^2} \cdot T \qquad \text{(Eq. 1-28)}$$

So converting a current, AASHTO code-based acceleration spectrum produces a displacement spectrum with no cap. The spectral displacement increases without bound as the period increases. It is a well-established fact that displacement spectra of real earthquakes eventually reach a limiting value – equal to some multiple of the maximum ground displacement. This limiting displacement occurs at the so-called "corner period". Modern scaling procedures are designed to use acceleration spectra as the target for matching as well. This is one major shortcoming of current design methods. As the science moves towards a displacement based approach for seismic loading, it will be preferable to develop displacement spectra, including the corner period estimation, rather than acceleration spectra.

To illustrate the potential discrepancy between code-based and real displacement spectra for large magnitude earthquake ground shaking, observe, in Figure 1.6.5-1, the overlaid code spectrum for a fault-normal component (NGA #2114) of the 2002 Denali, Alaska earthquake of 2002 scaled to match the 7% probability of exceedance in 75 year acceleration spectrum for Site No. 1 (A_S = 0.366 g). The two spectra are fairly close at periods around 1 second, yet vary widely at higher periods. A reasonable question to ask might relate to possible scaling strategies in such a situation.

Literature on the subject of corner-period estimation is fairly abundant. One finding concludes that strike-slip events have larger corner periods than thrust fault events, at least in Japan (Lyskova, et al., 1998). In the same study, an expression is given for corner period, T_C, in terms of fault length, L, fault width, W, and fault rupture velocity, V_r.

$$T_C = \frac{\pi}{V_r} \cdot \sqrt{\frac{LW}{2}} \qquad \text{(Eq. 1-29)}$$

Eurocode8 sets the corner period at 1.2 seconds for earthquakes having a magnitude of 5.5 or less and at 2.0 seconds for earthquakes having a magnitude of greater than 5.5. Eurocode8 also sets the maximum ordinate of the displacement spectrum at 2.5 times the maximum ground displacement (Faccioli, et al., May 2004). The particular study referenced was based on strong ground motion data from Taiwan, Japan, Italy, and Greece.

A Chinese study, using strong ground motion data from the United States, suggests that the corner period of the displacement spectrum is primarily a function of soil type and ranges from values as small as 1.15 seconds for sound rock up to as much as 6.05 seconds for deep, soft soils (Xiang & Li, 2000).

An EERI Monograph (Chopra, 2005) depicts response spectra implying corner period values of 3.14 seconds for mean spectra and 4.12 seconds for 84^{th} percentile spectra.

Research at the Multidisciplinary Center for Earthquake Engineering (MCEER) estimated corner periods ranging from 1.02 seconds for small magnitude-small distance locations up to 5.07 seconds for large magnitude-small distance locations (Warn & Whittaker, 2007).

ASCE7-05 (American Society of Civil Engineers, 2005) and NEHRP P-750 (Federal Emergency Management Agency, 2009) each establish a corner period of 12 seconds in the New Madrid Seismic Zone.

With the gradual move towards a displacement-based seismic design philosophy, the need for directly generating a design displacement spectrum instead of an acceleration spectrum exists. Measures have been taken towards this end. A paper presented at the 12^{th} World Conference on Earthquake Engineering (Bommer, et al., 2000) proposed empirical equations for displacement spectra similar to those currently used for acceleration spectra. Regression

coefficients were established for PGA, PGV, and PGD in terms of magnitude, distance, and site conditions.

Modifying ground motions to match a design elastic displacement spectrum will likely produce very different results than matching to a design acceleration spectrum. So this problem is one of the most glaring in current seismic design philosophy. The choice of some other parameter, such as spectral velocity or peak ground velocity, would produce yet another set of scale factors for a given set of records. Ideally, it would be possible to incorporate inelastic displacement spectra as targets for ground motion selection and modification since inelastic displacement has become generally accepted as the soundest engineering choice in evaluating structural response to earthquake loading.

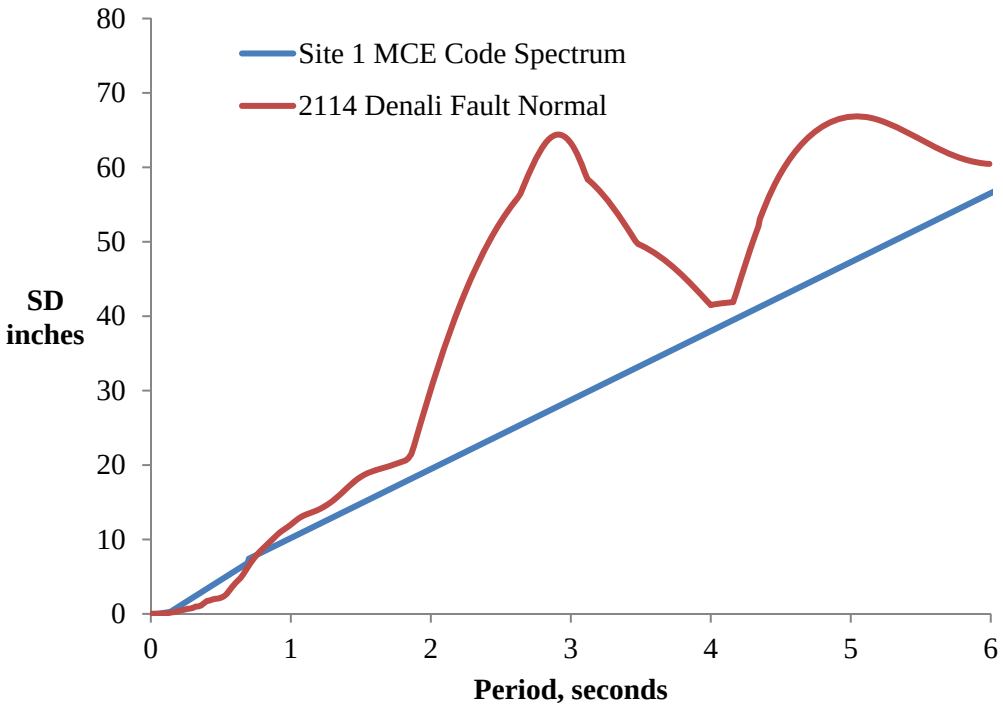

Figure 1.6.5-1. Displacement Response Spectra

1.7 Research Modeling Methods: A Summary

The Mississippi Embayment of the New Madrid Seismic Zones consists of soil profiles over 1 kilometer deep in some places and lies over an intraplate fault system. These factors make the use of code-based design spectra potentially problematic since:

- current specifications are based on data which is largely from active tectonic, interplate regions and
- current specifications make no distinction between two sites - one characterized by a soil profile 30 meters deep to bedrock and another 1 kilometer deep to bedrock - as long as the upper 30 meters of the two sites are similar.

This problem will be addressed by including NMSZ-specific spectral shapes from previous research at Georgia Tech along with code-based spectral shapes and comparisons between the two will be made.

Bridge design by current AASHTO specifications is primarily conducted using a linear response spectrum analysis with initial (cracked) stiffness properties and 5% viscous damping. The design of isolation systems for bridges is typically accomplished using simplified, equivalent linear analysis with effective (secant) stiffness properties and an assumed elastic damping (typically 5%) combined with equivalent viscous damping from hysteretic behavior of the isolation bearings. Nonlinear response history analysis is the most rigorous analysis technique. Explicit nonlinear properties of the isolators and/or the structural elements (beams, columns, piles, etc.) are incorporated into a model of the bridge and ground motion histories are applied to the base of the structure. Each of these three methods will be employed in this study:

- linear response spectrum analysis will be used in CHAPTER 5 to determine ductility requirements of the non-isolated bridges;
- equivalent linear analysis will be used in CHAPTER 6 for preliminary design of isolation systems for each of the bridges;
- nonlinear response history analysis will be used both in CHAPTER 4 for comparisons among various ground motion sets and in CHAPTER 7 for detailed assessment of the isolated bridges.

CHAPTER 2 - SEISMIC ISOLATION: AN OVERVIEW OF IMPLEMENTATION AND THEORY

CHAPTER 1 described the process used to establish the seismic hazard at the two bridge sites in terms of:

- AASHTO Site Classification
- Deaggregated M_W,R combinations
- Code-based and NMSZ-specific target response spectra

CHAPTER 1 also provided a discussion of 4 analysis tools for earthquake loading of structures. Prior to developing a process for ground motion selection in CHAPTER 3, a review of some historical implementation of isolation devices and some important principles in the theory of seismic isolation is necessary to completely understand and interpret CHAPTER 4 results and CHAPTER 7 results.

To begin with and prior to a discussion of some history, it is a good place to state the primary two mechanisms whereby the benefits of isolation are realized: (1) a shift in the natural period of the structure toward longer values and (2) an increase in effective damping through hysteretic behavior of the isolation devices.

2.1 History

One of the first examples of isolation methods applied to a real bridge structure is the Rangitikei Railway Bridge in New Zealand, constructed in 1974 (Buckle, et al., 2006). Transverse rocking was permitted at the base of 70 meter tall piers supporting the six-span

bridge. Torsional steel dampers with stops were used to add energy dissipation characteristics and prevent over-turning. Modern isolation strategies differ from this first innovative example in that the isolation system is typically located at the interface between sub-structure and super-structure in modern applications.

Modern isolation systems have included lead-rubber bearings (LRB), friction pendulum systems (FPS), and laminated elastomeric bearings (without the lead plug) among others. Laminated elastomers have been used for buildings in the United States and in Japan, as well as for bridges in Italy. The LRB isolators have been used extensively for bridges in New Zealand and in the United States (Skinner, et al., 1993). Figure 2.1-1 shows an LRB bearing and Figure 2.1-2 shows an FPS bearing. A laminated elastomeric bearing is essentially an LRB without the lead plug.

Isolation of bridges began in the United States in California near San Francisco with the replacement of fixed bearings using lead-rubber isolators for the Sierra Point Overhead at US-101. The bridge was isolated in 1985, some 35 years or so after original construction. Current estimates place the number of isolated bridges in North America in excess of 200.

As of 2006, some 14 bridges in Illinois, 10 in Missouri and 3 in Tennessee have incorporated some form of isolation device into the design (Buckle, et al., 2006). Of the Tennessee bridges, all three are located in Shelby County near Memphis, the most densely populated city in the heart of the Mississippi Embayment of the New Madrid Seismic Zone. Typical conditions in each of these three areas include embayment depths between 600 and 1200 meters with AASHTO Site Class “D” or “E” (stiff to soft soil) conditions. The bridges are:

- I-55 over Nonconnah Creek (Lead-Rubber Bearings)
- Fite Road over Big Creek Canal (Lead-Rubber Bearings)
- Interstate-40 over the Mississippi River (Lead-Rubber and Friction-Pendulum)

The expected seismic loading for any of these three bridges would be similar to that for Site No. 1 in this study. The Interstate-40 Mississippi River project is a retrofit of the Hernando de Soto bridge in Memphis. The bridge consists of 2 main-span arches of 274 meters (900') length each. Approach spans include concrete I-girders, steel I-girders, and steel box-girders. The retrofit of the three main arch-support piers included 2.69 meter (8'-10") diameter friction-pendulum bearings with a displacement capacity of over 0.69 meters (27 inches).

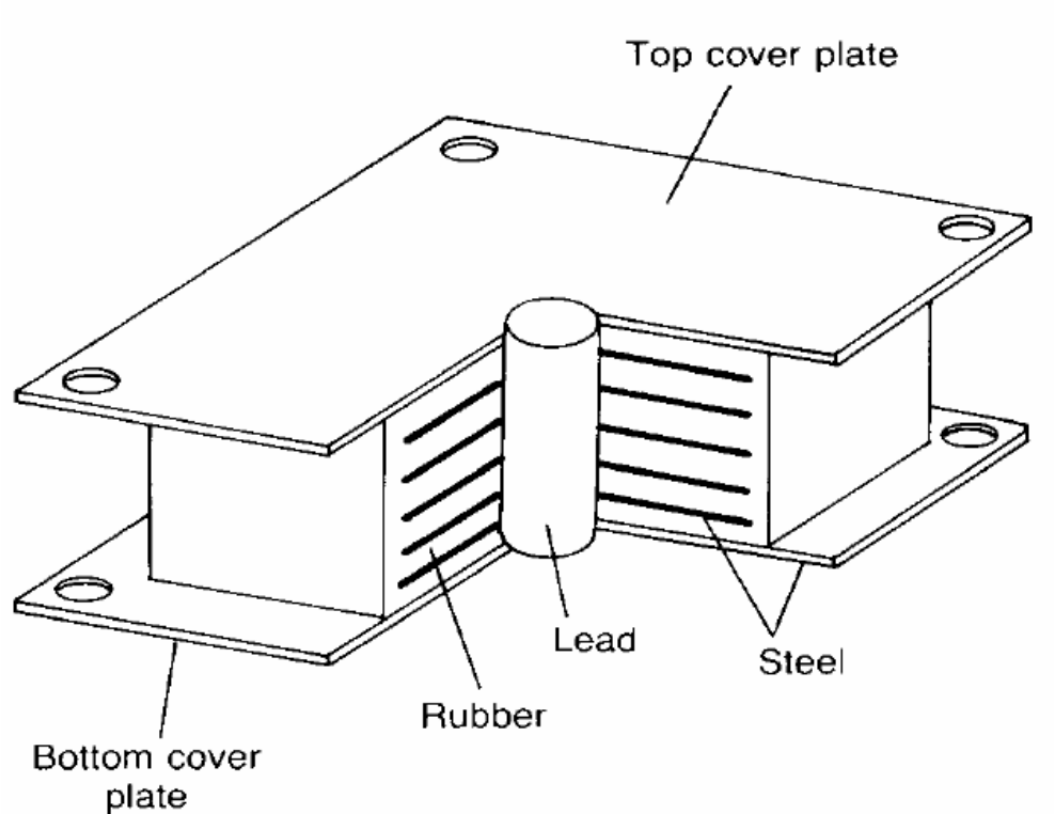

Figure 2.1-1. LRB Isolator (from Kunde and Jangid, 2003)

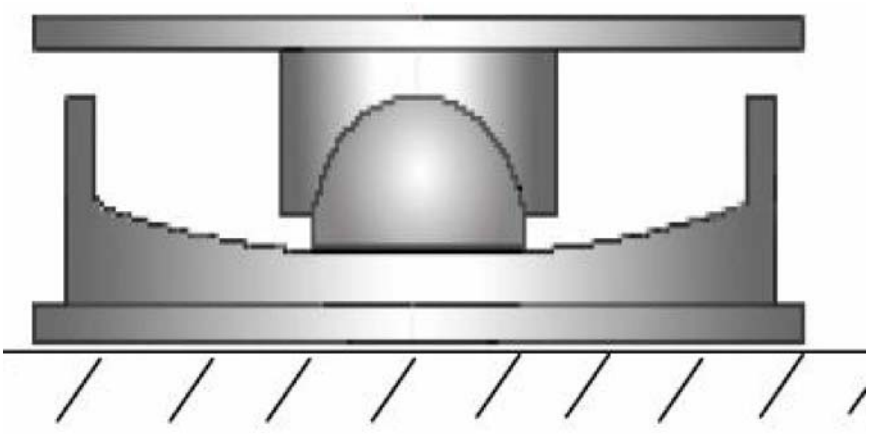

Figure 2.1-2. FPS Isolator (from FEMA 451, 2006)

2.2 Isolator Use and Behavior

To re-state a previous contention: the two primary effects of isolation are an increase in the natural period of the structure and an increase in the effective damping of the structure as a whole. In addition, the isolators provide a means whereby other structural elements may be designed for either completely elastic behavior or limited ductile behavior - limited in the sense that ductility demands are typically much smaller on isolated substructures compared to their non-isolated counterparts. The superstructure and substructures are, in effect, de-coupled.

Isolation devices are typically characterized by a bi-linear force-displacement relationship. An isolation device may be completely defined by the three parameters (see Figure 2.2-1):

1. Characteristic Strength, Q_d
2. Post-yield stiffness, K_d
3. Yield Displacement, D_y

The ratio of the post-yield stiffness, K_d, to the initial stiffness, K_i, is given the symbol α for the purposes of this study. The yield displacement, D_y, is related to α, Q_d and K_d as follows:

$$D_y = \frac{Q_d}{K_d} \cdot \frac{\alpha}{1-\alpha} \qquad \text{(Eq. 2-1)}$$

For LRB isolators, α is frequently taken equal to 0.10, though a range of values is possible. The initial stiffness is due to the lead plug and elastomer stiffness values in parallel with one another. Pure lead does not work-harden at room temperature, unlike most metals (Buckle, et al., 2006). Once the lead plug has yielded in shear, only the stiffness contribution from the elastomer remains. For FPS systems, α is theoretically equal to 0.0 since K_i is virtually infinite, but a small value is typically assigned to the yield displacement (say 0.01 inches). For the work presented here, α is taken to be 0.0001 for FPS systems and 0.10 for LRB systems.

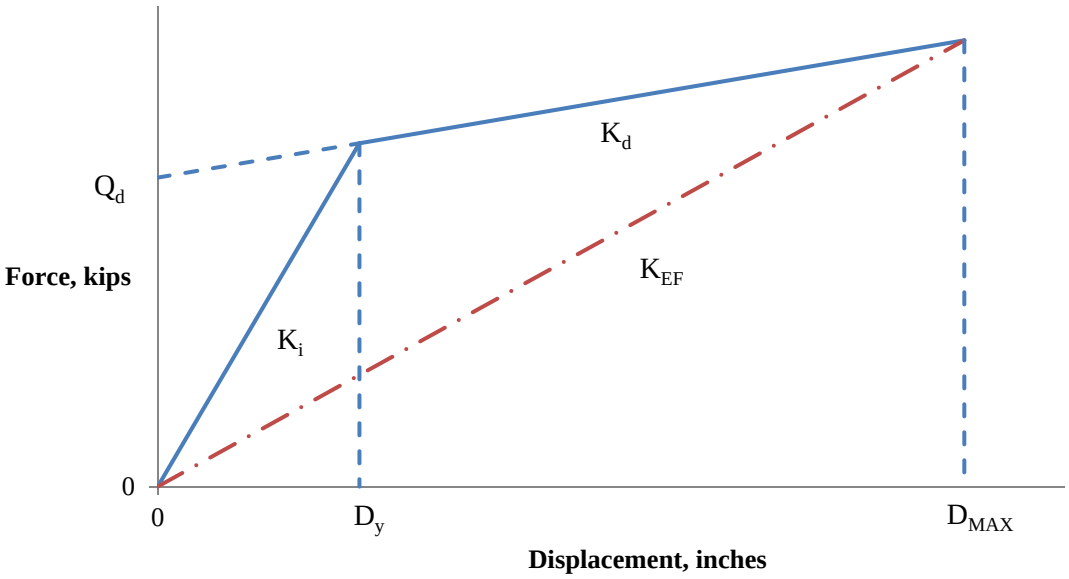

Figure 2.2-1. Isolator Parameters

Note that Q_d is an artificial, or effective, parameter, not the true yield strength, used for convenience in mathematical computations for isolators. The true yield strength is related to the characteristic strength by the expression in equation 2-2.

$$F_y = \frac{Q_d}{1-\alpha} \quad \text{(Eq. 2-2)}$$

For the FPS system, Q_d and K_d are determined by the supported weight, W, the radius of curvature of the articulated slider, R, and the dynamic coefficient of friction, μ_{dyn}, between the sliding surfaces of the FPS.

$$Q_d = \mu_{dyn} W \quad \text{(Eq. 2-3)}$$

$$K_d = \frac{W}{R} \quad \text{(Eq. 2-4)}$$

The effective coefficient of friction for FPS bearings is not a constant. The most important factor affecting the coefficient of friction at any given instant are (1) bearing pressure, (2) sliding velocity and (3) temperature (Buckle, et al., 2006). A large friction values is applicable at breakaway. At low velocities, the slider operates at a friction lower than that at breakaway. A maximum, constant friction value is attained at a velocity of about 100 m/sec. Nonetheless, for performance criteria in contract documents, the effective dynamic coefficient of friction, μ_{dyn}, is specified.

One feature unique to the FPS system is the need to accommodate vertical displacements due to the curved sliding surfaces. This vertical displacement is simple enough to compute and typically poses no serious limitations but should be considered in the design of the isolation system. For a horizontal isolator displacement equal to D_{ISO}, the corresponding vertical displacement is given by equation 2-5.

$$D_{VERT} = R\left[1 - cos\left(sin^{-1}\left(\frac{D_{ISO}}{R}\right)\right)\right] \cong \frac{D_{ISO}^2}{2R} \qquad \text{(Eq. 2-5)}$$

Because the mechanism of breakaway for the system is a sudden slip between sliding surfaces, the FPS system has an infinite theoretical, pre-yield stiffness so all flexibility prior to break-away of the isolator is from the substructures. The effective stiffness ratio, α, is therefore zero. So an FPS-isolated bridge may operate at quite a low period prior to break-away of the bearings. The LRB system can be designed to have quite a low pre-yield stiffness so that the LRB-isolated bridge may operate at a higher period prior to break-away compared to the FPS-isolated bridge. But the theoretical maximum damping is much higher for the FPS system compared to the LRB-system. So there are trade-offs for each system.

It can be shown (APPENDIX C) that, for two isolators with identical values of Q_d, K_d, and D_{ISO}, but different post-yield stiffness ratios, α_1 and α_2, that the ratio of effective damping values for the two systems as a function of the displacement ductility of the second system is given by:

$$\frac{\xi_1}{\xi_2} = \frac{\left(\mu_2\alpha_2 \cdot \frac{1-\alpha_1}{1-\alpha_2} - \alpha_1\right)(1 + \alpha_2\mu_2 - \alpha_2)}{\alpha_2(\mu_2 - 1)\left(1 + \mu_2\alpha_2 \cdot \frac{1-\alpha_1}{1-\alpha_2} - \alpha_1\right)} \qquad \text{(Eq. 2-6)}$$

Choosing $\alpha_2 = 0.10$ as representative of an LRB device (Hameed, et al., 2008) for the second system and $\alpha_1 = 0.00$ as representative of an FPS device for the first system, the expression reduces to:

$$\frac{\xi_1}{\xi_2} = \frac{\mu_2}{\mu_2 - 1} \qquad \text{(Eq. 2-7)}$$

So the FPS will always have higher effective damping than the LRB system for the same Q_d and K_d values at a given isolator displacement, D_{ISO}.

For any isolation system whose behavior is modeled by the bi-linear parameters discussed here, the effective (secant) stiffness and the effective hysteretic damping each are a function of the maximum horizontal displacement in the isolator. Equation 2-8 may be found in the literature (Buckle, et al., 2006) or simply derived from Figure 2.2-1. Equation 2-9 is from the AASHTO Guide Specifications for Seismic Isolation Design (AASHTO, 2010).

$$K_{EFF} = K_d + \frac{Q_d}{D_{ISO}} \qquad \text{(Eq. 2-8)}$$

$$\xi_{EFF} = \frac{2Q_d\left(D_{ISO} - D_y\right)}{\pi(D_{ISO})^2 K_{EFF}} \qquad \text{(Eq. 2-9)}$$

An important distinction is in the stiffness and damping values assigned to individual isolators, to individual sub-structures, and to the entire system as a whole. The above expressions for K_{EFF} and ξ_{EFF} are an isolator. When the isolator is installed at a particular sub-structure possessing damping equal to ξ_{SUB} and stiffness equal to K_{SUB}, then the composite stiffness and damping of the isolator and sub-structure in series are computed from equation 2-10 (AASHTO, 2010) and equation 2-11 (Priestley, et al., 2007), respectively.

$$K_{COMP} = \frac{K_{SUB}K_{EFF}}{K_{SUB} + K_{EFF}} \qquad \text{(Eq. 2-10)}$$

$$\xi_{COMP} = \frac{\xi_{SUB}D_{SUB} + \xi_{EFF}D_{ISO}}{D_{SUB} + D_{ISO}} \qquad \text{(Eq. 2-11)}$$

When a bridge composed of multiple sub-structures, with or without isolators, is modeled as a single-degree-of-freedom system, then the system damping depends upon the distribution of total shears at each sub-structure.

$$\xi_{SYS} = \frac{\sum[(V_i)(\xi_{COMP})_i]}{\sum V_i} \qquad \text{(Eq. 2-12)}$$

For the case of an isolator on a rigid sub-structure, it is informative to examine the effect of the post-yield stiffness ratio, $\alpha = K_d/K_i$, upon effective damping. There is no hard and fast rule for determining whether a substructure qualifies as "rigid" and engineering judgment is required in practice to determine whether or not a "rigid" assumption is valid. But suppose that the "rigid" assumption is valid. Then re-arranging the expression for ξ in equation 2-9 will make the comparisons among various parameter effects more convenient.

$$\xi_{EFF} = \frac{2Q_d\left(D_{ISO} - D_y\right)}{\pi D_{ISO}^2 K_{EFF}} \qquad \text{(Eq. 2-13)}$$

$$\xi_{EFF} = \frac{2Q_d\left(D_{ISO} - \frac{Q_d}{K_d}\cdot\frac{\alpha}{1-\alpha}\right)}{\pi D_{ISO}^2\left(K_d + \frac{Q_d}{D_{ISO}}\right)} \qquad \text{(Eq. 2-14)}$$

$$\xi_{EFF} = \frac{2}{\pi}\cdot\left(\frac{Q_d}{K_d D_{ISO}}\right)\cdot\frac{1 - \left(\frac{Q_d}{K_d D_{ISO}}\right)\cdot\left(\frac{\alpha}{1-\alpha}\right)}{1 + \left(\frac{Q_d}{K_d D_{ISO}}\right)} \qquad \text{(Eq. 2-15)}$$

So, for a given actual isolator displacement, D_{ISO}, the effective damping is a function of the two ratios: Q_d/K_d and $\alpha/(1-\alpha)$. Figures G2.2-2 through G2.2-6 (APPENDIX G2) provide plots of the damping reduction factor, $B_L = (\xi_{EFF}/0.05)^{0.3}$, for various values of Q_d/K_d. In particular, it is clear that the FPS system can possess significantly larger damping reduction for a given displacement and Q_d/K_d value. The effect is stronger at high Q_d/K_d values. No units are given on the charts

because the values are valid for any consistent system of units and the LRB plots begin at higher displacements than their FPS counterparts because for a given Q_d/K_d the LRB isolator has a higher yield displacement that the FPS isolator. Note also that the yield displacement - the displacement at which damping reduction begins to take effect - is given by equation 2-16, so that the plots for different Q_d/K_d values start at different values on the x-axis. Starting from Figure 2.2-1 equation 2-16 is derived as follows.

$$K_i D_y = Q_d + K_d D_y$$

$$\frac{K_d}{\alpha} D_y = Q_d + K_d D_y$$

$$D_y \left(\frac{K_d}{\alpha} - K_d\right) = Q_d$$

$$D_y K_d \left(\frac{1}{\alpha} - 1\right) = Q_d$$

$$D_y \left(\frac{1-\alpha}{\alpha}\right) = \frac{Q_d}{K_d}$$

$$D_y = \frac{Q_d}{K_d}\left(\frac{\alpha}{1-\alpha}\right) \qquad \text{(Eq. 2-16)}$$

No cap is placed on B_L in developing the plots. However, AASHTO (AASHTO, 2010) imposes a limit of 1.7 – corresponding to a damping value of 29.3% - on the value which may be assigned to B_L. This is due to the fact that the simplified procedures in AASHTO are thought to diverge from more accurate response history results at effective damping levels beyond about 30%.

2.3 Simplified Analysis Procedures

When a simplified, response spectrum-based analysis and design procedure is adopted for an isolated bridge, the procedure is generally an iterative one. After setting a trial value of the total displacement, the isolator displacement is calculated and the effective stiffness and damping are determined from relationships presented in Section 2.2. The procedure typically adopted in practice uses the effective stiffness analysis with equivalent damping, rather than an initial stiffness analysis with elastic damping. It is further assumed that the design acceleration response spectrum follows the shape currently specified in the AASHTO Specifications and is thus inversely proportional to period - i.e., that the isolated period falls within a constant velocity region of the design spectrum - so that the following relationships are established.

$$T_{EFF} = 2\pi\sqrt{\frac{W}{gK_{COMP}}} \qquad \text{(Eq. 2-17)}$$

$$SD = \frac{SA}{B_L}\cdot g\cdot\left(\frac{T_{EFF}}{2\pi}\right)^2 = \frac{S_{D1}}{T_{EFF}}\cdot\frac{g}{B_L}\cdot\left(\frac{T_{EFF}}{2\pi}\right)^2 = \frac{g}{4\pi^2}\cdot\frac{S_{D1}}{B_L}\cdot T_{EFF} \qquad \text{(Eq. 2-18)}$$

Here, SD is the spectral displacement (inches) at T_{EFF}, SA is the spectral acceleration (g's) at T_{EFF}, and S_{D1} is the spectral acceleration (g's) at a period of 1 second. In CHAPTER 3, the assumption of the isolated period falling within a constant spectral velocity region of the design response spectrum will be shown to be questionable for sites in the ME of the NMSZ. But for now, the purpose is to present the design method as it currently exists in AASHTO. Proposed modifications to spectral shape for NMSZ sites will be explored in CHAPTER 3 as well. To account for the increased effective viscous damping due to hysteretic behavior of the isolator, the 5%-damped elastic response spectrum is reduced in AASHTO (AASHTO, 2010) by the factor B_L.

$$B_L = \left(\frac{\xi_{COMP}}{0.05}\right)^{0.30} \leq 1.70 \qquad \text{(Eq. 2-19)}$$

The spectral displacement thus computed is the total displacement of the mass. This is compared to the assumed displacement. When the assumed displacement and the calculated displacement agree within some desired level - say 5% - the process is complete and the design displacement has been determined. The process will become clear in CHAPTER 6 when a detailed preliminary design of isolators for Bridge No. 1 at Site No. 1 is carried out using this very process.

Other means of computing the damping reduction have been proposed. Included among these are the following (Priestley, et al., 2007):

$$1/B_L = R_\xi = \left(\frac{0.10}{0.05 + \xi}\right)^{0.50}, Eurocode \qquad \text{(Eq. 2-20)}$$

$$1/B_L = R_\xi = \left(\frac{0.07}{0.02 + \xi}\right)^{0.25}, Velocity\ pulse\ conditions \qquad \text{(Eq. 2-21)}$$

$$1/B_L = R_\xi = 1.31 - 0.19 \cdot \ln(100\xi), Newmark - Hall \qquad \text{(Eq. 2-22)}$$

The second of these is similar in form to the first and is intended to be appropriate for sites where forward directivity velocity pulses might be expected in the design ground motion. Velocity pulses are generally considered for near-field sites - sites with a source-to-site distance less than about 12 kilometers (AASHTO, 2009). A comparison among AASHTO's method and the three alternate methods is made in Figure 2.3-1.

AASHTO and Eurocode modifiers for damping are very similar up to about 14% equivalent viscous damping at which point Eurocode begins to indicate larger reductions compared to AASHTO. Both AASHTO and Eurocode methods indicate larger reductions than

either Newmark-Hall or the velocity pulse condition methods. The use of an alternative reduction for damping would be a logical place to refine simplified procedures in AASHTO.

Duration dependent damping formulations have also been proposed (Stafford, et al., August, 2008). Damping correction factors were reported to be "mildly" dependent upon damping and "strongly" dependent upon duration. Three separate measures of duration were studied, including:

- $D_{5\text{-}95\%}$: significant duration from 5% to 95% of Arias intensity
- $D_{5\text{-}75\%}$: significant duration from 5% to 75% of Arias intensity
- $N_{rr}(2.0)$: number of equivalent cycles of ground motion

The general form of the developed function for each measure of duration is given here with symbols adjusted to agree with those used in this study. For a detailed definition of Arias intensity, refer to the literature (Kramer, 1996).

$$R_{\xi}(D_{5-95\%},\xi) = \frac{SD(\xi)}{SD(5\%)} = 1 - \frac{-0.631 + 0.421ln(\xi) - 0.015ln(\xi)^2}{1 + exp\left\{\frac{-[ln(D_{5-95\%}) - 2.047]}{0.930}\right\}} \quad \text{(Eq. 2-23)}$$

$$R_{\xi}(D_{5-75\%},\xi) = \frac{SD(\xi)}{SD(5\%)} = 1 - \frac{-0.652 + 0.435ln(\xi) - 0.016ln(\xi)^2}{1 + exp\left\{\frac{-[ln(D_{5-75\%}) - 1.168]}{1.283}\right\}} \quad \text{(Eq. 2-24)}$$

$$R_{\xi}(N_{rr},\xi) = \frac{SD(\xi)}{SD(5\%)} = 1 - \frac{-0.558 + 0.369ln(\xi) - 0.011ln(\xi)^2}{1 + exp\left\{\frac{-[ln(N_{rr}) - 1.791]}{1.181}\right\}} \quad \text{(Eq. 2-25)}$$

Figure 2.3-2 consists of plots for damping reduction versus effective damping for several different values of significant duration, $D_{5\text{-}95\%}$. This parameter has been chosen simply because it is the most readily available from the software used in this study and is, thus, frequently used in

the literature, as is the case for the referenced work. From this figure it is inferred that the AASHTO damping reduction rules correspond roughly to a significant duration of 10 to 15 seconds - the curve for AASHTO lies between the 10-second duration curve and the 15-second duration curve. This could be important in modifying damping correction factors for sites where significant durations of roughly 30 seconds are prevalent in design ground motions.

Regardless of the choice for modeling of effective damping, the effect is sensitive to both displacement ductility and post-yield stiffness ratio. Figure 2.3-3 shows the variation of effective damping from hysteretic behavior of the isolation system with displacement ductility demand - defined as the ratio of actual displacement to yield displacement - using the AASHTO method for various ratios of the post-yield stiffness, α.

Other approximate, simplified analysis procedures have been proposed. One such method (Ryan & Chopra, March, 2004) attempts to account for bi-directional excitation of the isolator. An interesting feature of the proposed method is dependence of the isolator response on peak ground velocity (PGV) rather than spectral acceleration. The final form of the estimated isolator displacement (with nomenclature modified to reflect that used here) is:

$$D_{ISO} = \frac{6.51}{4\pi^2} T_d^{0.19} \eta^{-0.46} PGV \qquad \text{(Eq. 2-26)}$$

$$T_d = 2\pi \sqrt{\frac{W}{g K_d}} \qquad \text{(Eq. 2-27)}$$

$$\eta = \frac{Q_d \cdot g \cdot T_{CP}}{2\pi \cdot W \cdot PGV} \qquad \text{(Eq. 2-28)}$$

Note that the expression as presented in the referenced document has been based on an assumed corner period (T_{CP}, the period at which the displacement spectrum initially reaches its peak value) of 2.06 seconds – which will be shown in CHAPTER 3 to be significantly smaller than that expected in the NMSZ. Additionally, the reported bi-directional effect incorporated into the expression is a simple 13% increase over uni-directional displacement demand based on statistical analyses.

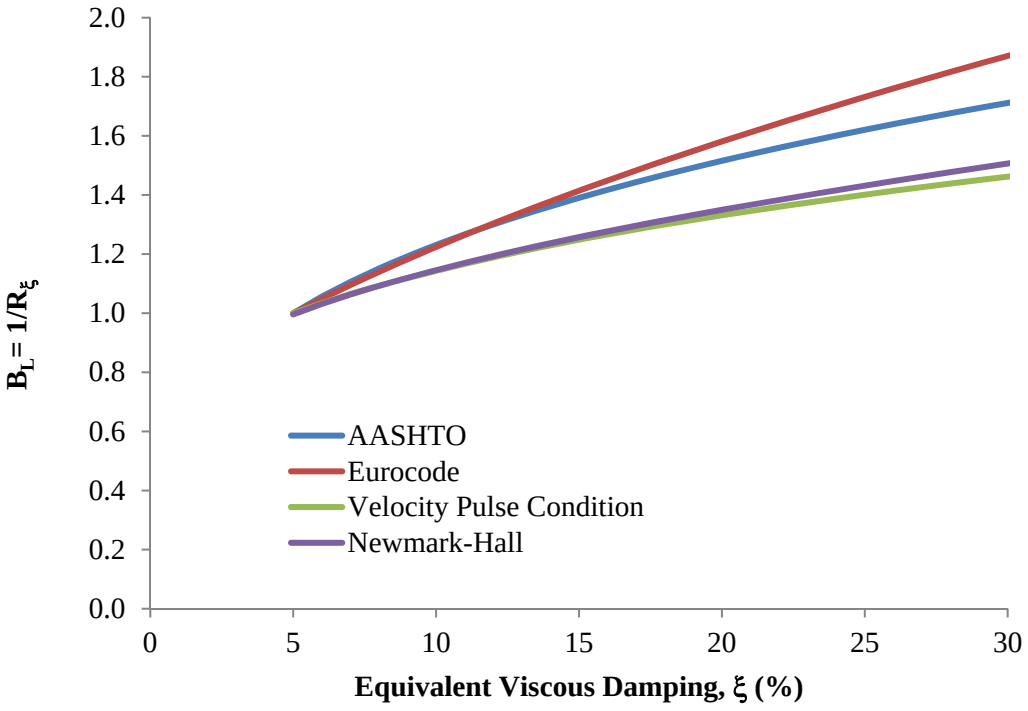

Figure 2.3-1. Response Modifier for Damping

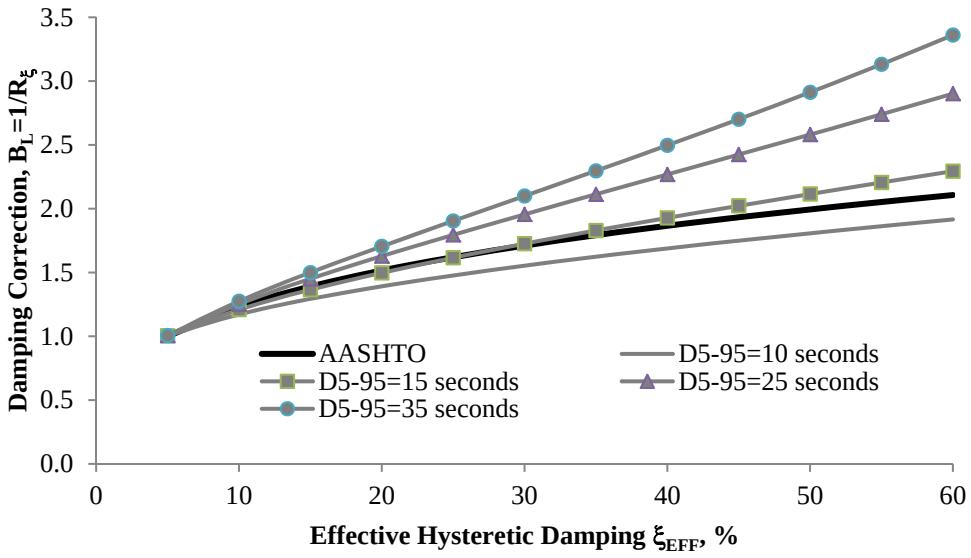

Figure 2.3-2. Duration Dependent Damping Correction

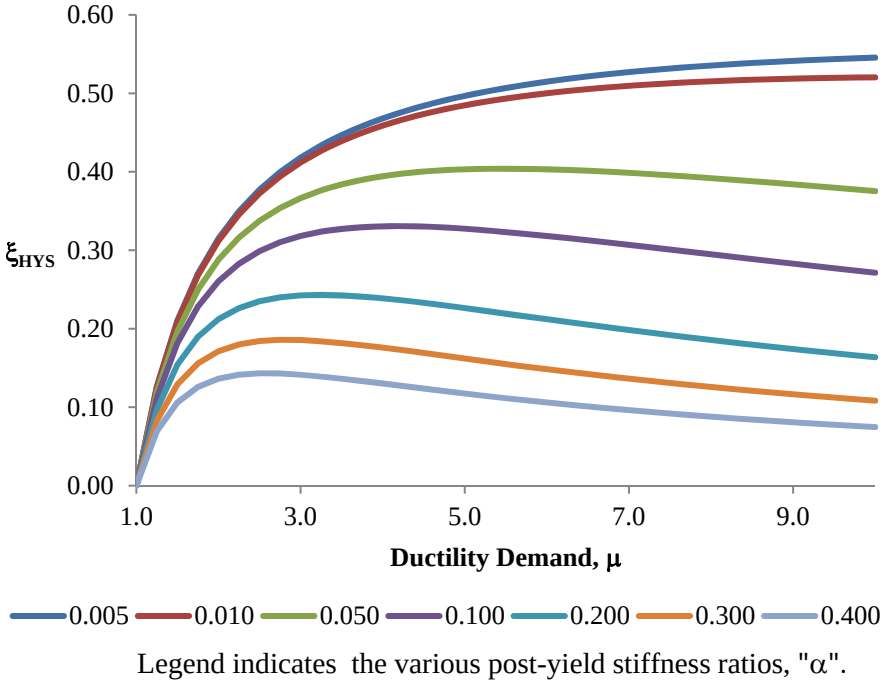

Figure 2.3-3. Variation in Damping Reduction for Various α-values

2.4 Code Requirements

Requirements for isolation devices from the AASHTO Guide Specifications for Seismic Isolation Design (AASHTO, 2010) are summarized here. An important feature of the Guide Specification is its consideration of ground motions larger than those corresponding to a return period of 1,000 years - the DBE event of CHAPTER 1. While the design in the Guide Specification is explicitly for the DBE-level hazard, provisions are made for isolator demands meeting 2,500 year return period criteria (See Article C3.1 and Article 12.3 of the Guide Specification).

Isolation design of bridges may typically be accomplished using the simplified, equivalent stiffness and damping, procedures introduced in Section 2.3. In cases where damping in the isolation system itself exceeds 30% or when the effective period exceeds 3 seconds, nonlinear time history analyses are required by the AASHTO Guide Specifications for Seismic Isolation Design (AASHTO, 2010).

Isolation systems must be designed not only at the specified values of K_d and Q_d, but also at upper-bound and lower-bound values of each parameter. Specified values for K_d and Q_d are multiplied by λ-factors which account for aging, velocity, contamination, wear, and temperature. A scragging λ-factor is also required for LRB isolators.

Adequate horizontal clearances are required for isolators. Movement due to braking forces, wind, centrifugal forces in curved bridges, uniform temperature changes, and temperature gradients are to be accommodated in isolation designs. These are accounted for in design using Extreme Event Load combinations from the AASHTO LRFD Bridge Design Specifications.

The resistance of isolation systems to braking, wind, centrifugal, and thermal effects is to be verified through prototype testing. Prototype testing also serves to verify assumed damping and deformation characteristics of isolators.

There are 3 types of tests which may be required by the AASHTO Guide Specifications for Seismic Isolation Design (AASHTO, 2010) for a proposed isolation system:

1. System characterization tests – tests required when a new system is being developed, these tests serve to establish fundamental properties controlling isolator behavior.
2. Prototype tests – these tests are performed on systems which have already been through system characterization testing and have been successfully implemented in practice.
3. Quality Control tests – these are tests performed on all isolator units specified for a particular project in order to verify properties such as compression capacity, combined compression-shear capacity, bonding adequacy between dis-similar elements of the bearing, geometry of the various parts, friction coefficients, etc.

It is possible to design isolation systems with zero post-yield stiffness. AASHTO currently requires a minimum restoring force in most isolation systems used for bridges. The restoring force in an LRB isolator is provided by the elastomer stiffness. The restoring force in an FPS isolator is provided by the curvature of the sliding surfaces. An example of a system with zero post-yield stiffness - i.e., zero restoring force bearings - would be a flat slider assembly. The

minimum post-yield stiffness must be such that the post-yield (tangent stiffness) period is less than 6 seconds.

$$T_d = 2\pi\sqrt{\frac{W}{gK_d}} < 6 \qquad \text{(Eq. 2-29)}$$

$$K_d > \frac{\pi^2 W}{9g} \qquad \text{(Eq. 2-30)}$$

Secondly, the restoring force at the total design displacement must be greater than the restoring force at one-half the design displacement by at least W/80. Assuming that the isolator is yielded at one-half the design displacement, this is equivalent to requiring that:

$$K_d \geq \frac{W}{40D_{ISO}} \qquad \text{(Eq. 2-31)}$$

In addition to code limitations, it is good practice to impose the following limit on FPS systems:

$$\mu \leq \frac{D_{ISO}}{R} \leq 0.15 \qquad \text{(Eq. 2-32)}$$

The lower limit on D_{ISO}/R establishes superior re-centering capability of the bearing after an earthquake and the upper limit is somewhat arbitrary, but larger values for D_{ISO}/R violate the assumptions of small angular rotations about the center of curvature of the concave surface of the bearing inherent in developed theories.

In summary, the main points of this chapter to be applied in subsequent material are as follows:

1. An isolation system, whether LRB or FPS, may be completely defined by three parameters:

- Q_d, the characteristic strength

- K_d, the post-yield stiffness
- D_y, the yield displacement

2. The design of most isolation systems may be carried out using a simplified, secant-stiffness analysis, with added damping from hysteretic behavior of the isolators. When the effective damping of the system exceeds 30%, AASHTO requires nonlinear response history analysis for design.

3. A modified spectral shape with duration-dependent damping reduction formulation may be appropriate for isolation design in the New Madrid Seismic Zone.

With some basics of isolation theory in hand, and with the seismic hazard definition from CHAPTER 1, the foundation is in place for beginning the process of ground motion selection and modification.

CHAPTER 3 - GROUND MOTION SELECTION AND MODIFICATION

To perform a nonlinear response history analysis of an isolated structure, a set of ground motions is required. This is one distinguishing feature of nonlinear analysis - the loading must be defined in terms of acceleration time histories applied at the base of the structure, whereas in a linear analysis, the loading may be expressed simply as a design response spectrum. These ground motions may be either actual recorded accelerograms from real earthquakes or synthetic motions generated from seismological models of faulting mechanisms.

The ground motion selection process begins with a definition of the seismic hazard at the site in question. This was a significant portion of CHAPTER 1 - hazard deaggregation produced a set of M_W,R combinations for each of the two study sites and PSHA results produced target response spectra, both code-based and NMSZ-specific. Subsurface conditions were used to establish AASHTO site classification and embayment depth estimates for each study site. With M_W,R pairs, target response spectra, and site characterization in hand, this entire chapter is devoted to ground motion selection and modification to be used for nonlinear structural analysis of (a) model isolators in CHAPTER 4 and (b) isolated bridge models in CHAPTER 7.

The selection and modification of real earthquake records for nonlinear analysis of structures is a developing science - at least in practice - in that most code-based guidance is somewhat vague. The process for sites in the NMSZ is further complicated given the shortage of strong ground motion records from large magnitude, intraplate events with recordings on deep soil sites.

Regarding the inter-versus-intra-plate issue, a study presented at the 10th World Conference on Earthquake Engineering in Rotterdam concluded that “the extrapolation of interplate derived design spectra to intraplate regions appears conservative, particularly for structures with periods greater than 0.3 seconds" (Chandler, et al., 1992). Other research suggests that ground shaking from New Madrid earthquakes might be comparable to ground shaking from California earthquakes one magnitude unit larger (Stein, 2007). And some evidence suggests that code-based spectral shapes in the period range of 1-3 seconds may be un-conservative for large magnitude, intraplate events (Nichols, 2005). Later, in Section 3.5.2, a discussion of potential un-conservatism in code-based spectral shapes due to subsurface profile depth effects will make it more clear that in the Mississippi Embayment of the New Madrid Seismic Zone, code-based spectra may not be appropriate - both intraplate and embayment depth effects are likely to modify the spectral shape in the typical isolated period range.

After summarizing frequently used modification procedures, code-based selection and modification requirements are discussed, firstly for bridges specifically and secondly for structures in general. Sources for both real and synthetic ground motion time histories are discussed followed by the development of criteria to be used for the initial selection of records. Sets of accelerograms are then selected and modified first for purposes of comparative study of the model isolators in CHAPTER 4 and, secondly for the design of the isolated bridges in CHAPTER 7.

3.1 Ground Motion Modification Procedures

Ground motions may be modified in a number of ways. Four of these are summarized here.

1. Single-period-based time domain scaling
2. Multi-period-based time domain scaling
3. SRSS-based (square-root-sum-of-squares) amplitude scaling
4. Spectral matching in the time domain or in the frequency domain

3.1.1 Single-period-based Time Domain Scaling

Amplitude scaling at a single period of interest may be used. The ground motion is scaled in the time domain such that the spectral acceleration of the scaled accelerogram matches the design spectral acceleration at a single period. This might be the fundamental period of the structure being analyzed or some other predetermined value.

3.1.2 Multi-period-based Time Domain Scaling

Amplitude scaling in a manner such that the mean-square error between the scaled spectrum of the actual earthquake and the design (target) spectrum is minimized within a window of periods is another option. The range of periods might be centered on the fundamental period of the structure being analyzed, or it might be at a set of discrete periods. The nuclear industry has used this method with five discrete periods: 0.3, 0.6, 1.0, 2.0, and 4.0 seconds (Huang & Whittaker, August, 2007). The Pacific Earthquake Engineering Research (PEER) Program proposes this method using a set of 301 logarithmically spaced periods between 0.01 and 10.0 seconds (PEER, Beta Version, October 1, 2010).

Appropriate amplitude scaling of ground motion records must account for the nature of the acceleration target spectrum to be matched. Historically and currently, design specification response spectra represent the geometric mean of two horizontal components. While the building industry is currently moving towards defining design spectra as maximum horizontal component

spectra, the same is not true for AASHTO. Amplitude scaling without regard to the nature of the design target spectrum can lead to extremely erroneous results as has been reported by the National Institute of Standards and Technology (NEHRP Consultants Joint Venture, 2011) and as will be further demonstrated in Section 3.3 of this chapter.

The scaled spectrum is taken as the target-compatible geometric mean of the two scaled, horizontal orthogonal components of the same earthquake record. Each record has a unique scale factor when this method is selected. The scale factor, *f*, for a given record pair is summarized in equations 3-1 through 3-3. Varying weights are assigned to the discrete periods through the use of the weighting factors, $w(T_i)$. SA_{H1} and SA_{H2} are the spectral values for the two horizontal components at the period in question. SA_{GM} is the geometric mean of the two components. SA_{TARGET} is the target spectral value at the period in question. The mean-square-error is denoted *MSE*.

$$SA_{GM}(T_i) = \sqrt{SA_{H1}(T_i) \cdot SA_{H2}(T_i)} \qquad \text{(Eq. 3-1)}$$

$$\ln f = \frac{\sum \left[w(T_i) \cdot ln \frac{SA_{TARGET}(T_i)}{SA_{GM}(T_i)} \right]}{\sum w(T_i)} \qquad \text{(Eq. 3-2)}$$

$$MSE = \frac{\sum w(T_i) \cdot \{ln[SA_{TARGET}(T_i)] - ln[f \cdot SA_{GM}(T_i)]\}^2}{\sum w(T_i)} \qquad \text{(Eq. 3-3)}$$

Further, realize that there is not a single geometric mean for a given record pair. The two used in current USGS data are the as-recorded geometric mean, GMAR, and a particular rotated geometric mean, GMRotI50. The as-recorded geometric mean is self-explanatory - take the geometric mean of the spectra from each of two horizontal components at every period as the basis for comparison to a target spectrum. GMRotI50 is that median, geometric mean at a

particular angle of rotation - namely, that which minimizes the "spread of the rotation-dependent geometric mean" (Boore, et al., August 2006). Dave Boore at the USGS has developed software to enable the computation of the geometric mean of two horizontal components at various angles, including the computation of GMRotI50 (Boore, 2009). It is useful to keep in mind that the two most often used data sets in establishing design response spectra in the CEUS (Central and Eastern United States) are the 2002 and updated 2008 USGS versions. The crucial parameter is the dependent variable used in the GMPM's (ground motion prediction models) making up the PSHA (probabilistic seismic hazard analysis) used to develop design spectra. The following dependent variables were used in the two PSHA's (Boore, August 2010):

- For the 2002 USGS PSHA data, GMPM's used the as-recorded geometric mean
- For the updated 2008 USGS PSHA, GMPM's used GMRotI50.

So, the analyst using a target response spectrum based upon 2002 USGS data should use the as-recorded geometric mean of selected records as the basis for comparison to target spectra while the analyst using targets based upon updated 2008 USGS data should use the rotated geometric mean, GMRotI50. The difference is typically small but this cannot be guaranteed. A set of records appropriate for Site 1 conditions was selected and scale factors were computed first using GMRotI50 - determined using TSPP - for each record (the correct way since the targets in this study are based upon 2008 USGS data), and secondly using GMAR (the incorrect way in this particular case). The results are summarized in Table 3.1.2-1 (Refer to Section 3.4 for data on the events listed in the table). Scale factors were based upon the minimization of the MSE at periods of 0.5, 0.8, 1.0, 2.0, and 4.0 seconds to achieve compatibility over a wide range of periods. The scale factor computed by the two methods may be quite close, as with Chi-Chi,

Taiwan record 1265 for which the GMRotI50-based scale factor is 2.132 and the GMAR-based scale factor is 2.134 at the DBE-hazard level. On the other hand, the scale factor computed by the two methods differs by about 5% for Landers record 900.

It might be tempting to conclude that, since the averages are so close, either basis is equally valid. However, when nonlinear behavior is concerned, unnecessarily over-scaling one record and under-scaling another will not have the same mean structural effect as correctly scaling the records, with the same average scale factor. The analyst is well-advised to use the target-compatible intensity measure - GMAR, GMRotI50, or some other measure - in the scaling of ground motions to be used in the nonlinear analysis of structures. This is discussed in more detail in APPENDIX D.

To illustrate the detailed calculation of a unique scale factor to minimize the mean-square-error at discrete periods, suppose the target spectrum is taken as the Site 2 DBE level uniform hazard spectrum and suppose that the ground motion to be scaled is that recorded at station MZQ during the 2008 Wenchuan, China M7.9 earthquake. Acceleration, velocity, and displacement plots of the uncorrected records obtained from Dr. Zhenming Wang of the Kentucky Geological Survey are shown in APPENDIX G3, Figure G3.1.2-1 for the North/South component and in Figure G3.1.2-2 for the East/West component.

The integrated velocity and displacement time histories clearly show the need for baseline correction and filtering of the records. SeismoSpect (SeismoSoft, 2011) is used to perform the necessary modification to the original records. Linear baseline correction and 4^{th} order Butterworth band-pass filtering produce the corrected and filtered time histories shown in

APPENDIX G3, Figure G3.1.2-3 for the North/South component and in Figure G3.1.2-4 for the East/West component.

Once the corrected accelerograms have been saved, response spectra - 5% damping - may then be generated for each of the two components. This is completed, again using SeismoSpect. The spectral accelerations for the Site 2 DBE-hazard level target, for each of the two components of the Wenchuan record, and for the GMRotI50 geometric mean (the geometric mean of "n" numbers is the "n"th root of the product of the "n" numbers) of the two components are given in Table 3.1.2-2. For this example, periods of 0.5, 0.8, 1.0, 2.0, and 4.0 seconds have been chosen for the scaling and equal weights are used for each of the periods. For the un-scaled, corrected records, the MSE is:

$$MSE = \frac{1.0 \cdot 0.379 + 1.0 \cdot 0.156 + 1.0 \cdot 0.314 + 1.0 \cdot 0.227 + 1.0 \cdot 0.061}{1.0 + 1.0 + 1.0 + 1.0 + 1.0} = 0.227$$

The scale factor which minimizes MSE at the 5 selected periods is:

$$\ln f = \frac{1.0 \cdot 0.616 + 1.0 \cdot 0.395 + 1.0 \cdot 0.561 + 1.0 \cdot 0.476 + 1.0 \cdot 0.248}{1.0 + 1.0 + 1.0 + 1.0 + 1.0} = 0.459$$

$$f = \exp(0.459) = 1.583$$

For the scaled, corrected record, the MSE is:

$$MSE = \frac{1.0 \cdot 0.024 + 1.0 \cdot 0.004 + 1.0 \cdot 0.010 + 1.0 \cdot 0.000 + 1.0 \cdot 0.045}{1.0 + 1.0 + 1.0 + 1.0 + 1.0} = 0.017$$

The various spectra are shown in APPENDIX G3, Figure 3.1.2-5.

For any strategy involving amplitude scaling, the following two points are important to remember.

- First, it is most preferable to use the same scale factor for both components of a given record (Buckle, et al., 2006). The relative intensities of recorded ground motion components is an important aspect of the probabilistic nature of structural analysis for ground motion. This first point is automatically satisfied when geometric mean target and record spectra are used.
- Secondly, some sort of limit on deviation from the target should be established. This is necessary because scaling to minimize the MSE between target and record spectra can still leave a poorly matched result. Again, the procedure recommended in the FHWA retrofit manual (Buckle, et al., 2006) provides perhaps the best criteria among modern codes and specifications. Namely, the mean of all amplitude-scaled record spectra in a set of motions to be used for analysis must (a) be no more than 15 percent lower than the target at any period within the range of interest and (b) possess an average ratio to the target of 1.0 or higher over the range of periods. Naturally, it is also desirable to put some upper limit on the deviation between the mean scaled and the target spectra. It would prove unduly conservative to adopt a set of records which produced a mean scaled spectrum 25% (just to give an example) above the target at all periods of interest.

Table 3.1.2-1. GMRotI vs. GMAR Scaling

Event	Station Code	DBE Scale Factor		MCE Scale Factor	
		GMRotI50	GMAR	GMRotI50	GMAR
Taiwan SMART1(45)	0570	2.115	2.102	3.082	3.062
	0575	2.009	1.962	2.927	2.859
Landers	0900	1.863	1.956	2.714	2.850
Kocaeli, Turkey	1147	1.446	1.390	2.106	2.025
	1155	3.077	3.066	4.482	4.466
	1158	1.098	1.092	1.599	1.591
Chi-Chi, Taiwan	1187	1.926	2.000	2.807	2.913
	1203	1.140	1.129	1.661	1.645
	1265	2.132	2.134	3.106	3.109
	1498	1.545	1.498	2.251	2.183
	1513	1.251	1.238	1.822	1.803
	1536	1.078	1.055	1.570	1.538
Duzce, Turkey	1605	0.831	0.801	1.210	1.167
Manjil, Iran	1640	2.862	2.950	4.169	4.298
Denali, Alaska	2114	0.885	0.879	1.289	1.281
Darfield, New Zealand	CHHC	1.750	1.717	2.549	2.501
	DSLC	2.149	2.039	3.131	2.971
	HORC	0.880	0.876	1.282	1.275
	LINC	1.043	1.112	1.520	1.620
	REHS	1.342	1.414	1.955	2.059
Sierra El Mayor	M412	1.039	1.056	1.513	1.538
	M01711	1.088	1.076	1.585	1.568
	M5057	2.332	2.280	3.397	3.321
	M5058	1.040	1.017	1.515	1.481
	M-DRE	1.883	1.867	2.743	2.720
Average		**1.592**	**1.588**	**2.319**	**2.314**

Table 3.1.2-2. Spectral ordinates - example scaling problem

Period sec	SA_{NS} g	SA_{EW} g	SA_{GM} g	SA_{TARGET} g	Un-scaled SE	ln (SA_{TARGET}/SA_{GM})	Scaled SE
0.5	0.808	0.967	0.884	1.636	0.379	0.616	0.024
0.8	0.656	0.724	0.689	1.023	0.156	0.395	0.004
1.0	0.401	0.544	0.467	0.818	0.314	0.561	0.010
2.0	0.201	0.320	0.254	0.409	0.227	0.476	0.000
4.0	0.128	0.200	0.160	0.205	0.061	0.248	0.045

3.1.3 SRSS-based Amplitude Scaling

A third amplitude scaling approach takes the scaled spectrum equal to the square-root-of-sum-of-squares (SRSS) of the spectra for the two horizontal components. A suite of records, each consisting of horizontal pairs, is scaled such that the mean of the scaled spectra does not fall below some multiple of the design (target) spectrum. There is no unique solution for the various scale factors applied to the records in this method. Many different sets of scale factors for a given suite of records will produce a mean spectrum which meets the requirement. FEMA 450 requires that the mean of the scaled SRSS spectra not fall below 1.3 times the target spectrum by more than 10% within the range of periods equal to 0.5 times the fundamental period up to 1.25 times the fundamental period (Building Seismic Safety Council, 2004). This is equivalent to requiring that the mean scaled SRSS spectrum not fall below 0.9 x 1.3 = 1.17 times the target spectrum.

For example, suppose a record pair were scaled using the geometric mean of the components and the target at a single period. Let *x* be the ratio of the spectral accelerations of the two components. Then the true required scale factor is simply:

$$f = \frac{SA_{TAR}}{\sqrt{SA_{H1} \cdot SA_{H2}}} \qquad \text{(Eq. 3-4)}$$

The scaled SRSS spectral ordinate for the record is then:

$$SA_{SRSS} = \sqrt{(f \cdot SA_{H1})^2 + (f \cdot SA_{H2})^2} = f\sqrt{SA_{H1}^2 + SA_{H2}^2}$$

$$= \frac{SA_{TAR}}{\sqrt{SA_{H1} \cdot SA_{H2}}} \cdot \sqrt{SA_{H1}^2 + SA_{H2}^2} \qquad \text{(Eq. 3-5)}$$

$$= SA_{TAR} \cdot \sqrt{\frac{SA_{H1}}{SA_{H2}} + \frac{SA_{H2}}{SA_{H1}}}$$

The question then becomes: "When will the geometric-mean-based scale factor at a given period produce a scaled spectral ordinate at least equal to 1.17 times the target?"

$$SA_{TAR} \cdot \sqrt{\frac{SA_{H1}}{SA_{H2}} + \frac{SA_{H2}}{SA_{H1}}} \geq 1.17 \cdot SA_{TAR}$$

$$\frac{SA_{H1}}{SA_{H2}} + \frac{SA_{H2}}{SA_{H1}} \geq 1.17^2$$

$$x + \frac{1}{x} \geq 1.17^2$$

So, when is the left-hand-side greater than the right-hand-side? The left-hand-side has a local minimum at a particular value of *x*, namely at *x*=1 (i.e., when the two components have equal spectral ordinates at the period in question) and the minimum is 2.

$$\frac{d}{dx}\left(x + \frac{1}{x}\right) = 1 - \frac{1}{x^2} = 0 \rightarrow x = 1$$

$$1 + \frac{1}{1} = 2 > 1.17^2$$

In other words, the geometric-mean-based scale factor will always produce a scaled spectral ordinate greater than the minimum required based on SRSS-scaling. This opens the door for SRSS-based scaling to give un-conservative scale factors in the sense that the geometric mean of the scaled components can be less than the design spectrum, which is a geometric mean spectrum to start with. This method will be explored no further for use in this study and it is not recommended for future code-based scaling procedures in which the design target spectrum represents the geometric mean of two horizontal components. This inconsistency has been identified in previous work as well (NEHRP Consultants Joint Venture, 2011).

To further clarify the problem with SRSS-based scaling to geometric-mean-based target spectra, consider a simple example. Suppose that the target spectral acceleration at a particular period is SA_{TAR} = 0.5 g and that a record pair has been selected with spectral acceleration values of SA_{H1} = 0.1 and SA_{H2} = 0.9 g for the two horizontal components. Then by the SRSS scaling rule, an admissible scale factor would be:

$$SF_{SRSS} = 1.3 \times 0.9 \times \frac{0.5}{\sqrt{0.1^2 + 0.9^2}} = 0.646$$

So, after scaling, the spectral ordinates of the components at the period in question are SA_{H1} = 0.1 x 0.646 = 0.0646 and SA_{H2} = 0.9 x 0.646 = 0.5814. The geometric mean of the two scaled components is:

$$SA_{GM} = \sqrt{0.0646 \times 0.5814} = 0.194$$

So it would seem that the SRSS scaling procedure often specified fails to account for the fact that design response spectra are typically geometric mean spectra. The target geometric mean in the

simple example is 0.5 g and the geometric mean of the two scaled components is 0.194 g, quite a lot less than the target - in fact, by a factor of 2.58. The effect is more pronounced when the spectral ordinates for the two components are dissimilar, as is the case with the example just presented. But even if the two components are identical, the possibility for under-estimating the appropriate scale factor still exists. Had the two components each had un-scaled spectral values of 0.3, then the SRSS-based scale factor and resulting geometric mean acceleration would be:

$$SF_{SRSS} = 1.3 \times 0.9 \times \frac{0.5}{\sqrt{0.3^2 + 0.3^2}} = 1.379$$

$$SA_{GM} = \sqrt{(1.379 \times 0.3) \times (1.379 \times 0.3)} = 0.414$$

So the scaled geometric mean (0.414) is still less than the required design geometric mean (0.5).

3.1.4 Spectral Matching

Wavelet (brief, wave-like oscillations) algorithms may be used to modify earthquake records such that the response spectrum of the modified record matches the design (target) spectrum within some desired tolerance of a specified range of periods. This method is not a scaling in the time domain and is philosophically different than amplitude scaling. Ground motion parameters such as significant duration, predominant period, PGD/PGV (the ratio of peak ground displacement to peak ground velocity) and others which are typically unaltered by amplitude scaling can be drastically changed through the process of spectral matching using wavelets. Efforts to mitigate some of these undesirable effects are being made (Al Atik & Abrahamson, 2010).

The purpose of this section is not to develop a general theory of wavelet algorithms, but to present some basic options available in spectral matching techniques. Within spectral matching procedures there are various wavelet options available. Among the wavelet forms incorporated into software - *RspMatch* (Al Atik & Abrahamson, 2010), *RspMatchBi* (Grant, 2011), *SeismoMatch* (SeismoSoft, 2011), etc. - are impulse functions, tapered cosine waves, sinusoidal displacement-compatible wavelets, and polynomial functions. *RspMatchBi*, in fact, is unique in that simultaneous matching of two components to major and minor target spectra is possible. This of course, has the disadvantage that the definition of a minor target spectrum is required. One solution to this problem is to set the minor target equal to the major target. The geometric mean of the two components is then equal to the target. However, the relative amplitude differences between the two components are lost when this approach is adopted since both components are matched to the same spectrum, but may have very different spectrum shapes themselves.

Spectral matching will be used in this study for ground motion modification so a strategy is developed here to maintain the relative magnitudes of component spectra. The spectral accelerations of the two components at a period of 1 second will be determined as will the geometric mean of the two at this same period. The ratio of each component to the geometric mean will be maintained in the matching process. So for example, suppose that $SA_{H1}(1)$ = 0.475 and $SA_{H2}(1)$ = 0.396. Then the geometric mean and the corresponding ratios are:

$$SA_{GM}(1) = \sqrt{0.475 \cdot 0.396} = 0.434$$

$$\frac{SA_{H1}(1)}{SA_{GM}(1)} = \frac{0.475}{0.434} = 1.094$$

$$\frac{SA_{H2}(1)}{SA_{GM}(1)} = \frac{0.396}{0.434} = 0.912$$

In this example, the H1 component would be matched to 1.094 times the target spectrum and H2 would be matched to 0.912 times the target spectrum.

For near field sites - sites within 10 kilometers (6 miles) of a fault (AASHTO Guide Specification Article 3.4.4) - it is considered important that records with pulse-type characteristics are included (NEHRP Consultants Joint Venture, 2011). Site No. 2 (R = 11.9 kilometers or 7.4 miles) is slightly outside the "near-field" range. Given the hypothetical nature of fault geometry and location in the NMSZ, Site No. 2 will be considered as near-field and pulse type records will be included in the sets to be used in design of the bridges for this study. This will affect the usefulness of spectral matching when applied to Site No. 2. Examination of pre and post-matched record displacement and velocity histories will be necessary to ensure that the pulse-type character has not been lost in the matching process.

For example, consider the record from Yarmica station (NGA sequence number 1176) of the 1999 Kocaeli, Turkey (M_W 7.51) earthquake for the fault-normal (FN) component (see Section 3.4). The record is first scaled by a factor of 2.08 to produce a seed motion with acceleration spectrum closer to the target spectrum (1.04 times the Site 2 UHRS for this example). The scaled record is then matched using *SeismoMatch* (SeismoSoft, 2011) for a period range of 0.1-6.0 seconds. APPENDIX G3, Figure G3.1.4-1 shows both the pre-matched and the post-matched ground displacement histories for the record. The general character of the motion has been preserved and the matched record can be considered a pulse-type record. On the other hand, consider the fault-normal record from Duzce station (NGA sequence number 1650) of the

1999 Duzce, Turkey (M_W 7.14) earthquake (see Section 3.4). The record is first scaled by a factor of 1.24 and then matched to 0.85 times a Site 2 NMSZ-specific target spectrum. The matching period range is again 0.10-6.0 seconds. APPENDIX G3, Figure G3.1.4-2 shows the pre-matched and post-matched ground displacement histories and it is evident that the general character of the motion has been altered in such a manner that the classification of the post-matched record as pulse-type is questionable at best. These differences in pre and post-matched records are typically not evident in the acceleration time histories, but in the velocity and displacement time histories.

3.2 AASHTO Code-based Selection and Modification Requirements

While most code-based guidance on requirements for the selection and modification of earthquake ground motions for nonlinear analysis is in a developing stage and still rather vague, there are provisions which, at least, make an attempt to establish criteria. At least four bridge-specific documents contain sections on ground motion selection and modification:

1. AASHTO LRFD Bridge Design Specifications (AASHTO, 2012), hereafter referred to as the *LRFD Specification*;
2. AASHTO Guide Specification for LRFD Seismic Bridge Design (AASHTO, 2011), hereafter referred to as the *LRFD Guide Spec*;
3. FHWA Seismic Retrofitting Manual for Highway Structures (Buckle, et al., 2006), hereafter referred to as the *Retrofit Manual*;
4. AASHTO Guide Specification for Seismic Isolation Design (AASHTO, 2010), hereafter referred to as the *Isolation Guide Spec*.

The following paragraphs discuss requirements found in the above documents.

The *LRFD Specification* requires that time histories used for the analysis of bridges have characteristics that are "representative of the seismic environment of the site and the local site conditions" (Article 4.7.4.3.4b). Characteristics to be considered include tectonic environment, magnitude, fault type, source-to-site distance, local site conditions, and "expected ground motion characteristics". Recorded time histories are to be scaled to the design spectrum "in the period range of significance" using "the time domain procedure". All three orthogonal components are to be applied simultaneously. Records are to correspond to the spectra for ground motion having a 7% probability of exceedance in 75 years. When seven or more records are used, the design response is taken as the mean response in each direction. If fewer than seven records are used, the design response is taken as the maximum in each direction. At least 3 records are required. For near-field sites (within 6 miles of a fault) are encountered, the as-recorded motions are to be transformed to fault-normal (major principal component) and fault-parallel (minor principal component) directions. The *LRFD Specification* Commentary permits spectral matching in the frequency domain to achieve a close match with the design spectrum. The use of a single scaling factor for each of the three orthogonal components is encouraged in time-domain modification.

The *LRFD Guide Spec* (Article 3.4.4) language is virtually identical to that of the *LRFD Specification* with a few exceptions noted here. The Commentary explains that "compromises are usually required" in time history selection because of the "multiple attributes of the seismic environment" and the sometimes "limited data bank of recorded time histories".

The Isolation Guide Spec (Article 7.4) requires that time histories be selected in accordance with the *LRFD Specification*.

FHWA's *Retrofit Manual* (Articles 2.8.2 and 2.8.3) permits both recorded time histories "scaled for the bridge location" and spectrum-matched time histories. Scaling of time histories is to be performed so that the scaled spectrum is "approximately at the level of the design spectrum in the range of periods of structural significance". For cases like the NMSZ where sufficient recorded motions are not available, simulated ground motions which incorporate soil column effects are permitted. When spectrum matching is used, "it is desirable that the overall shape of the spectrum of the recorded or simulated time history be similar to the shape of design response spectrum and that the time history initially be scaled so that its spectrum is at the approximate level of the design spectrum before spectral matching". For sites where deaggregation of the seismic hazard indicated that different seismic sources dominate contributions to different period ranges of the design spectrum, two or more sets of time histories (consisting of 3 or 7 or more records per set) may be required instead of a single set. For each set of ground motion records, the mean scaled spectrum is calculated and compared to the design spectrum. The calculated mean spectrum is to be no more than "15 percent lower than the design spectrum" at any period in the "range of periods of structural significance" and the average ratio of the mean scaled-to-design spectrum over the same range is to be no less than 1.0. All time histories are to be integrated to obtain velocity and displacement histories which are to be "examined for reasonableness". Requirements for number of accelerograms are identical to those found in any of the AASHTO documents.

So, for now, it may be necessary to incorporate provisions from a combination of documents in the process of selecting and modifying ground motions in a manner appropriate for nonlinear response history analysis of bridges.

3.3 Other Code-based Selection and Modification Requirements

A comprehensive summary of ground motion selection and modification criteria from various U.S codes has been developed at the National Institute of Standards and Technology with NIST GCR 11-917-15 (NEHRP Consultants Joint Venture, 2011). Included are requirement summaries for each of the following.

- ASCE/SEI 7, Minimum Design Loads for Buildings and Other Structures (ASCE, 2006 and 2010)
- ASCE/SEI 41-06, Seismic Rehabilitation of Existing Buildings (ASCE, 2007)
- AASHTO Guide Specifications for Seismic Isolation Design (AASHTO 2010)
- AASHTO LRFD Bridge Design Specifications (AASHTO, 2012)
- ASCE/SEI 43-05, Seismic Design Criteria for Structures, Systems, and Components in Nuclear Facilities (ASCE, 2007)
- Seismic Design Guidelines and Data Submittal Requirements for LNG Facilities (FERC, 2007)
- FEMA 65, Federal Guidelines for Dam Safety (FEMA, 2005)
- EC1110-2-600, Selection of Design Earthquakes and Associated Ground Motions (U.S. Army Corps of Engineers, 2009)
- UFC 3-310-04, Seismic Design for Buildings (Department of Defense, 2004, 2007, and 2010)

AASHTO requirements have already been summarized in Section 3.2. Rather than list all available requirements, a discussion of the most significant findings from the report as well as

recommendation from the report are summarized. Refer to the NIST GCR 11-917-15 for details from each Code.

NIST GCR 11-917-15, Article 3.2.4, identifies SRSS-based scaling as having “no solid technical basis because the design spectrum is a geometric mean spectrum”. This point was discussed earlier in Section 3.1.3 of this study. ASCE/SEI 41-06 and ASCE/SEI 43-05 both set limits on the correlation coefficient between orthogonal components of a record pair - the correlation coefficient is to be no more than 0.30. ASCE/SEI 43-05 permits the use of synthetic records only for linear time history analysis. Actual recorded ground motions, either raw or modified, are required for nonlinear seismic analysis. While most codes are consistent in requiring at least three records, EC1110-2-6000 requires a minimum of five time history records for nonlinear analysis, with three records being sufficient only for linear analysis. Similar to the FHWA Retrofit Manual, EC1110-2-6000 places limits on the ratio of mean-scaled-to-design spectrum of no less than 1.0 on average over the “period range of significance”, but is more strict than the Retrofit Manual on the minimum allowable value at any single period within the range - the Retrofit Manual permits a minimum 15 percent lower than the design spectrum while EC1110-2-6000 limits the value to 10 percent lower than the design spectrum at any single period within the range. EC1110-2-6000 encourages the use of identical scaling for two orthogonal components and no limits are placed on scaling factors - the contention being made that the “magnitude of the scaling factor is of secondary importance as long as time history sets after scaling have characteristics that correspond with those developed for the design ground motions”. While spectrum-matched records are said to show less variation in response compared to scaled records, EC1110-2-6000 requires that spectral matching not be used as a means of

decreasing the number of records used in nonlinear analysis. An observation is made in the NEHRP Consultants Joint Venture document (2011) that EC-1110-2-6000 guidelines are the "most comprehensive of those used in design practice at the time of this writing".

The NEHRP Consultants Joint Venture refers to three distinct types of performance assessment using nonlinear structural analysis:

- Intensity-based assessments for a specified intensity of ground shaking, usually a 5% damped elastic design spectrum
- Scenario-based assessments for a specified earthquake event
- Risk-based assessments providing response information over a specified period of time (the most comprehensive of the three)

Ground motion selection and modification requirements depend on the assessment type being used for a particular project.

Three target spectrum options are identified in NIST GCR 11-917-15:

- Uniform Hazard Response Spectra (UHS)
- Conditional Spectra (CS)
- Conditional Mean Spectra (CMS)

The UHS is the typical, code-based spectrum generated using USGS data and code rules for spectrum shape and generally envelopes multiple ground motion sources, thereby often resulting in matched records possessing characteristics not known to be naturally occurring and more conservative than records matched to a CS or a CMS for the same site. The CS and the CMS condition spectral shape on spectral acceleration at a single period, ensuring that matched records will have "appropriate properties for naturally occurring events".

The USGS has also published guidelines for ground motion selection and modification (Kalkan & Chopra, 2010). The report includes recommendations for “ordinary standard” bridges. Various engineering demand parameters (EDP) were determined in nonlinear analyses of standard bridges subjected to recorded ground motion records. A modal pushover-based scaling procedure is advocated, and examples are shown in which the MPS procedure produced accurate estimates of mean EDP’s with lower dispersion compared to results obtained using un-scaled records. In this respect, the MPS procedure and spectral matching can be viewed as having similar effects - accurate estimates of mean response with less dispersion in results.

3.4 Sources for Ground Motion Records

Anticipating the need to combine real records with synthetic and/or artificial records for the design of isolated structures in the NMSZ, a data search for each is summarized here. Real record search results are followed by synthetic record search results.

3.4.1 Records from Actual Earthquakes

Ten sources for strong ground motion recordings have been used for the initial search of records from historic earthquakes:

1. PEER (Pacific Earthquake Engineering Research Center, 2011)
2. NOAA (National Oceanic and Atmospheric Administration, 2011)
3. COSMOS (Consortium of Organizations for Strong Motion Observation Systems, 2007)
4. Kyoshen Network of Japan for Japanese recordings (National Research Institute for Earth Science and Disaster Prevention, n.d.)
5. USGS Strong Motion Program (United States Geological Survey, n.d.)

6. European Strong Motion Database
7. Italian Accelerometric Archive (Anon., 2010)
8. Center for Engineering Strong Motion Data (USGS and California Geological Survey, 2011)
9. New Zealand GeoNET (Anon., 2012)
10. Dr. Zhenming Wang (Kentucky Geological Survey) - Wenchuan records

The candidate events are listed in Table 3.4.1-1. Initial selection was based on those events with magnitude from 7.0 to 8.1, inclusive. A total of 724 record pairs were initially identified as potential candidates.

APPENDIX A lists the various station, distance, and site class parameters for the selected ground motion records. The data are sorted first by site class, secondly by ascending distance, and finally by ascending shear wave velocity. In this format, the data may be a useful guide for selecting ground motion records to be used at a particular site. When site class data were not readily available, station latitude and longitude were used to establish inferred V_{S30} (average shear wave velocity in the upper 30 meters) values using the OpenSHA software (Field, et al., 2003). When using OpenSHA for these sites in the ME of the NMSZ, the “Global VS30 from Topographic Slope” option and the “Stable Continent” (as opposed to “Active Tectonic”) options were selected.

Table 3.4.1-1. Events Considered for Analysis

Event	No. of Record Pairs	Date	Mw	Source
Cape Mendocino	6	25-Apr-92	7.01	PEER
Darfield, New Zealand	20	03-Sep-10	7.10	CESMD
Hector Mine	84	16-Oct-99	7.13	PEER
Duzce, Turkey	23	12-Nov-99	7.14	PEER
Sierra el Mayor	17	04-Apr-2010	7.20	CESMD
Landers	67	28-Jun-92	7.28	PEER
Taiwan, SMART1(45)	15	14-Nov-86	7.30	PEER
India-Burma Border	8	6-Aug-88	7.30	COSMOS
Tabas, Iran	7	16-Sep-78	7.35	PEER
Kern County	1	21-Jul-52	7.36	PEER
Manjil, Iran	6	20-Jun-90	7.37	PEER
Bucharest, Romania	1	3-Apr-77	7.50	ESD
Limon, Costa Rica	8	22-Apr-91	7.50	COSMOS
Kocaeli, Turkey	26	17-Aug-99	7.51	PEER
St. Elias, Alaska	2	28-Feb-79	7.54	PEER
Peru	2	3-Oct-74	7.60	COSMOS
Tangshan, China	1	27-Jul-76	7.60	NOAA
Chi Chi, Taiwan	371	20-Sep-99	7.62	PEER
Sitka, Alaska	1	12-Nov-99	7.68	PEER
El Salvador	11	13-Jan-01	7.70	USGS
Japan 01 (Aftershock)	6	11-Mar-11	7.70	KikNET
Bhuj, India	1	26-Jan-01	7.70	COSMOS
Valparaiso, Chile	3	3-Mar-85	7.80	COSMOS
Denali, Alaska	23	3-Nov-02	7.90	PEER
Indonesia (Aftershock)	1	12-Sep-07	7.90	USGS
Japan 02	4	26-Sep-03	8.00	KikNET
Michoacan, Mexico	5	19-Sep-85	8.10	COSMOS
Peru Coast	1	17-Oct-66	8.10	COSMOS
Wenchuan, China	3	12-May-2008	7.90	Dr. Zhenming Wang

3.4.2 Synthetic and Artificial Records

Previous research into the seismic hazard in the NMSZ has produced synthetic motions. Three separate studies generated ground motions for the NMSZ including site condition effects.

Atkinson (Atkinson & Beresnev, 2002) used a finite-fault simulation (FINSIM) and studied a wide range of input variables - the most important of which were found to be magnitude, hypocenter location, and maximum slip velocity - to generate ground motion for the cities of St. Louis, Missouri and Memphis, Tennessee for magnitude 7.5 and magnitude 8.0 events. Six ground motions were produced for rock, linear soil, and nonlinear soils conditions at each magnitude and each city. A generic soil profile for Memphis was used and is reproduced in Table 3.4.2-1.

Fernandez and Rix (Fernández, 2007) took McGuire's (McGuire, et al., 2001) records and wavelet-matched them to independently generated spectra from a probabilistic seismic hazard analysis for various site in the NMSZ including: Memphis and Jackson in Tennessee; Jonesboro, Blytheville, and Little Rock in Arkansas; Paducah, Kentucky and Cape Girardeau, Missouri. Further distinction was made between "uplands" and "lowlands" for the Memphis data. Mean annual return periods of 475 years, 975 years, and 2,475 years were included in the subsequently generated ground motions.

A NEHRP (National Earthquake Hazards Reduction Program) study (Olsen, 2011) produced synthetic seismograms for Memphis, Evansville, and St. Louis based on the simulation of spontaneous rupture on planar faulting. Three different fault segments believed to be part of the system which generated the 1811-1812 sequence of event in the NMSZ were studied: (1) the

140 km long by 22 km wide SW strike-slip segment, (2) the 70 km long by 22 km wide NE strike-slip segment, and (3) the 60 km long by 40 km wide central, dipping, thrust segment. Site effects were accounted for using amplitude dependent site correction factors.

Twenty-four accelerograms from Atkinson-Beresnev and sixty accelerograms from Fernandez-Rix will be used for this study.

Table 3.4.2-1. Generic Soil Profile for Memphis (Atkinson & Beresnev, 2002)

Layer	Type	Thickness, m	Shear Wave Velocity, m/sec	Density, g/cm^3
1	Alluvium	7	360	1.9
2	Alluvium	5	360	2.0
3	Alluvium	15	360	2.1
4	Loess	9	360	2.2
5	Fluvial deposits	8	360	2.0
6	Jackson formation	47	520	2.1
7	Memphis sand	246	667	2.3
8	Wilex group	83	733	2.4
9	Midway group	580	820	2.5
10	Paleozoic rock	500	3280	2.5
11	Paleozoic rock	8000	3600	2.7
12	Paleozoic rock	10000	3700	2.9
13	Paleozoic rock	20000	4200	3.0

3.5 Criteria for the Selection of Records

It is not typically permissible under modern code requirements to randomly select ground motion records without regard to certain selection criteria. These may be divided into three categories:

1. Seismological Criteria
2. Site-Characterization-based Criteria
3. Spectral Shape-based Criteria

3.5.1 Seismological Criteria

The major seismological parameters considered by modern codes are magnitude (usually moment magnitude), source-to-site distance (epicentral, hypocentral, Joyner-Boore, closest-distance-to-fault, etc.), and tectonic environment. Tectonic environment refers to fault location (inter-plate or intra-plate) and fault type (strike-slip, thrust, subduction zones, etc.).

Magnitude and distance will be retained here as criteria for selection of candidate records. It is interesting to note, however, that studies (Katsanos, et al., 2009) have shown that magnitude shows “some significance” and that closest source-to-site distance is “statistically insignificant” with regard to nonlinear displacement demand analysis. Given that it will be impossible to obtain real records from deep soil profile, intra-plate conditions because they are scarce and the ones we do have are for lower magnitude earthquakes, a broad range of magnitude and distance combinations will be used for initial screening. It is still desirable to make an attempt at selecting records which reasonably match the magnitude and source-to-site-distance obtained from hazard deaggregation at a given study site. If the matching process fails, then the M,R criteria may be expanded or synthetic motions can be used.

3.5.2 Site Characterization-based Criteria

The primary site characterization-based criteria are V_{S30} (shear wave velocity in the upper 30 meters of the subsurface profile) and embayment depth to bedrock for NMSZ sites. Modern code-based site amplification factors based on are based on V_{S30}.

For isolated structures (or any structure with a period of 1 second or more, for that matter) in the NMSZ, at least until the NGA-East project (Pacific Earthquake Engineering Research Center, 2012) is completed, the most reliable spectral value we have is the 1 second spectral acceleration. While spectral accelerations at 2 seconds are available, these values are good only at the B/C boundary. AASHTO provides generic site amplification factors at a period of 1 second, but not at a period of 2 seconds. While generic site amplification factors are certainly less than ideal, at least they are based on some scientific premise. Much of the Mississippi Embayment (ME) consists of deep soils - up to 1000 meters or more in some places - which alter the character of bedrock motions. Nonlinear site response studies (Park & Hashash, 2005) of the ME have shown that code-based site factors may be too high at low periods and too low at long periods when the embayment depth is greater than 30 meters. In other words, F_v may be un-conservative for sites where the embayment depth is greater than 30 meters. This will be particularly important for isolated bridges since isolated effective periods will most likely be longer than about 1.5 seconds. For this reason, the focus for this study is on the UHRS spectral acceleration at a period of 1-second in ground motion selection and modification. Implicit in code spectra is a constant site factor for periods equal to 1 second and longer. While deaggregation of the seismic hazard at deep sites in the ME provides a 2-second spectral acceleration at the B/C boundary, the choice is made to avoid the use of code site factors at

periods beyond 1 second for deep soil sites in the NMSZ. This choice will be reflected in the scaling of ground motions to match the target spectrum at a single period of 1 second rather than scaling to minimize mean-square-error (MSE) between the scaled record and the target within a range of periods applicable for isolated structures.

On pages 195-196 of a PEER Report (Stewart, et al., 2001) the authors recommend consideration of permitting spectral shapes of selected ground motions to "deviate from the design spectrum" at longer periods when basin effects are not include in the design spectrum of sites where basin effects are possible. The PEER Report also recommends scaling of selected records to match the design spectrum even in cases for which magnitude, distance, and site condition criteria are met. In a Georgia Tech study (Romero & Rix, 2005), site effects in the Mississippi Embayment, described as a basin, including depth of the soil profile were studied and the observation made that "current" code-based site provisions "may significantly underestimate ground motions at periods longer than 1 second." See page 397 of the referenced study.

3.5.3 Spectral Shape Criteria

NIST GCR 11-917-15 identifies spectral shape over the "period range of interest" as the most important factor in selecting ground motions for scaling to a target spectrum for distant sites (>10km from a fault). For sites closer than 10 km to a fault, NIST GCR 11-917-15 identifies two factors as being equally important: (1) spectral shape and (2) the presence of velocity pulses. Three parameters are used as measures of spectral shape match in this study:

1. Epsilon, ε
2. SA_{RMS}

3. Post-scaled MSE

The parameter ε (epsilon) has a significant impact upon the results of any nonlinear analysis which requires the selection of ground motions prior to modification. This is because epsilon has been shown to have a significant impact upon the resulting mean spectral shape. In short, a high epsilon value at a particular period suggests the likelihood that a spectral peak exists at that period. So let's define epsilon.

Ground motion prediction models (GMPM's) presume a lognormal distribution of spectral acceleration and thus generate estimates of the natural logarithm of spectral acceleration - *ln(SA)* - and the corresponding standard deviation - σ*(ln(SA))*. Given a specific ground motion record, a specific mean spectrum derived from a GMPM with parameters corresponding to the ground motion record, and a particular period, the distance between the record - $ln(SA_o)$ - and the GMPM mean - μ - log-spectral values may be expressed in terms of the number of logarithmic standard deviations - σ - also a parameter from the GMPM (Harmsen, 2001).

$$\varepsilon = \frac{ln(SA_o) - \mu}{\sigma} \qquad \text{(Eq. 3-6)}$$

USGS deaggregations provide mean and modal epsilons at a period of 1 second as follows for the sites considered in this study.

- Site 1 DBE: mean ε = -0.05, modal ε = -0.10
- Site 1 MCE: mean ε = +0.62, modal ε = +0.74
- Site 2 DBE: mean ε = -0.29, modal ε = -0.44
- Site 2 MCE: mean ε = +0.50, modal ε = +0.43

So this could be interpreted to signify that Site 1 and 2 ground motion selection at the DBE level should include records with slightly lower 1-second spectral accelerations than the UHRS values, while ground motion selection at the MCE level should include records with 1-second spectral accelerations slightly higher than the UHRS values.

Understand that epsilon primarily affects the mean spectral shape of the selected records. The implication is not that un-scaled records selected from the appropriate epsilon-group should be used. The records should still be scaled to the appropriate design spectrum level. It is just that the choice of records from inappropriate epsilon bins will skew results, and possibly in a really significant fashion. For example, Haselton (Haselton, et al., 2011) reported on collapse capacity computations in which the calculated collapse capacity was 70% higher when correct epsilon ranges were considered in record selection compared to the case in which epsilon was ignored during the record selection process. Haselton points out that the tendency for high-epsilon records to be spectrally peaked at the period of interest is not always apparent in individual records but "statistically defensible" based upon additional work (Baker & Jayaram, 2008).

An analysis of the Atkinson-Beresnev and Fernandez-Rix synthetic ground motion records will show the effect as well. The records are grouped into epsilon-bins corresponding to the following ranges:

$$\varepsilon < -0.50$$

$$-0.50 < \varepsilon < 0.00$$

$$\varepsilon > 0.00$$

Rather than a single ground motion prediction model to estimate μ and σ, use all 52 synthetic ground motions - 40 from Fernandez-Rix (975 year and 2,475 year return periods for Uplands

and for Lowlands in Memphis) and 12 from Atkinson-Beresnev (nonlinear soil effects, 6 each from Mw7.5 and Mw 8.0) to estimate the standard deviation of ln(SA) and use the UHRS 1-second spectral acceleration. This gives:

$$\mu = 0.555$$

$$\sigma = 0.482$$

Examination of APPENDIX G3, Figure G3.5.3-1 reveals the significant impact consideration of epsilon would have. In this case, the greatest difference is in the low period range. So higher mode effects would be vastly different for the case in which records are selected from the low-epsilon bin versus the high-epsilon bin. In general, however, the effect will be visible on both sides of a particular period in question.

So it is to the benefit of the engineer to give due consideration to epsilon in selecting records for nonlinear structural response.

The spectral shape compatibility of a record to a target may also be measured by the root-mean-square-difference parameter D_{RMS} (Katsanos, et al., 2009) for an un-scaled record and the mean-square-error (*MSE*) of a scaled record (see Section 3.1.2) over "*N*" periods.

$$D_{RMS} = \frac{1}{N}\sqrt{\sum_{i=1}^{N}\left(\frac{SA_{GM}(T_i)}{PGA_{GM}} - \frac{SA_{TAR}(T_i)}{PGA_{TAR}}\right)^2} \qquad \text{(Eq. 3-7)}$$

$$MSE = \frac{\sum w(T_i)\cdot\{ln[SA_{TARGET}(T_i)] - ln[f\cdot SA_{GM}(T_i)]\}^2}{\sum w(T_i)} \qquad \text{(Eq. 3-8)}$$

A visual inspection of spectral shape match to the target can be made by scaling records from a single event and examining the resulting fit to the target spectrum. A separate APPENDIX - APPENDIX E summarizes, in both tabular and graphic format, the results of scaling records from various events to each of the target spectra for the two sites.

3.6 Ground Motion Selection and Modification for Comparative Studies

Each ground motion modification procedure discussed in previous sections of this Chapter is valid provided one thing: that the target spectrum is, in fact, a valid target spectrum. While an AASHTO Specification-based design spectrum can be generated for a site in the NMSZ, the engineer is well-advised to take a step back and think about what is involved in generating such a spectrum. First, the USGS PSHA in the NMSZ includes spectral accelerations at period of 0.0 seconds, 0.2seconds, and 1.0 second, and 2.0 seconds. And these spectral accelerations are only valid at the Site Class B/C boundary. USGS PSHA results for Western United States sites include spectral acceleration values at periods of 3, 4, and 5 seconds in addition to those for the NMSZ. And Western sites include V_{S30}, the shear wave velocity characterizing a site, in the PSHA.

The frequency content of intra-plate earthquakes is likely to be different from shallow, crustal, active tectonic region (ATR) earthquakes of similar magnitude. So, adopting ATR ground motion records on soft soil sites to the NMSZ is suspect as well. It seems that the use of synthetic records generated specifically for the NMSZ and including site effects is the best choice.

To assess the effect of NMSZ-specific synthetic records applied to the model isolators, five sets of 14 ATR record pairs and two sets of 14 NMSZ-specific synthetic records are formulated. Herein is one shortcoming of the use of these synthetic records - only a single accelerogram is obtained whereas a record pair is characteristic of recorded motions. The problem is not insurmountable - for uni-directional analysis, the response to a record pair is simply taken as the geometric mean of the response to the individual components, which have been amplified by the same scale factor to make them compatible with the target spectrum. For bi-directional analysis, the synthetic motion is applied simultaneously in each of two perpendicular directions. Ideally, however, synthetic records should be ground motion pairs.

Five sets of 14 real ATR record pairs, a single set form Darfield, New Zealand, and two sets of 14 single component synthetic records are selected. Darfield has been included here because this earthquake occurred on an SCR, similar to conditions in the NMSZ. For ATR record pairs, the geometric mean of the two components is first computed and the result scaled to 0.555g - the DBE target - at a period of 1 second. Synthetic records are each individually scaled to 0.555g at a period of 1 second. This would imply that the single component should be applied simultaneously in two perpendicular horizontal directions for a 3-dimanesional nonlinear analysis. If the component is itself scaled to the target, then the geometric mean of the component with itself is still equal to the target. The result for both the ATR and the SCR cases is that the target 1-second spectral acceleration is exactly matched. Ideally, synthetic ground motion generation should consist of pairs of records rather than a single component.

The reason for choosing single-period matching is really twofold. First, the AASHTO Guide Specification for Seismic Isolation Design provides simplified analytic procedures which

are based solely upon the 1-second spectral acceleration. The assumption being that there is an abrupt transition from constant acceleration and constant velocity regions of the design spectrum. Exactly matching the 1-second period will provide a means of assessing the validity of this assumption for the various sets of motions. Secondly, as mentioned previously, both bedrock values and site amplification factors are available at a period of 1-second and this is the longest period for which both factors may be readily obtained for a site in the NMSZ.

Data for each selected record, including scale factors, are summarized in Tables 3.6-1 through 3.6-8. Ground motion parameters for the records are given in Tables 3.6-9 and 3.6-10.

The selected ground motions were baseline adjusted and filtered, prior to scaling, where necessary, using SeismoSpect (SeismoSoft, 2011). The spectra of the scaled records are shown against the Site 1 DBE target spectra in APPENDIX G3, Figures G3.6-1 through G3.6-9.

Some general observations are inferred from the ground motion parameters. The percentages given are only rounded approximations and not hard rules. For detailed definitions of RMS parameters, Arias Intensity, cumulative absolute velocity, etc., refer to the Help System for SeismoSpect (SeismoSoft, 2011).

- Peak ground displacement in NMSZ records is about 30% less than that for similar magnitude ATR records (ATR-3, ATR-4, and ATR-5), but peak spectral displacement is about 25% higher in the NMSZ. This results in a ratio of spectral displacement to peak ground displacement about 75% higher for the NMSZ records.
- Both acceleration RMS and Arias intensity are about 50% higher in the NMSZ records compared to similar magnitude ATR records.

- Both velocity RMS and peak spectral velocity are about 35% higher for NMSZ records compared to similar magnitude ATR records.
- Significant duration, cumulative absolute velocity, and velocity spectrum intensity are about 10-20% higher for NMSZ records compared to similar magnitude ATR records.
- Displacement RMS is about 15% lower for NMSZ records compared to similar magnitude ATR records.

Spectral velocities and displacements reveal the challenge of designing longer period structures in the NMSZ. For the records studies here, NMSZ spectral shapes do not closely follow the target spectra and are more severe than those for ATR record sets. While bedrock motions on an SCR may possess less long period content than ATR bedrock motions, the effect of the deep soil profiles characteristic of the Mississippi Embayment may have a pronounced effect - there is no clear transition between constant acceleration and constant velocity regions of the ground motion spectra as implied in design spectra generation found in modern codes and specifications. The result is higher spectral velocities and displacements within the range of periods typical for isolated structures.

The Darfield, New Zealand event, while lower in magnitude that the modal event for the NMSZ, possesses spectral shape similar to that for the NMSZ. While scaling for the Darfield event is generally (and expectedly, owing the magnitude difference) a bit higher than that required for the NMSZ synthetic motions, displacement and velocity spectra for both cases clearly diverge from the target on the severe side. The Darfield earthquake could be classified as intra-plate as the hypocenter was about 80 km from a plate boundary.

The AASHTO simplified procedure for isolation design is appropriate for uni-directional displacement demands for Chi-Chi, but not for New Zealand and not for NMSZ record sets. The simplified treatment of bi-directional demand is inappropriate and un-conservative for each of the large magnitude, soft soil record sets studied.

These observations imply that the AASHTO simplified design method for isolated bridges may not be applicable in the NMSZ. It may be that the AASHTO simplified procedure for isolation design may still be applicable, after modification, in the NMSZ. Most specifications - including AASHTO - express the spectral acceleration beyond the constant acceleration period as:

$$S_a(T) = \frac{S_{D1}}{T} \qquad \text{(Eq. 3-9)}$$

$$\Rightarrow S_v(T) = \frac{S_a(T)}{\omega} = \frac{S_{D1} \cdot g}{T} \cdot \frac{T}{2\pi} = \frac{S_{D1} \cdot g}{2\pi} \qquad \text{(Eq. 3-10)}$$

Rather than assuming spectral acceleration inversely proportional to period in this range, it may be that the proportionality could be estimated as inverse with respect to some power of period, or even some other period-dependent function. Future work on this project will consider this possibility.

Without readily available data from SCR events, the selection of ground motion records for nonlinear structural analysis in the NMSZ can be based upon design response spectra and modified accelerograms from appropriate magnitude events. Seismological setting cannot be ignored however. It has been demonstrated that ATR vs. SCR spectral shapes for similar magnitude events cannot be assumed equal.

Following the reasoning used for Site No. 1, NMSZ specific synthetic records are selected and scaled to the Site 2 DBE-level 1-second spectral acceleration, 0.818g. The purpose is to estimate various ground motion parameters applicable to Site No. 2 having a small source to site distance of about 12 km. Blytheville, Arkansas records from Fernandez-Rix are used for Set NMSZ-3. Memphis records form both Fernandez-Rix and from Atkinson-Beresnev are used for set No. NMSZ-4.

The spectra for the geometric mean of the 14 records per set are shown in APPENDIX G3, Figures G3.6-10 through G3.6-15. Ground motion parameters are summarized in Table 3.16-13. Clearly, there is quite a deviation between the AASHTO design spectra and those from synthetic ground motions specific to the NMSZ, and the deviation increases as the site-to-source distance decreases and as site conditions approach those in Blytheville as opposed to those in Memphis.

The isolator demands on site conditions similar to Blytheville would likely be much more severe than those similar to Memphis due to the even richer longer period content in Blytheville. The modal magnitude is the same in Blytheville as in Memphis - M_W7.7. But the source-to-site distance is smaller in Blytheville compare to Memphis - 12 kilometers compared to 60 kilometers. Estimated embayment depths for the two sites are similar - 900 meters.

Table 3.6-1 Selected Ground Motions - Set ATR-1 (M6.69-M7.01)

Event	Mw	Station	R, km	Vs30	Site Class	S1DBE SF
Erzican, Turkey	6.69	NGA 0821	9	275	D	0.781
Kobe, Japan	6.90	NGA 1120	2	256	D	0.472
Kobe, Japan	6.90	NGA 1106	1	312	D	0.604
Kobe, Japan	6.90	NGA 1119	0	312	D	0.633
Kobe, Japan	6.90	NGA 1107	23	312	D	1.650
Kobe, Japan	6.90	NGA 1116	19	256	D	2.049
Kobe, Japan	6.90	NGA 1113	21	256	D	2.840
Kobe, Japan	6.90	NGA 1105	96	256	D	2.848
Irpinia, Italy	6.90	NGA 0290	30	350	D	3.228
Loma Prieta	6.93	NGA 0786	31	210	D	1.350
Loma Prieta	6.93	NGA 0768	14	222	D	1.612
Loma Prieta	6.93	NGA 0799	59	190	D	2.009
Imperial Valley	6.95	NGA 0006	13	213	D	1.685
Cape Mendocino	7.01	NGA 0829	23	312	D	1.241

Table 3.6-2. Selected Ground Motions - Set ATR-2 (M7.14-M7.37)

Event	Mw	Station	R, km	Vs30	Site Class	S1DBE SF
Duzce, Turkey	7.14	NGA 1602	41	326	D	0.600
Duzce, Turkey	7.14	NGA 1605	7	276	D	0.882
Landers	7.28	NGA 0900	24	354	D	1.645
Landers	7.28	NGA 0850	22	345	D	1.981
Landers	7.28	NGA 0832	69	271	D	2.708
Landers	7.28	NGA 0884	36	207	D	2.507
Landers	7.28	NGA 0881	17	345	D	2.509
Taiwan SMART1(45)	7.30	NGA 0576	55	274	D	1.380
Taiwan SMART1(45)	7.30	NGA 0571	54	274	D	1.475
Taiwan SMART1(45)	7.30	NGA 0579	55	274	D	1.529
Taiwan SMART1(45)	7.30	NGA 0581	54	274	D	1.652
Taiwan SMART1(45)	7.30	NGA 0575	57	274	D	1.685
Manjil, Iran	7.37	NGA 1634	76	275	D	2.429
Manjil, Iran	7.37	NGA 1640	94	275	D	3.329

Table 3.6-3. Selected Ground Motions - Set ATR-3 (M7.50-M7.90)

Event	Mw	Station	R, km	Vs30	Site Class	S1DBE SF
Kocaeli, Turkey	7.51	NGA 1158	14	276	D	1.055
Kocaeli, Turkey	7.51	NGA 1176	1	297	D	1.527
Kocaeli, Turkey	7.51	NGA 1149	56	274	D	2.318
Kocaeli, Turkey	7.51	NGA 1166	31	274	D	2.418
Kocaeli, Turkey	7.51	NGA 1155	60	275	D	2.820
Kocaeli, Turkey	7.51	NGA 1167	145	275	D	3.469
Kocaeli, Turkey	7.51	NGA 1177	52	274	D	3.774
Kocaeli, Turkey	7.51	NGA 1147	70	175	E	1.045
Bucharest, Romania	7.50	STA155	116	130	E	1.224
Denali, Alaska	7.90	NGA 2114	0	329	D	0.726
St. Elias, Alaska	7.54	NGA 1628	26	275	D	1.969
El Salvador	7.60	CIG-ST	98	338	D	1.292
El Salvador	7.60	CIG-DB	92	304	D	1.746
Valparaiso, Chile	7.80	VTS	125	356	D	0.641

Table 3.6-4. Selected Ground Motions - Set ATR-4 (Chi-Chi 1)

Event	Mw	Station	R, km	Vs30	Site Class	S1DBE SF
Chi-Chi, Taiwan	7.62	NGA 1503	1	306	D	0.456
Chi-Chi, Taiwan	7.62	NGA 1244	10	259	D	0.735
Chi-Chi, Taiwan	7.62	NGA 1513	0	364	D	0.842
Chi-Chi, Taiwan	7.62	NGA 1536	12	213	D	1.075
Chi-Chi, Taiwan	7.62	NGA 1498	17	230	D	1.147
Chi-Chi, Taiwan	7.62	NGA 1292	60	259	D	1.258
Chi-Chi, Taiwan	7.62	NGA 1203	16	233	D	1.296
Chi-Chi, Taiwan	7.62	NGA 1456	108	201	D	1.380
Chi-Chi, Taiwan	7.62	NGA 1411	106	201	D	1.461
Chi-Chi, Taiwan	7.62	NGA 1419	98	201	D	1.466
Chi-Chi, Taiwan	7.62	NGA 1410	101	212	D	1.593
Chi-Chi, Taiwan	7.62	NGA 1547	15	242	D	1.601
Chi-Chi, Taiwan	7.62	NGA 1317	82	201	D	1.657
Chi-Chi, Taiwan	7.62	NGA 1246	18	223	D	1.658

Table 3.6-5. Selected Ground Motions - Set ATR-5 (Chi-Chi 2)

Event	Mw	Station	R, km	Vs30	Site Class	S1DBE SF
Chi-Chi, Taiwan	7.62	NGA 1194	19	277	D	1.750
Chi-Chi, Taiwan	7.62	NGA 1415	100	226	D	1.806
Chi-Chi, Taiwan	7.62	NGA 1294	47	279	D	1.857
Chi-Chi, Taiwan	7.62	NGA 1454	104	324	D	1.897
Chi-Chi, Taiwan	7.62	NGA 1297	50	357	D	1.912
Chi-Chi, Taiwan	7.62	NGA 1187	38	229	D	1.916
Chi-Chi, Taiwan	7.62	NGA 1542	25	199	D	1.918
Chi-Chi, Taiwan	7.62	NGA 1412	104	185	E	1.934
Chi-Chi, Taiwan	7.62	NGA 1269	52	244	D	2.012
Chi-Chi, Taiwan	7.62	NGA 1264	51	231	D	2.019
Chi-Chi, Taiwan	7.62	NGA 1262	49	242	D	2.021
Chi-Chi, Taiwan	7.62	NGA 1265	57	229	D	2.102
Chi-Chi, Taiwan	7.62	NGA 1481	25	229	D	2.118
Chi-Chi, Taiwan	7.62	NGA 1336	87	200	D	2.120

Table 3.6-6. Selected Ground Motions - Set DNZ

Event	Mw	Station	R, km	Vs30	Site Class	S1DBE SF
Darfield, NZ	7.10	GDLC	8	276	D	0.608
Darfield, NZ	7.10	LINC	25	235	D	0.996
Darfield, NZ	7.10	DFHS	9	278	D	1.421
Darfield, NZ	7.10	ROLC	17	264	D	1.451
Darfield, NZ	7.10	REHS	37	240	D	1.467
Darfield, NZ	7.10	CCCC	38	231	D	1.587
Darfield, NZ	7.10	PPHS	35	242	D	1.751
Darfield, NZ	7.10	KPOC	44	216	D	1.981
Darfield, NZ	7.10	DSLC	13	259	D	2.011
Darfield, NZ	7.10	PRPC	41	204	D	2.197
Darfield, NZ	7.10	SHLC	39	192	D	2.677
Darfield, NZ	7.10	TPLC	24	250	D	2.756
Darfield, NZ	7.10	RHSC	31	223	D	2.890
Darfield, NZ	7.10	NNBS	44	217	D	3.054

Table 3.6-7. Selected Ground Motions - Set NMSZ-1

Source	Identifier	Region	S1DBE SF
Fernandez-Rix	975 year - 01	Memphis Lowlands	1.182
Fernandez -Rix	975 year - 02	Memphis Lowlands	1.138
Fernandez -Rix	975 year - 06	Memphis Lowlands	1.472
Fernandez -Rix	975 year - 10	Memphis Lowlands	0.992
Fernandez -Rix	975 year - 07	Memphis Uplands	1.238
Fernandez -Rix	2475 year - 01	Memphis Lowlands	1.031
Fernandez -Rix	2475 year - 03	Memphis Lowlands	0.951
Fernandez -Rix	2475 year - 09	Memphis Lowlands	0.917
Fernandez -Rix	2475 year - 10	Memphis Lowlands	1.001
Fernandez -Rix	2475 year - 03	Memphis Uplands	1.073
Fernandez -Rix	2475 year - 08	Memphis Uplands	1.084
Fernandez -Rix	2475 year - 09	Memphis Uplands	1.110
Atkinson-Beresnev	M8.0-02	Nonlinear Soil	1.132
Atkinson-Beresnev	M8.0-05	Nonlinear Soil	1.009

Table 3.6-8. Selected Ground Motions - Set NMSZ-2

Source	Identifier	Region	S1DBE SF
Atkinson-Beresnev	M7.5-01	Nonlinear Soil	2.966
Atkinson-Beresnev	M7.5-02	Nonlinear Soil	2.354
Atkinson-Beresnev	M7.5-03	Nonlinear Soil	2.905
Atkinson-Beresnev	M7.5-04	Nonlinear Soil	2.249
Atkinson-Beresnev	M7.5-05	Nonlinear Soil	2.552
Atkinson-Beresnev	M7.5-06	Nonlinear Soil	2.730
Atkinson-Beresnev	M8.0-01	Nonlinear Soil	1.969
Atkinson-Beresnev	M8.0-02	Nonlinear Soil	1.132
Atkinson-Beresnev	M8.0-03	Nonlinear Soil	1.393
Atkinson-Beresnev	M8.0-04	Nonlinear Soil	1.288
Atkinson-Beresnev	M8.0-05	Nonlinear Soil	1.009
Atkinson-Beresnev	M8.0-06	Nonlinear Soil	1.701
Fernandez -Rix	975 year - 10	Memphis Lowlands	0.992
Fernandez -Rix	2475 year - 10	Memphis Lowlands	1.001

Table 3.6-9. Ground Motion Parameter Summary - ATR

Intensity Measure	Set ATR-1	Set ATR-2	Set ATR-3	Set ATR-4	Set ATR-5
PGA (g)	0.4033	0.3204	0.3388	0.2432	0.2428
PGV (cm/sec)	46.61	46.63	53.58	50.87	53.21
PGD (cm)	15.25	22.10	33.62	33.46	44.75
Acc RMS (g)	0.0596	0.0622	0.0497	0.0332	0.0344
Vel RMS (cm/sec)	8.5915	12.1028	10.6326	9.2264	10.0299
Displ RMS (cm)	3.7807	7.1084	8.4342	7.7340	10.8773
Arias Intensity (cm/sec)	6.2063	7.0355	6.9229	5.0050	5.0399
Specific Energy Density (cm^2/sec)	3,491	7,115	7,763	11,959	12,581
CAV (cm/sec)	1,432	1,761	1,874	1,845	1,863
Acc Spectrum Intensity (g*sec)	0.3616	0.2904	0.2840	0.1796	0.2015
Vel Spectrum Intensity (cm)	191.0109	184.2213	192.8240	178.9176	184.2161
Housner Intensity (cm)	177.6963	179.4874	190.6181	177.8535	182.1947
Sustained Max.Acceleration (g)	0.2871	0.2480	0.2624	0.1869	0.1892
Sustained Max.Velocity (cm/sec)	33.7665	37.0451	39.7985	37.8829	40.5150
Effective Design Acceleration (g)	0.4008	0.3132	0.3272	0.2368	0.2403
A95 parameter (g)	0.3969	0.3124	0.3334	0.2392	0.2392
Predominant Period (sec)	0.3808	0.4773	0.5753	0.5365	0.7256
Significant Duration (sec)	17.48	21.56	28.74	29.17	29.72
PSA Max	0.9516	0.7880	0.6792	0.5749	0.5821
SV Max (cm/sec)	92.58	86.70	95.8574	87.26	93.71
SD Max (cm)	24.89	38.55	46.7336	60.42	63.5717
PGV/PGA (sec)	0.1179	0.1484	0.1613	0.2134	0.2236
PGD/PGV (sec)	0.3271	0.4739	0.6275	0.6576	0.8410
SV-Max/PSA (sec)	0.0992	0.1122	0.1439	0.1548	0.1642
SD-Max/SV-Max (sec)	0.269	0.445	0.488	0.692	0.678

Table 3.6-10. Ground Motion Parameter Summary - SCR

Intensity Measure	Set DNZ	Set NMSZ-1	Set NMSZ-2
PGA (g)	0.4881	0.2815	0.3034
PGV (cm/sec)	65.76	54.12	54.25
PGD (cm)	28.43	27.67	25.37
Acc RMS (g)	0.0603	0.0594	0.0648
Vel RMS (cm/sec)	11.5705	13.8357	13.6409
Displ RMS (cm)	6.4359	7.7019	7.4987
Arias Intensity (cm/sec)	11.9484	7.9557	8.4929
Specific Energy Density (cm^2/sec)	11,596	11,762	10,182
CAV (cm/sec)	2,360	2,316	2,245
Acc Spectrum Intensity (g*sec)	0.4422	0.2284	0.2679
Vel Spectrum Intensity (cm)	241.7265	205.1622	212.5024
Housner Intensity (cm)	236.1627	206.5377	212.1502
Sustained Max.Acceleration (g)	0.3642	0.2377	0.2614
Sustained Max.Velocity (cm/sec)	50.1292	44.9502	43.2374
Effective Design Acceleration (g)	0.4626	0.2588	0.2979
A95 parameter (g)	0.4753	0.2727	0.2941
Predominant Period (sec)	0.3430	0.6757	0.5629
Significant Duration (sec)	19.4817	33.6800	30.8111
PSA Max	1.1565	0.5858	0.7457
SV Max (cm/sec)	138.7526	131.96	119.08
SD Max (cm)	75.0436	87.01	61.20
PGV/PGA (sec)	0.1374	0.1961	0.1824
PGD/PGV (sec)	0.4323	0.5114	0.4676
SV-Max/PSA (sec)	0.1224	0.2298	0.1629
SD-Max/SV-Max (sec)	0.541	0.659	0.514

Table 3.6-11. Selected Ground Motions - Set NMSZ-3

Source	Identifier	Region	S2DBE SF
Fernandez-Rix	975 year - 03	Blytheville	1.187
Fernandez -Rix	975 year - 06	Blytheville	1.346
Fernandez -Rix	975 year - 08	Blytheville	1.291
Fernandez -Rix	975 year - 10	Blytheville	1.175
Fernandez -Rix	2475 year - 01	Blytheville	0.642
Fernandez -Rix	2475 year - 02	Blytheville	0.678
Fernandez -Rix	2475 year - 03	Blytheville	0.716
Fernandez -Rix	2475 year - 04	Blytheville	0.726
Fernandez -Rix	2475 year - 05	Blytheville	0.716
Fernandez -Rix	2475 year - 06	Blytheville	0.690
Fernandez -Rix	2475 year - 07	Blytheville	0.982
Fernandez -Rix	2475 year - 08	Blytheville	0.668
Fernandez -Rix	2475 year - 09	Blytheville	0.841
Fernandez -Rix	2475 year - 10	Blytheville	0.762

Table 3.6-12. Selected Ground Motions - Set NMSZ-4

Source	Identifier	Region	S2DBE SF
Atkinson-Beresnev	M8.0-02	Nonlinear Soil	1.669
Atkinson-Beresnev	M8.0-05	Nonlinear Soil	1.488
Fernandez -Rix	975 year-10	Memphis Lowlands	1.463
Fernandez -Rix	2475 year - 02	Memphis Lowlands	0.950
Fernandez -Rix	2475 year - 04	Memphis Lowlands	1.046
Fernandez -Rix	2475 year - 05	Memphis Lowlands	1.263
Fernandez -Rix	2475 year - 06	Memphis Lowlands	1.120
Fernandez -Rix	2475 year - 07	Memphis Lowlands	1.288
Fernandez -Rix	2475 year - 08	Memphis Lowlands	1.108
Fernandez -Rix	2475 year - 09	Memphis Lowlands	1.352
Fernandez -Rix	2475 year - 01	Memphis Uplands	1.322
Fernandez -Rix	2475 year - 06	Memphis Uplands	1.252
Fernandez -Rix	2475 year - 07	Memphis Uplands	0.890
Fernandez -Rix	2475 year - 10	Memphis Uplands	1.130

Table 3.6-13. Ground Motion Parameter Summary - SCR Site 2

Intensity Measure	Set NMSZ-3	Set NMSZ-4
PGA (g)	0.406	0.372
PGV (cm/sec)	106.9	77.3
PGD (cm)	65.31	37.8
Acc RMS (g)	0.0778	0.0786
Vel RMS (cm/sec)	23.02	18.46
Displ RMS (cm)	26.04	9.77
Arias Intensity (cm/sec)	12.497	14.931
Specific Energy Density (cm^2/sec)	28,547	21,717
CAV (cm/sec)	2,524	3,337
Acc Spectrum Intensity (g*sec)	0.245	0.291
Vel Spectrum Intensity (cm)	399.4	292.5
Housner Intensity (cm)	418.7	294.2
Sustained Max.Acceleration (g)	0.347	0.309
Sustained Max.Velocity (cm/sec)	81.42	60.80
Effective Design Acceleration (g)	0.378	0.350
A95 parameter (g)	0.396	0.361
Predominant Period (sec)	1.727	0.809
Significant Duration (sec)	20.8	36.8
PSA Max	0.922	0.828
SV Max (cm/sec)	293.8	198.8
SD Max (cm)	129.5	128.0
PGV/PGA (sec)	0.268	0.211
PGD/PGV (sec)	0.611	0.490
SV-Max/PSA (sec)	0.325	0.245
SD-Max/SV-Max (sec)	0.441	0.644

3.7 Ground Motion Selection and Modification for Design of the Bridges

While visual inspection of scaled spectra provides valuable insight, a systematic approach is needed to select records for structural analysis and design of the bridges. To facilitate this selection, post-scaled *MSE* (previously defined) is used as a measure of spectral shape compatibility for each Site and each of two target spectra:

1. the DBE-level uniform hazard response spectrum
2. an alternate NMSZ-specific spectrum from the Georgia Tech ground motion prediction model (Fernandez & Rix, 2006) scaled to the DBE-level spectral acceleration at a period of 1 second

The anticipated usefulness of a dual target spectrum approach is a substructure design controlled by the UHRS and an isolation system design controlled by the site-specific spectrum. Much evidence in the literature of un-conservative long-period spectral shape in deep soil sites of the Mississippi Embayment is the justification for the long-period content in the selected NMSZ-specific spectrum (Hashash & Park, 2001), (Hashash, et al., 2008), (Park & Hashash, 2004).

The design of substructure components will be affected not only by loads transmitted from the superstructure, but also by local high-frequency vibration modes. So ground motions which do not create high nonlinearity in the soil and possess high frequency (low period) content, while not likely to control the design of isolation devices themselves, could well control the sub-structure design and cannot be ignored.

To establish the alternate, NMSZ-specific spectra, the choice is made to average six spectra for each of the two sites:

- Site No. 1, Shelby County, estimated profile depth = 900 meters: the low, median, and high stress drop spectra - both Uplands and Lowlands - of the 610-1220 meter profile depth Bin for a Magnitude 7.7 earthquake and an epicentral distance of 59.5 kilometers (to match the USGS deaggregation values)
- Site No. 2, Lake County, estimated profile depth = 900 meters: the low, median, and high stress drop spectra - both Uplands and Lowlands - of the 610-1220 meter profile depth Bin for a Magnitude 7.7 earthquake and an epicentral distance of 11.9 kilometers (to match the USGS deaggregation values)

This provides for the design of the isolation system, expected to be controlled by the NMSZ-based records, and for the design of the substructures, expected to be controlled by the code UHRS-based records. The target spectra are shown in Figures 3.7-1 and 3.7-2 for Sites 1 and 2 respectively. The MCE-level spectra are shown for reference only. The MCE-level spectra are not used as targets. Figures 3.7-3 through 3.7-6 depict the velocity and displacement spectra corresponding to the targets.

For Site 2 record selection will include pulse-type records. One set will be chosen with no pulse-type records and another set of records with only pulse-type records for Site 2. This site has a deaggregated (M, R) pair of (7.7, 11.9 km). The break-point between “near-field” and “far-field” sites is 10 kilometers in AASHTO. Strictly speaking, pulse-type motions would not be a necessary criterion for this site. Given the uncertainty in fault geometry and location in the NMSZ, the site will be considered “near-field” for ground motion selection at Site 2.

The PEER ground motion database is searched for records matching the target acceleration spectra. The online selection tool is used for the PEER record search. Records from

all other databases and synthetic records are processed separately and checked for compatibility to the various target spectra based on post-scaled MSE. The goal will be to produce a set of 14 record pairs for each of the 4 target spectra: (1) Site 1 DBE UHRS, (2) Site 1 DBE NMSZ-specific, (3) Site 2 DBE UHRS, and (4) Site 2 DBE NMSZ-specific.

Site No. 2 is only slightly outside (11.8 km) of the source-to-site distance criteria (10 km) used to classify sites as “near-field” or “far-field”. This is close enough to warrant consideration of pulse-type records for Site 2. Two additional sets of pulse-type records will thus be selected for Site 2. The total number of record sets for design is seven:

1. Design Set No. 1UHRS: Ground motion record pairs scaled to Site No.1 uniform hazard spectrum at the DBE hazard-level
2. Design Set No. 1NMSZ: Ground motion record pairs scaled to Site No.1 NMSZ-specific spectrum
3. Design Set No. 1NMSZ-B: Ground motions scaled prior to spectrum-matching to a composite spectrum enveloping 1UHRS and 1NMSZ; seed motions will be taken only from large magnitude (M_W7.28-M_W7.90) recorded at Site Class D and E stations
4. Design Set No. 2UHRS: Non-pulse type ground motion record pairs scaled to Site No. 2 uniform hazard spectrum at the DBE hazard-level
5. Design Set No. 2NMSZ: Non-pulse type ground motion record pairs scaled to Site No. 2 NMSZ-specific spectrum
6. Design Set No. 2UHRS-P: Pulse-type ground motion record pairs scaled to Site No. 2 uniform hazard spectrum at the DBE hazard-level

7. Design Set No. 2NMSZ-P: Pulse-type ground motion record pairs scaled to Site No. 2 NMSZ-specific spectrum

The primary factor in the design of the isolated bridges will be mean responses (isolator displacement demand, pile bending moment, etc.). Seven records would thus be acceptable according to AASHTO specifications and most other code requirements. The choice is made to include 14 records in each set here.

For synthetic and artificial cases, the records used here are single component accelerograms. All loads need to be applied simultaneously in orthogonal directions so the synthetic records will be paired. This must be done carefully however. Application of the same record simultaneously in two directions - as was done for the comparative studies in Section 3.6 - is not recommended for final design ground motions. The correlation coefficient of two orthogonal records will be limited to 0.30 in accordance with NIST GCR 11-917-15. Only records from the same source will be combined. The durations must be approximately the same. With these criteria in hand, Table 3.7-1 summarizes the paired synthetic and artificial accelerograms. Included in the last two lines of the table are pairings which resulted in correlation outside the recommended limits - these two pairs will not be used for design of the bridges. Spectral values at a period of 1 second are shown for each component with the intention of preserving the ratio in the event spectral matching is used. The idea would be to match each component to the target using wavelets, and then to scale each component such that (a) the geometric mean at a period of 1 second is exactly equal to the target value and (b) the ratio of the two spectral values at a period of 1 second is maintained.

Tables 3.7-2 through 3.7-8 summarize the selected record sets and Figures 3.7-7 through 3.7-14 depict the spectra, both target and mean scaled. Observation of Figures 3.7-10 and 3.7-12 reveals a poor mean-scaled-to-target ratio for sets 2NMSZ (non-pulse-type) and 2NMSZ-P (pulse-type). To remedy the poor shapes spectral matching using SeismoMatch (SeismoSoft, 2011) was performed for these two record sets to produce two additional sets: 2NMSZ-M (non-pulse-type, spectrum matched) and 2NMSZ-PM (pulse-type, spectrum matched). A period range for the matching was set equal to 0.10-6.0 seconds in each case and the resulting matched-to-target ratios were excellent as shown in Figures 3.7-15 and 3.7-16.

The minimum and average record mean-to-target ratios for the sets are as follows:

- Set No. 1UHRS: Minimum = 0.85, Average = 1.02 (0.2-6 second range)
- Set No. INMSZ: Minimum = 0.78, Average = 0.95 (1-6 second range)
- Set No. 2UHRS: Minimum = 0.91, Average = 1.00 (0.2-6.0 second range)
- Set No. 2NMSZ: Minimum = 0.66, Average = 0.87 (1-6 second range)
- Set No. 2UHRS-P: Minimum = 0.73, Average = 1.43 (0.2-6.0 second range)
- Set No. 2NMSZ-P: Minimum = 0.48, Average = 0.64 (1-6 second range)
- Set No. 2NMSZ-M: Minimum = 0.94, Average = 0.98 (0.2-6.0 second range)
- Set No. 2NMSZ-PM: Minimum = 0.95, Average = 0.99 (0.2-6.0 second range)
- Set No. 1NMSZ-BM: Minimum = 0.99, Average = 1.01 (0.2-6.0 second range)

Another method of adjusting record sets was used for set 1NMSZ. The retrofit manual limits the minimum mean-to-target ratio to no less than 0.85 and the average ratio to no less than 1.0. So, for set 1NMSZ, the final scale factors were increased by the larger of (a) 0.85/0.78 =

1.05 and (b) 1.00/0.95 = 1.09. Final scale factors for set NMSZ1 were amplified by a factor of 1.09 and these are the values shown in Table 3.7-3.

APPENDIX B contains detailed tables of many ground motion parameters for each individual ground motion pair and for the mean of the record sets selected for bridge design at the two sites. Inelastic Displacement Spectra for each of the record sets is included as APPENDIX F. While not used in current design practice, the increasing focus upon displacement-based design and the recognition that inelastic behavior is inherent in current design practice create a research atmosphere in which inelastic displacement spectra are likely to be a major component of future work in the NMSZ, and globally for that matter. The inelastic spectra are computed using SeismoSpect (SeismoSoft, 2011) for post-yield stiffness ratios of α = 0.0 and α = 0.10, corresponding roughly to FPS and LRB isolation systems, respectively. Displacement ductility vales ranging from μ = 2 to μ = 10 in increments of 2 are included in APPENDIX F. While bridge design in AASHTO for non-isolated cases is limited to ductility vales of μ = 8 at most, isolation systems typically require displacement ductility demands much larger than μ = 8. This is the reason for including μ = 10 in the analysis. APPENDIX F also contains a discussion of estimates for the inelastic displacement ratio, C_μ. This topic is ripe for future work.

Table 3.7-1. Synthetic Record Pairs

#	H1	H2	Correlation	Duration	$SA_{H1}(1)$	$SA_{H2}(1)$
	Atkinson-Beresnev Records					
1	7.5L-03	7.5L-01	0.0690	40.32	0.2262	0.3153
2	7.5L-02	7.5L-06	0.1418	40.32	0.2607	0.2436
3	7.5L-04	7.5L-05	-0.0286	40.32	0.1709	0.1535
4	7.5N-03	7.5N-05	-0.1662	40.32	0.1911	0.2174
5	7.5N-01	7.5N-06	0.0044	40.32	0.1871	0.2033
6	7.5N-02	7.5N-04	-0.0882	40.32	0.2358	0.2468
7	8.0L-05	8.0L-04	0.1021	64.68	0.4881	0.4705
8	8.0L-02	8.0L-06	0.0907	64.68	0.3470	0.5506
9	8.0L-03	8.0L-01	-0.0360	64.68	0.3914	0.3940
10	8.0N-02	8.0N-06	0.1346	64.68	0.4900	0.3263
11	8.0N-01	8.0N-04	-0.0624	64.68	0.2819	0.4310
12	8.0N-03	8.0N-05	0.0485	64.68	0.3985	0.5498
	Fernandez Memphis Lowlands					
13	0975-07	0975-08	0.1867	59.71	0.2008	0.2379
14	0975-01	0975-02	-0.0668	55.335	0.4695	0.4878
15	0975-09	0975-10	-0.0492	43.64	0.2427	0.5593
16	0975-05	0975-06	0.0358	71.75	0.2149	0.3771
17	2475-09	2475-10	-0.1350	43.59	0.6050	0.5545
18	2475-03	2475-07	-0.0456	59.525	0.5837	0.6349
19	2475-05	2475-06	0.0472	73.35	0.6476	0.7301
	Fernandez Memphis Uplands					
20	0975-07	0975-08	0.1665	59.56	0.4483	0.2144
21	0975-10	0975-09	0.0009	44.83	0.1905	0.2515
22	0975-05	0975-06	-0.0071	72.75	0.2565	0.2381
23	2475-08	2475-07	0.1837	58.825	0.5121	0.9196
24	2475-05	2475-06	0.0499	73.495	0.4319	0.6535
25	2475-09	2475-10	-0.0215	43.74	0.5000	0.7240
	Fernandez Blytheville					
26	0975-09	0975-08	0.2695	43.445	0.5224	0.6339
27	0975-05	0975-02	0.1301	83.00	0.4966	0.5679
28	0975-03	0975-06	0.1911	52.78	0.6894	0.6078
29	2475-01	2475-08	0.0025	39.49	1.2741	1.2240
30	2475-04	2475-10	0.0650	75.685	1.1266	1.0729
31	2475-05	2475-02	-0.0668	82.745	1.1424	1.2063
32	2475-08	2475-09	**0.5315**	43.19	1.2240	0.9729
33	2475-06	2475-03	**-0.3832**	52.595	1.1849	1.1426

Table 3.7-2. Record Set No. 1UHRS

Source	Event	Station	M_W	R, km	V_{S30}, m/s	SF
PEER NGA-1214	Chi-Chi, Taiwan	CHY057	7.62	56.7	411	8.371
PEER NGA-1190	Chi-Chi, Taiwan	CHY019	7.62	50.0	478	7.658
PEER NGA-1245	Chi-Chi, Taiwan	CHY102	7.62	36.1	680	8.803
PEER NGA-779	Loma Prieta	LGPC	6.93	0.0	478	0.690
PEER NGA-802	Loma Prieta	Saratoga	6.93	7.6	371	1.302
PEER NGA-746	Loma Prieta	Bear Valley	6.93	53.5	391	5.788
PEER NGA-1816	Hector Mine	North Pair	7.13	61.8	345	5.631
PEER NGA-1827	Hector Mine	San Bernadino	7.13	101.7	271	7.333
PEER NGA-1791	Hector Mine	Indio	7.13	73.5	345	4.654
PEER NGA-832	Landers	Amboy	7.28	69.2	271	2.766
PEER NGA-880	Landers	MC Fault	7.28	27.0	345	4.386
PEER NGA-900	Landers	Yermo	7.28	23.6	354	1.886
PEER NGA-1177	Kocaeli, Turkey	Zeytinburr	7.51	52.0	274	4.093
PEER NGA-1153	Kocaeli, Turkey	Botas	7.51	126.0	274	5.629

Table 3.7-3. Record Set No. 1NMSZ

Source	Event	Station	M_W	R, km	V_{S30}, m/s	SF
PEER NGA-1527	Chi-Chi, Taiwan	TCU100	7.62	11.4	474	2.722
PEER NGA-1497	Chi-Chi, Taiwan	TCU057	7.62	11.8	474	2.843
PEER NGA-1189	Chi-Chi, Taiwan	CHY017	7.62	59.1	191	5.374
PEER NGA-1194	Chi-Chi, Taiwan	CHY025	7.62	19.1	278	2.026
PEER NGA-1800	Hector Mine	Pico	7.13	186.8	270	20.894
PEER NGA-1790	Hector Mine	Lake Street	7.13	184.0	371	11.305
PEER NGA-1795	Hector Mine	Keys View	7.13	50.4	685	15.305
PEER NGA-2115	Denali, Alaska	PS#11	7.90	126.4	376	10.441
PEER NGA-1605	Duzce, Turkey	Duzce	7.14	0.0	276	1.388
Fernandez	GT-Synthetic	SYN27	-	-	-	1.051
Fernandez	GT-Synthetic	SYN21	-	-	-	2.713
Fernandez	GT-Synthetic	SYN24	-	-	-	1.263
Fernandez	GT-Synthetic	SYN17	-	-	-	1.336
Fernandez	GT-Synthetic	SYN22	-	-	-	2.983

Table 3.7-4. Record Set No. 2UHRS

Source	Event	Station	M_W	R, km	V_{S30}, m/s	SF
PEER NGA-1521	Chi-Chi, Taiwan	TCU089	7.62	0.0	680	2.721
PEER NGA-1507	Chi-Chi, Taiwan	TCU071	7.62	0.0	625	1.519
PEER NGA-880	Landers	MC Fault	7.28	27.0	345	7.562
PEER NGA-836	Landers	Baker FS	7.28	87.9	271	8.299
PEER NGA-855	Landers	MC Fault	7.28	63.0	345	7.631
PEER NGA-882	Landers	N Palm Spr	7.28	26.8	345	5.479
PEER NGA-761	Loma Prieta	Fremont EC	6.93	39.9	285	6.275
PEER NGA-762	Loma Prieta	Fremont MSJ	6.93	39.5	368	7.318
PEER NGA-807	Loma Prieta	Sunol FFS	6.93	47.6	401	9.716
PEER NGA-1153	Kocaeli, Turkey	Botas	7.51	127.0	274	9.704
PEER NGA-1149	Kocaeli, Turkey	Atakoy	7.51	56.5	274	6.678
PEER NGA-2107	Denali, Alaska	Carlo	7.90	49.9	964	10.927
PEER NGA-2111	Denali, Alaska	R109	7.90	43.0	964	10.988
PEER NGA-143	Tabas, Iran	Tabas	7.35	2.0	767	0.903

Table 3.7-5. Record Set No. 2NMSZ

Source	Event	Station	M_W	R, km	V_{S30}, m/s	SF
PEER NGA-1195	Chi-Chi, Taiwan	CHY026	7.62	29.5	226	4.850
PEER NGA-1540	Chi-Chi, Taiwan	TCU115	7.62	21.8	215	3.796
PEER NGA-1542	Chi-Chi, Taiwan	TCU117	7.62	25.4	199	3.075
PEER NGA-1238	Chi-Chi, Taiwan	CHY092	7.62	22.7	254	3.626
PEER NGA-1840	Hector Mine	Whittier	7.13	169.8	299	7.203
PEER NGA-883	Landers	Northridge	7.28	172.3	281	10.457
PEER NGA-853	Landers	El Monte	7.28	135.9	309	10.522
CESMD	Darfield, NZ	ROLC	7.10	2.9	264	2.757
CESMD	Darfield, NZ	HPSC	7.10	28.3	188	3.440
CESMD	Darfield, NZ	LRSC	7.10	12.5	269	8.488
Fernandez	GT-Synthetic	SYN28	-	-	-	1.387
Fernandez	GT-Synthetic	SYN27	-	-	-	1.688
Fernandez	GT-Synthetic	SYN26	-	-	-	1.473
Fernandez	GT-Synthetic	SYN23	-	-	-	1.519

Table 3.7-6. Record Set No. 2UHRS-P

Source	Event	Station	M_W	R, km	V_{S30}, m/s	SF
PEER NGA-1148	Kocaeli, Turkey	Arcelik	7.51	10.6	523	5.675
PEER NGA-1176	Kocaeli, Turkey	Yarmica	7.51	1.4	297	2.080
PEER NGA-292	Irpinia, Italy	Sturno	6.90	6.8	1000	2.246
PEER NGA-779	Loma Prieta	LGPC	6.93	0.0	478	1.190
PEER NGA-803	Loma Prieta	Saratoga	6.93	8.5	371	2.303
PEER NGA-767	Loma Prieta	Gilroy	6.93	12.2	350	2.242
PEER NGA-738	Loma Prieta	Alameda	6.93	70.9	190	3.957
PEER NGA-825	Cape Mendocino	Cape M	7.01	0.0	514	1.437
PEER NGA-828	Cape Mendocino	Petrolia	7.01	0.0	713	1.659
PEER NGA-1528	Chi-Chi, Taiwan	TCU101	7.62	2.1	504	2.840
PEER NGA-1526	Chi-Chi, Taiwan	TCU098	7.62	47.7	230	4.616
PEER NGA-1481	Chi-Chi, Taiwan	TCU038	7.62	25.4	229	3.682
PEER NGA-1505	Chi-Chi, Taiwan	TCU068	7.62	0.0	487	1.241
PEER NGA-1550	Chi-Chi, Taiwan	TCU136	7.62	8.3	538	3.711

Table 3.7-7. Record Set No. 2NMSZ-P

Source	Event	Station	M_W	R, km	V_{S30}, m/s	SF
PEER NGA-292	Irpinia, Italy	Sturno	6.90	6.8	1000	1.861
PEER NGA-1605	Duzce, Turkey	Duzce	7.14	0.0	276	1.244
PEER NGA-838	Landers	Barstow	7.28	34.9	371	4.995
PEER NGA-900	Landers	Yermo FS	7.28	23.6	354	2.685
PEER NGA-779	Loma Prieta	LGPC	6.93	0.0	478	0.984
PEER NGA-803	Loma Prieta	Saratoga	6.93	8.5	371	1.903
PEER NGA-1176	Kocaeli, Turkey	Yarmica	7.51	1.4	297	1.714
PEER NGA-2114	Denali, Alaska	PS#10	7.90	0.2	329	1.528
PEER NGA-1505	Chi-Chi, Taiwan	TCU068	7.62	0.0	487	1.020
PEER NGA-1548	Chi-Chi, Taiwan	TCU128	7.62	13.2	600	2.920
PEER NGA-1473	Chi-Chi, Taiwan	TCU018	7.62	66.2	490	7.654
PEER NGA-1529	Chi-Chi, Taiwan	TCU102	7.62	1.5	714	1.904
PEER NGA-1531	Chi-Chi, Taiwan	TCU104	7.62	12.9	544	4.264
PEER NGA-1480	Chi-Chi, Taiwan	TCU036	7.62	19.8	495	2.987

Table 3.7-8. Record Set No. 1NMSZ-B

Source	Event	Station	M_W	R, km	V_{S30}, m/s	SF
PEER NGA-1176	Kocaeli, Turkey	Yarmica	7.51	1.4	297	1.300
PEER NGA-1175	Kocaeli, Turkey	Usak	7.51	226.7	274	31.52
PEER NGA-1151	Kocaeli, Turkey	Balikesir	7.51	180.2	339	21.95
PEER NGA-2109	Denali, Alaska	Ester FS	7.90	139.3	274	25.16
PEER NGA-2102	Denali, Alaska	NOAA WF	7.90	275.1	274	18.71
PEER NGA-2095	Denali, Alaska	DOI	7.90	272.5	279	17.91
COSMOS	Michoacan	CALE	8.00	38.3	180	3.270
PEER NGA-851	Landers	DCMB	7.28	157.5	272	6.617
PEER NGA-1189	Chi-Chi, Taiwan	CHY017	7.62	59.1	191	1.020
PEER NGA-1194	Chi-Chi, Taiwan	CHY025	7.62	19.1	277	2.920
PEER NGA-1217	Chi-Chi, Taiwan	CHY060	7.62	68.9	229	7.654
PEER NGA-1242	Chi-Chi, Taiwan	CHY099	7.62	65.3	229	1.904
PEER NGA-1310	Chi-Chi, Taiwan	ILA004	7.62	86.6	124	4.264
PEER NGA-1311	Chi-Chi, Taiwan	ILA005	7.62	84.9	239	2.987

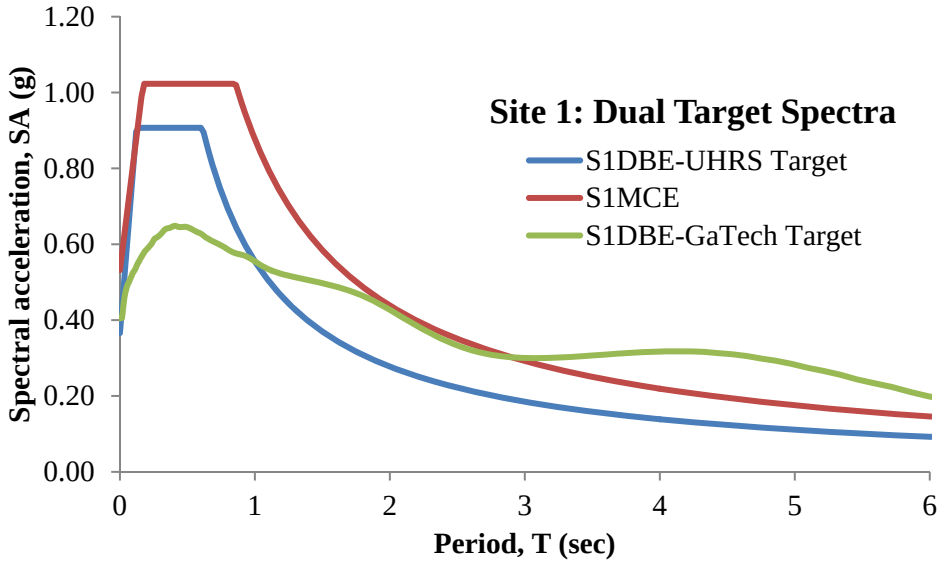

Figure 3.7-1. Dual Target Acceleration Spectra - Site No. 1

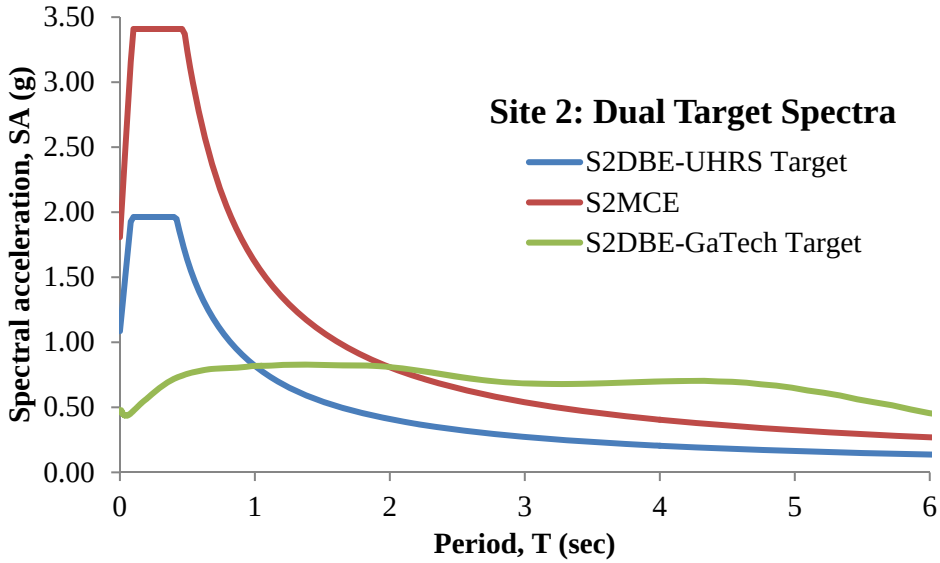

Figure 3.7-2. Dual Target Acceleration Spectra - Site No. 2

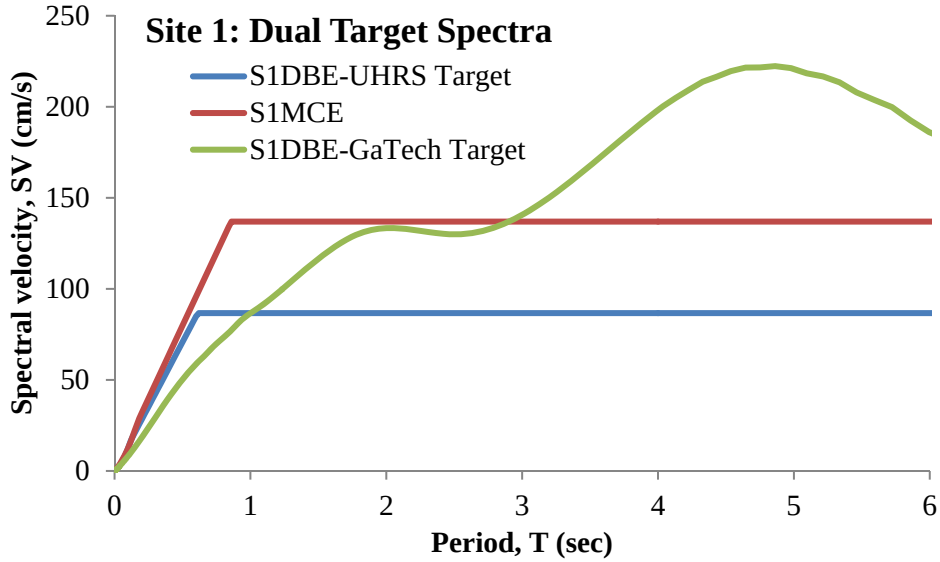

Figure 3.7-3. Dual Target Velocity Spectra - Site No. 1

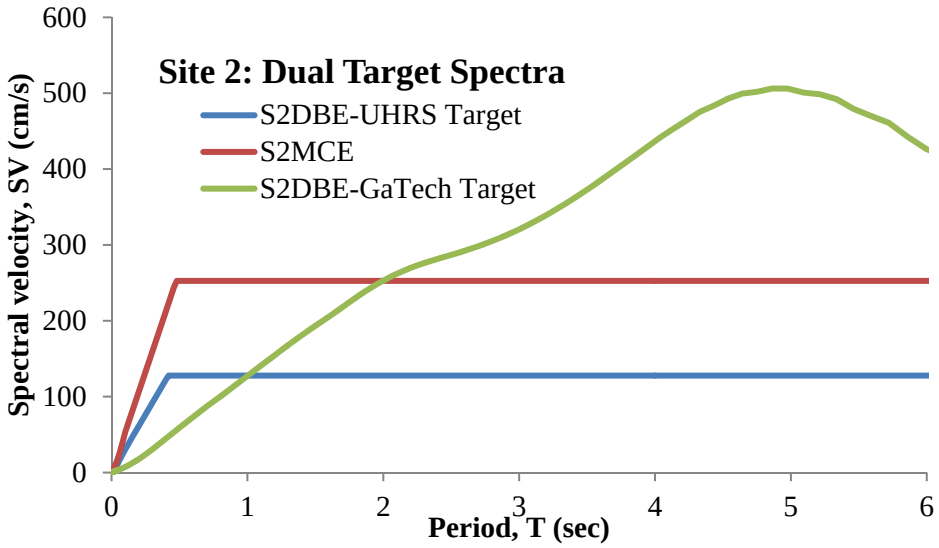

Figure 3.7-4. Dual Target Velocity Spectra - Site No. 2

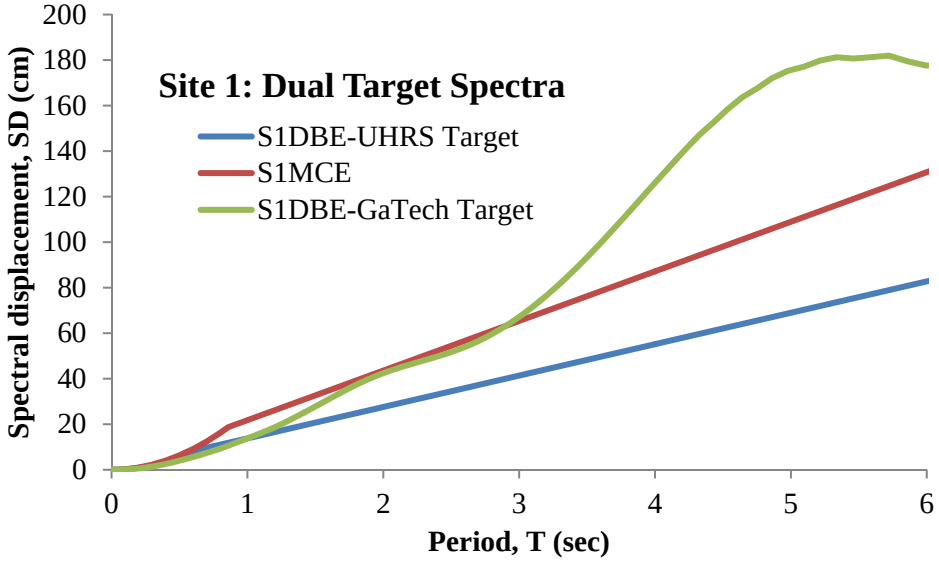

Figure 3.7-5. Dual Target Displacement Spectra - Site No. 1

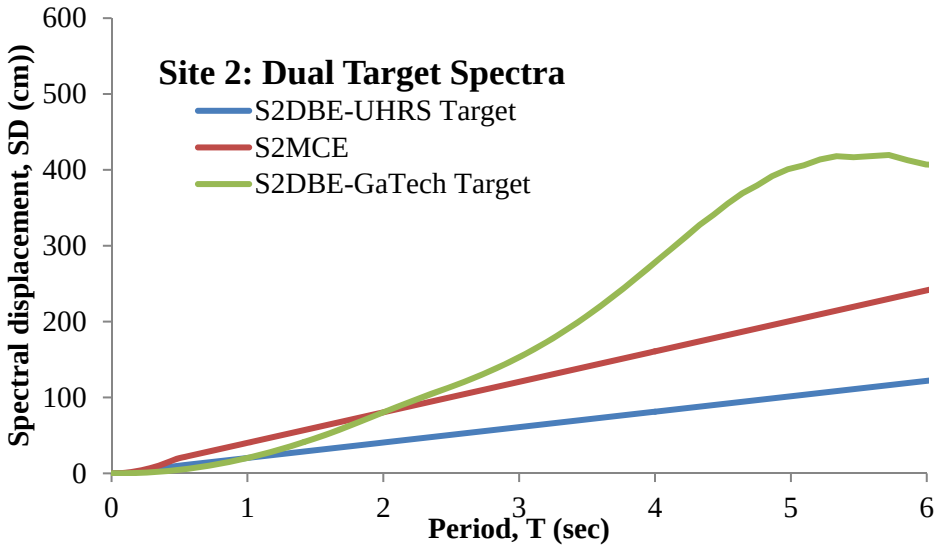

Figure 3.7-6. Dual Target Displacement Spectra - Site No. 2

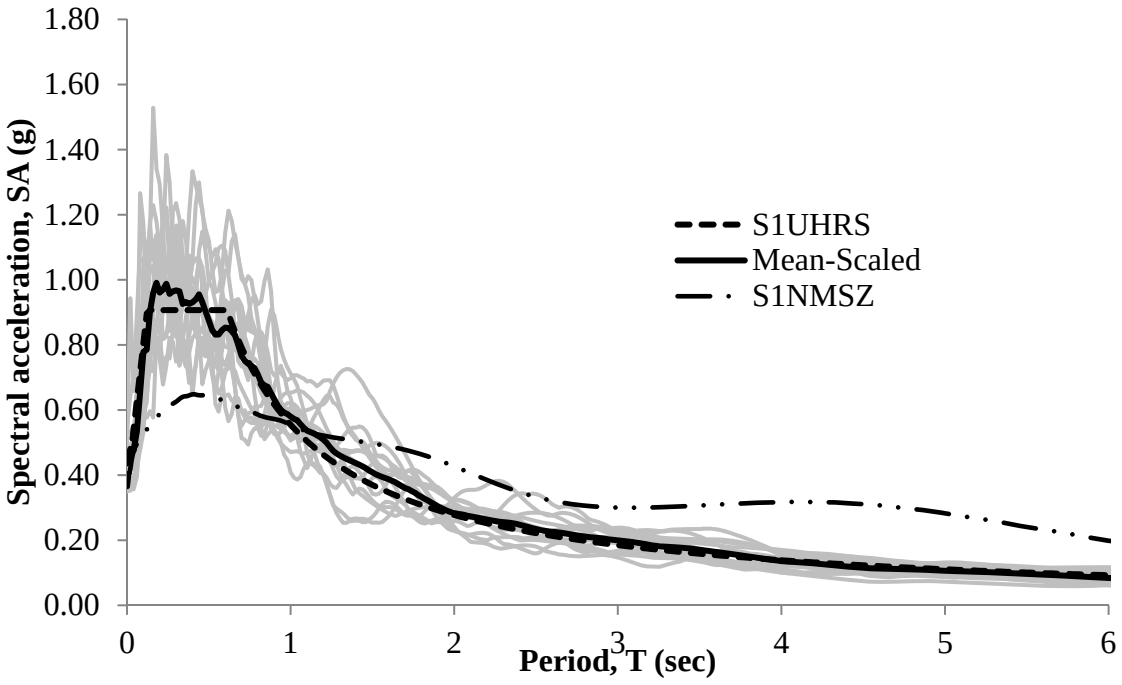

Figure 3.7-7. Acceleration Spectra - Record Set No. 1UHRS

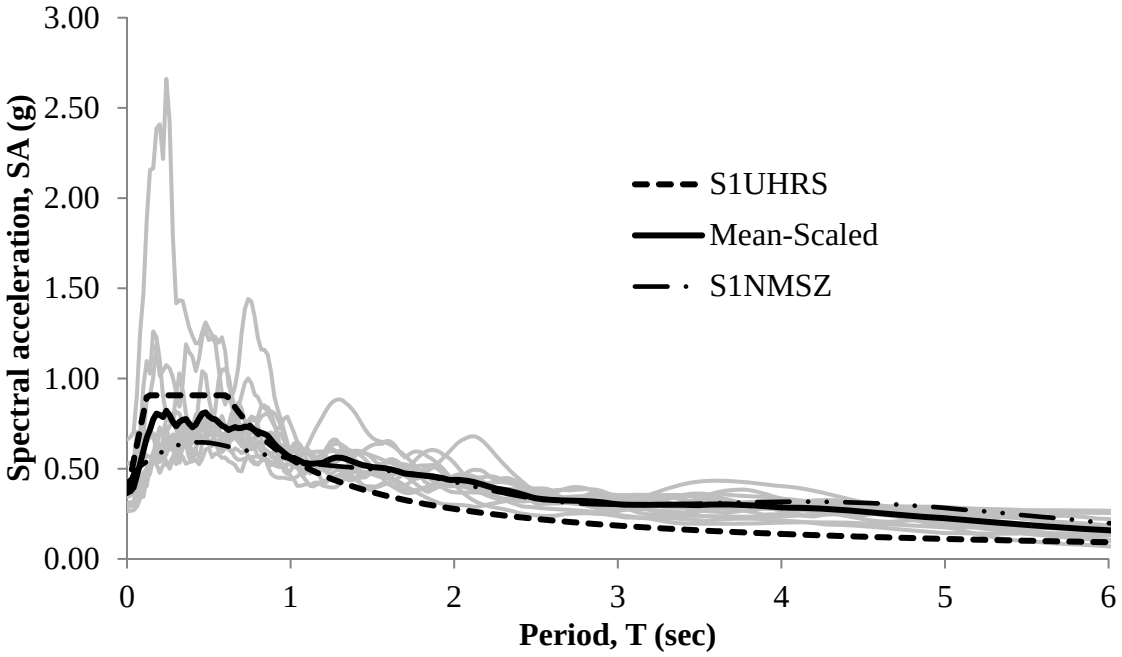

Figure 3.7-8. Acceleration Spectra - Record Set No. 1NMSZ

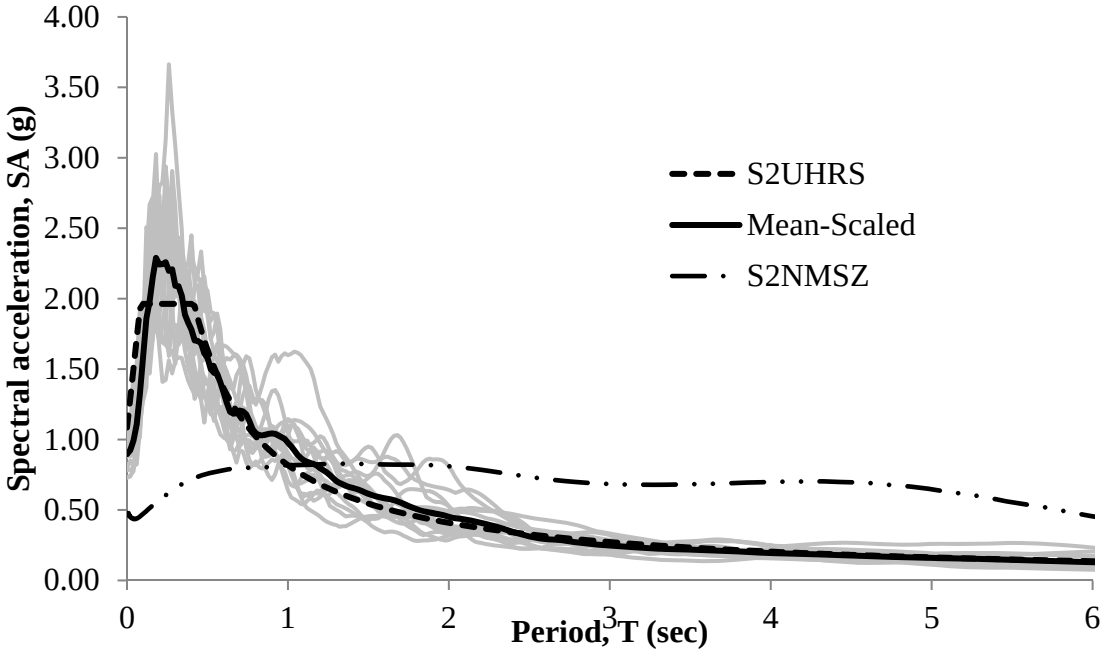

Figure 3.7-9. Acceleration Spectra - Record Set No. 2UHRS

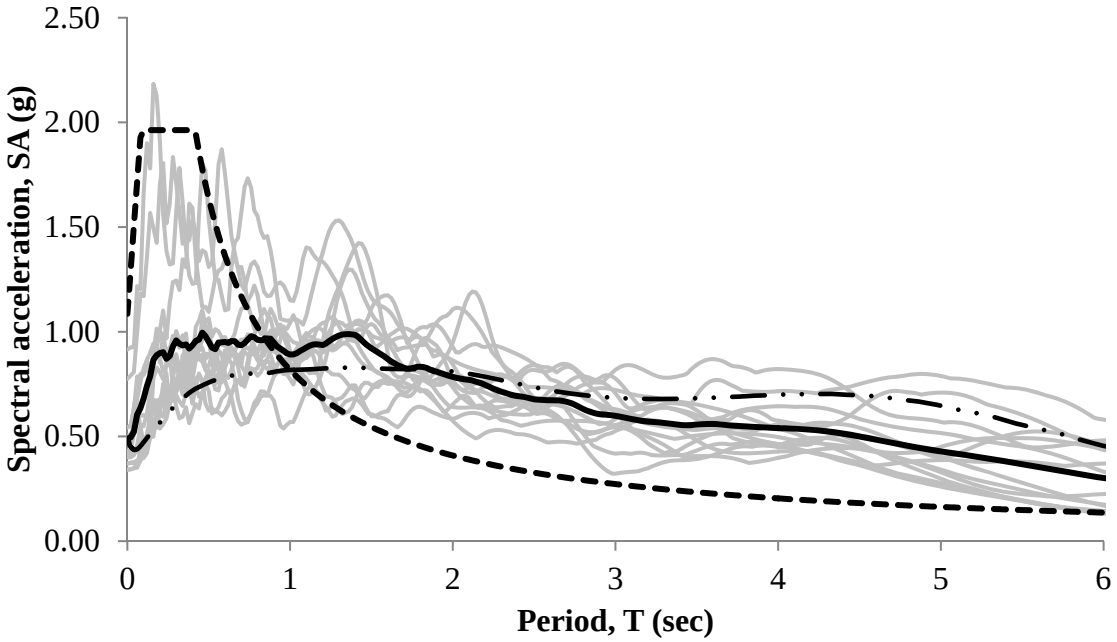

Figure 3.7-10. Acceleration Spectra - Record Set No. 2NMSZ

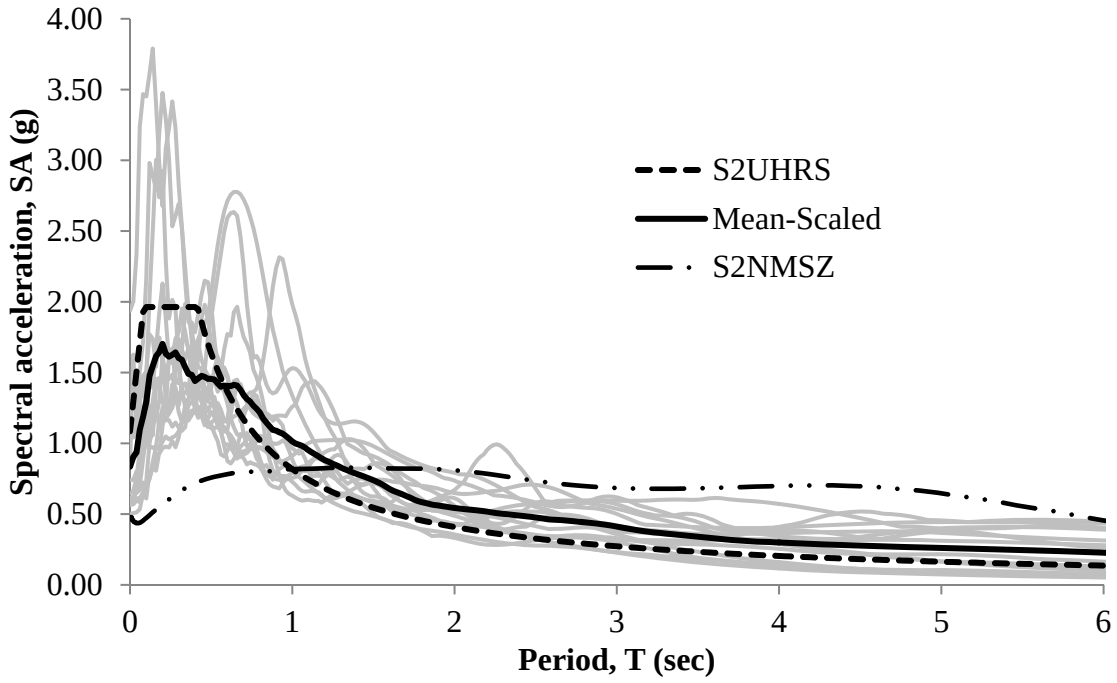

Figure 3.7-11. Acceleration Spectra - Record Set No. 2UHRS-P

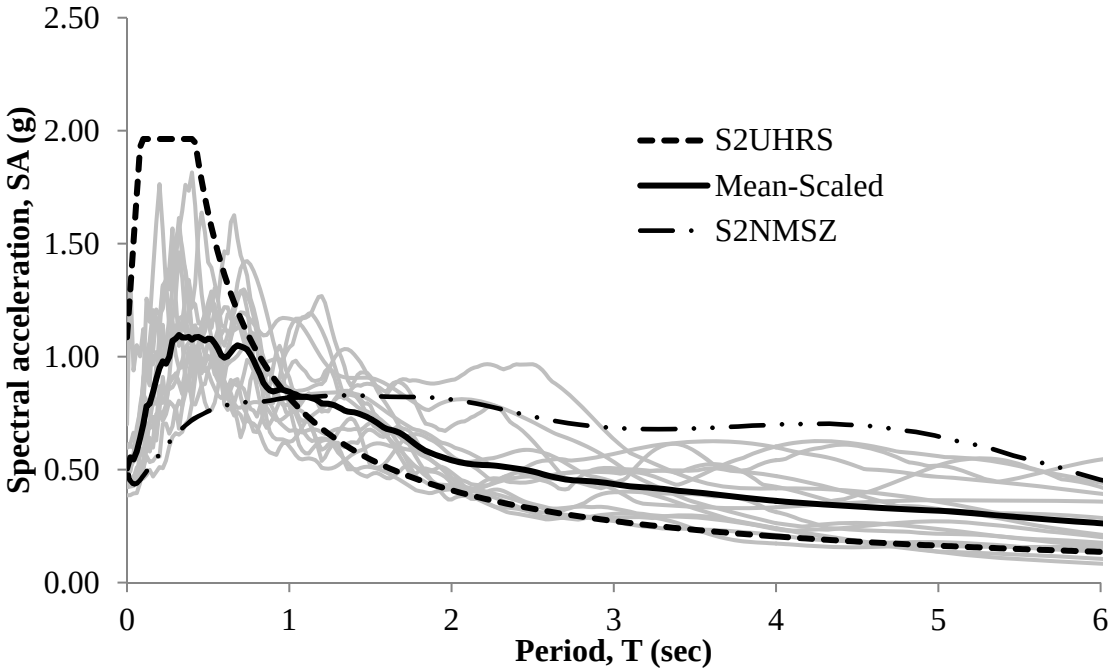

Figure 3.7-12. Acceleration Spectra - Record Set No. 2NMSZ-P

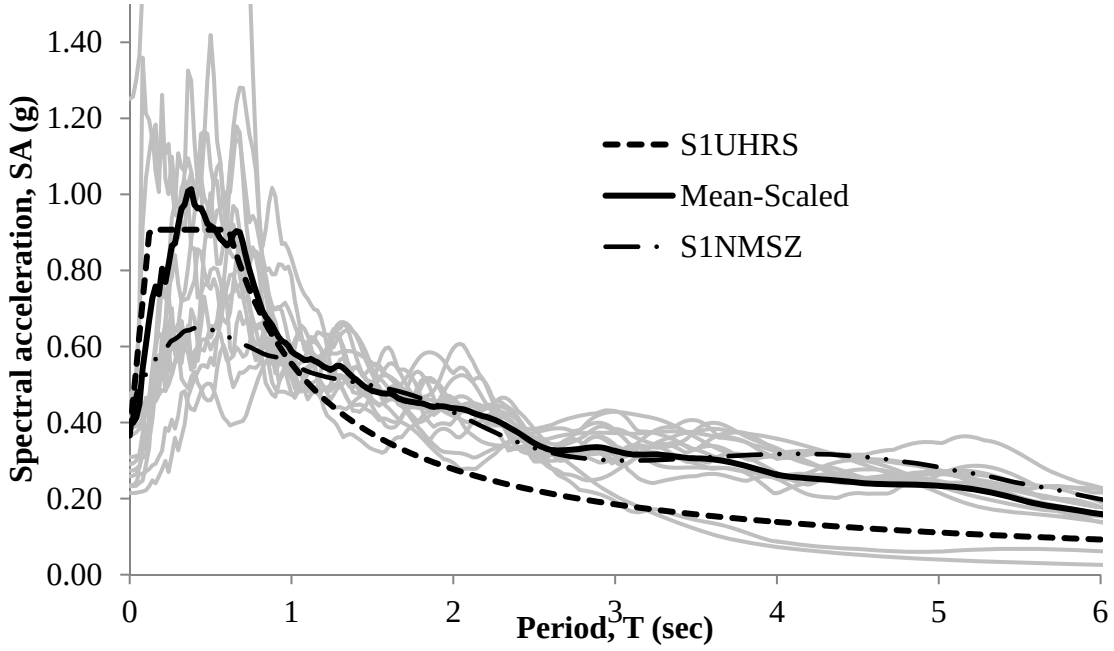

Figure 3.7-13. Acceleration Spectra - Record Set No. 1NMSZ-B

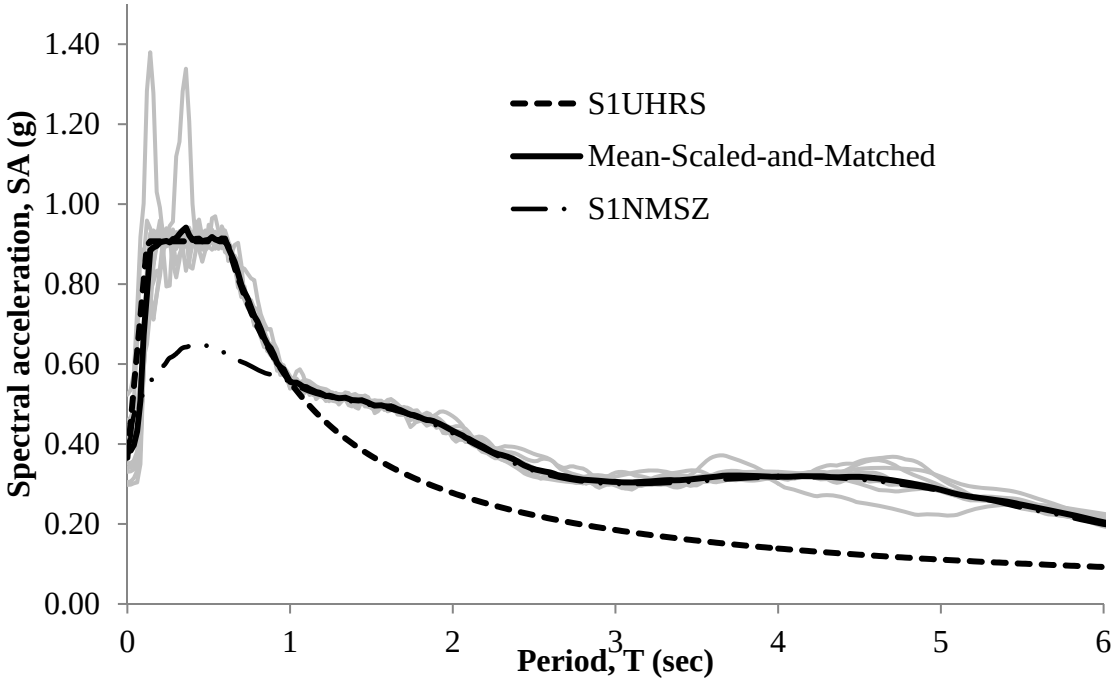

Figure 3.7-14. Acceleration Spectra - Record Set No. 1NMSZ-BM

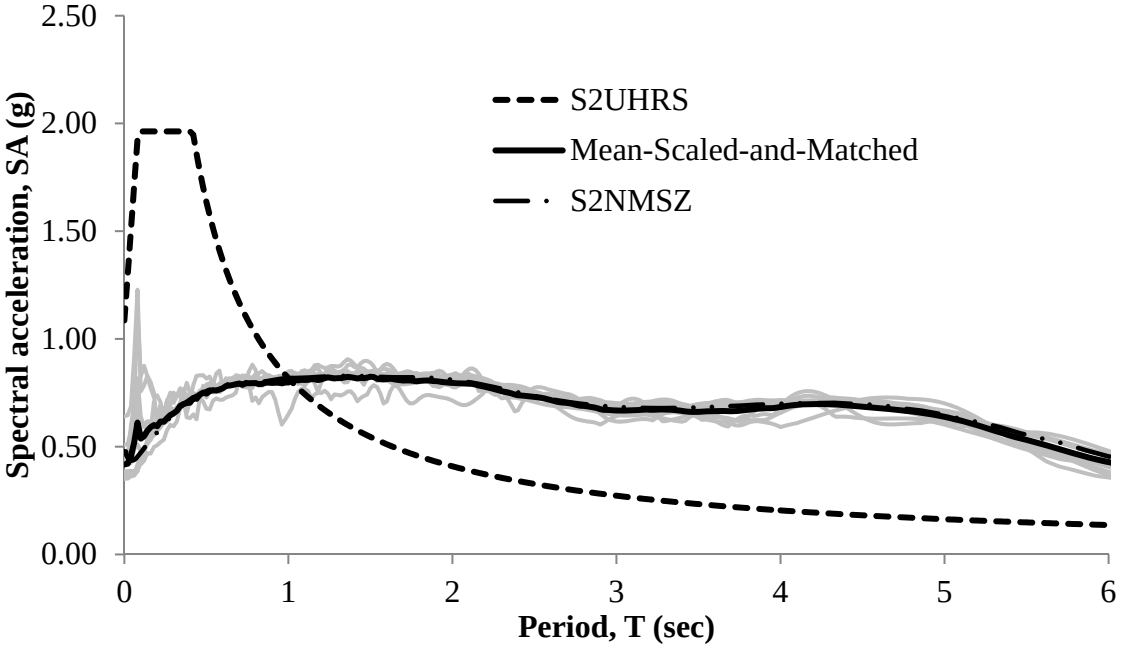

Figure 3.7-15. Acceleration Spectra - Record Set No. 2NMSZ-M

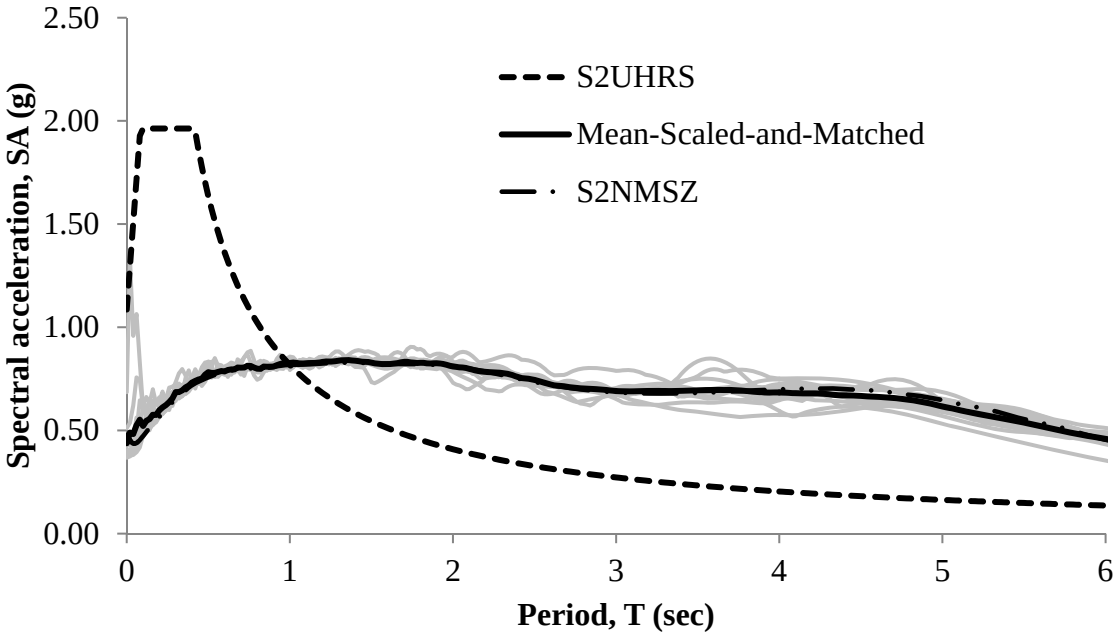

Figure 3.7-16. Acceleration Spectra - Record Set No. 2NMSZ-PM

CHAPTER 4 - MODEL ISOLATORS

In CHAPTER 3, ground motion sets were developed for two reasons. First, to make comparisons among nonlinear response to records of varying magnitude and tectonic environment, record sets from actual recorded ground motions of historic earthquakes were formed and modified by amplitude scaling to the Site 1 DBE-level hazard. Eight sets were formed for Site 1:

1. ATR-1: records from active tectonic regions, M_W=6.69-7.01, Site Class D stations
2. ATR-2: records from active tectonic regions, M_W =7.14-7.37, Site Class D stations
3. ATR-3: records from active tectonic regions, M_W =7.50-7.90, Site Class D/E stations
4. ATR-4: records from Chi-Chi, Taiwan, M_W =7.62, Site Class D stations (Chi-Chi 1)
5. ATR-5: records from Chi-Chi, Taiwan, M_W =7.62, Site Class D/E stations (Chi-Chi 2)
6. DNZ: records from Darfield, New Zealand, M_W =7.10, Site Class D stations
7. NMSZ-1: synthetic NMSZ-specific records, M_W =7.50-8.0
8. NMSZ-2: synthetic NMSZ-specific records, M_W =7.50-8.0

Two additional sets were formed for Site 2: NMSZ-3 and NMSZ-4. Secondly, sets of ground motion records were developed with the intent of using them in structural analysis of the isolated bridges in CHAPTER 7 - these record sets were formed using criteria from various codes and specifications to qualify as appropriate for final design.

The purpose of the current chapter is to take 5 of the 8 record sets for Site 1 from the first category and perform analyses of simple, bi-linear isolators. Maximum isolator demand, both uni-directional and bi-directional, as well as residual displacements were computed for each

record set, and for various combinations of the post-yield stiffness ratio (α) and the normalized characteristic strength (Q_d/W). The responses were computed from non-linear response history analyses. SAP2000 non-linear link elements were used to create the models. The average of these responses were computed and compared to results of simplified analytical procedures - specifically the simplified, effective stiffness-based procedure used in AASHTO for isolation design. The characteristics of the representative isolators are presented in Table 4-1.

Table 4-1. Model Isolator Properties

Isolator	Q_d kN (kips)	k_d kN/m (kips/inch)	T_d (sec)	FPS D_Y (mm)	LRB D_Y (mm)	W/k_d meters
1	111 (25)	438(2.5)	5.66	0.025	28.2	7.95
2		1,313(7.5)	3.27	0.008	9.4	2.65
3		2,189(12.5)	2.53	0.005	5.6	1.59
4		3,153(18.0)	2.11	0.004	3.9	1.10
5		4,380(25.0)	1.79	0.003	2.8	0.79
6	222 (50)	438(2.5)	5.66	0.051	56.4	7.95
7		1,313(7.5)	3.27	0.017	18.8	2.65
8		2,189(12.5)	2.53	0.010	11.3	1.59
9		3,153(18.0)	2.11	0.007	7.8	1.10
10		4,380(25.0)	1.79	0.005	5.6	0.79
11	334 (75)	438(2.5)	5.66	0.076	84.7	7.95
12		1,313(7.5)	3.27	0.025	28.2	2.65
13		2,189(12.5)	2.53	0.015	16.9	1.59
14		3,153(18.0)	2.11	0.011	11.8	1.10
15		4,380(25.0)	1.79	0.008	8.5	0.79
16	400 (90)	438(2.5)	5.66	0.091	101.6	7.95
17		1,313(7.5)	3.27	0.030	33.9	2.65
18		2,189(12.5)	2.53	0.018	20.3	1.59
19		3,153(18.0)	2.11	0.013	14.1	1.10
20		4,380(25.0)	1.79	0.009	10.2	0.79

The weight, 782 kips, assigned to each model isolator is approximately equal to the supported weight at one pier of Bridge No. 1. The post-yield stiffness ratio, α is varied to examine the effect on isolator response. Current manufacturers of LRB isolators typically recommend a post-stiffness ratio of $\alpha = 0.10$ for their products, which is in agreement with the AASHTO LRFD Specifications. To model FPS-systems, a very small value of $\alpha = 0.0001$ is selected. The characteristic strength, Q_d, values were selected to encompass typical ranges for both LRB isolators FPS isolators carrying 782 kips. Post-yield stiffness values were selected to produce post-yield period in the 1.5-6.0 second range, the expected approximate limits for isolated bridges. The purpose of this study of 2-DOF bi-linear response was to identify any peculiarities in response to the ground motions considered and to evaluate nonlinear, biaxial THA results in relation to AASHTO simplified, uniaxial RSA results. Keep in mind, however, that these are results for isolators rigidly connected to the ground. Real isolators installed between a bridge superstructure and substructure may behave quite differently. For example, it may be that an actual isolator reaches yield in say, the transverse direction but not in the longitudinal direction due to differences in stiffness.

For the simplified response spectrum analyses, a standard practice cap of 30% on effective damping (AASHTO, 2010) has been imposed. In other words, in situations for which the theoretical, calculated, effective damping was greater than 30%, then effective damping was taken to be 30%. For comparison purposes, the simplified analysis has also been performed without the 30% cap on effective damping for the FPS system since theoretical damping is much higher than 30% for this isolator while the theoretical maximum for the LRB system is 33.1% of critical. The simplified response spectrum analysis is that used by AASHTO in the Guide

Specification for Seismic Isolation Design (AASHTO, 2010). The procedure may be briefly summarized in 5 steps:

1. Assume a displacement.
2. Determine the effective (secant) stiffness, effective period, and equivalent viscous damping.
3. From the design, 5%-damping response spectrum, establish the spectral displacement at the effective period.
4. Determine the reduction factor for effective damping in excess of 5% and apply the factor to the spectral displacement to establish the calculated displacement demand on the isolator.
5. If the calculated displacement equals the assumed displacement within a reasonable margin of error, the displacement demand on the isolator has been determined. Otherwise, return to step 1 with a revised assumed displacement.

The simplified response spectrum analysis approach currently used for initial design will be shown to under-estimate the final design displacements from a nonlinear response history analysis - significantly in some cases - for two reasons:

1. The simplified approach is essentially uni-directional in nature because no coupling may be accounted for. The response history analysis involves the simultaneous application of 2 horizontal components with coupling between horizontal degrees of freedom explicitly included in the analysis.

2. The simplified method of handling bi-directional effects (the commonly used 100-30 rule) amounts to, at most an approximate 4% increase - as seen in equation 4-1 - in uni-directional response estimates, which is shown to be insufficient in some cases.

$$TDD = \sqrt{D_{ISO-x}^2 + (0.3D_{ISO-x})^2} = 1.044D_{ISO-x} \qquad \text{(Eq. 4-1)}$$

Another contributing factor is likely related to the fact that soft soil records are required for the subject sites. Other research (Warn & Whittaker, 2007) has asserted that the AASHTO simplified procedure significantly under-estimates isolator response for soft soil sites.

4.1 Nonlinear Displacement Response of the Model Isolators

Table 4.1-1 summarizes statistics for the ratio of uni-directional demands from AASHTO simplified procedures to those from response history analysis (RHA).

The simplified procedure under-estimated uni-directional isolator demand in:

- 2 out of 20 isolators, Chi-Chi 1
- 3 out of 20 isolators, Chi-Chi 2
- 20 out of 20 isolators for each of New Zealand, NMSZ1 and NMSZ2

The following additional observations are made with percentages rounded to the rough values.

- For New Zealand and the NMSZ records, the simplified procedure under-estimated uni-directional response by 25-30% on average and by as much as 45%.
- For the Chi-Chi sets of records, the simplified procedure actually over-estimated response history analysis uni-directional results by about 10-20% on average and never under-estimated uni-directional response by more than 7%.

Regarding bi-directional response, the AASHTO simplified procedures under-estimate LRB isolator demand in most cases, often by a large margin. Table 4.1-2 summarizes the statistics for bi-directional response. In only 4 instances, all in set Chi-Chi 1 and all less than 12% did the simplified procedure over-estimate RHA results for bi-directional displacement demand. The following general observations regarding bi-directional response are approximate.

- The AASHTO simplified procedure under-estimates bi-directional response by about 45-50% on average and by as much as 60% for New Zealand and NMSZ record sets.
- The AASHTO simplified procedure under-estimates bi-directional response by about 5-15% on average and by as much as 25% for the Chi-Chi record sets.

Other research (Warn & Whittaker, 2007) has also concluded that the AASHTO simplified procedure significantly under-estimates bi-directional isolator response for soft soil sites.

So the simplified analysis for uni-directional response is found to be reasonable and conservative only for the Chi-Chi record sets. Other researchers (Warn, 2002) have also identified cases in which uni-directional estimates by the AASHTO method were on the conservative side.

The AASHTO simplified procedure for isolation design is appropriate for uni-directional displacement demands for Chi-Chi, but not for New Zealand and not for NMSZ record sets. The simplified treatment of bi-directional demand is inappropriate and un-conservative for each of the large magnitude, soft soil record sets studied. It may be that the AASHTO simplified procedure for isolation design may still be applicable, after modification, in the NMSZ. Most

specifications - including AASHTO - express the spectral acceleration beyond the constant acceleration period as:

$$S_a(T) = \frac{S_{D1}}{T} \qquad \text{(Eq. 4-2)}$$

$$\Rightarrow S_v(T) = \frac{S_a(T)}{\omega} = \frac{S_{D1} \cdot g}{T} \cdot \frac{T}{2\pi} = \frac{S_{D1} \cdot g}{2\pi} \qquad \text{(Eq. 4-3)}$$

Rather than assuming spectral acceleration inversely proportional to period in this range, it may be that the proportionality could be estimated as inverse with respect to some power of period, or even some other period-dependent function. This will be explored further in Section 4.3.

Figures G4.1-1 through G4.1-8 in APPENDIX G4 are graphical representations of the results reported here.

Table 4.1-1. AASHTO / THA Isolator Demand (Uni-directional)

	$(D_{ISO})_{AASHTO}/(D_{ISO})_{RHA}$				
	DNZ	Chi-Chi 1	Chi-Chi 2	NMSZ 1	NMSZ 2
average	0.715	1.183	1.114	0.760	0.754
minimum	0.557	0.956	0.934	0.627	0.655
maximum	0.852	1.414	1.307	0.964	0.920
std. dev.	0.072	0.108	0.098	0.094	0.066

Table 4.1-2. AASHTO / THA Isolator Demand (Bi-directional)

	$(TDD)_{AASHTO}/(TDD)_{RHA}$				
	DNZ	Chi-Chi 1	Chi-Chi 2	NMSZ 1	NMSZ 2
average	0.508	0.947	0.869	0.561	0.556
minimum	0.394	0.770	0.754	0.463	0.483
maximum	0.612	1.119	0.990	0.712	0.679
std. dev.	0.054	0.084	0.062	0.069	0.049

4.2 Residual Displacements

A residual displacement analysis was completed for the model isolators under the scaled record sets. Results were normalized to report residual-to-maximum displacement ratios. Figures 4.2-2 and 4.2-3 are graphical summaries of these results for $\alpha = 0.0001$ (FPS systems) and for $\alpha = 0.10$ (LRB systems), respectively.

Residual displacement ratios tend to be significantly lower for LRB systems compared to FPS systems, for comparable values of Q_d/W and T_d, the yielded period. FPS systems may result in excessive residual displacements, particularly when Q_d/W is high and when T_d is high.

The results reported here are in basic agreement with previous work (Kawashima, et al., May, 1998) which has concluded that the single most important variable in residual displacement results is the post-yield stiffness ratio, α. The results were based on 14 bi-directional nonlinear load cases on each of the 20 model isolators for a total of 280 bi-directional, coupled plasticity analyses. All of the effective damping in the model was that due to hysteretic behavior of the isolators.

When simplified procedures are used to estimate isolator maximum displacements, it may still be possible to estimate isolator residual displacements. A research project in Europe, LESSLOSS (http://www.lessloss.org/main/), has provided a great deal of information relevant to displacement-based seismic design. This information includes methods of estimating residual displacements in seismic isolation systems. Results from theoretical considerations along with over 100,000 nonlinear analyses of 180 different single-degree-of-freedom systems were included in a report produced by the project (Fardis & Pinto, 2007). In the report it is demonstrated that residual-to-maximum displacement ratios may be estimated as follows.

$$\frac{D_{res}}{D_{rm}} = \frac{C_o}{\left(1 + C_1 \frac{D_{rm}}{D_r}\right)\left(1 + C_2 \frac{D_y}{D_r}\right)} \quad \text{(Eq. 4-4)}$$

$$\frac{D_{rm}}{D_r} = max\left[0, min\left(1, \frac{D_{max} - D_y}{D_r + D_y}\right)\right] \quad \text{(Eq. 4-5)}$$

$$D_r = \frac{Q_d}{k_d} \quad \text{(Eq. 4-6)}$$

C_0, C_1, *and* C_2 are non-linear regression coefficients developed in the LESSLOSS report. Statistical analysis was performed to arrive at coefficient values necessary to estimate D_{res}/D_{rm} at the mean, median (50th percentile), 80th percentile, and 90th percentile levels. For each of these levels, the corresponding coefficients from the study are:

- Mean estimate of D_{res}/D_{rm}: C_0 = 0.539, C_1 = 4.298, C_2 = 30.769
- Median estimate of D_{res}/D_{rm}: C_0 = 0.552, C_1 = 6.180, C_2 = 41.139
- 80th percentile estimate of D_{res}/D_{rm}: C_0 = 0.869, C_1 = 4.276, C_2 = 31.683
- Mean estimate of D_{res}/D_{rm}: C_0 = 0.972, C_1 = 3.300, C_2 = 25.508

With the goal of making it more convenient to compare different isolation systems the above equations can be transformed to the format presented next by introducing the post-yield stiffness ration of the isolator, α, into the equations. Note also that we are primarily concerned with the case in which the isolators actually yield during the strong ground motion so the zero-value case for residual displacement is dismissed in this study.

$$D_y = \frac{Q_d}{k_d} \cdot \frac{\alpha}{1 - \alpha} = D_r \cdot \frac{\alpha}{1 - \alpha} \quad \text{(Eq. 4-7)}$$

$$\frac{D_{rm}}{D_r} = 0.000 \; if \; \frac{D_{max}}{D_r} < \frac{\alpha}{1 - \alpha} \quad \text{(Eq. 4-8)}$$

$$\frac{D_{rm}}{D_r} = 1.000 \; if \; \frac{D_{max}}{D_r} > \frac{1+\alpha}{1-\alpha} \qquad \text{(Eq. 4-9)}$$

$$\frac{D_{rm}}{D_r} = \left[\frac{D_{max}}{D_r} \cdot (1-\alpha) - \alpha\right] \; if \; \frac{\alpha}{1-\alpha} \leq \frac{D_{max}}{D_r} \leq \frac{1+\alpha}{1-\alpha} \qquad \text{(Eq. 4-10)}$$

$$\frac{D_{res}}{D_{rm}} = \frac{C_o}{\left(1 + C_1 \frac{D_{rm}}{D_r}\right)\left(1 + C_2 \cdot \frac{\alpha}{1-\alpha}\right)} \qquad \text{(Eq. 4-11)}$$

$$\frac{D_{res}}{D_{max}} = \frac{D_{res}}{D_{rm}} \cdot \frac{D_{rm}}{D_r} \cdot \frac{D_r}{D_{max}} \qquad \text{(Eq. 4-12)}$$

It now becomes clear that the two primary factors determining residual displacement are the post-yield stiffness ratio, α, and the ratio of maximum displacement, D_{max}, to the quantity (Q_d/k_d).

For either an LRB or an FPS bearing, μ is not to be confused with displacement ductility demand in the context of this report, but is the characteristic strength to weight ratio.

$$\mu = \frac{Q_d}{W} \qquad \text{(Eq. 4-13)}$$

$$\frac{W}{k_d} = \frac{Q_d}{k_d} \cdot \frac{1}{\mu} \qquad \text{(Eq. 4-14)}$$

Note also that for friction-pendulum systems (FPS) we have:

$$\frac{Q_d}{k_d} = \frac{\mu \cdot W}{\left(W/R\right)} = \mu R \qquad \text{(Eq. 4-15)}$$

$$\frac{W}{k_d} = \frac{W}{\left(W/R\right)} = R \qquad \text{(Eq. 4-16)}$$

The LESLOSS parametric study included:

- μ-values of 0.03, 0.045, 0.06, 0.075, and 0.09

- W/k_d values of 2m, 3m, 4m, 5m, 6m, and 100m
- D_y-values of 0.125mm, 0.250mm, 0.500mm, 10 mm, and 15mm

Table 4-1 lists the model isolator properties used here for reference to values used in the LESSLOSS study. These same model isolators were analyzed for various ground motions of this study scaled to a 1-second spectral acceleration of 0.55g, corresponding to the Site No. 1 DBE. Figure 4.2-1 sheds some additional light on residual displacement potential for FPS systems compared to LRB systems. Figures 4.2-2 and 4.2-3 summarize the relationships between residual and maximum displacements for FPS and LRB systems, respectively.

There is a pronounced difference in LRB residual displacements for the NMSZ2 record set (see Figure 4.2-3), which is comprised of 12 Atkinson/Beresnev records and 2 Fernandez/Rix records. A response characteristic was observed in the analysis results for the NMSZ2 record set (in particular for records M7.504 and M8.004 of the Atkinson/Beresnev synthetic motions) which was not observed in any other record. Figure 4.2-4 shows a typical LRB response history, in this case for Isolator No. 1 subjected to the M8.001 Atkinson/Beresnev record. A typical response history for an FPS system with high Q_d and low k_d is presented in Figure 4.2-5. The unexpected behavior for an LRB isolator with low Q_d and low k_d is evident in Figure 4.2-6. Examination of the ground motion parameters for the NMSZ2 record set reveals no glaring differences to set them apart from all other record sets.

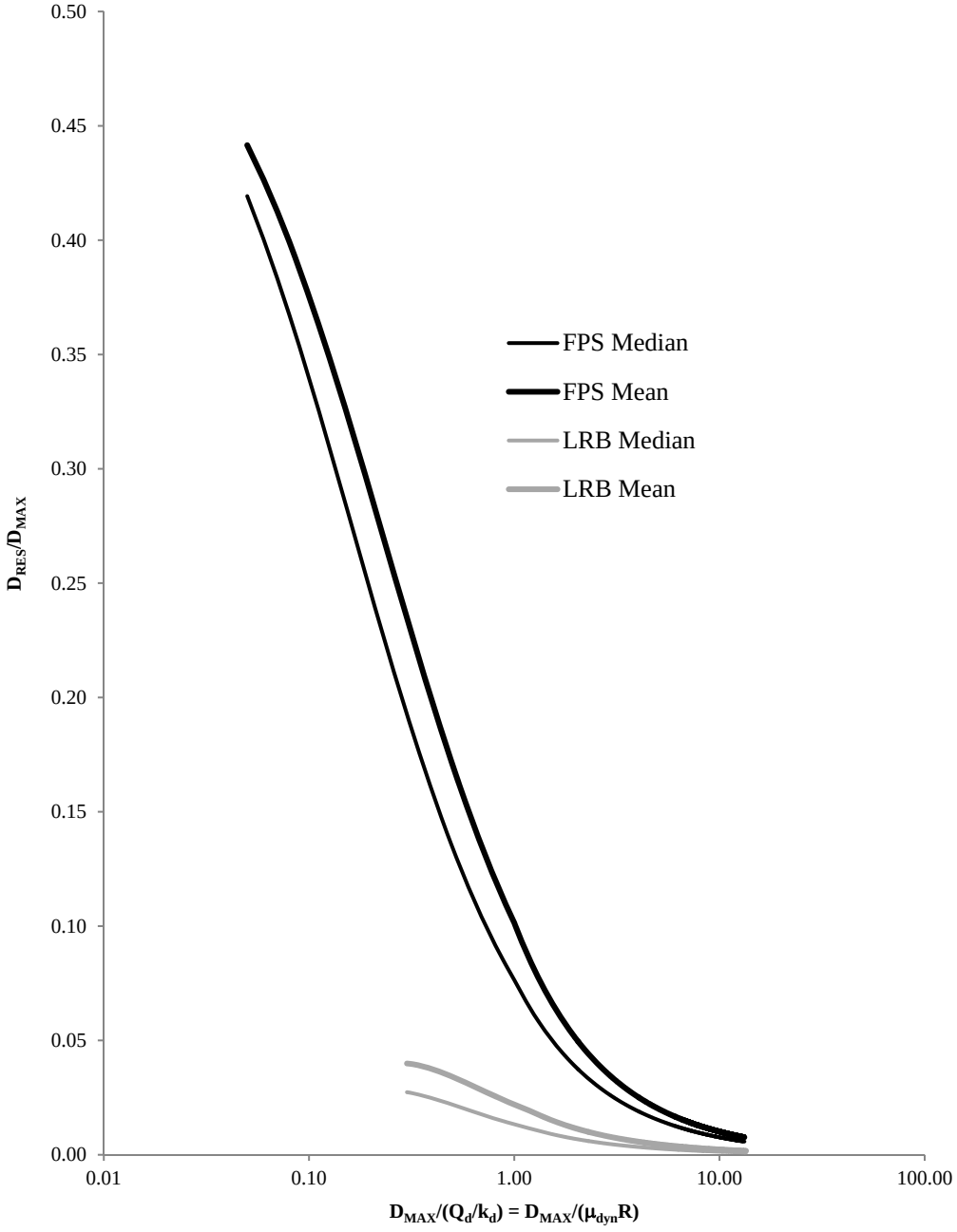

Figure 4.2-1. LESSLOSS Residual Displacement Estimates: FPS vs. LRB

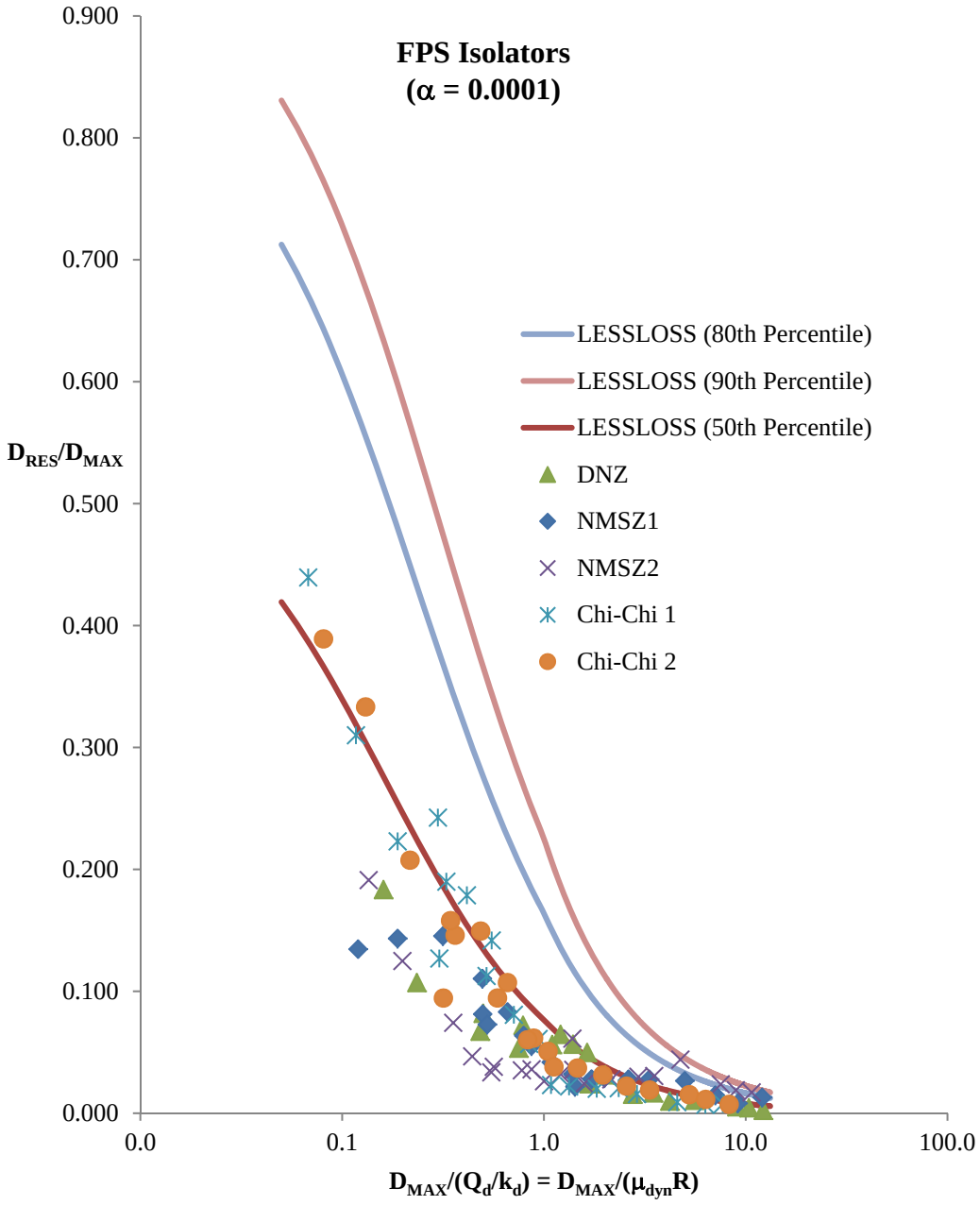

Figure 4.2-2. Residual Displacements: Estimated and Observed - FPS

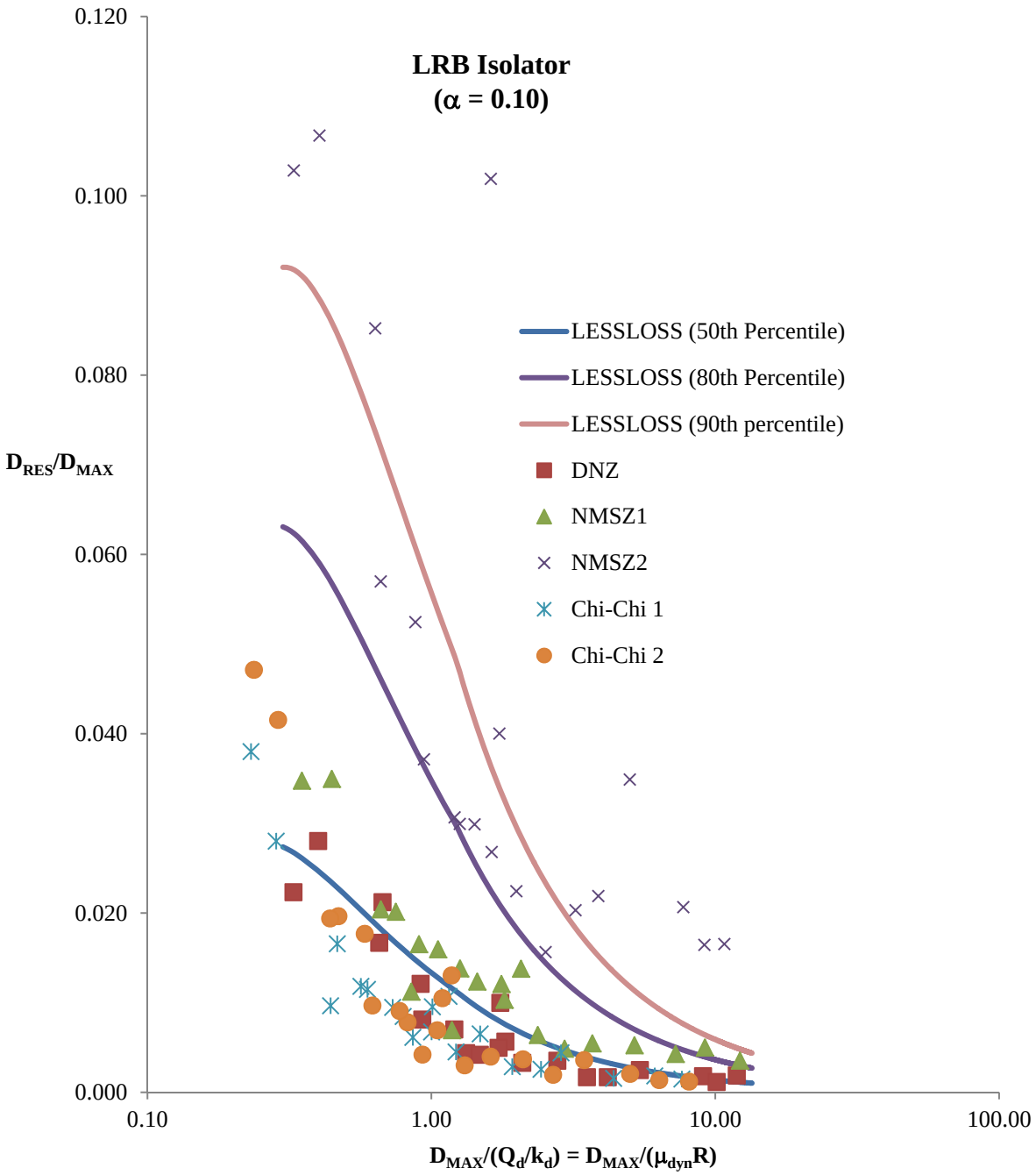

Figure 4.2-3. Residual Displacements: Estimated and Observed - LRB

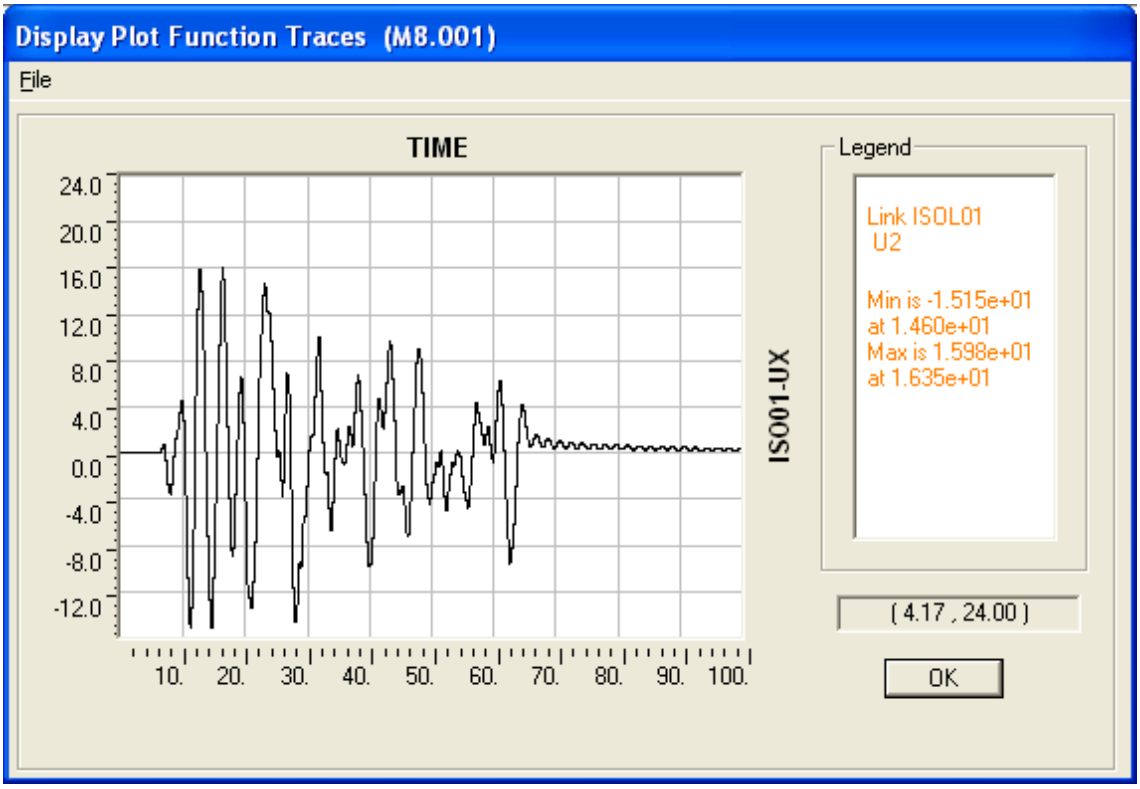

Figure 4.2-4. Typical Response: LRB

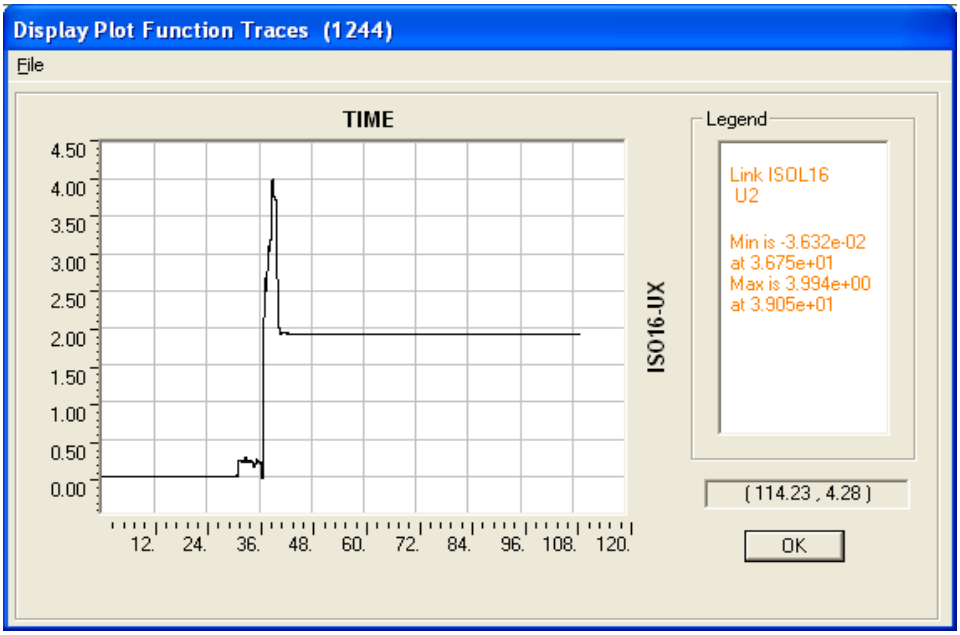

Figure 4.2-5. Typical Response: FPS with Large Q_d, Low k_d

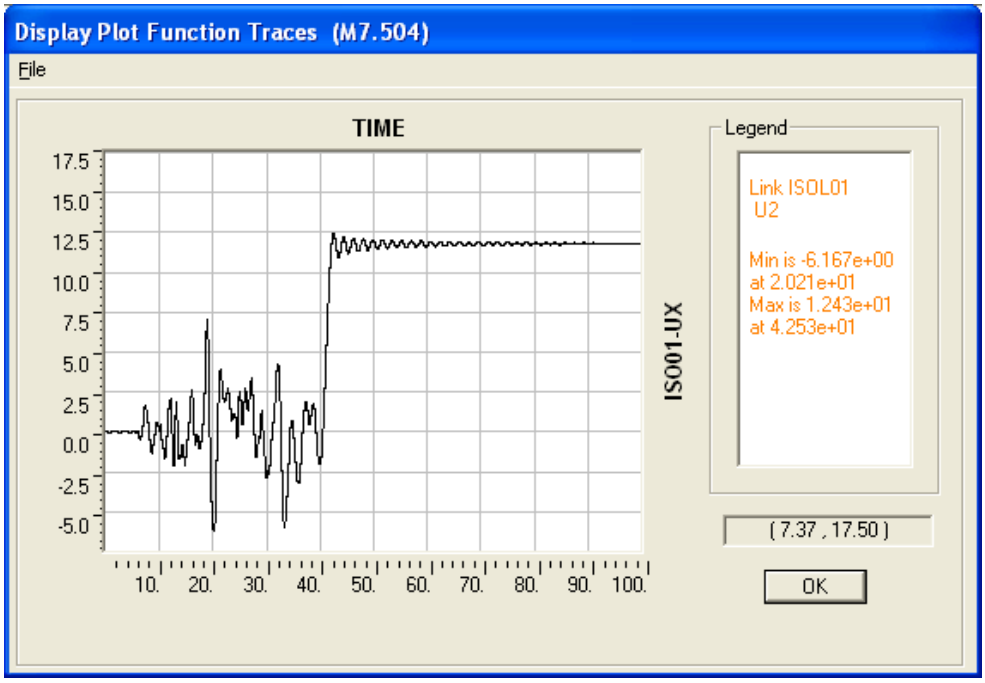

Figure 4.2-6. Unexpected Response: LRB

4.3 Spectral Shape Modification

It is clear from spectral plots of mean scaled ground motions that the effect of deep soils on intra-plate settings is to broaden the constant acceleration plateau and to impart a transition region from constant acceleration to constant velocity portions of the spectra. In effect, spectral acceleration is not inversely proportional to period on the descending branch of the acceleration spectrum. Operating on the premise that this proportionality should be expressed as some power of T, plots of the exponent "k" at various periods between 1.5 and 6 seconds and for various record sets are presented in Figure 4.3-1.

$$SA(T) = \frac{SA(1)}{T^k} \qquad \text{(Eq. 4-17)}$$

$$SD(T) = \frac{S_{D1}}{T^k} \cdot g \cdot \left(\frac{T}{2\pi}\right)^2 = \frac{S_{D1} \cdot g}{4\pi^2} \cdot T^{2-k} \qquad \text{(Eq. 4-18)}$$

The calculation of the exponent "k" is made by re-arranging the expression for spectral acceleration and making the calculation at each period and for each record set from periods in the 1.3-6.0 second range.

$$T^k = \frac{SA(1)}{SA(T)} \qquad \text{(Eq. 4-19)}$$

$$\rightarrow k = \frac{ln[SA(1)] - ln[SA(T)]}{ln(T)} \qquad \text{(Eq. 4-20)}$$

From Figure 4.3-1 observe that an exponent of 1.0 corresponds to the assumption made by AASHTO and in most all specification-based spectra generation rules. An exponent greater than 1.0 would represent a spectral shape for which AASHTO would produce conservative results. An exponent less than 1.0 would represent a spectral shape for which AASHTO would produce an un-conservative result. Notice that all 5 ATR sets - the Chi-Chi record sets and the three magnitude dependent sets - all generally either obey the AASHTO assumption or lie above the AASHTO assumption (on the conservative side). Both NMSZ sets and the Darfield, New Zealand set lie on the un-conservative side out to periods of about 4.3-5.3 seconds. A general trend may be inferred from the NMSZ2 record set. The exponent "k" appears to follow an approximately linear, period-dependent straight line given by the following approximate expression.

$$k = \frac{2}{15} \cdot (T + 3) \qquad \text{(Eq. 4-21)}$$

If we use this alternate spectral shape combined with duration dependent damping reduction coefficient, the iterative, simplified procedure used in AASHTO Guide Specifications for Seismic Isolation Design will produce more realistic estimates of isolator demand in the NMSZ. The significant duration, D5-95%, is taken as 30 seconds for the NMSZ. The revised spectral

shape is valid between periods of 1.5 to 6.0 seconds. To summarize, the following modifications to the procedure are proposed:

$$SD(T) = \frac{S_{D1} \cdot g}{4\pi^2} \cdot T^{\left[2-\frac{2}{15}\cdot(T+3)\right]} \qquad \text{(Eq. 4-22)}$$

$$R_\xi(D_{5-95\%}, \xi) = \frac{1}{B_L} = 1 - \frac{-0.631 + 0.421ln(\xi) - 0.015ln(\xi)^2}{1 + exp\left\{\frac{-[ln(30) - 2.047]}{0.930}\right\}} \qquad \text{(Eq. 4-23)}$$

In addition, the duration-dependent damping correction is recommended for high magnitude ATR regions. The prediction of uni-directional isolator demands using these modifications for highly-damped FPS systems is plotted in Figures G4.3-2 through G4.3-5, APPENDIX G4. To clarify, the record set plots are nonlinear response history analysis results, averaged for 14 records in each set, while the other plots are various permutations of the simplified procedure.

For LRB systems, the maximum theoretical damping is only slightly larger than the AASHTO cap of 30%. So a modified spectral shape in accord with that outlined above combined with the standard AASHTO damping rule is recommended. Response results from simplified method analyses compared to nonlinear RHA results are summarized in Tables G4.3-6 through G4.3-9. Figures G4.3-10 through G4.3-13 illustrate the effect on response in moving from an ATR site to a NMSZ site of similar distance to a near-field NMSZ site.

The final topic of this chapter is a study on sample size requirements for estimating isolator demand.

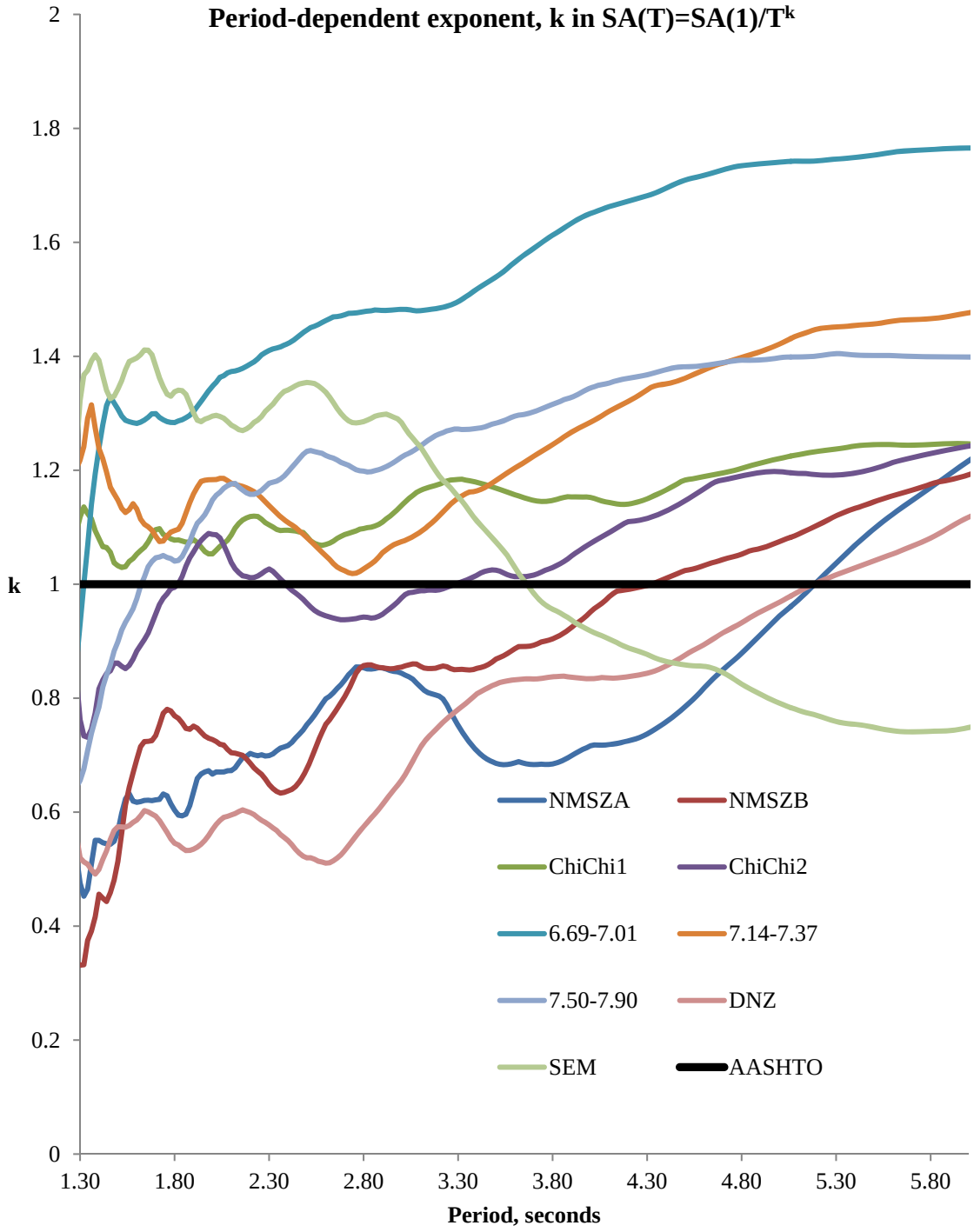

Figure 4.3-1. Exponent on Period for Various Ground Motion Record Sets

4.4 Sample Size Considerations

Seismic input is generally taken to be log-normally distributed. That is to say, PSHA spectral accelerations themselves are not normally distributed, but the logarithm of spectral acceleration is normally distributed. This is reflected in ground motion prediction equations, which predict ln(SA) and standard deviation of ln(SA) as opposed to SA and standard deviation of SA.

So it seems logical to consider the response to seismic loading as be log-normally distributed as well. This point has been identified by previous researchers as well (Hancock, et al., 2008). This is the underlying reason that the geometric mean is the appropriate measure of response to a series of nonlinear response history results. If the logarithm of response is normally distributed then:

$$\overline{ln(x)} = \frac{1}{n}\sum ln(x_i) \qquad \text{(Eq. 4-24)}$$

$$\bar{x} = e^{\overline{ln(x)}} = e^{\frac{1}{n}\sum ln(x_i)} = \left[\prod x_i\right]^{\frac{1}{n}} \qquad \text{(Eq. 4-25)}$$

The final result in the second expression is nothing more than the geometric mean of the sample.

Continuing under the assumption that nonlinear response to seismic input is log-normally distributed, it is possible to place confidence intervals on our estimate of mean (geometric mean) response. For sample sizes less than 30, it is more accurate to use the student's t-distribution instead of the normal distribution when the true standard deviation is unknown, as is the case here. For sample sizes greater than about 30, the t-distribution approaches the normal distribution. So we can use the t-distribution along with our estimate of the geometric mean and standard deviation of *ln(x)*.

Suppose we wish to cap the geometric mean response within ***q***% with a confidence level of ***p***%. We know the sample mean of *ln(x)*, the standard deviation of *ln(x)*, and t_{cr} - the t-value which provides the desired level of confidence. In order to cap the estimated geometric mean within ***q***%, we require:

$$e^{\left[\overline{ln(x)}+\frac{t_{cr}s_{ln(x)}}{\sqrt{n}}\right]} \leq \bar{x}\left(1+\frac{p}{100}\right) \qquad \text{(Eq. 4-26)}$$

$$\overline{ln(x)}+\frac{t_{cr}s_{ln(x)}}{\sqrt{n}} \leq ln\left[\bar{x}\left(1+\frac{p}{100}\right)\right] \qquad \text{(Eq. 4-27)}$$

$$n \geq \left\{\frac{t_{cr}s_{ln(x)}}{ln\left[\bar{x}\left(1+\frac{p}{100}\right)\right]-\overline{ln(x)}}\right\}^2 \qquad \text{(Eq. 4-28)}$$

The equation cannot be solved in closed form because t_{cr} is actually a function of the sample size ***n***. The iterative procedure can be automated and has been to compute results for the data set obtained from the nonlinear analyses here. For automating the process, it is actually more convenient to solve the above for t_{cr} and change ***n*** until the desired confidence interval is obtained.

$$t_{cr} \leq \left\{ln\left[\bar{x}\left(1+\frac{p}{100}\right)\right]-\overline{ln(x)}\right\}\frac{\sqrt{n}}{s_{\ln(x)}} \qquad \text{(Eq. 4-29)}$$

The data sets obtained from the nonlinear analyses obtained for the LRB and FPS model isolators are given in Tables 4.4-1 through 4.4-5.

As an example, suppose we wish to estimate the geometric mean of LRB-ISOLATOR 06 subjected to the Chi-Chi 1 record set. The desired confidence level is 90% and the desired error is 20%. From Table 4.4-4, find the following.

$$\bar{x} = (D_{ISO})_{GM} = 9.319\ inches$$

$$\overline{ln(x)} = 2.232$$

$$S_{ln(x)} = 0.690$$

Initially, assume a sample size ***n*** = 7 - the typical value required in design specifications. Recall that the number of degrees of freedom for the t-distribution is ***(n-1)***. From statistical tables for the student's t-distribution or from the Excel function:

T.INV(0.90,6), determine t_{cr} = 1.440

To obtain the desired accuracy with the desired level of confidence, we require:

$$t_{cr} \leq \left\{ln\left[\bar{x}\left(1+\frac{p}{100}\right)\right] - \overline{ln(x)}\right\}\frac{\sqrt{n}}{s_{\ln(x)}}$$

$$t_{cr} \leq \left\{ln\left[9.319\left(1+\frac{20}{100}\right)\right] - 2.232\right\}\frac{\sqrt{7}}{0.690} = 0.699$$

$$1.440 > 0.699 \rightarrow No\ good$$

In fact, successive iteration will demonstrate that a sample size of ***n****=25* is required to obtain the desired result.

The procedure has been automated in Excel and results for LRB and FPS systems are summarized in Tables 4.4-6 and 4.4-7. The tables are based on achieving a 90% confidence level on capping the estimated mean within 20% of the true mean.

Trends can be identified by plotting required sample size versus $\mu = Q_d/W$ for various yielded periods. These plots are presented in Figures G4.4-1, G4.4-2, and G4.4-3 for LRB Isolators, for FPS Isolators, and for the case in which all Isolators - both FPS and LRB - have been combined into a data set. For FPS isolators, at yielded periods within the 1.7-3.3 second range, it appears that the dependence of sample size upon Qd/W value is not as significant as for

LRB isolators. Regardless, it is evident that sample size requirements are dependent upon both $\mu = Q_d/W$ and the yielded period, T_d.

Another way of looking at the problem is to determine the accuracy of the estimate of the geometric mean at the 90% confidence level using the standard sample size of $\boldsymbol{n} = 7$. This is shown in Figure G4.4-4. Clearly, the accuracy obtained is a function of yielded period, T_d, and $\mu = Q_d/W$ with the possible exception on the case in which $T_d = 1.79$ seconds, for which the accuracy appears independent of μ. The figure has been produced by combining LRB and FPS data sets above.

Estimates of isolator demand depend upon sample size as well as on type of mean adopted. To demonstrate this arithmetic-mean-based and geometric-mean-based statistics were computed and are summarized in Figures G4.4-5 through G4.4-16 for some of the record sets. Other plots not shown have similar characteristics. Clearly, two researchers - one adopting a geometric mean and the other adopting an arithmetic mean - will come up with different conclusions in nonlinear response history analysis. It is noted that the arithmetic mean is frequently an approximation to the geometric-mean plus one-sigma and the geometric mean is frequently approximated by the arithmetic mean minus one-sigma.

Table 4.4-1. Darfield, NZ Data Set for Sample Size Analysis

ISOLATOR	LRB, $\alpha = 0.10$			FPS, $\alpha = 0.0001$		
	$x = (D_{ISO})_{GM}$	ln(x)	$S_{ln(x)}$	$x = (D_{ISO})_{GM}$	ln(x)	$S_{ln(x)}$
01	17.496	2.862	0.559	16.733	2.817	0.576
02	18.087	2.895	0.572	18.615	2.924	0.566
03	18.118	2.897	0.666	18.065	2.894	0.648
04	14.048	2.643	0.505	14.394	2.667	0.484
05	11.906	2.477	0.407	12.208	2.502	0.398
06	13.457	2.600	0.471	9.992	2.302	0.526
07	12.153	2.498	0.611	11.410	2.435	0.670
08	11.111	2.408	0.631	11.003	2.398	0.686
09	9.811	2.284	0.537	9.678	2.270	0.584
10	8.369	2.125	0.483	8.410	2.129	0.498
11	11.976	2.483	0.410	7.033	1.951	0488
12	9.164	2.215	0.545	7.498	2.015	0.614
13	7.952	2.073	0.532	7.251	1.981	0.632
14	7.187	1.972	0.494	6.824	1.920	0.599
15	6.270	1.836	0.456	6.033	1.797	0.524
16	11.761	2.465	0.393	5.765	1.752	0.467
17	7.861	2.062	0.491	5.792	1.756	0576
18	6.688	1.900	0.472	5.672	1.736	0.580
19	6.023	1.796	0.454	5.492	1.703	0.571
20	5.336	1.674	0.421	5.016	1.613	0.531

Table 4.4-2. NMSZ1 Data Set for Sample Size Analysis

ISOLATOR	LRB, α = 0.10			FPS, α = 0.0001		
	$x = (D_{ISO})_{GM}$	ln(x)	$S_{ln(x)}$	$x = (D_{ISO})_{GM}$	ln(x)	$S_{ln(x)}$
01	20.678	3.029	0.767	17.208	2.845	0.843
02	17.301	2.851	0.611	16.630	2.811	0.630
03	14.495	2.674	0.470	14.137	2.649	0.489
04	12.769	2.547	0.525	12.680	2.540	0.556
05	12.219	2.503	0.528	12.067	2.490	0.517
06	14.986	2.707	0.633	9.941	2.297	0.735
07	11.765	2.465	0.526	9.498	2.251	0.655
08	9.481	2.249	0.461	7.978	2.077	0.537
09	8.182	2.102	0.486	7.294	1.987	0.565
10	7.380	1.999	0.475	6.656	1.895	0.541
11	13.371	2.593	0.433	5.648	1.731	0.619
12	9.041	2.202	0.441	5.236	1.656	0.658
13	7.084	1.958	0.437	4.765	1.561	0.575
14	6.043	1.799	0.447	4.527	1.510	0.543
15	5.427	1.691	0.359	4.167	1.427	0.505
16	12.588	2.533	0.367	4.316	1.462	0.634
17	7.963	2.075	0406	3.789	1.332	0.610
18	6.114	1.811	0.400	3.567	1.272	0.602
19	5.275	1.663	0.391	3.302	1.195	0.573
20	4.543	1.514	0.322	3.124	1.139	0.537

Table 4.4-3. NMSZ2 Data Set for Sample Size Analysis

ISOLATOR	LRB, $\alpha = 0.10$			FPS, $\alpha = 0.0001$		
	$x = (D_{ISO})_{GM}$	ln(x)	$S_{ln(x)}$	$x = (D_{ISO})_{GM}$	ln(x)	$S_{ln(x)}$
01	16.196	2.785	0.471	13.840	2.628	0.524
02	16.665	2.813	0.563	15.810	2.761	0.589
03	15.426	2.736	0.348	15.033	2.710	0.356
04	12.719	2.543	0.341	12.416	2.519	0.333
05	10.758	2.376	0.377	10.702	2.370	0.413
06	12.681	2.540	0.386	8.822	2.177	0.474
07	11.568	2.448	0.445	9.326	2.233	0.541
08	10.098	2.312	0.312	8.629	2.155	0.366
09	8.943	2.191	0.316	8.169	2.100	0.354
10	7.745	2.047	0.331	7.039	1.952	0.361
11	12.099	2.493	0.321	5.966	1.786	0.455
12	8.783	2.173	0.273	5.485	1.702	0.518
13	7.554	2.022	0.338	5.209	1.650	0.517
14	6.795	1.916	0.368	5.050	1.619	0.491
15	5.977	1.788	0.390	4.750	1.558	0.460
16	11.793	2.467	0.280	4.871	1.583	0.482
17	7.959	2.074	0.272	4.263	1.450	0.507
18	6.778	1.914	0.358	4.064	1.402	0.543
19	6.033	1.797	0.379	3.886	1.357	0.546
20	5.108	1.631	0.415	3.607	1.283	0.523

Table 4.4-4. Chi-Chi 1 Data Set for Sample Size Analysis

ISOLATOR	LRB, $\alpha = 0.10$			FPS, $\alpha = 0.0001$		
	$x = (D_{ISO})_{GM}$	ln(x)	$S_{ln(x)}$	$x = (D_{ISO})_{GM}$	ln(x)	$S_{ln(x)}$
01	11.539	2.446	0.949	10.846	2.384	0.988
02	9.535	2.255	0.724	9.639	2.266	0.737
03	8.774	2.172	0.711	9.159	2.215	0.709
04	8.502	2.140	0.631	8.765	2.171	0.641
05	7.628	2.032	0.491	7.709	2.042	0.489
06	9.319	2.232	0.690	6.061	1.802	0.802
07	6.722	1.905	0.521	5.636	1.729	0.640
08	5.940	1.782	0.500	5.330	1.673	0.600
09	5.354	1.678	0.502	5.077	1.625	0.569
10	4.867	1.583	0.437	4.695	1.547	0.476
11	8.518	2.142	0.502	3.513	1.256	0.632
12	5.645	1.731	0.365	3.285	1.189	0.569
13	4.771	1.563	0.371	3.118	1.137	0543
14	4.172	1.428	0.364	2.958	1.085	0.520
15	3.664	1.298	0.340	2.822	1.037	0.496
16	8.336	2.121	0.430	2.444	0.894	0564
17	5.299	1.668	0.284	2.260	0.815	0.543
18	4.288	1.456	0.293	2.148	0.765	0.551
19	3.652	1.295	0.293	2.075	0.730	0.553
20	3.097	1.130	0.309	1.983	0.685	0.555

Table 4.4-5. Chi-Chi 2 Data Set for Sample Size Analysis

ISOLATOR	LRB, α = 0.10			FPS, α = 0.0001		
	$x = (D_{ISO})_{GM}$	ln(x)	$S_{ln(x)}$	$x = (D_{ISO})_{GM}$	ln(x)	$S_{ln(x)}$
01	11.790	2.467	0.916	10.482	2.350	0.991
02	11.511	2.443	0.605	11.134	2.410	0.634
03	10.026	2.305	0.583	10.500	2.351	0.604
04	8.818	2.177	0.570	8.797	2.174	0.550
05	8.088	2.090	0.401	8.279	2.114	0.406
06	9.411	2.242	0.587	6.353	1.849	0.775
07	7.291	1.987	0.540	5.924	1.779	0.651
08	6.468	1.867	0.480	5.865	1.769	0622
09	5.840	1.765	0.460	5.443	1.694	0.540
10	5.371	1.681	0.370	5.131	1.635	0.418
11	8.655	2.158	0.495	3.921	1.366	0.673
12	5.823	1.762	0.427	3.630	1.289	0.611
13	4.946	1.599	0.372	3.531	1.262	0.550
14	4.371	1.475	0.330	3.460	1.241	0.491
15	3.929	1.368	0.312	3.365	1.214	0.441
16	8.534	2.144	0.452	2.911	1.069	0.672
17	5.280	1.664	0.378	2.604	0.957	0.629
18	4.465	1.496	0.303	2.482	0.909	0.582
19	3.865	1.352	0.293	2.430	0.888	0.527
20	3.351	1.209	0.291	2.374	0.865	0.485

Table 4.4-6. Sample Size Requirements - LRB Model Isolators

ISOLATOR	*Req'd Sample Size, n (90% CL, capped within 20%)*					
	DNZ	**NMSZ1**	**NMSZ2**	**ChiChi1**	**ChiChi2**	**Average**
01	17	31	13	46	43	30
02	18	20	18	28	20	21
03	24	13	8	27	19	19
04	14	15	8	22	18	16
05	10	16	9	14	10	12
06	13	22	9	25	19	18
07	20	16	12	15	16	16
08	22	12	7	14	13	14
09	16	14	7	14	12	13
10	13	13	7	11	9	11
11	10	11	7	14	14	12
12	17	12	6	9	11	11
13	16	11	8	9	9	11
14	14	12	9	8	7	10
15	12	8	9	8	7	9
16	10	9	6	11	12	10
17	14	10	6	6	9	9
18	13	10	8	6	7	9
19	12	9	9	6	6	9
20	11	7	10	7	6	9

Table 4.4-7. Sample Size Requirements - FPS Model Isolators

ISOLATOR	*Req'd Sample Size, n (90% CL, capped within 20%)*					
	DNZ	**NMSZ1**	**NMSZ2**	**ChiChi1**	**ChiChi2**	**Average**
01	18	37	15	50	50	34
02	18	21	19	29	22	22
03	23	14	8	27	20	19
04	13	17	7	22	17	16
05	10	15	10	14	10	12
06	16	29	13	34	32	25
07	24	23	16	22	23	22
08	25	16	9	20	21	19
09	19	18	8	18	16	16
10	14	16	8	13	11	13
11	14	21	12	22	24	19
12	21	23	15	18	20	20
13	22	18	15	16	17	18
14	20	16	14	15	14	16
15	15	14	12	14	12	14
16	13	22	13	18	24	18
17	18	20	15	16	21	18
18	19	20	16	17	19	19
19	18	18	17	17	16	18
20	16	16	15	17	13	16

CHAPTER 5 – NON-ISOLATED STRUCTURE DETAILS

With a set of design ground motions from CHAPTER 3, it is now possible to design isolators for each of the six bridges. Before taking on that task, however, it will be beneficial to evaluate design details of the non-isolated structures. This chapter provides a summary of the structural details pertinent to the non-isolated (Type 1 construction) seismic response of the selected structures. Of primary interest are the details of piling for the steel pile bent bridges (1 through 4) and design requirements for pile caps and pre-stressed piling for the multi-post bent bridges (5 and 6). These are the elements which will potentially be affected the most by the incorporation of isolation devices at the bearings.

First, the plastic shear and the yield displacement for substructures will be determined in Section 5.1. In order for isolation to be effective for pile bent bridges 1-4, the piling shears experienced during strong ground shaking must be well below the plastic shear. Otherwise, the piles would be required to form plastic hinges and meet requirements for ductile elements, which are much more stringent than requirements for elements which behave elastically. Effectiveness of isolation for multi-column bents for bridges 5 and 6 will be largely dependent upon the savings in number of piles, with additional savings possible in column and bent cap reinforcement. The plastic shears and yield displacements will also be needed for the preliminary design of the isolators in CHAPTER 6.

Next, in Section 5.2, various code requirements for the substructures are summarized to support the choices made for the proposed type of piling for the bridges.

In Section 5.3, results from a response spectrum analysis for each bridge in the non-isolated condition are summarized. This chapter is devoted primarily to analysis of the non-

isolated bridges so that comparisons to the isolated bridges may be made in CHAPTER 7. These results are presented in the form of displacement ductility requirements for each non-isolated structure at each bridge site. Displacement ductility demands are compared to values permitted by the AASHTO Specifications for LRFD Seismic Bridge Design (AASHTO, 2009) discussed in Section 5.3.

5.1 Yield Displacement and Plastic Shear

Before describing the piling required for the non-isolated bridges, a discussion of pile types frequently used in bridges similar to the ones used for this study is appropriate. Standard piling types currently used in Tennessee for friction pile applications include each of the following:

1. Prestressed concrete piling - 36 cm, 41 cm, and 46 cm (14”, 16”, and 18”) square
2. Steel pipe piling

Un-factored pile loads are typically in the range of 445-667 kN (100-150 kips) with driving loads in the range of 800-1334 kN (180-300 kips). A pile axial load of 623 kN (140 kips) is used to establish approximate values for yield displacements and shears.

The following standard pile cross-sections are considered for this study.

1. 51 cm x 0.8 cm (20” x 5/16”) steel pipe piles, F_y = 241 MPa (35 ksi); this cross-section would qualify as “essentially elastic” (see Section 5.2) with a D/t ratio of 64;
2. 51 cm x 1.6 cm (20” x 5/8”) steel pipe piles, F_y = 241 MPa (35 ksi); this cross-section would qualify as “ductile” (see Section 5.2) with a D/t ratio of 32;

Full fixity is assumed at both the in-ground hinge and at the top of the pile, resulting in rigid-frame behavior in the transverse direction. Cantilever-type behavior is assumed in the longitudinal direction. Care must be taken to track substructure displacements at the top of the piles from computer model results in order to be consistent with the stiffness calculations made here. The in-ground hinge is assumed to be coincident with the effective point of fixity which is taken to be approximately 5 pile diameters below the ground surface (Priestley, et al., 1996). The term "approximate" is appropriate here since no modification to the depth to fixity was made for the various pile types. A point of contra-flexure is assumed at mid-height of each pile.

The AASHTO LRFD Bridge Design Specifications (commentary to Article 10.7.3.13.4) provide estimates of fixity depths for piles in either clay or sand as follows.

For clays:

$$D_F = 1.4\left(\frac{E_P I_P}{E_S}\right)^{0.25} \qquad \text{(Eq. 5-1)}$$

$$E_S = 0.465 S_u, ksi - soil\ modulus$$

$$S_u = undrained\ shear\ strength, ksf$$

$$E_P = elastic\ modulus\ for\ pile, ksi$$

$$I_P = moment\ of\ inertia\ for\ pile, ft^4$$

For sands:

$$D_F = 1.8\left(\frac{E_P I_P}{n_h}\right)^{0.20} \qquad \text{(Eq. 5-2)}$$

$$n_h = rate\ of\ increase\ of\ soil\ modulus\ with\ depth, ksi/ft$$

Furthermore, for a pile spacing of 3 diameters, the effective soil modulus is reduced to 25% of the single pile value. For a spacing of 8 diameters, group effects are negligible. For intermediate pile spacing, liner interpolation is used.

With these assumptions in hand, the yield displacement and shear may be calculated from basic equations for rigid frame (transverse) and cantilever (longitudinal) behavior.

$$\left(V_{yT}\right)_{PILE} = \frac{2M_n}{L_C} \quad \text{(Eq. 5-3)}$$

$$\left(D_{yT}\right)_{PILE} = \frac{\left(V_{yT}\right)_{PILE} L_C^3}{12(EI_{EFF})} = \frac{M_n L_C^2}{6(EI_{EFF})} \quad \text{(Eq. 5-4)}$$

$$\left(V_{yL}\right)_{PILE} = \frac{M_n}{H} \quad \text{(Eq. 5-5)}$$

$$\left(D_{yL}\right)_{PILE} = \frac{M_n L_C^2}{3(EI_{EFF})} \cdot \left(\frac{3}{2} - \frac{L_C}{2H}\right) \quad \text{(Eq. 5-6)}$$

The effective moment of inertia, I_{EFF}, for all steel pipe piles is taken to be I_G (I_G is the gross moment of inertia). The expression for longitudinal yield displacement has been derived by applying the conjugate beam principle and assuming a rigid zone between the top of the pile and the superstructure center of gravity. In the above equations, L_C is the clear height of the pile from the point of fixity in the ground to the top of the pile and H is the distance from the center of gravity of the superstructure to the point of fixity. The results are summarized in Tables 5.1-1 through 5.1-8 for each of the pile types considered in pile bent bridge structures Nos. 1 through 4.

Noting that each bent consists of 9 piles for Bridges No. 1 and 2 and 7 piles for Bridges No. 3 and No. 4, the total plastic shear at each substructure may then be computed. This value will be important in selecting and designing appropriate isolators, whether LRB or FPS systems, for the bridges. The idea being that the isolators should limit the shear into each substructure to a value well below the plastic shear calculated here.

For Bridges 5 and 6 with reinforced concrete column bents, similar equations will be used to estimate yield displacements. Approximate axial loads are 2313 kN (520 kips) per column (2-post bent) for Bridge No. 5 and 3336 kN (750 kips) per column (3-post bent) for Bridge No. 6. The columns are 107 cm (42 inches) square, but with 22 25 mm (No. 8) bars arranged in a circular pattern – a common configuration in West Tennessee multi-post bent bridges. The resulting nominal moment capacities are 2995 kN-m (2,209 ft-kips) per column for Bridge No. 5 and 3334 kN-m (2,459 ft-kips) per column for Bridge No. 6. Yield displacements are estimated from the approximate expression for yield curvature common in displacement based seismic design of reinforced concrete columns from the literature (Priestley, et al., 2007). A detailed section analysis may be performed to verify results, but the equation has been shown to be valid and to provide reasonable estimates of yield curvature. The ensuing expression for yield displacement has been derived for fixity at both column ends and for a strain penetration distance of 23 cm (9”) at each hinge location – top and bottom.

$$\phi_y = \frac{2.1\varepsilon_y}{h_c} = \frac{2.1 \times 60}{29{,}000 \times 42} = 0.00010345\ in^{-1} \qquad \text{(Eq. 5-7)}$$

$$D_y = \frac{2}{3}\phi_y \left(\frac{L_C}{2} + 9\right)^2 \qquad \text{(Eq. 5-8)}$$

The issue remains as to modeling of the abutment piles. Literature is available which outlines theoretical load-deflection behavior of fixed head embedded piles. A somewhat soft, cohesion-less material will be assumed for purposes of this study. No rigorous parametric study of abutment piles stiffness and strength will be attempted. Rather, reasonable values based on equations in the literature (Song, et al., 2004) have been used to establish the following modeling parameters for abutment piles. It is clear from the literature that a wide range of values is possible for various fill materials and a detailed parametric study would be a separate research topic in itself.

$$K_{PILE} = 35\ \frac{kN}{cm}\left(20\frac{kips}{inch}\right)\ per\ pile \qquad \text{(Eq. 5-9)}$$

$$D_y = 5\ cm\ (2.00)\ inches \qquad \text{(Eq. 5-10)}$$

Some designers rely upon passive pressure on abutment back-walls to assist in carrying longitudinal seismic effects. The practice is permitted – with Owner's consent – in the AASHTO Guide Specification for LRFD Seismic Bridge Design (AASHTO, 2009) but will not be used here. The sole source of stiffness contribution from the abutments to lateral response will be the pile stiffness.

An interaction equation for yield displacement during biaxial bending is needed. Using the above expressions for rigid frame behavior transversely and cantilever behavior longitudinally the development proceeds as follows.

$$M_L = V_L H = \frac{6EID_{SUB-L}}{L_C^2\left(3 - \frac{L_C}{H}\right)} \qquad \text{(Eq. 5-11)}$$

$$M_T = V_T\frac{L_C}{2} = \frac{6EID_{SUB-T}}{L_C^2} \qquad \text{(Eq. 5-12)}$$

Yield is reached when the resultant moment is equal to M_n.

$$M_r = \sqrt{\left[\frac{6EID_{SUB-L}}{L_C^2\left(3-\frac{L_C}{H}\right)}\right]^2 + \left[\frac{6EID_{SUB-T}}{L_C^2}\right]^2} = M_n \qquad \text{(Eq. 5-13)}$$

$$\frac{6EI}{L_C^2}\sqrt{\left[\frac{D_{SUB-L}}{3-\frac{L_C}{H}}\right]^2 + [D_{SUB-T}]^2} = M_n \qquad \text{(Eq. 5-14)}$$

$$\sqrt{\left[\frac{D_{SUB-L}}{3-\frac{L_C}{H}}\right]^2 + [D_{SUB-T}]^2} = \frac{M_n L_C^2}{6EI} = \frac{\phi_y L_C^2}{6} \qquad \text{(Eq. 5-15)}$$

Table 5.1-1. Bridge 1 Bent Analysis – 20” x 5/8” Steel Pipe

Direction	Bent	L_C, in.	H, in.	M_n, ft-k	V_y, k/pile	D_y, inches	K_{SUB}, k/in
Trans. (9 Piles)	1	180	270	682	90.9	0.852	960
	2	180	270		90.9	0.852	960
	3	180	270		90.9	0.852	960
	4	180	270		90.9	0.852	960
Long. (9 Piles)	1	180	270	682	30.3	1.990	137
	2	180	270		30.3	1.990	137
	3	180	270		30.3	1.990	137
	4	180	270		30.3	1.990	137

Table 5.1-2. Bridge 2 Bent Analysis – 20” x 5/8” Steel Pipe

Direction	Bent	L_C, in.	H, in	M_n, ft-k	V_y, k/pile	D_y, inches	K_{SUB}, k/in
Trans. (9 Piles)	1	180	270	682	90.9	0.852	960
	2	180	270		90.9	0.852	960
	3	420	510		39.0	4.643	76
	4	420	510		39.0	4.643	76
Long. (9 Piles)	1	180	270	682	30.3	1.990	137
	2	180	270		30.3	1.990	137
	3	420	510		16.0	10.105	161
	4	420	510		16.0	10.105	59

Table 5.1-3. Bridge 3 Bent Analysis – 20” x 5/8” Steel Pipe

Direction	Bent	L_C, in.	H, in.	M_n, ft-k	V_y, k/pile	D_y, inches	K_{SUB}, k/in
Trans. (7 Piles)	1	180	283	682	90.9	0.852	746
	2	180	283		90.9	0.852	746
	3	180	283		90.9	0.852	746
	4	180	283		90.9	0.852	746
	5	180	283		90.9	0.852	746
	6	180	283		90.9	0.852	746
	7	180	283		90.9	0.852	746
Long. (7 Piles)	1	180	283	682	28.9	2.016	100
	2	180	283		28.9	2.016	100
	3	180	283		28.9	2.016	100
	4	180	283		28.9	2.016	100
	5	180	283		28.9	2.016	100
	6	180	283		28.9	2.016	100
	7	180	283		28.9	2.016	100

Table 5.1-4. Bridge 4 Bent Analysis – 20” x 5/8” Steel Pipe

Direction	Bent	L_C, in.	H, in.	M_n, ft-k	V_y, k/pile	D_y, inches	K_{SUB}, k/in
Trans. (7 Piles)	1	180	283	682	90.9	0.852	746
	2	180	283		90.9	0.852	746
	3	300	403		54.6	2.369	161
	4	420	523		39.0	4.640	76
	5	300	403		54.6	2.369	161
	6	180	283		90.9	0.852	746
	7	180	283		90.9	0.852	746
Long. (7 Piles)	1	180	283	682	28.9	2.016	100
	2	180	283		28.9	2.016	100
	3	300	403		20.3	5.343	27
	4	420	523		15.6	10.200	11
	5	300	403		20.3	5.343	27
	6	180	283		28.9	2.016	100
	7	180	283		28.9	2.016	100

Table 5.1-5. Bridge 1 Bent Analysis – 20” x 5/16” Steel Pipe

Direction	Bent	L_C, in.	H, in.	M_n, ft-k	V_y, k/pile	D_y, inches	K_{SUB}, k/in
Trans. (9 Piles)	1	180	270	345	46.0	0.823	503
	2	180	270		46.0	0.823	503
	3	180	270		46.0	0.823	503
	4	180	270		46.0	0.823	503
Long. (9 Piles)	1	180	270	345	15.3	1.920	72
	2	180	270		15.3	1.920	72
	3	180	270		15.3	1.920	72
	4	180	270		15.3	1.920	72

Table 5.1-6. Bridge 2 Bent Analysis – 20” x 5/16” Steel Pipe

Direction	Bent	L_C, in.	H, in	M_n, ft-k	V_y, k/pile	D_y, inches	K_{SUB}, k/in
Trans. (9 Piles)	1	180	270	345	46.0	0.823	503
	2	180	270		46.0	0.823	503
	3	420	510		19.7	4.481	40
	4	420	510		19.7	4.481	40
Long. (9 Piles)	1	180	270	345	15.3	1.920	72
	2	180	270		15.3	1.920	72
	3	420	510		8.1	9.752	7.5
	4	420	510		8.1	9.752	7.5

Table 5.1-7. Bridge 3 Bent Analysis – 20” x 5/16” Steel Pipe

Direction	Bent	L_C, in.	H, in.	M_n, ft-k	V_y, k/pile	D_y, inches	K_{SUB}, k/in
Trans. (7 Piles)	1	180	283	345	46.0	0.823	391
	2	180	283		46.0	0.823	391
	3	180	283		46.0	0.823	391
	4	180	283		46.0	0.823	391
	5	180	283		46.0	0.823	391
	6	180	283		46.0	0.823	391
	7	180	283		46.0	0.823	391
Long. (7 Piles)	1	180	283	345	14.6	1.945	53
	2	180	283		14.6	1.945	53
	3	180	283		14.6	1.945	53
	4	180	283		14.6	1.945	53
	5	180	283		14.6	1.945	53
	6	180	283		14.6	1.945	53
	7	180	283		14.6	1.945	53

Table 5.1-8. Bridge 4 Bent Pile Analysis – 20” x 5/16” Steel Pipe

Direction	Bent	L_C, in.	H, in.	M_n, ft-k	V_y, k/pile	D_y, inches	K_{SUB}, k/in
Trans. (7 Piles)	1	180	283	345	46.0	0.823	391
	2	180	283		46.0	0.823	391
	3	300	403		27.6	2.286	84
	4	420	523		19.7	4.481	31
	5	300	403		27.6	2.286	84
	6	180	283		46.0	0.823	391
	7	180	283		46.0	0.823	391
Long. (7 Piles)	1	180	283	345	14.6	1.945	53
	2	180	283		14.6	1.945	53
	3	300	403		10.3	5.156	14
	4	420	523		7.9	9.844	5.6
	5	300	403		10.3	5.156	14
	6	180	283		14.6	1.945	53
	7	180	283		14.6	1.945	53

Table 5.1-9. Bridge 5 Column Analysis – 42" Square Columns

Direction	Bent	L_C, in.	H, in.	M_n, ft-k	V_y, k/col	D_y, inches	K_{SUB}, k/in
Trans. (2 columns)	1	180	303	2,209	294.5	0.676	871
	2	180	303		294.5	0.676	871
Long. (2 columns)	1	180	303	2,209	87.5	1.625	107
	2	180	303		87.5	1.625	107

Table 5.1-10. Bridge 6 Column Analysis – 42" Square Columns

Direction	Bent	L_C, in.	H, in.	M_n, ft-k	V_y, k/col	D_y, inches	K_{SUB}, k/in
Trans. (3 Columns)	1	180	308	2,459	327.9	0.676	1,454
Long. (3 columns)	1	180	308	2,459	95.8	1.634	176

5.2 Code Requirements

The AASHTO Guide Specification for LRFD Seismic Bridge Design (AASHTO, 2009) is the basis for the design of the piling for seismic effects.

The pile bent substructures are treated as multi-column bents for seismic design purposes. Guide Specification Article 4.9 limits the displacement ductility demand on multi-column bents to:

$$\mu_D =\leq 6 \qquad \text{(Eq. 5-16)}$$

Article 4.9 of the Guide Specification further limits the displacement ductility for prestressed concrete piling to:

$$\mu_D =\leq 4 \qquad \text{(Eq. 5-17)}$$

Article 5.2.4.2 states the following additional requirement for piles at the abutments:

> "For pile-supported abutment foundations, the stiffness contribution of piles less than or equal to 18 in. in diameter or width shall be ignored if the abutment displacement is

greater than 4 in. unless a displacement capacity analysis of the piles is performed and the piles are shown to be capable of accommodating the demands."

Therefore, for displacements greater than 4 inches at abutments and for displacement ductility demands greater than 4 at bents, pipe piles will be required.

The Guide Specification distinguishes between "ductile" and "essentially elastic" structural steel elements. Article 7.4 sets the following limits on member dimensions for pipe piling.

For ductile elements:

$$\lambda_c = \left(\frac{KL}{r\pi}\right)\sqrt{\frac{F_y}{E}} \leq 0.75 \qquad \text{(Eq. 5-18)}$$

$$\lambda_b = \frac{L}{r_y} \leq \frac{0.086E}{F_y} \qquad \text{(Eq. 5-19)}$$

$$\frac{D}{t} \leq \frac{0.044E}{F_y} \qquad \text{(Eq. 5-20)}$$

For essentially elastic elements:

$$\lambda_c = \left(\frac{KL}{r\pi}\right)\sqrt{\frac{F_y}{E}} \leq 1.50 \qquad \text{(Eq. 5-21)}$$

$$\lambda_b = \frac{L}{r_y} \leq 4.40\sqrt{\frac{E}{F_y}} \qquad \text{(Eq. 5-22)}$$

$$\frac{D}{t} \leq \frac{0.09E}{F_y} \qquad \text{(Eq. 5-23)}$$

The D/t requirement alone provides evidence that there may be a distinct cost advantage with regard to piling if inelastic behavior in the piling can be avoided.

Further, for any type piling in a pile bent used for Seismic Design Category C or D, AASHTO places a limit on the P-Delta effects to preclude geometric instability.

$$P_{DL}\Delta_r \leq 0.25M_n \qquad \text{(Eq. 5-24)}$$

In equation 5-24, Δ_r is the relative displacement between the point of contra-flexure and the maximum moment point.

5.3 Response Spectrum Analysis Results – Non-isolated Structures

Linear response spectrum analyses for each level of earthquake hazard at each site were conducted for the non-isolated bridges to determine the estimated displacement ductility demands at each substructure. In order to capture behavior at both extremes of the possible piling options for bridges 1 through 4, analyses were conducted for the case in which 20” x 5/16” steel pipe piles are used at each bent and for the case in which 20” x 5/8” steel pipe piles are used at each bent. All response spectrum analyses were for the 5% damped elastic spectra.

It is not unusual for structures of the types studied here to fall within the so-called “short-period” classification and require amplification of linear response spectrum results to estimate nonlinear response. The AASHTO requirements (AASHTO, 2010) state that response spectrum displacements should be magnified by R_d when T*/T is greater than 1.0.

$$T^* = 1.25T_S = 1.25\frac{S_{D1}}{S_{DS}} \qquad \text{(Eq. 5-25)}$$

$$R_d = \left(1 - \frac{1}{\mu_D}\right)\frac{T^*}{T} + \frac{1}{\mu_D} \qquad \text{(Eq. 5-26)}$$

So that, given the response spectrum displacement, D_{RSA}, one may determine the displacement demand, D_{DEM}, as follows:

$$D_{DEM} = R_d D_{RSA} \qquad \text{(Eq. 5-27)}$$

Note, however, that R_d is a function of the displacement ductility demand, μ_D, which is in turn, a function of total displacement, D_{DEM}. So, a little algebra is required to arrive at a final result unless an iterative procedure is implemented.

$$D_{DEM} = \mu_D D_y = D_{RSA}\left[\left(1 - \frac{1}{\mu_D}\right)\frac{T^*}{T} + \frac{1}{\mu_D}\right]$$

$$\mu_D^2 D_y = D_{RSA}\left(\mu_D \frac{T^*}{T} - \frac{T^*}{T} + 1\right)$$

$$\mu_D^2 D_y - \mu_D\left(D_{RSA}\frac{T^*}{T}\right) + D_{RSA}\left(\frac{T^*}{T} - 1\right) = 0$$

$$\mu_D = \frac{\left(D_{RSA}\frac{T^*}{T}\right) \pm \sqrt{\left(D_{RSA}\frac{T^*}{T}\right)^2 - 4D_{RSA}\left(\frac{T^*}{T} - 1\right)D_y}}{2D_y} \qquad \text{(Eq. 5-28)}$$

So, whenever T*/T is greater than 1.0, the above quadratic equation will be solved to establish the displacement ductility demand. Otherwise, the demand is determined as the ratio of the response spectrum displacement to the yield displacement.

Non-isolated periods for the bridges along with displacement ductility demands are summarized in Tables 5.3-1 through 5.3-12. Figures G5.3-1 through G5.3-10 - APPENDIX G5 - depict the displacement ductility required at each of the two sites for the 6 bridges. Also included in the figures are code limits on permissible displacement ductility demands.

Table 5.3-1. Non-Isolated Natural Periods – Pile Bent Bridges

Structure	Piles	T, seconds	
		Trans.	Long.
Bridge No. 1	20” x 5/16”	0.37	0.36
	20” x 5/8”	0.29	0.29
Bridge No. 2	20” x 5/16”	0.59	0.46
	20” x 5/8”	0.53	0.38
Bridge No. 3	20” x 5/16”	0.50	0.54
	20” x 5/8”	0.37	0.42
Bridge No. 4	20” x 5/16”	0.56	0.66
	20” x 5/8	0.48	0.52

Table 5.3-2. Non-Isolated Natural Periods – Bridges 5 and 6

Structure	T, seconds	
	Trans.	Long.
Bridge No. 5	0.34	0.35
Bridge No. 6	0.47	0.42

Table 5.3-3. Displacement Demand – Bridge 1: 20” x 5/8” Pipe Piles

Spectrum	Substructure	$(D_{RSA})_T$	$(D_{RSA})_L$	D_{RSA}	μ_D
Site 1 DBE	Abutment 1	0.87	0.26	0.91	0.45
	Bent 1	0.72	0.26	0.77	0.85
	Bent 2	0.64	0.26	0.69	0.75
	Bent 3	0.64	0.26	0.69	0.75
	Bent 4	0.72	0.26	0.77	0.85
	Abutment 2	0.87	0.26	0.91	0.45
Site 1 MCE	Abutment 1	0.98	0.30	1.02	0.51
	Bent 1	0.81	0.30	0.86	0.96
	Bent 2	0.72	0.30	0.78	0.84
	Bent 3	0.72	0.30	0.78	0.84
	Bent 4	0.81	0.30	0.86	0.96
	Abutment 2	0.98	0.30	1.02	0.51
Site 2 DBE	Abutment 1	1.88	0.57	1.96	0.98
	Bent 1	2.38	0.57	2.44	2.79
	Bent 2	2.03	0.57	2.11	2.39
	Bent 3	2.03	0.57	2.11	2.39
	Bent 4	2.38	0.57	2.44	2.79
	Abutment 2	1.88	0.57	1.96	0.98
Site 2 MCE	Abutment 1	5.46	0.98	5.54	2.77
	Bent 1	5.12	1.37	5.30	6.00
	Bent 2	4.46	1.37	4.66	5.23
	Bent 3	4.46	1.37	4.66	5.23
	Bent 4	5.12	1.37	5.30	6.00
	Abutment 2	5.46	0.98	5.54	2.77

Table 5.3-4. Displacement Demand – Bridge 1: 20” x 5/16” Pipe Piles

Spectrum	Substructure	$(D_{RSA})_T$	$(D_{RSA})_L$	D_{RSA}	μ_D
Site 1 DBE	Abutment 1	1.29	0.41	1.35	0.68
	Bent 1	1.99	0.41	2.03	2.43
	Bent 2	1.92	0.41	1.97	2.35
	Bent 3	1.92	0.41	1.97	2.35
	Bent 4	1.99	0.41	2.03	2.43
	Abutment 2	1.29	0.41	1.35	0.68
Site 1 MCE	Abutment 1	1.45	0.46	1.52	0.76
	Bent 1	3.34	0.46	3.37	4.08
	Bent 2	3.24	0.46	3.28	3.96
	Bent 3	3.24	0.46	3.28	3.96
	Bent 4	3.34	0.46	3.37	4.08
	Abutment 2	1.45	0.46	1.52	0.76
Site 2 DBE	Abutment 1	3.20	0.89	3.32	1.66
	Bent 1	3.47	0.93	3.59	4.24
	Bent 2	3.38	0.93	3.50	4.14
	Bent 3	3.38	0.93	3.50	4.14
	Bent 4	3.47	0.93	3.59	4.24
	Abutment 2	3.20	0.89	3.32	1.66
Site 2 MCE	Abutment 1	6.85	1.54	7.02	3.51
	Bent 1	7.03	2.13	7.35	8.62
	Bent 2	6.86	2.13	7.18	8.41
	Bent 3	6.86	2.13	7.18	8.41
	Bent 4	7.03	2.13	7.35	8.62
	Abutment 2	6.85	1.54	7.02	3.51

Table 5.3-5. Displacement Demand – Bridge 2 – 20” x 5/8” Pipe Piles

Spectrum	Substructure	$(D_{RSA})_T$	$(D_{RSA})_L$	D_{RSA}	μ_D
Site 1 DBE	Abutment 1	1.44	0.45	1.50	0.75
	Bent 1	0.86	0.45	0.97	1.03
	Bent 2	0.99	0.45	1.09	1.19
	Bent 3	1.65	0.45	1.71	0.36
	Bent 4	2.46	0.45	2.50	0.53
	Abutment 2	3.92	0.45	3.95	1.97
Site 1 MCE	Abutment 1	1.62	0.51	1.70	0.85
	Bent 1	1.31	0.51	1.41	1.56
	Bent 2	1.53	0.51	1.61	1.81
	Bent 3	1.86	0.51	1.93	0.40
	Bent 4	2.77	0.51	2.82	0.60
	Abutment 2	6.13	0.51	6.15	3.08
Site 2 DBE	Abutment 1	2.92	0.98	3.08	1.54
	Bent 1	1.84	1.04	2.11	2.21
	Bent 2	1.78	1.04	2.07	2.15
	Bent 3	2.94	0.98	3.10	0.64
	Bent 4	4.34	0.98	4.45	0.94
	Abutment 2	5.62	0.98	5.71	2.85
Site 2 MCE	Abutment 1	5.67	1.70	5.92	2.96
	Bent 1	3.51	2.29	4.19	4.27
	Bent 2	3.64	2.29	4.30	4.42
	Bent 3	5.85	1.70	6.09	1.27
	Bent 4	8.96	1.70	9.12	1.94
	Abutment 2	12.19	1.70	12.31	6.15

Table 5.3-6. Displacement Demand – Bridge 2 – 20” x 5/16” Pipe Piles

Spectrum	Substructure	$(D_{RSA})_T$	$(D_{RSA})_L$	D_{RSA}	μ_D
Site 1 DBE	Abutment 1	1.69	0.67	1.82	0.91
	Bent 1	1.37	0.67	1.52	1.70
	Bent 2	1.84	0.67	1.96	2.27
	Bent 3	2.47	0.67	2.55	0.55
	Bent 4	3.37	0.67	3.44	0.76
	Abutment 2	4.95	0.67	4.99	2.50
Site 1 MCE	Abutment 1	1.91	0.75	2.05	1.03
	Bent 1	2.06	0.75	2.19	2.54
	Bent 2	2.82	0.75	2.92	3.45
	Bent 3	2.78	0.75	2.88	0.63
	Bent 4	3.80	0.75	3.88	0.85
	Abutment 2	7.60	0.75	7.64	3.82
Site 2 DBE	Abutment 1	3.39	1.33	3.64	1.82
	Bent 1	2.42	1.40	2.79	3.02
	Bent 2	2.53	1.40	2.89	3.16
	Bent 3	3.89	1.33	4.11	0.88
	Bent 4	5.18	1.33	5.35	1.16
	Abutment 2	6.07	1.33	6.21	3.11
Site 2 MCE	Abutment 1	6.27	2.68	6.82	3.41
	Bent 1	4.61	3.00	5.50	5.82
	Bent 2	5.26	3.00	6.06	6.58
	Bent 3	7.74	2.50	8.13	1.75
	Bent 4	10.54	2.50	10.83	2.37
	Abutment 2	13.17	2.68	13.43	6.72

Table 5.3-7. Displacement Demand – Bridge 3 – 20” x 5/8” Pipe Piles

Spectrum	Substructure	$(D_{RSA})_T$	$(D_{RSA})_L$	D_{RSA}	μ_D
Site 1 DBE	Abutment 1	4.57	0.49	4.59	2.30
	Bent 1	1.73	0.49	1.80	2.05
	Bent 2	1.53	0.49	1.60	1.81
	Bent 3	2.25	0.49	2.30	2.65
	Bent 4	2.50	0.49	2.55	2.94
	Bent 5	2.25	0.49	2.30	2.65
	Bent 6	1.53	0.49	1.60	1.81
	Bent 7	1.73	0.49	1.80	2.05
	Abutment 2	4.57	0.49	4.59	2.30
Site 1 MCE	Abutment 1	7.76	0.55	7.78	3.89
	Bent 1	2.99	0.55	3.04	3.52
	Bent 2	2.69	0.55	2.75	3.17
	Bent 3	3.77	0.55	3.81	4.42
	Bent 4	4.15	0.55	4.19	4.88
	Bent 5	3.77	0.55	3.81	4.42
	Bent 6	2.69	0.55	2.75	3.17
	Bent 7	2.99	0.55	3.04	3.52
	Abutment 2	7.76	0.55	7.78	3.89
Site 2 DBE	Abutment 1	7.10	1.05	7.18	3.59
	Bent 1	2.86	1.11	3.07	3.40
	Bent 2	2.90	1.11	3.10	3.44
	Bent 3	3.86	1.11	4.02	4.56
	Bent 4	4.21	1.11	4.36	4.97
	Bent 5	3.86	1.11	4.02	4.56
	Bent 6	2.90	1.11	3.10	3.44
	Bent 7	2.86	1.11	3.07	3.40
	Abutment 2	7.10	1.05	7.18	3.59
Site 2 MCE	Abutment 1	16.16	1.84	16.27	8.13
	Bent 1	6.36	2.32	6.77	7.55
	Bent 2	5.92	2.32	6.36	7.04
	Bent 3	7.82	2.32	8.15	9.24
	Bent 4	8.51	2.32	8.82	10.05
	Bent 5	7.82	2.32	8.15	9.24
	Bent 6	5.92	2.32	6.36	7.04
	Bent 7	6.36	2.32	6.77	7.55
	Abutment 2	16.16	1.84	16.27	8.13

Table 5.3-8. Displacement Demand – Bridge 3 – 20” x 5/16” Pipe Piles

Spectrum	Substructure	$(D_{RSA})_T$	$(D_{RSA})_L$	D_{RSA}	μ_D
Site 1 DBE	Abutment 1	4.73	0.80	4.79	2.40
	Bent 1	3.25	0.80	3.35	3.97
	Bent 2	2.72	0.80	2.83	3.32
	Bent 3	3.26	0.80	3.36	3.98
	Bent 4	3.56	0.80	3.65	4.34
	Bent 5	3.26	0.80	3.36	3.98
	Bent 6	2.72	0.80	2.83	3.32
	Bent 7	3.25	0.80	3.35	3.97
	Abutment 2	4.73	0.80	4.79	2.40
Site 1 MCE	Abutment 1	7.49	0.90	7.54	3.77
	Bent 1	5.14	1.13	5.27	6.28
	Bent 2	4.30	1.13	4.44	5.25
	Bent 3	5.16	1.13	5.28	6.29
	Bent 4	5.63	1.13	5.74	6.87
	Bent 5	5.16	1.13	5.28	6.29
	Bent 6	4.30	1.13	4.44	5.25
	Bent 7	5.14	1.13	5.27	6.28
	Abutment 2	7.49	0.90	7.54	3.77
Site 2 DBE	Abutment 1	6.14	1.37	6.29	3.14
	Bent 1	4.06	1.35	4.28	4.98
	Bent 2	3.72	1.35	3.95	4.57
	Bent 3	4.49	1.35	4.69	5.50
	Bent 4	4.88	1.35	5.06	5.97
	Bent 5	4.49	1.35	4.69	5.50
	Bent 6	3.72	1.35	3.95	4.57
	Bent 7	4.06	1.35	4.28	4.98
	Abutment 2	6.14	1.37	6.29	3.14
Site 2 MCE	Abutment 1	13.62	2.76	13.90	6.95
	Bent 1	9.02	2.87	9.47	11.06
	Bent 2	8.15	2.87	8.64	10.01
	Bent 3	9.83	2.87	10.24	12.03
	Bent 4	10.68	2.87	11.06	13.06
	Bent 5	9.83	2.87	10.24	12.03
	Bent 6	8.15	2.87	8.64	10.01
	Bent 7	9.02	2.87	9.47	11.06
	Abutment 2	13.62	2.76	13.90	6.95

Table 5.3-9. Displacement Demand – Bridge 4 – 20” x 5/8” Piles

Spectrum	Substructure	$(D_{RSA})_T$	$(D_{RSA})_L$	D_{RSA}	μ_D
Site 1 DBE	Abutment 1	4.93	0.74	4.99	2.49
	Bent 1	1.73	0.74	1.89	2.07
	Bent 2	1.43	0.74	1.61	1.72
	Bent 3	4.32	0.74	4.38	1.83
	Bent 4	5.29	0.74	5.34	1.14
	Bent 5	4.32	0.74	4.38	1.83
	Bent 6	1.43	0.74	1.61	1.72
	Bent 7	1.73	0.74	1.89	2.07
	Abutment 2	4.93	0.74	4.99	2.49
Site 1 MCE	Abutment 1	7.97	0.84	8.02	4.01
	Bent 1	2.81	0.84	2.93	3.32
	Bent 2	2.71	0.84	2.84	3.21
	Bent 3	8.78	0.84	8.82	3.71
	Bent 4	11.62	0.84	11.65	2.50
	Bent 5	8.78	0.84	8.82	3.71
	Bent 6	2.71	0.84	2.84	3.21
	Bent 7	2.81	0.84	2.93	3.32
	Abutment 2	7.97	0.84	8.02	4.01
Site 2 DBE	Abutment 1	7.43	1.34	7.55	3.77
	Bent 1	2.75	1.34	3.05	3.29
	Bent 2	2.14	1.34	2.53	2.60
	Bent 3	5.33	1.34	5.50	2.26
	Bent 4	7.64	1.34	7.75	1.65
	Bent 5	5.33	1.34	5.50	2.26
	Bent 6	2.14	1.34	2.53	2.60
	Bent 7	2.75	1.34	3.05	3.29
	Abutment 2	7.43	1.34	7.55	3.77
Site 2 MCE	Abutment 1	16.19	2.69	16.42	8.21
	Bent 1	5.92	2.85	6.57	7.08
	Bent 2	4.49	2.85	5.32	5.45
	Bent 3	11.92	2.64	12.20	5.05
	Bent 4	17.02	2.60	17.22	3.68
	Bent 5	11.92	2.64	12.20	5.05
	Bent 6	4.49	2.85	5.32	5.45
	Bent 7	5.91	2.85	6.56	7.07
	Abutment 2	16.19	2.69	16.42	8.21

Table 5.3-10. Displacement Demand – Bridge 4 – 20” x 5/16” Piles

Spectrum	Substructure	$(D_{RSA})_T$	$(D_{RSA})_L$	D_{RSA}	μ_D
Site 1 DBE	Abutment 1	5.59	1.11	5.70	2.85
	Bent 1	3.12	1.16	3.33	3.84
	Bent 2	2.54	1.16	2.79	3.15
	Bent 3	5.80	1.11	5.91	2.55
	Bent 4	7.25	1.11	7.34	1.63
	Bent 5	5.80	1.11	5.91	2.55
	Bent 6	2.54	1.16	2.79	3.15
	Bent 7	3.12	1.16	3.33	3.84
	Abutment 2	5.59	1.11	5.70	2.85
Site 1 MCE	Abutment 1	8.97	1.34	9.07	4.53
	Bent 1	4.89	1.79	5.21	6.01
	Bent 2	5.28	1.79	5.58	6.49
	Bent 3	13.14	1.34	13.21	5.76
	Bent 4	16.77	1.34	16.82	3.75
	Bent 5	13.14	1.34	13.21	5.76
	Bent 6	5.28	1.79	5.58	6.49
	Bent 7	4.89	1.79	5.21	6.02
	Abutment 2	8.97	1.34	9.07	4.53
Site 2 DBE	Abutment 1	7.13	1.65	7.32	3.66
	Bent 1	3.89	1.49	4.16	4.78
	Bent 2	3.04	1.49	3.39	3.77
	Bent 3	6.74	1.65	6.94	2.96
	Bent 4	9.14	1.65	9.29	2.05
	Bent 5	6.74	1.65	6.94	2.96
	Bent 6	3.04	1.49	3.39	3.77
	Bent 7	3.89	1.49	4.16	4.78
	Abutment 2	7.13	1.65	7.32	3.66
Site 2 MCE	Abutment 1	15.55	3.11	15.86	7.93
	Bent 1	8.52	2.99	9.03	10.46
	Bent 2	6.58	2.99	7.22	8.14
	Bent 3	14.65	3.14	14.98	6.44
	Bent 4	19.57	3.23	19.84	4.38
	Bent 5	14.65	3.14	14.98	6.44
	Bent 6	6.58	2.99	7.22	8.14
	Bent 7	8.52	2.99	9.03	10.46
	Abutment 2	15.55	3.11	15.86	7.93

Table 5.3-11. Displacement Demand – Bridge 5

Spectrum	Substructure	$(D_{RSA})_T$	$(D_{RSA})_L$	D_{RSA}	μ_D
Site 1 DBE	Abutment 1	1.25	0.37	1.31	0.65
	Bent 1	1.70	0.37	1.74	2.78
	Bent 2	1.70	0.37	1.74	2.78
	Abutment 2	1.25	0.37	1.31	0.65
Site 1 MCE	Abutment 1	1.41	0.42	1.47	0.74
	Bent 1	2.90	0.42	2.93	4.73
	Bent 2	2.90	0.42	2.93	4.73
	Abutment 2	1.41	0.42	1.47	0.74
Site 2 DBE	Abutment 1	3.25	0.84	3.35	1.68
	Bent 1	2.96	0.97	3.12	4.88
	Bent 2	2.96	0.97	3.12	4.88
	Abutment 2	3.25	0.84	3.35	1.68
Site 2 MCE	Abutment 1	7.16	1.40	7.30	3.65
	Bent 1	6.05	2.06	6.39	9.96
	Bent 2	6.05	2.06	6.39	9.96
	Abutment 2	7.16	1.40	7.30	3.65

Table 5.3-12. Displacement Demand – Bridge 6

Spectrum	Substructure	$(D_{RSA})_T$	$(D_{RSA})_L$	D_{RSA}	μ_D
Site 1 DBE	Abutment 1	2.50	0.52	2.56	1.28
	Bent 1	2.34	0.52	2.39	3.44
	Abutment 2	2.50	0.52	2.56	1.28
Site 1 MCE	Abutment 1	4.23	0.59	4.27	2.14
	Bent 1	3.78	0.59	3.83	5.55
	Abutment 2	4.23	0.59	4.27	2.14
Site 2 DBE	Abutment 1	4.73	0.97	4.82	2.41
	Bent 1	3.53	1.05	3.68	5.21
	Abutment 2	4.73	0.97	4.82	2.41
Site 2 MCE	Abutment 1	10.20	1.77	10.35	5.18
	Bent 1	7.61	2.28	7.94	11.23
	Abutment 2	10.20	1.77	10.35	5.18

5.4 Foundation Springs at Multi-column Bents

The analysis of the bents for yield displacement has been based upon perfect fixity at the column bases. In reality, a series of foundation springs corresponding to the various degrees of freedom at each column base could be estimated and included in the analysis. A simple procedure to include these effects is the addition of a horizontal spring, k_h, at the base of each column in each of the transverse and longitudinal directions. This will increase the displacement at which yield in the column occurs, but will have no effect upon plastic deformation. So, an analysis of this type is preferred when analyzing non-isolated structures due to the decreased displacement ductility capacity. For example, suppose that the yield displacement with fixed base columns is 1 inch and the plastic displacement capacity is 3 inches. Then for the fixed base case, the displacement ductility capacity is (1+3)/1 = 4.0. Now suppose that foundation springs are included and the resulting yield displacement is 1.5 inches. The plastic displacement capacity is unchanged, still 3 inches. So the displacement ductility capacity including foundation spring effects is (1.5+3)/1.5 = 3.0. For determining the displacement ductility capacity of non-isolated multi-column bents, foundation springs should be included in the analysis.

For analyzing isolated bridge bents and establishing isolator demands, the opposite is true. The stiffer the column, the higher will be the ensuing displacement demand upon the isolator itself. So for this study, fixed base multi-column bents have been modeled for bridges 5 and 6. Note that for bridges 1 through 4 - pile bent bridges - this issue does not exist. The whole trick for pile bent bridges is to as accurately as possible estimate the depth to fixity. For actual bridge design in which detailed foundation explorations permit, p-y curves should be established

to assist the designer in setting depths to fixity. For the purposes of this study, the 5-diameter rule to depth of fixity has been used.

To include the effects of a simple, linear horizontal spring at the base of columns in a multi-column bent, the following equations may be useful. Subscripts “L” and “T” refer to the longitudinal and transverse directions respectively. L_C is the clear column height. H is the distance from the center of mass of the superstructure to the column base. k_{oL} and k_{oT} are stiffness values for a single column without consideration of the foundation spring - i.e., for the fixed base condition. k_L and k_T are the stiffness values for a single column including foundation spring effects. k_h is the foundation spring at a single column. Cantilever type behavior is assumed for longitudinal response and rigid-frame behavior for transverse response. It is crucial to remember that these expressions give displacement values at the top of the columns, so results from a computer model must be carefully retrieved. Comparing yield displacements from these equations to computer results at the center of gravity of the superstructure nodes could likely result in serious error, particularly in the longitudinal direction.

$$k_{oL} = \frac{3EI_{EFF}}{\lambda L_C^3} \quad \text{(Eq. 5-29)}$$

$$\lambda = \frac{3}{2} - \frac{L_C}{2H} \quad \text{(Eq. 5-30)}$$

$$k_L = k_{oL}\left(\frac{1}{1+\frac{k_{oL}}{k_h}}\right) \quad \text{(Eq. 5-31)}$$

$$k_{oT} = \frac{12EI_{EFF}}{L_C^3} \quad \text{(Eq. 5-32)}$$

$$k_T = k_{oT}\left(\frac{1}{1+\frac{k_{oT}}{k_h}}\right) \quad \text{(Eq. 5-33)}$$

$$\Delta_{yL} = \frac{M_P}{k_{oL}H}\left(1 + \frac{k_{oL}}{k_h}\right) \quad \text{(Eq. 5-34)}$$

$$\Delta_{yT} = \frac{2M_P}{k_{oT}L}\left(1 + \frac{k_{oT}}{k_h}\right) \quad \text{(Eq. 5-35)}$$

CHAPTER 6 – PRELIMINARY DESIGN OF ISOLATORS

The AASHTO Guide Specifications for Seismic Isolation Design (AASHTO, 2010) permit the design of many isolation systems using a simplified analysis procedure. In CHAPTER 3, ground motions were selected for design of isolation systems using the more rigorous and more accurate method of nonlinear response history analysis. In the present chapter, the AASHTO simplified procedure is used to estimate displacements for preliminary design, even though these estimates may be on the low side of response history results to be determined in CHAPTER 7. A slight variation of the AASHTO simplified procedure will present advantages in the preliminary design stage. Namely, direct displacement based design offers the advantage of a target displacement established up front. The designer then determines the isolator properties required to achieve this displacement. It would seem that this slight modification of the method - selecting a target displacement up front - gives the designer more control in the initial stages of design and will be used for the preliminary design of isolation systems for this research.

Section 6.1 provides details of the direct displacement-based design procedure as it applies to the preliminary design of isolation systems. A detailed step-by-step procedure used in this study is presented. In Section 6.2 this detailed procedure is applied to Bridge No. 1, located on Site No. 1, but with a code-based spectral shape to match the shape used in the AASHTO simplified procedure. Finally, in Section 6.3, results of this same procedure, automated in spreadsheet format, are summarized for each of the six bridges, with designs obtained for both code-based spectral shape (referred to as “ATR”) and the modified NMSZ spectral shape outlined in CHAPTER 4, Section 4.3. Results of the preliminary design will be used in

CHAPTER 7 for comparison to results obtained there from nonlinear response history analyses of each bridge for Site No. 1 conditions with ground motions scaled to match both the code-based (ATR) spectral shape and the NMSZ-specific, modified spectral shape.

6.1 Direct Displacement Based Design

The details of direct displacement based design applied to isolation systems used in bridges have been rigorously studied and outlined (Pietra, et al., 2008). This method with target displacements taken to be uniform along the bridge will be adopted here. A uniform target displacement is viewed as ideal in that superstructure stresses are thus minimized and adverse effects due to unsymmetrical pier stiffness configurations are somewhat alleviated. The procedure is briefly outlined followed by results of preliminary isolator design for each of the 6 bridges.

1. Establish a target displacement, Δ_{TAR}.
2. Determine the stiffness, K_{SUB}, yield displacement, D_{SUB}, and yield shear, V_Y at each substructure.
3. Assume a ratio of substructure displacement to yield displacement at each substructure. This should generally be limited to 0.8 to ensure that the substructures remain elastic, one of the major benefits of seismic isolation applied to bridges.

$$\mu_i \left(= \frac{D_{SUB-i}}{D_{Y-i}} \right)$$

4. Establish the appropriate substructure damping, ξ_{SUB} (usually takes as 5% of critical) and an effective viscous damping ratio desired for the isolators at each

substructure, ξ_{ISO}. The designer may decide the extent to which each isolator to be worked. This is another advantage of direct displacement based design.

5. Determine the fraction of total seismic shear carried by each substructure. For a uniform target displacement, this is simply the tributary length of superstructure for each substructure divided by the bridge length.

$$f_i = \frac{L_{TRIB-i}}{L_{TOT}} \quad \text{(Eq. 6-1)}$$

6. With the assumed actual-to-yield displacement and target displacement at each sub-structure, determine how much of the target displacement is taken up by each substructure, D_{SUB}, and how much is taken up in each isolator, D_{ISO}.

$$D_{SUB} = \mu_i \times D_Y \quad \text{(Eq. 6-2)}$$

$$D_{ISO} = \Delta_{TAR} - D_{SUB} \quad \text{(Eq. 6-3)}$$

7. Calculate the composite damping at each substructure.

$$\xi_{COMP} = \frac{\xi_{SUB} D_{SUB} + \xi_{EFF} D_{ISO}}{D_{SUB} + D_{ISO}} \quad \text{(Eq. 6-4)}$$

8. Calculate the system damping of the entire bridge.

$$\xi_{SYS} = \frac{\sum[(V_i)(\xi_{COMP})_i]}{\sum V_i} \quad \text{(Eq. 6-5)}$$

9. Calculate the effective period of the structure and the resulting effective stiffness required to achieve the target displacement reduced by the appropriate factor accounting for effective viscous damping in excess of 5%. The equations below correspond to active tectonic region spectral shape and AASHTO damping correction. Duration dependent damping correction and alternate spectral shapes

would simply require modifying these equations. The basic procedure remains unchanged.

$$B_L = \left(\frac{\xi_{SYS}}{0.05}\right)^{0.30} \leq 1.7 \qquad \text{(Eq. 6-6)}$$

$$T_{EFF} = \frac{B_L \cdot 4\pi^2 \cdot \Delta_{TAR}}{g \cdot S_{D1}} \qquad \text{(Eq. 6-7)}$$

$$K_{EFF} = \left(\frac{2\pi}{T_{EFF}}\right)^2 \cdot \frac{W_{TOT}}{g} \qquad \text{(Eq. 6-8)}$$

10. Find the total seismic shear and distribute to each substructure according to tributary lengths supported.

$$V_{SEIS} = K_{EFF} \cdot \Delta_{TAR} \qquad \text{(Eq. 6-9)}$$

$$V_i = f_i \cdot V_{SEIS} \qquad \text{(Eq. 6-10)}$$

11. Calculate the actual displacement-to-yield ratio at each substructure. When the calculated value is equal to the assumed value at each substructure within a reasonable margin of error, the solution has converged and the next step may be approached. Otherwise, return to step number 3.

$$\mu_i = \frac{V_i}{K_{SUB-i} \cdot D_{Y-i}} \qquad \text{(Eq. 6-11)}$$

12. Calculate the isolator properties, Q_d and k_d, required to achieve the converged response.

The calculation of required isolator properties in Step 12 is given detailed treatment here. Once this step in the preliminary design has been reached, the designer will have the desired values of isolator displacement, D_{ISO}, isolator effective damping, ξ_{EFF}, and the maximum isolator force, V. For a bi-linear isolator in general, the effective damping is given by equation 6-12. For

FPS systems, D_{YISO} is zero and the solution for required Q_d and k_d is straightforward by equations 6-13 and 6-14.

$$\xi_{EFF} = \frac{2Q_d(D_{ISO} - D_{YISO})}{\pi D_{ISO}(Q_d + k_d D_{ISO})} = \frac{2Q_d(D_{ISO} - D_{YISO})}{\pi D_{ISO} V} \qquad \text{(Eq. 6-12)}$$

$$(Q_d)_{FPS} = \frac{\pi V \xi_{EFF}}{2} \qquad \text{(Eq. 6-13)}$$

$$(k_d)_{FPS} = \frac{V - Q_d}{D_{ISO}} \qquad \text{(Eq. 6-14)}$$

For LRB systems, the isolator yield displacement, D_{YISO}, is not zero and the solution is just a bit more complicated. The ratio of post-yield stiffness to initial stiffness is assigned the value α (typically 0.10 for LRB bearings) and the calculations proceed as follows.

$$\alpha = \frac{k_d}{k_i} \qquad \text{(Eq. 6-15)}$$

$$\theta = \frac{1 - \alpha}{\alpha} \qquad \text{(Eq. 6-16)}$$

The algebraic details are omitted here, but the solution reduces to a quadratic generally admitting two solutions each of which will provide the required displacement, damping, and effective stiffness properties.

$$(Q_d)_{LRB} = \frac{V \cdot \left(2\theta + \xi_{EFF}\pi\theta \pm \sqrt{(2\theta + \xi_{EFF}\pi\theta)^2 - 8(1+\theta)(\xi_{EFF}\pi\theta)}\right)}{4(1+\theta)} \qquad \text{(Eq. 6-17)}$$

$$(k_d)_{LRB} = \frac{V - Q_d}{D_{ISO}} \qquad \text{(Eq. 6-18)}$$

The detailed solution will be carried out in Section 5.2 for Bridge No. 1 using ATR spectral shape and AASHTO damping correction.

6.2 Bridge No. 01 with ATR Spectral Shape

Preliminary design for the DBE at Site No. 1 is carried out by the direct method outlined in Section 5.1. The pipe piles are assumed to be 51 cm x 0.8 cm (20" x 5/16") essentially elastic piles with F_y = 241 MPa (35 ksi). The 1-second spectral displacement of the 5% damping elastic spectrum for Site 1 at the DBE-level hazard is S_{D1} = 0.555g. Yield displacements are 5 cm (2 inches) at the abutments and 2.1 cm (0.835 inches) at each of the piers. Yield shears are 3203 kN (720 kips) at each of the abutments and 1855 kN (417 kips) at each pier. Elastic substructure stiffness values are 630 kN/cm (360 kips/inch) for the abutments and 874 kN/cm (499 kips/inch) for the piers. The superstructure weight is 136 kN/m (9.344 klf) and each substructure includes 752 kN (169 kips) of additional weight from caps and diaphragms and end-walls.

$$W_{TOT} = 9.344 \times 250 + 6 \times 169 = 3{,}350\ kips \qquad \text{(Eq. 6-19)}$$

A target displacement of 12.7 cm (5 inches) is selected in an effort to avoid extremely large expansion joint requirements at the abutments. Isolators will be designed to achieve an effective viscous damping in the isolator of 30% of critical. Substructure viscous damping is taken as 5% of critical.

Step 1. Establish the target displacement.

$$\Delta_{TAR} = 5\ inches \qquad \text{(Eq. 6-20)}$$

Step 2. Determine the stiffness, K_{SUB}, yield displacement, D_{SUB}, and yield shear, V_Y at each substructure.

$$K_{SUB} = 360\frac{kips}{inch}, abutments\ 1\ and\ 2 \qquad \text{(Eq. 6-21)}$$

$$K_{SUB} = 499\frac{kips}{inch}, pier\ nos.\ 1, 2, 3, and\ 4 \qquad \text{(Eq. 6-22)}$$

$$V_{YSUB} = 720\ kips, abutments\ 1\ and\ 2 \quad \text{(Eq. 6-23)}$$

$$V_{YSUB} = 417\ kips, pier\ nos.\ 1, 2, 3, and\ 4 \quad \text{(Eq. 6-24)}$$

$$D_{YSUB} = 2\ inches, abutments\ 1\ and\ 2 \quad \text{(Eq. 6-25)}$$

$$D_{YSUB} = 0.835\ inches, pier\ nos.\ 1, 2, 3, and\ 4 \quad \text{(Eq. 6-26)}$$

Step 3. Assume a ratio of substructure displacement to yield displacement at each substructure. This should generally be limited to 0.8 to ensure that the substructures remain elastic, one of the major benefits of seismic isolation applied to bridges. For the first iteration, use 0.8 at each substructure.

$$\mu = 0.8, all\ substructures \quad \text{(Eq. 6-27)}$$

Step 4. Establish the appropriate substructure damping, ξ_{SUB} (usually takes as 5% of critical) and an effective viscous damping ratio desired for the isolators at each substructure, ξ_{ISO}. The designer may decide the extent to which she wishes each isolator to be worked. This is another advantage of direct displacement based design.

$$\xi_{SUB} = 0.05 \quad \text{(Eq. 6-28)}$$

$$\xi_{ISO} = 0.30 \quad \text{(Eq. 6-29)}$$

Step 5. Determine the fraction of total seismic shear carried by each substructure. For a uniform target displacement, this is simply the tributary length of superstructure for each substructure divided by the bridge length.

$$f_1 = f_6 = \frac{25}{250} = 0.10, abutments\ 1\ and\ 2 \quad \text{(Eq. 6-30)}$$

$$f_2 = f_3 = f_4 = f_5 = \frac{50}{250} = 0.20, piers\ 1, 2, 3, and\ 4 \quad \text{(Eq. 6-31)}$$

Step 6. With the assumed actual-to-yield displacement and target displacement at each sub-structure, determine how much of the target displacement is taken up by each substructure, D_{SUB}, and how much is taken up in each isolator, D_{ISO}.

$$D_{SUB-1} = D_{SUB-6} = 0.8 \times 2 = 1.6", abutments \quad \text{(Eq. 6-32)}$$

$$D_{ISO-1} = D_{ISO-6} = 5 - 1.6 = 3.4", abutments \quad \text{(Eq. 6-33)}$$

$$D_{SUB-2} = D_{SUB-3} = D_{SUB-4} = D_{SUB-5} = 0.8 \times 0.835 = 0.668", piers \quad \text{(Eq. 6-34)}$$

$$D_{ISO-2} = D_{ISO-3} = D_{ISO-4} = D_{ISO-5} = 5 - 0.668 = 4.332", piers \quad \text{(Eq. 6-35)}$$

Step 7. Calculate the composite damping at each substructure.

$$\xi_{COMP-1} = \xi_{COMP-6} = \frac{0.05 \times 1.6 + 0.30 \times 3.4}{5} = 0.220, abutments \quad \text{(Eq. 6-36)}$$

$$\xi_{COMP-2} = \xi_{COMP-3} = \xi_{COMP-4} = \xi_{COMP-5} = \frac{0.05 \times 0.668 + 0.30 \times 4.332}{5} = 0.267, piers \quad \text{(Eq. 6-37)}$$

Step 8. Calculate the system damping of the entire bridge.

$$\xi_{SYS} = 0.10 \times 0.220 \times 2 + 0.20 \times 0.267 \times 4 = 0.258 \quad \text{(Eq. 6-38)}$$

Step 9. Calculate the effective period of the structure and the resulting effective stiffness required to achieve the target displacement reduced by the appropriate factor accounting for effective viscous damping in excess of 5%.

$$B_L = \left(\frac{0.258}{0.05}\right)^{0.30} = 1.636 \quad \text{(Eq. 6-39)}$$

$$T_{EFF} = \frac{1.636 \cdot 4\pi^2 \cdot 5}{386 \cdot 0.555} = 1.507\ seconds \quad \text{(Eq. 6-40)}$$

$$K_{EFF} = \left(\frac{2\pi}{1.507}\right)^2 \cdot \frac{3{,}350}{386} = 151\ kips/inch \quad \text{(Eq. 6-41)}$$

Step 10. Find the total seismic shear and distribute to each substructure according to tributary lengths supported.

$$V_{TOT} = 151 \times 5 = 755\ kips \quad \text{(Eq. 6-42)}$$

$$V_1 = V_6 = 755 \times 0.1 = 75.5\ kips \quad \text{(Eq. 6-43)}$$

$$V_2 = V_3 = V_4 = V_5 = 755 \times 0.2 = 151\ kips \quad \text{(Eq. 6-44)}$$

Step 11. Calculate the actual displacement-to-yield ratio at each substructure.

$$\mu_1 = \mu_6 = \frac{75.5}{360 \cdot 2} = 0.105, abutments \quad \text{(Eq. 6-45)}$$

$$\mu_2 = \mu_3 = \mu_4 = \mu_5 = \frac{151}{499 \cdot 0.835} = 0.362, piers \quad \text{(Eq. 6-46)}$$

These values are very different from the assumed values of 0.80 at each substructure. Convergence is typically achieved quite quickly and, using these new μ-values as the new assumed values for a new iteration, one obtains:

$$\mu_1 = \mu_6 = 0.098, abutments \quad \text{(Eq. 6-47)}$$

$$\mu_2 = \mu_3 = \mu_4 = \mu_5 = 0.340, piers \quad \text{(Eq. 6-48)}$$

Finally, using these revised μ-values as assumed values, convergence is complete to 3 decimal places and the solution has been reached. The pertinent data from the final iteration needed for step 12 are as follows.

$$D_{ISO} = 4.803", abutments \quad \text{(Eq. 6-49)}$$

$$D_{ISO} = 4.716", piers \quad \text{(Eq. 6-50)}$$

$$V = 70.77\ kips, abutments \quad \text{(Eq. 6-51)}$$

$$V = 141.53\ kips, piers \quad \text{(Eq. 6-52)}$$

$$\xi_{EFF} = 0.30, all\ isolators \quad \text{(Eq. 6-53)}$$

Thus, for the preliminary design of FPS bearings on Bridge No. 1, we would have:

$$(Q_d)_{FPS} = \frac{\pi V \xi_{EFF}}{2} = \frac{\pi \cdot 70.77 \cdot 0.30}{2} = 33.35\ kips, abutments \quad \text{(Eq. 6-54)}$$

$$(Q_d)_{FPS} = \frac{\pi V \xi_{EFF}}{2} = \frac{\pi \cdot 141.53 \cdot 0.30}{2} = 66.69\ kips, piers \quad \text{(Eq. 6-55)}$$

$$(k_d)_{FPS} = \frac{V - Q_d}{D_{ISO}} = \frac{70.77 - 33.35}{4.803} = 7.79 \frac{kips}{inch}, abutments \quad \text{(Eq. 6-56)}$$

$$(k_d)_{FPS} = \frac{V - Q_d}{D_{ISO}} = \frac{141.53 - 66.69}{4.716} = 15.87 \frac{kips}{inch}, piers \quad \text{(Eq. 6-57)}$$

Note that these are total Q_d and k_d values for each substructure and need to be divided by the number of bearings to obtain values per bearing to be specified in the design documents to the bearing manufacturer. Check to see that the values obtained are within acceptable limits for current code requirements.

$$\mu_{DYN} = \frac{Q_d}{W} = \frac{33.35}{9.344 \cdot 25 + 169} = 0.083, abutments \quad \text{(Eq. 6-58)}$$

$$\mu_{DYN} = \frac{Q_d}{W} = \frac{66.69}{9.344 \cdot 50 + 169} = 0.105, piers \quad \text{(Eq. 6-59)}$$

FPS bearings should generally be designed such that μ_{DYN} is in the range (0.03-0.12). Thus, the above designs are acceptable with regard to the required dynamic coefficient of friction. Values outside these limits may eventually be used in particular designs but would likely require more stringent testing requirements, so it is best to stay within the limits whenever possible.

The second parameter to be checked for FPS systems is the radius of curvature for the concave surface. Values should be within the range of R = (39”-244”) to avoid the possibility of more stringent test requirements for isolators outside the range of those which have been used in practice to date already.

$$R = \frac{W}{k_d} = \frac{402.6}{7.79} = 51.7", abutments \quad \text{(Eq. 6-60)}$$

$$R = \frac{W}{k_d} = \frac{636.2}{15.87} = 40.1", piers \quad \text{(Eq. 6-61)}$$

Finally, a check should be made to ensure that the specified Q_d values are larger than the Strength Limit State loadings from wind and braking forces.

The design wind loading for the bridge is 0.35 klf. The maximum Strength Limit State load factor for WS (Wind on Structure) loading is 1.4. So the total wind force on the bridge is:

$$V_{WS} = 0.35 \times 250 \times 1.40 = 122.5\ kips \quad \text{(Eq. 6-62)}$$

The design braking force on the entire bridge is taken to be that due to two HL-93 trucks with a load factor at the Strength Limit State of 1.75.

$$V_{BR} = 0.25 \times 72 \times 2 \times 1.75 = 63.0\ kips \quad \text{(Eq. 6-63)}$$

The sum of Q_d values for the entire bridge is found to be larger than either the wind or the braking force.

$$\sum Q_d = 2 \times 33.35 + 4 \times 66.69 = 333.5\ kips \quad \text{(Eq. 6-64)}$$

With 5 girders, the specification of the bearing properties at each location is thus:

$$Q_d = \frac{33.35}{5} = 6.67\ kips\ per\ bearing, abutments \quad \text{(Eq. 6-65)}$$

$$k_d = \frac{7.79}{5} = 1.56\frac{kips}{inch}\ perbearing, abutments \quad \text{(Eq. 6-66)}$$

$$Q_d = \frac{66.69}{5} = 13.34\ kips\ per\ bearing, piers \quad \text{(Eq. 6-67)}$$

$$k_d = \frac{15.87}{5} = 3.18\frac{kips}{inch}\ perbearing, piers \quad \text{(Eq. 6-68)}$$

For a design incorporating LRB bearings, assume that the post-yield stiffness ratio, α, is equal to 0.10. This is typical for LRB devices.

$$\theta = \frac{1 - 0.1}{0.1} = 9 \quad \text{(Eq. 6-69)}$$

$$(Q_d)_{LRB} = \frac{V \cdot \left(2\theta + \xi_{EFF}\pi\theta \pm \sqrt{(2\theta + \xi_{EFF}\pi\theta)^2 - 8(1+\theta)(\xi_{EFF}\pi\theta)}\right)}{4(1+\theta)} \quad \text{(Eq. 6-70)}$$

For the abutments:

$$(Q_d)_{LRB} = \frac{70.77 \cdot \left(18 + 2.7\pi \pm \sqrt{(18 + 2.7\pi)^2 - 8(10)(2.7\pi)}\right)}{4(10)} = 55.29, 38.42\ kips \quad \text{(Eq. 6-71)}$$

For the higher Q_d, the corresponding k_d would be:

$$k_d = \frac{70.77 - 55.29}{4.803} = 3.22\frac{kips}{inch}total = 0.64\frac{kips}{inch}per\ bearing \quad \text{(Eq. 6-72)}$$

For the lower Q_d, the corresponding k_d would be:

$$k_d = \frac{70.77 - 38.4}{4.803} = 6.74\frac{kips}{inch}total = 1.35\frac{kips}{inch}per\ bearing \quad \text{(Eq. 6-73)}$$

And for the piers:

$$(Q_d)_{LRB} = \frac{141.53 \cdot \left(18 + 2.7\pi \pm \sqrt{(18 + 2.7\pi)^2 - 8(10)(2.7\pi)}\right)}{4(10)} = 110.57, 76.83\ kips \qquad \text{(Eq. 6-74)}$$

For the higher Q_d, the corresponding k_d would be:

$$k_d = \frac{141.53 - 110.57}{4.716} = 6.56\frac{kips}{inch}total = 1.31\frac{kips}{inch}per\ bearing \qquad \text{(Eq. 6-75)}$$

For the lower Q_d, the corresponding k_d would be:

$$k_d = \frac{141.53 - 76.83}{4.716} = 13.72\frac{kips}{inch}total = 2.74\frac{kips}{inch}per\ bearing \qquad \text{(Eq. 6-76)}$$

To reiterate - a low value for the actual to yield displacement ratio, μ, will be desired in most, if not all, cases to leave some room for local displacements from the influence of higher modes. For this bridge the effect could be easily estimated for a pier by using the cap weight - 134 kips - plus one-third of the pipe pile weights - 5 kips - along with the transverse stiffness of 499 kips/inch. This gives a local period of:

$$T_{LOCAL} = 2\pi\sqrt{\frac{139}{386 \cdot 499}} = 0.17\ seconds \qquad \text{(Eq. 6-77)}$$

This puts the local mode in the acceleration plateau of the design response spectrum so that the pier displacement from higher mode effects may be estimated as:

$$D_{SUB-LOCAL} = S_{DS} \cdot g \cdot \left(\frac{T_{LOCAL}}{2\pi}\right)^2 = 0.907 \cdot 386 \cdot \left(\frac{0.17}{2\pi}\right)^2 = 0.27\ inches \quad \text{(Eq. 6-78)}$$

Adding this to the displacement from the analysis of the isolated mode gives a total pier displacement of:

$$D_{SUB} = \frac{141.53}{499} + 0.27 = 0.28 + 0.27 = 0.55\ inches \quad \text{(Eq. 6-79)}$$

This is a conservative estimate since it implies that the maximum displacements of the two modes occur simultaneously. While this is still less than the yield displacement of 0.823 inches, it is clear that the effect is significant in this case and should be included in preliminary analyses.

6.3 Bridges 1-6 Summary

Preliminary isolator designs for each of the bridges are presented here. Automated solutions for NMSZ-specific conditions and comparisons with ATR-specific conditions are included.

From CHAPTER 4, the following recap of recommendations is given to establish the criteria for making comparisons between LRB and FPS isolation systems in a given tectonic setting and between ATR and NMSZ spectral shapes for a given isolator type.

- For LRB isolators in the NMSZ, use the Mod-A spectral shape with AASHTO damping correction.
- For LRB isolators in an ATR, use the AASHTO spectral shape with AASHTO damping correction.

- For FPS isolators in the NMSZ, use the Mod-A spectral shape and duration-dependent damping correction with $D_{5\text{-}95\%}$ = 30 seconds.
- For FPS isolators in an ATR, use the AASHTO spectral shape with duration-dependent damping correction and a $D_{5\text{-}95\%}$ significant duration corresponding to the appropriate magnitude of design event in the ATR.

Tables 6.3-1 through 6.3-6 summarize the results for calculations following the procedure outlined in Sections 5.1 and 5.2 for each of the 6 bridges. The ATR-specific tabular values of Q_d and k_d for each isolator type are used for the nonlinear time history analyses of CHAPTER 7.

The preliminary design process is doubly-iterative because sub-structure μ-values are assumed for a given target displacement until convergence is attained for that target displacement. Should that target result in required Q_d and k_d values outside the normal range, or yielding in the piers, then a different target displacement was assigned and the process repeated. Tables 6.3-13 and 6.3-14 summarize the target displacement used for each bridge and FPS parameters required to produce the desired behavior. Tables 6.3-15 and 6.3-16 summarize the dynamic properties of the FPS and LRB isolated bridges.

Table 6.3-1. Bridge No. 1 Preliminary Isolator Design - ATR

Substructure	FPS Design		LRB Design	
	Q_d, k/beam	k_d, k/in/beam	Q_d, k/beam	k_d, k/in/beam
Abutment 1	23.73	5.48	38.42	6.74
Pier 1	47.46	11.10	76.83	13.72
Pier 2	47.46	11.10	76.83	13.72
Pier 3	47.46	11.10	76.83	13.72
Pier 4	47.46	11.10	76.83	13.72
Abutment 2	23.73	5.48	38.42	6.74

Table 6.3-2. Bridge No. 1 Preliminary Isolator Design - NMSZ

Substructure	FPS Design		LRB Design	
	Q_d, k/beam	k_d, k/in/beam	Q_d, k/beam	k_d, k/in/beam
Abutment 1	33.91	7.93	50.16	8.90
Pier 1	67.82	16.15	100.32	18.25
Pier 2	67.82	16.15	100.32	18.25
Pier 3	67.82	16.15	100.32	18.25
Pier 4	67.82	16.15	100.32	18.25
Abutment 2	33.91	7.93	50.16	8.90

Table 6.3-3. Bridge No. 2 Preliminary Isolator Design - ATR

Substructure	FPS Design		LRB Design	
	Q_d, k/beam	k_d, k/in/beam	Q_d, k/beam	k_d, k/in/beam
Abutment 1	9.85	1.81	12.59	2.12
Pier 1	19.70	3.62	25.18	4.26
Pier 2	19.70	3.62	25.18	4.26
Pier 3	19.70	4.16	25.18	5.05
Pier 4	19.70	4.16	25.18	5.05
Abutment 2	9.85	1.81	12.59	2.12

Table 6.3-4. Bridge No. 2 Preliminary Isolator Design - NMSZ

Substructure	FPS Design		LRB Design	
	Q_d, k/beam	k_d, k/in/beam	Q_d, k/beam	k_d, k/in/beam
Abutment 1	16.06	2.96	20.94	3.55
Pier 1	32.12	5.95	41.89	7.15
Pier 2	32.12	5.95	41.89	7.15
Pier 3	32.12	7.53	41.89	9.68
Pier 4	32.12	7.53	41.89	9.68
Abutment 2	16.06	2.96	20.94	3.55

Table 6.3-5. Bridge No. 3 Preliminary Isolator Design - ATR

Substructure	FPS Design		LRB Design	
	Q_d, k/beam	k_d, k/in/beam	Q_d, k/beam	k_d, k/in/beam
Abutment 1	29.21	3.83	39.98	3.97
Pier 1	58.41	7.55	79.97	7.81
Pier 2	58.41	7.55	79.97	7.81
Pier 3	58.41	7.55	79.97	7.81
Pier 4	58.41	7.55	79.97	7.81
Pier 5	58.41	7.55	79.97	7.81
Pier 6	58.41	7.55	79.97	7.81
Pier 7	58.41	7.55	79.97	7.81
Abutment 2	29.21	3.83	39.98	3.97

Table 6.3-6. Bridge No. 3 Preliminary Isolator Design - NMSZ

Substructure	FPS Design		LRB Design	
	Q_d, k/beam	k_d, k/in/beam	Q_d, k/beam	k_d, k/in/beam
Abutment 1	47.72	6.47	63.64	6.57
Pier 1	95.43	12.62	127.29	12.76
Pier 2	95.43	12.62	127.29	12.76
Pier 3	95.43	12.62	127.29	12.76
Pier 4	95.43	12.62	127.29	12.76
Pier 5	95.43	12.62	127.29	12.76
Pier 6	95.43	12.62	127.29	12.76
Pier 7	95.43	12.62	127.29	12.76
Abutment 2	47.72	6.47	63.64	6.57

Table 6.3-7. Bridge No. 4 Preliminary Isolator Design - ATR

Substructure	FPS Design		LRB Design	
	Q_d, k/beam	k_d, k/in/beam	Q_d, k/beam	k_d, k/in/beam
Abutment 1	19.11	1.56	26.08	1.61
Pier 1	38.21	3.11	52.15	3.19
Pier 2	38.21	3.11	52.15	3.19
Pier 3	38.21	3.29	52.15	3.42
Pier 4	38.21	3.77	52.15	4.03
Pier 5	38.21	3.29	52.15	3.42
Pier 6	38.21	3.11	52.15	3.19
Pier 7	38.21	3.11	52.15	3.19
Abutment 2	19.11	1.56	26.08	1.61

Table 6.3-8. Bridge No. 4 Preliminary Isolator Design - NMSZ

Substructure	FPS Design		LRB Design	
	Q_d, k/beam	k_d, k/in/beam	Q_d, k/beam	k_d, k/in/beam
Abutment 1	8.64	0.70	8.14	0.49
Pier 1	17.27	1.39	16.28	0.98
Pier 2	17.27	1.39	16.28	0.98
Pier 3	17.27	1.43	16.28	1.01
Pier 4	17.27	1.51	16.28	1.05
Pier 5	17.27	1.43	16.28	1.01
Pier 6	17.27	1.39	16.28	0.98
Pier 7	17.27	1.39	16.28	0.98
Abutment 2	8.64	0.70	8.14	0.49

Note: The required design at the selected target displacement for Bridge No. 4, NMSZ case, are outside of the range currently applied and readily available.

Table 6.3-9. Bridge No. 5 Preliminary Isolator Design - ATR

Substructure	FPS Design		LRB Design	
	Q_d, k/beam	k_d, k/in/beam	Q_d, k/beam	k_d, k/in/beam
Abutment 1	20.36	2.94	33.05	3.63
Pier 1	57.94	8.27	94.07	10.15
Pier 2	57.94	8.27	94.07	10.15
Abutment 2	20.36	2.94	33.05	3.63

Table 6.3-10. Bridge No. 5 Preliminary Isolator Design - NMSZ

Substructure	FPS Design		LRB Design	
	Q_d, k/beam	k_d, k/in/beam	Q_d, k/beam	k_d, k/in/beam
Abutment 1	33.61	4.96	52.81	5.96
Pier 1	95.66	13.82	150.30	16.47
Pier 2	95.66	13.82	150.30	16.47
Abutment 2	33.61	4.96	52.81	5.96

Table 6.3-11. Bridge No. 6 Preliminary Isolator Design - ATR

Substructure	FPS Design		LRB Design	
	Q_d, k/beam	k_d, k/in/beam	Q_d, k/beam	k_d, k/in/beam
Abutment 1	57.16	8.75	92.33	11.02
Pier 1	114.33	16.38	184.66	20.02
Abutment 2	57.16	8.75	92.33	11.02

Table 6.3-12. Bridge No. 6 Preliminary Isolator Design - NMSZ

Substructure	FPS Design		LRB Design	
	Q_d, k/beam	k_d, k/in/beam	Q_d, k/beam	k_d, k/in/beam
Abutment 1	96.13	15.71	149.02	19.38
Pier 1	192.27	27.95	298.05	32.92
Abutment 2	96.13	15.71	149.02	19.38

Table 6.3-13. Target Displacements and FPS Parameters - ATR

Bridge	D_{TAR}, in	Substructure	μ_{DYN}	R, in
1	5	Abutments 1-2	0.059	73.5
		Piers 1-4	0.075	57.3
2	12	Abutment 1-2	0.024	223.1
		Piers 1-2	0.031	175.7
		Pier 3-4	0.031	153.1
3	9	Abutment 1-2	0.054	141.1
		Piers 1-7	0.063	123.5
4	14	Abutments 1-2	0.035	345.7
		Piers 1,2,6,7	0.041	299.8
		Piers 3,5	0.041	283.4
		Pier 4	0.041	247.5
5	8	Abutments 1-2	0.036	190.4
		Piers 1-2	0.047	149.3
6	8	Abutments 1-2	0.043	152.4
		Pier	0.047	148.3

Table 6.3-14. Target Displacements and FPS Parameters - NMSZ

Bridge	D_{TAR}, in	Substructure	μ_{DYN}	R, in
1	5	Abutments 1-2	0.084	50.8
		Piers 1-4	0.107	39.4
2	12	Abutment 1-2	0.040	136.2
		Piers 1-2	0.050	107.0
		Pier 3-4	0.050	84.5
3	9	Abutment 1-2	0.088	83.6
		Piers 1-7	0.102	73.8
4	14	Abutments 1-2	0.016	773.8
		Piers 1,2,6,7	0.019	668.9
		Piers 3,5	0.019	652.4
		Pier 4	0.019	616.6
5	8	Abutments 1-2	0.060	113.0
		Piers 1-2	0.077	89.4
6	8	Abutments 1-2	0.072	85.0
		Pier	0.079	86.9

Table 6.3-15. Dynamic Properties of Isolated Bridges - FPS

	ξ_{SYS}, %		T_{EFF}, sec		T_d, sec	
Bridge	**ATR**	**NMSZ**	**ATR**	**NMSZ**	**ATR**	**NMSZ**
1	29.0	28.6	1.84	1.54	2.49	2.06
2	19.1	18.5	3.62	2.84	4.23	3.23
3	18.2	17.8	2.66	2.08	3.59	2.77
4	17.8	18.3	4.10	6.09	5.48	**8.28**
5	29.5	29.1	2.97	2.31	4.05	3.13
6	28.7	27.8	2.93	1.96	3.92	2.96

Table 6.3-16. Dynamic Properties of Isolated Bridges - LRB

	ξ_{SYS}, %		T_{EFF}, sec		T_d, sec	
Bridge	**ATR**	**NMSZ**	**ATR**	**NMSZ**	**ATR**	**NMSZ**
1	28.7	28.3	1.56	1.36	2.08	1.81
2	18.9	18.2	3.30	2.56	3.82	2.86
3	18.0	17.6	2.44	1.93	3.28	2.56
4	17.6	18.4	3.76	6.38	5.00	**9.18**
5	29.3	28.8	2.50	1.98	3.39	2.66
6	28.2	27.0	2.48	1.95	3.27	2.51

CHAPTER 7 - ANALYSIS OF ISOLATED BRIDGES

In CHAPTER 6, preliminary designs of both FPS and LRB isolation systems were carried out for all 6 bridges at both sites for the DBE-level seismic hazard conditions. Both code-based spectral shape (termed ATR spectral shape here) and NMSZ-specific spectral shape from studies conducted in CHAPTER 4 were considered. In CHAPTER 7, a nonlinear response history analysis is conducted for each bridge, for Site No. 1 DBE-level hazard conditions, and for each of the three design ground motion sets developed in CHAPTER 3:

- Record Set 1UHRS: 14 ground motion record pairs amplitude scaled to the Site No. 1 DBE code-based spectral shape
- Record Set 1NMSZ: 14 ground motion record pairs amplitude scaled to the Site No. 1 DBE NMSZ-specific spectral shape
- Record Set 1NMSZB: 14 ground motion record pairs, first amplitude scaled and then spectrum matched using wavelets, to a composite spectral shape which envelopes the code based (ATR) spectral shape and the NMSZ-specific spectral shape. Recall from CHAPTER 3 that the code-based spectral shape for the study sites is more severe than the NMSZ-specific spectral shape at periods shorter than about 1 second, and the NMSZ-specific spectral shape is the more severe of the two at periods beyond about 1 second.

The analysis for record set 1UHRS is intended to provide an evaluation of the simplified procedure results from CHAPTER 6 for a site where code-based spectral shape is appropriate. The purpose of the analysis for record set 1NMSZ is to compare results for a site with the same

bedrock (AASHTO B/C boundary) design accelerations as for record set 1UHRS, but with design spectral shape corresponding to the NMSZ-specific shape for deep emabyment depths developed in CHAPTER 3 for Site No.1. Spectral matching to a composite spectrum with set 1NMSZB serves to provide a comparison between amplitude-scaled and spectrum-matched ground motion records for isolator design in the NMSZ.

In Section 7.1, the modeling of the isolators in CSiBridge is discussed. The specific results reported here - in Section 7.2 - include bi-directional superstructure displacement demands for the isolated bridges, bi-directional isolator demands for both LRB and FPS isolators for each bridge, bi-directional substructure displacement demands at both abutments and intermediate bents, seismic expansion joint requirements for each bridge, yield strength requirements for steel pipe piles to remain elastic at pile-bent bridges 1 through 4, and pre-stressed concrete pile requirements for multi-column bent bridges 5 and 6. Revised isolator designs for other hazard levels besides Site No. 1, DBE-level, are discussed in Section 7.3. Potential material savings from isolation are presented in Section 7.4. Finally, in Section 7.5, partial isolation is explored as a design alternative.

The first step in nonlinear modal time history analysis (Fast Nonlinear Analysis - FNA) is, logically, a modal analysis, dependent upon the mass and initial stiffness distribution and exclusive of any time history loading. Results from the modal analysis are then used in an iterative FNA.

Table 7-1 summarizes the modal analysis results for the six bridges. As mentioned in previous chapters, FPS systems generally operate at a higher stiffness - and consequently lower

period - prior to yielding than LRB counterparts and this is reflected in the Table. T_T is the dominant transverse mode, T_L is the dominant longitudinal mode, and N3 is the number of modes required to capture 100% of the mass in each of the transverse, longitudinal, and vertical translational degrees of freedom.

Some explanation of the apparent discrepancies between the modal analysis results listed here and those listed for the non-isolated bridges in Chapter 5 will be helpful. At first glance, it might seem that the natural periods for the isolated bridge should be the same as those for the non-isolated bridge, at least until the isolators yield. But such is not the case for two reasons. First, the non-isolated superstructure is rigidly attached to the piers for displacement, while the isolated superstructure is attached to the pier with a spring which is nonlinear in nature. For Fast Nonlinear Analysis (FNA), an initial effective stiffness is required by the user and this is the basis for initial natural period calculations. The stiffness properties are adjusted during the analysis to match the exact nonlinear behavior specified by the user, so the initial stiffness is only an estimate, though as mentioned in the CSiBridge Analysis Reference Manual, better estimates of effective stiffness may result in faster convergence of the solution. So the modal analysis results listed here could theoretically be completely different had other initial effective stiffness estimates been used, but since convergence has been reached in each case reported, the final response histories would be the same.

Figures G1.4-1 through G1.4-10 are CSiBridge models and cross sections for Bridges 1 through 6. These were introduced in CHAPTER 1 and are not repeated here. Superstructures for each bridge are modeled as spine elements possessing the appropriate computed properties about

each principal axis and with total mass corresponding to the actual calculated value, distributed in a linear fashion through the elements.

A preliminary summary of results in the form of average actual-to-target isolator demand is provided in Table 7-2. As evident from the table, isolator demands on this soft soil site (Site No. 1) are considerably higher when the analysis includes ground motions scaled or matched to a response spectrum which accounts for site-specific amplification (NMSZ-specific), as opposed to code-based site amplification (ATR).

Table 7-1. Modal Analysis Results for FNA

	LRB System			**FPS System**		
	T_T, sec	**T_L, sec**	**N3**	**T_T, sec**	**T_L, sec**	**N3**
Bridge No. 1	0.69	1.01	341	0.37	0.71	341
Bridge No. 2	1.38	1.73	333	0.63	0.81	335
Bridge No. 3	1.17	1.79	480	0.61	1.26	470
Bridge No. 4	1.87	2.50	450	1.07	1.43	474
Bridge No. 5	1.09	1.64	115	0.40	1.14	112
Bridge No. 6	1.15	1.74	85	0.39	0.90	93

Table 7-2. Actual-to-Target Transverse Isolator Demand

Structure	Loading	$(D_{ISO})_{NLRHA} / (D_{ISO})_{TARGET}$	
		FPS	**LRB**
Bridge No. 1	1UHRS	0.433	0.710
	1NMSZ	0.690	1.027
	NMSZB	0.494	0.728
Bridge No. 2	1UHRS	0.462	0698
	1NMSZ	1.165	1.968
	NMSZB	0.906	1.411
Bridge No. 3	1UHRS	0.460	0.629
	1NMSZ	1.040	1.320
	NMSZB	0.852	1.106
Bridge No. 4	1UHRS	0.420	0.612
	1NMSZ	1.559	2.232
	NMSZB	1.116	1.454
Bridge No. 5	1UHRS	0.497	0.718
	1NMSZ	1.124	1.644
	NMSZB	0.845	1.288
Bridge No. 6	1UHRS	0.560	0.786
	1NMSZ	1.327	1.854
	NMSZB	1.023	1.446

7.1 Modeling the Isolators

Some points regarding the nonlinear time history analysis of bridge models consisting of link type elements are important to note. Most of these points are found in the help system of programs such as SAP2000 and SeismoStruct. Isolators are modeled in SAP2000 using link type elements. The element formulation includes a coupled plasticity model based on hysteretic behavior. The model incorporated into SAP2000 is that proposed by Wen (Wen, 1976) and recommended for isolators by Nagarajaiah, et al (Nagarajaiah, et al., 1991). The isolators have been modeled with non-linear properties for both shear directions and linear properties for each of the other 4 degrees-of-freedom. Finite length (rather than zero-length) links with geometry determined by the superstructure center of mass at the top and top of pier cap at the bottom have been used.

The coupling behavior is important in accurately modeling isolator behavior. Consider the calculated response of the same isolator, once under uni-directional loading to represent uncoupled behavior, and a second time under bi-directional loading with coupled behavior included in the formulation of the elements. Figures 7.1-1 and 7.1-2 show the difference in behavior of isolators without and with coupled degrees of freedom, respectively. The smooth hysteresis curve seen under uni-directional response becomes somewhat chaotic with coupling effects included.

Body constraints provide a seemingly convenient means of modeling pier diaphragms - the movement of the superstructure center of mass and the tops of the isolators as a unit in space. However, when fixed degrees of freedom are assigned to link type elements, constraining link

nodes can produce incorrect results in dynamics. Large stiffness values - but not too large - are preferred over fixed degrees of freedom when links have constrained nodes.

Ritz vector modal analysis is preferred over eigenvector modal analysis. Consequently, small masses and rotational inertias should be assigned to the links. This is necessary for the appropriate Ritz vectors to be generated in the mathematics of the model solution. In situations where all modes can be solved, eigenvector solutions are fine.

Structural damping has been set to 0.5 % (not the usual 5%) of critical for all analyses to obtain displacement estimates based on most of the energy dissipation being taken in the isolators, not the abutments and piers. This is likely to produce somewhat conservative isolator demands, but not as conservative as might be thought. The treatment of damping in multi-degree-of-freedom (MDOF) models has a significant impact upon the results. It is difficult to accurately model damping and most software and textbook solutions treat damping as viscous as a matter of convenience more than a matter of precise reality. Rayleigh damping is often specified for MDOF structures. In Rayleigh damping the damping matrix is a linear combination of the mass and stiffness matrices, as shown by Equation 7-1.

$$\boldsymbol{C} = \alpha \boldsymbol{M} + \beta \boldsymbol{K} \qquad \text{(Eq. 7-1)}$$

This assumption leads to a critical damping ratio - given by Equation 7-2 -which varies from mode to mode as a function of the circular frequency, ω.

$$\xi_i = \frac{1}{2}\left(\frac{\gamma}{\omega_i} + \beta \omega_i\right) \qquad \text{(Eq. 7-2)}$$

Priestley (Priestley, et al., 2007) has demonstrated that tangent-stiffness-based, as opposed to initial-stiffness-based damping is more appropriate for the nonlinear analysis of structures. Given the two parameters, γ and β, it is possible to obtain the desired critical damping ratio, ξ, at two distinct modes of vibration. With the higher frequency taken equal to κ times the lower frequency, ω_1, Priestley shows that the following relationships are necessarily true.

$$\frac{\gamma}{2\omega_1} = \xi \frac{\kappa}{\kappa + 1} \quad \text{(Eq. 7-3)}$$

$$\frac{1}{2}\beta\omega_1 = \xi \frac{1}{\kappa + 1} \quad \text{(Eq. 7-4)}$$

The first term represents that portion of damping which is mass-proportional while the second term represents that portion of damping which is stiffness-proportional. The salient point being that most of the damping in the first mode is mass-proportional when the two chosen frequencies are far apart (i.e., when $\kappa > 1$), thus making it unlikely that tangent-stiffness based damping can be achieved for Rayleigh damping models in the significant, lower modes of vibration.

Priestley suggests an approximate, artificial critical damping ratio, ξ^*, be substituted for the desired actual critical damping ratio, ξ, in accordance with the expression given in Equation 7-5.

$$\xi^* = \xi \frac{1 - 0.1(\mu - 1)(1 - \alpha)}{\sqrt{\frac{\mu}{1 + \alpha\mu - \alpha}}} \quad \text{(Eq. 7-5)}$$

Figure 7.1-3 shows the relationship between ξ^*/ξ and μ for various values of α. For LRB systems, $\alpha = 0.10$ and the above becomes zero when $\mu = 12.111$. For FPS systems, $\alpha = 0.0001$ and a value of zero is reached when $\mu = 11.001$. So, at least for the case of Rayleigh damping, it

would appear that the choice of 0.5% damping is appropriate for the nonlinear analysis of isolated structures given that it is not at all uncommon for isolated systems to have μ-values well above 12.

Priestley and Grant (Priestley & Grant, 2005) proposed the modification presented in Equations 7-6 through 7-8. The nomenclature has been modified to match that used elsewhere in this study.

$$\xi^* = \xi \cdot \lambda_1 \lambda_2 \qquad \text{(Eq. 7-6)}$$

$$\lambda_1 = \sqrt{\frac{\mu}{1 + \alpha\mu - \alpha}} \qquad \text{(Eq. 7-7)}$$

$$\lambda_2 = \alpha + \left(\frac{1-\alpha}{\pi}\right)\left[cos^{-1}\left(\frac{\mu-2}{\mu}\right) - \frac{2(\mu-2)\sqrt{\mu-1}}{\mu^2}\right] \qquad \text{(Eq. 7-8)}$$

Figure 7.1-4 is a plot of this reduction model as a function of displacement ductility for both LRB and FPS systems. While this model proposes somewhat higher ξ*/ξ values, the ratio is still small enough, for μ-values larger than 10, to justify the use of elastic damping much less than the typically assumed value of 5% for both LRB and FPS isolators.

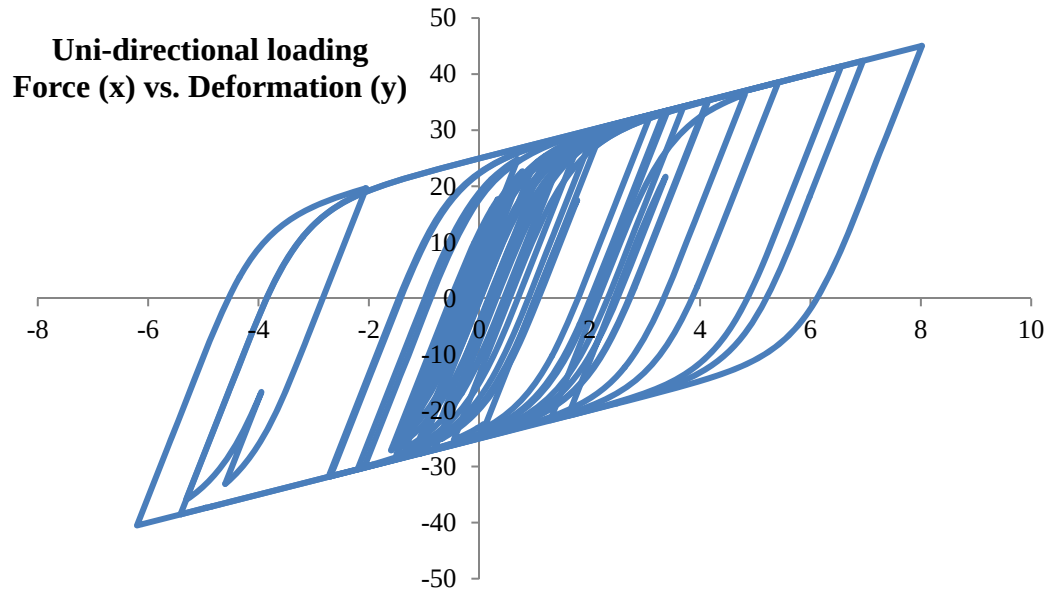

Figure 7.1-1. Uni-directional, Uncoupled Isolator Response

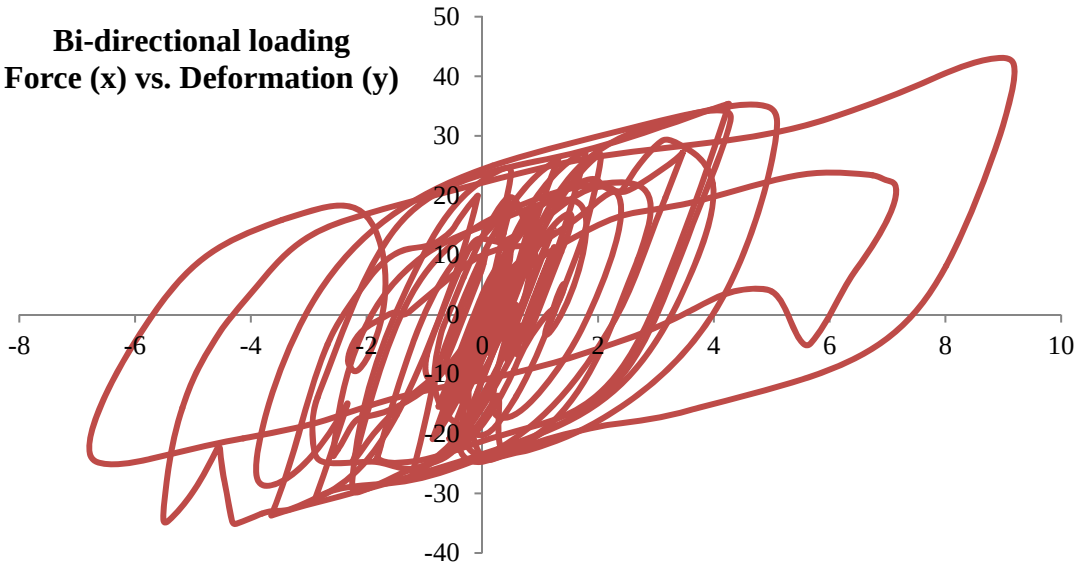

Figure 7.1-2. Bi-directional, Coupled Isolator Response

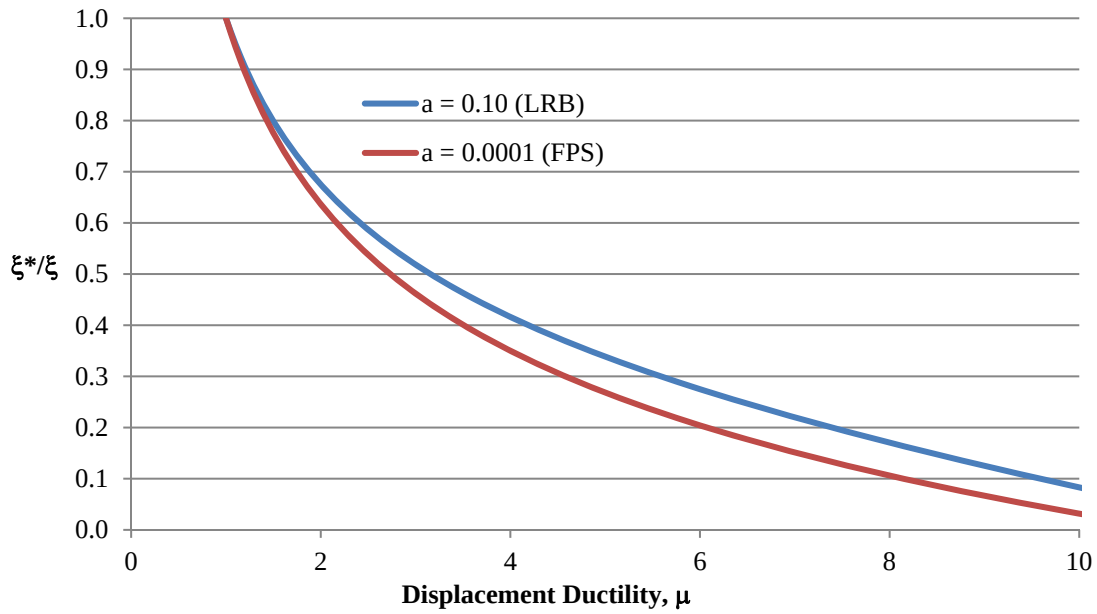

Figure 7.1-3. Reduction in Effective Equivalent Viscous Damping - A

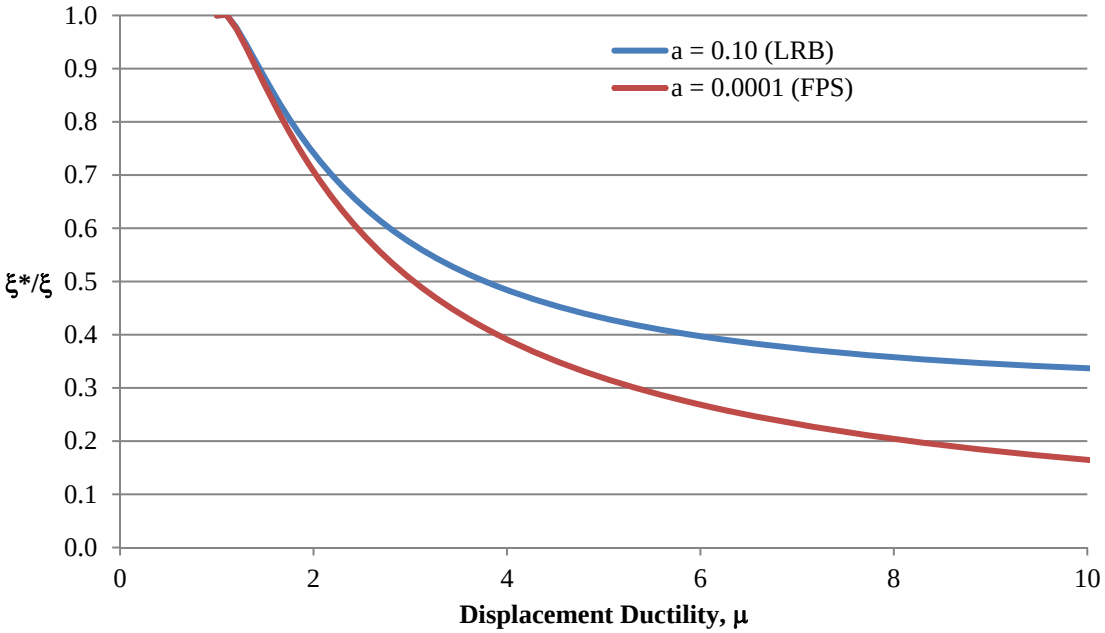

Figure 7.1-4. Reduction in Effective Equivalent Viscous Damping - B

7.2 Site No. 01 - DBE Hazard Level

The primary focus is on response at the Design Basis Event hazard level since this is the basis for AASHTO requirements in both the Standard Specifications for LRFD Bridge Design and in the Guide Specification for Seismic Isolation Design. This corresponds to ground shaking with a 7% probability of exceedance over 75 years for bridges.

Bridges 1 through 4 were analyzed for nonlinear behavior when subjected to loads from the 1UHRS, 1NMSZ, and 1NMSZB record sets. Isolator properties from the preliminary designs in CHAPTER 6 are used for the link-elements in CSiBridge. Recall that the records sets have been formulated as follows:

- Set 1UHRS consists of real records from large magnitude events recorded on Site Class D and E stations and amplitude-scaled to minimize the MSE from the Site 1 DBE-UHRS target.
- Set 1NMSZ consists of both real and artificial records from large magnitude events amplitude-scaled to minimize the MSE from the Site 1 NMSZ-specific acceleration target spectrum.
- Set 1NMSZB consists of real records from large magnitude events recorded on Site Class D and E stations spectrum-matched with wavelets to a composite spectrum which envelopes the Site 1 UHRS and the Site 1 NMSZ-specific spectra.

7.2.1 Superstructure Displacement Results: Bridges 1-4

Superstructure displacements are determined in the transverse and longitudinal directions for each of the three record sets and for each Pile Bent Bridges - nos. 1 through 4.

Superstructure target displacements are shown in each of APPENDIX G7, Figure numbers G7.2.1-1 through G7.2.1-8 for reference. Recall that transverse displacement targets were established in CHAPTER 6 - PRELIMINARY DESIGN OF THE ISOLATORS. Table numbers 7.2.1-1 through 7.2.1-8 summarize the superstructure displacements in each direction from nonlinear analysis.

Longitudinal displacements are typically significantly larger than the transverse displacements for each bridge. This is primarily due to the more flexible substructure conditions in the longitudinal direction relative to transverse. In some cases, in order to limit expansion device requirements, it may be advisable to establish longitudinal, rather than transverse, target displacements. The procedure is identical and requires only an adjustment in substructure stiffness values adopted for the preliminary analysis.

Comparison of the Figures for Bridge Nos. 1 and 2 show the importance of stiffness symmetry in the design of isolated bridges, whether in the NMSZ or otherwise. An unsymmetrical distribution of pier height, and thus substructure stiffness, produces much larger displacement demands on the isolated superstructure.

A similar effect is evident in comparing transverse displacement of Bridge Nos. 3 and 4. While Bridge No. 4 does have a symmetric substructure distribution, it does not possess the property of a uniform substructure stiffness distribution while Bridge No. 3 possesses both. Again, a stark contrast in displacement demands for the two structures is evident.

Table 7.2.1-1. Superstructure Displacements - Bridge No. 1 (inches)

		Longitudinal		Transverse	
Loading-Type	**Location**	**Positive**	**Negative**	**Positive**	**Negative**
1UHRS-FPS	AB1-SS	4.09	3.87	2.21	2.20
	PR1-SS	4.09	3.87	2.20	2.20
	PR2-SS	4.09	3.87	2.20	2.21
	PR3-SS	4.09	3.87	2.20	2.21
	PR4-SS	4.09	3.87	2.20	2.20
	AB2-SS	4.09	3.87	2.21	2.20
1UHRS-LRB	AB1-SS	5.04	4.82	3.53	3.56
	PR1-SS	5.04	4.82	3.52	3.56
	PR2-SS	5.04	4.82	3.52	3.56
	PR3-SS	5.04	4.82	3.52	3.56
	PR4-SS	5.04	4.82	3.52	3.56
	AB2-SS	5.04	4.82	3.53	3.56
1NMSZ-FPS	AB1-SS	4.93	5.46	3.48	3.33
	PR1-SS	4.93	5.46	3.48	3.34
	PR2-SS	4.93	5.46	3.48	3.35
	PR3-SS	4.93	5.46	3.48	3.35
	PR4-SS	4.93	5.46	3.48	3.34
	AB2-SS	4.93	5.46	3.48	3.33
1NMSZ-LRB	AB1-SS	6.36	6.78	4.70	5.07
	PR1-SS	6.36	6.78	4.70	5.08
	PR2-SS	6.36	6.78	4.70	5.09
	PR3-SS	6.36	6.78	4.70	5.09
	PR4-SS	6.36	6.78	4.70	5.08
	AB2-SS	6.36	6.78	4.70	5.07
NMSZB-FPS	AB1-SS	4.65	4.29	2.52	2.47
	PR1-SS	4.65	4.29	2.52	2.47
	PR2-SS	4.65	4.29	2.52	2.47
	PR3-SS	4.65	4.29	2.52	2.47
	PR4-SS	4.65	4.29	2.52	2.47
	AB2-SS	4.65	4.29	2.52	2.47
NMSZB-LRB	AB1-SS	6.05	5.45	3.61	3.65
	PR1-SS	6.05	5.45	3.61	3.65
	PR2-SS	6.05	5.45	3.61	3.66
	PR3-SS	6.05	5.45	3.61	3.66
	PR4-SS	6.05	5.45	3.61	3.65
	AB2-SS	6.05	5.45	3.61	3.65

Table 7.2.1-2. Superstructure Displacements - Bridge No. 2 (inches)

		Longitudinal		Transverse	
Loading-Type	**Location**	**Positive**	**Negative**	**Positive**	**Negative**
1UHRS-FPS	AB1-SS	9.25	9.87	5.04	4.72
	PR1-SS	9.25	9.87	5.25	5.02
	PR2-SS	9.25	9.87	5.48	5.34
	PR3-SS	9.25	9.87	5.81	5.67
	PR4-SS	9.25	9.87	6.19	6.02
	AB2-SS	9.25	9.87	6.57	6.42
1UHRS-LRB	AB1-SS	11.86	11.98	7.31	7.77
	PR1-SS	11.86	11.98	7.54	8.01
	PR2-SS	11.86	11.98	7.80	8.26
	PR3-SS	11.87	11.98	8.10	8.53
	PR4-SS	11.87	11.98	8.43	8.84
	AB2-SS	11.87	11.98	8.78	9.16
1NMSZ-FPS	AB1-SS	21.59	21.80	13.44	11.86
	PR1-SS	21.59	21.80	13.77	12.28
	PR2-SS	21.59	21.80	14.14	12.76
	PR3-SS	21.59	21.80	14.53	13.34
	PR4-SS	21.59	21.80	14.95	13.93
	AB2-SS	21.59	21.80	15.36	14.52
1NMSZ-LRB	AB1-SS	30.30	31.88	22.96	22.98
	PR1-SS	30.30	31.88	23.29	23.32
	PR2-SS	30.30	31.88	23.62	23.67
	PR3-SS	30.30	31.88	23.96	24.01
	PR4-SS	30.30	31.89	24.29	24.35
	AB2-SS	30.30	31.88	24.64	24.74
NMSZB-FPS	AB1-SS	18.17	17.79	10.37	10.24
	PR1-SS	18.17	17.79	10.68	10.55
	PR2-SS	18.17	17.79	11.02	10.86
	PR3-SS	18.17	17.79	11.38	11.19
	PR4-SS	18.17	17.79	11.74	11.61
	AB2-SS	18.17	17.79	12.10	12.03
NMSZB-LRB	AB1-SS	27.70	26.68	15.74	16.61
	PR1-SS	27.70	26.69	15.99	16.86
	PR2-SS	27.70	26.69	16.24	17.11
	PR3-SS	27.70	26.69	16.48	17.35
	PR4-SS	27.70	26.69	16.77	17.60
	AB2-SS	27.70	26.69	17.14	17.83

Table 7.2.1-3. Superstructure Displacements - Bridge No. 3 (inches)

		Longitudinal		Transverse	
Loading-Type	**Location**	**Positive**	**Negative**	**Positive**	**Negative**
1UHRS-FPS	AB1-SS	7.00	6.91	4.22	4.05
	PR1-SS	7.00	6.91	4.30	4.09
	PR2-SS	7.00	6.91	4.32	4.11
	PR3-SS	7.00	6.91	4.30	4.10
	PR4-SS	7.00	6.91	4.29	4.11
1UHRS-LRB	AB1-SS	8.43	8.08	5.69	5.20
	PR1-SS	8.43	8.08	5.76	5.25
	PR2-SS	8.43	8.08	5.78	5.27
	PR3-SS	8.43	8.08	5.77	5.28
	PR4-SS	8.43	8.08	5.77	5.29
1NMSZ-FPS	AB1-SS	13.73	14.37	9.10	9.02
	PR1-SS	13.73	14.37	9.30	9.26
	PR2-SS	13.73	14.37	9.44	9.42
	PR3-SS	13.73	14.37	9.51	9.50
	PR4-SS	13.73	14.37	9.54	9.54
1NMSZ-LRB	AB1-SS	16.45	16.80	11.49	11.58
	PR1-SS	16.45	16.80	11.73	11.74
	PR2-SS	16.45	16.80	11.89	11.83
	PR3-SS	16.45	16.80	11.99	11.88
	PR4-SS	16.45	16.80	12.03	11.89
NMSZB-FPS	AB1-SS	12.66	10.86	7.46	7.18
	PR1-SS	12.66	10.86	7.68	7.38
	PR2-SS	12.66	10.86	7.82	7.50
	PR3-SS	12.66	10.86	7.89	7.57
	PR4-SS	12.66	10.86	7.92	7.60
NMSZB-LRB	AB1-SS	14.38	12.93	9.81	9.02
	PR1-SS	14.38	12.93	10.00	9.23
	PR2-SS	14.38	12.93	10.11	9.37
	PR3-SS	14.38	12.93	10.16	9.45
	PR4-SS	14.38	12.93	10.18	9.47

Table 7.2.1-4. Superstructure Displacements - Bridge No. 4 (inches)

		Longitudinal		Transverse	
Loading-Type	**Location**	**Positive**	**Negative**	**Positive**	**Negative**
1UHRS-FPS	AB1-SS	10.64	11.13	5.85	5.63
	PR1-SS	10.64	11.13	6.08	5.78
	PR2-SS	10.64	11.13	6.43	6.16
	PR3-SS	10.64	11.13	6.66	6.45
	PR4-SS	10.65	11.13	6.75	6.62
1UHRS-LRB	AB1-SS	12.16	12.67	7.56	8.50
	PR1-SS	12.16	12.67	7.78	8.73
	PR2-SS	12.16	12.67	8.15	9.00
	PR3-SS	12.16	12.67	8.48	9.28
	PR4-SS	12.16	12.67	8.64	9.38
1NMSZ-FPS	AB1-SS	29.53	30.12	21.84	20.38
	PR1-SS	29.53	30.12	22.08	20.51
	PR2-SS	29.53	30.12	22.24	20.59
	PR3-SS	29.53	30.12	22.31	20.64
	PR4-SS	29.54	30.12	22.33	20.66
1NMSZ-LRB	AB1-SS	34.97	36.17	31.61	29.69
	PR1-SS	34.97	36.17	31.46	29.82
	PR2-SS	34.97	36.17	31.29	29.88
	PR3-SS	34.98	36.17	31.18	29.88
	PR4-SS	34.98	36.17	31.16	29.88
NMSZB-FPS	AB1-SS	22.98	22.96	15.37	14.40
	PR1-SS	22.98	22.97	15.76	14.64
	PR2-SS	22.98	22.97	16.12	15.00
	PR3-SS	22.98	22.97	16.39	15.24
	PR4-SS	22.98	22.97	16.50	15.33
NMSZB-LRB	AB1-SS	28.13	27.89	20.06	19.32
	PR1-SS	28.13	27.89	20.41	19.47
	PR2-SS	28.13	27.89	20.68	19.60
	PR3-SS	28.13	27.89	20.86	19.68
	PR4-SS	28.13	27.89	20.94	19.71

Table 7.2.1-5. Superstructure Displacements - Bridge No. 1 (cm)

		Longitudinal		Transverse	
Loading-Type	**Location**	**Positive**	**Negative**	**Positive**	**Negative**
1UHRS-FPS	AB1-SS	10.40	9.83	5.60	5.59
	PR1-SS	10.40	9.83	5.59	5.60
	PR2-SS	10.40	9.83	5.59	5.61
	PR3-SS	10.40	9.83	5.59	5.61
	PR4-SS	10.40	9.83	5.59	5.60
	AB2-SS	10.40	9.83	5.60	5.59
1UHRS-LRB	AB1-SS	12.79	12.24	8.96	9.04
	PR1-SS	12.79	12.24	8.95	9.04
	PR2-SS	12.79	12.24	8.95	9.05
	PR3-SS	12.79	12.24	8.95	9.05
	PR4-SS	12.79	12.24	8.95	9.04
	AB2-SS	12.79	12.24	8.96	9.04
1NMSZ-FPS	AB1-SS	12.52	13.88	8.85	8.47
	PR1-SS	12.52	13.88	8.84	8.49
	PR2-SS	12.52	13.88	8.84	8.50
	PR3-SS	12.52	13.88	8.84	8.50
	PR4-SS	12.52	13.88	8.84	8.49
	AB2-SS	12.52	13.88	8.85	8.47
1NMSZ-LRB	AB1-SS	16.16	17.22	11.94	12.88
	PR1-SS	16.16	17.22	11.94	12.90
	PR2-SS	16.16	17.23	11.94	12.92
	PR3-SS	16.16	17.23	11.94	12.92
	PR4-SS	16.16	17.22	11.94	12.90
	AB2-SS	16.16	17.22	11.94	12.88
NMSZB-FPS	AB1-SS	11.80	10.89	6.40	6.29
	PR1-SS	11.80	10.89	6.40	6.28
	PR2-SS	11.80	10.89	6.40	6.28
	PR3-SS	11.80	10.89	6.40	6.28
	PR4-SS	11.80	10.89	6.40	6.28
	AB2-SS	11.80	10.89	6.40	6.29
NMSZB-LRB	AB1-SS	15.37	13.85	9.16	9.27
	PR1-SS	15.37	13.85	9.16	9.28
	PR2-SS	15.37	13.85	9.18	9.29
	PR3-SS	15.37	13.85	9.18	9.29
	PR4-SS	15.37	13.85	9.16	9.28
	AB2-SS	15.37	13.85	9.16	9.27

Table 7.2.1-6. Superstructure Displacements - Bridge No. 2 (cm)

		Longitudinal		Transverse	
Loading-Type	**Location**	**Positive**	**Negative**	**Positive**	**Negative**
1UHRS-FPS	AB1-SS	23.48	25.06	12.79	11.99
	PR1-SS	23.48	25.06	13.34	12.74
	PR2-SS	23.48	25.07	13.92	13.55
	PR3-SS	23.49	25.07	14.76	14.39
	PR4-SS	23.49	25.07	15.73	15.29
	AB2-SS	23.49	25.07	16.68	16.31
1UHRS-LRB	AB1-SS	30.13	30.42	18.57	19.74
	PR1-SS	30.13	30.42	19.16	20.34
	PR2-SS	30.14	30.42	19.82	20.99
	PR3-SS	30.14	30.42	20.58	21.66
	PR4-SS	30.14	30.42	21.41	22.46
	AB2-SS	30.14	30.42	22.31	23.27
1NMSZ-FPS	AB1-SS	54.83	55.36	34.14	30.13
	PR1-SS	54.83	55.36	34.98	31.20
	PR2-SS	54.83	55.36	35.91	32.42
	PR3-SS	54.83	55.36	36.92	33.88
	PR4-SS	54.83	55.37	37.96	35.38
	AB2-SS	54.83	55.36	39.00	36.89
1NMSZ-LRB	AB1-SS	76.95	80.98	58.32	58.38
	PR1-SS	76.95	80.98	59.17	59.24
	PR2-SS	76.95	80.98	60.01	60.11
	PR3-SS	76.96	80.99	60.85	60.98
	PR4-SS	76.96	80.99	61.69	61.86
	AB2-SS	76.96	80.99	62.59	62.85
NMSZB-FPS	AB1-SS	46.16	45.18	26.33	26.01
	PR1-SS	46.16	45.18	27.13	26.79
	PR2-SS	46.16	45.19	28.00	27.58
	PR3-SS	46.16	45.19	28.91	28.43
	PR4-SS	46.16	45.19	29.82	29.49
	AB2-SS	46.16	45.19	30.73	30.55
NMSZB-LRB	AB1-SS	70.36	67.78	39.99	42.18
	PR1-SS	70.36	67.78	40.61	42.82
	PR2-SS	70.37	67.78	41.24	43.46
	PR3-SS	70.37	67.79	41.87	44.08
	PR4-SS	70.37	67.79	42.59	44.69
	AB2-SS	70.37	67.79	43.54	45.30

Table 7.2.1-7. Superstructure Displacements - Bridge No. 3 (cm)

		Longitudinal		Transverse	
Loading-Type	**Location**	**Positive**	**Negative**	**Positive**	**Negative**
1UHRS-FPS	AB1-SS	17.78	17.54	10.73	10.28
	PR1-SS	17.78	17.54	10.91	10.38
	PR2-SS	17.78	17.55	10.96	10.45
	PR3-SS	17.78	17.55	10.92	10.42
	PR4-SS	17.78	17.55	10.90	10.43
1UHRS-LRB	AB1-SS	21.41	20.51	14.45	13.20
	PR1-SS	21.41	20.51	14.64	13.34
	PR2-SS	21.41	20.51	14.68	13.39
	PR3-SS	21.41	20.52	14.66	13.42
	PR4-SS	21.41	20.52	14.66	13.43
1NMSZ-FPS	AB1-SS	34.88	36.50	23.11	22.92
	PR1-SS	34.88	36.50	23.62	23.52
	PR2-SS	34.88	36.50	23.97	23.92
	PR3-SS	34.88	36.50	24.16	24.14
	PR4-SS	34.88	36.50	24.22	24.22
1NMSZ-LRB	AB1-SS	41.78	42.67	29.18	29.42
	PR1-SS	41.78	42.67	29.78	29.82
	PR2-SS	41.79	42.67	30.20	30.05
	PR3-SS	41.79	42.68	30.45	30.17
	PR4-SS	41.79	42.68	30.55	30.21
NMSZB-FPS	AB1-SS	32.15	27.59	18.96	18.25
	PR1-SS	32.15	27.59	19.52	18.74
	PR2-SS	32.15	27.59	19.87	19.06
	PR3-SS	32.15	27.60	20.05	19.24
	PR4-SS	32.16	27.60	20.11	19.30
NMSZB-LRB	AB1-SS	36.53	32.83	24.93	22.91
	PR1-SS	36.53	32.83	25.40	23.45
	PR2-SS	36.53	32.83	25.67	23.80
	PR3-SS	36.54	32.83	25.81	23.99
	PR4-SS	36.54	32.84	25.85	24.05

Table 7.2.1-8. Superstructure Displacements - Bridge No. 4 (cm)

		Longitudinal		Transverse	
Loading-Type	**Location**	**Positive**	**Negative**	**Positive**	**Negative**
1UHRS-FPS	AB1-SS	27.03	28.26	14.87	14.30
	PR1-SS	27.03	28.26	15.45	14.68
	PR2-SS	27.03	28.26	16.33	15.64
	PR3-SS	27.04	28.27	16.92	16.38
	PR4-SS	27.04	28.27	17.13	16.83
1UHRS-LRB	AB1-SS	30.88	32.19	19.20	21.58
	PR1-SS	30.88	32.19	19.77	22.17
	PR2-SS	30.88	32.19	20.71	22.86
	PR3-SS	30.89	32.19	21.53	23.57
	PR4-SS	30.89	32.19	21.94	23.84
1NMSZ-FPS	AB1-SS	75.01	76.51	55.48	51.76
	PR1-SS	75.01	76.51	56.08	52.09
	PR2-SS	75.01	76.51	56.50	52.30
	PR3-SS	75.02	76.51	56.67	52.41
	PR4-SS	75.02	76.52	56.71	52.47
1NMSZ-LRB	AB1-SS	88.83	91.87	80.30	75.41
	PR1-SS	88.83	91.87	79.92	75.73
	PR2-SS	88.83	91.87	79.47	75.88
	PR3-SS	88.84	91.88	79.20	75.89
	PR4-SS	88.84	91.88	79.15	75.91
NMSZB-FPS	AB1-SS	58.37	58.33	39.05	36.58
	PR1-SS	58.37	58.33	40.04	37.20
	PR2-SS	58.37	58.34	40.94	38.10
	PR3-SS	58.37	58.34	41.63	38.70
	PR4-SS	58.38	58.34	41.91	38.93
NMSZB-LRB	AB1-SS	71.44	70.84	50.96	49.08
	PR1-SS	71.44	70.84	51.84	49.45
	PR2-SS	71.45	70.84	52.52	49.77
	PR3-SS	71.45	70.84	52.98	49.98
	PR4-SS	71.45	70.85	53.20	50.06

7.2.2 Material Yield Strength Requirements: Bridges 1-4

The most critical factor in assessing the feasibility of isolation for pile bents is the yield strength necessary to maintain linear, elastic behavior in the pile, thus enabling thinner wall piles to be used. Required values were determined using yield criteria developed in Chapter 4 and are summarized in Table 7.2.2-1 for FPS isolation and in Table 7.2.2-2 for LRB systems. Note that Bridge No. 3 and Bridge No. 4 are symmetric about Pier No. 4. The values are based on the use of 51 cm x 0.8 cm (20” x 5/16”) pipe piles. So it would be possible to decrease the required yield strength values in the tables by increasing the wall thickness of the piles and re-running the analyses with the revised properties. Of course, if the thickness were to be increased all the way up to 5/8”, then the benefits of isolation have been completely negated since the 5/8” piles qualify as ductile and are able to form plastic hinges.

The table illustrates the difficulty - not the impossibility - of applying isolation in the NMSZ. While the values for Bridge No. 4 are somewhat smaller than those for Bridge No. 3, recall that the isolator properties identified from the preliminary design and used in the detailed, nonlinear model for this bridge are outside of the range applied in practice to date. Certainly Bridges 1 and 2 - shorter and wider in a relative sense than the others - present the greatest potential for the application of isolation.

Of course, if elastic behavior is designed for in the pipe piles, then some multiple of the values required should be specified in the design documents. A reasonable value would be 1.25 times the tabulated requirement. Figures G7.2.2-1 through G7.2.2-16 in APPENDIX G7 summarize the results graphically.

Some general observations from the referenced figures and tables are made here.

- Required piling strengths are higher for NMSZ loading cases - scaled 1NMSZ and spectrum-matched 1NMSZB, compared to the 1UHRS loading condition.
- The effect is more pronounced when unsymmetrical and/or non-uniform substructure stiffness distribution effects are included. This can be seen by comparing results for Bridge No. 1 vs. Bridge No. 2, and as well in comparing results for Bridge No. 3 vs. Bridge No. 4. The increase in piling strength requirements for NMSZ-specific record sets compared to UHRS record sets is greater for irregular and non-symmetric Bridge No. 2 (compared to its symmetric and regular counterpart, Bridge No. 1) and irregular Bridge No.4 (compared to its symmetric, yet irregular counterpart, Bridge No. 3).
- Strength requirements in the piles when LRB isolators were modeled are slightly higher than the corresponding values for the same structure modeled using FPS isolators.
- Strength requirements for spectrum-matched record set 1NMSZB are consistently a bit less than those for scaled set 1NMSZ, but still considerably less than those for scaled record set 1UHRS.

Table 7.2.2-1. Pipe Pile Required Yield Strength - FPS Isolation System

		Pipe Pile $(F_y)_{REQD}$, MPa (ksi)			
Pier	**Record Set**	**Bridge 1**	**Bridge 2**	**Bridge 3**	**Bridge 4**
1UHRS	**Pier 1**	340 (49.2)	305 (44.2)	541 (78.4)	436 (63.3)
	Pier 2	340 (49.2)	306 (44.4)	541 (78.4)	433 (62.8)
	Pier 3	340 (49.2)	314 (45.5)	542 (78.7)	469 (68.0)
	Pier 4	340 (49.2)	317 (45.9)	544 (78.9)	419 (60.8)
1NMSZ	**Pier 1**	367 (53.2)	472 (68.4)	751 (109)	723 (105)
	Pier 2	367 (53.2)	465 (67.5)	749 (109)	729 (106)
	Pier 3	367 (53.2)	516 (74.9)	755 (109)	775 (112)
	Pier 4	367 (53.2)	518 (75.2)	761 (110)	771 (112)
1NMSZB	**Pier 1**	364 (52.8)	409 (59.4)	703 (102)	618 (89.6)
	Pier 2	364 (52.8)	406 (58.9)	705 (102)	616 (89.3)
	Pier 3	364 (52.8)	438 (63.6)	707 (103)	659 (95.5)
	Pier 4	364 (52.8)	440 (63.8)	712 (103)	656 (95.1)

Table 7.2.2-2. Pipe Pile Required Yield Strength - LRB Isolation System

		Pipe Pile $(F_y)_{REQD}$, MPa (ksi)			
Pier	**Record Set**	**Bridge 1**	**Bridge 2**	**Bridge 3**	**Bridge 4**
1UHRS	**Pier 1**	352 (51.0)	354 (51.3)	577 (83.6)	471 (68.3)
	Pier 2	352 (51.0)	354 (51.3)	581 (84.3)	472 (68.5)
	Pier 3	352 (51.0)	333 (48.2)	583 (84.5)	496 (72.0)
	Pier 4	352 (51.0)	334 (48.5)	583 (84.5)	436 (63.2)
1NMSZ	**Pier 1**	411 (59.6)	618 (89.6)	818 (119)	765 (111)
	Pier 2	411 (59.6)	618 (89.6)	827 (120)	767 (111)
	Pier 3	411 (59.6)	703 (102)	827 (120)	875 (127)
	Pier 4	411 (59.6)	705 (102)	825 (120)	901 (131)
1NMSZB	**Pier 1**	383 (55.5)	532 (77.2)	752 (109)	658 (95.4)
	Pier 2	383 (55.5)	532 (77.2)	759 (110)	660 (95.7)
	Pier 3	383 (55.5)	601 (87.1)	759 (110)	742 (108)
	Pier 4	383 (55.5)	602 (87.3)	759 (110)	755 (109)

7.2.3 Displacement Results: Bridges 5-6

Bridges 5 and 6 are very symmetric and regular structures, with the superstructure behaving as a rigid block in the isolated condition.

Results for Bridge No. 6 are very similar to that of Bridge No. 5. Symmetric structures with low span length to deck width ratios are likely to have the benefit of a uniform transverse displacement response for either LRB or FPS isolation systems when properly designed.

Substructure displacements are well below the 4” maximum permitted by AASHTO Guide Specification (AASHTO, 2009) Article 5.2.4.2 at the abutments, so linear behavior would be expected in these areas and isolation has been effective in this respect. These results are summarized in Tables 7.2.3-2 and 7.2.3-4.

Isolator demands are shown graphically for Bridges 5 and 6 in Figures 7.2.3-1 and 7.2.3-2. Transverse and longitudinal demands are comparable in all cases. FPS results are lower than LRB results in all cases. Isolator demands for Bridges 5 and 6 were considerably higher for the load cases 1NMSZ and NMSZB compared to those for load case 1UHRS. Recall that load case 1NMSZ consists of 14 records amplitude scaled to minimize MSE between the scaled set and a target response spectrum incorporating site specific amplification effects. Load case 1UHRS consists of 14 record pairs scaled to match a code-based response spectrum. Load case NMSZB consists of 14 record pairs spectrum-matched using wavelets to the NMSZ-specific target spectrum. A trend is noticeable in the graphs - isolator demands from analysis using the spectrum-matched record set are consistently slightly lower than demands from analysis using the amplitude-scaled record set with the same target spectrum.

Table 7.2.3-1. Superstructure Displacements: Bridge No. 5

		FPS		LRB		Transverse
Location	**Loading**	**Trans. cm (in)**	**Longit. cm (in)**	**Trans. cm (in)**	**Longit. cm (in)**	**Target cm (in)**
Abutment	1UHRS	9.8 (3.88)	10.8 (4.26)	14.3 (5.63)	15.2 (5.97)	20.3 (8.00)
	1NMSZ	22.6 (8.89)	21.4 (8.41)	32.5 (12.79)	28.8 (11.33)	20.3 (8.00)
	NMSZB	17.0 (6.67)	17.7 (6.97)	25.7 (10.11)	25.7 (10.12)	20.3 (8.00)
Bent	1UHRS	9.9 (3.89)	10.8 (4.26)	14.3 (5.64)	15.2 (5.97)	20.3 (8.00)
	1NMSZ	22.6 (8.90)	21.4 (8.41)	32.5 (12.81)	28.8 (11.33)	20.3 (8.00)
	NMSZB	17.0 (6.69)	17.7 (6.97)	25.7 (10.13)	25.7 (10.12)	20.3 (8.00)

Table 7.2.3-2. Substructure Displacements: Bridge No. 5

		FPS		LRB	
Location	**Loading**	**Trans. cm (in)**	**Longit. cm (in)**	**Trans. cm (in)**	**Longit. cm (in)**
Abutment	1UHRS	1.7 (0.67)	1.8 (0.70)	2.1 (0.83)	2.2 (0.87)
	1NMSZ	2.0 (0.78)	2.0 (0.79)	2.6 (1.03)	2.6 (1.03)
	NMSZB	1.7 (0.68)	0.6 (0.25)	2.2 (0.86)	2.3 (0.92)
Bent	1UHRS	0.5 (0.20)	0.6 (0.25)	0.6 (0.23)	0.7 (0.28)
	1NMSZ	0.6 (0.24)	0.7 (0.27)	0.8 (0.30)	0.8 (0.31)
	NMSZB	0.5 (0.21)	0.6 (0.25)	0.6 (0.23)	0.7 (0.27)

Table 7.2.3-3. Superstructure Displacements: Bridge No. 6

		FPS		LRB		Transverse
Location	**Loading**	**Trans. cm (in)**	**Longit. cm (in)**	**Trans. cm (in)**	**Longit. cm (in)**	**Target cm (in)**
Abutment	1UHRS	11.0 (4.33)	12.2 (4.79)	15.4 (6.07)	16.1 (6.34)	20.3 (8.00)
	1NMSZ	25.7 (10.13)	25.8 (10.15)	35.9 (14.13)	32.4 (12.76)	20.3 (8.00)
	NMSZB	20.1 (7.90)	22.3 (8.77)	28.4 (11.17)	28.5 (11.24)	20.3 (8.00)
Bent	1UHRS	11.1 (4.37)	12.2 (4.79)	15.3 (6.03)	16.1 (6.34)	20.3 (8.00)
	1NMSZ	25.9 (10.19)	25.8 (10.15)	35.7 (14.05)	32.4 (12.76)	20.3 (8.00)
	NMSZB	20.2 (7.95)	22.3 (8.77)	28.2 (11.11)	28.5 (11.24)	20.3 (8.00)

Table 7.2.3-4. Substructure Displacements: Bridge No. 6

		FPS		LRB	
Location	**Loading**	**Trans. cm (in)**	**Longit. cm (in)**	**Trans. cm (in)**	**Longit. cm (in)**
Abutment	1UHRS	2.0 (0.77)	2.2 (0.85)	2.2 (0.88)	2.4 (0.94)
	1NMSZ	2.5 (0.99)	2.6 (1.02)	3.2 (1.27)	2.9 (1.15)
	NMSZB	2.2 (0.87)	09 (0.34)	2.6 (1.02)	2.7 (1.07)
Bent	1UHRS	0.2 (0.08)	0.4 (0.16)	0.2 (0.08)	0.4 (0.14)
	1NMSZ	0.3 (0.10)	0.5 (0.18)	0.3 (0.13)	0.5 (0.19)
	NMSZB	0.6 (0.25)	0.9 (0.34)	0.7 (0.28)	0.9 (036)

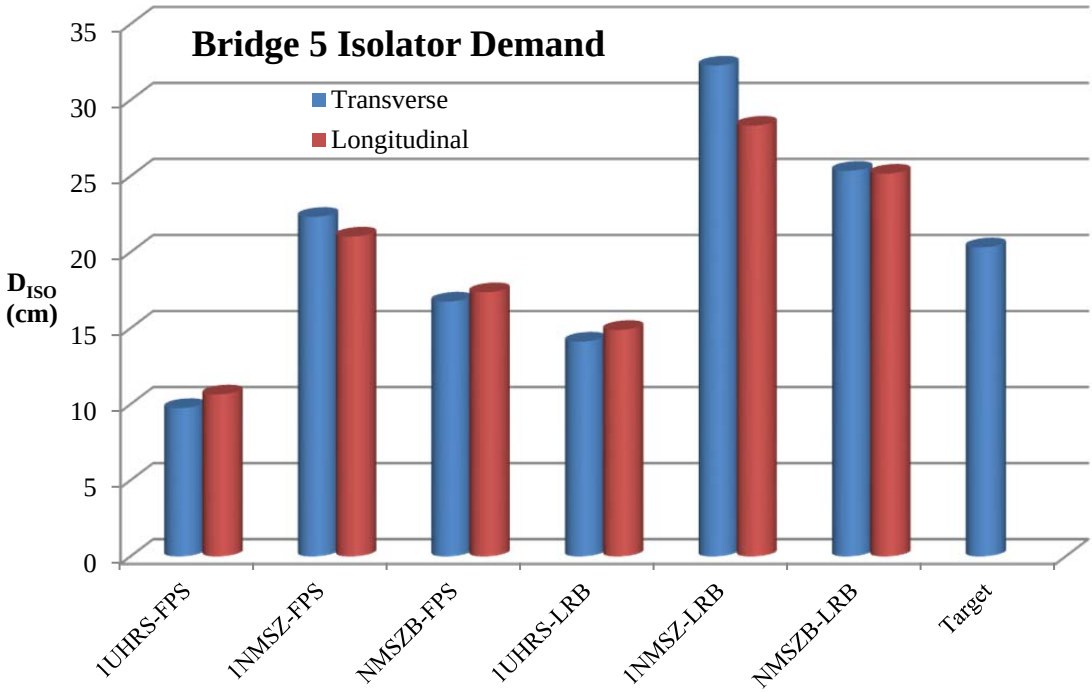

Figure 7.2.3-1. Bridge No. 5 Isolator Demand

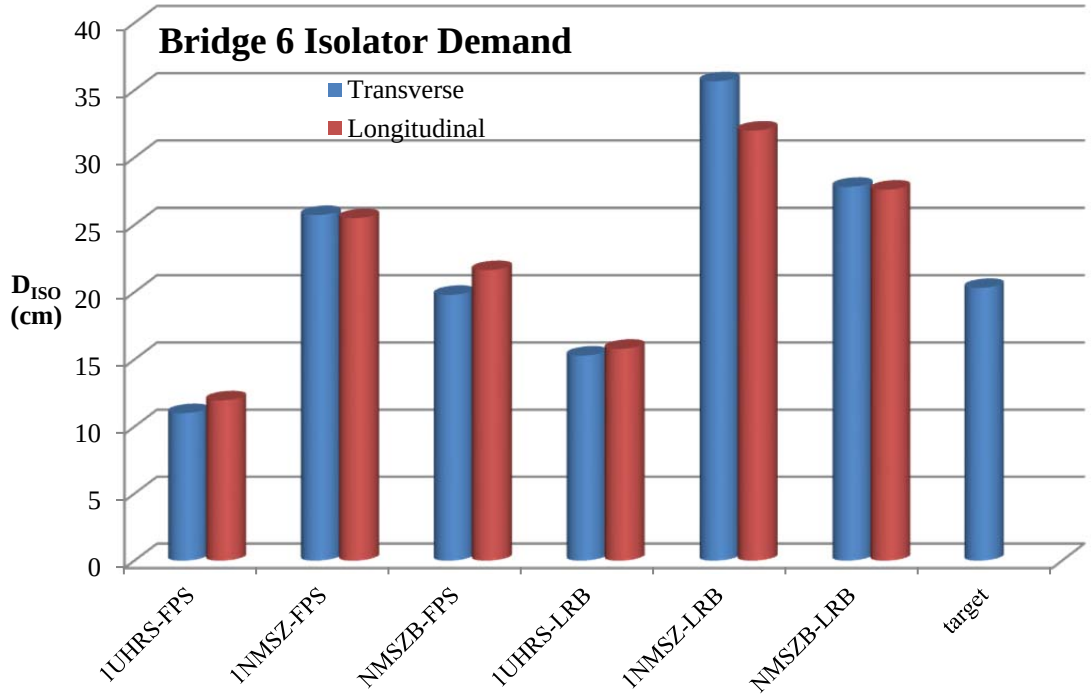

Figure 7.2.3-2. Bridge No. 6 Isolator Demand

7.2.4 Required Seismic Joint Movements

One of the most significant side-effects of complete isolation is the need to provide expansion joints at both abutments. And these joints are not typical expansion joints in that they must have movement capabilities on both transverse and longitudinal directions. Note that the isolator demands reported above are only the seismic movement requirements and would need to be added to thermal movements in the longitudinal direction. While the movements could likely be somewhat reduced in most cases by tweaking isolator properties, the difficulties presented in the form of expensive, maintenance intensive joints is significant. Special seismic joints with large bi-directional movement capacity in the horizontal plane and simultaneous rotation capacities are available for such purposes. See, for example, the Maurer / D. S. Brown swivel expansion joint assembly (http://www.dsbrown.com/Bridges/)

7.2.5 Isolator Demands: Bridges 1-4

The transverse and longitudinal isolator demands for Bridges 1 through 4 are reported in Tables 7.2.5-1 through 7.2.5-8 and in Figures G7.2.5-1 through G7.2.5-8, APPENDIX G7. The “target” plots are in the transverse direction from preliminary design of the isolators, but are shown on both the longitudinal and transverse graphs for reference.

The preliminary design, based upon substitute structure simplified analyses for the code-based target spectral shape, has conservatively estimated isolator response only for the record set matched to the code-base target spectrum. As was the case for Bridges 5 and 6, isolator demands in the NMSZ should be expected to be considerably higher due to (a) deep soil site amplification effects and (b) failure of code-based elastic displacement amplification (R_d in AASHTO) to fully capture nonlinear response at ductility values beyond about 4.

Table 7.2.5-1. Isolator Demand - Bridge No. 1 (inches)

		Longitudinal		Transverse	
Loading-Type	**Location**	**Positive**	**Negative**	**Positive**	**Negative**
1UHRS-FPS	AB1-SS	3.86	3.66	2.05	2.04
	PR1-SS	2.66	2.43	2.05	2.06
	PR2-SS	2.66	2.43	2.05	2.06
	PR3-SS	2.66	2.43	2.05	2.06
	PR4-SS	2.66	2.43	2.05	2.06
	AB2-SS	3.86	3.66	2.05	2.04
1UHRS-LRB	AB1-SS	4.80	4.64	3.36	3.40
	PR1-SS	3.26	3.08	3.32	3.35
	PR2-SS	3.26	3.07	3.32	3.35
	PR3-SS	3.26	3.07	3.32	3.35
	PR4-SS	3.26	3.08	3.32	3.35
	AB2-SS	4.80	4.64	3.36	3.40
1NMSZ-FPS	AB1-SS	4.67	5.19	3.24	3.16
	PR1-SS	3.43	3.76	3.29	3.14
	PR2-SS	3.43	3.76	3.29	3.15
	PR3-SS	3.43	3.76	3.29	3.15
	PR4-SS	3.43	3.76	3.29	3.14
	AB2-SS	4.67	5.19	3.24	3.16
1NMSZ-LRB	AB1-SS	6.11	6.49	4.46	4.93
	PR1-SS	4.39	4.64	4.47	4.84
	PR2-SS	4.40	4.63	4.47	4.84
	PR3-SS	4.40	4.63	4.47	4.84
	PR4-SS	4.39	4.64	4.47	4.84
	AB2-SS	6.11	6.49	4.46	4.93
NMSZB-FPS	AB1-SS	4.36	4.03	2.34	2.31
	PR1-SS	3.08	2.80	2.35	2.30
	PR2-SS	3.08	2.80	2.35	2.30
	PR3-SS	3.08	2.80	2.35	2.30
	PR4-SS	3.08	2.80	2.35	2.30
	AB2-SS	4.36	4.03	2.34	2.31
NMSZB-LRB	AB1-SS	5.69	5.15	3.38	3.45
	PR1-SS	3.87	3.46	3.42	3.46
	PR2-SS	3.87	3.46	3.41	3.46
	PR3-SS	3.87	3.46	3.41	3.46
	PR4-SS	3.87	3.46	3.42	3.46
	AB2-SS	5.69	5.15	3.38	3.45

Table 7.2.5-2. Isolator Demand - Bridge No. 2 (inches)

		Longitudinal		Transverse	
Loading-Type	**Location**	**Positive**	**Negative**	**Positive**	**Negative**
1UHRS-FPS	AB1-SS	9.23	9.84	5.04	4.76
	PR1-SS	8.22	8.78	5.19	4.96
	PR2-SS	8.21	8.79	5.42	5.28
	PR3-SS	2.95	3.23	4.56	4.35
	PR4-SS	3.01	3.27	4.80	4.67
	AB2-SS	9.24	9.85	6.55	6.37
1UHRS-LRB	AB1-SS	11.88	12.13	7.33	7.84
	PR1-SS	10.59	10.68	7.55	7.98
	PR2-SS	10.59	10.69	7.80	8.24
	PR3-SS	4.09	4.02	6.80	7.07
	PR4-SS	4.15	4.05	7.06	7.32
	AB2-SS	11.88	12.14	8.82	9.23
1NMSZ-FPS	AB1-SS	21.45	21.55	13.37	11.85
	PR1-SS	19.41	19.50	13.59	12.15
	PR2-SS	19.45	19.48	13.96	12.62
	PR3-SS	8.88	9.19	11.57	10.76
	PR4-SS	8.91	9.24	11.87	11.22
	AB2-SS	21.46	21.56	15.25	14.47
1NMSZ-LRB	AB1-SS	30.11	31.61	22.88	22.89
	PR1-SS	27.08	28.50	23.08	23.15
	PR2-SS	27.09	28.51	23.41	23.49
	PR3-SS	12.55	12.99	19.83	19.97
	PR4-SS	12.58	13.00	20.14	20.26
	AB2-SS	30.12	31.61	24.55	24.69
NMSZB-FPS	AB1-SS	17.94	17.59	10.24	10.13
	PR1-SS	16.30	15.88	10.53	10.39
	PR2-SS	16.31	15.87	10.87	10.70
	PR3-SS	7.59	6.83	9.02	8.91
	PR4-SS	7.63	6.89	9.32	9.23
	AB2-SS	17.95	17.59	11.96	11.92
NMSZB-LRB	AB1-SS	27.42	26.44	15.63	16.50
	PR1-SS	24.61	23.78	15.79	16.64
	PR2-SS	24.61	23.79	16.03	16.88
	PR3-SS	11.14	10.41	13.61	14.22
	PR4-SS	11.14	10.43	13.88	14.42
	AB2-SS	27.43	26.44	17.06	17.73

Table 7.2.5-3. Isolator Demand - Bridge No. 3 (inches)

		Longitudinal		Transverse	
Loading-Type	**Location**	**Positive**	**Negative**	**Positive**	**Negative**
1UHRS-FPS	AB1-SS	6.52	6.39	3.84	3.76
	PR1-SS	4.32	4.26	3.96	3.80
	PR2-SS	4.24	4.21	3.99	3.82
	PR3-SS	4.22	4.22	4.00	3.83
	PR4-SS	4.20	4.21	3.99	3.83
1UHRS-LRB	AB1-SS	7.90	7.59	5.34	4.82
	PR1-SS	5.12	5.00	5.41	4.93
	PR2-SS	5.07	4.94	5.43	4.95
	PR3-SS	5.07	4.95	5.43	4.96
	PR4-SS	5.08	4.96	5.42	4.95
1NMSZ-FPS	AB1-SS	13.07	13.61	8.64	8.56
	PR1-SS	9.86	10.06	8.88	8.87
	PR2-SS	9.78	9.98	9.00	9.00
	PR3-SS	9.80	9.99	9.06	9.07
	PR4-SS	9.77	9.95	9.09	9.10
1NMSZ-LRB	AB1-SS	15.68	15.95	10.95	11.07
	PR1-SS	11.78	11.87	11.23	11.23
	PR2-SS	11.71	11.79	11.39	11.31
	PR3-SS	11.71	11.79	11.49	11.36
	PR4-SS	11.71	11.80	11.52	11.37
NMSZB-FPS	AB1-SS	11.98	10.25	7.01	6.74
	PR1-SS	8.71	7.48	7.27	6.97
	PR2-SS	8.59	7.40	7.38	7.08
	PR3-SS	8.62	7.39	7.46	7.14
	PR4-SS	8.58	7.36	7.50	7.17
NMSZB-LRB	AB1-SS	13.57	12.21	9.24	8.46
	PR1-SS	9.69	8.89	9.45	8.72
	PR2-SS	9.63	8.84	9.56	8.85
	PR3-SS	9.63	8.84	9.62	8.92
	PR4-SS	9.63	8.83	9.63	8.94

Table 7.2.5-4. Isolator Demand - Bridge No. 4 (inches)

		Longitudinal		Transverse	
Loading-Type	**Location**	**Positive**	**Negative**	**Positive**	**Negative**
1UHRS-FPS	AB1-SS	10.39	10.90	5.70	5.51
	PR1-SS	8.72	9.37	5.89	5.60
	PR2-SS	8.75	9.38	6.24	5.99
	PR3-SS	5.37	5.78	5.73	5.63
	PR4-SS	1.88	1.68	4.13	4.01
1UHRS-LRB	AB1-SS	11.98	12.46	7.44	8.38
	PR1-SS	10.03	10.65	7.62	8.59
	PR2-SS	10.06	10.64	7.97	8.85
	PR3-SS	6.30	6.36	7.55	8.32
	PR4-SS	2.37	2.19	5.82	6.18
1NMSZ-FPS	AB1-SS	28.90	29.51	21.40	20.04
	PR1-SS	25.89	26.31	21.71	20.20
	PR2-SS	25.88	26.35	21.85	20.27
	PR3-SS	18.74	19.14	20.54	18.82
	PR4-SS	10.32	10.63	17.08	15.71
1NMSZ-LRB	AB1-SS	34.42	35.57	31.14	29.28
	PR1-SS	30.68	31.90	31.01	29.45
	PR2-SS	30.70	31.89	30.83	29.51
	PR3-SS	22.83	23.50	29.01	27.78
	PR4-SS	12.71	13.32	24.80	23.75
NMSZB-FPS	AB1-SS	22.49	22.44	15.06	14.11
	PR1-SS	19.92	19.70	15.48	14.36
	PR2-SS	19.93	19.73	15.82	14.70
	PR3-SS	13.94	13.81	14.86	13.80
	PR4-SS	6.79	7.06	12.22	11.22
NMSZB-LRB	AB1-SS	27.54	27.33	19.75	18.92
	PR1-SS	24.56	23.97	20.09	19.11
	PR2-SS	24.53	23.95	20.37	19.23
	PR3-SS	17.26	16.73	19.11	17.99
	PR4-SS	8.45	8.47	16.28	14.92

Table 7.2.5-5. Isolator Demand - Bridge No. 1 (cm)

		Longitudinal		Transverse	
Loading-Type	**Location**	**Positive**	**Negative**	**Positive**	**Negative**
1UHRS-FPS	AB1-SS	9.79	9.29	5.22	5.19
	PR1-SS	6.76	6.17	5.22	5.22
	PR2-SS	6.76	6.17	5.21	5.22
	PR3-SS	6.76	6.17	5.21	5.22
	PR4-SS	6.76	6.17	5.22	5.22
	AB2-SS	9.79	9.29	5.22	5.19
1UHRS-LRB	AB1-SS	12.20	11.79	8.53	8.64
	PR1-SS	8.29	7.82	8.43	8.51
	PR2-SS	8.29	7.81	8.42	8.51
	PR3-SS	8.29	7.81	8.42	8.51
	PR4-SS	8.29	7.82	8.43	8.51
	AB2-SS	12.20	11.79	8.53	8.64
1NMSZ-FPS	AB1-SS	11.87	13.17	8.23	8.03
	PR1-SS	8.71	9.54	8.35	7.98
	PR2-SS	8.71	9.54	8.35	8.00
	PR3-SS	8.71	9.54	8.35	8.00
	PR4-SS	8.71	9.54	8.35	7.98
	AB2-SS	11.87	13.17	8.23	8.03
1NMSZ-LRB	AB1-SS	15.51	16.47	11.33	12.53
	PR1-SS	11.15	11.78	11.35	12.30
	PR2-SS	11.17	11.77	11.35	12.30
	PR3-SS	11.17	11.77	11.35	12.30
	PR4-SS	11.15	11.78	11.35	12.30
	AB2-SS	15.51	16.47	11.33	12.53
NMSZB-FPS	AB1-SS	11.06	10.23	5.95	5.86
	PR1-SS	7.82	7.11	5.96	5.84
	PR2-SS	7.82	7.11	5.96	5.84
	PR3-SS	7.82	7.11	5.96	5.84
	PR4-SS	7.82	7.11	5.96	5.84
	AB2-SS	11.06	10.23	5.95	5.86
NMSZB-LRB	AB1-SS	14.46	13.08	8.58	8.77
	PR1-SS	9.83	8.78	8.67	8.78
	PR2-SS	9.83	8.78	8.67	8.78
	PR3-SS	9.83	8.78	8.67	8.78
	PR4-SS	9.83	8.78	8.67	8.78
	AB2-SS	14.46	13.08	8.58	8.77

Table 7.2.5-6. Isolator Demand - Bridge No. 2 (cm)

		Longitudinal		Transverse	
Loading-Type	**Location**	**Positive**	**Negative**	**Positive**	**Negative**
1UHRS-FPS	AB1-SS	23.45	25.00	12.79	12.09
	PR1-SS	20.87	22.30	13.19	12.61
	PR2-SS	20.86	22.34	13.77	13.40
	PR3-SS	7.50	8.21	11.57	11.04
	PR4-SS	7.65	8.29	12.19	11.87
	AB2-SS	23.47	25.01	16.64	16.19
1UHRS-LRB	AB1-SS	30.17	30.82	18.62	19.91
	PR1-SS	26.90	27.13	19.17	20.28
	PR2-SS	26.91	27.14	19.80	20.92
	PR3-SS	10.38	10.22	17.28	17.95
	PR4-SS	10.53	10.28	17.94	18.60
	AB2-SS	30.19	30.83	22.39	23.46
1NMSZ-FPS	AB1-SS	54.49	54.73	33.97	30.10
	PR1-SS	49.31	49.53	34.53	30.86
	PR2-SS	49.40	49.47	35.45	32.05
	PR3-SS	22.56	23.35	29.38	27.33
	PR4-SS	22.62	23.46	30.15	28.51
	AB2-SS	54.51	54.75	38.75	36.75
1NMSZ-LRB	AB1-SS	76.49	80.29	58.11	58.15
	PR1-SS	68.79	72.39	58.62	58.80
	PR2-SS	68.81	72.40	59.45	59.65
	PR3-SS	31.89	32.99	50.36	50.73
	PR4-SS	31.96	33.03	51.15	51.45
	AB2-SS	76.51	80.30	62.35	62.71
NMSZB-FPS	AB1-SS	45.58	44.67	26.01	25.73
	PR1-SS	41.40	40.34	26.75	26.40
	PR2-SS	41.42	40.32	27.60	27.17
	PR3-SS	19.28	17.34	22.92	22.62
	PR4-SS	19.38	17.49	23.67	23.45
	AB2-SS	45.60	44.68	30.37	30.27
NMSZB-LRB	AB1-SS	69.65	67.17	39.69	41.92
	PR1-SS	62.50	60.41	40.09	42.26
	PR2-SS	62.50	60.42	40.71	42.88
	PR3-SS	28.29	26.44	34.58	36.12
	PR4-SS	28.29	26.49	35.24	36.64
	AB2-SS	69.66	67.17	43.32	45.03

Table 7.2.5-7. Isolator Demand - Bridge No. 3 (cm)

		Longitudinal		Transverse	
Loading-Type	**Location**	**Positive**	**Negative**	**Positive**	**Negative**
1UHRS-FPS	AB1-SS	16.56	16.23	9.76	9.54
	PR1-SS	10.98	10.81	10.05	9.64
	PR2-SS	10.77	10.69	10.13	9.70
	PR3-SS	10.73	10.71	10.16	9.72
	PR4-SS	10.66	10.69	10.15	9.73
1UHRS-LRB	AB1-SS	20.07	19.27	13.58	12.25
	PR1-SS	13.00	12.69	13.74	12.52
	PR2-SS	12.87	12.55	13.79	12.57
	PR3-SS	12.88	12.57	13.78	12.59
	PR4-SS	12.91	12.59	13.77	12.58
1NMSZ-FPS	AB1-SS	33.19	34.56	21.94	21.74
	PR1-SS	25.05	25.56	22.56	22.53
	PR2-SS	24.83	25.36	22.85	22.87
	PR3-SS	24.88	25.38	23.02	23.04
	PR4-SS	24.82	25.26	23.09	23.11
1NMSZ-LRB	AB1-SS	39.83	40.50	27.80	28.13
	PR1-SS	29.91	30.15	28.54	28.52
	PR2-SS	29.74	29.95	28.94	28.73
	PR3-SS	29.73	29.95	29.18	28.85
	PR4-SS	29.74	29.97	29.27	28.88
NMSZB-FPS	AB1-SS	30.44	26.04	17.80	17.13
	PR1-SS	22.14	19.01	18.46	17.70
	PR2-SS	21.83	18.79	18.75	17.97
	PR3-SS	21.89	18.76	18.94	18.14
	PR4-SS	21.79	18.69	19.04	18.21
NMSZB-LRB	AB1-SS	34.47	31.00	23.47	21.48
	PR1-SS	24.61	22.58	24.01	22.15
	PR2-SS	24.45	22.46	24.28	22.48
	PR3-SS	24.46	22.44	24.43	22.65
	PR4-SS	24.47	22.43	24.47	22.72

Table 7.2.5-8. Isolator Demand - Bridge No. 4 (cm)

		Longitudinal		Transverse	
Loading-Type	**Location**	**Positive**	**Negative**	**Positive**	**Negative**
1UHRS-FPS	AB1-SS	26.40	27.68	14.47	13.99
	PR1-SS	22.15	23.80	14.97	14.23
	PR2-SS	22.22	23.83	15.84	15.20
	PR3-SS	13.63	14.69	14.56	14.29
	PR4-SS	4.78	4.27	10.50	10.19
1UHRS-LRB	AB1-SS	30.44	31.66	18.89	21.30
	PR1-SS	25.47	27.06	19.34	21.82
	PR2-SS	25.54	27.03	20.24	22.48
	PR3-SS	15.99	16.15	19.16	21.14
	PR4-SS	6.02	5.55	14.79	15.71
1NMSZ-FPS	AB1-SS	73.42	74.95	54.37	50.90
	PR1-SS	65.76	66.82	55.13	51.31
	PR2-SS	65.73	66.93	55.50	51.49
	PR3-SS	47.61	48.62	52.17	47.79
	PR4-SS	26.22	27.00	43.38	39.91
1NMSZ-LRB	AB1-SS	87.44	90.34	79.09	74.38
	PR1-SS	77.93	81.01	78.76	74.80
	PR2-SS	77.97	81.00	78.32	74.96
	PR3-SS	57.98	59.70	73.69	70.57
	PR4-SS	32.29	33.84	63.00	60.34
NMSZB-FPS	AB1-SS	57.12	56.99	38.25	35.84
	PR1-SS	50.58	50.03	39.31	36.47
	PR2-SS	50.63	50.11	40.19	37.34
	PR3-SS	35.42	35.07	37.76	35.06
	PR4-SS	17.24	17.93	31.04	28.49
NMSZB-LRB	AB1-SS	69.95	69.42	50.15	48.06
	PR1-SS	62.39	60.89	51.04	48.55
	PR2-SS	62.31	60.84	51.73	48.84
	PR3-SS	43.84	42.50	48.53	45.71
	PR4-SS	21.45	21.52	41.36	37.91

7.3 Other Hazard Levels

The simplified analysis procedure is used to obtain transverse isolator demand estimates for the other hazard levels - namely at the Site 2 Design Base hazard level (S_{D1} = 0.818), the Site 1 MCE hazard level (S_{D1} - 0.877), and the Site 2 MCE hazard level (S_{D1} = 1.618). The standard spectral shape assumption and damping correction have been used to obtain these estimated properties. To assess the feasibility of isolation at these levels, the goal has been to keep the loading into the substructures equal to that at the Site 1 DBE hazard level. The FPS system properties are selected for comparison purposes as a single, unique solution exists, whereas multiple solutions are possible for LRB systems. A system will be feasible as long as the yielded period is less than 6 seconds - a requirement in AASHTO (AASHTO, 2010), and as long as the required FPS radius of curvature is less than 244 inches. Clearly, devices with larger radii are possible, but this is the current, approximate limit on devices that have been successfully used. Table 7.3-1 summarizes the analysis results for all 6 bridges. While the tabulated results are for transverse analysis only and would not be used for a final design, it is inferred that isolation alone is not feasible at the Site 2 (11.9 km fault distance) MCE hazard level for any of the 6 bridges using the desired strategy of inelastic pile action with no increase in pile size or strength. A combination of isolation and some limited inelastic behavior in the substructures may well be required for certain structures in near-field regions of the NMSZ. The greatest benefit of isolation can be attained when the structure is regular - equal pier heights symmetrically place - and stiff. The large expansion joint requirements could also result in cost prohibitive hardware for the bridges at the Site 1 (59.5 km fault distance) MCE hazard level or even at the Site 2 DBE hazard level.

Table 7.3-1. Isolation Parameters for Other Hazard Levels

Bridge	Hazard	S_{D1}, g	$(D_{ISO-T})_{TAR}$, in	T_{EFF}, sec	T_d, sec	R_{REQD}, in
1	S1DBE	0.555	5.0	1.56	2.08	52
	S2DBE	0.818	10.7	2.28	3.09	113
	S1MCE	0.877	12.3	2.44	3.32	130
	S2MCE	1.618	41.5	4.48	**6.15**	**444**
2	S1DBE	0.555	8.0	2.14	2.29	77
	S2DBE	0.818	16.6	3.08	3.55	161
	S1MCE	0.877	19.0	3.30	3.82	185
	S2MCE	1.618	63.0	6.00	**7.17**	**616**
3	S1DBE	0.555	6.0	1.60	2.08	46
	S2DBE	0.818	12.7	2.33	3.13	107
	S1MCE	0.877	14.5	2.49	3.35	123
	S2MCE	1.618	48.5	4.54	**6.21**	**427**
4	S1DBE	0.555	12.0	3.20	4.19	208
	S2DBE	0.818	25.3	4.65	**6.25**	**447**
	S1MCE	0.877	29.1	4.99	**6.74**	**517**
	S2MCE	1.618	97.3	9.11	**12.47**	**1740**
5	S1DBE	0.555	6.0	1.87	2.50	71
	S2DBE	0.818	12.9	2.74	3.73	161
	S1MCE	0.877	14.8	2.94	4.00	186
	S2MCE	1.618	49.8	5.38	**7.37**	**637**
6	S1DBE	0.555	6.0	1.83	2.32	56
	S2DBE	0.818	12.6	2.65	3.53	122
	S1MCE	0.877	14.4	2.83	3.78	141
	S2MCE	1.618	47.9	5.16	**7.04**	**502**

7.4 Potential Material Savings

The goal of the study has been to demonstrate the feasibility of isolation in certain cases, but also to identify areas where potential savings could be realized in order to offset the cost of the isolation bearings required to achieve the desired response.

For Bridges 1 through 4, the major saving is in pile material quantities and can be significant. If piles can be kept below yield to the extent that essentially elastic behavior is a valid design basis, then the pile quantity may be essentially halved for steel pipe piles, provided the required pipe pile material strength is available. The estimated quantity of piles for Bridge No. 1, for example, is 318,000 pounds for the essentially elastic condition and twice this much for the ductile condition. Some minimal savings would also be realized in lower design shears and moments in the cap beams at the Extreme Event Limit State. If the piles are kept essentially elastic, then it may be possible to relax capacity protection requirements for the caps. The added costs, however, are likely to be significant as well. These come in the form of isolation bearings, large bi-directional expansion joints at the abutments, and increased maintenance of these joints.

For Bridges 5 and 6, elastic column will again result in potentially relaxed capacity protection requirements for both the bent caps and the pile/pile cap systems of the multi-column bent bridges. This can be significant in some instances, but the largest benefit would be in those cases in which fewer piles and/or lower driving requirements for the piles are attainable through isolation. For the set of parameters studied here, the higher resistance factors permitted at the Extreme Event Limit State relative to those at the Strength Limit State for friction piles result in no major change in the number of piles required or in the required pile driving loads. So the

primary source of potential savings for these structures is in relaxed capacity protection of the caps at the top and bottom of the columns.

7.5 Partial Isolation

For structures such as Bridge No.1, the possibilities of partial isolation should be explored. If the abutments could be constructed integrally and only the piers isolated, then the expensive, maintenance-demanding expansion joints could be eliminated altogether. Some simple calculations will demonstrate the feasibility of this option.

Suppose the piers were completely isolated with friction-less, sliding devices. Then the entire contribution to structure stiffness in both the longitudinal and transverse directions is that from the abutments. With Owner's approval, seismic design relying upon the mobilization of passive pressures behind abutments is permitted by the AASHTO Guide Specification for LRFD Seismic Bridge Design (AASHTO, 2009). The permissible pressure behind an abutment back-wall is given in the referenced specification by:

$$p_p = 0.7 \times \frac{2}{3} H_w = 0.7 \times \frac{2}{3} \times 6 = 2.8\ ksf \qquad \text{(Eq. 7-9)}$$

Taking an average value for the backfill coefficient, $F_w = 0.03$, should certainly be justifiable given that backfill behind abutments walls is generally strictly controlled. The resulting initial stiffness from the passive pressure component behind the wall is then:

$$K_{eff1} = \frac{P_p}{F_w H_w} = \frac{2.8\ ksf \times 6' \times 50'}{0.03 \times 6} = \frac{840}{0.18} = 4{,}667\ k/ft = 389\ k/inch \qquad \text{(Eq. 7-10)}$$

The procedure is now to perform a simple analysis of the bridge, treated as a single-degree-of-freedom system in each of the longitudinal and transverse directions. In the longitudinal direction, the maximum permitted force in the back-wall is 840 kips. Should

analysis indicate a higher value, then the abutment spring would have to be softened and the bridge re-analyzed until the force is within the prescribed capacity limit.

For the simplified analysis, it is necessary to evaluate the abutment stiffness in both directions. Note also that the passive pressure at only one abutment back-wall is mobilized at any given instant of time. In the longitudinal direction the total stiffness of the bridge is thus that from the piles at each abutment and the back-wall at a single abutment. The transverse stiffness is that from the piles alone at each abutment combined.

$$K_L = 360 + 360 + 389 = 1{,}109\ kips/inch \qquad \text{(Eq. 7-11)}$$

$$K_T = 360 + 360 = 720\ kips/inch \qquad \text{(Eq. 7-12)}$$

The natural frequencies and response spectrum displacements are then easily determined. For structure mass, use the superstructure mass along with that of the abutments.

$$W = 9.344 \times 250' + 170 \times 2 = 2{,}676\ kips \qquad \text{(Eq. 7-13)}$$

$$T_L = 2\pi\sqrt{\frac{2{,}676}{386.1 \times 1{,}109}} = 0.497\ seconds \qquad \text{(Eq. 7-14)}$$

$$T_T = 2\pi\sqrt{\frac{2{,}676}{386.1 \times 720}} = 0.616\ seconds \qquad \text{(Eq. 7-15)}$$

Both periods are essentially within the constant acceleration plateau - T_S = 0.612 seconds - of the Site 1 DBE Hazard Level spectrum, for which S_{DS} = 0.907 g.

$$SD_L = 0.907 \times 386.1 \times \left(\frac{0.497}{2\pi}\right)^2 = 2.19\ inches \qquad \text{(Eq. 7-16)}$$

$$SD_T = 0.907 \times 386.1 \times \left(\frac{0.616}{2\pi}\right)^2 = 3.37\ inches \qquad \text{(Eq. 7-17)}$$

Back-calculate the force required to be carried in passive resistance at this design displacement in the longitudinal direction. Also, determine the fraction of total longitudinal load carried by the back-wall and the fraction carried in pile flexure.

$$(P_L)_{wall} = 389\frac{kips}{inch} \times 2.19\ inches = 852\ kips > 840\ kips\ \rightarrow No\ Good \qquad \text{(Eq. 7-18)}$$

The approximate softening required is easily calculated since the force is quite close to the limiting values already. Allow for a slight increase in the longitudinal displacement, say up to 2.5 inches.

$$K_{eff1} \cong \frac{840\ kips}{2.50\ inches} = 336\ kips/inch \qquad \text{(Eq. 7-19)}$$

$$K_L = 360 + 360 + 336 = 1{,}056\ kips/inch \qquad \text{(Eq. 7-20)}$$

$$T_L = 2\pi\sqrt{\frac{2{,}676}{386.1 \times 1{,}056}} = 0.509\ seconds \qquad \text{(Eq. 7-21)}$$

$$SD_L = 0.907 \times 386.1 \times \left(\frac{0.509}{2\pi}\right)^2 = 2.30\ inches \qquad \text{(Eq. 7-22)}$$

$$(P_L)_{wall} = 336\frac{kips}{inch} \times 2.30\ inches = 773\ kips < 840\ kips\ \rightarrow Good \qquad \text{(Eq. 7-23)}$$

$$(P_L)_{piles} = 720\frac{kips}{inch} \times 2.30\ inches = 1{,}656\ kips \qquad \text{(Eq. 7-24)}$$

$$(P_T)_{piles} = 720\frac{kips}{inch} \times 3.37\ inches = 2{,}426\ kips \qquad \text{(Eq. 7-25)}$$

$$(P_{Res})_{piles} = \sqrt{1{,}656^2 + 2{,}426^2} = 2{,}938\ kips \qquad \text{(Eq. 7-26)}$$

$$(V_{Res})_{piles} = \frac{2{,}938\ kips}{18\ piles} = 163\ kips\ per\ pile \qquad \text{(Eq. 7-27)}$$

The shear resistance of a circular tube may be taken in accordance with the AASSHTO Specifications, Article 6.12.1.2.3c.

$$V_n = 0.50 F_{cr} A_g \quad \text{(Eq. 7-28)}$$

$$F_{cr} = \frac{0.78E}{\left(\frac{D}{t}\right)^{1.5}} \leq 0.58F_y \quad \text{(Eq. 7-29)}$$

For 20" x 5/16" steel pipe piles, D/t = 64 and A_g = 19.33 in^2.

$$F_{cr} = \frac{0.78 \times 29{,}000}{(64)^{1.5}} = 44.2\ ksi > 0.58 \times 35 = 20.3\ ksi \rightarrow Take\ F_{cr} = 20.3 \quad \text{(Eq. 7-30)}$$

$$V_n = 0.50 \times 20.3 \times 19.33 = 196.2\ kips > 163\ kips \rightarrow OK \quad \text{(Eq. 7-31)}$$

So, even essentially elastic category pipe piles are capable of carrying the seismically induced shears for the partially isolated bridge and the back-wall pressures are below permissible values. The issue remains - do the piles indeed remain elastic. For our assumed yield displacement of 4.00 inches at the abutment piles, the answer is no.

$$D_{SUB} = \sqrt{2.30^2 + 3.37^2} = 4.08\ inches \quad \text{(Eq. 7-32)}$$

The thicker (t = 5/8"), ductile category pipe piles would be required at the abutments. So, essentially elastic 20" x 5/16" pipe piles could be used at the Piers and ductile 20" x 5/8" piles (A_g = 38.0) could be used at the abutments for the partially isolated bridge.

$$V_n = 0.50 \times 20.3 \times 38.0 = 386\ kips > 163\ kips \rightarrow OK \quad \text{(Eq. 7-33)}$$

There is conservatism built into this simplified analysis in that additional damping could be justified from both the abutment response and from the hysteretic behavior of the sliders at the piers.

The situation is a bit more difficult for a structure similar to Bridge No. 3, consisting of more spans, more mass, but of course, still only 2 abutments. An estimate of the partially isolated abutment displacements is developed below.

$$K_{eff1} = \frac{P_p}{F_w H_w} = \frac{2.8\ ksf \times 6' \times 26'}{0.03 \times 6} = \frac{437}{0.18} = 2{,}427\ k/ft = 202\ k/inch \qquad \text{(Eq. 7-34)}$$

$$K_L = 280 + 280 + 202 = 762\ kips/inch \qquad \text{(Eq. 7-35)}$$

$$W = \ 7.53 \times 832' + 150\ \times 2 = \ 6{,}565\ kips \qquad \text{(Eq. 7-36)}$$

$$T_L = 2\pi \sqrt{\frac{6{,}565}{386.1 \times 762}} = 0.939\ seconds \qquad \text{(Eq. 7-37)}$$

$$SA = \frac{0.555}{0.939} = 0.591\ g \qquad \text{(Eq. 7-38)}$$

$$SD_L = 0.591 \times 386.1 \times \left(\frac{0.939}{2\pi}\right)^2 = 5.10\ inches \qquad \text{(Eq. 7-39)}$$

$$T_T = 2\pi \sqrt{\frac{6{,}565}{386.1 \times 560}} = 1.095\ seconds \qquad \text{(Eq. 7-40)}$$

$$SA = \frac{0.555}{1.095} = 0.507\ g \qquad \text{(Eq. 7-41)}$$

$$SD_T = 0.507 \times 386.1 \times \left(\frac{1.095}{2\pi}\right)^2 = 5.95\ inches \qquad \text{(Eq. 7-42)}$$

So, while the displacements are considerably larger, it is not outside the realm of reason to envision the use of ductile piles at the abutments and essentially elastic piles at the piers, even for a longer structure like Bridge No. 3.

CHAPTER 8 - CONCLUSIONS AND RECOMMENDATIONS

In this final chapter, conclusions from the research are summarized in three areas: (1) conclusions regarding bridges in the NMSZ, (2) conclusions regarding ground motion selection and modification and (3) conclusions regarding analytical procedures. Recommendations for future research conclude the study.

8.1 Conclusions Regarding Bridges in the NMSZ

Isolation can be an effective means of protecting bridge structures from the effects of strong ground shaking during earthquakes in the New Madrid Seismic Zone under the right circumstances. Savings in substructure costs may offset or nearly offset the cost of isolators in certain cases. Displacement demands on isolators can be expected to be larger than those for the same system in a tectonic environment outside the intra-plate, deep soil realm found in the Mississippi Embayment. Bridges with short, stiff pile bent supports are one example where the economies of isolation are worth considering during design. Sites approximately 60 kilometers from the NMFS have been shown to be viable isolation candidates at the DBE Hazard Level (7% probability of exceedance in 75 year ground motion). This is the current hazard level basis in the AASHTO design specifications. Sites closer than about 12 kilometers to the NMFS will require much larger expansion joint and isolation bearing movements, but successful designs using standard devices may still be accomplished at the DBE Hazard Level, possibly with some limited inelastic behavior in the substructures. Design of isolation devices at the MCE Hazard Level (3% probability of exceedance in 75 year ground motion) for sites closer than 12 kilometers from the

NMFS will typically require devices outside the range of those which have been successfully used on bridges to date, and most likely will require limited inelastic behavior in the substructures as well. This is not an impossible obstacle to surmount, but would likely require even more expensive device and testing procedures.

When steel pipe piles bents are used, the piling quantity can potentially be halved for an isolated structure compared to that required for a non-isolated bridge. Though not specifically addressed in this study, it is not difficult to envision that isolation could also permit the use of prestressed concrete piles in situations where steel pipe piles might otherwise be required. Typical two and three span grade crossing structures supported on multi-column friction-pile foundations see little economic benefit from isolation relative to Type 2 construction, which relies upon hinging in columns. The potential benefit of a more useable post-event structure still exists for these types of bridges however.

The most significant benefits may be realized for symmetric structures. Non-symmetric pier height arrangements will result in larger displacement demands on isolators and either: (a) a highly non-uniform transverse displacement profile of the superstructure or (b) significantly different device requirements at each sub-structure, a somewhat more costly approach relative to arrangements of similar isolators across the entire bridge.

8.2 Conclusions Regarding Ground Motion Selection and Modification

Ground motion selection is not merely a trivial part of the design for isolation systems. In the New Madrid Seismic Zone, both intra-plate effects and deep soil effects are likely to require the use of modified spectral shapes at periods beyond about 1 second. Code-based site

amplification is un-conservative for deep soil, intra-plate sites appear to be un-conservative at periods longer than about 1 second..

For this study, the source earthquake for selection purposes was taken as the USGS modal event, a magnitude 7.7 earthquake. The most important factor for ground motion selection at far-field sites is spectral shape, with magnitude, site class, and distance being secondary factors. For near-field sites, the presence of pulses and spectral shape are the two most important factors in ground motion selection (NEHRP Consultants Joint Venture, 2011). Amplitude scaling - either at a single period or at a series of discrete periods to minimize mean-square-error between the as-recorded geometric mean and target spectra - provides the preferred option for ground motion modification. SRSS-based scaling often specified in codes has little technical basis when the target response spectrum is geometric-mean based, as is the case with AASHTO spectra definitions. A uniform hazard response spectrum and a New Madrid Seismic Zone specific spectrum were employed as dual target spectra. Matching to a composite spectrum - a spectrum which envelopes the dual targets - was investigated as well.

Spectrum matching through wavelet additions to the actual ground motion provides another option for modification, but preserves less of the character of the original motion compared to amplitude scaling. When pulse-type records are needed for a near-field (R<12 kilometers) site, velocity and displacement histories of the matched accelerogram should be examined to ensure that the pulse characteristics have been preserved through the matching process.

The following guidelines for ground motion selection and modification may be used for bridge sites in the Mississippi Embayment of the New Madrid Seismic Zone.

1. The modal event will most likely be a magnitude 7.7 earthquake but other magnitudes should not be ruled out for initial selection as long as the match to spectral shape is relatively acceptable.
2. Match to spectral shape may be best measured through calculation of the mean-square-error between the record geometric mean and the target.
3. The correlation coefficient between the orthogonal horizontal components of a record should be within the range of -0.30 to +0.30. This is particularly important in pairing synthetic or artificial records to form a pair.
4. Amplitude scaling to minimize the mean-square-error may provide an adequate match between mean scaled record and target spectra. If not, then spectral matching may be used to obtain a much closer fit to the target.
5. The adequacy of fit for a scaled record set to the target spectrum may be evaluated using the FHWA Seismic Retrofit Manual method. For a period range of interest, the minimum scaled-to-target ratio should be 0.85 at any single period. The average scaled-to-target ratio over the same period range should be no less than 1.0.
6. When spectral matching is used, the ratio of component spectral values at a period of 1 second should be maintained. This may be accomplished by matching each component to the appropriate multiple of the target instead of matching each component to the target.

$$Match\ component\ H1\ to\ \frac{SA_{H1}(1)}{SA_{GM}(1)}\ times\ the\ target$$

$$Match\ component\ H2\ to\ \frac{SA_{H2}(1)}{SA_{GM}(1)}\ times\ the\ target$$

7. Long duration records from large magnitude (M_w7.3-M_w8.0) earthquakes recorded at Class D and E sites produce superior results upon spectral matching to target spectra in the NMSZ. This is true in terms of the number of iterations required to perform the matching, the speed of the matching algorithm, the degree of convergence, and the preservation of the general characteristics of the original record.

Real records and synthetic records were obtained and analyzed for compatibility to the target spectra. Both types of ground motion records were used in the final design of the isolated bridges.

It is important that the target spectrum used for ground motion modification include the effects of (a) an intra-plate, stable continental tectonic setting and (b) deep soil profile. Code-based spectral shape - which ignores these effects - is likely to be un-conservative at periods longer than about 1 second for deep soil sites in the Mississippi Embayment of the New Madrid Seismic Zone.

8.3 Conclusions Regarding Analytical Procedures

Effects due to eccentricity in substructure stiffness distribution were found to be generally under-estimated by the AASHTO simplified design procedure. Isolated bridges in the Mississippi Embayment of the New Madrid Seismic Zone should be designed by the nonlinear analysis of the structure to ground motion sets scaled to a target response spectrum which accounts for deep soil amplification effects. Code based site amplification factors (F_{PGA}, F_a, F_v)

and code based displacement amplification factors (R_d) are questionable for the design of bridges in much of the NMSZ when large displacement ductility demands are imposed on the structure.

Duration-dependent damping correction has been demonstrated to be important in estimating FPS isolation demands using the simplified procedure. A modified spectral shape has been developed which provides better estimates for isolation response - both LRB and FPS - estimates from the simplified procedure in the New Madrid Seismic Zone for devices on infinitely rigid substructures. The modified spectral shape generally produces conservative estimates of isolator displacement demand for isolators on realistic stiffness sub-structures when compared to nonlinear response analysis results.

Nonlinear response history analysis should typically be used as the design tool of choice once preliminary design has been completed using simple, response spectrum methods with effective stiffness and equivalent viscous damping from hysteretic behavior. Link type elements available in programs like SAP2000 and SeismoStruct are ideally suited for use in modal time history analysis, which is generally considered to be even more accurate - and much faster - than direct integration time history analysis. Ritz vector modal analysis is preferred over eigenvector modal solution unless every possible mode is solved for and included in the analysis.

A direct displacement-based design procedure is presented and may be useful in certain situations as an alternative to the method found in current specifications. The principles used in the two methods are identical. In the direct displacement based procedure, the engineer decides on a target displacement up front and then determines the isolator properties necessary to give the target response. In the code methods, preliminary values of isolator properties are established

and the resulting displacement is calculated. It can be expected that displacement demands from this type of analysis would be somewhat lower than the appropriate design demand due to the uni-directional nature of these analyses.

Simplified means of accounting for bi-directional effects are found to significantly under-estimate total isolator demand. Hence, the preference for nonlinear time history analyses as a final design tool to complement the preliminary design process. The 100-30 rule currently specified in AASHTO for estimating bi-directional response is found to be inadequate. In particular, when damping is 30% or less, the simplified rule is likely to provide displacement estimates significantly lower than those from response history analysis results. The effect is significant and deserves further study. However, it is important to note that the effect could easily be exaggerated if researchers estimate bi-directional effects by taking design displacements equal to the vector resultant of two orthogonal maxima. The proper method of determining total design isolator displacements in nonlinear time history analyses for a given bi-directional loading is to find the vector resultant at each time step and find the maxima, not to find the vector resultant of the maxima in each direction. The error in taking the more conservative route was found to be virtually negligible for some ground motions used in the study and as much as 30% for other ground motions.

Regarding sites in which intra-plate and deep soil effects are absent, simplified analysis procedures are found to give reasonable estimates of uni-directional isolator response for LRB Systems and to over-estimate uni-directional FPS response when the effective hysteretic damping is greater than 30%. The 30% limit on effective hysteretic damping imposed by the AASHTO Guide Specification for Seismic Isolation Design has thus been found overly

conservative for the Friction Pendulum System in which theoretical damping can be as high as 63.7%. The effect the 30% cap upon Lead-Rubber Bearing system response is negligible since these systems typically possess post-yield ratios of $\alpha = 0.10$, giving a maximum theoretical damping of 33.1%, only minimally higher than the imposed 30% limit.

Regarding sites like the Mississippi Embayment of the New Madrid Seismic Zone, where intra-plate and deep soil effects are present, the simplified analysis (substitute structure) method often produces un-conservative estimates of isolator response if the spectral shape used in the method does not account for the intra-plate and deep soil effects.

Lead-Rubber Bearing systems have shown less scatter in residual displacement analysis results and generally lower residual displacements than Friction Pendulum Systems having dynamic friction coefficients in the high end on the range currently used in practice. Hence, the use of FPS bearing should keep specified dynamic friction coefficient values as low as possible.

The following useful reminders for nonlinear modal analysis applied to isolator-type elements have been identified and are summarized here.

- Ritz vector modal analysis is preferred over eigenvector modal analysis unless every possible mode is found and included in the analysis.
- Coupling between the two shear degrees of freedom in link-type isolators can be crucial to accurately evaluate displacement demands imposed on isolation systems.
- Care is essential in applying even small amounts of viscous damping to bridge models. This applies for constant modal damping and to Rayleigh damping in which the damping matrix is a combination of stiffness-proportional and mass-proportional components.

- FNA is much faster than direct-integration response history analysis, but is primarily applicable in situations where all of the nonlinear behavior occurs in link-type elements. When nonlinear behavior occurs in both isolators and frame elements of the superstructure or substructure, FNA may not be applicable and analysts are forewarned to consult software manuals and developers for guidance in such situations.
- In order to properly apply capacity-design principles to protected elements of the structure, it is essential to include higher-mode, local effects. While 90% of the total system mass may be fine for non-isolated structures, this has the possibility of completely ignoring local modes at substructures and severely under-estimating displacement demands on columns and piles. This can be solved by including enough modes to capture 100% of the translational mass in each direction or by hand calculations when this is not feasible.

8.4 Recommendation for Future Research

There is a need for work in the area of displacement spectra development for intra-plate earthquakes at deep soil sites such as those which are capable of occurring in the NMSZ. Specifically, ground motion prediction models for inelastic displacement spectra would be ideal since inelastic displacement is the most important design parameter in bridge design practice. Inelastic displacement spectra and amplification factors for ground motion sets used in this study are included as APPENDIX F of this study.

Future research into the use of both (a) modified spectral shape and (b) duration dependent damping factors in the AASHTO simplified method for seismic isolation design

would be an important addition to design specifications. Refinement of the formulations proposed here could form the basis of a major research effort.

There are implications for conventional design as well, seismic isolation aside. The AASHTO method of estimating inelastic displacement - the R_d method - is shown in APPENDIX F to be un-conservative for ground shaking during large magnitude events at high ductility demands. The substitute structure method (SSM) - based on effective stiffness and effective damping - provides better estimates of inelastic displacement response compared to the R_d method. The SSM holds promise for both the development of inelastic spectra and use in design provisions for conventionally designed (non-isolated) bridge structures.

Additional research is needed as well in the area of residual displacement estimation. It might seem, at first glance, that residual displacement following an earthquake for a nonlinear system might be impossible to determine with any degree of confidence. It has been observed (Ruiz-Garcia & Miranda, August 2005), however, that the statistical dispersion of residual-to-elastic displacement ratios may actually be less than that for inelastic-to-elastic displacements. A rational means of estimating residual displacements at the mean, median, 80^{th} percentile and 90^{th} percentile levels has been proposed based on procedures from the LESSLOSS project in Europe. So the development of residual displacement spectra might not be such a stretch after all and might provide valuable insight into the problem of determining when isolation is a better strategy compared to ductile substructure design.

The stiffness of abutments during earthquake loading in both the transverse and longitudinal directions of a bridge is a difficult number to evaluate and a wide range of values can be obtained. Work on appropriate stiffness of pile-supported abutments will prove valuable

to engineers working on the seismic design of bridges. Some researchers treat abutments as completely fixed to the moving ground. Others use estimates of stiffness which can potentially make the abutments actually softer than the piers of a bridge structure - the philosophy adopted for the analysis of all 6 bridges in this study.

The effects of the deep, soft soil deposits found in the Mississippi Embayment of the New Madrid Seismic Zone on near-field, pulse-type ground motions applied at bedrock deserves further attention. One study (Rahnama, 1993) stated in the conclusions that “soft soil amplifications of elastic and inelastic strength demands do not depend strongly on the rock motion spectral shape. In general, the results obtained from near-source rock motions are close to those obtained from the far-source rock motions.” This is one potential source of hazard relief in the ME.

More statistical analysis should be conducted on nonlinear response history results. Policy-makers and specification writers need to evaluate appropriate confidence levels and accuracy requirements to establish more realistic, scientifically-based sample size requirements.

There is no easy answer for the selection and modification of ground motions for nonlinear analysis of structures in the New Madrid Seismic Zone. Consider Site 1 in Memphis from this study. Assume that active tectonic region records are being matched to the target response spectrum. The modal source is an M7.7 earthquake at 59.5 kilometers and the Site Class is near the boundary between D and E. Assuming that intra-plate earthquakes do in fact attenuate more slowly than inter-plate earthquakes, set a range on distance of 20-80 kilometers, on magnitude of 7.3-7.9, and consider only recordings from stations on Site Class D or E subsurface conditions. Choose amplitude scaling to minimize mean-square-error at discrete

periods of 0.5, 1, 2, 3, and 4 seconds and a uniform hazard target spectrum. Starting with a database of 279 record pairs meeting the criteria outlined for Site 1, each of these record pairs was scaled and sorted by scale factor, from lowest to highest. Table 8.4-1 lists the first 7 records.

So for this site in Memphis, the design ground motion is a minimum of 34% higher than that recorded at any station under similar site conditions for all of the events considered. The events and stations considered are not the only ones meeting the criteria, but encompass a very wide range of candidates from around the world. Is the seismic hazard in the NMSZ really this severe? Perhaps. And the fact that we know less about the spectral shapes beyond a 1-second period for deep soil sites lends credence to the possibility that it is this severe. This is a key question which additional research needs to address. This is the price to be paid given the lack of data from strong motion recordings in the NMSZ.

If, on the other hand, a risk-targeted spectrum is chosen as the target, the resulting scale factors are those given in Table 8.4-2. This is one argument in favor of using risk-targeted spectra over uniform hazard spectra. It would seem somewhat logical for scale factors to be close to unity when appropriate events and stations are selected. These factors have been determined on the presumption that the standard AASHTO spectral shape is valid for the NMSZ - a questionable presumption. Again, however, the first priority is learning more about spectral shape at deep soil sites of the Mississippi Embayment and incorporating these shapes into codes and specifications so that we can be more clear about the nature of appropriate target spectra for the region.

The debate over the appropriate earthquake magnitude for initial screening of ground motions in the first place should and will continue. The effect can be significant. An earthquake

with moment magnitude M_W7.7 has been used as a basis in this study. What if the source were taken as an event of moment magnitude M_W7.0 instead? Some good candidates for selection would then be those summarized in Table 8.4-3. The risk-targeted spectrum has been used to come up with the scale factors shown. Of course, if the source were to be taken as an M_W7.0 event instead of an M_W7.7 event, then the target spectra would likely go down so that lower scale factors would be appropriate.

The science of scaling real records to be used in nonlinear analysis of structures deserves further development in codes and specifications. Due attention must be given to the nature of the design target spectrum. Without a clear knowledge of the variable depicted in the design spectrum, proper scaling is a mere matter of chance. Most codes and specifications have adopted geometric mean design spectra, not maximum component spectra. To further complicate matters, there is no single unique geometric mean spectrum for a given record pair, as introduced in CHAPTER 3. The as-recorded geometric mean - GMAR - is the most logical choice and the simplest in terms of the mathematical processing required. However, had the instrumentation ben oriented differently, then a different geometric mean spectrum would not only be possible, but likely. So a different scale factor could have been obtained for the same station.

Table 8.4-1. Site 1 Uniform Hazard DBE Scaled Records

NGA #	Event	Magnitude	R, km	Site Class	Scale Factor
1634	Manjil, Iran	7.37	76.0	D	1.34
1542	Chi-Chi, Taiwan	7.62	25.4	D	1.38
1147	Kocaeli, Turkey	7.51	70.0	E	1.50
1537	Chi-Chi, Taiwan	7.62	22.1	D	1.52
1540	Chi-Chi, Taiwan	7.62	21.8	D	1.59
1238	Chi-Chi, Taiwan	7.62	22.7	D	1.69
1180	Chi-Chi, Taiwan	7.62	25.0	D	1.74

Table 8.4-2. Site 1 Risk-Targeted DBE Scaled Records

NGA #	Event	Magnitude	R, km	Site Class	Scale Factor
1634	Manjil, Iran	7.37	76.0	D	1.14
1542	Chi-Chi, Taiwan	7.62	25.4	D	1.17
1147	Kocaeli, Turkey	7.51	70.0	E	1.28
1537	Chi-Chi, Taiwan	7.62	22.1	D	1.30
1540	Chi-Chi, Taiwan	7.62	21.8	D	1.35
1238	Chi-Chi, Taiwan	7.62	22.7	D	1.44
1180	Chi-Chi, Taiwan	7.62	25.0	D	1.48

Table 8.4-3. Site 1 Risk-Targeted DBE Scaled Records - M7.0 Source

NGA #	Event	Magnitude	R, km	Site Class	Scale Factor
1602	Duzce, Turkey ‘99	7.14	12.0	D	0.82
1605	Duzce, Turkey ‘99	7.14	6.6	D	0.70
1116	Kobe, Japan ‘95	6.90	19.1	D	1.55
1119	Kobe, Japan ‘95	6.90	0.0	D	0.63
0759	Loma Prieta ‘89	6.93	43.8	E	0.99
0778	Loma Prieta ‘89	6.93	24.5	D	1.17
0829	Cape Mendocino ‘92	7.01	7.9	D	1.59

BIBLIOGRAPHY

AASHTO, 2009. *Guide Specifications for LRFD Seismic Bridge Design.* shington, D.C.: American Association of State Highway and Transportation Officials.

AASHTO, 2010. *Guide Specifications for Seismic Isolation Design.* Washington, D. C.: American Association of State Highway and Transportation Officials.

Al Atik, L. & Abrahamson, N., 2010. An Improved Method for Nonstationary Spectral Matching. *Earthquake Spectra*, 26(3), pp. 301-617.

American Society of Civil Engineers, 2005. *ASCE 7-05: Minimum Design Loads For Buildings and Other Structures.* Reston, VA: ASCE/ANSI.

Angelopoulou, D., 2009. *Seismic Response Analysis of Multi-Span Isolated Bridges,* Patras, Greece: The University of Patras.

Applied Technology Council, June, 2005. *FEMA 440: Improvement of Nonlinear Static Seismic Analysis Procedures,* Washington, D. C.: Federal Emergency Management Agency.

Applied Technology Council, May, 2011. *Seismic Performance Assessment of Buildings: Volume 1 – Methodology (ATC-58-1, 75% Draft),* Redwood City, California: Federal Emergency Management Agency.

Atkinson, G. & Beresnev, I. A., 2002. Ground Motions at Memphis and St. Louis from M 7.5-8.0 Earthquakes in the New Madrid Seismic Zone. *Bulletin of the Seismological Society of America,* vol. 92, no. 3, pp. 1015-1024.

Atkinson, G. M. & Boore, D. M., 1995. Ground Motion Relations for Eastern North America. *Bulletin of the Seismological Society of America*, 85(1), pp. 17-30.

Atkinson, G. M. & Boore, D. M., 2006. Earthquake Ground-Motion Prediction Equations for Eastern North America. *Bulletin of the Seismological Society of America,* Vol. 96, No. 6, pp. 2181-2205.

Baker, J. W., 2011. The Conditional Mean Spectrum: A Tool for Ground Motion Selection. *ASCE Journal of Structural Engineering,* 137(3), pp. 322-331.

Baker, J. W. & Jayaram, N., 2008. Correlation of Spectral Acceleration Values from NGA Ground Motion Models. *Earthquake Spectra*, vol. 24, no. 1, pp. 299-317.

Baker, J. W. & Jayaram, N., 2008. Correlation of Spectral Acceleration Values from NGA Ground Motion Models. *Earthquake Spectra*, 24(1), pp. 299-317.

Bazzurro, P. & Cornell, C. A., April, 1999. Disaggregation of Seismic Hazard. *Bulletin of the Seismological Society of America,* 89(2), pp. 501-520.

Bommer, J., Elnashai, A. S. & Weir, A. G., 2000. *Compatible Acceleration and Displacement Spectra for Seismic Design Codes.* Auckland, New Zealand, New Zealand Society for Earthquake Engineering, pp. 1-8.

Boore, D. M., 2009. *TSPP---A Collection of FORTRAN Programs for Processing and Manipulating Time Series,* Reston, Virginia: U.S. Geological Survey Open-File Report 2008-1111.

Boore, D. M., August 2010. Orientation-Independent, Nongeometric-Mean Measures of Seismic Intensity from Two Horizontal Components of Motion. *Bulletin of the Seismological Society of America,* 100(4), pp. 1830-1835.

Boore, D. M., Watson-Lamprey, J. & Abrahamson, N. A., August 2006. Orientation-Independent Measures of Ground Motion. *Bulletin of the Seismological Society of America,* 96(4A), pp. 1502-1511.

Bozorgnia, Y., Hachem, M. M. & Campbell, K. W., February 2010. Deterministic and Probabilistic Predictions of Yield Strength and Inelastic Displacement Spectra. *Earthquake Spectra,* 26(1), p. 25–40.

Buckle, I., Constantinou, M., Dicleli, M. & Ghasemi, H., 2006. *Seismic Isolation of Highway Bridges (MCEER-06-SP07),* Buffalo, NY: Multidisciplinary Center for Earthquake Engineering Research.

Buckle, I. et al., 2006. *Seismic Retrofitting Manual for Highway Bridges (FHWA-HRT-06-032),* McLean, VA: Federal Highway Administration.

Building Seismic Safety Council, 2003. *FEMA 450: NEHRP Recommended Provisions for Seismic Regulations for New Buildings and Other Structures,* Washington, D. C.: Federal Emergency Management Agency.

Building Seismic Safety Council, 2004. *NEHRP Recommended Provisions for Seismic Regulations for New Buildings and Other Structures (FEMA 450),* Washington, D.C.: Federal Emergency Management Agency.

Campbell, K. W., 2003. Prediction of Strong Ground Motion Using the Hybrid Empirical Method and Its Use in the Development of Ground-Motion (Attenuation) Relations in Eastern North America. *Bulletin of the Seismological Society of America,* Vol. 93, No. 3, pp. 1012-1033.

Cardone, D., Dolce, M., Matera, F. & Palermo, G., 2008. *Application of Direct Displacement Based Design to Multi-Span Simply Supported Deck Bridges with Seismic Isolation: A Case Study*. Beijing, China, International Association for Earthquake Engineering, pp. 1-8.

Casarotti, C., 2004. *Bridge Isolation and Dissipation Devices,* Pavia, Italy: European School for Advanced Studies in Reduction of Seismic Risk (ROSE School).

Casarotti, C., Pinho, R. & Calvi, G. M., 2005. *Adaptive Pushover-Based Methods for Seismic Assessment and Design of Bridge Structures.* Pavia, Italy: IUSS Press.

Charney, F. A., 2010. *NONLIN 8.00 - Computer Program for Nonlinear Dynamic Time History Analysis of Single- and Multi-Degree-of-Freedom Systems,* Blacksburg, VA: Virginia Tech.

Chopra, A. K., 2005. *Earthquake Dynamics of Structures.* Oakland, CA: Earthquake Engineering Research Institute.

Christopoulos, C. & Filiatrault, A., 2006. *Principles of Passive Supplemental Damping and Seismic Isolation.* Pavia, Italy: IUSS Press.

Computers and Structures, Inc., 2011. *CSiBridge Version 15,* Berekely, CA: CSI.

Consortium of Organizations for Strong Motion Observation Systems, 2007. *COSMOS Virtual Data Center.*: http://db.cosmos-eq.org/scripts/default.plx.

Dimitriadou, O., May 2007. *Effect of Isolation on Bridge Seismic Design and Response,* Pavia, Italy: European School for Advanced Studies in Reuction of Seismic Risk (ROSE School).

Duc, T. L., March, 2007. *Verification of the Equations for Equivalent Viscous Damping for Single Degree of Freedom Systems,* Pavia, Italy: European School for Advanced Studies in Reduction of Seismic Risk (ROSE School).

Dynamic Isolations Systems Brochure, 2011. *Seismic Isolation for Buildings and Bridges,* McCarran, NV: Dynamic Isolation Systems.

Electric Power Research Institute, 1993. *Guidelines for Determining Design Basis Ground Motions - EPRI TR-102293,* Palo Alto, California: Electric Power Research Institute.

Faccioli, E., Paolucci, R. & Rey, J., May 2004. Displacement Spectra for Long Periods. *Earthquake Spectra,* 20(2), pp. 347–376.

Fardis, M. N. & Pinto, P. E., 2007. *Report No. 2007/05: Guidelines for Displacement-Based Design of Buildings and Bridges,* Pavia, Italy: LESSLOSS - Risk Mitigation for Earthquakes and Landslides.

Federal Emergency Management Agency, 2009. *FEMA P-750: NEHRP Recommended Seismic Provisions for New Buildings and Other Structures: Training and Instructional Materials,* Washington, D.C.: FEMA.

Fenz, D. M. & Constantinou, M. C., 2008. *Mechanical Behavior of Multi-Spherical Sliding Bearings (MCEER-08-007),* Buffalo, NY: Multidisciplinary Center for Earthquake Engineering Research.

Fernández, J. A., 2007. *Numerical Simulation of Earthquake Ground Motions in the Upper Mississippi Embayment,* Atlanta, GA: Doctoral Dissertation, Georgia Institute of Technology.

Fernandez, J. A. & Rix, G. J., 2006. *Soil Attenuation Relationships and Seismic Hazard Analyses in the Upper Mississippi Embayment.* San Francisco, CA.

Field, E. H., Jordan, T. H. & Cornell, C. A., 2003. OpenSHA: A Developing Community - Modeling Environment for Seismic Hazard Analysis. *Seismological Research Letters,* vol. 74, no. 4, pp. 406-419.

FIP Industriale, 2011. *Lead Rubber Bearings Product Catalog,* Selvazanno, Italy: FIP Industriale.

Frankel, A. et al., 1996. *National Seismic Hazard Maps: Documentation (OFR 96-532),* United States Geological Survey.

Frankel, A. et al., 1996. *National Seismic Hazard Maps—Documentation,* United States Geological Survey.

Gangopadhyay, A. & Talwani, P., November/December 2003. Symptomatic Features of Intraplate Earthquakes. *Seismological Research Letters,* 74(6), pp. 863-883.

Grant, D. N., 2011. Response Spectral Matching of Two Horizontal Ground Motion Components. *ASCE Journal of Structural Engineering,* 137(3), pp. 289-297.

Gulkan, P. & Sozen, M. A., December, 1974. Inelastic Response of Reinforced Concrete Structures to Earthquake Ground Motions. *Journal of the American Concrete Institute,* 71(12), pp. 604-610.

Hancock, J., Bommer, J. J. & Stafford, P. J., 2008. Number of Scaled and Matched Accelerograms Required for Inelastic Dynamic Analyses. *Earthquake Engineering and Structural Dynamics,* 37(1), pp. 1585-1607.

Harmsen, S. C., 2001. Mean and Modal Epsilon in the Deaggregation of Probabilistic Ground Motion. *Bulletin of the Seismological Society of America,* 91(6), pp. 1537-1552.

Haselton, C. B., Baker, J. W., Liel, A. B. & Deierlein, G. G., 2011. Accounting for Ground Motion Spectral Shape Characteristics in Structural Collapse Assessment through an Adjustment for Epsilon. *ASCE Journal of Structural Engineering,* pp. 332-344.

Hashash, Y. M. A., 2011. *DEEPSOIL 5: User's Manual and Tutorial,* Urbana-Champaign: UIUC.

Hashash, Y. M. A. & Park, D., 2001. Non-linear One-dimensional Seismic Ground Motion Propagation in the Mississippi Embayment. *Engineering Geology*, Volume 62, pp. 185-206.

Hashash, Y. M. A., Tsai, C.-C., Phillips, C. & Park, D., 2008. Soil-Column Depth-Dependent Seismic Site Coefficeints and Hazard Maps for the Upper Mississippi Embayment. *Bulletin of the Seismological Society of America*, 98(4), pp. 2004-2021.

Huang, Y.-N. & Whittaker, A., August, 2007. Scaling Earthquake Records for Response-History Analysis of Safety-Related Nuclear and Conventional Structures. *Transactions, SMiRT*.

Idriss, I. M. & Boulanger, R. W., 2008. *Soil Liquefaction During Earthquakes.* Oakland, CA: Earthquake Engineering Research Institute.

Iervolina, I., Maddaloni, G. & Cosenza, E., 2008. Eurocode 8 Compliant Real Record Sets for Seismic Analysis of Structures. *Journal of Earthquake Engineering,* Volume 12, p. 54–90.

Iervolina, I., Maddaloni, G. & Cosenza, E., 2009. A Note on Selection of Time-Histories for Seismic Analysis of Bridges in Eurocode 8. *Journal of Earthquake Engineering,* Volume 13, pp. 1125–1152.

Iervolinoa, I. & Cornell, C. A., August 2005. Record Selection for Nonlinear Seismic Analysis of Structures. *Earthquake Spectra*, 21(3), pp. 685–713.

Iervolino, I., Galasso, C. & Cosenza, E., 2010. REXEL: Computer Aided Record Selection for Code-based Seismic Structural Analysis. *Bulletin of Earthquake Engineering,* Volume 8, pp. 339–362.

Katsanos, E. I., Sextos, A. G. & Manolis, G. D., 2009. Selection of Earthquake Ground Motion Records: A State-of-the-art Review from a Structural Engineering Perspective. *Soil Dynamics and Earthquake Engineering*.

Kawashima, K., 2004. Seismic Isolation of Highway Bridges. *Journal of Japan Association for Earthquake Engineering,* 4(3), pp. 283-297.

Kawashima, K., MacRae, G. A., Hoshikuma, J.-i. & Nagaya, K., May, 1998. Residual Displacement Response Spectrum. *ASCE Journal of Structural Engineering,* pp. 523-530.

Kunde, M. C. & Jangid, R., 2003. Seismic Behavior of Isolated Bridges: A State-of-the-Art Review. *Electronic Journal of Structural Engineering,* Volume 3, pp. 140-170.

Kwai, T. F., 1986. *Seismic Behavior of Bridges on Isolating Bearings (Master's Thesis),* Christchurch, New Zealand: University of Canterbury.

Lam, N. & Wilson, J., March, 2004. Displacement Modelling of Intraplate Earthquakes. *ISET Journal of Earthquake Technology*, pp. 15-52.

Liao, W. I., Loh, C. H. & Wan, S., 2000. *Responses of Isolated Bridges to Near-Fault Ground Motions Recorded in Chi Chi Earthquake.* Taipei, Taiwan, National Center for Research in Earthquake Engineering.

Li, Q. L., Liu, M. & Yang, Y., 2002. The 01/26/2001 Bhuj, India, Earthquake: Intraplate or Interplate?. *Plate Boundary Zones - AGU Geophysical Monograph*, pp. 255-264.

Luco, N. et al., 2007. *Risk-Targeted versus Current Seismic Design Maps for the Conterminous United States.* California, SEAOC 2007 Convention Proceedings.

Lyskova, E. L., Yanovskaya, T. B. & Duda, S. J., 1998. Spectral Characteristics of Earthquakes Along Plate Boundaries. *GEOFIZIKA,* Volume 15, pp. 69-81.

M., B. D., Watson-Lamprey, J. & Abrahamson, N. A., August 2006. Orientation-Independent Measures of Ground Motion. *Bulletin of the Seismological Society of America,* 96(4A), pp. 1502-1511.

Macrae, G. A. & Kawashima, K., 1997. Post-Earthquake Residual Displacements of Bilinear Oscillators. *Earthquake Engineering and Structural Dynamics*, Volume 26, pp. 701-716.

Madabhushi, G., Knappett, J. & Haigh, S., 2010. *Design of Pile Foundations in Liquefiable Soils.* London: Imperial College Press.

Maurer, 2011. *Seismic Isolation Systems with Lead Rubber Bearings,* Munich, Germany: Maurer Sohne.

McGuire, R. K., Silva, W. J. & Costantino, C. J., 2001. *Technical Basis for Revision of Regulatory Guidance on Design Ground Motions (NUREG/CR-6728),* Washington, D.C.: U.S. Nuclear Regulatory Commission.

Mosqueda, G., Whittaker, A. S., Fenves, G. L. & Mahin, S. A., 2004. *Experimental and Analytical Studies of the Friction Pendulum System for the Seismic Protection of Simple Bridges,* Berkeley, CA: Earthquake Engineering Research Center.

Nagarajaiah, S., Reinhorn, A. M. & Constantinou, M. C., 1991. *3D- Basis: Nonlinear Dynamic Analysis of Three-Dimensional Base Isolated Structures: Part II, Technical Report NCEER-91-0005,* Buffalo, N.Y.: National Center for Earthquake Engineering Research, SUNY.

National Oceanic and Atmospheric Administration, 2011. *Earthquake Strong Motion Database.*: http://www.ngdc.noaa.gov/hazard/strong.shtml

National Research Institute for Earth Science and Disaster Prevention, n.d. *Kyoshen Network.*: http://www.k-net.bosai.go.jp/

NEHRP Consultants Joint Venture, 2011. *Selecting and Scaling Earthquake Ground Motions,* Redwood City, California: National Institute of Standards and Technology.

Olsen, K. B., 2011. *3D Broadband Ground Motion Estimation for Large Earthquakes on the New Madrid Seismic Zone, Central United States - NEHRP Final Report, Award #G10AP00007,* UCSD: National Earthquake Hazards Reduction Program.

Pacific Earthquake Engineering Research Center, 2011. *PEER Ground Motion Database.*: http://peer.berkeley.edu/peer_ground_motion_database

Pacific Earthquake Engineering Research Center, 2012. *Next Generation Attenuation Relationships for Central and Eastern North America.*: http://peer.berkeley.edu/ngaeast/

Park, D., 2004. *Estimation of Nonlinear Site Effects for Deep Deposits of the Mississippi Embayment - PhD Thesis,* Urbana-Champaign: University of Illinois.

Park, D. & Hashash, Y. M. A., 2004. *Probabilistic Seismic Hazard Analysis with Nonlinear Site Effects in the Mississippi Embayment.* Vancouver, B.C., Canada, Paper No. 1549.

Park, D. & Hashash, Y. M. A., 2005. Evaluation of Seismic Cite Factors in the Mississippi Embayment - II - Probabilistic Seismic Hazard Analysis with Nonlinear Site Effects. *Soil Dynamics and Earthquake Engineering,* pp. 145-156.

Park, D. & Hashash, Y. M. A., 2005. Evaluation of Seismic Site Factors in the Mississippi Embayment - I - Estimation of Dynamic Properties. *Soil Dynamics and Earthquake Engineering,* Volume 25, pp. 133-144.

Park, D. & Hashash, Y. M. A., October, 2004. *Estimation of Non-linear Seismic Site Effects for Deep Deposits of the Mississippi Embayment,* Urbana, Illinois: Mid America Earthquake Center.

PEER, Beta Version, October 1, 2010. *Technical Report for the PEER Ground Motion Database Web Application,* University of California, Berkeley, CA : Pacific Earthquake Engineering Research Center.

Petersen, M. D., 2008. *Documentation for the 2008 Update of the United States National Seismic Hazard Maps,* Reston, Virginia: U.S. Geological Survey.

Pezeshk, S., Zandieh, A. & Tavakoli, B., August, 2011. Hybrid Empirical Ground-Motion Prediction Equations fro Eastern North America Using NGA Models and Updated Seismological Parameters. *Bulletin of the Seismological Society of America,* 101(4), pp. 1859-1870.

Pietra, G. M., Calvi, G. M. & Pinho, R., 2008. *Displacement-Based Seismic Design of Isolated Bridges.* Pavia, Italy: IUSS Press.

Priestley, M. J. N., Calvi, G. M. & Kowalsky, M. J., 2007. *Displacement-Based Seismic Design of Structures.* Pavia, Italy: IUSS Press.

Priestley, M. J. N. & Grant, D. N., 2005. Viscous Damping in Seismic Design and Analysis. *Journal of Earthquake Engineering - Imperial College Press,* pp. 229-255.

Priestley, M. J. N., Seible, F. & Calvi, G. M., 1996. *Seismic Design and Retrofit of Bridges.* New York, NY: John Wiley & Sons.

Robinson Seismic LTD, 2011. *Catalog of Robinson Seismic Bearings,* Petone, New Zealand: Robinson Seismic LTD.

Ruiz-Garcia, J. & Miranda, E., August 2005. *Performance-Based Assessment of Existing Structures Accounting for Residual Displacements,* Stanford, CA: The John A. Blume Earthquake Engineering Center, Stanford University.

Ryan, K. L. & Chopra, A. K., March, 2004. Estimation of Seismic Demands on Isolators Based on Nonlinear Analysis. *ASCE Journal of Structural Engineering,* 130(3), pp. 392-402.

SeismoSoft, 2011. *SeismoMatch v 1.3.0.*: http://seismosoft.com/en/SeismoMatch.aspx.

SeismoSoft, 2011. *SeismoSpect v 1.3.0.*: http://www.seismosoft.com/en/HomePage.aspx

Shama, A. A., Mander, J. B., Blabac, B. B. & Chen, S. S., 2001. *Experimental Investigation and Retrofit of Steel Pile Foundations and Pile Bents Under Cyclic Lateral Loadings (MCEER-01-0006),* Buffalo, NY: Multidisciplinary Center for Earthquake Engineering Research.

Silva, W., Gregor, N. & and Darragh, R., 2002. *Development of Hard Rock Attenuation Relations for Central and Eastern North America,* El Cerrito, CA: Internal report from Pacific Engineering.

Silva, W., Gregor, N. & Darragh, R., 2003. *Development of Regional Hard Rock Attenuation Relations for Central and Eastern North America,* El Cerrito, California: Pacific Engineering and Analysis.

Skinner, R. I., Robinson, W. H. & McVerry, G. H., 1993. *An Introduction to Seismic Isolation.* Chichester, England: Wiley and Sons.

Somerville, P. et al., 2001. *Ground Motion Attenuation Relations for the Central and Eastern United States - Final Report,* Pasadena: United States Geological Survey.

Song, S. T., Chai, Y. H. & Hale, T. H., 2004. *Limit State Analysis of Fixed-Head Concrete Piles Under Lateral Loads.* Vancouver, B. C., Canada, 13th World Conference on Earthquake Engineering.

Stafford, P. J., Mendis, R. & Bommer, J. J., August, 2008. Dependence of Damping Correction Factors for Response Spectra on Duration and Number of Cycles. *ASCE Journal of Structural Engineering,* 134(8), pp. 1364-1373.

Stein, S., 2007. Approaches to continental intraplate earthquake issues. *Continental Intraplate Earthquakes: Science, Hazard, and Policy Issues: Geological Society of America,* Volume 425, pp. 1-16.

Suarez, V. A., 2008. *Implementation of Direct Displacement Based Design for Highway Bridges,* Raleigh, North Carolina: A dissertation submitted to the Graduate Faculty of North Carolina State University.

SUNY at Buffalo, 2005. *Engineering Seismology Laboratory.*: http://civil.eng.buffalo.edu/engseislab/products.htm.

Tavakoli, B. & Pezeshk, S., 2005. Empirical-Stochastic Ground-Motion Prediction for Eastern North America. *Bulletin of the Seismological Society of America,* Vol. 95, No. 6, pp. 2283-2296.

Toro, G., Abrahamson, N. & and Schneider, J., 1997. A Model of Strong Ground Motions from Earthquakes in Central and Eastern North America - Best Estimates and Uncertainties. *Seismological Research Letters,* v. 68, pp. 41-57.

Towhata, I., 2008. *Geotechnical Earthquake Engineering.* Berlin, Germany: Springer-Verlag.

United States Geological Survey, 2011. *2008 Interactive Deaggregations (Beta).*: https://geohazards.usgs.gov/deaggint/2008/.

United States Geological Survey, 2011. *Java Ground Motion Parameter Calculator.*: http://earthquake.usgs.gov/hazards/designmaps/javacalc.php

United States Geological Survey, 2011. *U.S. Seismic "DesignMaps" Web Application.*: https://geohazards.usgs.gov/secure/designmaps/us/.

United States Geological Survey, *USGS*: http://nsmp.wr.usgs.gov/

USGS and California Geological Survey, 2011. *Center for Engineering Strong Motion Data.*: http://strongmotioncenter.org.

Vamvatsikos, D. & Cornell, C. A., August 2005. *Seismic Performance, Capacity, and Reliability of Structures as Seen Through Incremental Dynamic Analysis,* Stanford, CA: The John A. Blume Earthquake Engineering Center, Stanford University.

Van Arsdale, R. & Ellis, M., 2004. *Characterization of Active Faults in the New Madrid Seismic Zone,* Urbana, Illinois: Mid America Earthquake Center.

Villaverde, R., 2009. *Fundamental Concepts of Earthquake Engineering.* Boca Raton, FL: CRC Press.

Wang, Y.-P., Chung, L.-L. & Liao, W.-H., 1998. Seismic Response Analysis of Bridges Isolated with Friction Pendulum Bearings. *Earthquake Engineering and Structural Dynamics,* Volume 27, pp. 1069-1093.

Warn, G. P., 2002. Displacement Estimates in Isolated Bridges. *MCEER Student Research Accomplishments.*

Warn, G. P. & Whittaker, A. S., 2007. *Performance Estimates for Seismically Isolated Bridges (MCEER-07-0024),* Buffalo, NY: Multidisciplinary Center for Earthquake Engineering Research.

Watson-Lamprey, J. A. & Boore, D. M., October 2007. Beyond SA-GMRotI: Conversion to SA-Arb, SA-SN, and SA-MaxRot. *Bulletin of the Seismological Society of America,* vol. 97, no. 5, pp. 1511-1524.

Wen, Y. K., 1976. Method for Random Vibration of Hysteretic Systems. *Journal of the Engineering Mechanics Division, ASCE,* 102(2), pp. 249-263.

Wong, Y. & Zhao, J. X., 2000. *Investigation on Attenuation Characteristics of Strong Ground Motions in China and Hong Kong.* Auckland, New Zealand, 12th World Conference on Earthquake Engineering.

Wu, C.-L. & Wen, Y., 1999. *Uniform Hazard Ground Motions and Response Spectra for Mid-America Cities,* Urbana, Illinois: Mid America Earthquake Center.

Xiang, Z. & Li, Y., 2000. *Statistical Characteristics of Long Period Response Spectra of Earthquake Ground Motion.* Auckland, New Zealand, New Zealand Society for Earthquake Engineering .

APPENDICES

APPENDIX A: MAGNITUDE-DISTANCE-SITE CLASS DATA

Code	Event	Year	Station	Mag	R(km)	Vs30 m/s	Site Class
1257	Chi-Chi- Taiwan	1999	HWA003	7.62	52.5	1525.8	A
2111	Denali- Alaska	2002	R109 (temp)	7.90	43.0	963.9	B
2107	Denali- Alaska	2002	Carlo (temp)	7.90	49.9	963.9	B
1518	Chi-Chi- Taiwan	1999	TCU085	7.62	55.1	999.7	B
1347	Chi-Chi- Taiwan	1999	ILA063	7.62	57.7	996.5	B
1587	Chi-Chi- Taiwan	1999	TTN042	7.62	62.1	845.3	B
1352	Chi-Chi- Taiwan	1999	KAU003	7.62	113.4	913.8	B
1446	Chi-Chi- Taiwan	1999	TAP077	7.62	117.3	1022.8	B
1440	Chi-Chi- Taiwan	1999	TAP065	7.62	120.8	1023.5	B
1165	Kocaeli, Turkey	1999	Izmit	7.51	7.2	811.0	B
143	Tabas, Iran	1978	Tabas	7.35	1.8	766.8	B
143	Tabas	1978	143	7.35	55.2	767.0	B
UNIO	Michoacan, Mexico	1985	UNIO	8.10	83.9	366.0	C
AZIH	Michoacan, Mexico	1985	AZIH	8.10	132.6	627.0	C
SCT	Michoacan, Mexico	1985	SCT	8.10	374.0	410.0	C
MZQ	Wenchuan	2008	MZQ	7.90	1.4	650.0	C
AXT	Wenchuan	2008	AXT	7.90	20.4	650.0	C
2113	Denali- Alaska	2002	TAPS Pump Station #09	7.90	53.0	382.5	C
GYS	Wenchuan	2008	GYS	7.90	61.1	518.0	C
2112	Denali- Alaska	2002	TAPS Pump Station #08	7.90	104.2	424.8	C
2115	Denali- Alaska	2002	TAPS Pump Station #11	7.90	126.4	376.1	C
2110	Denali- Alaska	2002	Fairbanks - Geophysic- CIGO	7.90	140.7	424.8	C
VEA	Valparaiso, Chile	1985	el Almendral	7.80	26.0	387.0	C
VAL	Valparaiso, Chile	1985	Valparaiso	7.80	129.2	387.0	C

Code	Event	Year	Station	Mag	R(km)	Vs30 m/s	Site Class
1626	Sitka, Alaska	1972	Sitka Observatory	7.68	34.6	659.6	C
1521	Chi-Chi- Taiwan	1999	TCU089	7.62	0.0	680.0	C
1507	Chi-Chi- Taiwan	1999	TCU071	7.62	0.0	624.9	C
1505	Chi-Chi- Taiwan	1999	TCU068	7.62	0.0	487.3	C
1508	Chi-Chi- Taiwan	1999	TCU072	7.62	0.0	468.1	C
1512	Chi-Chi- Taiwan	1999	TCU078	7.62	0.0	443.0	C
1509	Chi-Chi- Taiwan	1999	TCU074	7.62	0.0	549.4	C
1517	Chi-Chi- Taiwan	1999	TCU084	7.62	0.0	680.0	C
1492	Chi-Chi- Taiwan	1999	TCU052	7.62	0.0	579.1	C
1231	Chi-Chi- Taiwan	1999	CHY080	7.62	0.1	680.0	C
1504	Chi-Chi- Taiwan	1999	TCU067	7.62	0.6	433.6	C
1227	Chi-Chi- Taiwan	1999	CHY074	7.62	0.7	553.4	C
1510	Chi-Chi- Taiwan	1999	TCU075	7.62	0.9	573.0	C
1529	Chi-Chi- Taiwan	1999	TCU102	7.62	1.5	714.3	C
1528	Chi-Chi- Taiwan	1999	TCU101	7.62	2.1	504.4	C
1511	Chi-Chi- Taiwan	1999	TCU076	7.62	2.8	615.0	C
1197	Chi-Chi- Taiwan	1999	CHY028	7.62	3.1	542.6	C
1489	Chi-Chi- Taiwan	1999	TCU049	7.62	3.8	487.3	C
1520	Chi-Chi- Taiwan	1999	TCU088	7.62	4.7	680.0	C
1515	Chi-Chi- Taiwan	1999	TCU082	7.62	5.2	472.8	C
1494	Chi-Chi- Taiwan	1999	TCU054	7.62	5.3	460.7	C
1493	Chi-Chi- Taiwan	1999	TCU053	7.62	6.0	454.6	C
1530	Chi-Chi- Taiwan	1999	TCU103	7.62	6.1	494.1	C
1495	Chi-Chi- Taiwan	1999	TCU055	7.62	6.4	447.8	C

Code	Event	Year	Station	Mag	R(km)	Vs30 m/s	Site Class
1519	Chi-Chi- Taiwan	1999	TCU087	7.62	7.0	561.8	C
1545	Chi-Chi- Taiwan	1999	TCU120	7.62	7.4	459.3	C
1491	Chi-Chi- Taiwan	1999	TCU051	7.62	7.7	467.5	C
1550	Chi-Chi- Taiwan	1999	TCU136	7.62	8.3	538.0	C
1499	Chi-Chi- Taiwan	1999	TCU060	7.62	8.5	495.8	C
1546	Chi-Chi- Taiwan	1999	TCU122	7.62	9.3	475.5	C
1490	Chi-Chi- Taiwan	1999	TCU050	7.62	9.5	470.7	C
1193	Chi-Chi- Taiwan	1999	CHY024	7.62	9.6	427.7	C
1551	Chi-Chi- Taiwan	1999	TCU138	7.62	9.8	652.9	C
1182	Chi-Chi- Taiwan	1999	CHY006	7.62	9.8	438.2	C
1501	Chi-Chi- Taiwan	1999	TCU063	7.62	9.8	476.1	C
1496	Chi-Chi- Taiwan	1999	TCU056	7.62	10.5	440.2	C
1198	Chi-Chi- Taiwan	1999	CHY029	7.62	11.0	544.7	C
1527	Chi-Chi- Taiwan	1999	TCU100	7.62	11.4	479.3	C
1497	Chi-Chi- Taiwan	1999	TCU057	7.62	11.8	479.3	C
1541	Chi-Chi- Taiwan	1999	TCU116	7.62	12.4	493.1	C
1202	Chi-Chi- Taiwan	1999	CHY035	7.62	12.6	555.2	C
1531	Chi-Chi- Taiwan	1999	TCU104	7.62	12.9	543.8	C
1535	Chi-Chi- Taiwan	1999	TCU109	7.62	13.1	424.2	C
1548	Chi-Chi- Taiwan	1999	TCU128	7.62	13.2	599.6	C
1488	Chi-Chi- Taiwan	1999	TCU048	7.62	13.6	551.2	C
1201	Chi-Chi- Taiwan	1999	CHY034	7.62	14.8	378.8	C
1533	Chi-Chi- Taiwan	1999	TCU106	7.62	15.0	418.8	C
1534	Chi-Chi- Taiwan	1999	TCU107	7.62	16.0	418.7	C

Code	Event	Year	Station	Mag	R(km)	Vs30 m/s	Site Class
1486	Chi-Chi- Taiwan	1999	TCU046	7.62	16.7	465.6	C
1532	Chi-Chi- Taiwan	1999	TCU105	7.62	17.2	575.5	C
1506	Chi-Chi- Taiwan	1999	TCU070	7.62	19.0	401.3	C
1205	Chi-Chi- Taiwan	1999	CHY041	7.62	19.4	492.3	C
1480	Chi-Chi- Taiwan	1999	TCU036	7.62	19.8	495.0	C
1184	Chi-Chi- Taiwan	1999	CHY010	7.62	19.9	549.6	C
1482	Chi-Chi- Taiwan	1999	TCU039	7.62	19.9	540.7	C
1208	Chi-Chi- Taiwan	1999	CHY046	7.62	24.1	442.1	C
1484	Chi-Chi- Taiwan	1999	TCU042	7.62	26.3	424.0	C
1380	Chi-Chi- Taiwan	1999	KAU054	7.62	27.4	577.4	C
1206	Chi-Chi- Taiwan	1999	CHY042	7.62	27.5	680.0	C
1234	Chi-Chi- Taiwan	1999	CHY086	7.62	27.6	680.0	C
1476	Chi-Chi- Taiwan	1999	TCU029	7.62	28.1	426.3	C
1235	Chi-Chi- Taiwan	1999	CHY087	7.62	28.8	505.2	C
1477	Chi-Chi- Taiwan	1999	TCU031	7.62	30.2	489.2	C
1594	Chi-Chi- Taiwan	1999	TTN051	7.62	30.8	680.0	C
1186	Chi-Chi- Taiwan	1999	CHY014	7.62	33.2	560.3	C
1350	Chi-Chi- Taiwan	1999	ILA067	7.62	33.3	680.0	C
1377	Chi-Chi- Taiwan	1999	KAU050	7.62	35.7	680.0	C
1479	Chi-Chi- Taiwan	1999	TCU034	7.62	35.7	393.8	C
1301	Chi-Chi- Taiwan	1999	HWA056	7.62	35.9	511.3	C
1245	Chi-Chi- Taiwan	1999	CHY102	7.62	36.1	679.9	C
1236	Chi-Chi- Taiwan	1999	CHY088	7.62	37.5	366.2	C
1287	Chi-Chi- Taiwan	1999	HWA038	7.62	37.5	642.7	C

Code	Event	Year	Station	Mag	R(km)	Vs30 m/s	Site Class
1273	Chi-Chi- Taiwan	1999	HWA024	7.62	38.2	630.1	C
1211	Chi-Chi- Taiwan	1999	CHY052	7.62	38.7	574.7	C
1285	Chi-Chi- Taiwan	1999	HWA036	7.62	39.0	481.2	C
1283	Chi-Chi- Taiwan	1999	HWA034	7.62	39.5	379.2	C
1270	Chi-Chi- Taiwan	1999	HWA020	7.62	39.8	502.3	C
1248	Chi-Chi- Taiwan	1999	CHY109	7.62	40.4	557.4	C
1586	Chi-Chi- Taiwan	1999	TTN041	7.62	40.7	418.2	C
1478	Chi-Chi- Taiwan	1999	TCU033	7.62	40.9	423.4	C
1303	Chi-Chi- Taiwan	1999	HWA058	7.62	41.2	564.0	C
1288	Chi-Chi- Taiwan	1999	HWA039	7.62	41.3	497.2	C
1232	Chi-Chi- Taiwan	1999	CHY081	7.62	41.4	575.1	C
1286	Chi-Chi- Taiwan	1999	HWA037	7.62	41.6	476.9	C
1351	Chi-Chi- Taiwan	1999	KAU001	7.62	42.5	571.5	C
1279	Chi-Chi- Taiwan	1999	HWA030	7.62	42.5	487.4	C
1281	Chi-Chi- Taiwan	1999	HWA032	7.62	42.7	514.8	C
1300	Chi-Chi- Taiwan	1999	HWA055	7.62	43.0	497.6	C
1258	Chi-Chi- Taiwan	1999	HWA005	7.62	43.2	489.2	C
1289	Chi-Chi- Taiwan	1999	HWA041	7.62	43.4	501.4	C
1259	Chi-Chi- Taiwan	1999	HWA006	7.62	43.5	490.8	C
1284	Chi-Chi- Taiwan	1999	HWA035	7.62	44.0	500.8	C
1585	Chi-Chi- Taiwan	1999	TTN040	7.62	44.0	728.0	C
1210	Chi-Chi- Taiwan	1999	CHY050	7.62	44.7	432.9	C
1304	Chi-Chi- Taiwan	1999	HWA059	7.62	44.9	421.6	C
1302	Chi-Chi- Taiwan	1999	HWA057	7.62	46.5	678.6	C

Code	Event	Year	Station	Mag	R(km)	Vs30 m/s	Site Class
1230	Chi-Chi- Taiwan	1999	CHY079	7.62	46.6	550.8	C
1573	Chi-Chi- Taiwan	1999	TTN020	7.62	46.6	507.1	C
1295	Chi-Chi- Taiwan	1999	HWA049	7.62	46.6	389.8	C
1268	Chi-Chi- Taiwan	1999	HWA017	7.62	47.0	446.0	C
1272	Chi-Chi- Taiwan	1999	HWA023	7.62	47.1	552.1	C
1280	Chi-Chi- Taiwan	1999	HWA031	7.62	47.4	473.0	C
1293	Chi-Chi- Taiwan	1999	HWA046	7.62	47.8	617.5	C
1275	Chi-Chi- Taiwan	1999	HWA026	7.62	48.0	457.5	C
1282	Chi-Chi- Taiwan	1999	HWA033	7.62	49.3	395.6	C
1574	Chi-Chi- Taiwan	1999	TTN022	7.62	49.4	507.0	C
1471	Chi-Chi- Taiwan	1999	TCU015	7.62	49.8	426.0	C
1274	Chi-Chi- Taiwan	1999	HWA025	7.62	49.9	425.7	C
1190	Chi-Chi- Taiwan	1999	CHY019	7.62	50.0	478.3	C
1278	Chi-Chi- Taiwan	1999	HWA029	7.62	50.5	614.0	C
1575	Chi-Chi- Taiwan	1999	TTN023	7.62	50.5	527.5	C
1375	Chi-Chi- Taiwan	1999	KAU047	7.62	52.9	564.2	C
1557	Chi-Chi- Taiwan	1999	TTN001	7.62	52.9	424.0	C
1256	Chi-Chi- Taiwan	1999	HWA002	7.62	53.3	418.8	C
1305	Chi-Chi- Taiwan	1999	HWA060	7.62	53.9	422.4	C
1582	Chi-Chi- Taiwan	1999	TTN032	7.62	54.1	424.2	C
1472	Chi-Chi- Taiwan	1999	TCU017	7.62	54.3	558.8	C
1525	Chi-Chi- Taiwan	1999	TCU096	7.62	54.5	421.2	C
1523	Chi-Chi- Taiwan	1999	TCU094	7.62	54.5	589.9	C
1291	Chi-Chi- Taiwan	1999	HWA044	7.62	54.7	419.5	C

Code	Event	Year	Station	Mag	R(km)	Vs30 m/s	Site Class
1588	Chi-Chi- Taiwan	1999	TTN044	7.62	55.5	548.4	C
1475	Chi-Chi- Taiwan	1999	TCU026	7.62	56.0	487.5	C
1576	Chi-Chi- Taiwan	1999	TTN024	7.62	56.6	645.5	C
1214	Chi-Chi- Taiwan	1999	CHY057	7.62	56.7	411.5	C
1218	Chi-Chi- Taiwan	1999	CHY061	7.62	57.5	495.3	C
1589	Chi-Chi- Taiwan	1999	TTN045	7.62	57.8	503.1	C
1271	Chi-Chi- Taiwan	1999	HWA022	7.62	58.8	417.9	C
1577	Chi-Chi- Taiwan	1999	TTN025	7.62	62.7	705.0	C
1590	Chi-Chi- Taiwan	1999	TTN046	7.62	62.8	542.7	C
1191	Chi-Chi- Taiwan	1999	CHY022	7.62	63.2	486.5	C
1560	Chi-Chi- Taiwan	1999	TTN004	7.62	63.8	493.5	C
1338	Chi-Chi- Taiwan	1999	ILA050	7.62	63.8	497.2	C
1322	Chi-Chi- Taiwan	1999	ILA024	7.62	64.8	557.7	C
1558	Chi-Chi- Taiwan	1999	TTN002	7.62	65.7	427.4	C
1473	Chi-Chi- Taiwan	1999	TCU018	7.62	66.2	490.5	C
1578	Chi-Chi- Taiwan	1999	TTN026	7.62	67.4	557.0	C
1387	Chi-Chi- Taiwan	1999	KAU069	7.62	67.8	556.1	C
1348	Chi-Chi- Taiwan	1999	ILA064	7.62	69.5	409.9	C
1555	Chi-Chi- Taiwan	1999	TCU147	7.62	70.6	537.9	C
1572	Chi-Chi- Taiwan	1999	TTN018	7.62	71.7	546.7	C
1361	Chi-Chi- Taiwan	1999	KAU020	7.62	72.2	373.3	C
1464	Chi-Chi- Taiwan	1999	TCU006	7.62	72.5	533.1	C
1579	Chi-Chi- Taiwan	1999	TTN027	7.62	73.5	501.0	C
1321	Chi-Chi- Taiwan	1999	ILA021	7.62	74.3	462.3	C

Code	Event	Year	Station	Mag	R(km)	Vs30 m/s	Site Class
1333	Chi-Chi- Taiwan	1999	ILA043	7.62	74.5	425.2	C
1580	Chi-Chi- Taiwan	1999	TTN028	7.62	75.9	506.9	C
1339	Chi-Chi- Taiwan	1999	ILA051	7.62	76.5	503.5	C
1360	Chi-Chi- Taiwan	1999	KAU018	7.62	76.7	432.1	C
1335	Chi-Chi- Taiwan	1999	ILA046	7.62	77.1	396.9	C
1592	Chi-Chi- Taiwan	1999	TTN048	7.62	77.1	460.2	C
1584	Chi-Chi- Taiwan	1999	TTN036	7.62	77.5	420.9	C
1315	Chi-Chi- Taiwan	1999	ILA010	7.62	77.6	417.6	C
1516	Chi-Chi- Taiwan	1999	TCU083	7.62	80.2	512.5	C
1400	Chi-Chi- Taiwan	1999	NCU	7.62	80.3	473.9	C
1561	Chi-Chi- Taiwan	1999	TTN005	7.62	80.4	417.9	C
1391	Chi-Chi- Taiwan	1999	KAU077	7.62	80.5	680.0	C
1325	Chi-Chi- Taiwan	1999	ILA031	7.62	80.9	649.2	C
1313	Chi-Chi- Taiwan	1999	ILA007	7.62	81.7	417.6	C
1468	Chi-Chi- Taiwan	1999	TCU010	7.62	82.2	483.5	C
1340	Chi-Chi- Taiwan	1999	ILA052	7.62	82.7	552.1	C
1319	Chi-Chi- Taiwan	1999	ILA015	7.62	83.0	552.1	C
1433	Chi-Chi- Taiwan	1999	TAP047	7.62	83.6	400.3	C
1358	Chi-Chi- Taiwan	1999	KAU012	7.62	83.7	422.4	C
1466	Chi-Chi- Taiwan	1999	TCU008	7.62	85.0	467.6	C
1428	Chi-Chi- Taiwan	1999	TAP036	7.62	86.2	552.1	C
1463	Chi-Chi- Taiwan	1999	TCU003	7.62	86.6	517.3	C
1392	Chi-Chi- Taiwan	1999	KAU078	7.62	86.7	531.9	C
1593	Chi-Chi- Taiwan	1999	TTN050	7.62	87.0	418.2	C

Code	Event	Year	Station	Mag	R(km)	Vs30 m/s	Site Class
1465	Chi-Chi- Taiwan	1999	TCU007	7.62	87.6	474.0	C
1522	Chi-Chi- Taiwan	1999	TCU092	7.62	87.7	494.3	C
1427	Chi-Chi- Taiwan	1999	TAP035	7.62	87.7	438.1	C
1437	Chi-Chi- Taiwan	1999	TAP053	7.62	90.3	419.7	C
1426	Chi-Chi- Taiwan	1999	TAP034	7.62	90.6	425.2	C
1452	Chi-Chi- Taiwan	1999	TAP086	7.62	92.0	510.9	C
1470	Chi-Chi- Taiwan	1999	TCU014	7.62	92.3	480.6	C
1425	Chi-Chi- Taiwan	1999	TAP032	7.62	93.2	417.8	C
1442	Chi-Chi- Taiwan	1999	TAP067	7.62	95.3	596.9	C
1436	Chi-Chi- Taiwan	1999	TAP052	7.62	98.5	559.3	C
1444	Chi-Chi- Taiwan	1999	TAP072	7.62	99.8	554.2	C
1307	Chi-Chi- Taiwan	1999	ILA001	7.62	101.2	417.6	C
1453	Chi-Chi- Taiwan	1999	TAP087	7.62	101.7	443.0	C
1435	Chi-Chi- Taiwan	1999	TAP051	7.62	102.5	403.2	C
1458	Chi-Chi- Taiwan	1999	TAP098	7.62	106.1	467.6	C
1434	Chi-Chi- Taiwan	1999	TAP049	7.62	107.3	431.4	C
1445	Chi-Chi- Taiwan	1999	TAP075	7.62	107.4	594.7	C
1381	Chi-Chi- Taiwan	1999	KAU057	7.62	112.5	514.0	C
1341	Chi-Chi- Taiwan	1999	ILA054	7.62	114.3	425.2	C
1432	Chi-Chi- Taiwan	1999	TAP046	7.62	116.6	426.3	C
1438	Chi-Chi- Taiwan	1999	TAP059	7.62	117.6	552.1	C
1448	Chi-Chi- Taiwan	1999	TAP079	7.62	117.7	552.1	C
1447	Chi-Chi- Taiwan	1999	TAP078	7.62	118.3	552.1	C
1439	Chi-Chi- Taiwan	1999	TAP060	7.62	119.5	552.1	C

Code	Event	Year	Station	Mag	R(km)	Vs30 m/s	Site Class
1450	Chi-Chi- Taiwan	1999	TAP083	7.62	120.9	415.8	C
1443	Chi-Chi- Taiwan	1999	TAP069	7.62	121.9	552.6	C
1449	Chi-Chi- Taiwan	1999	TAP081	7.62	122.2	552.1	C
1368	Chi-Chi- Taiwan	1999	KAU038	7.62	141.8	522.5	C
1394	Chi-Chi- Taiwan	1999	KAU082	7.62	168.7	573.2	C
PURI	Limon, Costa Rica	1991	Puriscal	7.60	32.7	760.0	C
SM	El Salvador	2001	Santiago de Maria	7.60	52.5	622.0	C
QC	El Salvador	2001	De Septiembre Dam	7.60	63.9	399.0	C
CACHI	Limon, Costa Rica	1991	Cachi	7.60	80.4	465.0	C
LIMA	Peru	1974	Las Gardenias, Lima	7.60	88.5	421.0	C
OB	El Salvador	2001	Observatorio	7.60	91.0	433.0	C
CART	Limon, Costa Rica	1991	Cartago	7.60	93.8	486.0	C
SS	El Salvador	2001	Seminario San Jose	7.60	94.9	433.0	C
RS	El Salvador	2001	Relaciones Exteriores	7.60	95.6	472.0	C
GUAT	Limon, Costa Rica	1991	Guatuso	7.60	106.0	493.0	C
GOLF	Limon, Costa Rica	1991	Golfito	7.60	111.0	760.0	C
ALAJ	Limon, Costa Rica	1991	Alajuela	7.60	113.0	407.0	C
1148	Kocaeli, Turkey	1999	Arcelik	7.51	13.5	523.0	C
1162	Kocaeli, Turkey	1999	Goynuk	7.51	32.0	425.0	C
1164	Kocaeli, Turkey	1999	Istanbul	7.51	52.0	425.0	C
1170	Kocaeli, Turkey	1999	Mecidiyekoy	7.51	53.0	425.0	C
1169	Kocaeli, Turkey	1999	Maslak	7.51	55.0	660.0	C
1163	Kocaeli, Turkey	1999	Hava Alani	7.51	60.0	425.0	C
1154	Kocaeli, Turkey	1999	Bursa Sivil	7.51	66.0	660.0	C

Code	Event	Year	Station	Mag	R(km)	Vs30 m/s	Site Class
1159	Kocaeli, Turkey	1999	Eregli	7.51	142.0	660.0	C
1172	Kocaeli, Turkey	1999	Tekirdag	7.51	165.0	660.0	C
1168	Kocaeli, Turkey	1999	Manisa	7.51	293.0	660.0	C
139	Tabas, Iran	1978	Dayhook	7.35	0.0	659.6	C
139	Tabas	1978	139	7.35	20.6	660.0	C
142	Tabas, Iran	1978	Sedeh	7.35	150.3	424.8	C
572	Taiwan SMART1(45)	1986	SMART1 E02	7.30	52.0	659.6	C
HAJA	India-Burma Border	1988	HAJA	7.30	206.5	465.0	C
BAIG	India-Burma Border	1988	BAIG	7.30	247.1	454.0	C
BAIT	India-Burma Border	1988	BAIT	7.30	284.3	426.0	C
879	Landers	1992	Lucerne	7.28	2.2	685.0	C
864	Landers	1992	Joshua Tree	7.28	11.0	379.0	C
838	Landers	1992	Barstow	7.28	35.0	371.0	C
897	Landers	1992	Twentynine Palms	7.28	41.0	685.0	C
879	Landers	1992	879	7.28	44.0	685.0	C
891	Landers	1992	Silent Valley - Poppet Flat	7.28	51.0	685.0	C
886	Landers	1992	Puerta La Cruz	7.28	94.0	371.0	C
887	Landers	1992	Riverside Airport	7.28	96.0	371.0	C
858	Landers	1992	Glendora - N Oakbank	7.28	123.0	446.0	C
852	Landers	1992	Duarte - Mel Canyon Rd.	7.28	126.0	446.0	C
835	Landers	1992	Arcadia - Campus Dr	7.28	135.0	368.0	C
889	Landers	1992	San Gabriel - E Grand Ave	7.28	142.0	401.0	C
840	Landers	1992	Big Tujunga, Angeles Nat F	7.28	144.0	446.0	C
875	Landers	1992	La Crescenta - New York	7.28	148.0	446.0	C

Code	Event	Year	Station	Mag	R(km)	Vs30 m/s	Site Class
857	Landers	1992	Glendale - Las Palmas	7.28	148.0	446.0	C
868	Landers	1992	LA - N Figueroa St	7.28	149.0	405.0	C
894	Landers	1992	Sunland - Mt Gleason Ave	7.28	152.0	446.0	C
867	Landers	1992	LA - Fletcher Dr	7.28	153.0	446.0	C
872	Landers	1992	LA - W 15th St	7.28	161.0	405.0	C
846	Landers	1992	Chatsworth - Devonshire	7.28	172.0	376.0	C
CMHS	NZ-10	2010	CMHS	7.10	36.0	410.6	C
HVSC	NZ-10	2010	HVSC	7.10	43.0	760.0	C
LPCC	NZ-10	2010	LPCC	7.10	44.0	631.1	C
828	CapeM	1992	828	7.01	4.5	713.0	C
825	CapeM	1992	825	7.01	10.4	514.0	C
126	Gazli	1976	126	6.80	12.8	660.0	C
VILE	Michoacan, Mexico	1985	VILE	8.10	47.8	327.0	D
2114	Denali- Alaska	2002	TAPS Pump Station #10	7.90	0.2	329.4	D
2109	Denali- Alaska	2002	Fairbanks - Ester Fire Station	7.90	139.3	274.5	D
2116	Denali- Alaska	2002	TAPS Pump Station #12	7.90	164.7	338.6	D
VTS	Valparaiso, Chile	1985	Ventanas	7.80	124.9	356.0	D
AHMD	Bhuj, India	2001	Ahmedabad	7.70	239.0	197.0	D
1513	Chi-Chi- Taiwan	1999	TCU079	7.62	0.0	364.0	D
1503	Chi-Chi- Taiwan	1999	TCU065	7.62	0.6	305.9	D
1244	Chi-Chi- Taiwan	1999	CHY101	7.62	10.0	258.9	D
1536	Chi-Chi- Taiwan	1999	TCU110	7.62	11.6	212.7	D
1547	Chi-Chi- Taiwan	1999	TCU123	7.62	14.9	241.7	D
1203	Chi-Chi- Taiwan	1999	CHY036	7.62	16.1	233.1	D

Code	Event	Year	Station	Mag	R(km)	Vs30 m/s	Site Class
1502	Chi-Chi- Taiwan	1999	TCU064	7.62	16.6	357.5	D
1498	Chi-Chi- Taiwan	1999	TCU059	7.62	17.1	230.3	D
1500	Chi-Chi- Taiwan	1999	TCU061	7.62	17.2	320.3	D
1246	Chi-Chi- Taiwan	1999	CHY104	7.62	18.0	223.2	D
1194	Chi-Chi- Taiwan	1999	CHY025	7.62	19.1	277.5	D
1540	Chi-Chi- Taiwan	1999	TCU115	7.62	21.8	215.3	D
1483	Chi-Chi- Taiwan	1999	TCU040	7.62	22.1	362.0	D
1537	Chi-Chi- Taiwan	1999	TCU111	7.62	22.1	237.5	D
1238	Chi-Chi- Taiwan	1999	CHY092	7.62	22.7	253.7	D
1209	Chi-Chi- Taiwan	1999	CHY047	7.62	24.1	291.9	D
1553	Chi-Chi- Taiwan	1999	TCU141	7.62	24.2	209.2	D
1180	Chi-Chi- Taiwan	1999	CHY002	7.62	25.0	235.1	D
1481	Chi-Chi- Taiwan	1999	TCU038	7.62	25.4	229.3	D
1542	Chi-Chi- Taiwan	1999	TCU117	7.62	25.4	198.6	D
1543	Chi-Chi- Taiwan	1999	TCU118	7.62	26.8	201.0	D
1538	Chi-Chi- Taiwan	1999	TCU112	7.62	27.5	201.0	D
1195	Chi-Chi- Taiwan	1999	CHY026	7.62	29.5	226.0	D
1539	Chi-Chi- Taiwan	1999	TCU113	7.62	31.1	230.3	D
1204	Chi-Chi- Taiwan	1999	CHY039	7.62	31.9	201.2	D
1552	Chi-Chi- Taiwan	1999	TCU140	7.62	33.0	201.0	D
1554	Chi-Chi- Taiwan	1999	TCU145	7.62	35.3	201.0	D
1199	Chi-Chi- Taiwan	1999	CHY032	7.62	35.4	192.7	D
1233	Chi-Chi- Taiwan	1999	CHY082	7.62	36.1	193.7	D
1240	Chi-Chi- Taiwan	1999	CHY094	7.62	37.1	221.9	D

Code	Event	Year	Station	Mag	R(km)	Vs30 m/s	Site Class
1544	Chi-Chi- Taiwan	1999	TCU119	7.62	38.0	201.0	D
1187	Chi-Chi- Taiwan	1999	CHY015	7.62	38.1	228.7	D
1183	Chi-Chi- Taiwan	1999	CHY008	7.62	40.4	210.7	D
1196	Chi-Chi- Taiwan	1999	CHY027	7.62	42.0	210.0	D
1200	Chi-Chi- Taiwan	1999	CHY033	7.62	43.8	197.6	D
1266	Chi-Chi- Taiwan	1999	HWA015	7.62	47.0	334.6	D
1181	Chi-Chi- Taiwan	1999	CHY004	7.62	47.3	271.3	D
1294	Chi-Chi- Taiwan	1999	HWA048	7.62	47.4	278.6	D
1276	Chi-Chi- Taiwan	1999	HWA027	7.62	47.6	282.9	D
1526	Chi-Chi- Taiwan	1999	TCU098	7.62	47.7	229.7	D
1267	Chi-Chi- Taiwan	1999	HWA016	7.62	48.2	344.0	D
1262	Chi-Chi- Taiwan	1999	HWA011	7.62	49.3	241.7	D
1296	Chi-Chi- Taiwan	1999	HWA050	7.62	49.4	239.6	D
1297	Chi-Chi- Taiwan	1999	HWA051	7.62	49.7	357.5	D
1239	Chi-Chi- Taiwan	1999	CHY093	7.62	49.8	190.5	D
1277	Chi-Chi- Taiwan	1999	HWA028	7.62	50.0	241.7	D
1264	Chi-Chi- Taiwan	1999	HWA013	7.62	50.5	231.1	D
1265	Chi-Chi- Taiwan	1999	HWA014	7.62	51.5	228.7	D
1269	Chi-Chi- Taiwan	1999	HWA019	7.62	51.9	244.1	D
1261	Chi-Chi- Taiwan	1999	HWA009	7.62	52.4	325.1	D
1260	Chi-Chi- Taiwan	1999	HWA007	7.62	52.6	255.6	D
1581	Chi-Chi- Taiwan	1999	TTN031	7.62	52.6	353.1	D
1263	Chi-Chi- Taiwan	1999	HWA012	7.62	53.0	278.6	D
1243	Chi-Chi- Taiwan	1999	CHY100	7.62	53.5	230.1	D

Code	Event	Year	Station	Mag	R(km)	Vs30 m/s	Site Class
1290	Chi-Chi- Taiwan	1999	HWA043	7.62	54.5	228.6	D
1207	Chi-Chi- Taiwan	1999	CHY044	7.62	55.1	194.5	D
1583	Chi-Chi- Taiwan	1999	TTN033	7.62	56.0	229.3	D
1237	Chi-Chi- Taiwan	1999	CHY090	7.62	58.4	201.0	D
1185	Chi-Chi- Taiwan	1999	CHY012	7.62	59.0	198.4	D
1189	Chi-Chi- Taiwan	1999	CHY017	7.62	59.1	190.6	D
1215	Chi-Chi- Taiwan	1999	CHY058	7.62	59.8	237.6	D
1292	Chi-Chi- Taiwan	1999	HWA045	7.62	60.2	259.0	D
1569	Chi-Chi- Taiwan	1999	TTN014	7.62	60.3	315.5	D
1242	Chi-Chi- Taiwan	1999	CHY099	7.62	65.3	228.8	D
1188	Chi-Chi- Taiwan	1999	CHY016	7.62	66.7	200.9	D
1349	Chi-Chi- Taiwan	1999	ILA066	7.62	67.4	306.0	D
1217	Chi-Chi- Taiwan	1999	CHY060	7.62	68.9	228.9	D
1346	Chi-Chi- Taiwan	1999	ILA062	7.62	70.4	278.6	D
1220	Chi-Chi- Taiwan	1999	CHY063	7.62	71.9	246.9	D
1216	Chi-Chi- Taiwan	1999	CHY059	7.62	73.3	191.1	D
1345	Chi-Chi- Taiwan	1999	ILA061	7.62	76.0	241.7	D
1318	Chi-Chi- Taiwan	1999	ILA014	7.62	78.2	300.8	D
1226	Chi-Chi- Taiwan	1999	CHY071	7.62	78.7	201.0	D
1562	Chi-Chi- Taiwan	1999	TTN006	7.62	78.7	259.0	D
1568	Chi-Chi- Taiwan	1999	TTN013	7.62	78.9	259.0	D
1567	Chi-Chi- Taiwan	1999	TTN012	7.62	79.2	249.4	D
1563	Chi-Chi- Taiwan	1999	TTN007	7.62	79.6	239.6	D
1320	Chi-Chi- Taiwan	1999	ILA016	7.62	79.9	271.1	D

Code	Event	Year	Station	Mag	R(km)	Vs30 m/s	Site Class
1564	Chi-Chi- Taiwan	1999	TTN008	7.62	80.4	230.3	D
1323	Chi-Chi- Taiwan	1999	ILA027	7.62	80.8	201.0	D
1570	Chi-Chi- Taiwan	1999	TTN015	7.62	80.9	232.0	D
1192	Chi-Chi- Taiwan	1999	CHY023	7.62	81.1	279.8	D
1250	Chi-Chi- Taiwan	1999	CHY116	7.62	81.3	201.0	D
1565	Chi-Chi- Taiwan	1999	TTN009	7.62	81.4	230.3	D
1566	Chi-Chi- Taiwan	1999	TTN010	7.62	81.5	246.6	D
1317	Chi-Chi- Taiwan	1999	ILA013	7.62	81.7	201.0	D
1329	Chi-Chi- Taiwan	1999	ILA037	7.62	81.7	210.2	D
1326	Chi-Chi- Taiwan	1999	ILA032	7.62	81.8	295.5	D
1241	Chi-Chi- Taiwan	1999	CHY096	7.62	82.2	291.9	D
1314	Chi-Chi- Taiwan	1999	ILA008	7.62	82.4	229.7	D
1312	Chi-Chi- Taiwan	1999	ILA006	7.62	82.7	279.4	D
1221	Chi-Chi- Taiwan	1999	CHY065	7.62	82.8	344.0	D
1324	Chi-Chi- Taiwan	1999	ILA030	7.62	83.2	201.0	D
1332	Chi-Chi- Taiwan	1999	ILA042	7.62	83.3	209.4	D
1225	Chi-Chi- Taiwan	1999	CHY070	7.62	83.5	282.9	D
1223	Chi-Chi- Taiwan	1999	CHY067	7.62	83.6	228.0	D
1330	Chi-Chi- Taiwan	1999	ILA039	7.62	83.8	227.2	D
1344	Chi-Chi- Taiwan	1999	ILA059	7.62	84.0	236.8	D
1311	Chi-Chi- Taiwan	1999	ILA005	7.62	84.9	239.3	D
1331	Chi-Chi- Taiwan	1999	ILA041	7.62	85.7	196.9	D
1337	Chi-Chi- Taiwan	1999	ILA049	7.62	85.7	201.0	D
1316	Chi-Chi- Taiwan	1999	ILA012	7.62	85.9	237.6	D

Code	Event	Year	Station	Mag	R(km)	Vs30 m/s	Site Class
1224	Chi-Chi- Taiwan	1999	CHY069	7.62	86.0	201.0	D
1396	Chi-Chi- Taiwan	1999	KAU085	7.62	86.0	260.8	D
1336	Chi-Chi- Taiwan	1999	ILA048	7.62	86.7	199.6	D
1328	Chi-Chi- Taiwan	1999	ILA036	7.62	87.7	229.3	D
1342	Chi-Chi- Taiwan	1999	ILA055	7.62	88.0	266.8	D
1222	Chi-Chi- Taiwan	1999	CHY066	7.62	89.4	212.0	D
1343	Chi-Chi- Taiwan	1999	ILA056	7.62	89.8	223.7	D
1431	Chi-Chi- Taiwan	1999	TAP043	7.62	90.0	239.6	D
1309	Chi-Chi- Taiwan	1999	ILA003	7.62	90.6	263.8	D
1327	Chi-Chi- Taiwan	1999	ILA035	7.62	91.3	241.7	D
1376	Chi-Chi- Taiwan	1999	KAU048	7.62	91.5	296.5	D
1384	Chi-Chi- Taiwan	1999	KAU063	7.62	92.8	201.0	D
1559	Chi-Chi- Taiwan	1999	TTN003	7.62	92.9	262.6	D
1424	Chi-Chi- Taiwan	1999	TAP028	7.62	94.7	231.1	D
1308	Chi-Chi- Taiwan	1999	ILA002	7.62	95.5	229.3	D
1423	Chi-Chi- Taiwan	1999	TAP026	7.62	95.8	201.0	D
1397	Chi-Chi- Taiwan	1999	KAU086	7.62	95.9	201.0	D
1362	Chi-Chi- Taiwan	1999	KAU022	7.62	96.8	202.0	D
1457	Chi-Chi- Taiwan	1999	TAP097	7.62	97.3	201.0	D
1356	Chi-Chi- Taiwan	1999	KAU010	7.62	97.5	201.0	D
1419	Chi-Chi- Taiwan	1999	TAP017	7.62	97.7	201.0	D
1409	Chi-Chi- Taiwan	1999	TAP	7.62	98.3	201.0	D
1459	Chi-Chi- Taiwan	1999	TAP100	7.62	98.3	201.0	D
1386	Chi-Chi- Taiwan	1999	KAU066	7.62	99.1	201.0	D

Code	Event	Year	Station	Mag	R(km)	Vs30 m/s	Site Class
1421	Chi-Chi- Taiwan	1999	TAP021	7.62	99.5	201.0	D
1415	Chi-Chi- Taiwan	1999	TAP010	7.62	99.9	226.4	D
1385	Chi-Chi- Taiwan	1999	KAU064	7.62	100.0	201.0	D
1363	Chi-Chi- Taiwan	1999	KAU030	7.62	100.1	201.0	D
1416	Chi-Chi- Taiwan	1999	TAP012	7.62	100.1	201.0	D
1417	Chi-Chi- Taiwan	1999	TAP013	7.62	100.8	201.0	D
1410	Chi-Chi- Taiwan	1999	TAP003	7.62	101.3	212.4	D
1418	Chi-Chi- Taiwan	1999	TAP014	7.62	101.6	201.0	D
1414	Chi-Chi- Taiwan	1999	TAP008	7.62	102.8	201.0	D
1389	Chi-Chi- Taiwan	1999	KAU074	7.62	103.7	201.0	D
1454	Chi-Chi- Taiwan	1999	TAP090	7.62	103.7	324.4	D
1412	Chi-Chi- Taiwan	1999	TAP006	7.62	104.2	184.8	D
1411	Chi-Chi- Taiwan	1999	TAP005	7.62	105.5	201.0	D
1430	Chi-Chi- Taiwan	1999	TAP042	7.62	105.5	228.9	D
1354	Chi-Chi- Taiwan	1999	KAU007	7.62	105.9	252.4	D
1359	Chi-Chi- Taiwan	1999	KAU015	7.62	106.5	320.3	D
1355	Chi-Chi- Taiwan	1999	KAU008	7.62	107.0	285.9	D
1382	Chi-Chi- Taiwan	1999	KAU058	7.62	107.8	201.0	D
1456	Chi-Chi- Taiwan	1999	TAP095	7.62	107.8	201.0	D
1455	Chi-Chi- Taiwan	1999	TAP094	7.62	107.9	262.6	D
1388	Chi-Chi- Taiwan	1999	KAU073	7.62	108.8	201.0	D
1399	Chi-Chi- Taiwan	1999	KAU088	7.62	108.9	201.0	D
1395	Chi-Chi- Taiwan	1999	KAU083	7.62	109.1	201.0	D
1429	Chi-Chi- Taiwan	1999	TAP041	7.62	110.3	229.3	D

Code	Event	Year	Station	Mag	R(km)	Vs30 m/s	Site Class
1364	Chi-Chi- Taiwan	1999	KAU032	7.62	111.0	201.0	D
1398	Chi-Chi- Taiwan	1999	KAU087	7.62	111.7	276.1	D
1383	Chi-Chi- Taiwan	1999	KAU062	7.62	112.2	201.0	D
1353	Chi-Chi- Taiwan	1999	KAU006	7.62	113.4	218.5	D
1390	Chi-Chi- Taiwan	1999	KAU075	7.62	114.8	201.0	D
1365	Chi-Chi- Taiwan	1999	KAU033	7.62	119.3	201.0	D
1373	Chi-Chi- Taiwan	1999	KAU044	7.62	120.0	221.2	D
1451	Chi-Chi- Taiwan	1999	TAP084	7.62	122.1	224.2	D
1367	Chi-Chi- Taiwan	1999	KAU037	7.62	135.0	283.2	D
1393	Chi-Chi- Taiwan	1999	KAU081	7.62	161.2	255.6	D
1374	Chi-Chi- Taiwan	1999	KAU046	7.62	161.6	204.2	D
MG	El Salvador	2001	San Miguel	7.60	70.0	330.0	D
SANISI	Limon, Costa Rica	1991	San Isidro	7.60	72.9	315.0	D
AREQ	Peru	1974	Arequippa	7.60	83.5	335.0	D
DB	El Salvador	2001	Ciudadela Don Bosco	7.60	92.4	304.0	D
ST	El Salvador	2001	Santa Tecia	7.60	98.0	338.0	D
BIBLIO	Limon, Costa Rica	1991	San Jose, Biblioteque	7.60	110.0	347.0	D
HEBEI	Tangshan	1976	Hongshan, Hebei	7.60	391.0	252.0	D
1628	St. Elias, Alaska	1979	Icy Bay	7.54	26.5	275.0	D
1629	St. Elias, Alaska	1979	Yakutat	7.54	80.0	275.0	D
1176	Kocaeli, Turkey	1999	Yarimca	7.51	1.4	297.0	D
1158	Kocaeli, Turkey	1999	Duzce	7.51	13.6	276.0	D
1166	Kocaeli, Turkey	1999	Iznik	7.51	30.7	274.5	D
1177	Kocaeli, Turkey	1999	Zeytinburnu	7.51	52.0	274.5	D

Code	Event	Year	Station	Mag	R(km)	Vs30 m/s	Site Class
1160	Kocaeli, Turkey	1999	Fatih	7.51	55.0	339.0	D
1149	Kocaeli, Turkey	1999	Atakoy	7.51	56.5	274.5	D
1155	Kocaeli, Turkey	1999	Bursa Tofas	7.51	60.0	275.0	D
1157	Kocaeli, Turkey	1999	Cekmece	7.51	67.0	346.0	D
1153	Kocaeli, Turkey	1999	Botas	7.51	127.0	275.0	D
1167	Kocaeli, Turkey	1999	Kutahya	7.51	145.0	275.0	D
1151	Kocaeli, Turkey	1999	Balikesir	7.51	180.0	339.0	D
1175	Kocaeli, Turkey	1999	Usak	7.51	227.0	275.0	D
1156	Kocaeli, Turkey	1999	Canakkale	7.51	266.0	275.0	D
1152	Kocaeli, Turkey	1999	Bornova	7.51	316.0	275.0	D
1636	Manjil, Iran	1990	Qazvin	7.37	50.0	274.5	D
1637	Manjil, Iran	1990	Rudsar	7.37	64.0	275.0	D
1634	Manjil, Iran	1990	Abhar	7.37	76.0	275.0	D
1640	Manjil, Iran	1990	Tonekabun	7.37	94.0	275.0	D
1639	Manjil, Iran	1990	Tehran - Sarif University	7.37	172.0	275.0	D
1638	Manjil, Iran	1990	Tehran - Building & Housing	7.37	175.0	275.0	D
12	Kern County	1952	LA - Hollywood Stor FF	7.36	118.0	316.0	D
0012	KernCo	1952	0012	7.36	118.0	316.0	D
138	Tabas, Iran	1978	Boshrooyeh	7.35	24.1	338.6	D
140	Tabas, Iran	1978	Ferdows	7.35	89.8	274.5	D
137	Tabas, Iran	1978	Bajestan	7.35	120.0	338.6	D
141	Tabas, Iran	1978	Kashmar	7.35	193.9	274.5	D
571	Taiwan SMART1(45)	1986	SMART1 E01	7.30	54.0	274.5	D
580	Taiwan SMART1(45)	1986	SMART1 O06	7.30	54.0	274.5	D

Code	Event	Year	Station	Mag	R(km)	Vs30 m/s	Site Class
581	Taiwan SMART1(45)	1986	SMART1 O07	7.30	54.0	274.5	D
576	Taiwan SMART1(45)	1986	SMART1 M07	7.30	55.0	274.5	D
579	Taiwan SMART1(45)	1986	SMART1 O04	7.30	55.0	274.5	D
582	Taiwan SMART1(45)	1986	SMART1 O08	7.30	55.0	274.5	D
570	Taiwan SMART1(45)	1986	SMART1 C00	7.30	56.0	274.5	D
573	Taiwan SMART1(45)	1986	SMART1 I01	7.30	56.0	274.5	D
574	Taiwan SMART1(45)	1986	SMART1 I07	7.30	56.0	274.5	D
575	Taiwan SMART1(45)	1986	SMART1 M01	7.30	57.0	274.5	D
578	Taiwan SMART1(45)	1986	SMART1 O02	7.30	57.0	274.5	D
583	Taiwan SMART1(45)	1986	SMART1 O10	7.30	57.0	274.5	D
577	Taiwan SMART1(45)	1986	SMART1 O01	7.30	58.0	274.5	D
584	Taiwan SMART1(45)	1986	SMART1 O12	7.30	58.0	274.5	D
BOKA	India-Burma Border	1988	BOKA	7.30	189.9	297.0	D
DIPU	India-Burma Border	1988	DIPU	7.30	210.1	290.0	D
BERL	India-Burma Border	1988	Berlanger	7.30	220.1	310.0	D
PANI	India-Burma Border	1988	PANI	7.30	257.1	263.0	D
SAIT	India-Burma Border	1988	SAIT	7.30	296.3	235.0	D
881	Landers	1992	Morongo Valley	7.28	17.3	345.0	D
850	Landers	1992	Desert Hot Springs	7.28	21.8	345.0	D
900	Landers	1992	Yermo Fire Station	7.28	23.6	354.0	D
882	Landers	1992	North Palm Springs	7.28	26.8	345.0	D
880	Landers	1992	Mission Creek Fault	7.28	27.0	345.0	D
884	Landers	1992	Palm Springs Airport	7.28	36.0	207.0	D
862	Landers	1992	Indio - Coachella Canal	7.28	54.0	345.0	D

Code	Event	Year	Station	Mag	R(km)	Vs30 m/s	Site Class
855	Landers	1992	Fort Irwin	7.28	63.0	345.0	D
832	Landers	1992	Amboy	7.28	69.0	271.0	D
860	Landers	1992	Hemet Fire Station	7.28	69.0	339.0	D
888	Landers	1992	San Bern. - E & Hospitality	7.28	80.0	271.0	D
848	Landeers	1992	848	7.28	82.0	271.0	D
836	Landers	1992	Baker Fire Station	7.28	88.0	271.0	D
841	Landers	1992	Boron Fire Station	7.28	90.0	345.0	D
885	Landers	1992	Pomona - 4th & Locust FF	7.28	118.0	230.0	D
854	Landers	1992	Featherly Park - Maint	7.28	122.0	309.0	D
849	Landers	1992	Covina - W Badillo	7.28	128.0	271.0	D
837	Landers	1992	Baldwin Park - N Holly	7.28	132.0	309.0	D
877	Landers	1992	La Puente - Rimgrove Av	7.28	132.0	309.0	D
899	Landers	1992	West Covina - S Orange Ave	7.28	132.0	309.0	D
898	Landers	1992	Villa Park - Serrano Ave	7.28	133.0	309.0	D
853	Landers	1992	El Monte - Fairview Av	7.28	136.0	309.0	D
859	Landers	1992	Hacienda Heights - Colima	7.28	136.0	309.0	D
834	Landers	1992	Arcadia - Arcadia Av	7.28	137.0	309.0	D
842	Landers	1992	Brea - S Flower Av	7.28	137.0	309.0	D
896	Landers	1992	Tustin - E Sycamore	7.28	137.0	235.0	D
876	Landers	1992	La Habra - Briarcliff	7.28	143.0	361.0	D
833	Landers	1992	Anaheim - W Ball Rd	7.28	145.0	235.0	D
856	Landers	1992	Fountain Valley - Euclid	7.28	147.0	270.0	D
843	Landers	1992	Buena Park - La Palma	7.28	150.0	309.0	D
890	Landers	1992	Santa Fe Springs - E.Joslin	7.28	150.0	309.0	D

Code	Event	Year	Station	Mag	R(km)	Vs30 m/s	Site Class
870	Landers	1992	LA - Obregon Park	7.28	152.0	349.0	D
839	Landers	1992	Bell Gardens - Jaboneria	7.28	154.0	309.0	D
861	Landers	1992	Huntington Bch - Waikiki	7.28	156.0	235.0	D
851	Landers	1992	Downey - Co Maint Bldg	7.28	157.0	272.0	D
878	Landers	1992	Lakewood - Del Amo Blvd	7.28	157.0	235.0	D
844	Landers	1992	Burbank - N Buena Vista	7.28	158.0	271.0	D
893	Landers	1992	Sun Valley - Sunland	7.28	158.0	271.0	D
869	Landers	1992	LA - N Westmoreland	7.28	159.0	315.0	D
847	Landers	1992	Compton - Castlegate St	7.28	161.0	309.0	D
874	Landers	1992	LB - Orange Ave	7.28	161.0	270.0	D
871	Landers	1992	LA - S Grand Ave	7.28	162.0	309.0	D
865	Landers	1992	LA - 116th St School	7.28	164.0	301.0	D
873	Landers	1992	LA - W 70th St	7.28	164.0	294.0	D
892	Landers	1992	Sun Valley - Roscoe Blvd	7.28	164.0	309.0	D
863	Landers	1992	Inglewood - Union Oil	7.28	167.0	316.0	D
883	Landers	1992	Northridge - 17645 Saticoy St	7.28	172.0	281.0	D
895	Landers	1992	Tarzana - Cedar Hill	7.28	176.0	257.0	D
845	Landers	1992	Calabasas - N Las Virg	7.28	190.0	339.0	D
M931	Sierra el Mayor	2010	M931	7.20	16.7	209.0	D
M5058	Sierra el Mayor	2010	M5058	7.20	22.0	209.0	D
M5053	Sierra el Mayor	2010	M5053	7.20	23.1	209.0	D
M412	Sierra el Mayor	2010	M412	7.20	26.0	209.0	D
M1711	Sierra el Mayor	2010	M1711	7.20	26.0	209.0	D
M5165	Sierra el Mayor	2010	M5165	7.20	29.3	209.0	D

Code	Event	Year	Station	Mag	R(km)	Vs30 m/s	Site Class
M1794	Sierra el Mayor	2010	M1794	7.20	33.4	209.0	D
M464	Sierra el Mayor	2010	M464	7.20	33.5	209.0	D
M5028	Sierra el Mayor	2010	M5028	7.20	33.9	209.0	D
M5413	Sierra el Mayor	2010	M5413	7.20	35.6	209.0	D
M5054	Sierra el Mayor	2010	M5054	7.20	35.7	209.0	D
M-DRE	Sierra el Mayor	2010	M-DRE	7.20	35.7	209.0	D
M5055	Sierra el Mayor	2010	M5055	7.20	41.2	209.0	D
M955	Sierra el Mayor	2010	M955	7.20	41.3	209.0	D
M5057	Sierra el Mayor	2010	M5057	7.20	46.9	209.0	D
M5060	Sierra el Mayor	2010	M5060	7.20	48.9	209.0	D
M11369	Sierra el Mayor	2010	M11369	7.20	50.6	209.0	D
280	Trinidad	1980	280	7.20	76.8	311.8	D
281	Trinidad	1980	281	7.20	76.8	311.8	D
282	Trinidad	1980	282	7.20	76.8	311.8	D
M11628	Sierra el Mayor	2010	M11628	7.20	80.2	209.0	D
1605	Duzce	1999	1605	7.14	6.6	276.0	D
1602	Duzce	1999	1602	7.14	41.3	326.0	D
1762	HecM	1999	1762	7.13	43.0	271.0	D
1766	HecM	1999	1766	7.13	65.0	271.0	D
1792	HecM	1999	1792	7.13	74.0	207.0	D
GDLC	NZ-10	2010	GDLC	7.10	8.0	275.6	D
DFHS	NZ-10	2010	DFHS	7.10	9.0	277.8	D
DSLC	NZ-10	2010	DSLC	7.10	13.0	258.7	D
ROLC	NZ-10	2010	ROLC	7.10	17.0	264.2	D

Code	Event	Year	Station	Mag	R(km)	Vs30 m/s	Site Class
TPLC	NZ-10	2010	TPLC	7.10	24.0	250.1	D
LINC	NZ-10	2010	LINC	7.10	25.0	235.1	D
CACS	NZ-10	2010	CACS	7.10	29.0	258.0	D
RHSC	NZ-10	2010	RHSC	7.10	31.0	223.5	D
PPHS	NZ-10	2010	PPHS	7.10	35.0	242.4	D
REHS	NZ-10	2010	REHS	7.10	37.0	240.0	D
CCCC	NZ-10	2010	CCCC	7.10	38.0	231.1	D
SHLC	NZ-10	2010	SHLC	7.10	39.0	191.6	D
PRPC	NZ-10	2010	PRPC	7.10	41.0	204.1	D
KPOC	NZ-10	2010	KPOC	7.10	44.0	215.6	D
NNBS	NZ-10	2010	NNBS	7.10	44.0	217.4	D
829	CapeM	1992	829	7.01	22.6	312.0	D
6	ElCentro	1940	6	6.95	13.0	213.0	D
0768	LomaP	1989	0768	6.93	14.3	222.0	D
0786	LomaP	1989	0786	6.93	31.0	210.0	D
0799	LomaP	1989	0799	6.93	59.0	190.0	D
1119	Kobe	1995	1119	6.90	0.3	312.0	D
1106	Kobe	1995	1106	6.90	1.0	312.0	D
1120	Kobe	1995	1120	6.90	1.5	256.0	D
1116	Kobe	1995	1116	6.90	19.0	256.0	D
1113	Kobe	1995	1113	6.90	21.0	256.0	D
1107	Kobe	1995	1107	6.90	23.0	312.0	D
0290	Irpinia	1980	0290	6.90	30.0	350.0	D
0287	Irpinia	1980	0287	6.90	46.0	275.0	D

Code	Event	Year	Station	Mag	R(km)	Vs30 m/s	Site Class
1105	Kobe	1995	1105	6.90	96.0	256.0	D
1103	Kobe	1995	1103	6.90	159.0	256.0	D
821	Erzican	1992	821	6.69	9.0	275.0	D
CALE	Michoacan, Mexico	1985	CALE	8.10	38.3	180.0	E
SGMS2	SGMS	2012	SGMS2	7.70	11.9	180.0	E
RSCTH2	RSCTH	2012	RSCTH2	7.70	11.9	180.0	E
USGS1B	USGS	2012	USGS1B	7.70	59.0	180.0	E
SGMS1	SGMS	2012	SGMS1	7.70	59.5	180.0	E
RSCTH1	RSCTH	2012	RSCTH1	7.70	59.5	180.0	E
USGS1A	USGS	2012	USGS1A	7.70	59.5	180.0	E
USGS1C	USGS	2012	USGS1C	7.70	59.5	180.0	E
USGS2A	USGS	2012	USGS2A	7.70	59.5	180.0	E
USGS2B	USGS	2012	USGS2B	7.70	59.5	180.0	E
USGS2C	USGS	2012	USGS2C	7.70	59.5	180.0	E
1228	Chi-Chi- Taiwan	1999	CHY076	7.62	42.2	169.8	E
1212	Chi-Chi- Taiwan	1999	CHY054	7.62	48.5	172.1	E
1247	Chi-Chi- Taiwan	1999	CHY107	7.62	50.6	175.7	E
1229	Chi-Chi- Taiwan	1999	CHY078	7.62	77.2	160.7	E
1334	Chi-Chi- Taiwan	1999	ILA044	7.62	78.0	158.1	E
1310	Chi-Chi- Taiwan	1999	ILA004	7.62	86.6	124.3	E
1357	Chi-Chi- Taiwan	1999	KAU011	7.62	101.2	155.3	E
1147	Kocaeli, Turkey	1999	Ambarli	7.51	70.0	175.0	E
STA155	Bucharest, Romania	1977	Station 155	7.50	116.0	130.0	E
HORC	NZ-10	2010	HORC	7.10	18.0	180.0	E

Code	Event	Year	Station	Mag	R(km)	Vs30 m/s	Site Class
CHHC	NZ-10	2010	CHHC	7.10	36.0	180.0	E
0732	LomaP	1989	0732	6.93	63.5	133.1	E
0759	LomaP	1989	0759	6.93	64.0	116.4	E
0760	LomaP	1989	0760	6.93	65.7	126.4	E
0808	LomaP	1989	0808	6.93	77.0	155.0	E
0780	LomaP	1989	0780	6.93	95.0	170.0	E
0962	NorthR	1994	0962	6.69	50.3	160.6	E
0178	ImpVal	1979	0178	6.53	28.7	162.9	E

“Code” is the NGA database number for PEER records and a unique station identifier for all other records.

“Site Class” is AASHTO definition Site Class.

APPENDIX B: GROUND MOTION PARAMETERS - DESIGN RECORD SETS

1UHRS Scaled Accelerogram	1214FN	1214FP	GM	1190FN	1190FP	GM
Max Acceleration (g)	0.303	0.481	0.382	0.413	0.469	0.440
Max Velocity (cm/sec)	62.1	49.5	55.5	51.8	39.4	45.2
Max Displacement (cm)	55.2	36.2	44.7	46.8	33.0	39.3
Vmax/Amax (sec)	0.209	0.105	0.148	0.128	0.086	0.105
Acceleration RMS (g)	0.063	0.071	0.067	0.065	0.068	0.066
Velocity RMS (cm/sec)	12.8	12.2	12.5	10.8	10.6	10.7
Displacement RMS (cm)	16.9	13.3	15.0	15.1	11.1	13.0
Arias Intensity (cm/sec)	5.42	6.95	6.14	7.00	7.55	7.27
Characteristic Intensity	0.148	0.179	0.163	0.172	0.182	0.177
SED (cm2/sec)	14642	13377	13995	12584	12081	12330
Cum. Abs. Velocity (cm/sec)	3470	3875	3667	4033	4200	4116
Acc Spec. Intensity (g*sec)	0.348	0.416	0.381	0.409	0.431	0.420
Vel Spectrum Intensity (cm)	214	198	206	189	194	192
Housner Intensity (cm)	213	192	203	171	183	177
Sustained Max.Acc. (g)	0.300	0.366	0.331	0.358	0.387	0.372
Sustained Max.Vel. (cm/sec)	43.5	41.3	42.4	45.7	35.7	40.4
Effective Design Acc. (g)	0.308	0.474	0.382	0.382	0.442	0.411
A95 parameter (g)	0.298	0.471	0.374	0.402	0.458	0.429
Predominant Period (sec)	0.46	0.18	0.29	0.26	0.24	0.25
Significant Duration (sec)	36.4	39.3	37.8	38.0	38.7	38.3

GM: Geometric Mean
SED: Specific Energy Density

1UHRS Scaled Accelerogram	0779FN	0779FP	GM	1245FN	1245FP	GM
Max Acceleration (g)	0.651	0.370	0.491	0.432	0.506	0.467
Max Velocity (cm/sec)	66.9	49.8	57.7	52.4	53.2	52.8
Max Displacement (cm)	43.2	21.1	30.2	44.1	42.7	43.4
Vmax/Amax (sec)	0.105	0.137	0.120	0.124	0.107	0.115
Acceleration RMS (g)	0.101	0.065	0.081	0.066	0.066	0.066
Velocity RMS (cm/sec)	18.6	11.4	14.5	13.1	11.2	12.1
Displacement RMS (cm)	12.8	7.6	9.9	12.2	12.8	12.5
Arias Intensity (cm/sec)	3.93	1.62	2.52	6.08	6.02	6.05
Characteristic Intensity	0.160	0.083	0.115	0.162	0.160	0.161
SED (cm2/sec)	8630	3225	5276	15341	11231	13126
Cum. Abs. Velocity (cm/sec)	1464	976	1196	3523	3474	3499
Acc Spec. Intensity (g*sec)	0.421	0.272	0.339	0.328	0.356	0.342
Vel Spectrum Intensity (cm)	281	171	219	180	192	186
Housner Intensity (cm)	265	165	209	180	185	183
Sustained Max.Acc. (g)	0.542	0.303	0.405	0.343	0.367	0.355
Sustained Max.Vel. (cm/sec)	64.1	40.8	51.1	48.1	47.3	47.7
Effective Design Acc. (g)	0.394	0.352	0.372	0.360	0.442	0.399
A95 parameter (g)	0.640	0.364	0.483	0.418	0.494	0.454
Predominant Period (sec)	0.74	0.66	0.70	0.10	0.08	0.09
Significant Duration (sec)	10.0	10.9	10.4	37.1	34.8	36.0

GM: Geometric Mean
SED: Specific Energy Density

1UHRS Scaled Accelerogram	1816FN	1816FP	GM	1177FN	1177FP	GM
Max Acceleration (g)	0.317	0.387	0.350	0.441	0.441	0.441
Max Velocity (cm/sec)	53.8	45.1	49.3	76.1	62.3	68.9
Max Displacement (cm)	49.4	39.0	43.9	50.6	75.2	61.7
Vmax/Amax (sec)	0.173	0.119	0.143	0.176	0.144	0.159
Acceleration RMS (g)	0.052	0.054	0.053	0.047	0.053	0.050
Velocity RMS (cm/sec)	10.6	9.1	9.8	10.2	9.2	9.7
Displacement RMS (cm)	10.3	8.6	9.4	10.8	13.2	12.0
Arias Intensity (cm/sec)	3.87	4.25	4.06	4.32	5.63	4.93
Characteristic Intensity	0.114	0.123	0.118	0.114	0.139	0.126
SED (cm2/sec)	10389	7720	8955	13492	11052	12212
Cum. Abs. Velocity (cm/sec)	2648	2636	2642	3081	3479	3274
Acc Spec. Intensity (g*sec)	0.332	0.417	0.372	0.328	0.489	0.401
Vel Spectrum Intensity (cm)	214	189	201	236	198	216
Housner Intensity (cm)	208	177	192	222	187	204
Sustained Max.Acc. (g)	0.305	0.326	0.316	0.307	0.374	0.339
Sustained Max.Vel. (cm/sec)	48.2	42.2	45.1	55.9	51.5	53.7
Effective Design Acc. (g)	0.309	0.369	0.338	0.430	0.442	0.436
A95 parameter (g)	0.310	0.378	0.342	0.433	0.433	0.433
Predominant Period (sec)	0.20	0.18	0.19	0.64	0.44	0.53
Significant Duration (sec)	27.7	21.9	24.6	39.4	38.9	39.1

GM: Geometric Mean
SED: Specific Energy Density

1UHRS Scaled Accelerogram	0832FN	0832FP	GM	1827FN	1827FP	GM
Max Acceleration (g)	0.405	0.309	0.354	0.324	0.429	0.373
Max Velocity (cm/sec)	54.4	50.7	52.5	53.6	123.2	81.3
Max Displacement (cm)	20.5	31.9	25.6	24.8	134.1	57.6
Vmax/Amax (sec)	0.137	0.168	0.151	0.169	0.293	0.222
Acceleration RMS (g)	0.087	0.075	0.081	0.072	0.094	0.082
Velocity RMS (cm/sec)	13.1	14.6	13.9	11.4	28.6	18.0
Displacement RMS (cm)	6.9	11.8	9.0	7.6	37.7	16.9
Arias Intensity (cm/sec)	5.79	4.30	4.99	3.16	5.39	4.12
Characteristic Intensity	0.181	0.145	0.162	0.121	0.181	0.148
SED (cm2/sec)	8606	10713	9602	5157	32774	13001
Cum. Abs. Velocity (cm/sec)	2946	2575	2754	2096	2576	2324
Acc Spec. Intensity (g*sec)	0.403	0.322	0.360	0.323	0.396	0.358
Vel Spectrum Intensity (cm)	230	177	202	200	276	235
Housner Intensity (cm)	229	184	205	183	278	225
Sustained Max.Acc. (g)	0.344	0.271	0.305	0.277	0.344	0.309
Sustained Max.Vel. (cm/sec)	42.4	43.0	42.7	32.7	103.9	58.3
Effective Design Acc. (g)	0.376	0.295	0.333	0.329	0.428	0.375
A95 parameter (g)	0.381	0.285	0.330	0.320	0.421	0.367
Predominant Period (sec)	0.14	0.24	0.18	0.32	0.30	0.31
Significant Duration (sec)	25.2	29.9	27.4	26.2	21.4	23.6

GM: Geometric Mean
SED: Specific Energy Density

1UHRS Scaled Accelerogram	0802FN	0802FP	GM	0880FN	0880FP	GM
Max Acceleration (g)	0.472	0.490	0.481	0.536	0.554	0.545
Max Velocity (cm/sec)	72.3	56.3	63.8	101.6	30.2	55.4
Max Displacement (cm)	38.3	20.5	28.0	106.6	10.9	34.1
Vmax/Amax (sec)	0.156	0.117	0.135	0.193	0.056	0.104
Acceleration RMS (g)	0.062	0.056	0.059	0.070	0.080	0.075
Velocity RMS (cm/sec)	11.9	8.2	9.9	22.0	7.6	12.9
Displacement RMS (cm)	8.1	5.5	6.7	34.2	3.9	11.6
Arias Intensity (cm/sec)	2.37	1.93	2.14	5.33	6.94	6.09
Characteristic Intensity	0.098	0.084	0.090	0.156	0.190	0.172
SED (cm2/sec)	5648	2667	3881	33888	4017	11667
Cum. Abs. Velocity (cm/sec)	1194	1053	1121	3168	3662	3406
Acc Spec. Intensity (g*sec)	0.401	0.395	0.398	0.380	0.454	0.415
Vel Spectrum Intensity (cm)	243	171	203	228	161	192
Housner Intensity (cm)	232	159	192	233	148	186
Sustained Max.Acc. (g)	0.394	0.386	0.390	0.388	0.417	0.402
Sustained Max.Vel. (cm/sec)	53.0	30.6	40.2	71.4	27.2	44.1
Effective Design Acc. (g)	0.452	0.462	0.457	0.390	0.473	0.430
A95 parameter (g)	0.469	0.483	0.476	0.519	0.542	0.530
Predominant Period (sec)	0.18	0.16	0.17	0.28	0.18	0.22
Significant Duration (sec)	8.4	8.9	8.7	40.2	34.7	37.3

GM: Geometric Mean
SED: Specific Energy Density

1UHRS Scaled Accelerogram	0746FN	0746FP	GM	0900FN	0900FP	GM
Max Acceleration (g)	0.395	0.415	0.405	0.418	0.420	0.419
Max Velocity (cm/sec)	51.5	58.5	54.9	100.3	47.0	68.7
Max Displacement (cm)	26.0	39.0	31.9	85.4	31.8	52.1
Vmax/Amax (sec)	0.133	0.144	0.138	0.244	0.114	0.167
Acceleration RMS (g)	0.080	0.080	0.080	0.071	0.058	0.064
Velocity RMS (cm/sec)	15.4	18.2	16.7	21.4	11.1	15.4
Displacement RMS (cm)	10.5	14.4	12.3	24.2	7.8	13.7
Arias Intensity (cm/sec)	2.95	2.95	2.95	3.41	2.29	2.79
Characteristic Intensity	0.124	0.124	0.124	0.125	0.093	0.108
SED (cm2/sec)	6999	9820	8290	20071	5407	10418
Cum. Abs. Velocity (cm/sec)	1700	1687	1693	1825	1572	1694
Acc Spec. Intensity (g*sec)	0.389	0.392	0.391	0.341	0.341	0.341
Vel Spectrum Intensity (cm)	189	189	189	275	191	229
Housner Intensity (cm)	192	192	192	266	193	226
Sustained Max.Acc. (g)	0.326	0.278	0.301	0.377	0.267	0.317
Sustained Max.Vel. (cm/sec)	42.0	39.8	40.9	74.6	39.4	54.2
Effective Design Acc. (g)	0.363	0.431	0.396	0.408	0.415	0.412
A95 parameter (g)	0.386	0.410	0.398	0.407	0.411	0.409
Predominant Period (sec)	0.22	0.24	0.23	0.38	0.28	0.33
Significant Duration (sec)	17.6	17.8	17.7	17.2	19.6	18.3

GM: Geometric Mean
SED: Specific Energy Density

1UHRS Scaled Accelerogram	1153FN	1153FP	GM	1791FN	1791FP	GM
Max Acceleration (g)	0.569	0.489	0.527	0.517	0.362	0.433
Max Velocity (cm/sec)	54.2	67.7	60.6	66.5	58.4	62.3
Max Displacement (cm)	25.6	84.8	46.6	39.2	27.9	33.1
Vmax/Amax (sec)	0.097	0.141	0.117	0.131	0.164	0.147
Acceleration RMS (g)	0.045	0.042	0.043	0.066	0.049	0.057
Velocity RMS (cm/sec)	7.4	11.7	9.3	15.6	11.3	13.3
Displacement RMS (cm)	8.1	23.4	13.8	11.7	8.7	10.1
Arias Intensity (cm/sec)	3.19	2.72	2.95	4.03	2.23	3.00
Characteristic Intensity	0.097	0.086	0.091	0.131	0.084	0.105
SED (cm2/sec)	5557	14006	8822	14613	7664	10583
Cum. Abs. Velocity (cm/sec)	2131	1991	2060	2385	1845	2098
Acc Spec. Intensity (g*sec)	0.509	0.352	0.423	0.372	0.288	0.327
Vel Spectrum Intensity (cm)	214	212	213	295	172	225
Housner Intensity (cm)	197	199	198	282	172	220
Sustained Max.Acc. (g)	0.394	0.288	0.337	0.240	0.256	0.248
Sustained Max.Vel. (cm/sec)	38.1	45.2	41.5	56.2	46.8	51.3
Effective Design Acc. (g)	0.554	0.456	0.502	0.510	0.376	0.438
A95 parameter (g)	0.565	0.483	0.522	0.505	0.354	0.423
Predominant Period (sec)	0.40	0.40	0.40	1.18	0.60	0.84
Significant Duration (sec)	29.4	30.1	29.8	23.6	32.9	27.9

GM: Geometric Mean
SED: Specific Energy Density

1UHRS Scaled Accelerogram	Set Average	Set StdDev
Max Acceleration (g)	0.436	0.061
Max Velocity (cm/sec)	59.2	9.3
Max Displacement (cm)	40.9	11.1
Vmax/Amax (sec)	0.141	0.031
Acceleration RMS (g)	0.066	0.013
Velocity RMS (cm/sec)	12.8	2.7
Displacement RMS (cm)	11.8	2.7
Arias Intensity (cm/sec)	4.29	1.64
Characteristic Intensity	0.133	0.030
SED (cm2/sec)	10154	2953
Cum. Abs. Velocity (cm/sec)	2539	950
Acc Spec. Intensity (g*sec)	0.376	0.033
Vel Spectrum Intensity (cm)	208	16
Housner Intensity (cm)	201	15
Sustained Max.Acc. (g)	0.338	0.044
Sustained Max.Vel. (cm/sec)	46.7	6.0
Effective Design Acc. (g)	0.406	0.046
A95 parameter (g)	0.426	0.062
Predominant Period (sec)	0.34	0.21
Significant Duration (sec)	26.9	10.3

GM: Geometric Mean
SED: Specific Energy Density

1NMSZ Scaled Accelerogram	1527FN	1527FP	GM	1497FN	1497FP	GM
Max Acceleration (g)	0.286	0.274	0.280	0.301	0.237	0.267
Max Velocity (cm/sec)	88.9	115.9	101.5	90.3	107.2	98.4
Max Displacement (cm)	131.0	136.7	133.8	144.6	149.0	146.8
Vmax/Amax (sec)	0.317	0.431	0.370	0.306	0.462	0.376
Acceleration RMS (g)	0.054	0.050	0.052	0.055	0.052	0.053
Velocity RMS (cm/sec)	19.7	27.2	23.1	21.3	26.7	23.8
Displacement RMS (cm)	32.8	32.9	32.9	35.3	32.8	34.0
Arias Intensity (cm/sec)	4.02	3.49	3.74	4.14	3.71	3.92
Characteristic Intensity	0.119	0.107	0.112	0.121	0.112	0.116
SED (cm2/sec)	34800	66428	48080	40848	64130	51182
Cum. Abs. Velocity (cm/sec)	2600	2546	2573	2665	2734	2699
Acc Spec. Intensity (g*sec)	0.310	0.231	0.267	0.272	0.261	0.266
Vel Spectrum Intensity (cm)	217	222	220	242	198	219
Housner Intensity (cm)	218	236	227	245	206	225
Sustained Max.Acc. (g)	0.264	0.221	0.241	0.266	0.221	0.242
Sustained Max.Vel. (cm/sec)	76.4	89.5	82.7	74.8	98.4	85.8
Effective Design Acc. (g)	0.274	0.268	0.271	0.297	0.231	0.262
A95 parameter (g)	0.277	0.268	0.272	0.295	0.230	0.261
Predominant Period (sec)	0.42	0.58	0.49	0.80	0.40	0.57
Significant Duration (sec)	26.4	27.9	27.2	27.4	30.0	28.7

GM: Geometric Mean
SED: Specific Energy Density

1NMSZ Scaled Accelerogram	1189FN	1189FP	GM	1194FN	1194FP	GM
Max Acceleration (g)	0.237	0.282	0.259	0.297	0.285	0.291
Max Velocity (cm/sec)	56.5	101.5	75.7	89.9	70.0	79.3
Max Displacement (cm)	44.1	86.6	61.8	68.2	45.7	55.8
Vmax/Amax (sec)	0.243	0.366	0.298	0.308	0.250	0.278
Acceleration RMS (g)	0.044	0.053	0.048	0.055	0.050	0.053
Velocity RMS (cm/sec)	13.5	25.7	18.6	21.6	16.0	18.6
Displacement RMS (cm)	13.1	24.5	17.9	17.5	13.9	15.6
Arias Intensity (cm/sec)	4.53	6.49	5.42	4.24	3.47	3.83
Characteristic Intensity	0.114	0.149	0.131	0.123	0.106	0.114
SED (cm2/sec)	27417	99078	52120	42017	22993	31082
Cum. Abs. Velocity (cm/sec)	3871	5033	4414	2901	2618	2756
Acc Spec. Intensity (g*sec)	0.224	0.251	0.237	0.243	0.249	0.246
Vel Spectrum Intensity (cm)	209	239	223	245	246	246
Housner Intensity (cm)	215	248	231	258	240	249
Sustained Max.Acc. (g)	0.233	0.238	0.236	0.252	0.232	0.242
Sustained Max.Vel. (cm/sec)	51.9	80.7	64.7	81.8	52.6	65.6
Effective Design Acc. (g)	0.236	0.275	0.255	0.282	0.281	0.281
A95 parameter (g)	0.230	0.269	0.248	0.289	0.278	0.284
Predominant Period (sec)	0.60	0.46	0.53	0.52	0.68	0.59
Significant Duration (sec)	57.6	65.6	61.5	33.6	35.4	34.5

GM: Geometric Mean
SED: Specific Energy Density

1NMSZ Scaled Accelerogram	1800FN	1800FP	GM	2115FN	2115FP	GM
Max Acceleration (g)	0.274	0.333	0.302	0.784	0.680	0.730
Max Velocity (cm/sec)	64.4	120.7	88.1	119.9	102.0	110.6
Max Displacement (cm)	55.7	146.0	90.2	117.3	96.8	106.5
Vmax/Amax (sec)	0.240	0.369	0.298	0.156	0.153	0.154
Acceleration RMS (g)	0.059	0.071	0.065	0.106	0.112	0.109
Velocity RMS (cm/sec)	18.2	42.5	27.8	28.0	22.3	25.0
Displacement RMS (cm)	18.7	51.1	30.9	29.7	27.5	28.6
Arias Intensity (cm/sec)	3.17	4.71	3.86	28.30	31.52	29.87
Characteristic Intensity	0.110	0.148	0.127	0.441	0.479	0.460
SED (cm2/sec)	19829	108298	46341	128469	80981	101998
Cum. Abs. Velocity (cm/sec)	2505	3218	2839	11006	11287	11145
Acc Spec. Intensity (g*sec)	0.237	0.251	0.244	0.564	0.617	0.590
Vel Spectrum Intensity (cm)	231	234	232	221	291	253
Housner Intensity (cm)	232	255	243	221	277	247
Sustained Max.Acc. (g)	0.212	0.253	0.232	0.596	0.661	0.627
Sustained Max.Vel. (cm/sec)	50.2	106.3	73.1	118.9	97.6	107.7
Effective Design Acc. (g)	0.267	0.334	0.299	0.642	0.600	0.621
A95 parameter (g)	0.265	0.324	0.293	0.746	0.654	0.698
Predominant Period (sec)	0.80	0.32	0.51	0.12	0.12	0.12
Significant Duration (sec)	39.3	46.4	42.7	78.5	70.3	74.3

GM: Geometric Mean
SED: Specific Energy Density

1NMSZ Scaled Accelerogram	1605FN	1605FP	GM	1790FN	1790FP	GM
Max Acceleration (g)	0.456	0.663	0.550	0.186	0.292	0.233
Max Velocity (cm/sec)	79.4	101.4	89.7	90.6	119.5	104.1
Max Displacement (cm)	59.3	61.6	60.4	68.3	122.6	91.6
Vmax/Amax (sec)	0.177	0.156	0.166	0.497	0.417	0.455
Acceleration RMS (g)	0.105	0.109	0.107	0.041	0.048	0.044
Velocity RMS (cm/sec)	27.0	27.4	27.2	19.4	28.8	23.7
Displacement RMS (cm)	22.8	19.4	21.0	18.3	34.6	25.2
Arias Intensity (cm/sec)	4.39	4.76	4.57	2.49	3.50	2.95
Characteristic Intensity	0.173	0.184	0.178	0.081	0.105	0.092
SED (cm2/sec)	18859	19438	19146	36936	81374	54824
Cum. Abs. Velocity (cm/sec)	1743	1730	1736	2754	3166	2953
Acc Spec. Intensity (g*sec)	0.558	0.519	0.539	0.198	0.185	0.192
Vel Spectrum Intensity (cm)	233	324	275	174	258	212
Housner Intensity (cm)	244	330	284	190	264	224
Sustained Max.Acc. (g)	0.398	0.458	0.427	0.180	0.210	0.195
Sustained Max.Vel. (cm/sec)	78.2	80.3	79.3	54.6	91.6	70.8
Effective Design Acc. (g)	0.442	0.638	0.531	0.189	0.293	0.235
A95 parameter (g)	0.450	0.658	0.544	0.179	0.285	0.226
Predominant Period (sec)	0.42	0.22	0.30	0.46	1.32	0.78
Significant Duration (sec)	10.9	10.7	10.8	71.7	64.2	67.9

GM: Geometric Mean
SED: Specific Energy Density

1NMSZ Scaled Accelerogram	1799FN	1799FP	GM	SYN27 H1	SYN27 H2	GM
Max Acceleration (g)	0.426	0.420	0.423	0.292	0.331	0.311
Max Velocity (cm/sec)	67.2	104.4	83.8	65.4	76.3	70.6
Max Displacement (cm)	48.6	130.2	79.6	48.2	45.8	47.0
Vmax/Amax (sec)	0.161	0.253	0.202	0.229	0.235	0.232
Acceleration RMS (g)	0.067	0.073	0.070	0.035	0.052	0.042
Velocity RMS (cm/sec)	18.8	33.7	25.2	13.7	18.1	15.7
Displacement RMS (cm)	17.6	38.8	26.1	9.4	13.0	11.1
Arias Intensity (cm/sec)	5.55	6.51	6.01	1.54	3.41	2.29
Characteristic Intensity	0.155	0.175	0.165	0.059	0.107	0.079
SED (cm2/sec)	28144	90996	50606	15304	27331	20451
Cum. Abs. Velocity (cm/sec)	3503	3794	3646	1605	2726	2092
Acc Spec. Intensity (g*sec)	0.418	0.397	0.408	0.191	0.200	0.195
Vel Spectrum Intensity (cm)	268	247	257	193	225	208
Housner Intensity (cm)	264	255	260	214	228	221
Sustained Max.Acc. (g)	0.358	0.399	0.378	0.190	0.230	0.209
Sustained Max.Vel. (cm/sec)	55.0	98.4	73.5	60.4	65.2	62.8
Effective Design Acc. (g)	0.431	0.413	0.422	0.272	0.296	0.284
A95 parameter (g)	0.407	0.404	0.406	0.286	0.320	0.303
Predominant Period (sec)	0.28	0.54	0.39	0.74	1.34	1.00
Significant Duration (sec)	45.0	44.1	44.5	24.4	35.1	29.3

GM: Geometric Mean
SED: Specific Energy Density

1NMSZ Scaled Accelerogram	SYN21 H1	SYN21 H2	GM	SYN24 H1	SYN24 H2	GM
Max Acceleration (g)	0.506	0.490	0.498	0.342	0.442	0.389
Max Velocity (cm/sec)	100.5	89.0	94.6	77.6	101.1	88.6
Max Displacement (cm)	57.0	38.5	46.9	45.3	55.3	50.1
Vmax/Amax (sec)	0.202	0.185	0.194	0.231	0.233	0.232
Acceleration RMS (g)	0.099	0.088	0.093	0.070	0.088	0.078
Velocity RMS (cm/sec)	25.1	20.7	22.8	17.2	22.7	19.8
Displacement RMS (cm)	16.1	11.7	13.7	10.3	13.4	11.8
Arias Intensity (cm/sec)	6.80	5.18	5.93	5.47	8.55	6.84
Characteristic Intensity	0.209	0.172	0.190	0.157	0.221	0.186
SED (cm2/sec)	28184	18741	22983	21731	36831	28291
Cum. Abs. Velocity (cm/sec)	3119	2570	2832	3728	4548	4117
Acc Spec. Intensity (g*sec)	0.440	0.405	0.422	0.293	0.341	0.316
Vel Spectrum Intensity (cm)	243	305	272	241	229	235
Housner Intensity (cm)	262	305	283	248	241	245
Sustained Max.Acc. (g)	0.352	0.431	0.390	0.297	0.340	0.318
Sustained Max.Vel. (cm/sec)	85.3	61.5	72.5	43.4	73.7	56.6
Effective Design Acc. (g)	0.473	0.439	0.456	0.357	0.393	0.375
A95 parameter (g)	0.495	0.476	0.485	0.336	0.425	0.378
Predominant Period (sec)	0.14	0.26	0.19	0.70	0.32	0.47
Significant Duration (sec)	26.6	22.4	24.4	49.8	46.6	48.2

GM: Geometric Mean
SED: Specific Energy Density

1NMSZ Scaled Accelerogram	SYN17 H1	SYN17 H2	GM	SYN22 H1	SYN22 H2	GM
Max Acceleration (g)	0.460	0.371	0.413	0.544	0.585	0.564
Max Velocity (cm/sec)	62.3	94.0	76.5	76.6	85.5	80.9
Max Displacement (cm)	40.5	51.9	45.8	39.1	51.6	44.9
Vmax/Amax (sec)	0.138	0.258	0.189	0.144	0.149	0.146
Acceleration RMS (g)	0.064	0.083	0.073	0.092	0.104	0.098
Velocity RMS (cm/sec)	18.0	23.7	20.6	19.5	22.4	20.9
Displacement RMS (cm)	10.1	16.0	12.7	11.2	12.5	11.8
Arias Intensity (cm/sec)	2.79	4.59	3.58	9.51	12.15	10.75
Characteristic Intensity	0.108	0.157	0.130	0.238	0.287	0.262
SED (cm2/sec)	14068	24432	18540	27699	36112	31627
Cum. Abs. Velocity (cm/sec)	1821	2393	2088	4808	5507	5145
Acc Spec. Intensity (g*sec)	0.281	0.349	0.313	0.453	0.430	0.441
Vel Spectrum Intensity (cm)	249	260	255	244	266	254
Housner Intensity (cm)	253	267	260	239	273	256
Sustained Max.Acc. (g)	0.270	0.357	0.310	0.421	0.431	0.426
Sustained Max.Vel. (cm/sec)	58.7	76.9	67.2	67.6	82.3	74.6
Effective Design Acc. (g)	0.404	0.361	0.382	0.500	0.473	0.486
A95 parameter (g)	0.452	0.361	0.404	0.526	0.562	0.544
Predominant Period (sec)	0.14	0.48	0.26	0.40	0.12	0.22
Significant Duration (sec)	20.5	22.8	21.6	45.9	48.8	47.3

GM: Geometric Mean
SED: Specific Energy Density

1NMSZ Scaled Accelerogram	Set Average	Set StdDev
Max Acceleration (g)	0.394	0.146
Max Velocity (cm/sec)	88.7	11.8
Max Displacement (cm)	75.8	33.8
Vmax/Amax (sec)	0.256	0.094
Acceleration RMS (g)	0.070	0.023
Velocity RMS (cm/sec)	22.3	3.5
Displacement RMS (cm)	20.9	8.5
Arias Intensity (cm/sec)	6.68	7.00
Characteristic Intensity	0.167	0.097
SED (cm2/sec)	41234	22164
Cum. Abs. Velocity (cm/sec)	3645	2360
Acc Spec. Intensity (g*sec)	0.334	0.126
Vel Spectrum Intensity (cm)	240	22
Housner Intensity (cm)	247	20
Sustained Max.Acc. (g)	0.320	0.120
Sustained Max.Vel. (cm/sec)	74.1	12.5
Effective Design Acc. (g)	0.369	0.120
A95 parameter (g)	0.382	0.141
Predominant Period (sec)	0.46	0.24
Significant Duration (sec)	40.2	18.5

GM: Geometric Mean
SED: Specific Energy Density

1NMSZB Scaled Accelerogram	0851FN	0851FP	GM	1151FN	1151FP	GM
Max Acceleration (g)	0.324	0.356	0.340	0.321	0.467	0.387
Max Velocity (cm/sec)	77.6	124.7	98.4	91.5	127.3	107.9
Max Displacement (cm)	105.3	166.4	132.4	154.6	211.1	180.6
Vmax/Amax (sec)	0.244	0.356	0.295	0.291	0.278	0.284
Acceleration RMS (g)	0.067	0.078	0.072	0.046	0.054	0.050
Velocity RMS (cm/sec)	27.5	45.1	35.2	19.3	25.0	21.9
Displacement RMS (cm)	36.9	70.6	51.0	33.5	44.6	38.6
Arias Intensity (cm/sec)	4.78	6.58	5.61	4.00	5.69	4.77
Characteristic Intensity	0.144	0.183	0.162	0.109	0.142	0.124
SED (cm2/sec)	52811	142590	86777	46314	77450	59892
Cum. Abs. Velocity (cm/sec)	3345	3934	3628	3371	3492	3431
Acc Spec. Intensity (g*sec)	0.319	0.405	0.360	0.280	0.453	0.356
Vel Spectrum Intensity (cm)	210	266	236	186	293	234
Housner Intensity (cm)	212	270	239	189	307	241
Sustained Max.Acc. (g)	0.286	0.312	0.298	0.240	0.381	0.303
Sustained Max.Vel. (cm/sec)	65.1	108.1	83.9	85.4	123.3	102.6
Effective Design Acc. (g)	0.339	0.352	0.345	0.324	0.474	0.392
A95 parameter (g)	0.311	0.335	0.323	0.307	0.456	0.374
Predominant Period (sec)	0.18	0.42	0.27	0.68	0.36	0.49
Significant Duration (sec)	47.3	53.8	50.5	55.6	33.6	43.2

GM: Geometric Mean
SED: Specific Energy Density

1NMSZB Scaled Accelerogram	1175FN	1175FP	GM	1176FN	1176FP	GM
Max Acceleration (g)	0.451	0.392	0.421	0.386	0.544	0.458
Max Velocity (cm/sec)	110.0	160.2	132.8	80.1	157.3	112.3
Max Displacement (cm)	194.9	332.6	254.6	110.8	283.5	177.3
Vmax/Amax (sec)	0.249	0.416	0.322	0.212	0.295	0.250
Acceleration RMS (g)	0.064	0.046	0.054	0.071	0.070	0.070
Velocity RMS (cm/sec)	24.8	29.4	27.0	29.7	50.6	38.8
Displacement RMS (cm)	54.3	84.8	67.9	41.6	115.4	69.3
Arias Intensity (cm/sec)	8.21	4.20	5.88	2.72	2.63	2.67
Characteristic Intensity	0.185	0.112	0.144	0.112	0.109	0.110
SED (cm2/sec)	80051	112275	94804	30873	89741	52636
Cum. Abs. Velocity (cm/sec)	4754	3549	4107	1556	1498	1526
Acc Spec. Intensity (g*sec)	0.459	0.278	0.357	0.369	0.336	0.352
Vel Spectrum Intensity (cm)	312	192	245	241	224	232
Housner Intensity (cm)	313	188	243	250	233	241
Sustained Max.Acc. (g)	0.376	0.233	0.296	0.289	0.280	0.284
Sustained Max.Vel. (cm/sec)	99.3	150.2	122.1	71.7	130.7	96.8
Effective Design Acc. (g)	0.452	0.390	0.420	0.395	0.530	0.457
A95 parameter (g)	0.441	0.379	0.409	0.381	0.540	0.454
Predominant Period (sec)	0.22	0.48	0.32	0.42	0.54	0.48
Significant Duration (sec)	47.9	55.8	51.7	17.7	16.8	17.2

GM: Geometric Mean
SED: Specific Energy Density

1NMSZB Scaled Accelerogram	1189FN	1189FP	GM	1194FN	1194FP	GM
Max Acceleration (g)	0.326	0.355	0.340	0.298	0.312	0.305
Max Velocity (cm/sec)	75.2	69.6	72.4	87.4	62.0	73.6
Max Displacement (cm)	52.8	74.1	62.5	64.0	61.5	62.7
Vmax/Amax (sec)	0.235	0.200	0.217	0.299	0.203	0.246
Acceleration RMS (g)	0.050	0.052	0.051	0.055	0.057	0.056
Velocity RMS (cm/sec)	17.2	21.2	19.1	19.0	20.0	19.5
Displacement RMS (cm)	16.0	21.9	18.7	20.8	18.0	19.4
Arias Intensity (cm/sec)	5.70	6.25	5.97	4.27	4.44	4.35
Characteristic Intensity	0.136	0.145	0.140	0.124	0.128	0.126
SED (cm2/sec)	44548	67303	54756	32529	36154	34294
Cum. Abs. Velocity (cm/sec)	4323	4803	4557	2938	3093	3015
Acc Spec. Intensity (g*sec)	0.340	0.371	0.355	0.326	0.361	0.343
Vel Spectrum Intensity (cm)	231	246	238	233	246	239
Housner Intensity (cm)	240	248	244	235	245	240
Sustained Max.Acc. (g)	0.271	0.334	0.301	0.290	0.284	0.287
Sustained Max.Vel. (cm/sec)	64.5	66.0	65.3	62.4	59.3	60.8
Effective Design Acc. (g)	0.311	0.352	0.331	0.287	0.309	0.298
A95 parameter (g)	0.309	0.345	0.326	0.290	0.305	0.297
Predominant Period (sec)	0.24	0.46	0.33	0.44	0.44	0.44
Significant Duration (sec)	58.1	67.1	62.4	33.5	44.6	38.6

GM: Geometric Mean
SED: Specific Energy Density

1NMSZB Scaled Accelerogram	1217FN	1217FP	GM	1242FN	1242FP	GM
Max Acceleration (g)	0.310	0.286	0.298	0.327	0.379	0.352
Max Velocity (cm/sec)	89.6	76.6	82.9	56.4	75.3	65.2
Max Displacement (cm)	161.0	69.8	106.0	60.2	76.3	67.7
Vmax/Amax (sec)	0.294	0.273	0.284	0.176	0.203	0.189
Acceleration RMS (g)	0.065	0.057	0.061	0.038	0.048	0.043
Velocity RMS (cm/sec)	27.2	21.2	24.0	12.6	18.6	15.3
Displacement RMS (cm)	44.4	26.4	34.2	13.4	17.1	15.2
Arias Intensity (cm/sec)	5.88	4.43	5.10	4.35	7.15	5.58
Characteristic Intensity	0.158	0.127	0.142	0.103	0.150	0.124
SED (cm2/sec)	66481	40638	51978	31860	69219	46961
Cum. Abs. Velocity (cm/sec)	3794	3244	3508	4182	5283	4700
Acc Spec. Intensity (g*sec)	0.383	0.330	0.355	0.316	0.414	0.361
Vel Spectrum Intensity (cm)	253	219	236	206	272	236
Housner Intensity (cm)	257	223	239	209	275	239
Sustained Max.Acc. (g)	0.287	0.255	0.270	0.251	0.313	0.280
Sustained Max.Vel. (cm/sec)	88.4	67.3	77.2	51.1	73.6	61.3
Effective Design Acc. (g)	0.305	0.299	0.302	0.345	0.402	0.372
A95 parameter (g)	0.303	0.279	0.291	0.318	0.364	0.340
Predominant Period (sec)	0.24	0.42	0.32	0.20	0.48	0.31
Significant Duration (sec)	48.7	49.8	49.2	67.0	67.6	67.3

GM: Geometric Mean
SED: Specific Energy Density

1NMSZB Scaled Accelerogram	1310FN	1310FP	GM	1311FN	1311FP	GM
Max Acceleration (g)	0.341	0.470	0.400	0.445	0.262	0.341
Max Velocity (cm/sec)	72.6	73.5	73.0	87.1	82.2	84.6
Max Displacement (cm)	48.2	105.1	71.2	75.3	66.5	70.8
Vmax/Amax (sec)	0.217	0.159	0.186	0.199	0.320	0.253
Acceleration RMS (g)	0.039	0.045	0.042	0.042	0.035	0.038
Velocity RMS (cm/sec)	15.8	20.7	18.1	16.3	11.8	13.9
Displacement RMS (cm)	13.2	25.0	18.1	16.6	10.6	13.2
Arias Intensity (cm/sec)	3.20	4.22	3.67	4.57	3.20	3.83
Characteristic Intensity	0.090	0.111	0.100	0.111	0.085	0.097
SED (cm2/sec)	33556	57740	44018	45455	23923	32976
Cum. Abs. Velocity (cm/sec)	3033	3617	3312	3682	3031	3340
Acc Spec. Intensity (g*sec)	0.323	0.361	0.342	0.411	0.311	0.358
Vel Spectrum Intensity (cm)	221	243	232	282	203	240
Housner Intensity (cm)	228	250	239	277	207	240
Sustained Max.Acc. (g)	0.236	0.269	0.252	0.316	0.241	0.276
Sustained Max.Vel. (cm/sec)	47.6	63.6	55.0	63.8	59.1	61.4
Effective Design Acc. (g)	0.354	0.465	0.406	0.458	0.267	0.349
A95 parameter (g)	0.333	0.459	0.391	0.438	0.253	0.333
Predominant Period (sec)	0.32	0.28	0.30	0.38	0.16	0.25
Significant Duration (sec)	57.3	63.0	60.1	54.1	42.8	48.1

GM: Geometric Mean
SED: Specific Energy Density

1NMSZB Scaled Accelerogram	2095FN	2095FP	GM	2102FN	2102FP	GM
Max Acceleration (g)	0.432	0.354	0.391	0.363	0.301	0.331
Max Velocity (cm/sec)	86.8	66.4	75.9	68.6	86.6	77.1
Max Displacement (cm)	211.3	114.3	155.4	92.2	86.8	89.5
Vmax/Amax (sec)	0.205	0.191	0.198	0.193	0.293	0.238
Acceleration RMS (g)	0.062	0.052	0.057	0.062	0.059	0.060
Velocity RMS (cm/sec)	24.6	19.5	21.9	22.9	21.7	22.3
Displacement RMS (cm)	58.2	33.4	44.0	28.0	27.0	27.5
Arias Intensity (cm/sec)	10.24	7.13	8.55	9.72	8.68	9.18
Characteristic Intensity	0.203	0.155	0.177	0.198	0.182	0.190
SED (cm2/sec)	104377	65259	82532	85468	77019	81134
Cum. Abs. Velocity (cm/sec)	7824	6479	7120	7473	6828	7143
Acc Spec. Intensity (g*sec)	0.364	0.331	0.347	0.342	0.360	0.351
Vel Spectrum Intensity (cm)	261	228	244	241	241	241
Housner Intensity (cm)	258	226	241	243	245	244
Sustained Max.Acc. (g)	0.271	0.237	0.254	0.270	0.300	0.285
Sustained Max.Vel. (cm/sec)	66.2	57.0	61.5	64.3	74.7	69.3
Effective Design Acc. (g)	0.441	0.366	0.402	0.369	0.303	0.334
A95 parameter (g)	0.413	0.337	0.373	0.351	0.294	0.322
Predominant Period (sec)	0.36	0.42	0.39	0.24	0.50	0.35
Significant Duration (sec)	119.4	119.0	119.2	117.1	108.7	112.8

GM: Geometric Mean
SED: Specific Energy Density

1NMSZB Scaled Accelerogram	2109FN	2109FP	GM	CALE EW	CALE NS	GM
Max Acceleration (g)	0.457	0.600	0.523	0.513	0.383	0.443
Max Velocity (cm/sec)	75.5	106.2	89.6	92.6	85.3	88.9
Max Displacement (cm)	120.4	128.2	124.2	99.0	92.0	95.4
Vmax/Amax (sec)	0.169	0.181	0.174	0.184	0.227	0.204
Acceleration RMS (g)	0.068	0.081	0.075	0.102	0.079	0.090
Velocity RMS (cm/sec)	14.2	12.9	13.5	27.5	24.0	25.7
Displacement RMS (cm)	24.7	22.0	23.3	33.0	32.8	32.9
Arias Intensity (cm/sec)	21.59	30.70	25.75	8.15	4.86	6.29
Characteristic Intensity	0.309	0.403	0.353	0.232	0.158	0.192
SED (cm2/sec)	60444	49940	54942	38303	29166	33424
Cum. Abs. Velocity (cm/sec)	11963	14482	13162	3413	2757	3068
Acc Spec. Intensity (g*sec)	0.400	0.459	0.429	0.465	0.289	0.367
Vel Spectrum Intensity (cm)	239	269	253	310	188	241
Housner Intensity (cm)	229	256	242	309	189	241
Sustained Max.Acc. (g)	0.440	0.549	0.492	0.415	0.334	0.372
Sustained Max.Vel. (cm/sec)	71.4	86.7	78.7	87.7	72.3	79.6
Effective Design Acc. (g)	0.450	0.550	0.497	0.435	0.352	0.391
A95 parameter (g)	0.435	0.554	0.491	0.496	0.370	0.429
Predominant Period (sec)	0.12	0.14	0.13	0.08	0.12	0.10
Significant Duration (sec)	136.4	133.9	135.1	24.2	28.5	26.3

GM: Geometric Mean
SED: Specific Energy Density

1NMSZB Scaled Accelerogram	Set Average	Set StdDev
Max Acceleration (g)	0.381	0.064
Max Velocity (cm/sec)	88.2	18.8
Max Displacement (cm)	117.9	57.0
Vmax/Amax (sec)	0.239	0.046
Acceleration RMS (g)	0.058	0.014
Velocity RMS (cm/sec)	22.6	7.4
Displacement RMS (cm)	33.8	18.5
Arias Intensity (cm/sec)	6.94	5.69
Characteristic Intensity	0.156	0.064
SED (cm2/sec)	57937	20602
Cum. Abs. Velocity (cm/sec)	4687	2873
Acc Spec. Intensity (g*sec)	0.360	0.021
Vel Spectrum Intensity (cm)	239	6
Housner Intensity (cm)	241	2
Sustained Max.Acc. (g)	0.304	0.061
Sustained Max.Vel. (cm/sec)	76.8	19.2
Effective Design Acc. (g)	0.378	0.057
A95 parameter (g)	0.368	0.060
Predominant Period (sec)	0.32	0.11
Significant Duration (sec)	63.0	35.1

GM: Geometric Mean
SED: Specific Energy Density

2UHRS Scaled Accelerogram	1521FN	1521FP	GM	0880FN	0880FP	GM
Max Acceleration (g)	0.913	0.667	0.780	0.925	0.956	0.940
Max Velocity (cm/sec)	84.1	84.4	84.3	175.1	52.1	95.5
Max Displacement (cm)	50.6	87.6	66.6	183.8	18.8	58.8
Vmax/Amax (sec)	0.094	0.129	0.110	0.193	0.056	0.104
Acceleration RMS (g)	0.135	0.097	0.114	0.121	0.138	0.129
Velocity RMS (cm/sec)	17.5	14.8	16.1	37.9	13.1	22.3
Displacement RMS (cm)	13.0	17.7	15.1	59.0	6.8	20.0
Arias Intensity (cm/sec)	22.25	11.41	15.93	15.85	20.64	18.09
Characteristic Intensity	0.442	0.268	0.344	0.353	0.430	0.390
SED (cm2/sec)	24142	17404	20498	100724	11939	34678
Cum. Abs. Velocity (cm/sec)	5300	3927	4562	5462	6313	5872
Acc Spec. Intensity (g*sec)	0.961	0.693	0.816	0.655	0.783	0.716
Vel Spectrum Intensity (cm)	375	271	319	393	278	330
Housner Intensity (cm)	354	258	302	402	255	320
Sustained Max.Acc. (g)	0.751	0.541	0.637	0.669	0.719	0.694
Sustained Max.Vel. (cm/sec)	79.6	72.6	76.0	123.1	46.9	76.0
Effective Design Acc. (g)	0.929	0.676	0.792	0.673	0.816	0.741
A95 parameter (g)	0.897	0.655	0.767	0.894	0.934	0.914
Predominant Period (sec)	0.34	0.24	0.29	0.28	0.18	0.22
Significant Duration (sec)	24.1	24.9	24.5	40.2	34.7	37.3

GM: Geometric Mean
SED: Specific Energy Density

2UHRS Scaled Accelerogram	0761FN	0761FP	GM	0762FN	0762FP	GM
Max Acceleration (g)	0.799	1.232	0.992	1.056	0.995	1.025
Max Velocity (cm/sec)	69.3	104.6	85.1	69.4	99.5	83.1
Max Displacement (cm)	35.4	42.8	38.9	33.5	34.6	34.0
Vmax/Amax (sec)	0.088	0.087	0.087	0.067	0.102	0.083
Acceleration RMS (g)	0.130	0.154	0.142	0.135	0.165	0.149
Velocity RMS (cm/sec)	18.9	19.7	19.3	20.8	17.3	19.0
Displacement RMS (cm)	13.4	15.1	14.2	12.4	10.8	11.6
Arias Intensity (cm/sec)	10.38	14.58	12.30	11.14	16.72	13.65
Characteristic Intensity	0.296	0.382	0.336	0.312	0.423	0.363
SED (cm2/sec)	14269	15403	14825	17354	11910	14377
Cum. Abs. Velocity (cm/sec)	3181	3661	3412	3413	3960	3676
Acc Spec. Intensity (g*sec)	0.780	0.952	0.862	0.766	0.938	0.847
Vel Spectrum Intensity (cm)	260	370	310	305	350	327
Housner Intensity (cm)	250	341	292	292	307	299
Sustained Max.Acc. (g)	0.658	0.778	0.715	0.609	0.812	0.703
Sustained Max.Vel. (cm/sec)	52.2	59.8	55.9	63.5	54.8	59.0
Effective Design Acc. (g)	0.773	1.237	0.978	1.003	0.859	0.928
A95 parameter (g)	0.785	1.223	0.980	1.048	0.972	1.009
Predominant Period (sec)	0.28	0.20	0.24	0.20	0.18	0.19
Significant Duration (sec)	17.9	17.4	17.6	18.3	16.4	17.3

GM: Geometric Mean
SED: Specific Energy Density

2UHRS Scaled Accelerogram	2107FN	2107FP	GM	0143FN	0143FP	GM
Max Acceleration (g)	0.968	1.086	1.025	0.729	0.732	0.730
Max Velocity (cm/sec)	113.4	82.8	96.9	106.8	71.8	87.6
Max Displacement (cm)	58.8	40.6	48.9	87.6	36.9	56.9
Vmax/Amax (sec)	0.119	0.078	0.096	0.149	0.100	0.122
Acceleration RMS (g)	0.127	0.117	0.122	0.142	0.130	0.136
Velocity RMS (cm/sec)	17.9	12.9	15.2	29.8	17.7	23.0
Displacement RMS (cm)	15.9	9.6	12.4	24.3	12.7	17.5
Arias Intensity (cm/sec)	21.47	18.24	19.79	10.25	8.57	9.37
Characteristic Intensity	0.421	0.373	0.396	0.308	0.269	0.288
SED (cm2/sec)	27543	14321	19860	29133	10259	17288
Cum. Abs. Velocity (cm/sec)	5436	5260	5347	2867	2640	2751
Acc Spec. Intensity (g*sec)	0.779	0.814	0.796	0.882	0.665	0.766
Vel Spectrum Intensity (cm)	473	239	336	293	285	289
Housner Intensity (cm)	434	218	307	290	274	282
Sustained Max.Acc. (g)	0.793	0.819	0.806	0.566	0.627	0.596
Sustained Max.Vel. (cm/sec)	108.9	61.1	81.5	87.4	68.5	77.4
Effective Design Acc. (g)	0.895	0.768	0.829	0.801	0.738	0.769
A95 parameter (g)	0.941	1.056	0.997	0.705	0.712	0.708
Predominant Period (sec)	0.16	0.18	0.17	0.24	0.24	0.24
Significant Duration (sec)	19.7	24.7	22.0	16.9	15.8	16.4

GM: Geometric Mean
SED: Specific Energy Density

2UHRS Scaled Accelerogram	1153FN	1153FP	GM	0836FN	0836FP	GM
Max Acceleration (g)	0.981	0.843	0.909	0.924	0.852	0.887
Max Velocity (cm/sec)	93.4	116.7	104.4	73.6	90.8	81.7
Max Displacement (cm)	44.1	146.2	80.3	49.5	68.7	58.3
Vmax/Amax (sec)	0.097	0.141	0.117	0.081	0.109	0.094
Acceleration RMS (g)	0.078	0.072	0.075	0.147	0.153	0.150
Velocity RMS (cm/sec)	12.7	20.2	16.1	20.7	24.5	22.5
Displacement RMS (cm)	14.0	40.3	23.8	15.6	22.3	18.7
Arias Intensity (cm/sec)	9.49	8.07	8.75	16.59	18.06	17.31
Characteristic Intensity	0.219	0.194	0.206	0.398	0.424	0.410
SED (cm2/sec)	16516	41628	26220	21495	29887	25346
Cum. Abs. Velocity (cm/sec)	3673	3433	3551	4775	4781	4778
Acc Spec. Intensity (g*sec)	0.878	0.607	0.730	0.824	0.865	0.844
Vel Spectrum Intensity (cm)	369	365	367	314	377	344
Housner Intensity (cm)	339	343	341	306	373	338
Sustained Max.Acc. (g)	0.679	0.496	0.580	0.645	0.648	0.647
Sustained Max.Vel. (cm/sec)	65.8	77.9	71.6	61.9	76.7	68.9
Effective Design Acc. (g)	0.955	0.786	0.866	0.783	0.741	0.762
A95 parameter (g)	0.973	0.832	0.900	0.893	0.815	0.853
Predominant Period (sec)	0.40	0.40	0.40	0.22	0.44	0.31
Significant Duration (sec)	29.4	30.1	29.8	26.9	19.3	22.8

GM: Geometric Mean
SED: Specific Energy Density

2UHRS Scaled Accelerogram	0855FN	0855FP	GM	0807FN	0807FP	GM
Max Acceleration (g)	0.880	1.242	1.045	0.725	0.873	0.796
Max Velocity (cm/sec)	93.9	97.8	95.8	69.8	77.2	73.4
Max Displacement (cm)	129.4	113.3	121.1	49.6	55.8	52.6
Vmax/Amax (sec)	0.109	0.080	0.093	0.098	0.090	0.094
Acceleration RMS (g)	0.144	0.150	0.147	0.132	0.135	0.133
Velocity RMS (cm/sec)	32.8	30.4	31.6	26.1	23.9	25.0
Displacement RMS (cm)	45.7	42.1	43.9	18.0	20.6	19.3
Arias Intensity (cm/sec)	12.75	13.81	13.27	10.43	11.02	10.72
Characteristic Intensity	0.345	0.366	0.355	0.298	0.311	0.305
SED (cm2/sec)	43072	36995	39918	26607	22304	24361
Cum. Abs. Velocity (cm/sec)	3459	3362	3410	3441	3290	3365
Acc Spec. Intensity (g*sec)	0.861	1.012	0.934	0.686	0.900	0.786
Vel Spectrum Intensity (cm)	276	381	324	276	272	274
Housner Intensity (cm)	260	330	293	274	259	266
Sustained Max.Acc. (g)	0.612	0.820	0.708	0.554	0.638	0.594
Sustained Max.Vel. (cm/sec)	91.4	93.8	92.6	68.7	70.4	69.5
Effective Design Acc. (g)	0.754	1.156	0.933	0.692	0.881	0.781
A95 parameter (g)	0.856	1.226	1.024	0.708	0.858	0.779
Predominant Period (sec)	0.18	0.28	0.22	0.20	0.30	0.24
Significant Duration (sec)	14.1	13.1	13.6	21.3	17.2	19.1

GM: Geometric Mean
SED: Specific Energy Density

2UHRS Scaled Accelerogram	2111FN	2111FP	GM	1507FN	1507FP	GM
Max Acceleration (g)	1.209	0.655	0.890	0.859	1.005	0.929
Max Velocity (cm/sec)	144.4	62.9	95.3	68.2	106.3	85.1
Max Displacement (cm)	48.5	38.3	43.1	22.5	74.1	40.8
Vmax/Amax (sec)	0.122	0.098	0.109	0.081	0.108	0.093
Acceleration RMS (g)	0.110	0.091	0.100	0.124	0.126	0.125
Velocity RMS (cm/sec)	18.8	14.2	16.4	12.6	15.4	13.9
Displacement RMS (cm)	11.4	10.0	10.7	4.4	24.2	10.4
Arias Intensity (cm/sec)	13.56	9.40	11.29	21.49	22.00	21.74
Characteristic Intensity	0.311	0.236	0.271	0.417	0.424	0.420
SED (cm2/sec)	25919	14716	19530	14221	21389	17440
Cum. Abs. Velocity (cm/sec)	3916	3629	3770	5404	5188	5295
Acc Spec. Intensity (g*sec)	0.829	0.626	0.720	0.875	0.938	0.906
Vel Spectrum Intensity (cm)	552	271	387	362	306	333
Housner Intensity (cm)	560	260	381	324	268	295
Sustained Max.Acc. (g)	0.723	0.510	0.607	0.789	0.869	0.828
Sustained Max.Vel. (cm/sec)	63.2	61.2	62.2	58.8	71.4	64.8
Effective Design Acc. (g)	1.176	0.663	0.883	0.864	1.002	0.930
A95 parameter (g)	1.187	0.644	0.874	0.840	0.982	0.908
Predominant Period (sec)	0.40	0.22	0.30	0.26	0.26	0.26
Significant Duration (sec)	18.8	23.7	21.1	24.6	23.7	24.2

GM: Geometric Mean
SED: Specific Energy Density

2UHRS Scaled Accelerogram	0882FN	0882FP	GM	1149FN	1149FP	GM
Max Acceleration (g)	0.716	0.741	0.729	0.701	1.104	0.880
Max Velocity (cm/sec)	78.8	62.0	69.9	148.1	107.5	126.2
Max Displacement (cm)	30.5	28.1	29.2	157.4	76.8	110.0
Vmax/Amax (sec)	0.112	0.085	0.098	0.215	0.099	0.146
Acceleration RMS (g)	0.138	0.134	0.136	0.071	0.078	0.075
Velocity RMS (cm/sec)	22.2	16.7	19.2	18.9	13.1	15.7
Displacement RMS (cm)	10.7	7.9	9.2	26.9	17.5	21.7
Arias Intensity (cm/sec)	20.61	19.37	19.98	10.47	12.60	11.49
Characteristic Intensity	0.430	0.410	0.420	0.220	0.253	0.236
SED (cm2/sec)	34539	19466	25930	47664	22788	32957
Cum. Abs. Velocity (cm/sec)	6352	6181	6266	4548	4677	4612
Acc Spec. Intensity (g*sec)	0.650	0.713	0.681	0.541	0.970	0.724
Vel Spectrum Intensity (cm)	424	358	389	386	369	377
Housner Intensity (cm)	430	345	385	362	330	346
Sustained Max.Acc. (g)	0.545	0.628	0.585	0.575	0.754	0.659
Sustained Max.Vel. (cm/sec)	70.6	59.7	64.9	106.3	87.0	96.1
Effective Design Acc. (g)	0.688	0.687	0.688	0.696	1.138	0.890
A95 parameter (g)	0.696	0.721	0.708	0.692	1.096	0.871
Predominant Period (sec)	0.24	0.24	0.24	0.92	0.30	0.53
Significant Duration (sec)	37.0	36.3	36.7	35.9	31.7	33.8

GM: Geometric Mean
SED: Specific Energy Density

2UHRS Scaled Accelerogram	Set Average	Set StdDev
Max Acceleration (g)	0.897	0.106
Max Velocity (cm/sec)	90.3	14.0
Max Displacement (cm)	60.0	27.2
Vmax/Amax (sec)	0.103	0.017
Acceleration RMS (g)	0.124	0.025
Velocity RMS (cm/sec)	19.7	4.8
Displacement RMS (cm)	17.7	8.8
Arias Intensity (cm/sec)	14.55	4.24
Characteristic Intensity	0.339	0.069
SED (cm2/sec)	23802	7706
Cum. Abs. Velocity (cm/sec)	4333	1070
Acc Spec. Intensity (g*sec)	0.795	0.077
Vel Spectrum Intensity (cm)	336	34
Housner Intensity (cm)	318	36
Sustained Max.Acc. (g)	0.668	0.079
Sustained Max.Vel. (cm/sec)	72.6	11.8
Effective Design Acc. (g)	0.841	0.087
A95 parameter (g)	0.878	0.106
Predominant Period (sec)	0.27	0.09
Significant Duration (sec)	24.0	7.6

GM: Geometric Mean
SED: Specific Energy Density

2UHRS-P Scaled Accelerogram	1148FN	1148FP	GM	0779FN	0779FP	GM
Max Acceleration (g)	1.233	0.864	1.032	1.123	0.639	0.847
Max Velocity (cm/sec)	114.4	218.8	158.2	115.3	85.8	99.5
Max Displacement (cm)	90.1	196.6	133.1	74.4	36.3	52.0
Vmax/Amax (sec)	0.095	0.258	0.156	0.105	0.137	0.120
Acceleration RMS (g)	0.141	0.124	0.132	0.174	0.112	0.139
Velocity RMS (cm/sec)	25.8	56.8	38.3	32.0	19.6	25.0
Displacement RMS (cm)	34.9	71.6	50.0	22.0	13.2	17.0
Arias Intensity (cm/sec)	9.16	7.13	8.09	11.67	4.81	7.50
Characteristic Intensity	0.289	0.240	0.263	0.363	0.187	0.260
SED (cm2/sec)	20022	96808	44026	25647	9586	15680
Cum. Abs. Velocity (cm/sec)	2304	1998	2146	2524	1683	2061
Acc Spec. Intensity (g*sec)	0.754	0.683	0.718	0.726	0.470	0.584
Vel Spectrum Intensity (cm)	234	281	257	484	295	378
Housner Intensity (cm)	211	299	251	458	284	361
Sustained Max.Acc. (g)	0.698	0.660	0.679	0.934	0.523	0.699
Sustained Max.Vel. (cm/sec)	86.6	170.9	121.6	110.4	70.4	88.2
Effective Design Acc. (g)	1.186	0.805	0.977	0.679	0.606	0.641
A95 parameter (g)	1.224	0.853	1.022	1.103	0.627	0.832
Predominant Period (sec)	0.16	0.26	0.20	0.74	0.66	0.70
Significant Duration (sec)	11.0	10.3	10.6	10.0	10.9	10.4

GM: Geometric Mean
SED: Specific Energy Density

2UHRS-P Scaled Accelerogram	0825FN	0825FP	GM	0292FN	0292FP	GM
Max Acceleration (g)	1.824	2.057	1.937	0.521	0.686	0.598
Max Velocity (cm/sec)	82.8	170.0	118.7	93.0	102.1	97.4
Max Displacement (cm)	19.8	54.8	33.0	49.7	52.6	51.1
Vmax/Amax (sec)	0.046	0.084	0.062	0.182	0.152	0.166
Acceleration RMS (g)	0.114	0.156	0.133	0.091	0.116	0.103
Velocity RMS (cm/sec)	11.9	18.4	14.8	20.2	21.5	20.8
Displacement RMS (cm)	7.6	14.8	10.6	12.2	11.3	11.7
Arias Intensity (cm/sec)	6.00	11.24	8.21	5.02	8.12	6.38
Characteristic Intensity	0.211	0.337	0.266	0.172	0.247	0.206
SED (cm2/sec)	4269	10156	6585	16009	18110	17027
Cum. Abs. Velocity (cm/sec)	1531	1993	1747	2167	2475	2316
Acc Spec. Intensity (g*sec)	0.811	1.271	1.015	0.508	0.804	0.640
Vel Spectrum Intensity (cm)	266	366	312	297	413	350
Housner Intensity (cm)	230	311	267	302	434	362
Sustained Max.Acc. (g)	0.443	0.586	0.510	0.487	0.649	0.563
Sustained Max.Vel. (cm/sec)	31.4	53.6	41.0	76.4	93.4	84.5
Effective Design Acc. (g)	1.322	2.181	1.698	0.521	0.728	0.616
A95 parameter (g)	1.819	2.052	1.932	0.517	0.678	0.592
Predominant Period (sec)	0.14	0.26	0.19	0.20	0.32	0.25
Significant Duration (sec)	6.9	6.5	6.7	16.6	12.1	14.2

GM: Geometric Mean
SED: Specific Energy Density

2UHRS-P Scaled Accelerogram	0803FN	0803FP	GM	0767FN	0767FP	GM
Max Acceleration (g)	0.928	0.591	0.740	1.195	1.023	1.106
Max Velocity (cm/sec)	164.2	138.2	150.7	110.6	83.1	95.8
Max Displacement (cm)	47.9	68.6	57.4	24.6	37.6	30.4
Vmax/Amax (sec)	0.180	0.239	0.207	0.094	0.083	0.088
Acceleration RMS (g)	0.111	0.087	0.098	0.124	0.113	0.118
Velocity RMS (cm/sec)	23.8	22.3	23.0	13.1	13.3	13.2
Displacement RMS (cm)	14.9	17.5	16.1	5.0	6.8	5.9
Arias Intensity (cm/sec)	7.65	4.64	5.96	9.45	7.81	8.59
Characteristic Intensity	0.235	0.162	0.195	0.276	0.239	0.257
SED (cm2/sec)	22670	19798	21186	6843	7032	6937
Cum. Abs. Velocity (cm/sec)	2282	1824	2040	2233	2105	2168
Acc Spec. Intensity (g*sec)	0.608	0.545	0.576	1.031	0.988	1.009
Vel Spectrum Intensity (cm)	478	326	395	373	325	348
Housner Intensity (cm)	454	332	388	321	306	313
Sustained Max.Acc. (g)	0.546	0.485	0.514	0.712	0.707	0.710
Sustained Max.Vel. (cm/sec)	62.5	67.0	64.7	42.0	76.1	56.5
Effective Design Acc. (g)	0.939	0.583	0.740	1.182	1.021	1.099
A95 parameter (g)	0.921	0.583	0.733	1.186	1.010	1.095
Predominant Period (sec)	0.32	0.36	0.34	0.22	0.20	0.21
Significant Duration (sec)	11.0	12.4	11.7	7.7	8.9	8.3

GM: Geometric Mean
SED: Specific Energy Density

2UHRS-P Scaled Accelerogram	0828FN	0828FP	GM	1528FN	1528FP	GM
Max Acceleration (g)	1.020	1.044	1.032	0.617	0.676	0.646
Max Velocity (cm/sec)	135.8	100.2	116.7	194.2	150.4	170.9
Max Displacement (cm)	42.3	43.2	42.7	204.3	118.2	155.4
Vmax/Amax (sec)	0.136	0.098	0.115	0.321	0.227	0.270
Acceleration RMS (g)	0.135	0.133	0.134	0.107	0.098	0.103
Velocity RMS (cm/sec)	18.8	15.0	16.8	38.0	35.4	36.6
Displacement RMS (cm)	9.6	7.7	8.6	53.1	39.4	45.8
Arias Intensity (cm/sec)	10.09	9.82	9.95	8.69	7.29	7.96
Characteristic Intensity	0.297	0.291	0.294	0.246	0.216	0.230
SED (cm2/sec)	12682	8094	10132	70643	61288	65799
Cum. Abs. Velocity (cm/sec)	2465	2482	2473	3086	2952	3018
Acc Spec. Intensity (g*sec)	0.692	0.638	0.664	0.637	0.465	0.544
Vel Spectrum Intensity (cm)	501	376	434	353	316	334
Housner Intensity (cm)	449	314	375	359	307	332
Sustained Max.Acc. (g)	0.395	0.772	0.552	0.602	0.468	0.530
Sustained Max.Vel. (cm/sec)	40.6	45.8	43.1	108.4	110.6	109.5
Effective Design Acc. (g)	0.949	0.989	0.969	0.596	0.594	0.595
A95 parameter (g)	1.007	1.037	1.022	0.600	0.661	0.630
Predominant Period (sec)	0.66	0.64	0.65	0.28	0.40	0.33
Significant Duration (sec)	16.2	17.3	16.8	18.8	19.7	19.2

GM: Geometric Mean
SED: Specific Energy Density

2UHRS-P Scaled Accelerogram	0738FN	0738FP	GM	1526FN	1526FP	GM
Max Acceleration (g)	0.879	0.902	0.890	0.496	0.508	0.502
Max Velocity (cm/sec)	127.2	137.7	132.4	150.9	170.3	160.3
Max Displacement (cm)	40.5	43.6	42.0	127.1	234.7	172.7
Vmax/Amax (sec)	0.147	0.156	0.152	0.310	0.342	0.326
Acceleration RMS (g)	0.117	0.120	0.119	0.084	0.085	0.085
Velocity RMS (cm/sec)	23.3	22.5	22.9	31.6	39.5	35.3
Displacement RMS (cm)	10.2	12.0	11.1	35.2	50.8	42.3
Arias Intensity (cm/sec)	6.21	6.60	6.41	9.90	9.95	9.93
Characteristic Intensity	0.217	0.227	0.222	0.233	0.234	0.233
SED (cm2/sec)	16106	14921	15502	89924	140281	112315
Cum. Abs. Velocity (cm/sec)	1695	1648	1671	4343	4290	4317
Acc Spec. Intensity (g*sec)	0.541	0.500	0.520	0.558	0.477	0.516
Vel Spectrum Intensity (cm)	489	505	497	383	340	361
Housner Intensity (cm)	487	503	495	414	358	385
Sustained Max.Acc. (g)	0.463	0.536	0.498	0.421	0.418	0.420
Sustained Max.Vel. (cm/sec)	101.1	52.5	72.8	141.0	151.1	145.9
Effective Design Acc. (g)	0.805	0.903	0.853	0.518	0.507	0.513
A95 parameter (g)	0.868	0.895	0.881	0.487	0.494	0.491
Predominant Period (sec)	0.60	0.68	0.64	0.20	0.28	0.24
Significant Duration (sec)	6.0	4.6	5.3	33.2	27.8	30.4

GM: Geometric Mean
SED: Specific Energy Density

2UHRS-P Scaled Accelerogram	1481FN	1481FP	GM	1505FN	1505FP	GM
Max Acceleration (g)	0.519	0.614	0.564	0.698	0.496	0.588
Max Velocity (cm/sec)	187.3	168.2	177.5	236.7	295.1	264.3
Max Displacement (cm)	240.5	154.7	192.9	460.9	480.7	470.7
Vmax/Amax (sec)	0.368	0.279	0.321	0.346	0.606	0.458
Acceleration RMS (g)	0.086	0.101	0.093	0.063	0.057	0.060
Velocity RMS (cm/sec)	37.5	31.8	34.5	52.3	50.1	51.2
Displacement RMS (cm)	46.5	36.1	41.0	117.2	119.5	118.3
Arias Intensity (cm/sec)	10.18	14.12	11.99	5.49	4.54	5.00
Characteristic Intensity	0.238	0.304	0.269	0.150	0.130	0.139
SED (cm2/sec)	126534	91081	107354	245694	225897	235588
Cum. Abs. Velocity (cm/sec)	4129	4719	4414	2227	2267	2247
Acc Spec. Intensity (g*sec)	0.489	0.657	0.567	0.563	0.356	0.448
Vel Spectrum Intensity (cm)	282	380	327	385	333	358
Housner Intensity (cm)	311	364	336	451	371	409
Sustained Max.Acc. (g)	0.481	0.537	0.508	0.426	0.281	0.346
Sustained Max.Vel. (cm/sec)	159.7	139.5	149.3	215.6	129.4	167.0
Effective Design Acc. (g)	0.511	0.601	0.554	0.645	0.472	0.551
A95 parameter (g)	0.509	0.600	0.553	0.689	0.487	0.579
Predominant Period (sec)	0.74	0.34	0.50	0.40	1.40	0.75
Significant Duration (sec)	27.6	25.7	26.7	12.5	13.1	12.8

GM: Geometric Mean
SED: Specific Energy Density

2UHRS-P Scaled Accelerogram	1176FN	1176FP	GM	1550FN	1550FP	GM
Max Acceleration (g)	0.580	0.649	0.613	0.629	0.589	0.609
Max Velocity (cm/sec)	100.2	151.6	123.3	192.8	190.2	191.4
Max Displacement (cm)	89.5	116.4	102.0	223.6	197.7	210.2
Vmax/Amax (sec)	0.176	0.238	0.205	0.312	0.329	0.321
Acceleration RMS (g)	0.107	0.100	0.103	0.083	0.074	0.079
Velocity RMS (cm/sec)	34.6	42.9	38.6	33.1	37.7	35.4
Displacement RMS (cm)	33.7	37.6	35.6	51.1	45.7	48.3
Arias Intensity (cm/sec)	6.12	5.35	5.72	9.64	7.68	8.61
Characteristic Intensity	0.206	0.186	0.196	0.228	0.193	0.210
SED (cm2/sec)	41954	64517	52026	98851	128106	112532
Cum. Abs. Velocity (cm/sec)	2242	2028	2133	3571	3305	3436
Acc Spec. Intensity (g*sec)	0.500	0.434	0.466	0.491	0.392	0.438
Vel Spectrum Intensity (cm)	380	298	336	466	354	406
Housner Intensity (cm)	378	349	363	425	371	397
Sustained Max.Acc. (g)	0.482	0.421	0.450	0.529	0.400	0.460
Sustained Max.Vel. (cm/sec)	99.5	142.7	119.2	123.1	156.6	138.8
Effective Design Acc. (g)	0.555	0.625	0.589	0.644	0.594	0.619
A95 parameter (g)	0.570	0.640	0.604	0.621	0.585	0.603
Predominant Period (sec)	0.42	0.74	0.56	0.92	0.94	0.93
Significant Duration (sec)	15.4	14.9	15.2	19.8	24.1	21.8

GM: Geometric Mean
SED: Specific Energy Density

2UHRS-P Scaled Accelerogram	Set Average	Set StdDev
Max Acceleration (g)	0.836	0.374
Max Velocity (cm/sec)	146.9	45.9
Max Displacement (cm)	124.7	118.2
Vmax/Amax (sec)	0.212	0.113
Acceleration RMS (g)	0.107	0.024
Velocity RMS (cm/sec)	29.0	11.1
Displacement RMS (cm)	33.0	29.7
Arias Intensity (cm/sec)	7.88	1.92
Characteristic Intensity	0.232	0.041
SED (cm2/sec)	58763	64661
Cum. Abs. Velocity (cm/sec)	2585	883
Acc Spec. Intensity (g*sec)	0.622	0.184
Vel Spectrum Intensity (cm)	364	58
Housner Intensity (cm)	360	60
Sustained Max.Acc. (g)	0.531	0.105
Sustained Max.Vel. (cm/sec)	100.2	41.5
Effective Design Acc. (g)	0.787	0.321
A95 parameter (g)	0.826	0.375
Predominant Period (sec)	0.46	0.24
Significant Duration (sec)	15.0	7.4

GM: Geometric Mean
SED: Specific Energy Density

2NMSZ Scaled Accelerogram	1195FN	1195FP	GM	1540FN	1540FP	GM
Max Acceleration (g)	0.368	0.315	0.340	0.361	0.443	0.400
Max Velocity (cm/sec)	224.4	157.9	188.2	203.2	148.1	173.5
Max Displacement (cm)	171.5	130.1	149.4	141.8	127.4	134.4
Vmax/Amax (sec)	0.621	0.511	0.564	0.574	0.341	0.443
Acceleration RMS (g)	0.101	0.073	0.086	0.084	0.083	0.084
Velocity RMS (cm/sec)	54.5	40.1	46.8	39.3	40.7	40.0
Displacement RMS (cm)	43.5	39.8	41.6	33.4	32.9	33.1
Arias Intensity (cm/sec)	14.03	7.34	10.15	9.70	9.66	9.68
Characteristic Intensity	0.303	0.186	0.237	0.229	0.229	0.229
SED (cm2/sec)	267492	144874	196856	139195	149310	144163
Cum. Abs. Velocity (cm/sec)	5769	4136	4885	4711	4638	4674
Acc Spec. Intensity (g*sec)	0.299	0.268	0.283	0.319	0.281	0.299
Vel Spectrum Intensity (cm)	353	274	311	289	378	330
Housner Intensity (cm)	403	301	348	311	404	355
Sustained Max.Acc. (g)	0.348	0.263	0.303	0.328	0.321	0.325
Sustained Max.Vel. (cm/sec)	163.8	113.4	136.3	127.4	138.1	132.6
Effective Design Acc. (g)	0.364	0.312	0.337	0.341	0.440	0.387
A95 parameter (g)	0.358	0.309	0.333	0.351	0.435	0.391
Predominant Period (sec)	1.10	0.42	0.68	0.46	2.24	1.02
Significant Duration (sec)	43.2	44.6	43.9	43.6	44.1	43.9

GM: Geometric Mean
SED: Specific Energy Density

2NMSZ Scaled Accelerogram	1542FN	1542FP	GM	1238FN	1238FP	GM
Max Acceleration (g)	0.371	0.372	0.371	0.402	0.294	0.344
Max Velocity (cm/sec)	175.0	162.9	168.8	198.1	126.1	158.0
Max Displacement (cm)	150.3	139.7	144.9	135.0	111.3	122.6
Vmax/Amax (sec)	0.481	0.447	0.463	0.502	0.437	0.468
Acceleration RMS (g)	0.085	0.081	0.083	0.074	0.056	0.064
Velocity RMS (cm/sec)	35.0	34.6	34.8	36.0	28.3	31.9
Displacement RMS (cm)	35.5	31.1	33.2	28.4	26.2	27.3
Arias Intensity (cm/sec)	10.05	9.14	9.58	12.58	7.27	9.56
Characteristic Intensity	0.236	0.219	0.227	0.245	0.163	0.200
SED (cm2/sec)	110381	107703	109033	194514	119769	152632
Cum. Abs. Velocity (cm/sec)	4649	4463	4555	5964	4680	5284
Acc Spec. Intensity (g*sec)	0.281	0.260	0.270	0.306	0.235	0.268
Vel Spectrum Intensity (cm)	434	425	430	388	280	330
Housner Intensity (cm)	442	451	447	405	300	349
Sustained Max.Acc. (g)	0.319	0.347	0.332	0.376	0.264	0.315
Sustained Max.Vel. (cm/sec)	117.3	102.4	109.6	141.1	114.9	127.3
Effective Design Acc. (g)	0.371	0.371	0.371	0.402	0.293	0.343
A95 parameter (g)	0.363	0.367	0.365	0.391	0.284	0.334
Predominant Period (sec)	1.34	1.38	1.36	0.82	0.86	0.84
Significant Duration (sec)	32.6	40.9	36.5	43.5	51.0	47.1

GM: Geometric Mean
SED: Specific Energy Density

2NMSZ Scaled Accelerogram	0883FN	0883FP	GM	1840FN	1840FP	GM
Max Acceleration (g)	0.340	0.402	0.370	0.480	0.388	0.432
Max Velocity (cm/sec)	151.9	161.9	156.8	146.4	157.2	151.7
Max Displacement (cm)	138.6	139.8	139.2	103.1	211.8	147.7
Vmax/Amax (sec)	0.455	0.411	0.432	0.311	0.413	0.358
Acceleration RMS (g)	0.099	0.109	0.104	0.086	0.092	0.089
Velocity RMS (cm/sec)	43.6	48.3	45.9	29.5	57.7	41.2
Displacement RMS (cm)	41.0	51.0	45.7	29.6	71.1	45.9
Arias Intensity (cm/sec)	8.56	10.24	9.36	7.70	8.78	8.23
Characteristic Intensity	0.235	0.269	0.251	0.208	0.229	0.218
SED (cm2/sec)	107208	131407	118692	58172	223054	113910
Cum. Abs. Velocity (cm/sec)	4209	4319	4263	4048	4320	4181
Acc Spec. Intensity (g*sec)	0.306	0.326	0.316	0.260	0.332	0.294
Vel Spectrum Intensity (cm)	340	473	401	457	413	434
Housner Intensity (cm)	366	488	422	469	448	458
Sustained Max.Acc. (g)	0.315	0.378	0.345	0.342	0.359	0.351
Sustained Max.Vel. (cm/sec)	124.2	143.5	133.5	80.2	149.4	109.5
Effective Design Acc. (g)	0.342	0.398	0.369	0.477	0.380	0.426
A95 parameter (g)	0.327	0.378	0.352	0.472	0.379	0.423
Predominant Period (sec)	1.40	1.44	1.42	1.98	0.88	1.32
Significant Duration (sec)	39.0	32.9	35.8	43.1	37.1	40.0

GM: Geometric Mean
SED: Specific Energy Density

2NMSZ Scaled Accelerogram	0853FN	0853FP	GM	ROLC 151	ROLC 241	GM
Max Acceleration (g)	0.385	0.436	0.410	1.032	0.810	0.914
Max Velocity (cm/sec)	96.2	123.0	108.8	156.7	146.1	151.3
Max Displacement (cm)	73.9	66.3	70.0	101.3	48.6	70.2
Vmax/Amax (sec)	0.255	0.287	0.271	0.155	0.184	0.169
Acceleration RMS (g)	0.111	0.122	0.116	0.091	0.091	0.091
Velocity RMS (cm/sec)	33.1	39.3	36.1	23.4	20.2	21.7
Displacement RMS (cm)	20.7	25.6	23.0	16.4	10.3	13.0
Arias Intensity (cm/sec)	7.50	8.98	8.21	10.45	10.48	10.47
Characteristic Intensity	0.233	0.266	0.249	0.248	0.249	0.249
SED (cm2/sec)	43206	61003	51339	44831	33474	38739
Cum. Abs. Velocity (cm/sec)	3230	3628	3423	2979	3114	3046
Acc Spec. Intensity (g*sec)	0.305	0.275	0.290	0.651	0.652	0.651
Vel Spectrum Intensity (cm)	393	452	421	467	452	459
Housner Intensity (cm)	409	484	445	476	455	465
Sustained Max.Acc. (g)	0.336	0.351	0.343	0.712	0.666	0.689
Sustained Max.Vel. (cm/sec)	84.6	86.0	85.3	123.5	120.0	121.7
Effective Design Acc. (g)	0.380	0.430	0.404	0.910	0.792	0.849
A95 parameter (g)	0.360	0.415	0.387	1.014	0.788	0.894
Predominant Period (sec)	0.78	1.10	0.93	0.32	0.18	0.24
Significant Duration (sec)	26.7	27.0	26.8	11.1	11.3	11.2

GM: Geometric Mean
SED: Specific Energy Density

2NMSZ Scaled Accelerogram	HPSC 356	HPSC 266	GM	LRSC 311	LRSC 221	GM
Max Acceleration (g)	0.601	0.401	0.491	0.921	0.652	0.775
Max Velocity (cm/sec)	146.7	89.4	114.5	113.3	135.0	123.7
Max Displacement (cm)	58.2	53.7	55.9	64.8	44.9	54.0
Vmax/Amax (sec)	0.249	0.227	0.238	0.125	0.211	0.163
Acceleration RMS (g)	0.082	0.062	0.072	0.127	0.099	0.112
Velocity RMS (cm/sec)	23.2	19.0	21.0	27.0	20.7	23.6
Displacement RMS (cm)	12.5	11.3	11.9	17.4	10.2	13.3
Arias Intensity (cm/sec)	8.59	4.92	6.50	17.35	10.55	13.53
Characteristic Intensity	0.214	0.141	0.174	0.378	0.260	0.314
SED (cm2/sec)	44084	29540	36087	50662	29954	38955
Cum. Abs. Velocity (cm/sec)	3372	2774	3058	4770	3893	4309
Acc Spec. Intensity (g*sec)	0.540	0.384	0.455	0.800	0.468	0.612
Vel Spectrum Intensity (cm)	405	276	334	446	401	423
Housner Intensity (cm)	413	292	347	427	401	414
Sustained Max.Acc. (g)	0.487	0.374	0.427	0.603	0.520	0.560
Sustained Max.Vel. (cm/sec)	103.1	81.0	91.4	89.9	81.9	85.8
Effective Design Acc. (g)	0.612	0.404	0.498	0.813	0.643	0.723
A95 parameter (g)	0.581	0.388	0.475	0.890	0.624	0.745
Predominant Period (sec)	0.40	0.64	0.51	0.28	1.26	0.59
Significant Duration (sec)	17.4	26.7	21.5	23.3	23.6	23.4

GM: Geometric Mean
SED: Specific Energy Density

2NMSZ Scaled Accelerogram	SYN28 H1	SYN28 H2	GM	SYN27 H1	SYN27 H2	GM
Max Acceleration (g)	0.436	0.410	0.423	0.509	0.579	0.543
Max Velocity (cm/sec)	127.9	131.2	129.6	114.2	133.4	123.4
Max Displacement (cm)	58.8	52.9	55.8	84.3	80.1	82.2
Vmax/Amax (sec)	0.299	0.326	0.312	0.229	0.235	0.232
Acceleration RMS (g)	0.086	0.100	0.093	0.061	0.090	0.074
Velocity RMS (cm/sec)	27.4	29.7	28.5	23.9	31.7	27.5
Displacement RMS (cm)	14.7	15.0	14.8	16.4	22.8	19.3
Arias Intensity (cm/sec)	5.96	8.14	6.97	4.71	10.40	7.00
Characteristic Intensity	0.183	0.230	0.205	0.137	0.247	0.184
SED (cm2/sec)	39261	46539	42745	46729	83453	62447
Cum. Abs. Velocity (cm/sec)	2863	3729	3268	2804	4764	3655
Acc Spec. Intensity (g*sec)	0.276	0.272	0.274	0.333	0.349	0.341
Vel Spectrum Intensity (cm)	415	427	421	338	392	364
Housner Intensity (cm)	446	459	452	374	398	386
Sustained Max.Acc. (g)	0.381	0.373	0.377	0.332	0.402	0.365
Sustained Max.Vel. (cm/sec)	78.6	82.7	80.7	105.6	114.0	109.7
Effective Design Acc. (g)	0.428	0.396	0.412	0.476	0.517	0.496
A95 parameter (g)	0.426	0.401	0.413	0.500	0.560	0.529
Predominant Period (sec)	1.42	1.78	1.59	0.74	1.34	1.00
Significant Duration (sec)	23.0	29.9	26.2	24.4	35.1	29.3

GM: Geometric Mean
SED: Specific Energy Density

2NMSZ Scaled Accelerogram	SYN26 H1	SYN26 H2	GM	SYN23 H1	SYN23 H2	GM
Max Acceleration (g)	0.548	0.541	0.544	0.470	0.534	0.501
Max Velocity (cm/sec)	153.8	136.2	144.7	132.3	113.7	122.7
Max Displacement (cm)	63.1	63.9	63.5	68.5	62.0	65.1
Vmax/Amax (sec)	0.286	0.256	0.271	0.287	0.217	0.250
Acceleration RMS (g)	0.098	0.102	0.100	0.102	0.121	0.111
Velocity RMS (cm/sec)	31.3	29.5	30.4	32.0	26.2	29.0
Displacement RMS (cm)	18.2	15.8	16.9	19.8	14.8	17.1
Arias Intensity (cm/sec)	6.46	6.47	6.47	9.28	13.36	11.13
Characteristic Intensity	0.203	0.207	0.205	0.248	0.324	0.283
SED (cm2/sec)	42529	34727	38431	59436	40413	49010
Cum. Abs. Velocity (cm/sec)	2839	2659	2747	4179	5187	4656
Acc Spec. Intensity (g*sec)	0.354	0.373	0.363	0.343	0.416	0.378
Vel Spectrum Intensity (cm)	399	419	409	403	394	398
Housner Intensity (cm)	430	425	427	418	395	406
Sustained Max.Acc. (g)	0.384	0.438	0.410	0.417	0.441	0.429
Sustained Max.Vel. (cm/sec)	86.3	94.0	90.1	99.5	72.7	85.0
Effective Design Acc. (g)	0.529	0.488	0.508	0.443	0.472	0.457
A95 parameter (g)	0.538	0.529	0.533	0.457	0.511	0.483
Predominant Period (sec)	1.68	0.30	0.71	1.86	1.02	1.38
Significant Duration (sec)	23.5	18.5	20.8	36.8	39.7	38.2

GM: Geometric Mean
SED: Specific Energy Density

2NMSZ Scaled Accelerogram	Set Average	Set StdDev
Max Acceleration (g)	0.490	0.167
Max Velocity (cm/sec)	144.0	24.1
Max Displacement (cm)	96.8	39.7
Vmax/Amax (sec)	0.331	0.124
Acceleration RMS (g)	0.091	0.016
Velocity RMS (cm/sec)	32.7	8.4
Displacement RMS (cm)	25.4	12.4
Arias Intensity (cm/sec)	9.06	2.00
Characteristic Intensity	0.230	0.038
SED (cm2/sec)	85217	53117
Cum. Abs. Velocity (cm/sec)	4000	793
Acc Spec. Intensity (g*sec)	0.364	0.125
Vel Spectrum Intensity (cm)	390	47
Housner Intensity (cm)	409	44
Sustained Max.Acc. (g)	0.398	0.107
Sustained Max.Vel. (cm/sec)	107.0	20.6
Effective Design Acc. (g)	0.470	0.147
A95 parameter (g)	0.475	0.163
Predominant Period (sec)	0.97	0.40
Significant Duration (sec)	31.8	10.6

GM: Geometric Mean
SED: Specific Energy Density

2NMSZ-P Scaled Accelerogram	1473FN	1473FP	GM	1548FN	1548FP	GM
Max Acceleration (g)	0.368	0.519	0.437	0.548	0.389	0.461
Max Velocity (cm/sec)	162.4	256.6	204.1	229.6	140.9	179.8
Max Displacement (cm)	228.5	406.1	304.6	281.5	174.2	221.4
Vmax/Amax (sec)	0.450	0.504	0.476	0.427	0.369	0.397
Acceleration RMS (g)	0.076	0.091	0.083	0.070	0.064	0.067
Velocity RMS (cm/sec)	51.4	64.2	57.4	40.7	30.8	35.4
Displacement RMS (cm)	72.5	90.0	80.8	45.9	38.6	42.1
Arias Intensity (cm/sec)	6.77	9.74	8.12	6.71	5.68	6.17
Characteristic Intensity	0.183	0.240	0.209	0.174	0.154	0.164
SED (cm2/sec)	200913	313079	250802	149274	85641	113066
Cum. Abs. Velocity (cm/sec)	3724	4238	3973	3098	2891	2993
Acc Spec. Intensity (g*sec)	0.301	0.320	0.311	0.355	0.338	0.346
Vel Spectrum Intensity (cm)	288	442	357	268	295	281
Housner Intensity (cm)	303	477	380	321	285	303
Sustained Max.Acc. (g)	0.266	0.418	0.334	0.369	0.367	0.368
Sustained Max.Vel. (cm/sec)	159.0	196.6	176.8	115.1	104.4	109.7
Effective Design Acc. (g)	0.364	0.516	0.433	0.549	0.397	0.467
A95 parameter (g)	0.359	0.509	0.428	0.543	0.384	0.457
Predominant Period (sec)	0.48	0.50	0.49	0.42	0.50	0.46
Significant Duration (sec)	38.3	35.4	36.8	20.7	19.6	20.1

GM: Geometric Mean
SED: Specific Energy Density

2NMSZ-P Scaled Accelerogram	1529FN	1529FP	GM	1480FN	1480FP	GM
Max Acceleration (g)	0.558	0.319	0.422	0.402	0.371	0.386
Max Velocity (cm/sec)	203.2	147.6	173.2	186.5	143.4	163.6
Max Displacement (cm)	167.5	103.8	131.9	190.0	139.1	162.6
Vmax/Amax (sec)	0.371	0.472	0.419	0.473	0.394	0.432
Acceleration RMS (g)	0.072	0.067	0.070	0.070	0.067	0.069
Velocity RMS (cm/sec)	27.9	25.4	26.6	33.9	31.4	32.6
Displacement RMS (cm)	31.5	20.1	25.2	42.1	32.2	36.8
Arias Intensity (cm/sec)	7.24	6.31	6.76	6.86	6.30	6.57
Characteristic Intensity	0.184	0.166	0.175	0.177	0.166	0.171
SED (cm2/sec)	69855	57889	63591	103363	88793	95801
Cum. Abs. Velocity (cm/sec)	2937	3054	2995	3248	3260	3254
Acc Spec. Intensity (g*sec)	0.325	0.209	0.261	0.366	0.343	0.354
Vel Spectrum Intensity (cm)	442	431	437	283	271	277
Housner Intensity (cm)	488	457	472	293	293	293
Sustained Max.Acc. (g)	0.390	0.287	0.334	0.391	0.307	0.347
Sustained Max.Vel. (cm/sec)	102.7	90.8	96.6	156.3	133.5	144.5
Effective Design Acc. (g)	0.555	0.313	0.416	0.399	0.366	0.382
A95 parameter (g)	0.554	0.313	0.417	0.395	0.363	0.378
Predominant Period (sec)	0.72	2.30	1.29	0.30	0.44	0.36
Significant Duration (sec)	16.5	18.9	17.6	22.9	27.5	25.1

GM: Geometric Mean
SED: Specific Energy Density

2NMSZ-P Scaled Accelerogram	1531FN	1531FP	GM	1505FN	1505FP	GM
Max Acceleration (g)	0.471	0.388	0.427	0.573	0.408	0.483
Max Velocity (cm/sec)	134.7	199.5	163.9	194.5	242.5	217.2
Max Displacement (cm)	202.4	238.8	219.9	378.7	395.0	386.8
Vmax/Amax (sec)	0.291	0.525	0.391	0.346	0.606	0.458
Acceleration RMS (g)	0.079	0.074	0.077	0.052	0.047	0.049
Velocity RMS (cm/sec)	31.6	51.5	40.3	42.9	41.2	42.0
Displacement RMS (cm)	50.4	61.2	55.5	96.3	98.2	97.2
Arias Intensity (cm/sec)	8.75	7.60	8.15	3.71	3.07	3.37
Characteristic Intensity	0.212	0.191	0.201	0.112	0.097	0.104
SED (cm2/sec)	89823	239006	146521	165892	152525	159069
Cum. Abs. Velocity (cm/sec)	3822	3767	3794	1830	1863	1847
Acc Spec. Intensity (g*sec)	0.403	0.309	0.353	0.462	0.293	0.368
Vel Spectrum Intensity (cm)	336	254	292	316	274	294
Housner Intensity (cm)	323	300	311	370	305	336
Sustained Max.Acc. (g)	0.444	0.354	0.397	0.350	0.230	0.284
Sustained Max.Vel. (cm/sec)	119.5	193.2	151.9	177.1	106.3	137.2
Effective Design Acc. (g)	0.469	0.369	0.416	0.530	0.388	0.453
A95 parameter (g)	0.458	0.377	0.415	0.566	0.400	0.476
Predominant Period (sec)	0.40	0.50	0.45	0.40	1.40	0.75
Significant Duration (sec)	28.7	29.2	28.9	12.5	13.1	12.8

GM: Geometric Mean
SED: Specific Energy Density

2NMSZ-P Scaled Accelerogram	1176FN	1176FP	GM	2114FN	2114FP	GM
Max Acceleration (g)	0.478	0.535	0.505	0.501	0.418	0.457
Max Velocity (cm/sec)	82.6	125.0	101.6	146.0	185.4	164.5
Max Displacement (cm)	73.8	95.9	84.1	141.2	177.6	158.3
Vmax/Amax (sec)	0.176	0.238	0.205	0.297	0.452	0.367
Acceleration RMS (g)	0.088	0.082	0.085	0.053	0.049	0.051
Velocity RMS (cm/sec)	28.5	35.4	31.8	20.6	18.7	19.6
Displacement RMS (cm)	27.8	31.0	29.4	27.6	38.6	32.7
Arias Intensity (cm/sec)	4.16	3.64	3.89	3.85	3.33	3.58
Characteristic Intensity	0.154	0.139	0.146	0.115	0.103	0.109
SED (cm2/sec)	28496	43823	35338	38210	31368	34621
Cum. Abs. Velocity (cm/sec)	1848	1672	1758	2321	1951	2128
Acc Spec. Intensity (g*sec)	0.412	0.358	0.384	0.355	0.289	0.320
Vel Spectrum Intensity (cm)	313	245	277	358	416	386
Housner Intensity (cm)	311	287	299	404	448	426
Sustained Max.Acc. (g)	0.397	0.347	0.371	0.323	0.370	0.346
Sustained Max.Vel. (cm/sec)	82.0	117.6	98.2	83.5	66.5	74.5
Effective Design Acc. (g)	0.457	0.515	0.485	0.513	0.419	0.464
A95 parameter (g)	0.469	0.528	0.498	0.494	0.415	0.453
Predominant Period (sec)	0.42	0.74	0.56	0.76	1.04	0.89
Significant Duration (sec)	15.4	14.9	15.2	25.4	22.4	23.9

GM: Geometric Mean
SED: Specific Energy Density

2NMSZ-P Scaled Accelerogram	0838FN	0838FP	GM	1605FN	1605FP	GM
Max Acceleration (g)	0.689	0.431	0.545	0.445	0.646	0.536
Max Velocity (cm/sec)	151.6	55.6	91.8	77.4	98.9	87.5
Max Displacement (cm)	138.8	34.2	68.9	57.8	60.0	58.9
Vmax/Amax (sec)	0.224	0.131	0.172	0.177	0.156	0.166
Acceleration RMS (g)	0.103	0.081	0.092	0.102	0.107	0.104
Velocity RMS (cm/sec)	33.8	18.2	24.8	26.3	26.7	26.5
Displacement RMS (cm)	42.0	12.0	22.4	22.2	18.9	20.5
Arias Intensity (cm/sec)	6.56	4.07	5.17	4.18	4.53	4.35
Characteristic Intensity	0.210	0.146	0.175	0.167	0.177	0.172
SED (cm2/sec)	45719	13194	24561	17939	18490	18213
Cum. Abs. Velocity (cm/sec)	2542	2172	2350	1700	1687	1694
Acc Spec. Intensity (g*sec)	0.497	0.400	0.446	0.545	0.506	0.525
Vel Spectrum Intensity (cm)	347	232	284	228	316	268
Housner Intensity (cm)	333	236	280	238	322	277
Sustained Max.Acc. (g)	0.438	0.364	0.400	0.388	0.447	0.416
Sustained Max.Vel. (cm/sec)	75.9	46.3	59.3	76.3	78.3	77.3
Effective Design Acc. (g)	0.673	0.402	0.520	0.431	0.622	0.518
A95 parameter (g)	0.677	0.415	0.530	0.439	0.641	0.531
Predominant Period (sec)	0.34	0.32	0.33	0.42	0.22	0.30
Significant Duration (sec)	17.4	22.9	19.9	10.9	10.7	10.8

GM: Geometric Mean
SED: Specific Energy Density

2NMSZ-P Scaled Accelerogram	0803FN	0803FP	GM	0779FN	0779FP	GM
Max Acceleration (g)	0.767	0.488	0.612	0.929	0.528	0.701
Max Velocity (cm/sec)	135.7	114.2	124.5	95.4	71.0	82.3
Max Displacement (cm)	39.6	56.7	47.4	61.6	30.1	43.0
Vmax/Amax (sec)	0.180	0.239	0.207	0.105	0.137	0.120
Acceleration RMS (g)	0.092	0.072	0.081	0.144	0.092	0.115
Velocity RMS (cm/sec)	19.7	18.4	19.0	26.5	16.2	20.7
Displacement RMS (cm)	12.3	14.5	13.3	18.2	10.9	14.1
Arias Intensity (cm/sec)	5.22	3.17	4.07	7.99	3.30	5.13
Characteristic Intensity	0.177	0.121	0.146	0.273	0.141	0.196
SED (cm2/sec)	15474	13514	14461	17556	6562	10733
Cum. Abs. Velocity (cm/sec)	1885	1507	1685	2088	1393	1705
Acc Spec. Intensity (g*sec)	0.503	0.450	0.476	0.601	0.389	0.483
Vel Spectrum Intensity (cm)	395	270	326	400	244	313
Housner Intensity (cm)	375	274	321	379	235	298
Sustained Max.Acc. (g)	0.451	0.401	0.425	0.773	0.433	0.578
Sustained Max.Vel. (cm/sec)	51.6	55.4	53.5	91.4	58.2	72.9
Effective Design Acc. (g)	0.776	0.481	0.611	0.561	0.501	0.531
A95 parameter (g)	0.761	0.482	0.605	0.913	0.519	0.688
Predominant Period (sec)	0.32	0.36	0.34	0.74	0.66	0.70
Significant Duration (sec)	11.0	12.4	11.7	10.0	10.9	10.4

GM: Geometric Mean
SED: Specific Energy Density

2NMSZ-P Scaled Accelerogram	0900FN	0900FP	GM	0292FN	0292FP	GM
Max Acceleration (g)	0.595	0.598	0.597	0.431	0.569	0.495
Max Velocity (cm/sec)	142.7	67.0	97.8	77.0	84.6	80.7
Max Displacement (cm)	121.6	45.3	74.2	41.1	43.6	42.3
Vmax/Amax (sec)	0.244	0.114	0.167	0.182	0.152	0.166
Acceleration RMS (g)	0.101	0.083	0.091	0.075	0.096	0.085
Velocity RMS (cm/sec)	30.4	15.8	21.9	16.7	17.8	17.2
Displacement RMS (cm)	34.5	11.1	19.6	10.1	9.3	9.7
Arias Intensity (cm/sec)	6.91	4.64	5.66	3.45	5.57	4.38
Characteristic Intensity	0.213	0.158	0.183	0.130	0.186	0.155
SED (cm2/sec)	40673	10957	21111	10988	12430	11687
Cum. Abs. Velocity (cm/sec)	2597	2238	2411	1795	2050	1918
Acc Spec. Intensity (g*sec)	0.486	0.486	0.486	0.421	0.666	0.530
Vel Spectrum Intensity (cm)	391	271	326	246	342	290
Housner Intensity (cm)	379	274	322	250	360	300
Sustained Max.Acc. (g)	0.537	0.380	0.452	0.404	0.538	0.466
Sustained Max.Vel. (cm/sec)	106.1	56.1	77.2	63.3	77.4	70.0
Effective Design Acc. (g)	0.581	0.591	0.586	0.431	0.603	0.510
A95 parameter (g)	0.579	0.585	0.582	0.428	0.561	0.490
Predominant Period (sec)	0.38	0.28	0.33	0.20	0.32	0.25
Significant Duration (sec)	17.2	19.6	18.3	16.6	12.1	14.2

GM: Geometric Mean
SED: Specific Energy Density

2NMSZ-P Scaled Accelerogram	Set Average	Set StdDev
Max Acceleration (g)	0.505	0.086
Max Velocity (cm/sec)	138.0	47.9
Max Displacement (cm)	143.2	106.8
Vmax/Amax (sec)	0.296	0.133
Acceleration RMS (g)	0.080	0.018
Velocity RMS (cm/sec)	29.7	11.2
Displacement RMS (cm)	35.7	25.9
Arias Intensity (cm/sec)	5.38	1.58
Characteristic Intensity	0.165	0.031
SED (cm2/sec)	71398	72642
Cum. Abs. Velocity (cm/sec)	2465	800
Acc Spec. Intensity (g*sec)	0.403	0.086
Vel Spectrum Intensity (cm)	315	49
Housner Intensity (cm)	330	57
Sustained Max.Acc. (g)	0.394	0.073
Sustained Max.Vel. (cm/sec)	100.0	38.4
Effective Design Acc. (g)	0.485	0.066
A95 parameter (g)	0.496	0.085
Predominant Period (sec)	0.54	0.29
Significant Duration (sec)	19.0	7.6

GM: Geometric Mean
SED: Specific Energy Density

APPENDIX C. DERIVATIONS

Beginning with the customarily adopted expression for equivalent viscous damping it is possible to derive some useful relationships. The algebra is presented here for the derivations discussed in the main body of this dissertation.

First, for given values of Q_d, k_d, and D_{ISO}, but with different post-yield stiffness (α) values, the ratio of effective damping for the two systems is developed.

From the bi-linear force-displacement relationship:

$$D_{Y1} \cdot k_{i1} = Q_{d1} + k_{d1} \cdot D_{Y1}$$

$$D_{Y1} \cdot \frac{k_{d1}}{\alpha_1} = Q_{d1} + k_{d1} \cdot D_{Y1}$$

$$D_{Y1} \cdot \left(\frac{k_{d1}}{\alpha_1} - k_{d1}\right) = Q_{d1}$$

$$D_{Y1} \cdot k_{d1} \left(\frac{1}{\alpha_1} - 1\right) = Q_{d1}$$

$$D_{Y1} \cdot k_{d1} \left(\frac{1 - \alpha_1}{\alpha_1}\right) = Q_{d1}$$

$$\Rightarrow D_{Y1} = \frac{Q_{d1}}{k_{d1}} \cdot \frac{\alpha_1}{1 - \alpha_1} \text{ , } Similarly, D_{Y2} = \frac{Q_{d2}}{k_{d2}} \cdot \frac{\alpha_2}{1 - \alpha_2}$$

$$\frac{D_{Y1}}{D_{Y2}} = \frac{Q_{d1}}{k_{d1}} \cdot \frac{\alpha_1}{1 - \alpha_1} \cdot \frac{k_{d2}}{Q_{d2}} \cdot \frac{1 - \alpha_2}{\alpha_2}$$

So, if $Q_{d1} = Q_{d2}$ and $k_{d1} = k_{d2}$, we have:

$$\frac{D_{Y1}}{D_{Y2}} = \frac{\alpha_1(1 - \alpha_2)}{(1 - \alpha_1)\alpha_2}$$

Now provided $\mu_1 > 1$, $\mu_2 > 1$:

$$\xi_1 = \frac{2(\mu_1 - 1)(1 - \alpha_1)}{\pi\mu_1(1 + \alpha_1\mu_1 - \alpha_1)} \;\; and \;\; \xi_2 = \frac{2(\mu_2 - 1)(1 - \alpha_2)}{\pi\mu_2(1 + \alpha_2\mu_2 - \alpha_2)}$$

Note also that for a given value of isolator displacement, D_{ISO}, it is possible relate the two ductility value.

$$\mu_1 = \frac{D_{ISO}}{D_{Y1}} = \frac{D_{ISO}}{D_{Y2}} \cdot \frac{D_{Y2}}{D_{Y1}} = \frac{\mu_2\alpha_2(1 - \alpha_1)}{\alpha_1(1 - \alpha_2)}$$

$$\frac{\xi_1}{\xi_2} = \frac{2(\mu_1 - 1)(1 - \alpha_1)}{\pi\mu_1(1 + \alpha_1\mu_1 - \alpha_1)} \cdot \frac{\pi\mu_2(1 + \alpha_2\mu_2 - \alpha_2)}{2(\mu_2 - 1)(1 - \alpha_2)} = \frac{(\mu_1 - 1)(1 - \alpha_1)\mu_2(1 + \alpha_2\mu_2 - \alpha_2)}{\mu_1(1 + \alpha_1\mu_1 - \alpha_1)(\mu_2 - 1)(1 - \alpha_2)}$$

$$\frac{\xi_1}{\xi_2} = \frac{\left(\frac{\mu_2\alpha_2(1 - \alpha_1)}{\alpha_1(1 - \alpha_2)} - 1\right)(1 - \alpha_1)\mu_2(1 + \alpha_2\mu_2 - \alpha_2)}{\frac{\mu_2\alpha_2(1 - \alpha_1)}{\alpha_1(1 - \alpha_2)}\left(1 + \alpha_1\frac{\mu_2\alpha_2(1 - \alpha_1)}{\alpha_1(1 - \alpha_2)} - \alpha_1\right)(\mu_2 - 1)(1 - \alpha_2)}$$

$$\frac{\xi_1}{\xi_2} = \frac{\alpha_1\left(\frac{\mu_2\alpha_2(1 - \alpha_1)}{\alpha_1(1 - \alpha_2)} - 1\right)(1 + \alpha_2\mu_2 - \alpha_2)}{\alpha_2\left(1 + \frac{\mu_2\alpha_2(1 - \alpha_1)}{(1 - \alpha_2)} - \alpha_1\right)(\mu_2 - 1)}$$

$$\frac{\xi_1}{\xi_2} = \frac{\left(\mu_2\alpha_2 \cdot \frac{1 - \alpha_1}{1 - \alpha_2} - \alpha_1\right)(1 + \alpha_2\mu_2 - \alpha_2)}{\alpha_2(\mu_2 - 1)\left(1 + \mu_2\alpha_2 \cdot \frac{1 - \alpha_1}{1 - \alpha_2} - \alpha_1\right)}$$

Take system 1 =FPS, $\alpha_1 = 0$; system 2 = LRB, $\alpha_2 = 1/10$:

$$\frac{\xi_1}{\xi_2} = \frac{\xi_{FPS}}{\xi_{LRB}} = \frac{\left(\mu_2 \cdot \frac{1}{10} \cdot \frac{1}{9/10} - 0\right)\left(1 + \frac{1}{10}\mu_2 - \frac{1}{10}\right)}{\frac{1}{10}(\mu_2 - 1)\left(1 + \mu_2 \cdot \frac{1}{10} \cdot \frac{1}{9/10} - 0\right)}$$

$$\frac{\xi_1}{\xi_2} = \frac{\xi_{FPS}}{\xi_{LRB}} = \frac{10\left(\mu_2 \cdot \frac{1}{9}\right)\left(1 + \frac{1}{10}\mu_2 - \frac{1}{10}\right)}{(\mu_2 - 1)\left(1 + \mu_2 \cdot \frac{1}{9}\right)}$$

$$\frac{\xi_1}{\xi_2} = \frac{\xi_{FPS}}{\xi_{LRB}} = \frac{10(\mu_2)\left(1 + \frac{1}{10}\mu_2 - \frac{1}{10}\right)}{9(\mu_2 - 1)\left(1 + \mu_2 \cdot \frac{1}{9}\right)} = \frac{\mu_2}{\mu_2 - 1} \cdot \frac{9 + \mu_2}{9 + \mu_2} = \frac{\mu_2}{\mu_2 - 1} \qquad \text{(Eq. C-1)}$$

Also starting from the general expression for equivalent viscous damping, it is possible to determine the maximum possible equivalent damping for a specified post-yield stiffness ratio (α) and the ductility (μ) at which this maximum possible damping occurs.

$$\xi = \frac{2(\mu - 1)(1 - \alpha)}{\pi\mu(1 + \alpha\mu - \alpha)}$$

Differentiate with respect to μ:

$$\xi = \frac{u}{v}$$

$$u = 2(1 - \alpha)(\mu - 1)$$

$$v = \pi\mu(1 + \alpha\mu - \alpha) = \pi\mu - \pi\mu\alpha + \pi\mu^2\alpha$$

$$\frac{d}{d\mu}\xi = \frac{d}{d\mu}\left(\frac{u}{v}\right) = \frac{u'v - v'u}{v^2}$$

$$u' = 2(1 - \alpha)$$

$$v' = \pi - \pi\alpha + 2\pi\mu\alpha = \pi(1 - \alpha + 2\mu\alpha)$$

$$\frac{d}{d\mu}\xi = \frac{2(1 - \alpha)(\mu\pi)(1 + \alpha\mu - \alpha) - \pi(1 - \alpha + 2\mu\alpha)(2)(1 - \alpha)(\mu - 1)}{[\pi\mu(1 + \alpha\mu - \alpha)]^2}$$

To find the μ-value which maximizes ξ, set the derivative equal to zero.

$$2(1 - \alpha)(\mu\pi)(1 + \alpha\mu - \alpha) - \pi(1 - \alpha + 2\mu\alpha)(2)(1 - \alpha)(\mu - 1) = 0$$

$$(\mu)(1+\alpha\mu-\alpha)-(1-\alpha+2\mu\alpha)(\mu-1)=0$$

$$\mu+\alpha\mu^2-\alpha\mu-\mu+1+\alpha\mu-\alpha-2\alpha\mu^2+2\alpha\mu=0$$

$$\alpha\mu^2+1-\alpha-2\alpha\mu^2+2\alpha\mu=0$$

$$\alpha\mu^2-2\alpha\mu-(\alpha-1)=0$$

$$\mu=\frac{2\alpha\pm\sqrt{4\alpha^2+4\alpha(1-\alpha)}}{2\alpha}$$

$$\mu=\frac{2\alpha\pm\sqrt{4\alpha}}{2\alpha}=\frac{\alpha\pm\sqrt{\alpha}}{\alpha}\cdot\left(\frac{\sqrt{\alpha}}{\sqrt{\alpha}}\right)=\frac{\alpha\sqrt{\alpha}\pm\alpha}{\alpha\sqrt{\alpha}}$$

$$\mu=1\pm\frac{1}{\sqrt{\alpha}}$$

Since we are interested only in cases for which $\mu > 0$, the negative root has no physical meaning and may be disregarded.

$$\mu=1+\frac{1}{\sqrt{\alpha}} \qquad \text{(Eq. C-2)}$$

The expression in Equation C-2 is the ductility at which maximum possible damping occurs. To find the maximum possible damping, substitute Equation C-2 into the equivalent damping equation.

$$\mu=1+\frac{1}{\sqrt{\alpha}}$$

$$\mu-1=\frac{1}{\sqrt{\alpha}}$$

$$\xi_{max} = \frac{2\left(\frac{1}{\sqrt{\alpha}}\right)(1-\alpha)}{\pi\left(1+\frac{1}{\sqrt{\alpha}}\right)\left(1+\alpha\left(1+\frac{1}{\sqrt{\alpha}}\right)-\alpha\right)}$$

$$\xi_{max} = \frac{2\left(\frac{1}{\sqrt{\alpha}}\right)(1-\alpha)}{\pi\left(\frac{\sqrt{\alpha}+1}{\sqrt{\alpha}}\right)\left(1+\alpha+\frac{\alpha}{\sqrt{\alpha}}-\alpha\right)}$$

$$\xi_{max} = \frac{2\left(\frac{1}{\sqrt{\alpha}}\right)(1-\alpha)}{\pi\left(\frac{\sqrt{\alpha}+1}{\sqrt{\alpha}}\right)\left(1+\frac{\alpha}{\sqrt{\alpha}}\right)} = \frac{2\left(\frac{1}{\sqrt{\alpha}}\right)(1-\alpha)}{\pi\left(\frac{\sqrt{\alpha}+1}{\sqrt{\alpha}}\right)\left(1+\sqrt{\alpha}\right)}$$

$$\xi_{max} = \frac{2(1-\alpha)}{\pi\left(1+\sqrt{\alpha}\right)^2} \qquad \text{(Eq. C-3)}$$

Another problem which may arise is the estimation of inelastic displacement spectra from inelastic acceleration spectra. For the elastic case, this is simple enough. Equation C-4 provides the conversion.

$$SD_{EL}(T) = SA_{EL}(T) \cdot g \cdot \left(\frac{T}{2\pi}\right)^2 \qquad \text{(Eq. C-4)}$$

For the inelastic case, suppose that the available result is inelastic spectral acceleration, $SA_{INEL}(T)$. Figure C-1 presents the parameters necessary to estimate inelastic spectral displacement, $SD_{INEL}(T)$, from the inelastic spectral acceleration.

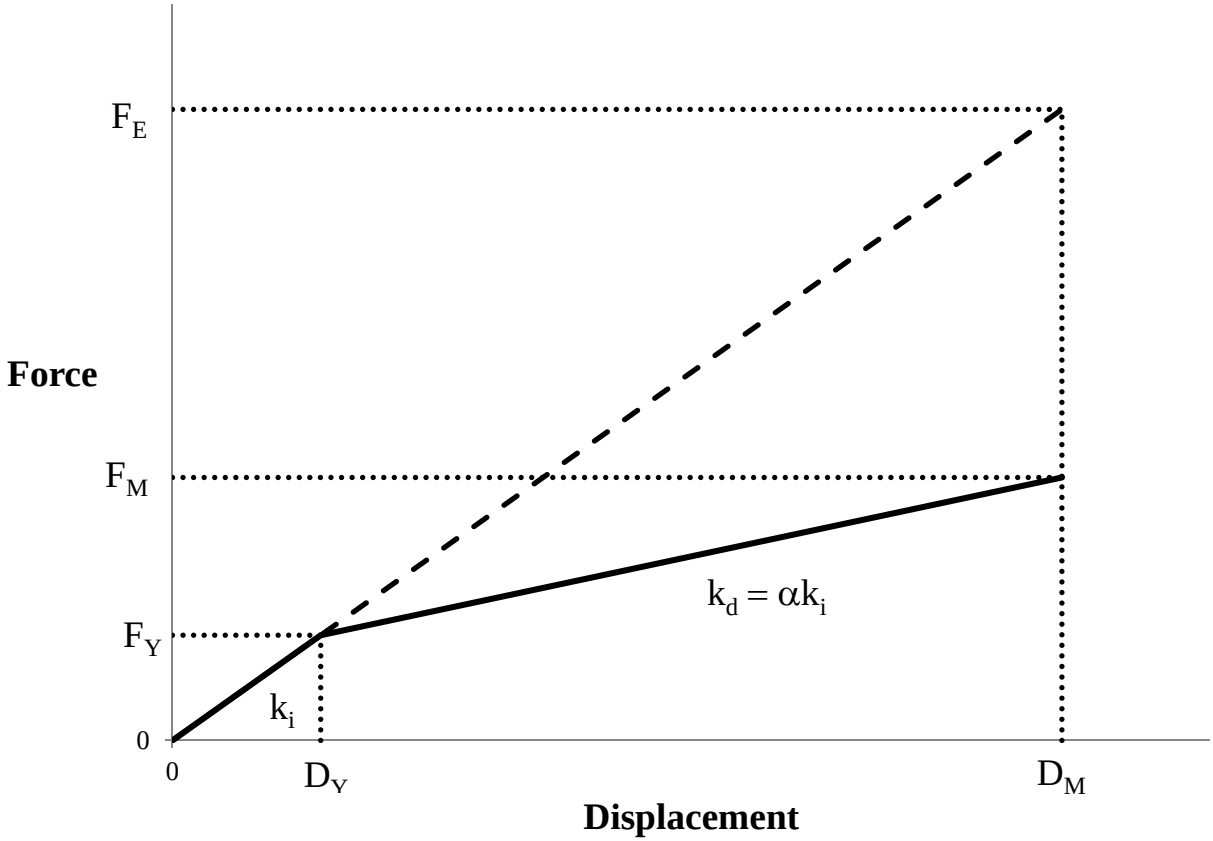

Figure C-1. Inelastic Displacement Parameters

From similar triangles and using the fact that $\mu = D_M/D_Y$:

$$\frac{F_E}{D_M} = \frac{F_Y}{D_Y} = \frac{F_M - \alpha k_i (D_M - D_Y)}{D_Y}$$

$$\frac{F_E}{D_M} = \frac{F_M - \alpha \frac{F_Y}{D_Y}(D_M - D_Y)}{D_Y}$$

$$\frac{F_E}{F_M} = \frac{D_M - \alpha \frac{F_Y}{D_Y}\frac{D_M}{F_M}(D_M - D_Y)}{D_Y}$$

$$\frac{F_E}{F_M} = \frac{D_M}{D_Y} - \alpha \frac{F_Y}{F_M}\frac{D_M^2}{D_Y^2} + \alpha \frac{F_Y}{F_M}\frac{D_M}{D_Y}$$

$$\frac{F_E}{F_M} = \mu - \alpha \frac{F_Y}{F_M}\mu^2 + \alpha \frac{F_Y}{F_M}\mu$$

$$\frac{F_E}{F_M} = \mu - \alpha\mu^2 \frac{F_Y}{F_E}\frac{F_E}{F_M} + \alpha\mu \frac{F_Y}{F_E}\frac{F_E}{F_M}$$

But $F_Y/F_E = 1/\mu$, so:

$$\frac{F_E}{F_M} = \mu - \alpha\mu \frac{F_E}{F_M} + \alpha \frac{F_E}{F_M}$$

$$\frac{F_E}{F_M}(1 + \alpha\mu - \alpha) = \mu$$

$$\frac{F_E}{F_M} = \frac{\mu}{(1 + \alpha\mu - \alpha)} \qquad \text{(Eq. C-5)}$$

For inelastic displacement spectra we want D_M as a function of the initial period, T_i.

$$T_i = 2\pi\sqrt{\frac{m}{k_i}} = 2\pi\sqrt{\frac{W}{g \cdot k_i}} = 2\pi\sqrt{\frac{W \cdot D_Y}{g \cdot F_Y}} = 2\pi\sqrt{\frac{W \cdot D_M}{g \cdot F_E}}$$

$$D_M = \frac{F_E}{W} \cdot g\left(\frac{T_i}{2\pi}\right)^2$$

$$D_M = \frac{F_M}{W} \cdot \frac{F_E}{F_M} \cdot g\left(\frac{T_i}{2\pi}\right)^2$$

But F_M/W is simply the inelastic spectral acceleration, $SA_{INEL}(T_i)$, D_M is the inelastic displacement, $SD_{INEL}(T_i)$, and F_E/F_M is given by equation C-5.

$$SD_{INEL}(T_i) = D_M = SA_{INEL}(T_i) \cdot \frac{\mu}{(1 + \alpha\mu - \alpha)} \cdot g\left(\frac{T_i}{2\pi}\right)^2 \qquad \text{(Eq. C-6)}$$

It will provide valuable insight to explore further into the substitute structure method - secant stiffness based, effective period simplified analysis - used in the AASHTO isolation design. Specifically, find the inelastic displacement amplification factor implied by the method. First, an expression for the effective period in terms of the initial period will be needed. This simply requires a relationship between the initial and secant stiffness values

.

$$k_E D_M = k_i D_Y + \alpha k_i (D_M - D_Y)$$

Divide through by $k_i D_M$.

$$\frac{k_E}{k_i} = \frac{D_Y}{D_M} + \frac{\alpha (D_M - D_Y)}{D_M}$$

$$\frac{k_E}{k_i} = \frac{1}{\mu} + \alpha - \frac{\alpha}{\mu} = \frac{1 + \alpha\mu - \alpha}{\mu}$$

Now the initial and effective periods are given by:

$$T_i = 2\pi \sqrt{\frac{W}{g \cdot k_i}} \qquad T_{EFF} = 2\pi \sqrt{\frac{W}{g \cdot k_E}} = 2\pi \sqrt{\frac{W}{g \cdot k_i \cdot \left(\frac{k_E}{k_i}\right)}}$$

$$T_{EFF} = T_i \sqrt{\frac{\mu}{1 + \alpha\mu - \alpha}} \qquad \text{Eq. (C-7)}$$

The elastic spectral displacement at period T_i is a function of the elastic spectral acceleration and is given by:

$$SD_{EL}(T_i) = SA_{EL}(T_i) \cdot g \cdot \left(\frac{T_i}{2\pi}\right)^2$$

The inelastic spectral displacement - also a function of elastic spectral acceleration, but at period T_{EFF} instead of period T_i - will require the use of a reduction factor, R_ξ, for increased damping in the inelastic case due to hysteretic behavior. The three rules for this factor used in this study are repeated here.

$$1/B_L = R_\xi = \left(\frac{0.05}{\xi_{EFF}}\right)^{0.30}, AASHTO$$

$$1/B_L = R_\xi = \left(\frac{0.10}{0.05 + \xi_{EFF}}\right)^{0.50}, Eurocode$$

$$1/B_L = R_\xi = \left(\frac{0.07}{0.02 + \xi_{EFF}}\right)^{0.25}, Velocity\ pulse\ conditions$$

$$\xi_{EFF} = \xi_o + \frac{2(\mu - 1)(1 - \alpha)}{\pi\mu(1 + \alpha\mu - \alpha)}$$

The substitute structure method estimates inelastic displacement as follows.

$$SD_{INEL}(T_i) = SA_{EL}(T_{EFF}) \cdot g \cdot \left(\frac{T_{EFF}}{2\pi}\right)^2 \cdot R_\xi$$

When code-based spectral shape is used in the analysis and the effective period is greater than T_S, the elastic spectral acceleration is determined by:

$$SA_{EL}(T_{EFF}) = \frac{S_{D1}}{T_{EFF}}$$

In this case, the elastic and inelastic spectral displacements may be simplified.

$$SD_{EL}(T_i) = \frac{S_{D1}}{T_i} \cdot g \cdot \left(\frac{T_i}{2\pi}\right)^2 = \frac{S_{D1} \cdot g}{4\pi^2} \cdot T_i$$

$$SD_{INEL}(T_i) = \frac{S_{D1}}{T_{EFF}} \cdot g \cdot \left(\frac{T_{EFF}}{2\pi}\right)^2 \cdot R_\xi = \frac{S_{D1} \cdot g}{4\pi^2} \cdot T_{EFF} \cdot R_\xi$$

$$C_\mu = \frac{SD_{INEL}(T_i)}{SD_{EL}(T_i)} = \frac{T_{EFF}}{T_i} \cdot R_\xi = R_\xi \cdot \sqrt{\frac{\mu}{1 + \alpha\mu - \alpha}}$$

So it is now clear that whenever both the initial and effective periods fall within the region of constant spectral velocity on the design response spectrum, then the inelastic displacement amplification factor is constant. In other regions of the design spectrum, the displacement amplification for inelastic behavior effects is either larger (at short periods) or smaller (at long periods) compared to this constant value.

APPENDIX D - ROTATION OF GROUND MOTION RECORDS

As discussed in CHAPTER 3, one measure of ground motion intensity is “GMRotD50”, the median value of the geometric mean spectrum at a particular period of interest over all rotation angles from 0 to 90 degrees. Note the periodicity of 90 degrees in ground motion rotation - once we have rotated the as-recorded components by 90 degrees we are, in essence back where we started form in term of the geometric mean - H1 is now H2 and H2 is now H1.

“GMRotD100” is the maximum value of the geometric mean over all rotation angles at a particular period of interest, and “GMRotD00” is the minimum value. The “D” in the terminology used for these parameters indicates that the particular rotation angle which produces the maximum response depends upon the period under question. So, the rotation angle which maximizes the geometric mean at a period of 1 second is not necessarily the same as the rotation angle which maximizes the PGA geometric mean. Another measure of seismic intensity is “GMRotI50” - the median geometric mean at a period-independent rotation angle determined for a particular ground motion so as to “minimize the spread of the rotation-dependent geometric mean” (Boore, et al., August 2006). The referenced study goes so far as to say that the ground motion intensity measure used in developing ground motion prediction equations for the Pacific Earthquake Engineering Research Center Next Generation Attenuation Project is “GMRotI50”.

The analyst must understand the basis of the GMPM’s used in the PSHA to develop the design, target spectrum. Codes and specifications must begin to be explicit in defining the basis of acceleration (or velocity or displacement) spectra generated by the provisions of said code or specification. The basis for most current code design spectrum requirements is either 2002 USGS data or updated 2008 USGS data. USGS data from 2002 is based upon PSHA which uses the as-recorded geometric mean - GMAR - as the dependent variable in the GMPM’s. The updated

2008 USGS data are based upon GMPM's which use GMRotI50 - the period-independent rotated geometric mean minimizing spread of the rotation-dependent geometric mean - as the dependent variable.

The tempting assumption to make is that the appropriate geometric mean to be used in determining scaling factors is the as-recorded geometric mean since the as-recorded motions are the ones which are typically applied to the computer models of structures. However, any time 2008 USGS data are used to obtain the design target spectra, GMRotI50 would be the more accurate choice. It thus seem logical to conclude that the appropriate measure to be used for scaling ground motions is not the as-recorded geometric mean, but "GMRotI50", provided 2008 USGS data sets are adopted. The answer is not clear, especially since ground motions are typically applied to structural models in the as-recorded orientation. Nevertheless, if "GMRotI50" is the parameter upon which predictive equations used to develop design target spectra are based, a strong argument should be made in favor of using "GMRotI50" to scale ground motion pairs, even if the as-recorded components are applied to the structure.

Software developed at the USGS to enable computation of the effect of rotation upon ground motion geometric mean response (Boore, 2009) has been used to analyze several of the scaled ground motions (at the Site 1 DBE Hazard Level) used in this study. Figures D-1 through D-5 represent the variation in geometric mean with angle of rotation at a period of 1 second. Similar plots could be done for a range of periods. The variation is great for some records and not so great for others. For example, consider the Landers record in Figure D-1. The geometric mean used for scaling is the chart value at a rotation angle of 0 degrees. Note how much higher the geometric mean is for a rotation angle of about 30 degrees. If "GMRotI50" happened to

correspond to an angle of about 30 degrees for this record, then it could be argued that the record was scaled much too severely in using the as-recorded data. On the other hand, the variation in geometric mean with rotation angle is observed to be minimal across the entire range for the AXT (Wenchuan, China) record in Figure D-4.

The subset of scaled real records was further analyzed using TSPP to generate spectra at discrete periods. These plots are shown in Figures D-6 through D-19.

The as-recorded spectra are generally reasonably aligned with the GMRotI50 spectra in an overall sense for most of the records. See, for example, Kocaeli NGA number 1155 in Figure D-10.The two deviate quite a lot for records such as Chi-Chi NGA number 1265, Figure D-14 and Landers NGA number 0900 in Figure D-8.

Should records which are only minimally affected by rotation be purposefully chosen to minimize scatter in nonlinear time history analysis results? Probably not, even though the possible error in calculated scale factors is thereby reduced. Should scale factors be based upon as-recorded geometric mean spectra or GMRotI50 spectra? Does the answer to this question depend upon how the ground motions records are applied to the structural model? For the ground motions selected for this study, the effect is minimal but this cannot be guaranteed. Further research into the conditions under which the as-recorded geometric mean may be used, even when the target spectrum is GMRotI50-based, could save time and expense in nonlinear analyses.

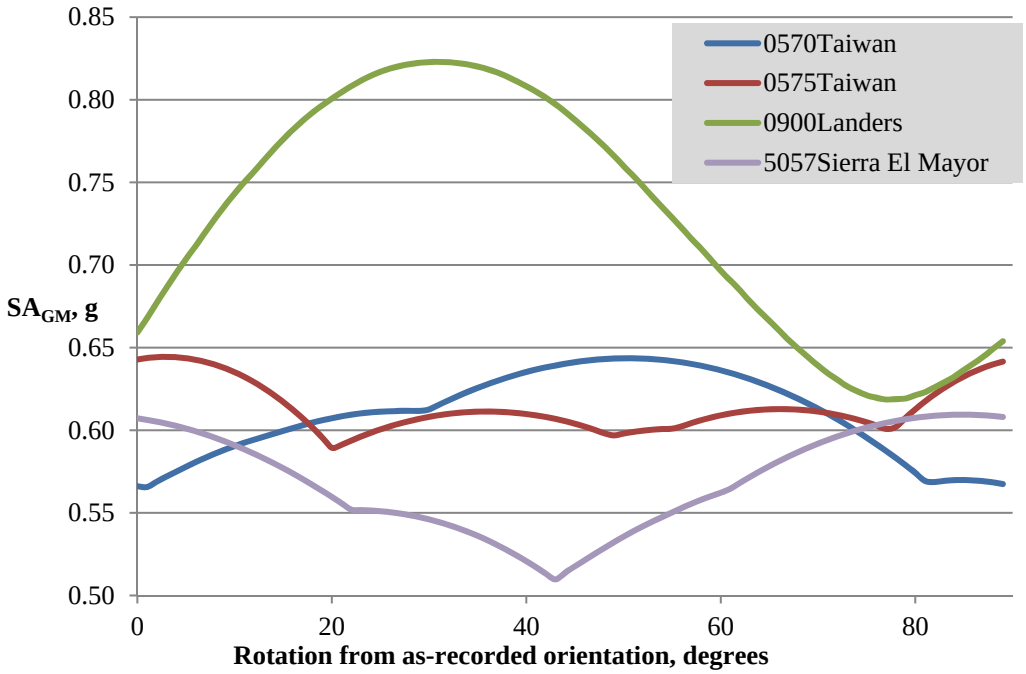

Figure D-1. Effect of Rotation on GM - Taiwan, Landers, SEM

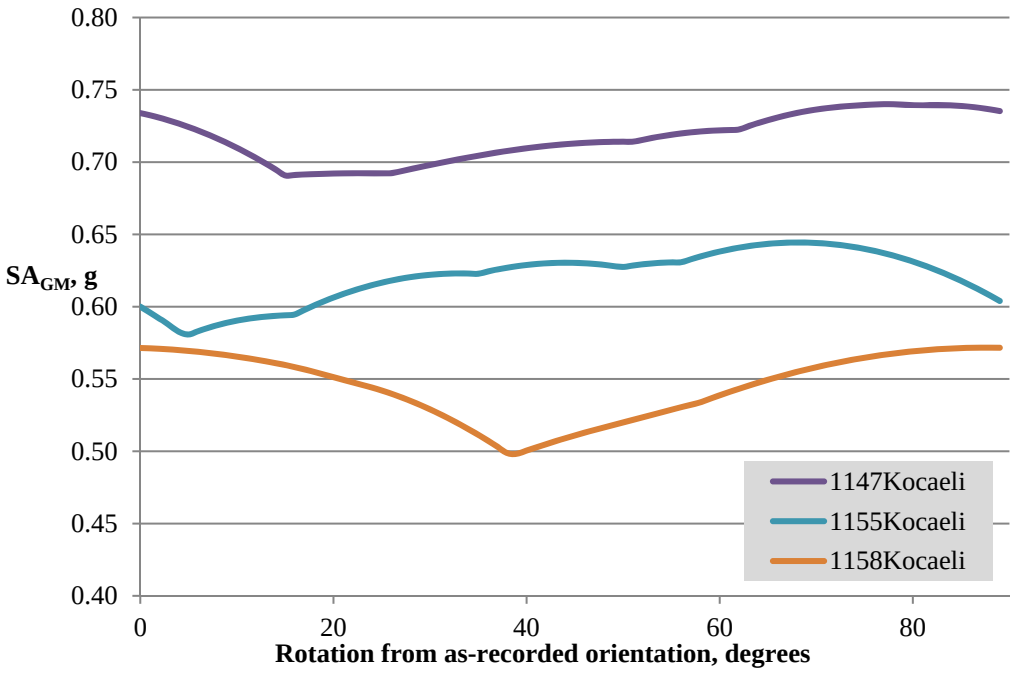

Figure D-2. Effect of Rotation on GM - Kocaeli

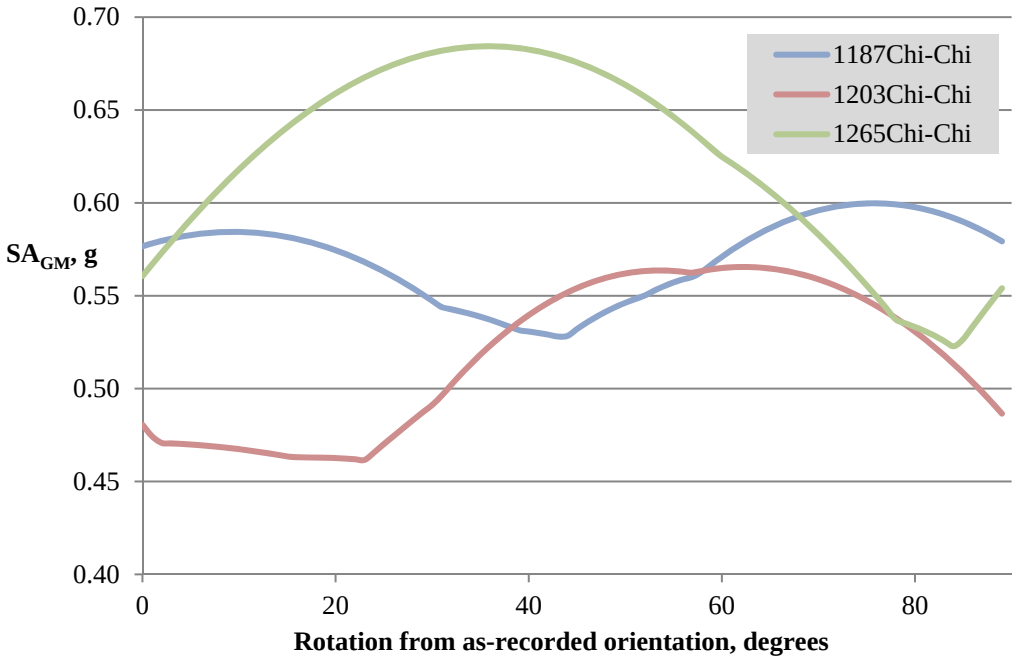

Figure D-3. Effect of Rotation on GM - Chi-Chi

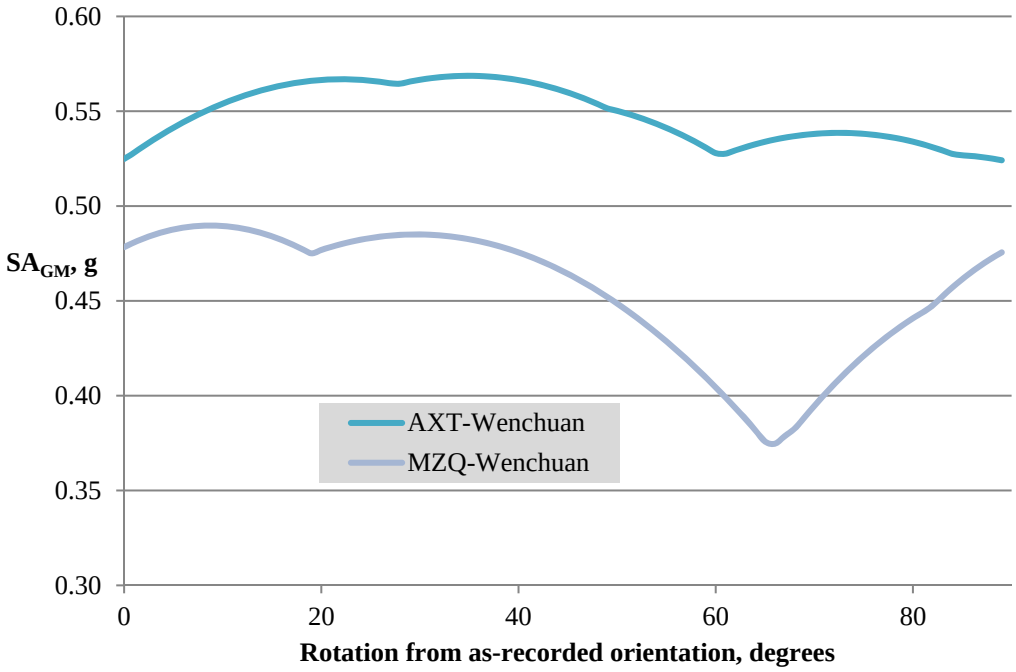

Figure D-4. Effect of Rotation on GM - Wenchuan

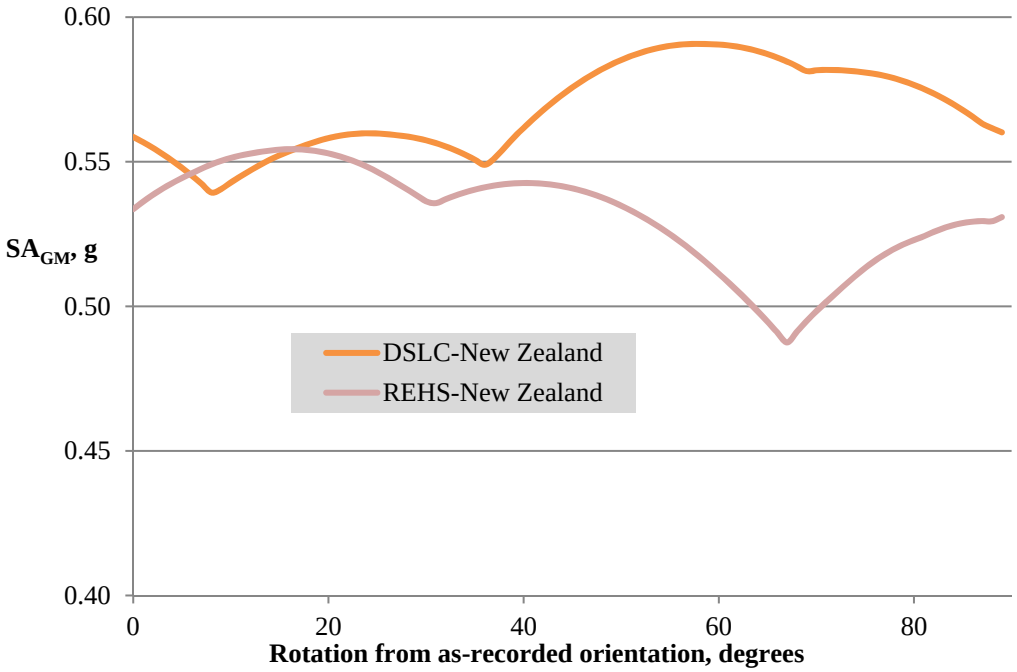

Figure D-5. Effect of Rotation on GM - Darfield, New Zealand

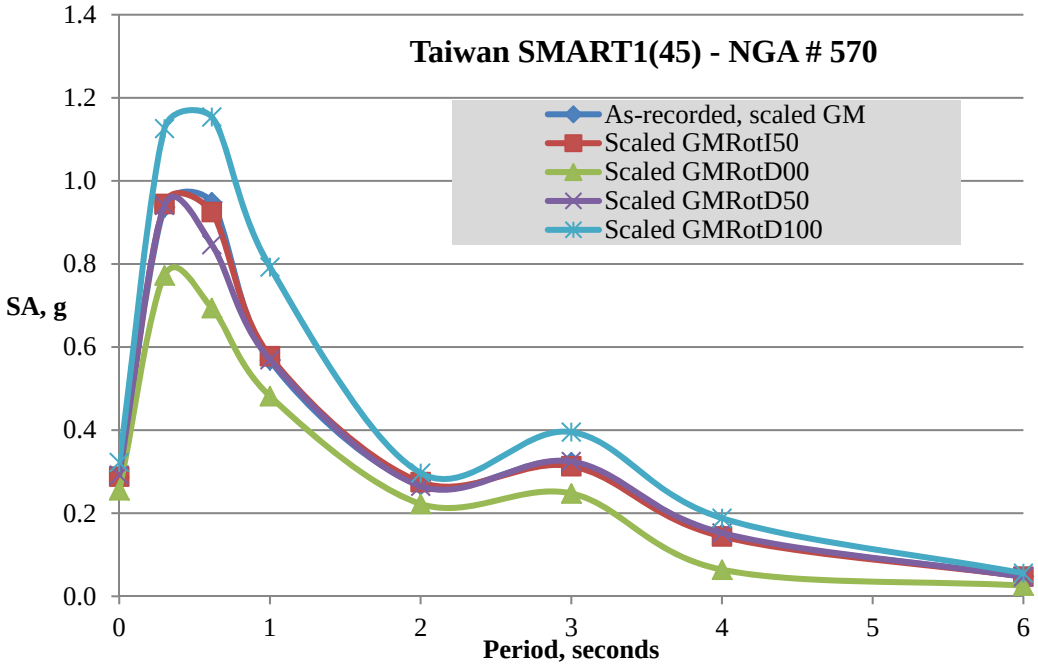

Figure D-6. GM Intensity Measures - 0570Taiwan

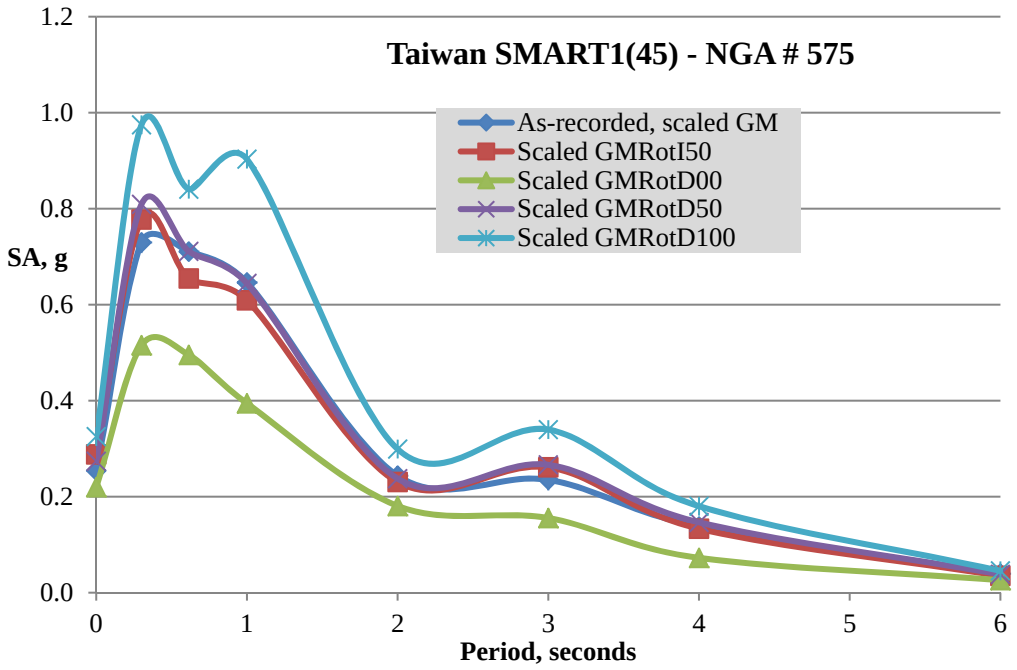

Figure D-7. GM Intensity Measures - 0575Taiwan

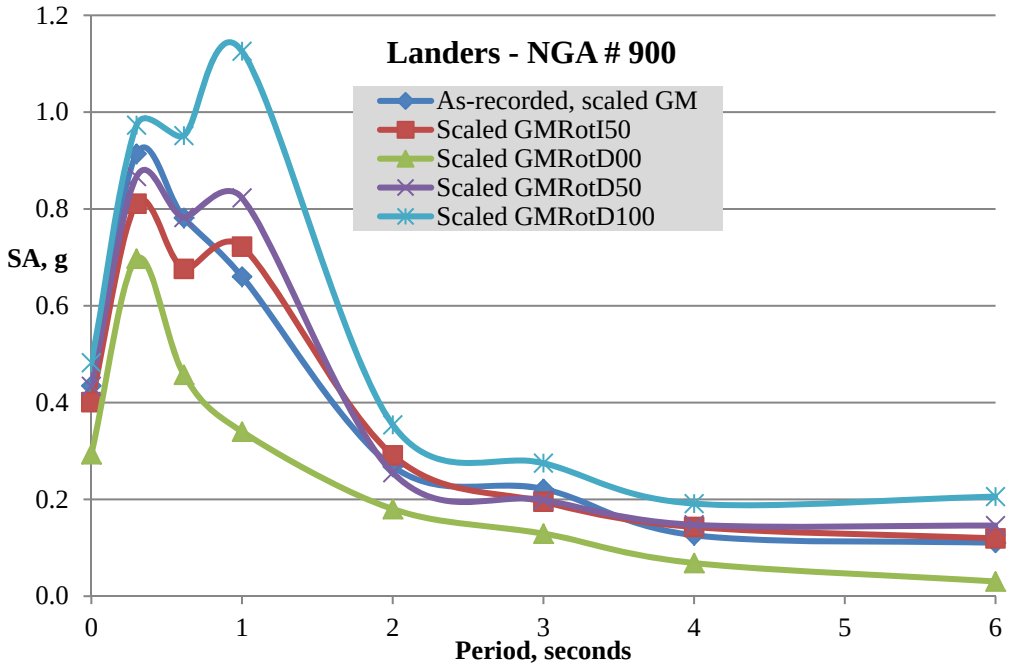

Figure D-8. GM Intensity Measures - 0900Landers

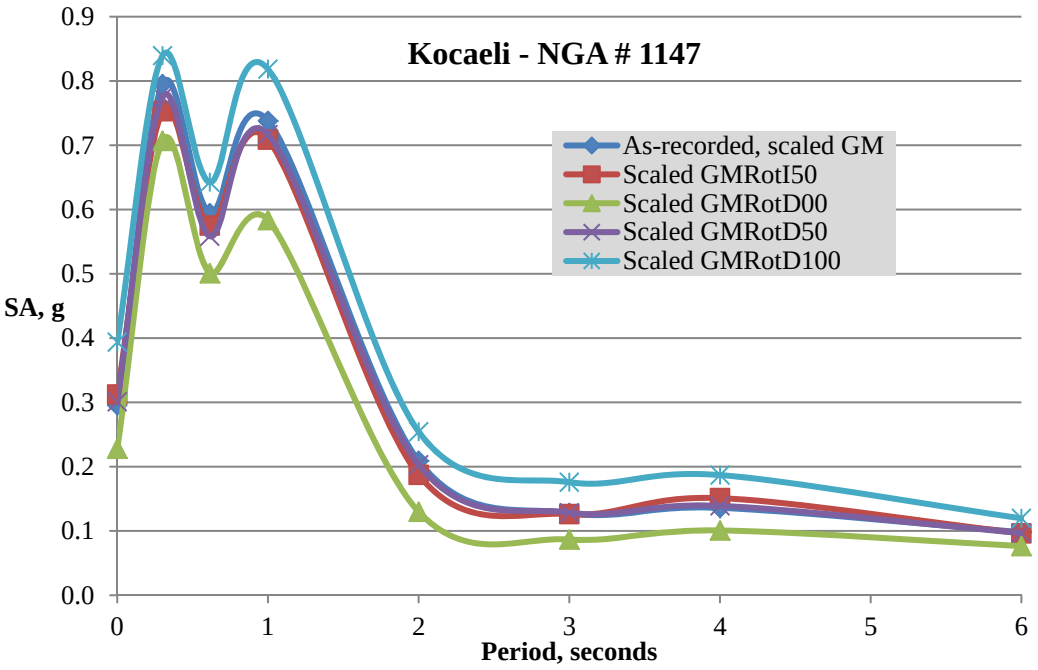

Figure D-9. GM Intensity Measures - 1147Kocaeli

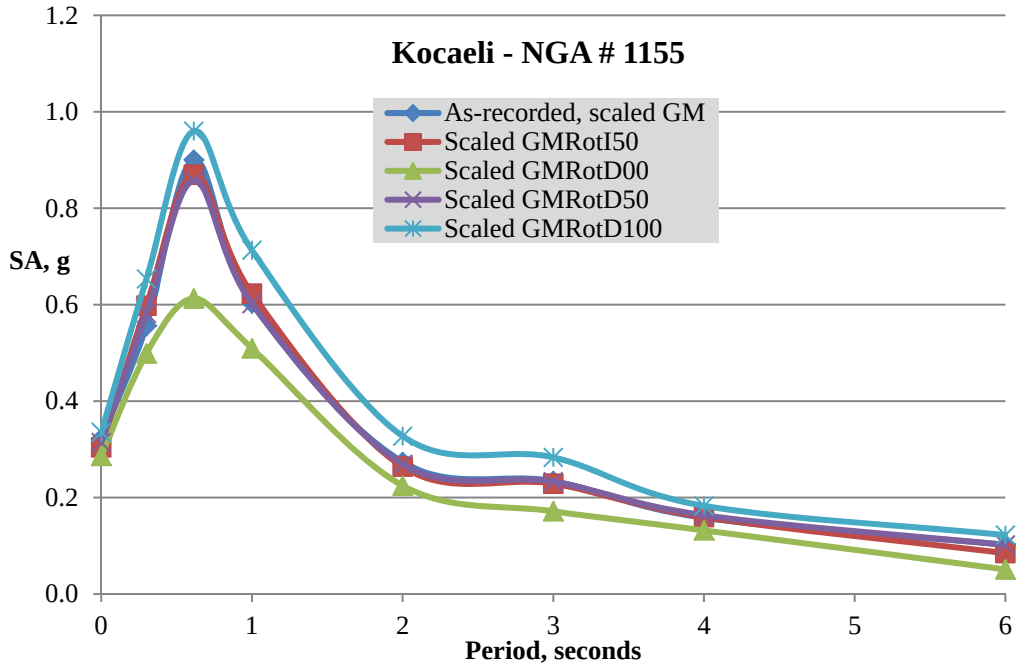

Figure D-10. GM Intensity Measures - 1155Kocaeli

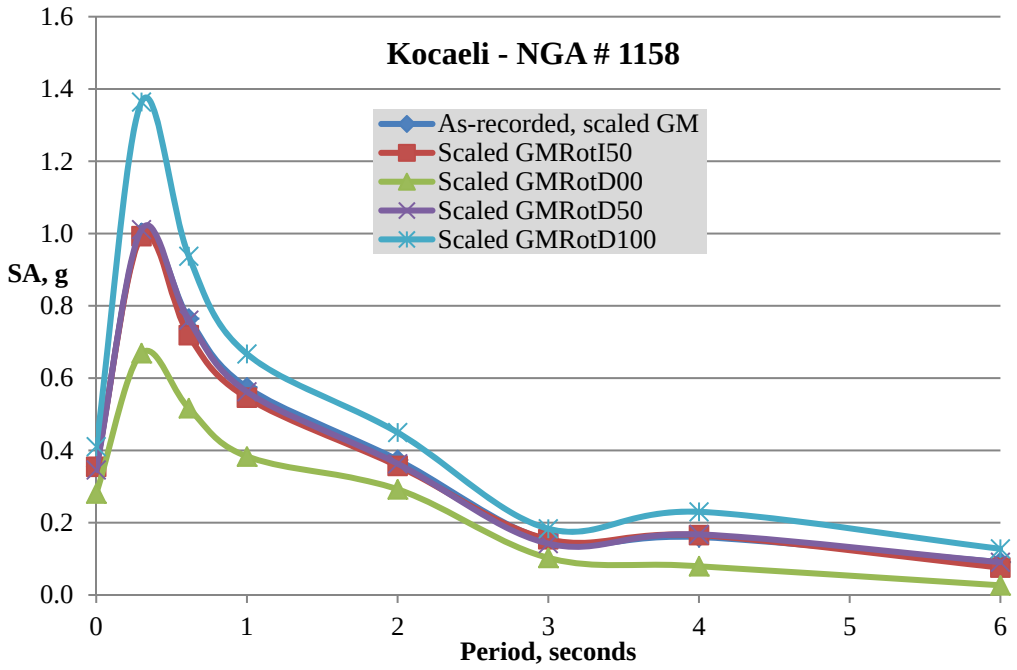

Figure D-11. GM Intensity Measures - 1158Kocaeli

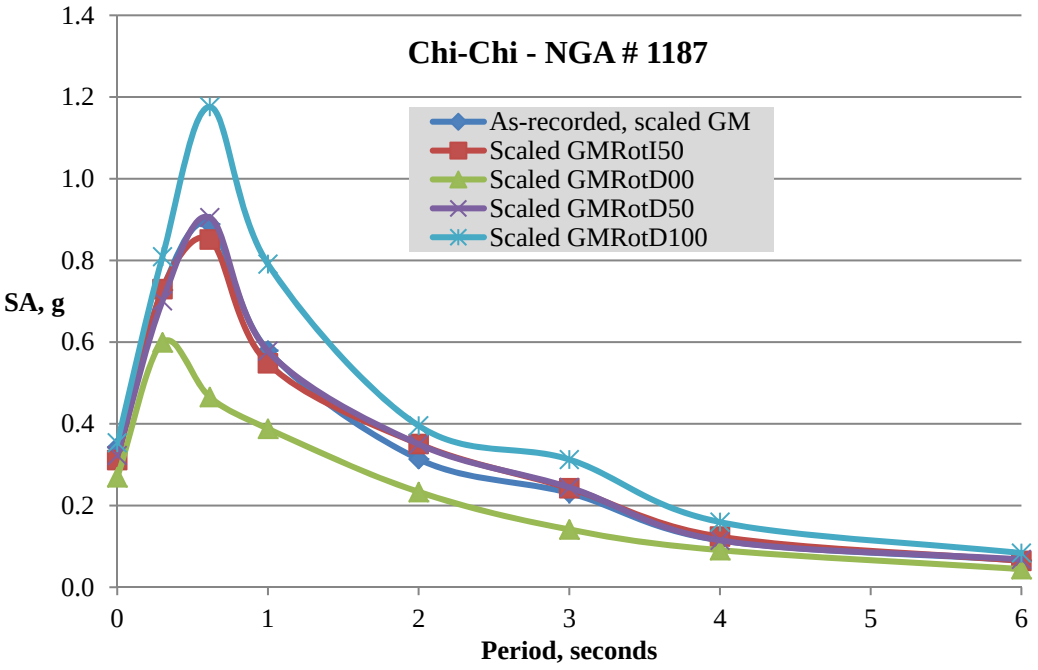

Figure D-12. GM Intensity Measures - 1187Chi-Chi

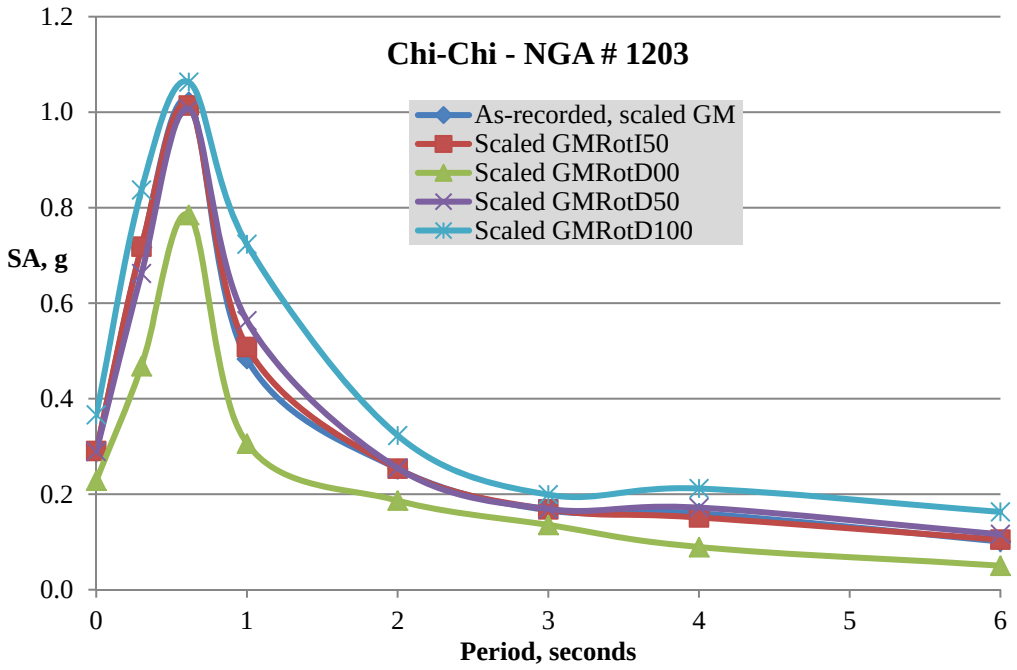

Figure D-13. GM Intensity Measures - 1203Chi-Chi

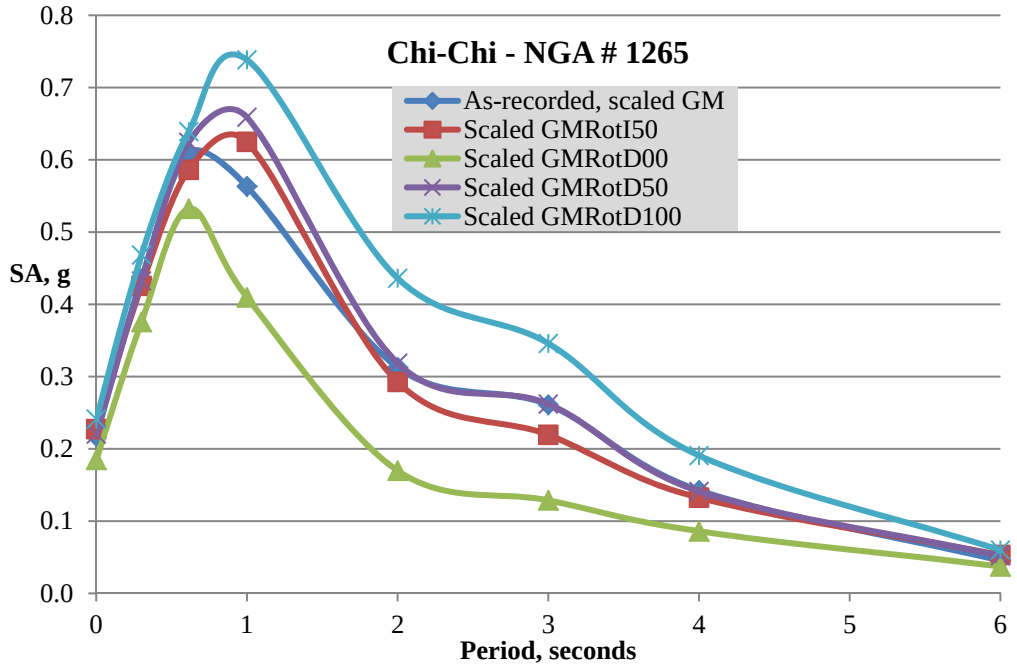

Figure D-14. GM Intensity Measures - 1265Chi-Chi

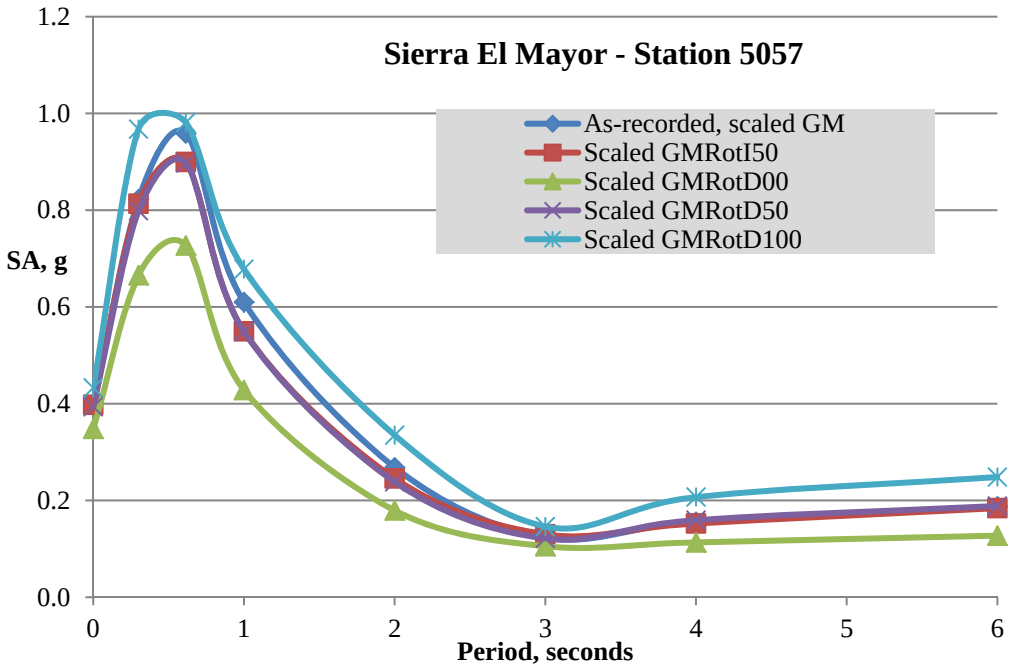

Figure D-15. GM Intensity Measures - 5057Sierra El Mayor

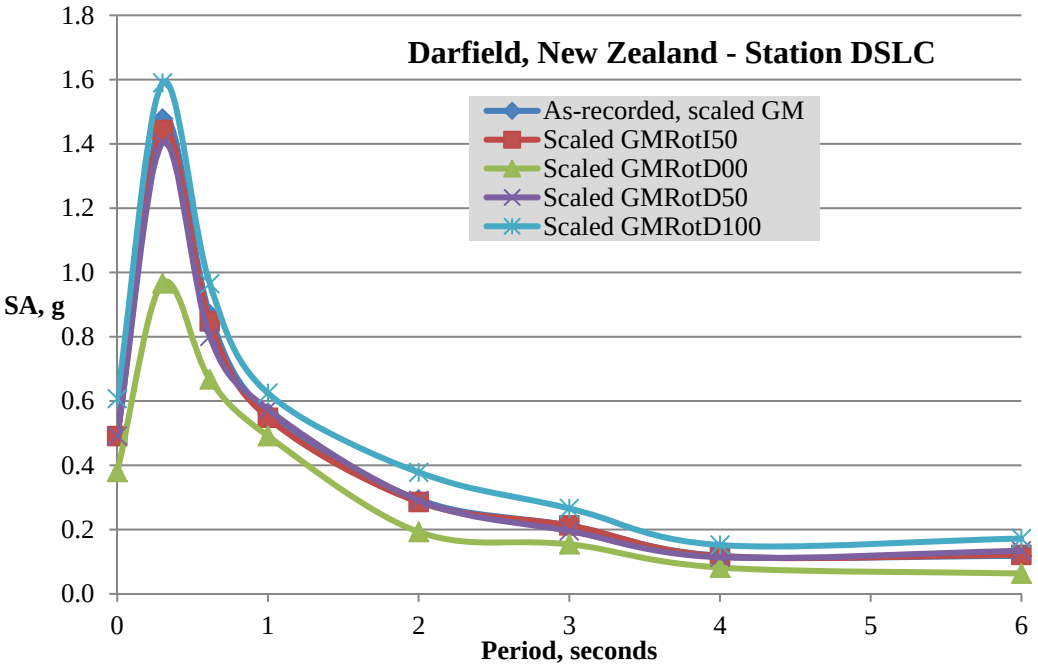

Figure D-16. GM Intensity Measures - DSLC-Darfield, NNZ

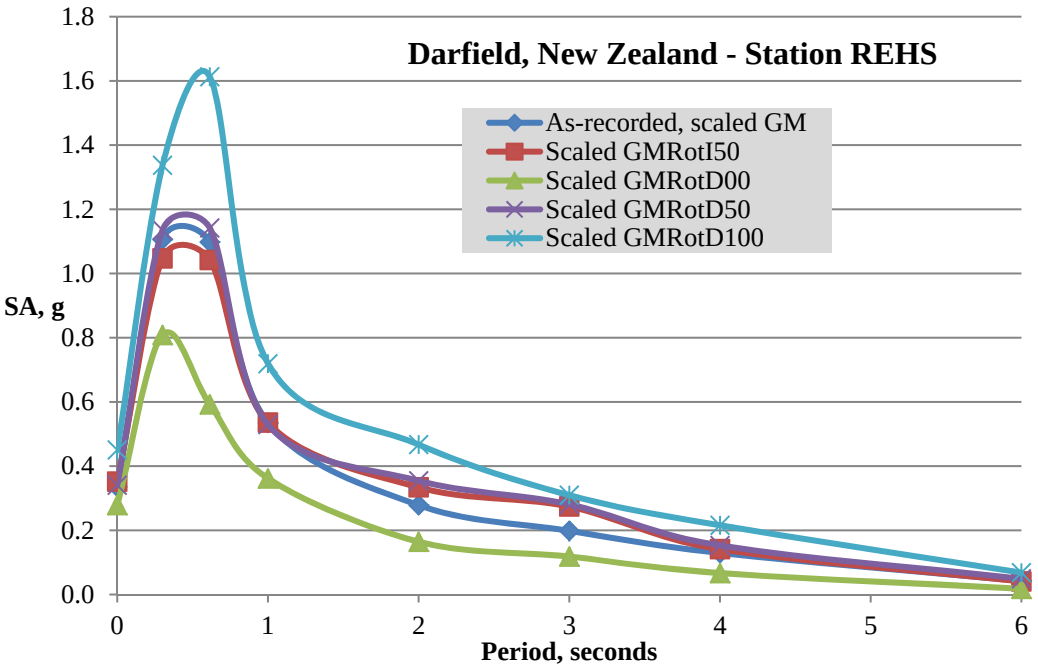

Figure D-17. GM Intensity Measures - REHS-Darfield

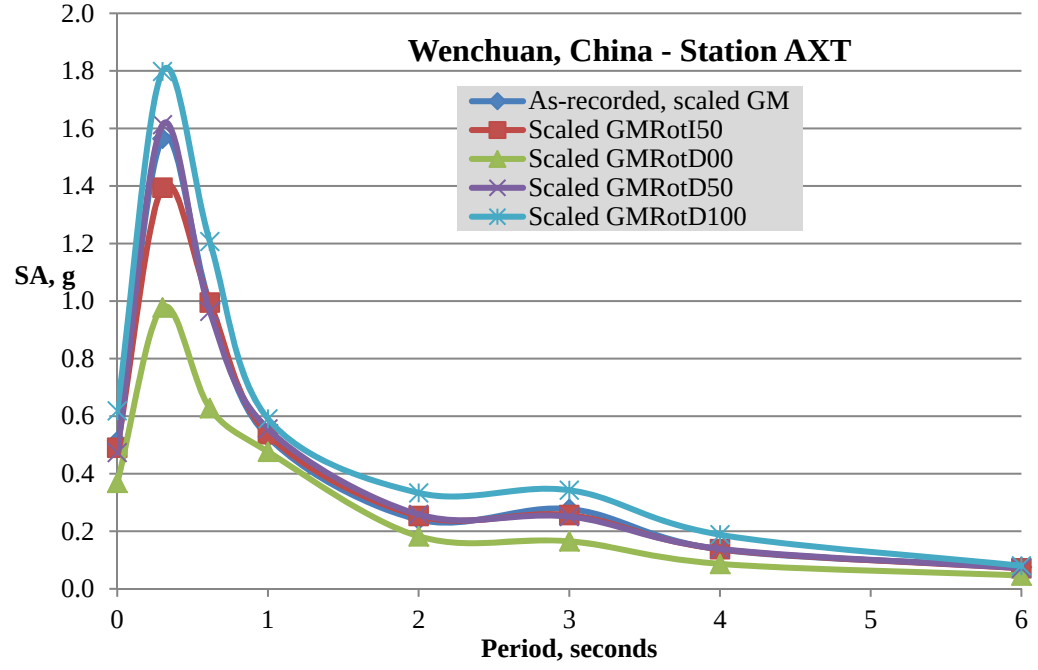

Figure D-18. GM Intensity Measures - AXT-Wenchuan

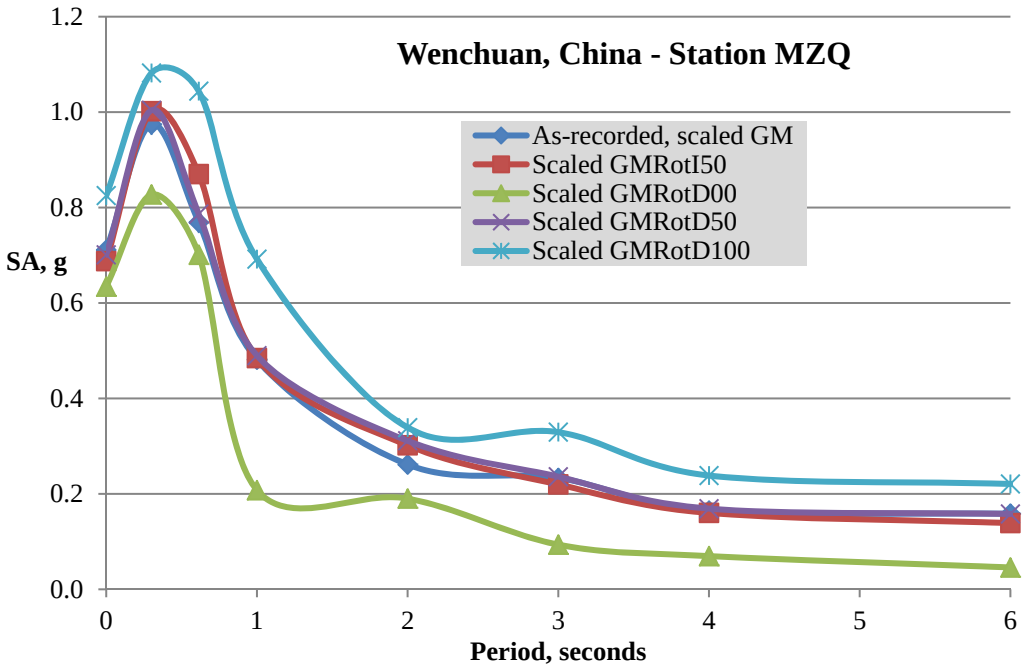

Figure D-19. GM Intensity Measures - MZQ-Wenchuan

APPENDIX E - GROUND MOTION SCALING EXAMPLES

The spectral shape compatibility of a record to a target may be measured by the root-mean-square-difference parameter D_{RMS} (Katsanos, et al., 2009) for an un-scaled record and the mean-square-error (MSE) of a scaled record (see Section 3.1.2).

$$D_{RMS} = \frac{1}{N}\sqrt{\sum_{i=1}^{N}\left(\frac{SA_{GM}(T_i)}{PGA_{GM}} - \frac{SA_{TAR}(T_i)}{PGA_{TAR}}\right)^2} \qquad \text{(E-1)}$$

$$MSE = \frac{\sum w(T_i)\cdot\{ln[SA_{TARGET}(T_i)] - ln[f\cdot SA_{GM}(T_i)]\}^2}{\sum w(T_i)} \qquad \text{(E-2)}$$

A visual inspection of spectral shape match to the target can be made by scaling records from a single event and examining the resulting fit to the target spectrum. Consider the 2010 Darfield (Canterbury) New Zealand earthquake. Scale eleven records from this event to minimize the MSE at five discrete periods (0.5, 0.8, 1, 2, and 4 seconds). This results in a mean spectrum as shown in Figure E-1.

Table E-1 lists the station data and the scale factors used to generate Figure E-1. Distances in the table are epicentral distance and shear wave velocity values are inferred, determined from station latitude and longitude along with the OpenSHA (Field, et al., 2003) software. The scale factors are all well within sometimes recommended limits of 0.25-4.0 and the visual match to the Site 1 DBE spectrum is quite good so the M7.1 Canterbury records appear to be good candidates for the NMSZ.

Figure E-2 provides a visual comparison of spectra from scaled records of the 1992 Landers earthquake (M7.28, a lower magnitude event than Canterbury) and the Site 1 DBE target. The scale factors for this event, given in Table E-2, are quite a bit higher than those for the Canterbury records and the fit is not quite as tight.

Several other plots and tabulated data sets are investigated. These include the Taiwan SMART1-45 (M7.30), Chi-Chi Taiwan (M7.62), Sierra El Mayor (M7.20), Kocaeli, Turkey (M7.52), and miscellaneous events which may not have met criteria for initial selection but which showed a good fit to the target spectra.

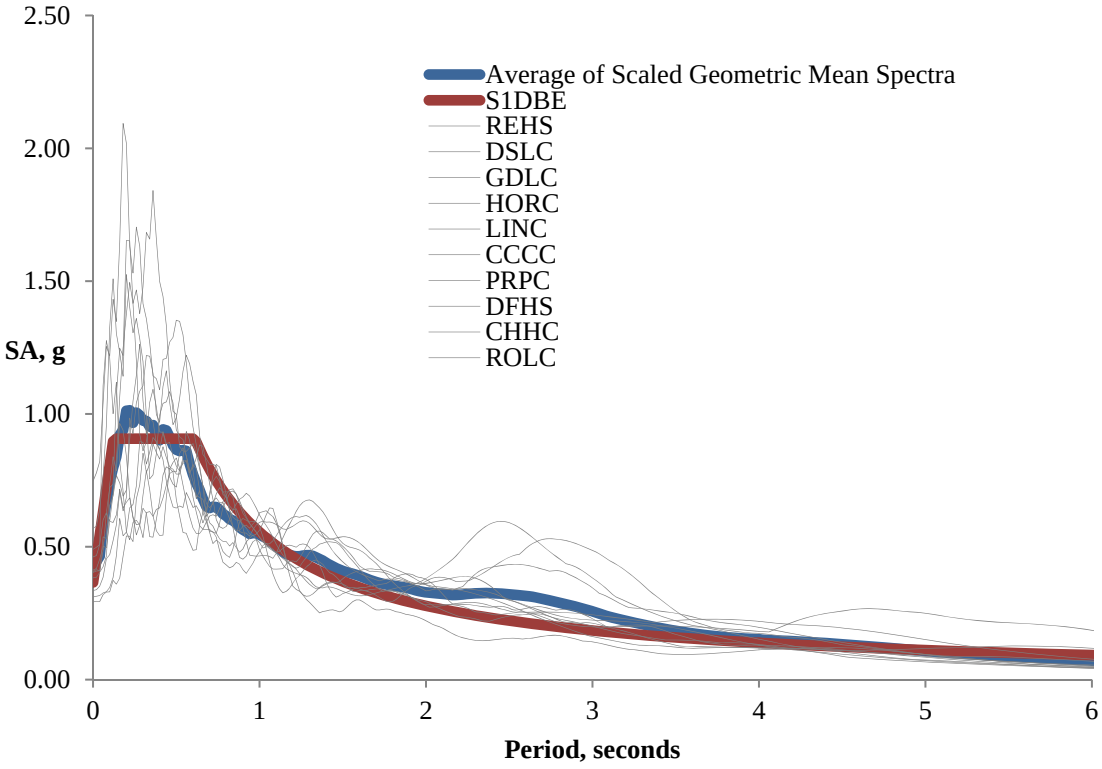

Figure E-1. Darfield, New Zealand Record Scaling - S1DBE

Table E-1. Darfield (Canterbury), New Zealand Station Data - S1DBE

Station	R_{EPI}, km	Vs30, m/s	Site Class	S1DBE SF
REHS	37	240	D	1.414
DSLC	13	259	D	2.039
GDLC	8	276	D	0.589
HORC	18	180	E	0.876
LINC	25	235	D	1.112
CCCC	38	231	D	1.476
PRPC	41	204	D	1.934
DFHS	9	278	D	1.610
CHHC	36	180	E	1.717
ROLC	17	264	D	1.217
TPLC	24	250	D	2.396

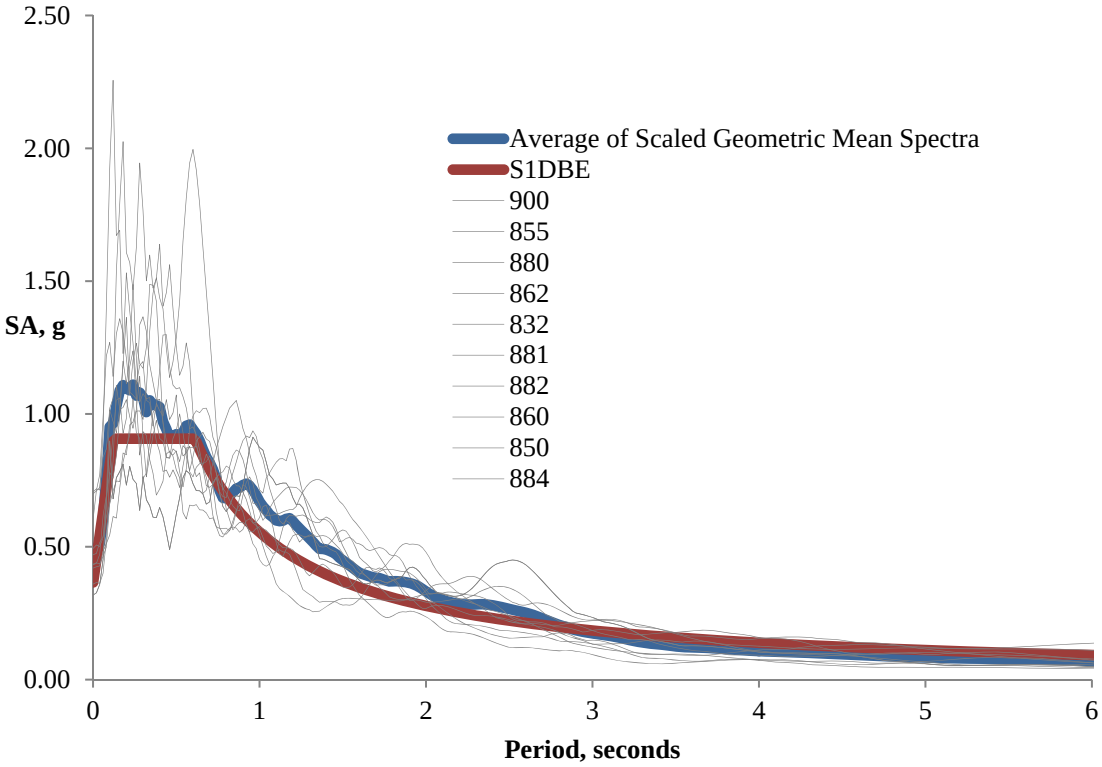

Figure E-2. Landers Record Scaling - S1DBE

Table E-2. Landers Station Data - S1DBE

NGA #	R_{jb}, km	Vs30, m/s	Site Class	S1DBE SF
900	24	354	D	1.956
855	63	345	D	5.106
880	27	345	D	4.848
862	54	345	D	3.883
832	69	271	D	2.812
881	17	345	D	2.872
882	27	345	D	3.252
860	69	339	D	7.870
850	22	345	D	3.073
844	36	207	D	3.951

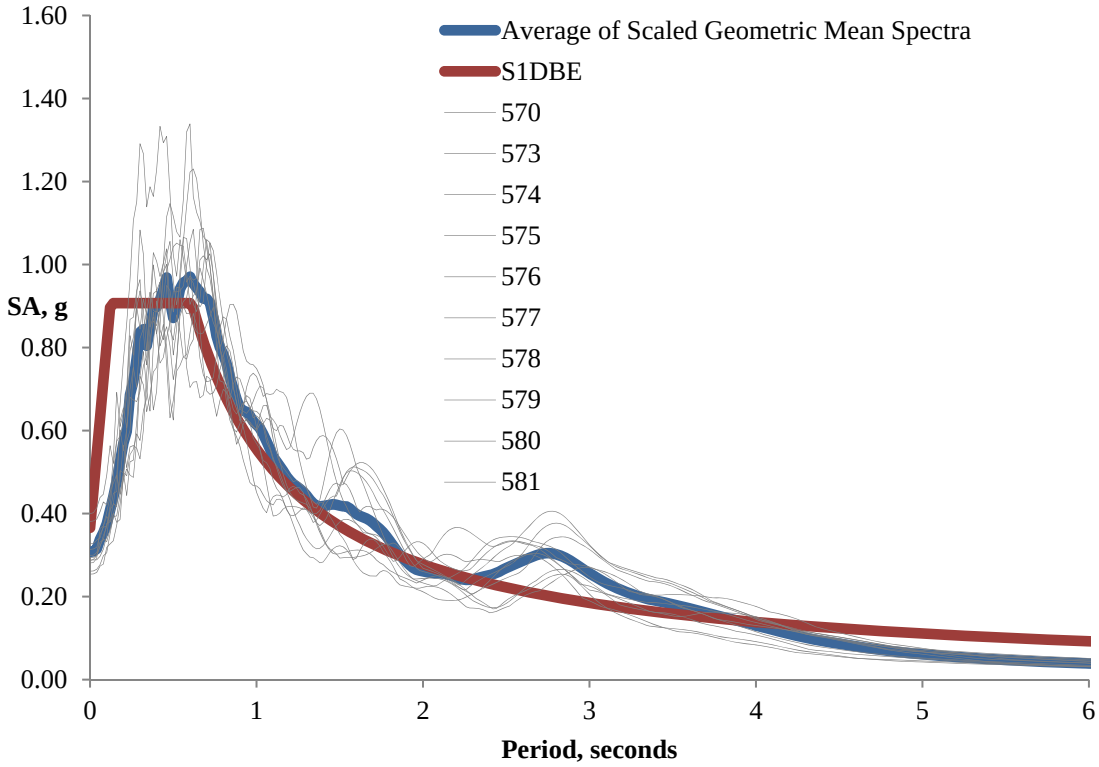

Figure E-3. Taiwan SMART1(45) Record Scaling - S1DBE

Table E-3. Taiwan SMART1(45) Station Data - S1DBE

NGA #	R_{jb}, km	Vs30, m/s	Site Class	S1DBE SF
570	56	274	D	2.102
573	56	274	D	2.059
574	56	274	D	2.183
575	57	274	D	1.962
576	55	274	D	1.864
577	58	274	D	2.025
578	57	274	D	2.028
579	55	274	D	2.013
580	54	274	D	2.113
581	54	274	D	2.063
582	55	274	D	2.057

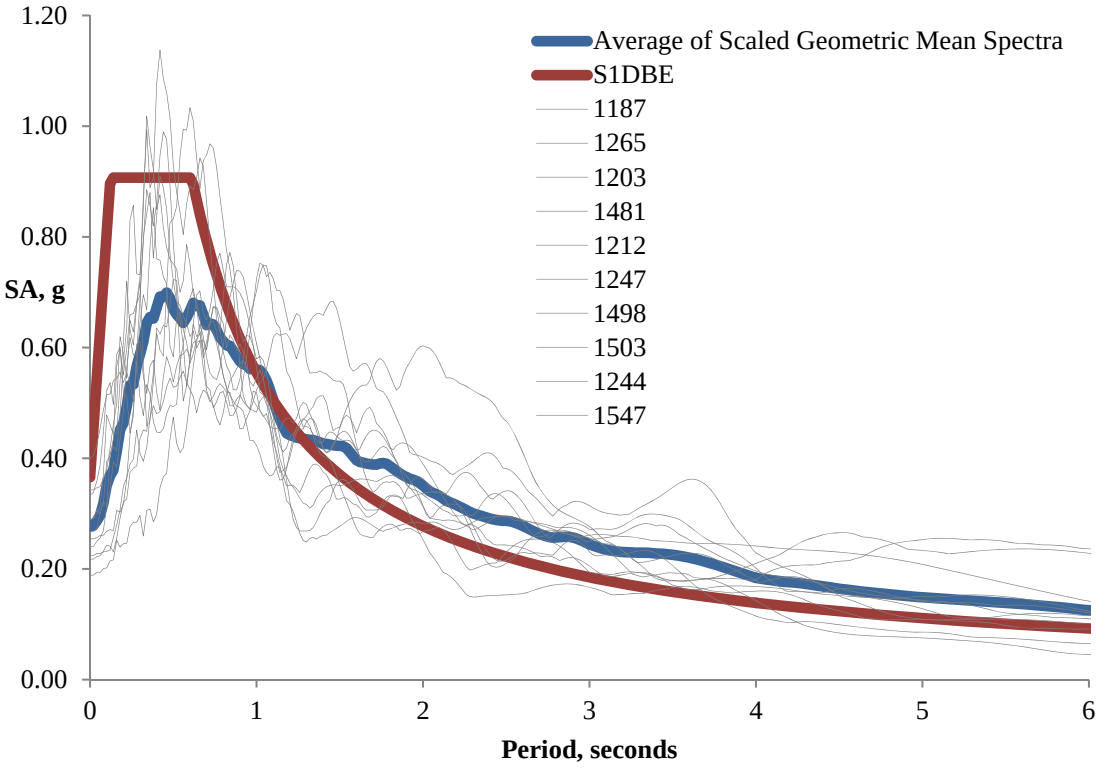

Figure E-4. Chi-Chi, Taiwan Record Scaling - S1DBE

Table E-4. Chi-Chi, Taiwan Station Data - S1DBE

NGA #	R_{jb}, km	Vs30, m/s	Site Class	S1DBE SF
1187	38	229	D	2.000
1265	55	229	D	2.134
1203	16	279	D	1.129
1481	25	229	D	1.888
1212	48	172	E	2.795
1247	51	176	E	2.783
1498	17	230	D	1.498
1503	1	306	D	0.578
1244	10	259	D	0.805
1547	15	242	D	1.510
1536	12	213	D	1.055

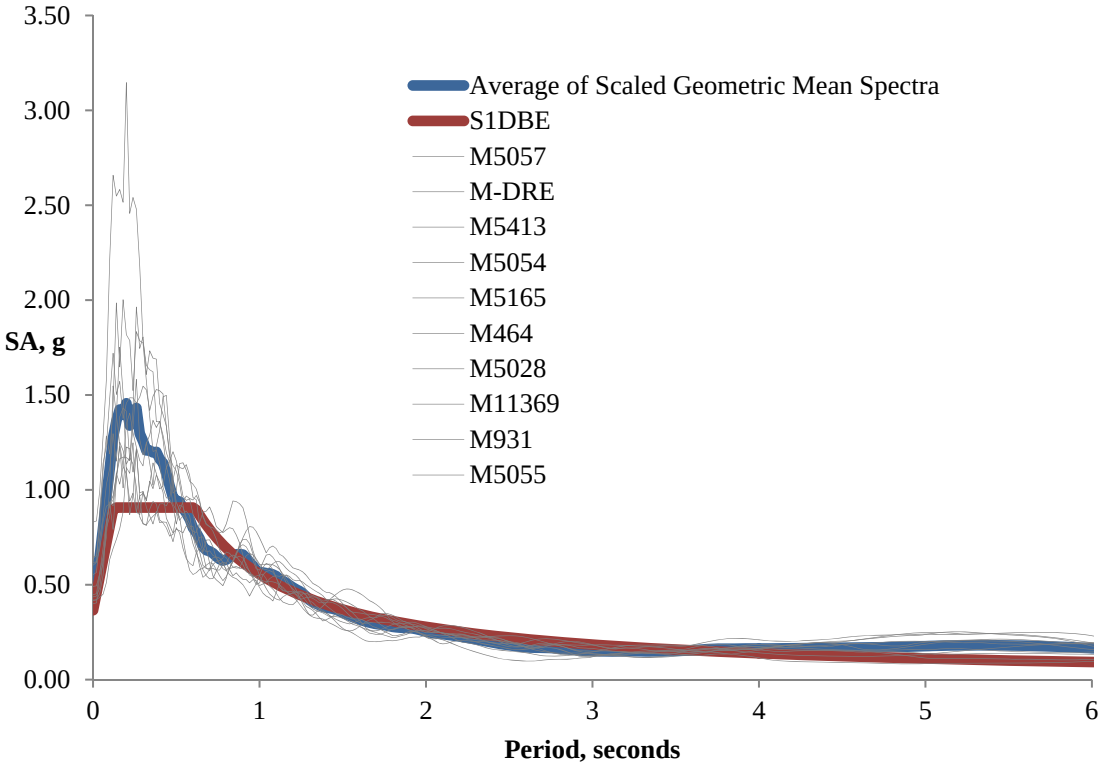

Figure E-5. Sierra El Mayor Record Scaling - S1DBE

Table E-5. Sierra El Mayor Station Data - S1DBE

Station	R_{EPI}, km	Vs30, m/s	Site Class	S1DBE SF
5057	71	209	D	2.280
DRE	62	209	D	1.867
5413	89	209	D	2.297
5054	48	209	D	2.549
5165	77	209	D	1.575
464	81	209	D	2.170
5028	66	209	D	2.350
11369	92	209	D	2.754
931	78	209	D	1.108
5055	62	209	D	2.600
955	87	209	D	2.232

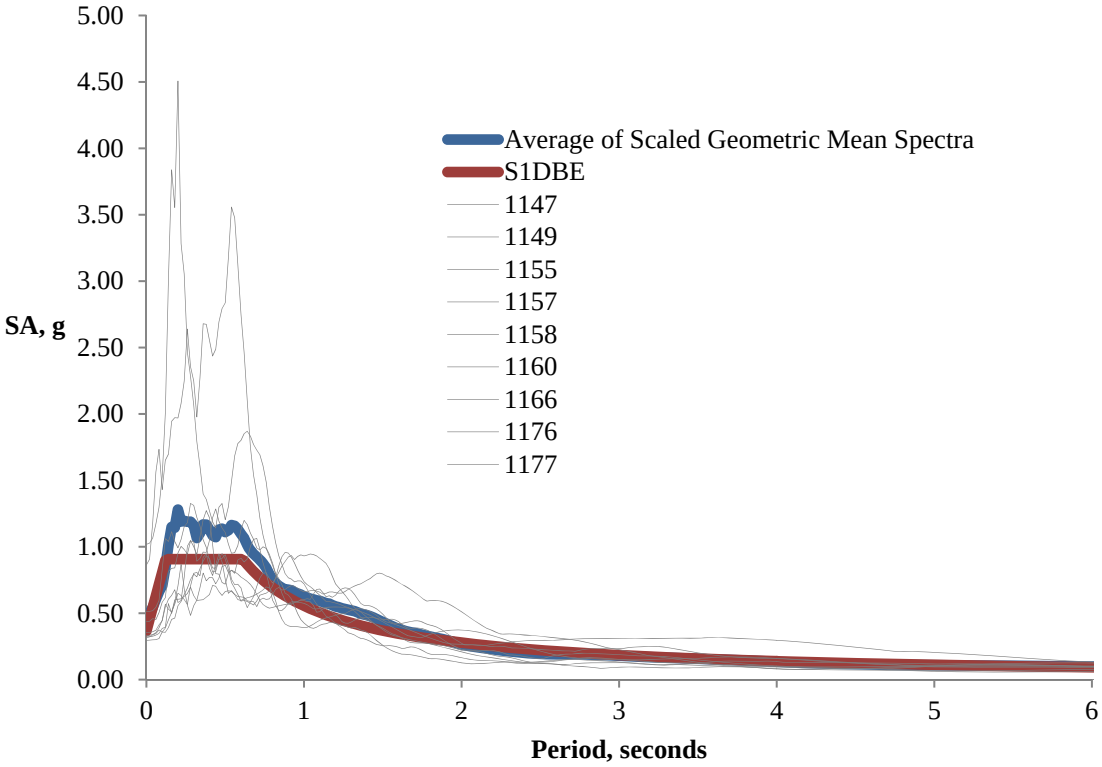

Figure E-6. Kocaeli, Turkey Record Scaling - S1DBE

Table E-6. Kocaeli, Turkey Station Data - S1DBE

NGA #	R_{jb}, km	Vs30, m/s	Site Class	S1DBE SF
1147	70	175	E	1.390
1149	56	275	D	3.891
1155	60	275	D	3.066
1157	67	346	D	6.583
1158	14	276	D	1.092
1160	55	339	D	4.985
1166	31	275	D	2.885
1176	1.4	297	D	1.077
1177	52	275	D	4.048

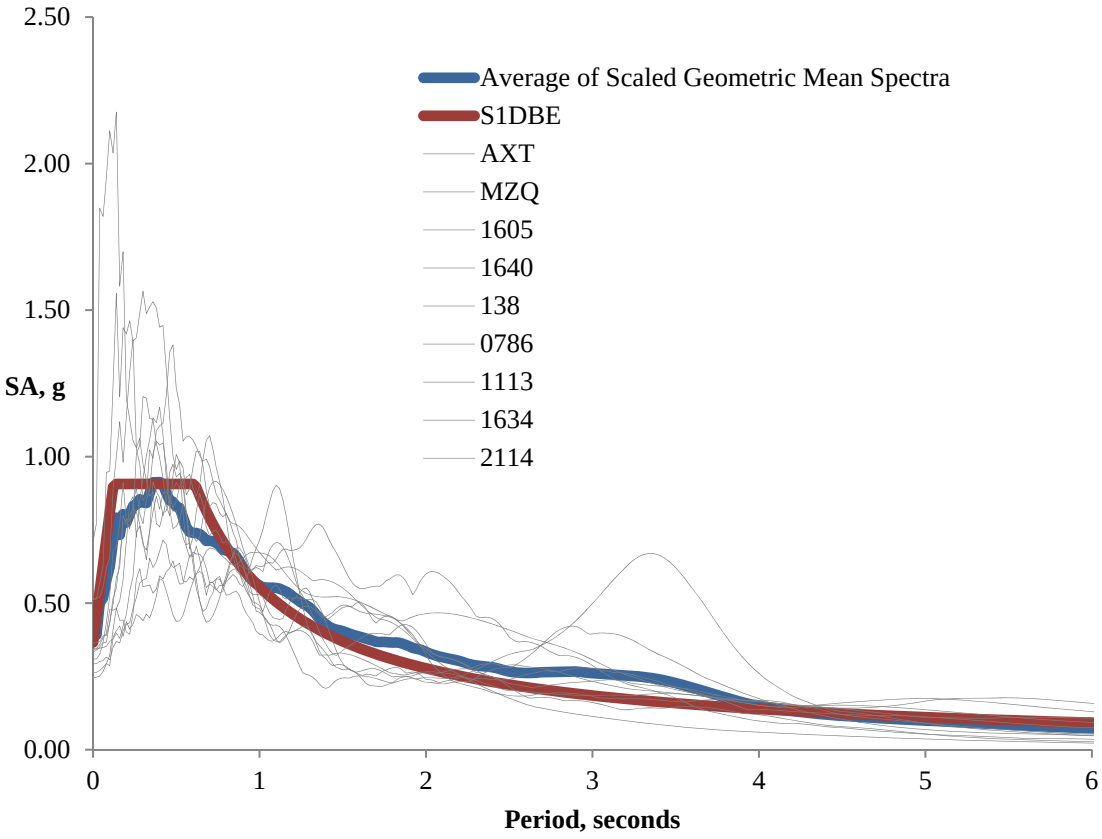

Figure E-7. Miscellaneous Record Scaling - S1DBE

Table E-7. Miscellaneous Station Data - S1DBE

Station	Event	R_{jb}, km	Vs30, m/s	Site Class	S1DBE SF
AXT	Wenchuan	20	650	C	1.918
MZQ	Wenchuan	1.4	650	C	1.031
1605	Duzce, Turkey	6.6	276	D	0.801
1640	Manjil, Iran	94	275	D	2.950
138	Tabas, Iran	24	339	D	3.429
786	Loma Prieta	31	210	D	1.740
1113	Kobe, Japan	21	256	D	3.156
1634	Manjil, Iran	76	275	D	1.727
2114	Denali, Alaska	0.2	329	D	0.879
1119	Kobe, Japan	0.3	312	D	0.767
1628	St. Elias, Alaska	26	275	D	2.220

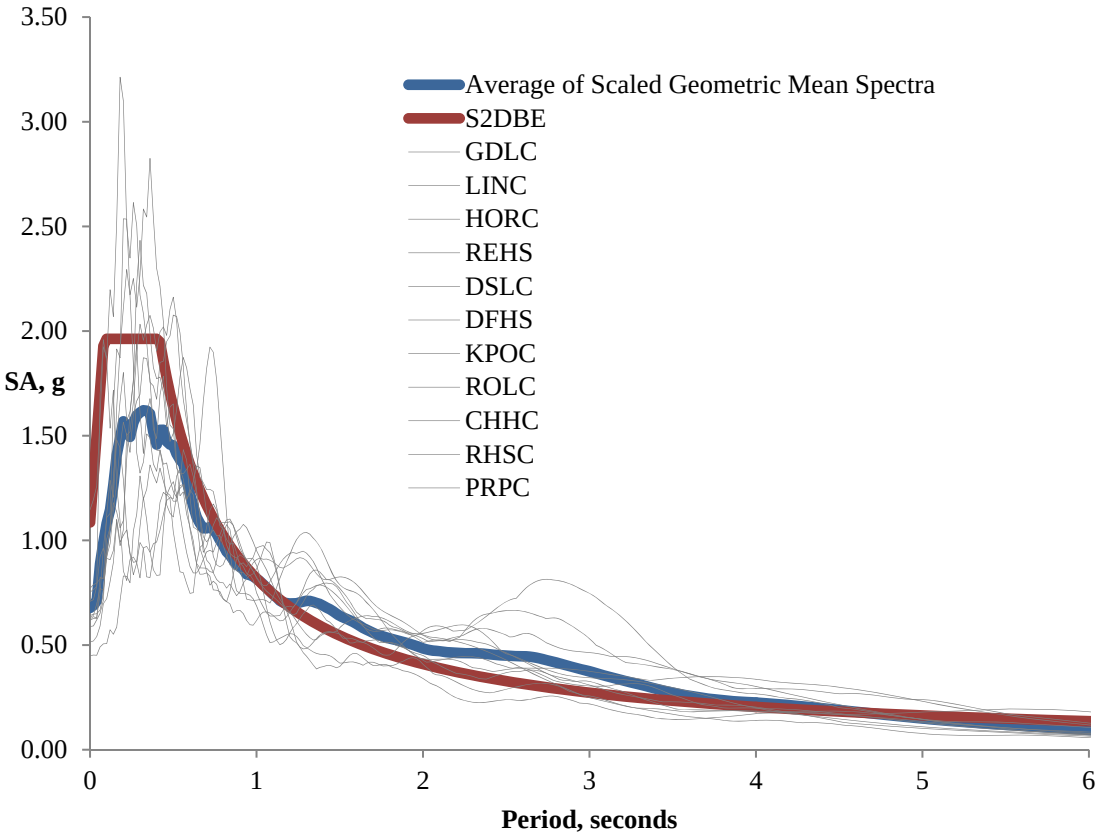

Figure E-8. Canterbury, New Zealand Record Scaling - S2DBE

Table E-8. Canterbury, New Zealand Station Data - S2DBE

Station	R_{EPI}, km	Vs30, m/s	Site Class	S2DBE SF
GDLC	8	276	D	0.907
LINC	25	235	D	1.706
HORC	18	180	E	1.344
REHS	37	240	D	2.170
DSLC	13	259	D	3.130
DFHS	9	278	D	2.470
KPOC	44	216	D	2.453
ROLC	17	264	D	1.868
CHHC	36	180	E	2.635
RHSC	31	223	D	3.213
PRPC	41	204	D	2.968

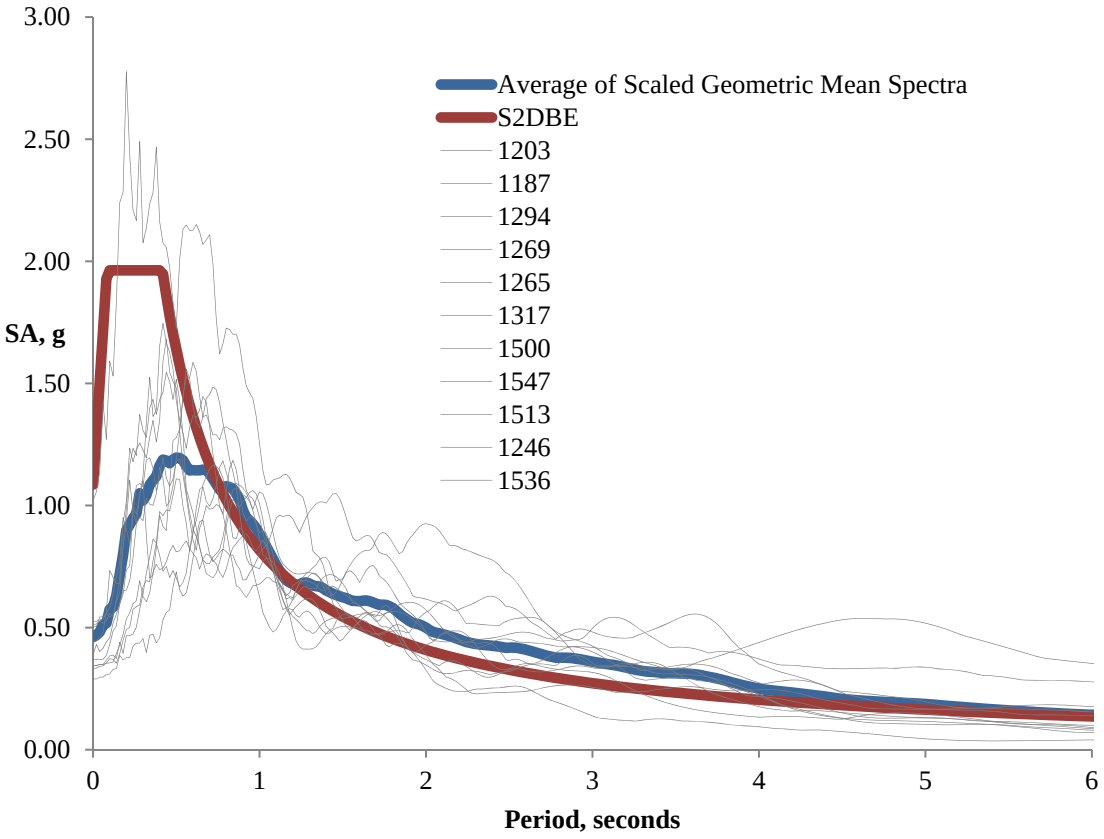

Figure E-9. Chi-Chi, Taiwan Record Scaling - S2DBE

Table E-9. Chi-Chi, Taiwan Station Data - S2DBE

NGA#	R_{jb}, km	Vs30, m/s	Site Class	S2DBE SF
1203	16	233	D	1.732
1187	38	229	D	3.069
1294	47	279	D	3.368
1269	52	244	D	3.829
1265	52	229	D	3.274
1317	82	201	D	2.841
1500	17	320	D	2.742
1547	15	242	D	2.317
1513	0	364	D	1.899
1246	18	223	D	1.874
1536	12	213	D	1.620

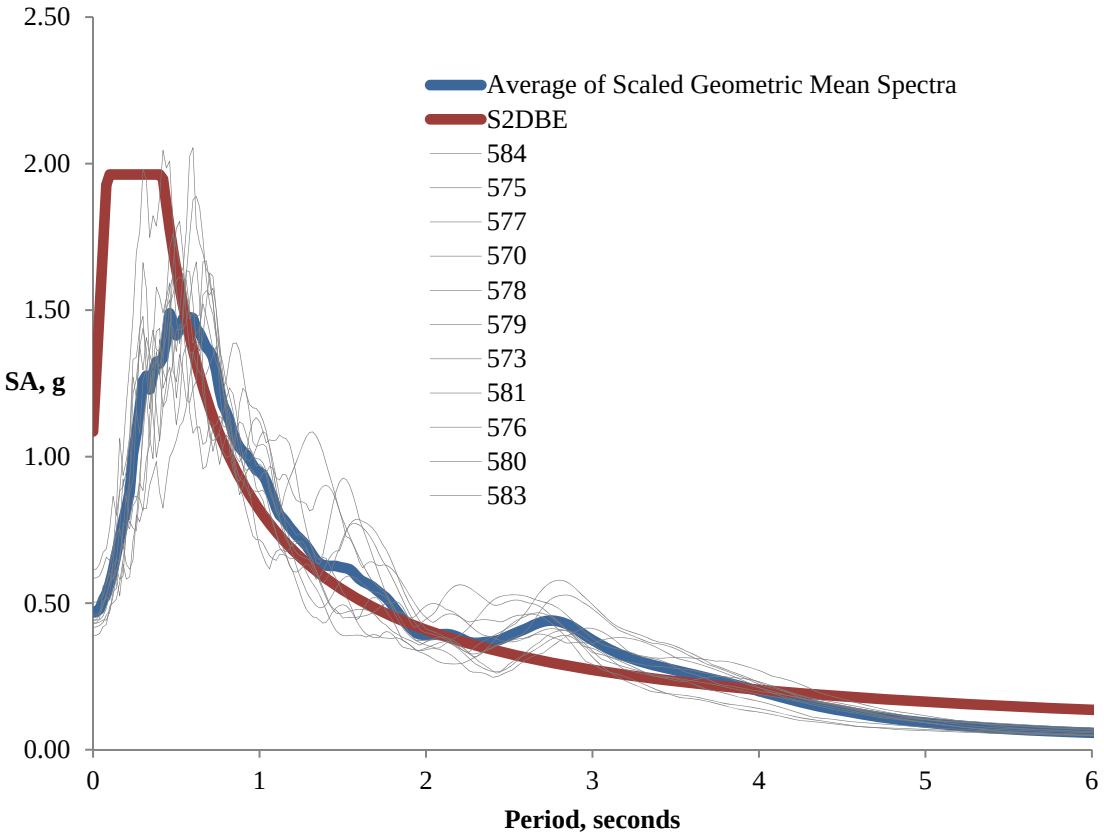

Figure E-10. Taiwan SMART1(45) Record Scaling - S2DBE

Table E-10. Taiwan SMART1(45) Station Data - S2DBE

NGA#	R_{jb}, km	Vs30, m/s	Site Class	S2DBE SF
584	58	275	D	2.804
575	57	275	D	3.012
577	58	275	D	3.108
570	56	275	D	3.226
578	57	275	D	3.113
579	55	275	D	3.089
573	56	275	D	3.160
581	54	275	D	3.165
576	55	275	D	2.860
580	54	275	D	3.243
583	57	275	D	3.297

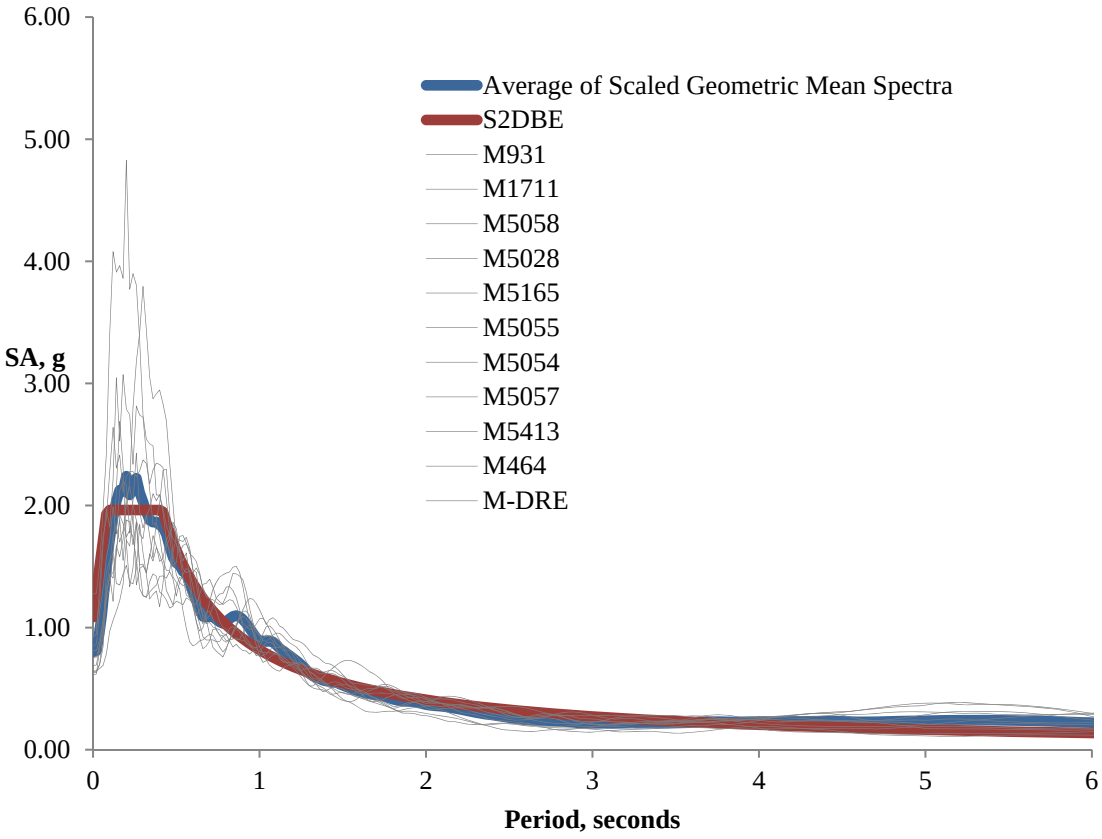

Figure E-11. Sierra El Mayor Record Scaling - S2DBE

Table E-11. Sierra El Mayor Station Data - S2DBE

Station	R_{jb}, km	Vs30, m/s	Site Class	S2DBE SF
M931	17	209	D	1.700
M1711	26	209	D	1.651
M5058	22	209	D	1.560
M5028	34	209	D	3.607
M5165	29	209	D	2.416
M5055	41	209	D	3.990
M5054	36	209	D	3.912
M5057	47	209	D	3.499
M5413	36	209	D	3.524
M464	34	209	D	3.331
M-DRE	36	209	D	2.865

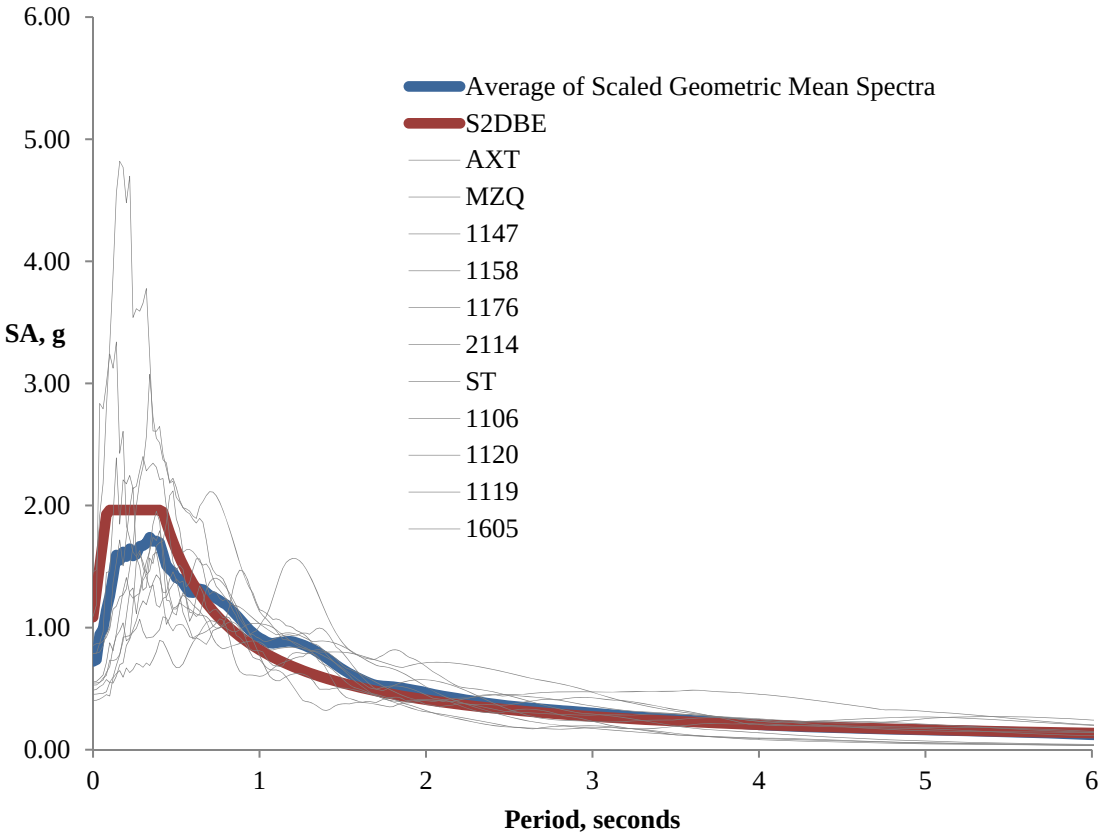

Figure E-12. Miscellaneous Record Scaling - S2DBE

Table E-12. Miscellaneous Station Data - S2DBE

Station	Event	R_{jb}, km	Vs30, m/s	Site Class	S2DBE SF
AXT	Wenchuan	20	650	C	2.943
MZQ	Wenchuan	1.4	650	C	1.583
1147	Kocaeli, Turkey	70	175	E	2.133
1158	Kocaeli, Turkey	14	276	D	1.676
1176	Kocaeli, Turkey	1.4	297	D	1.654
2114	Denali, Alaska	0.2	329	D	1.350
ST	El Salvador	98	338	D	2.128
1106	Kobe, Japan	1.0	312	D	1248
1120	Kobe, Japan	1.5	256	D	0.863
1119	Kobe, Japan	0.3	312	D	1.177
1605	Duzce, Turkey	6.6	276	D	1.229

Both the Atkinson and the Fernandez ground motions were obtained and various ground motion parameters, response spectra, and scale factors to minimize MSE for the uniform hazard design spectra were determined. Complete sets of scale factors are include in the tabulated results for comparison purposes only. For example, while scale factors are reported for Site 2 at the DBE and MCE hazard levels, the Atkinson ground motions are specifically for the Memphis area, Site 1. And the Blytheville records from Fernandez are probably the most appropriate for Site 2 since Blytheville source-to-site distances correspond more closely to Site 2 than to Site 1. Tables E-13 through E-19 summarize the computed scale factors.

The most logical choice of records for a synthetic set for Site 1 are Atkinson's six M8.0 records and Fernandez's 20 Memphis records - 10 from the Uplands data and 10 from the Lowlands data. The most logical choice for Site 2 is the set of 975-year and 2,475-year return period records for Blytheville. Figures E-13 through E-28 show the average scaled spectra vs. the various uniform hazard target spectra for Atkinson's ground motions at Site 1, and for Fernandez's ground motions at both Site 1 and Site 2.

The scaling presented here minimizes the MSE at 5 discrete periods - 0.5, 1, 2, and 4 seconds. There is a fairly consistent flattening of the mean spectra at long periods for NMSZ-specific synthetic records compared to ATR and generic synthetic records. This will have a significant impact upon isolation feasibility since isolators will lengthen the natural period of the structure and at longer periods, NMSZ-specific spectra are generally a more severe loading than the target, design spectrum. This agrees with findings in the literature from site-specific hazard analyses (Pezeshk, et al., August, 2011).

Table E-13. Scaling of Atkinson & Beresnev NMSZ Synthetic Ground Motions

Source	Scale Factors			
	S1DBE	S1MCE	S2DBE	S2MCE
A&B: Memphis M7.5-01	2.594	3.506	4.514	8.568
A&B: Memphis M7.5-02	2.948	3.984	5.129	9.735
A&B: Memphis M7.5-03	3.349	4.526	5.827	11.060
A&B: Memphis M7.5-04	2.937	3.969	5.109	9.699
A&B: Memphis M7.5-05	2.947	3.982	5.127	9.732
A&B: Memphis M7.5-06	2.919	3.944	5.078	9.640
A&B: Memphis M8.0-01	1.567	2.118	2.727	5.176
A&B: Memphis M8.0-02	1.365	1.845	2.375	4.509
A&B: Memphis M8.0-03	1.446	1.954	2.515	4.775
A&B: Memphis M8.0-04	1.544	2.086	2.686	5.098
A&B: Memphis M8.0-05	1.325	1.791	2.306	4.377
A&B: Memphis M8.0-06	1.739	2.350	3.026	5.743

Table E-14. Scaling of Fernandez Blytheville 975-yr Synthetic Ground Motions

Source	Scale Factors			
	S1DBE	S1MCE	S2DBE	S2MCE
Fernandez: Blyth0975-01	1.025	1.385	1.783	3.385
Fernandez: Blyth0975-02	0.974	1.316	1.695	3.217
Fernandez: Blyth0975-03	0.857	1.158	1.491	2.830
Fernandez: Blyth0975-04	1.124	1.519	1.956	3.712
Fernandez: Blyth0975-05	1.046	1.414	1.821	3.456
Fernandez: Blyth0975-06	0.831	1.123	1.446	2.745
Fernandez: Blyth0975-07	1.177	1.591	2.048	3.888
Fernandez: Blyth0975-08	0.835	1.128	1.453	2.757
Fernandez: Blyth0975-09	0.861	1.163	1.498	2.843
Fernandez: Blyth0975-10	0.804	1.087	1.399	2.656

Table E-15. Scaling of Fernandez Blytheville 2475-yr Synthetic Ground Motions

Source	Scale Factors			
	S1DBE	S1MCE	S2DBE	S2MCE
Fernandez: Blyth2475-01	0.638	0.862	1.109	2.106
Fernandez: Blyth2475-02	0.515	0.695	0.895	1.699
Fernandez: Blyth2475-03	0.445	0.602	0.775	1.471
Fernandez: Blyth2475-04	0.443	0.599	0.771	1.464
Fernandez: Blyth2475-05	0.476	0.643	0.828	1.571
Fernandez: Blyth2475-06	0.414	0.559	0.720	1.367
Fernandez: Blyth2475-07	0.637	0.860	1.108	2.103
Fernandez: Blyth2475-08	0.418	0.564	0.726	1.379
Fernandez: Blyth2475-09	0.478	0.646	0.831	1.578
Fernandez: Blyth2475-10	0.514	0.694	0.894	1.697

Table E-16. Scaling of Fernandez Lowlands 975-yr Synthetic Ground Motions

Source	Scale Factors			
	S1DBE	S1MCE	S2DBE	S2MCE
Fernandez: MemLo0975-01	1.409	1.904	2.452	4.654
Fernandez: MemLo0975-02	1.535	2.075	2.671	5.070
Fernandez: MemLo0975-03	2.283	3.086	3.973	7.541
Fernandez: MemLo0975-04	1.996	2.698	3.473	6.593
Fernandez: MemLo0975-05	2.064	2.790	3.592	6.818
Fernandez: MemLo0975-06	1.460	1.973	2.540	4.821
Fernandez: MemLo0975-07	2.369	3.201	4.121	7.822
Fernandez: MemLo0975-08	2.333	3.153	4.059	7.705
Fernandez: MemLo0975-09	1.856	2.508	3.228	6.128
Fernandez: MemLo0975-10	1.428	1.930	2.484	4.716

Table E-17. Scaling of Fernandez Lowlands 2,475-yr Synthetic Ground Motions

Source	Scale Factors			
	S1DBE	S1MCE	S2DBE	S2MCE
Fernandez: MemLo2475-01	1.037	1.402	1.805	3.426
Fernandez: MemLo2475-02	0.843	1.139	1.466	2.783
Fernandez: MemLo2475-03	1.127	1.523	1.960	3.721
Fernandez: MemLo2475-04	0.735	0.993	1.279	2.427
Fernandez: MemLo2475-05	1.007	1.360	1.752	3.325
Fernandez: MemLo2475-06	0.922	1.246	1.604	3.045
Fernandez: MemLo2475-07	1.004	1.356	1.746	3.315
Fernandez: MemLo2475-08	0.689	0.932	1.199	2.277
Fernandez: MemLo2475-09	1.053	1.422	1.831	3.476
Fernandez: MemLo2475-10	0.932	1.259	1.621	3.077

Table E-18. Scaling of Fernandez Uplands 975-yr Synthetic Ground Motions

Source	Scale Factors			
	S1DBE	S1MCE	S2DBE	S2MCE
Fernandez: MemUp0975-01	2.205	2.980	3.837	7.283
Fernandez: MemUp0975-02	1.668	2.255	2.903	5.510
Fernandez: MemUp0975-03	1.471	1.988	2.560	4.859
Fernandez: MemUp0975-04	2.209	2.985	3.843	7.295
Fernandez: MemUp0975-05	2.112	2.855	3.675	6.976
Fernandez: MemUp0975-06	1.995	2.696	3.471	6.588
Fernandez: MemUp0975-07	1.970	2.663	3.428	6.507
Fernandez: MemUp0975-08	1.733	2.342	3.015	5.723
Fernandez: MemUp0975-09	1.820	2.460	3.167	6.011
Fernandez: MemUp0975-10	1.689	2.282	2.939	5.578

Table E-19. Scaling of Fernandez Uplands 2,475-yr Synthetic Ground Motions

Source	Scale Factors			
	S1DBE	S1MCE	S2DBE	S2MCE
Fernandez: MemUp2475-01	0.838	1.133	1.459	2.769
Fernandez: MemUp2475-02	0.982	1.326	1.708	3.242
Fernandez: MemUp2475-03	0.965	1.304	1.678	3.186
Fernandez: MemUp2475-04	0.862	1.164	1.499	2.846
Fernandez: MemUp2475-05	1.087	1.469	1.892	3.591
Fernandez: MemUp2475-06	0.909	1.229	1.582	3.003
Fernandez: MemUp2475-07	0.825	1.115	1.436	2.725
Fernandez: MemUp2475-08	0.922	1.246	1.604	3.045
Fernandez: MemUp2475-09	0.943	1.275	1.641	3.116
Fernandez: MemUp2475-10	0.913	1.234	1.589	3.017

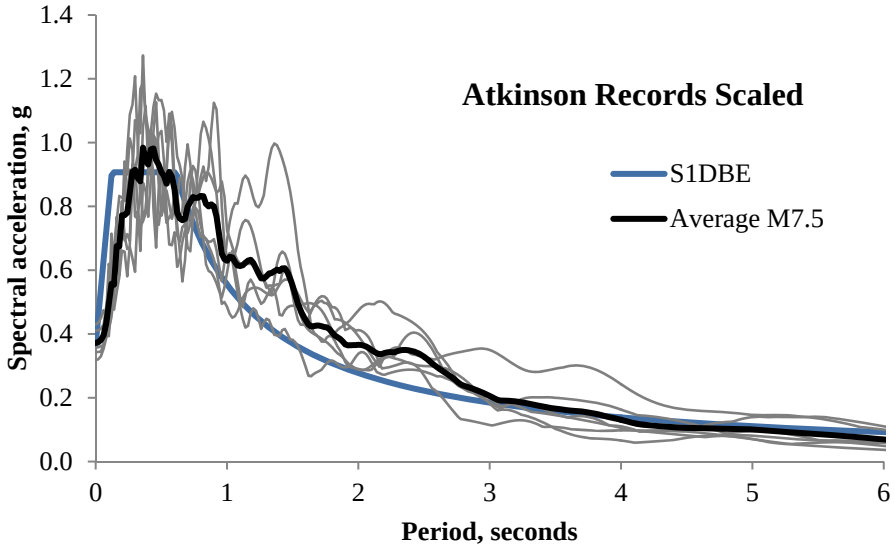

Figure E-13. Atkinson's M7.5 Records Scaled to S1DBE

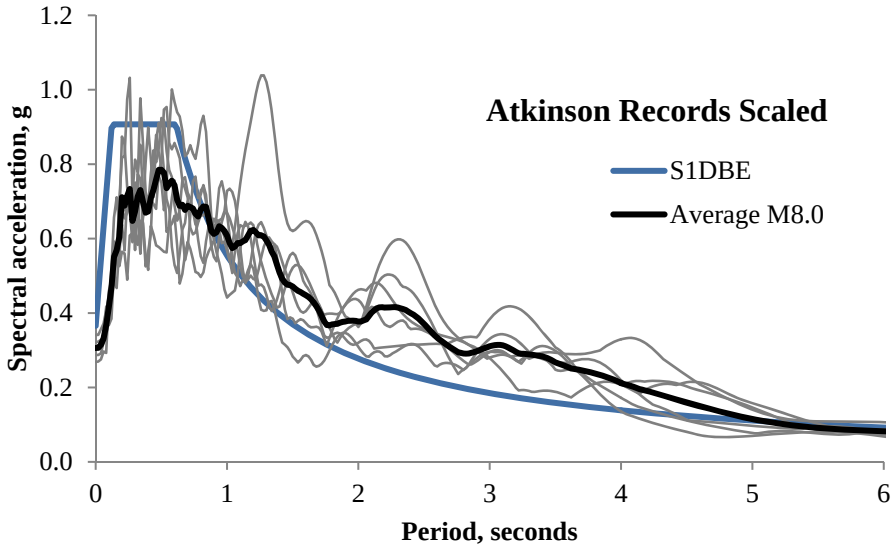

Figure E-14. Atkinson's M8.0 Records Scaled to S1DBE

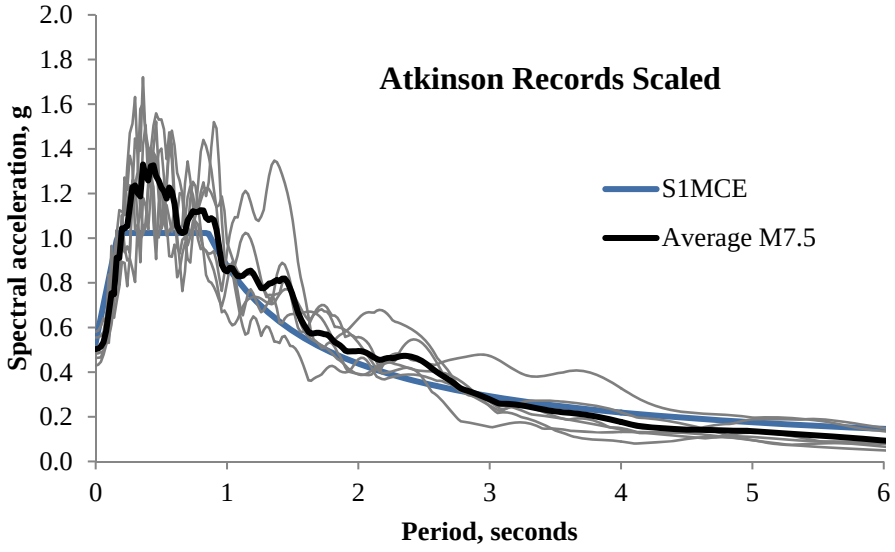

Figure E-15. Atkinson's M7.5 Records Scaled to S1MCE

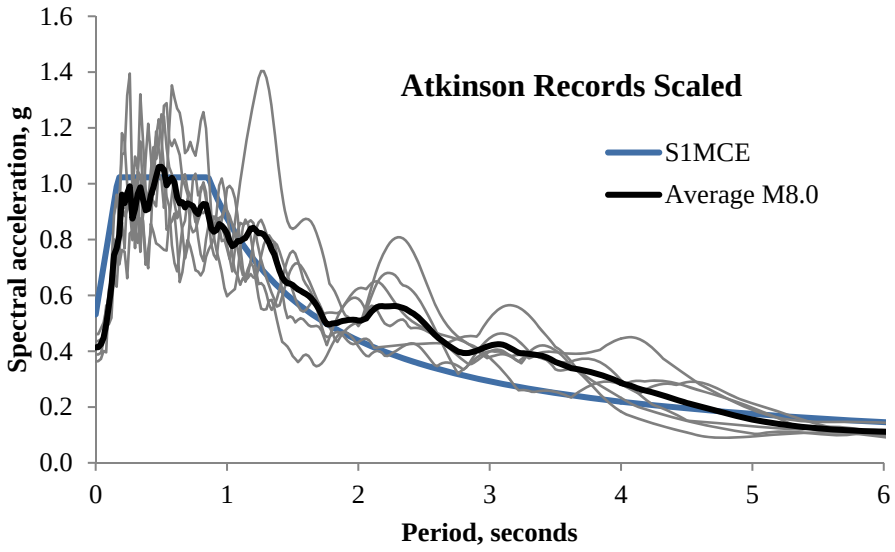

Figure E-16. Atkinson's M8.0 Records Scaled to S1MCE

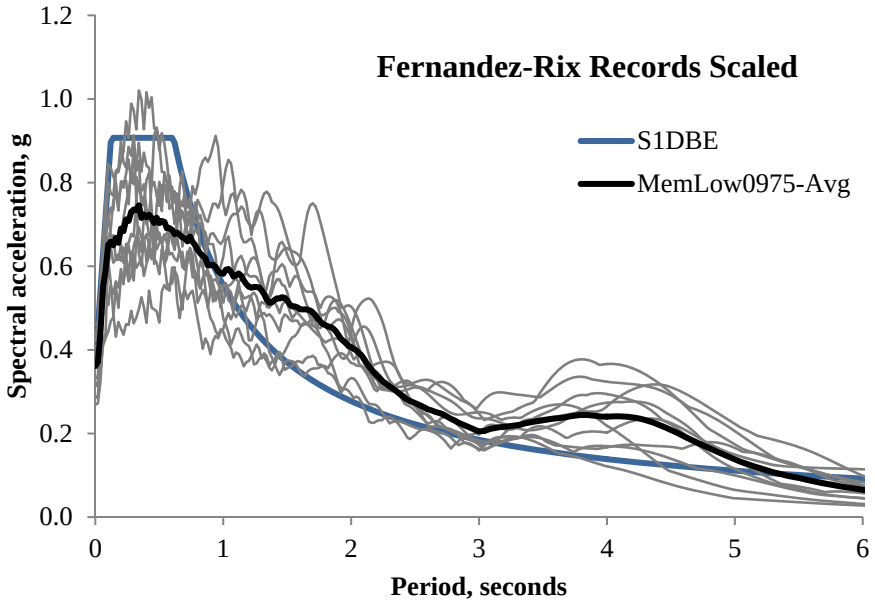

Figure E-17. Fernandez's 975-yr Memphis (Lowland) Records Scaled to S1DBE

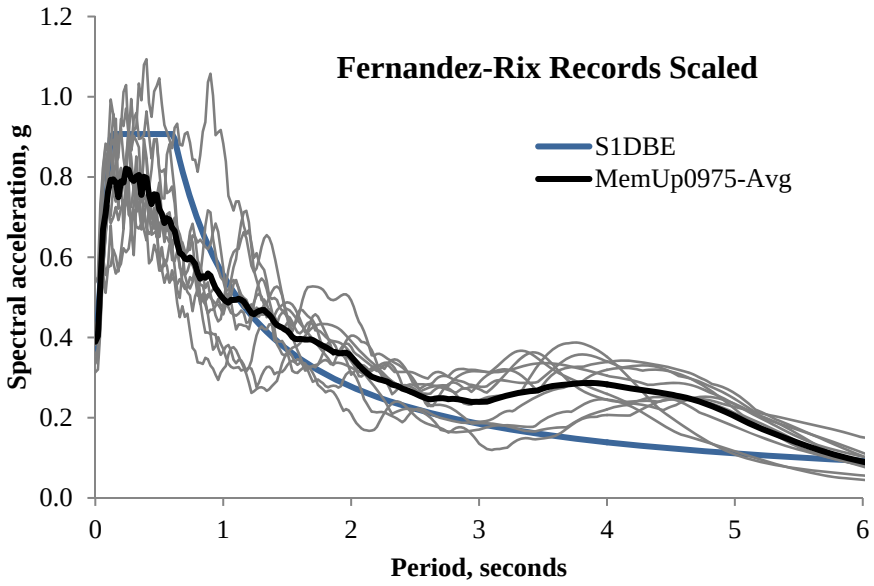

Figure E-18. Fernandez's 975-yr Memphis (Upland) Records Scaled to S1DBE

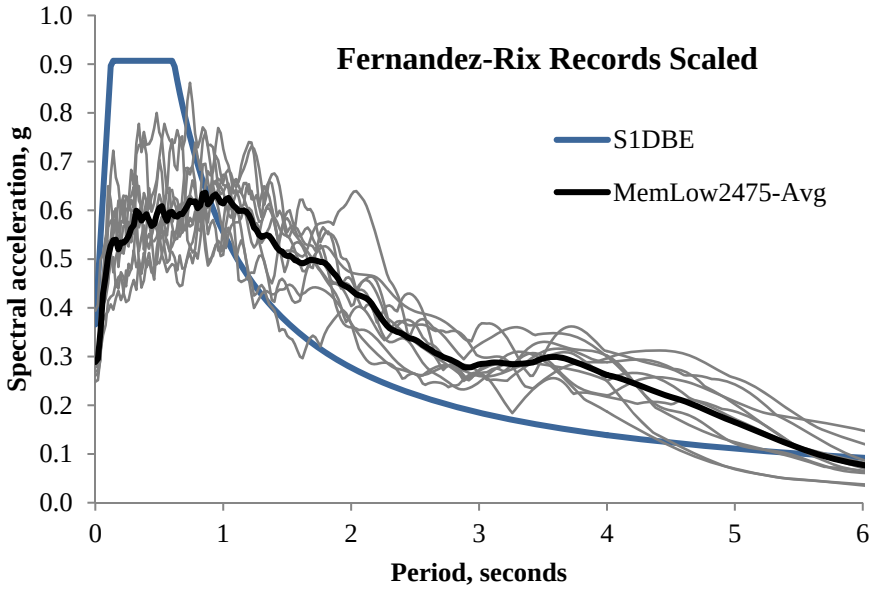

Figure E-19. Fernandez's 2475-yr Memphis (Lowland) Records Scaled to S1DBE

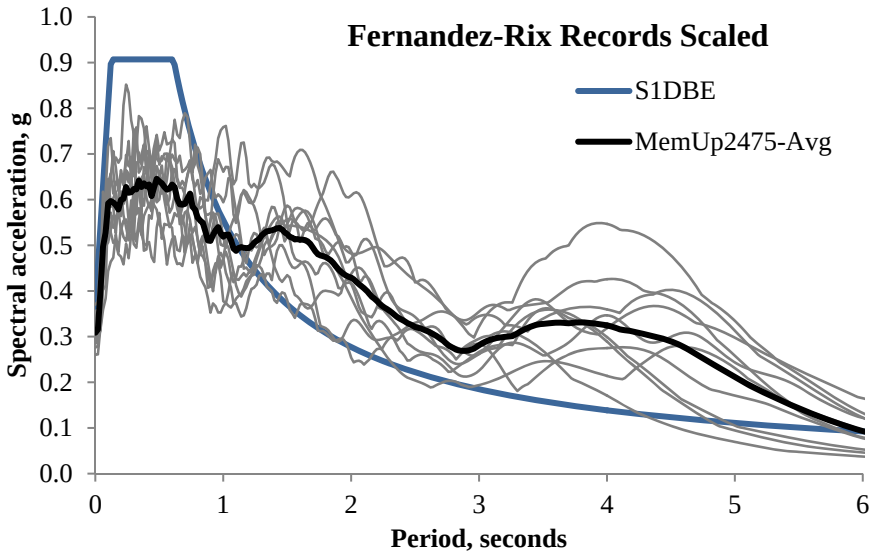

Figure E-20. Fernandez's 2475-yr Memphis (Upland) Records Scaled to S1DBE

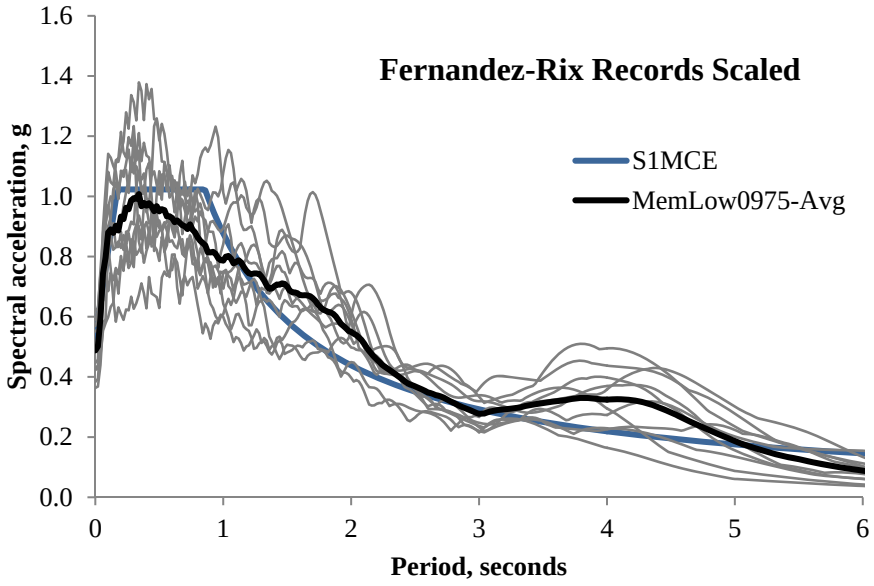

Figure E-21. Fernandez's 975-yr Memphis (Lowland) Records Scaled to S1MCE

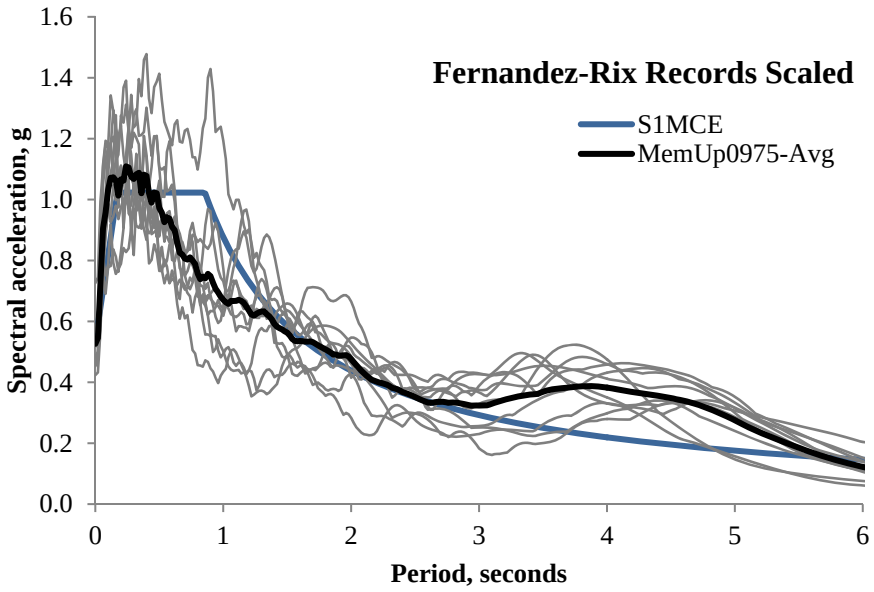

Figure E-22. Fernandez's 975-yr Memphis (Upland) Records Scaled to S1MCE

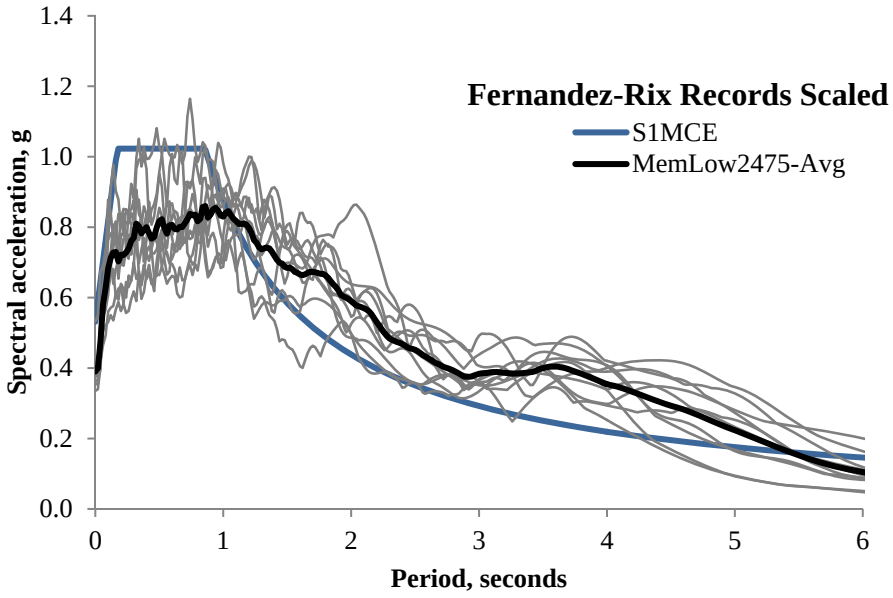

Figure E-23. Fernandez's 2475-yr Memphis (Lowland) Records Scaled to S1MCE

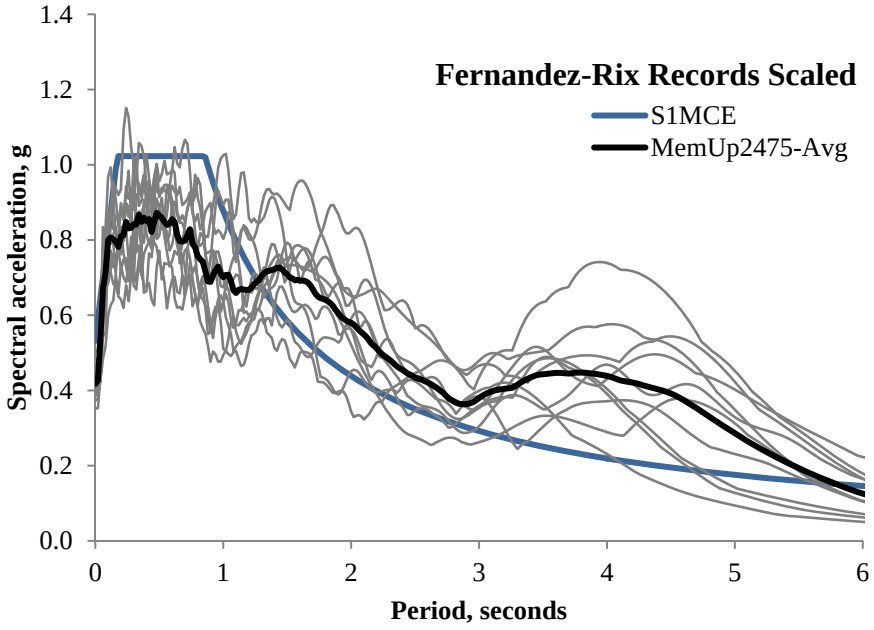

Figure E.-24. Fernandez's 2475-yr Memphis (Upland) Records Scaled to S1MCE

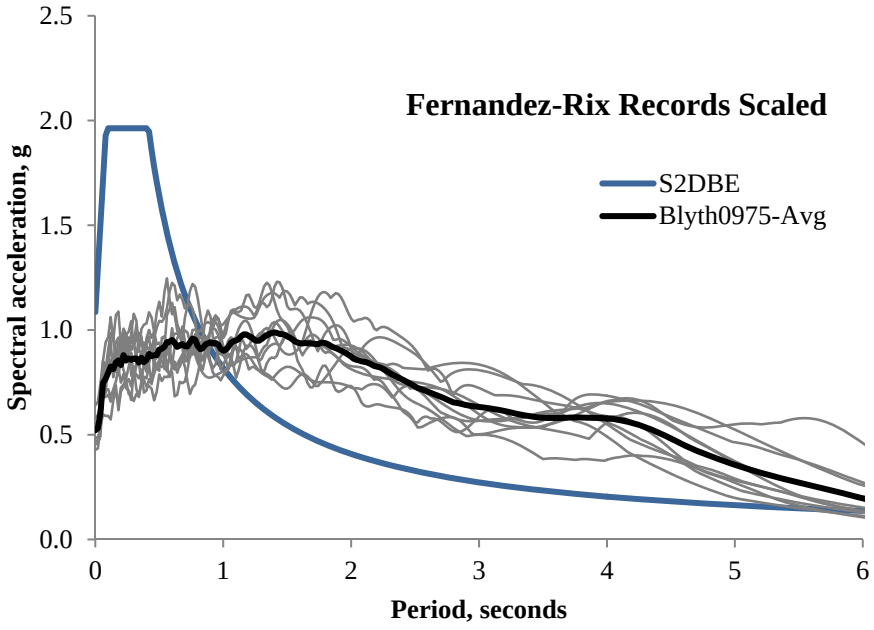

Figure E-25. Fernandez's 975-yr Blytheville Records Scaled to S2DBE

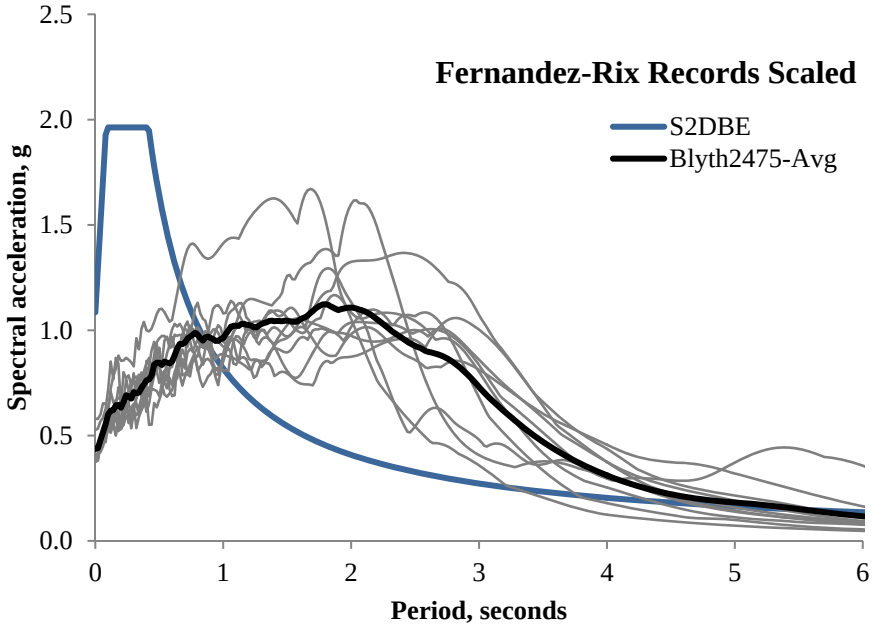

Figure E-26. Fernandez's 2475-yr Blytheville Records Scaled to S2DBE

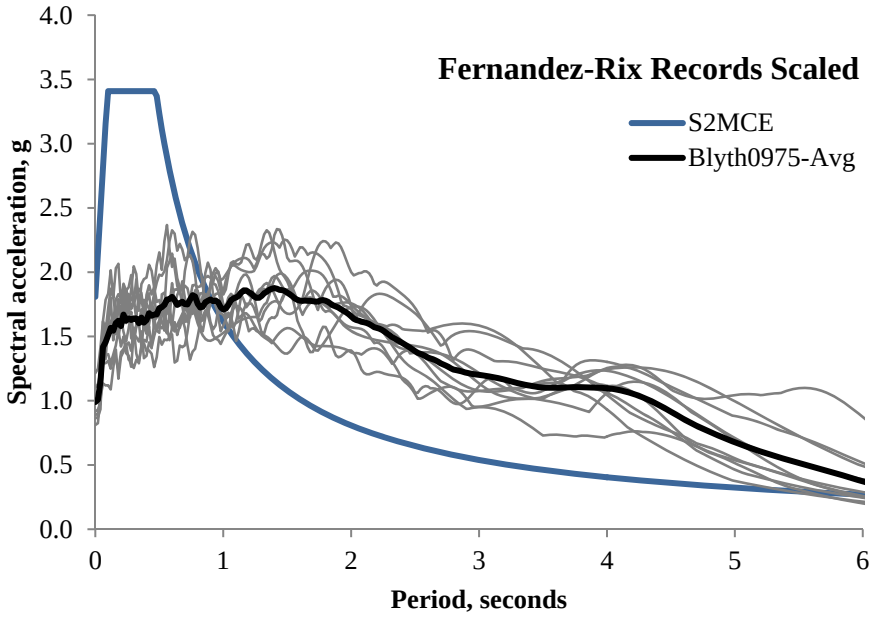

Figure E-27. Fernandez's 975-yr Blytheville Records Scaled to S2MCE

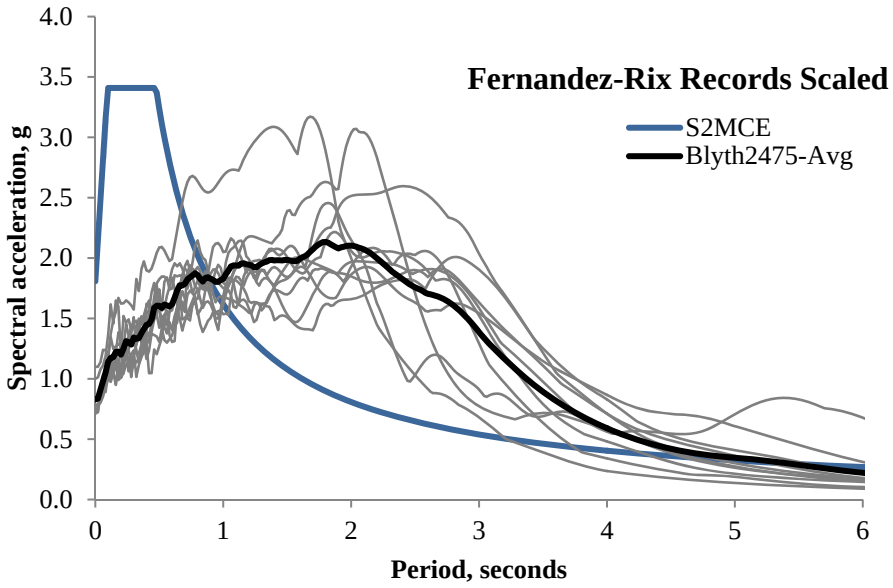

Figure E-28. Fernandez's 2475-yr Blytheville Records Scaled to S2MCE

APPENDIX F - INELASTIC DISPLACEMENT SPECTRA

A commonly used rule in estimating nonlinear displacements in structures subjected to earthquake loading is to assume that the nonlinear response exactly equals the response of a linear structure having period equal to the initial stiffness based period of the nonlinear system. The so-called “equal displacement” rule is now known to be valid for “short period” structures. But what defines a “short period” structure? Is the dividing line between a “short period” structure and a regular structure dependent on the set of ground motions being studied?

Much research has involved attempts to estimate inelastic acceleration spectra from elastic acceleration spectra without performing a rigorous nonlinear analysis for ground motion records. Miranda (Miranda, 2001) proposed a period-and-ductility-dependent model of the form given by equation F-1 based on 264 ground motions recorded on firm sites from 12 separate California earthquakes.

$$C_\mu = \left[1 + \left(\frac{1}{\mu} - 1\right) exp(-12T\mu^{-0.8})\right]^{-1} \quad \text{(Eq. F-1)}$$

AASHTO conventional seismic design uses a displacement amplifier for inelastic behavior, R_d, which is directly analogous to C_μ.

$$R_d = \left(1 - \frac{1}{\mu}\right)\frac{T^*}{T} + \frac{1}{\mu} \geq 1.0 \quad \text{(Eq. F-2)}$$

$$T^* = 1.25 \cdot \frac{S_{D1}}{S_{DS}} \quad \text{(Eq. F-3)}$$

AASHTO isolation design (AASHTO, 2010) incorporates non-linearity explicitly in the substitute structure method used for simplified design. The method can be used to develop both

inelastic displacement spectra and inelastic displacement amplification factors. A step by step procedure to do so is outlined here.

First, for a given value for the initial period, T_i, determine the elastic spectral displacement.

$$SD_{EL}(T_i) = SA_{EL}(T_i) \cdot g \cdot \left(\frac{T_i}{2\pi}\right)^2 \quad \text{(Eq. F-4)}$$

For given values of ductility demand, μ, and post-yield stiffness ratio, α, compute the inelastic spectral displacement using the effective stiffness and equivalent damping of the substitute structure.

$$\xi_{EFF} = \xi_o + \frac{2(\mu - 1)(1 - \alpha)}{\pi\mu(1 + \alpha\mu - \alpha)} \quad \text{(Eq. F-5)}$$

$$T_{EFF} = T_i \sqrt{\frac{\mu}{1 + \alpha\mu - \alpha}} \quad \text{(Eq. F-6)}$$

$$SD_{INEL}(T_i) = SA_{EL}(T_{EFF}) \cdot g \cdot \left(\frac{T_{EFF}}{2\pi}\right)^2 \cdot R_\xi \quad \text{(Eq. F-7)}$$

Different rules for the damping reduction factor may be used. Some of the most frequently used rules include:

$$R_\xi = \frac{1}{B_L} = \left(\frac{0.05}{\xi_{EFF}}\right)^{0.30} \geq \frac{1}{1.70} = 0.588\,, AASHTO \quad \text{(Eq. F-8)}$$

$$R_\xi = \left(\frac{0.10}{0.05 + \xi_{EFF}}\right)^{0.50}, Eurocode \quad \text{(Eq. F-9)}$$

$$R_\xi = \left(\frac{0.07}{0.02 + \xi_{EFF}}\right)^{0.25}, Velocity\ pulse\ conditions \qquad \text{(Eq. F-10)}$$

Now the inelastic displacement ratio is readily available by simply dividing the two demands.

$$C_\mu(T_i) = \frac{SA_{INEL}(T_i)}{SA_{EL}(T_i)} \qquad \text{(Eq. F-11)}$$

The AASHTO Rd method for conventional design and the substitute structure method, currently used by AASHTO for isolation design but applicable for any nonlinear, simplified analysis are compared for various values of α and μ in Figures F-1 through F-8.

Many other models have been proposed, but the only way to arrive at the true solution for a given set of ground motion records is to explicitly solve the nonlinear equations of motion in developing the inelastic displacement spectra.

Ground motion record sets proposed for bridge design in this study have been analyzed using SeismoSpect (SeismoSoft, 2011) to develop mean inelastic displacement spectra. SesimoSpect produces a true nonlinear response history analysis at each period to develop the inelastic spectra. The inelastic displacement spectrum is a valuable and informative tool in earthquake engineering given the design philosophy of designing for controlled nonlinear behavior. In fact, the growing focus on displacement-based, rather than force-based, seismic design may necessitate the use of inelastic displacement spectra instead of elastic acceleration spectra as the science becomes more fully developed and incorporated into design practice.

The graphs presented in this APPENDIX show that the equal-displacement rule does not apply to ground motions from large magnitude events on deep soil sites. In addition to the inelastic displacement spectra for each ground motion record set, plots of the inelastic displacement ratio, C_μ, are given. C_μ is the ratio of the inelastic displacement to the elastic displacement at the given period. The equal displacement rule provides a conservative estimate of displacement demand whenever C_μ is less than or equal to 1.0.

Results for post-yield stiffness values of $\alpha = 0$ and $\alpha = 0.10$ are given for each of the following record sets:

- Set 1UHRS
- Set 1NMSZ
- Set 1NMSZB
- Set 2UHRS
- Set 2UHRS-P
- Set 2NMSZ
- Set 2NMSZ-P

Comparison of Figures F-10 through F-36 with the theoretical plots of Figures F-1 through F-8 makes it possible to infer that the substitute structure approach (adopted by AASHTO for simplified design of isolation systems) is more appropriate than the Rd method employed by AASHTO for conventional design, for estimating inelastic displacements in the NMSZ when displacement ductility demands greater than about 2 are adopted for design.

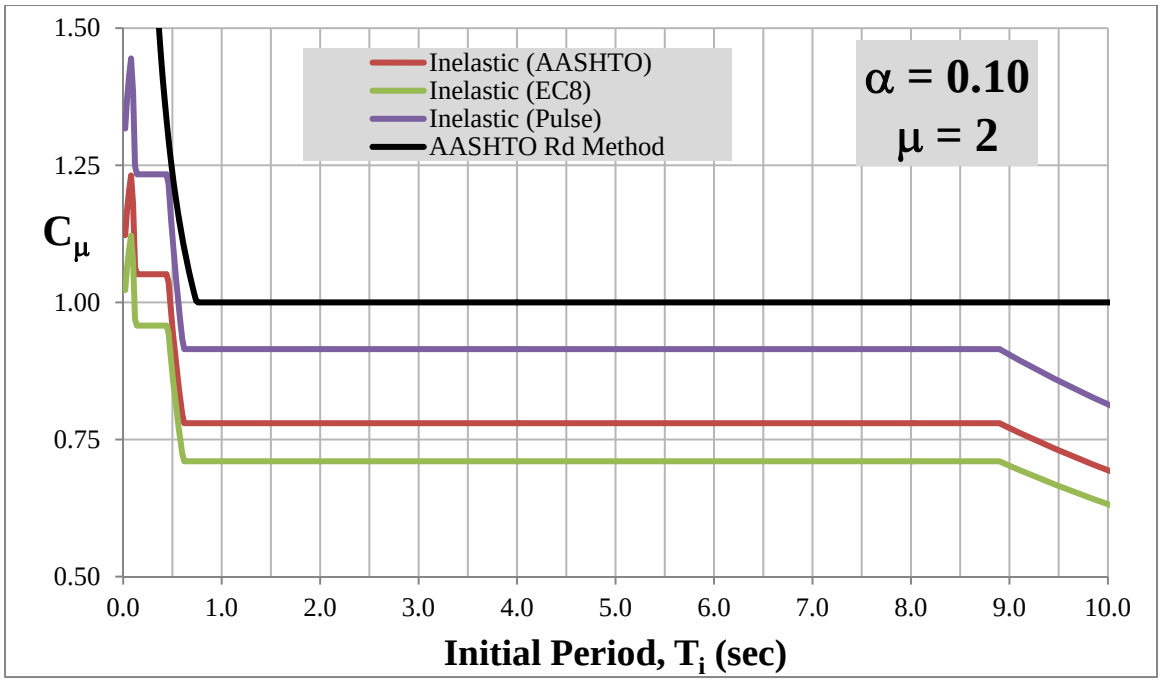

Figure F-1. Inelastic Displacement Ratios (α = 0.10, μ = 2)

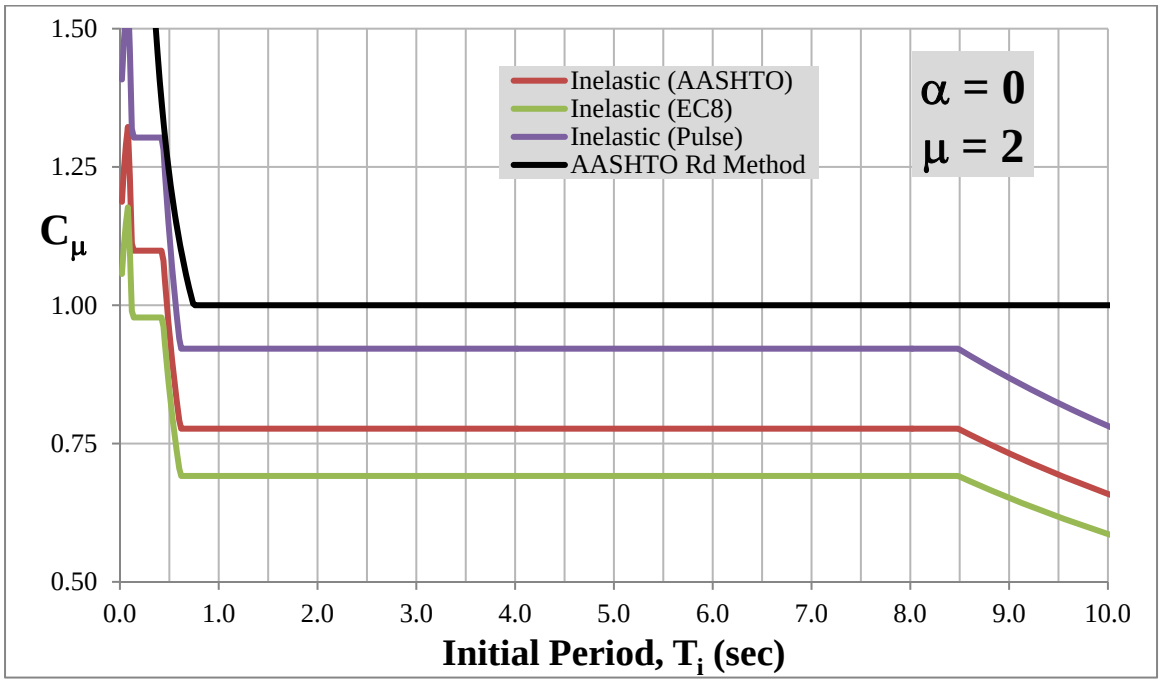

Figure F-2. Inelastic Displacement Ratios (α = 0, μ = 2)

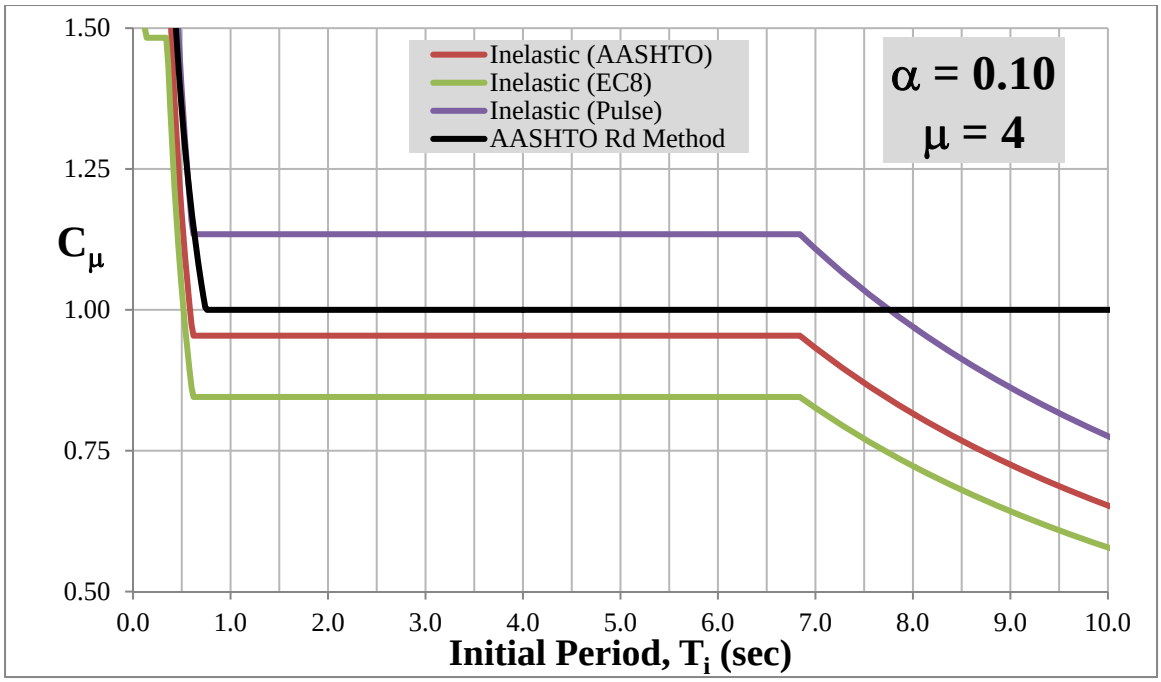

Figure F-3. Inelastic Displacement Ratios (α = 0.10, μ = 4)

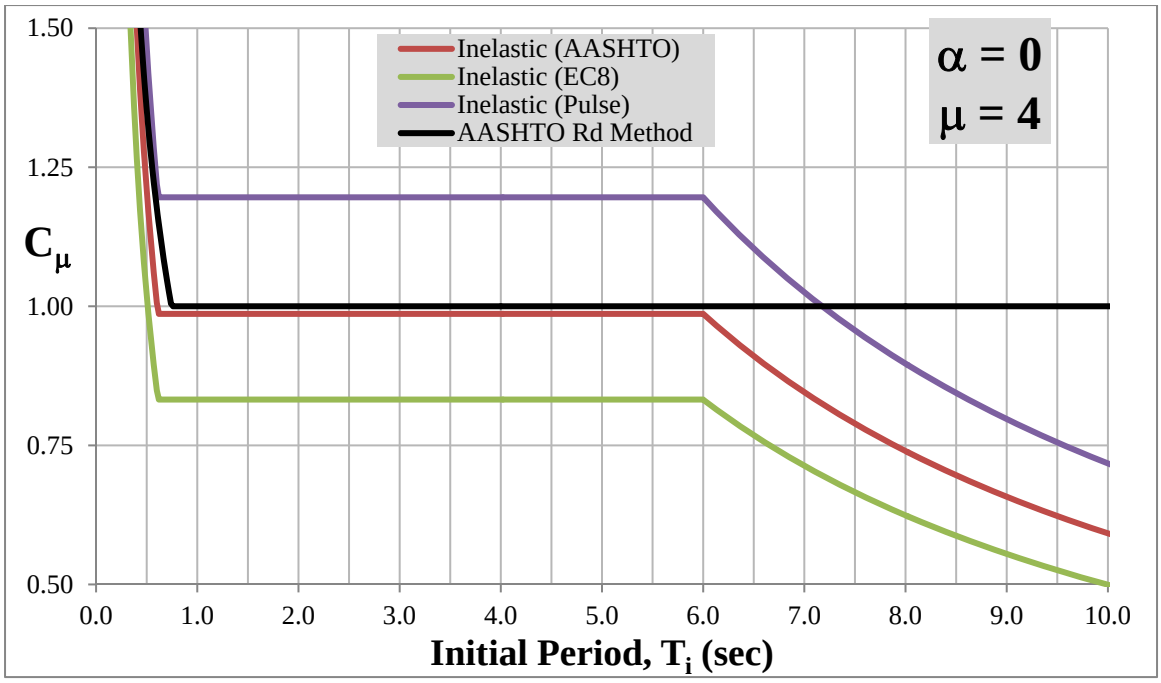

Figure F-4. Inelastic Displacement Ratios (α = 0, μ = 4)

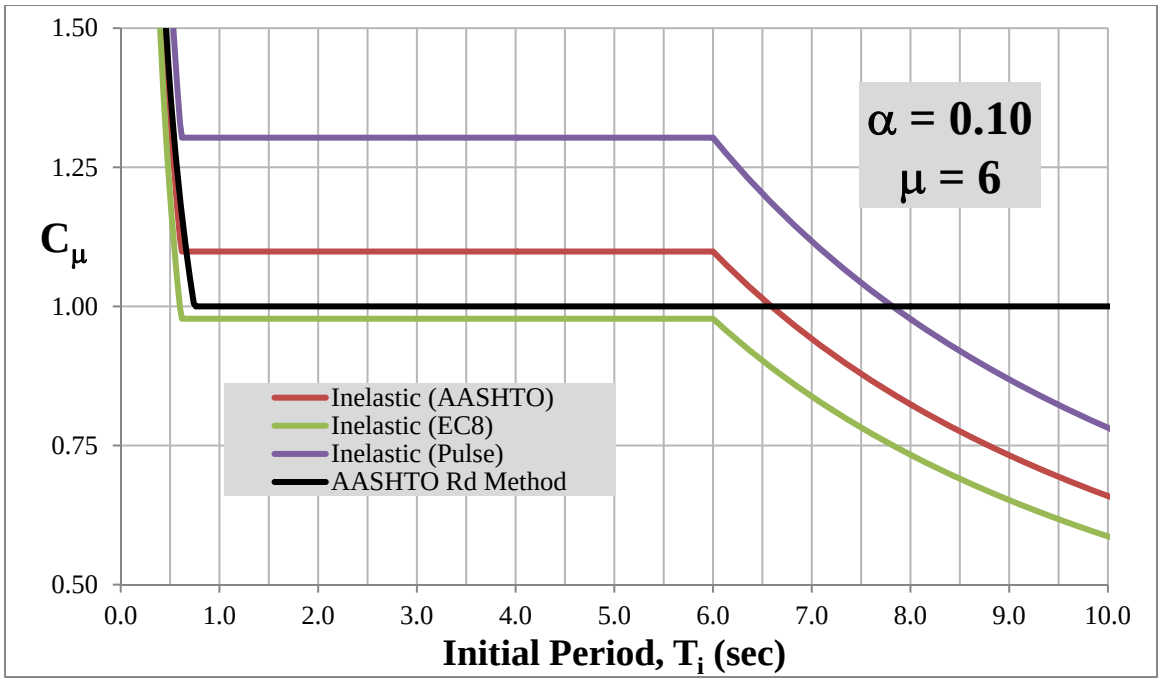

Figure F-5. Inelastic Displacement Ratios (α = 0.10, μ = 6)

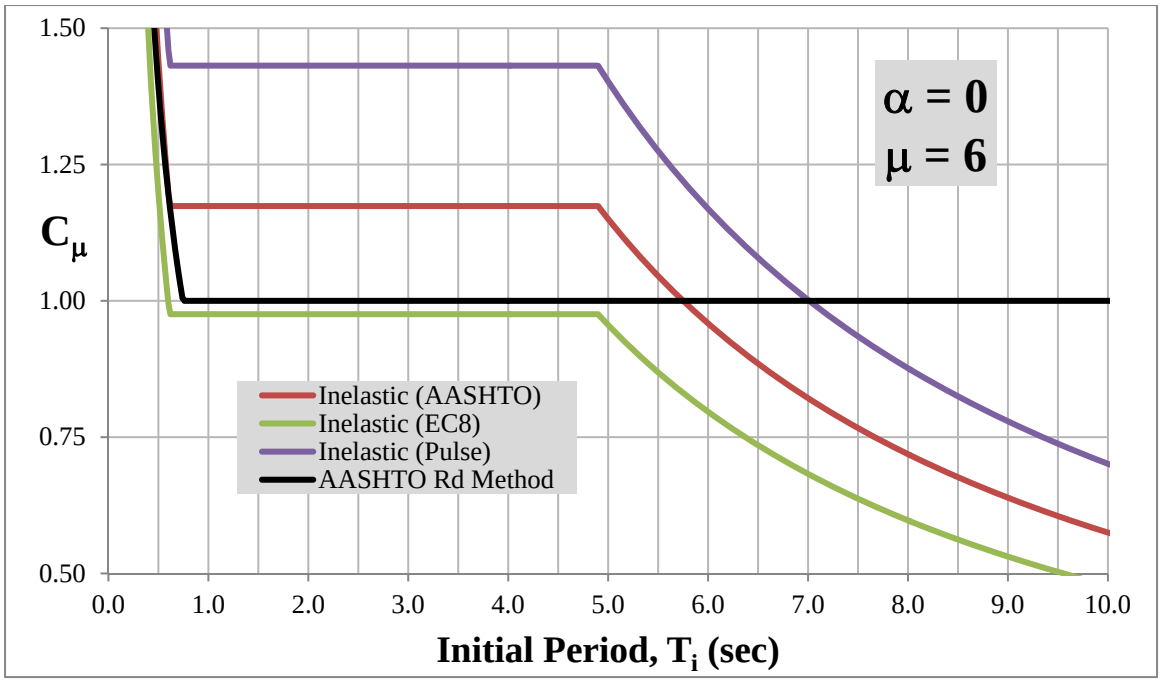

Figure F-6. Inelastic Displacement Ratios (α = 0, μ = 6)

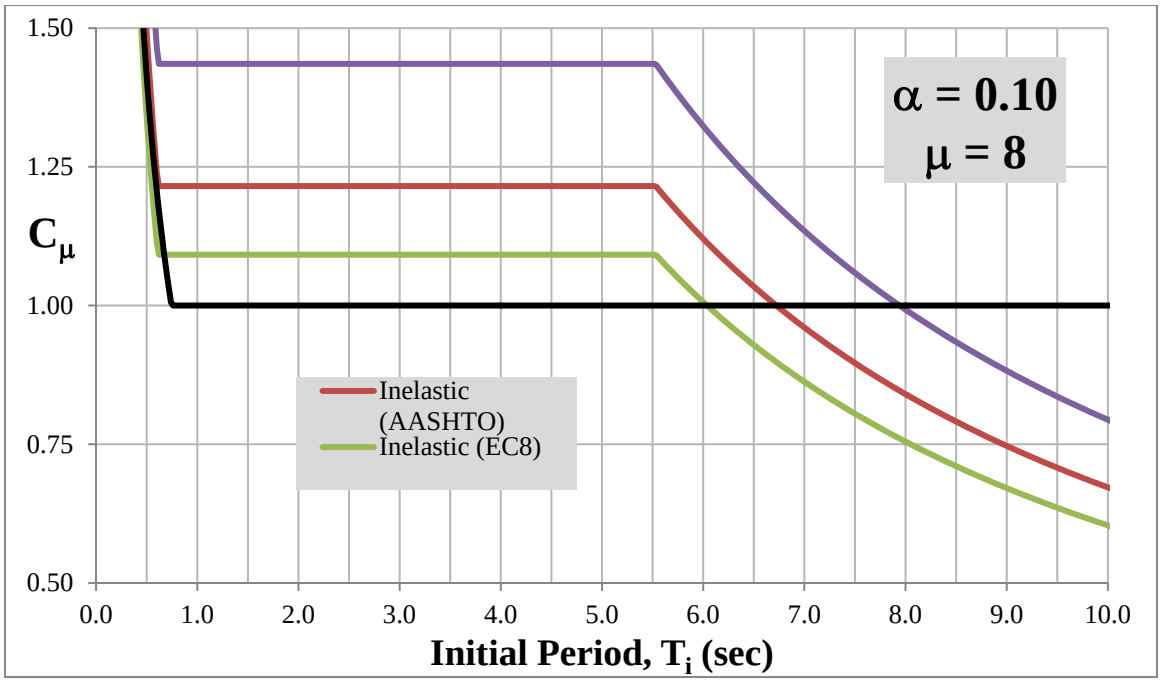

Figure F-7. Inelastic Displacement Ratios (α = 0.10, μ = 8)

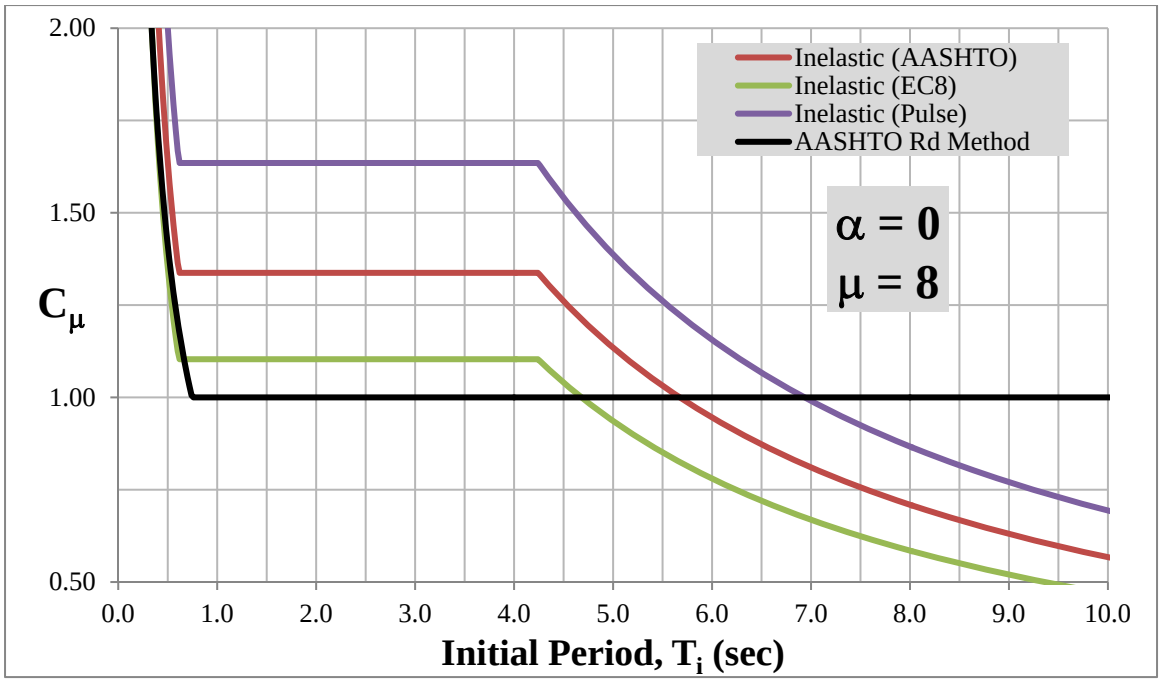

Figure F-8. Inelastic Displacement Ratios (α = 0, μ = 8)

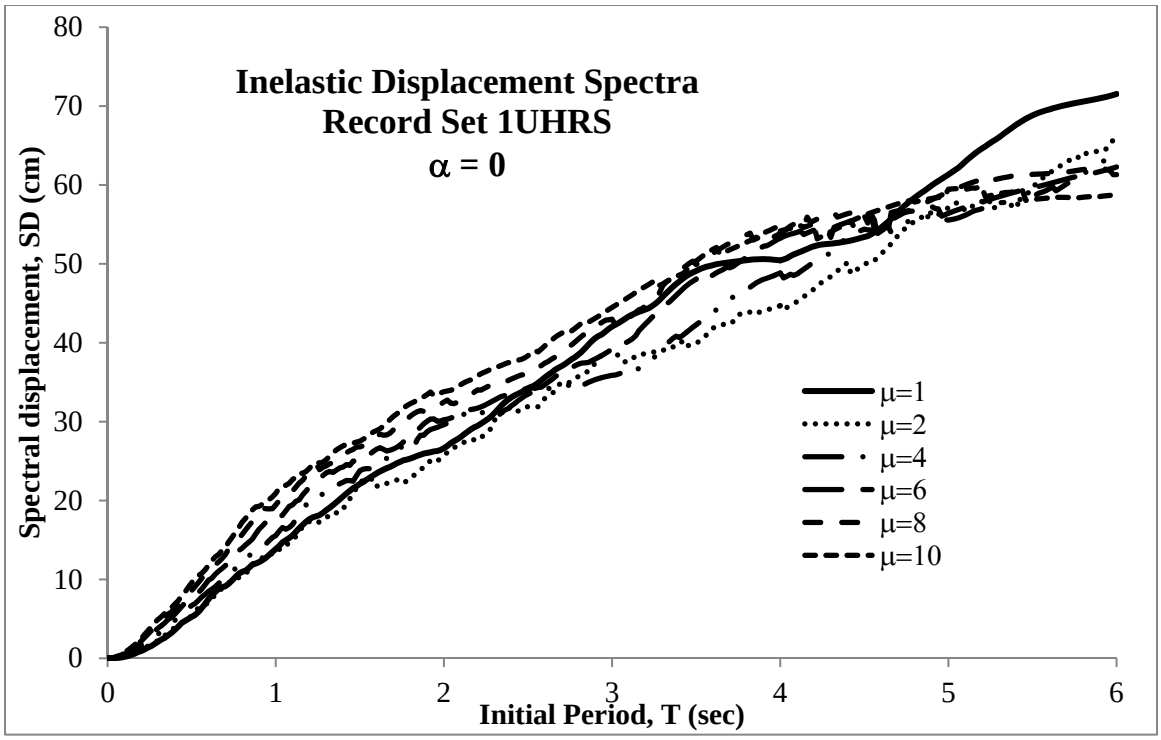

Figure F-9. Inelastic Displacement Spectra - Record Set 1UHRS (α = 0)

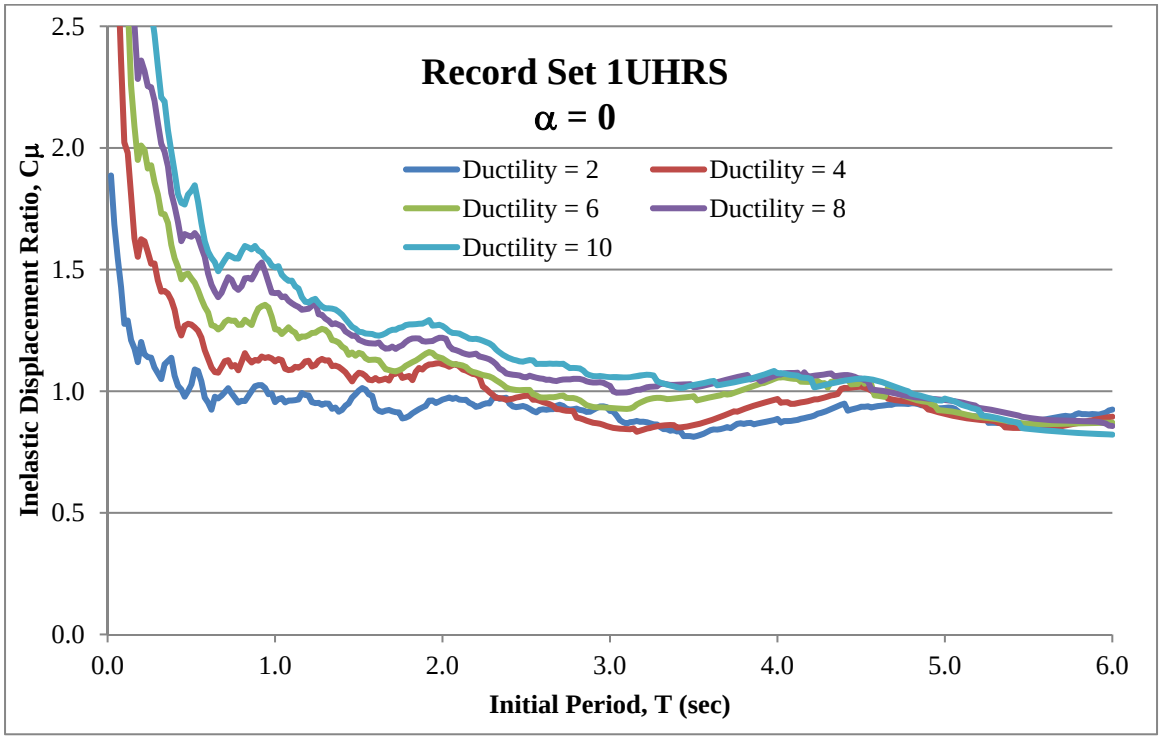

Figure F-10. Inelastic Displacement Ratio - Record Set 1UHRS (α = 0)

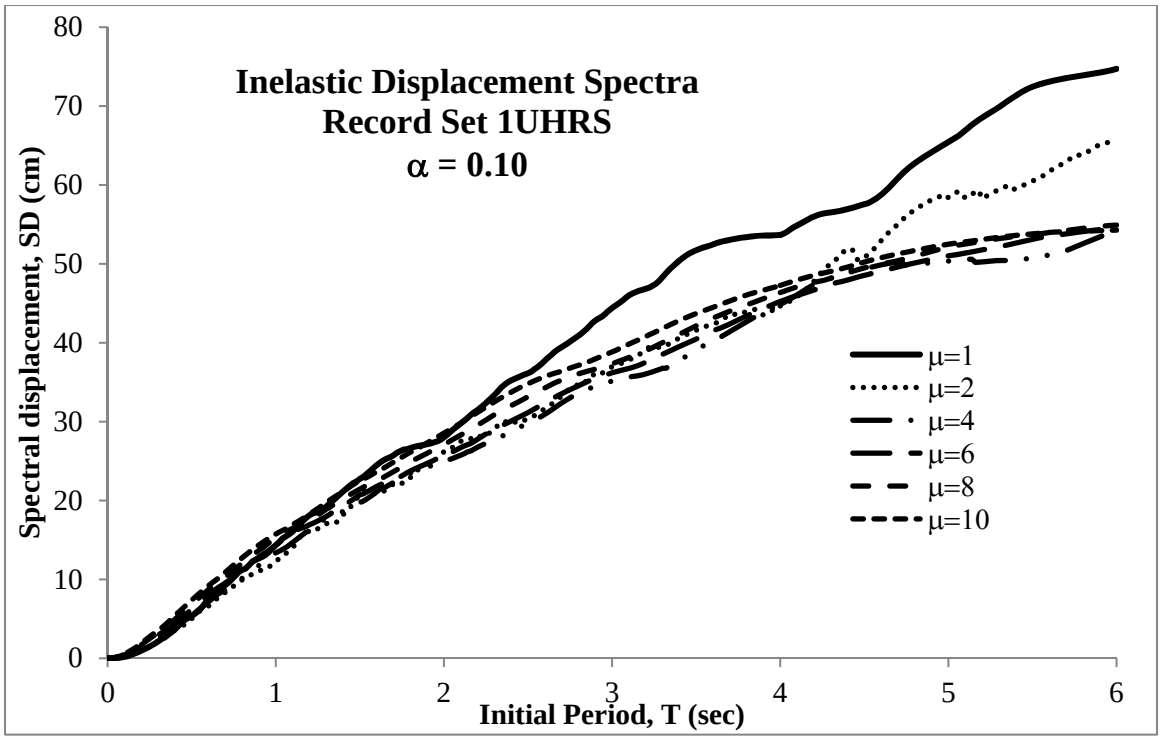

Figure F-11. Inelastic Displacement Spectra - Record Set 1UHRS (α = 0.10)

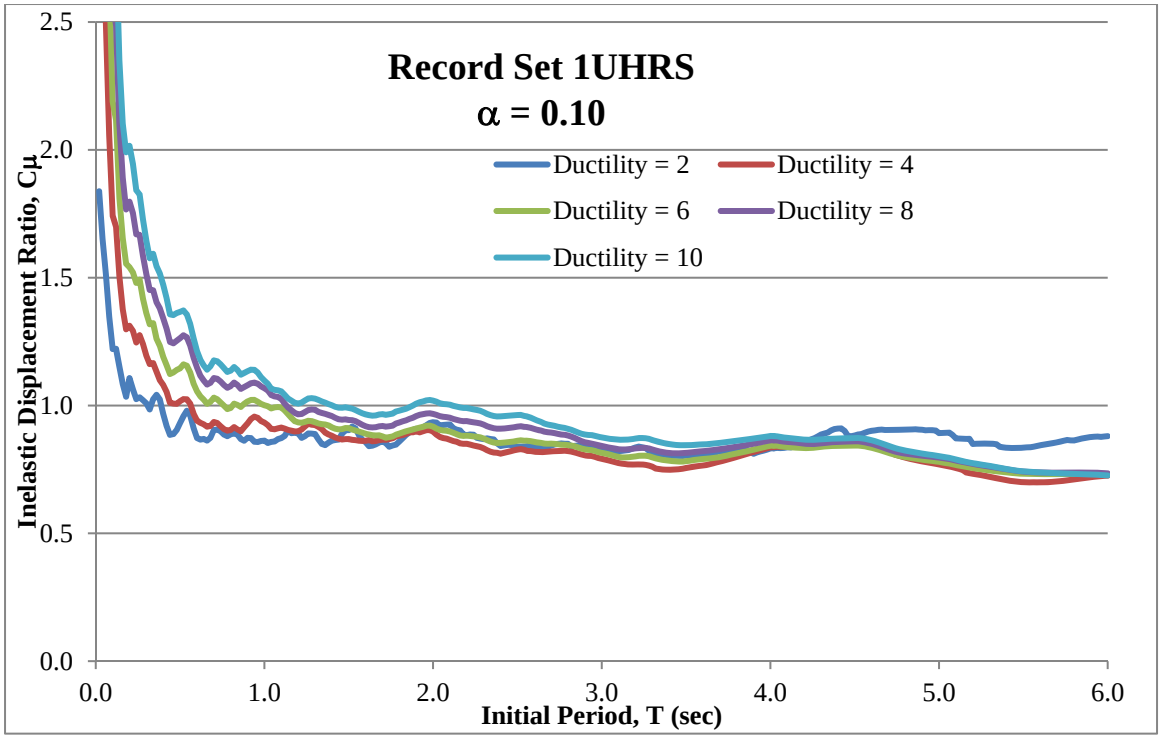

Figure F-12. Inelastic Displacement Ratio - Record Set 1UHRS (α = 0.10)

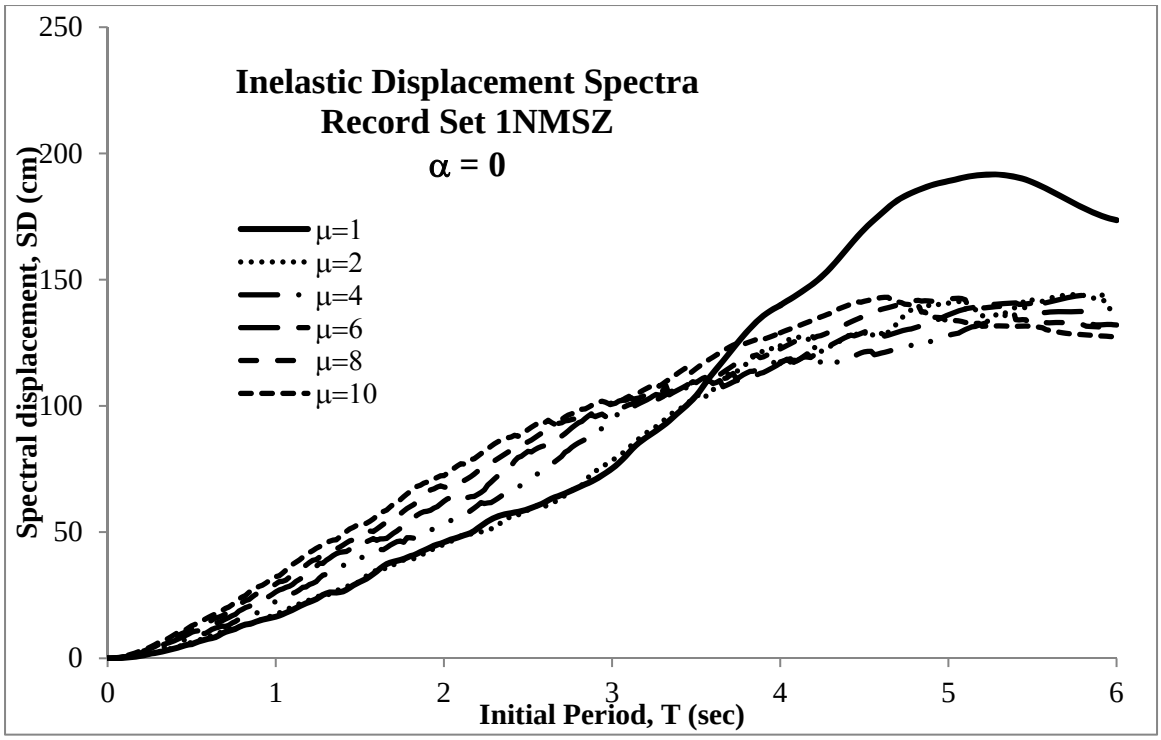

Figure F-13. Inelastic Displacement Spectra - Record Set 1NMSZ (α = 0)

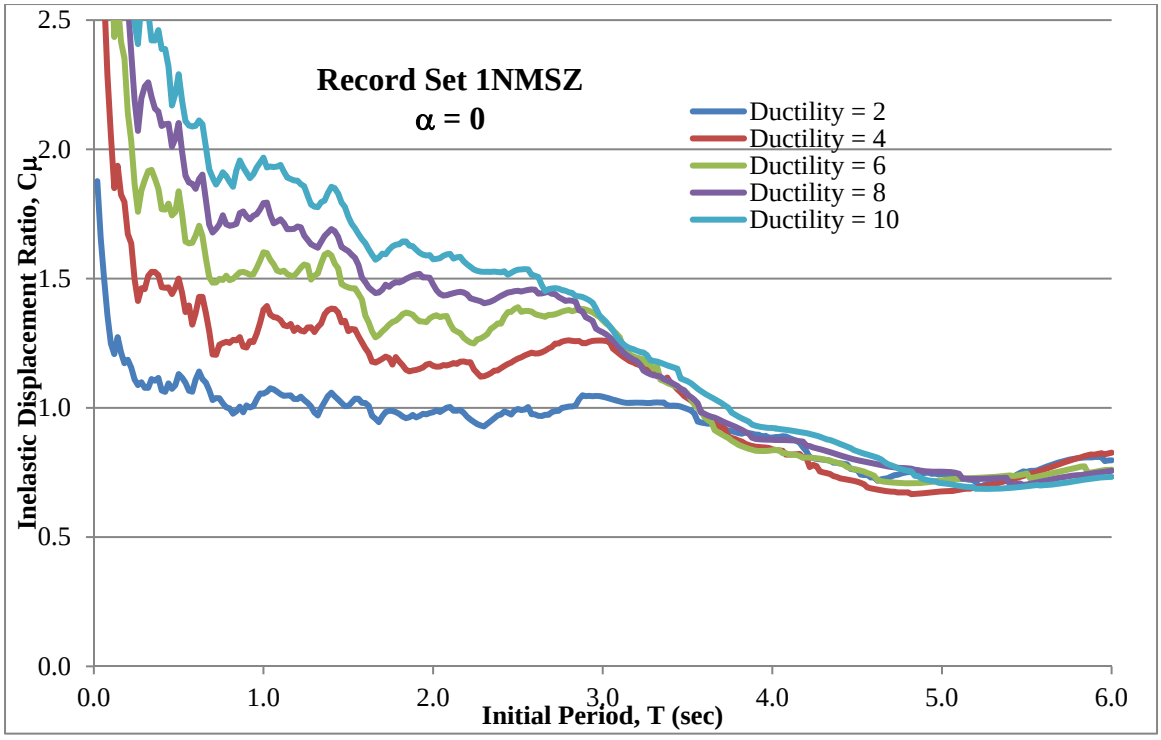

Figure F-14. Inelastic Displacement Ratio - Record Set 1NMSZ (α = 0)

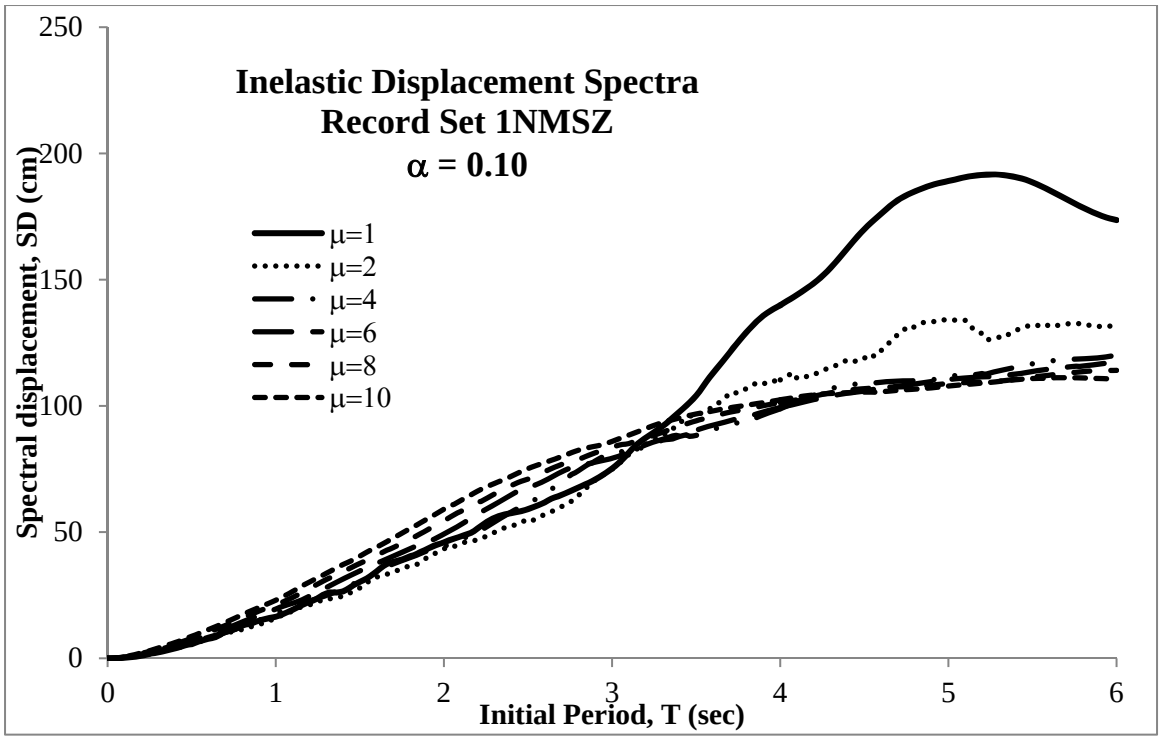

Figure F-15. Inelastic Displacement Spectra - Record Set 1NMSZ (α = 0.10)

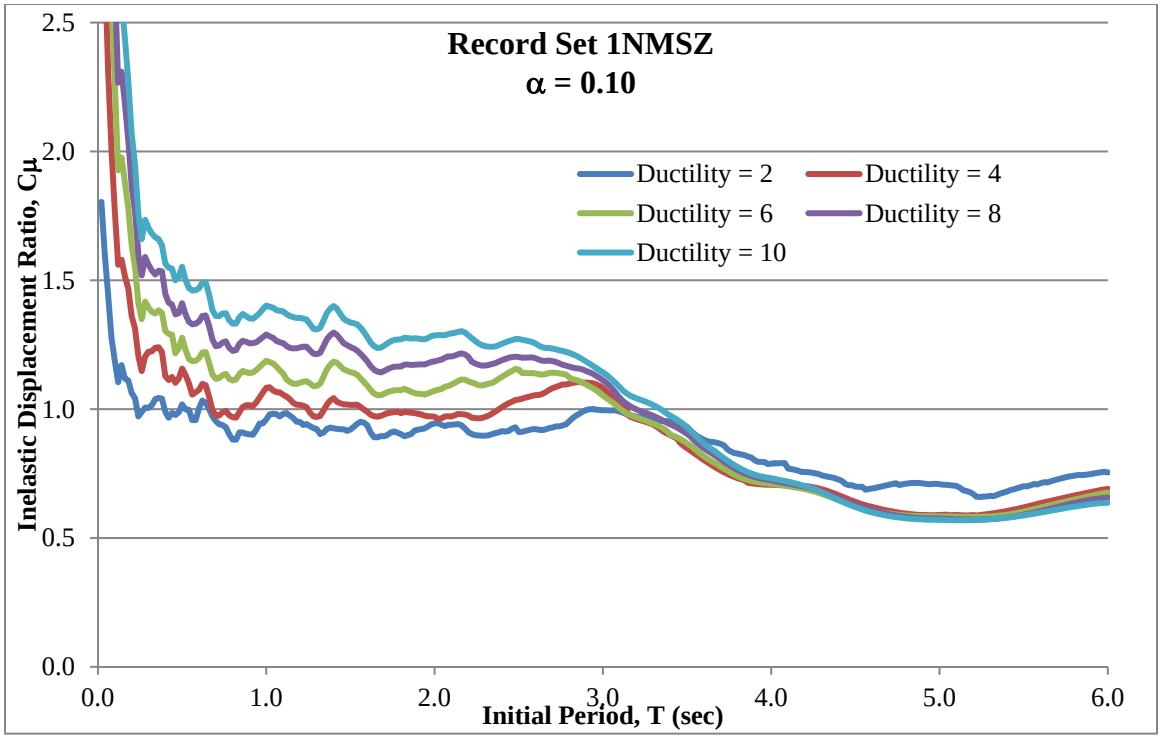

Figure F-16. Inelastic Displacement Ratio - Record Set 1NMSZ (α = 0.10)

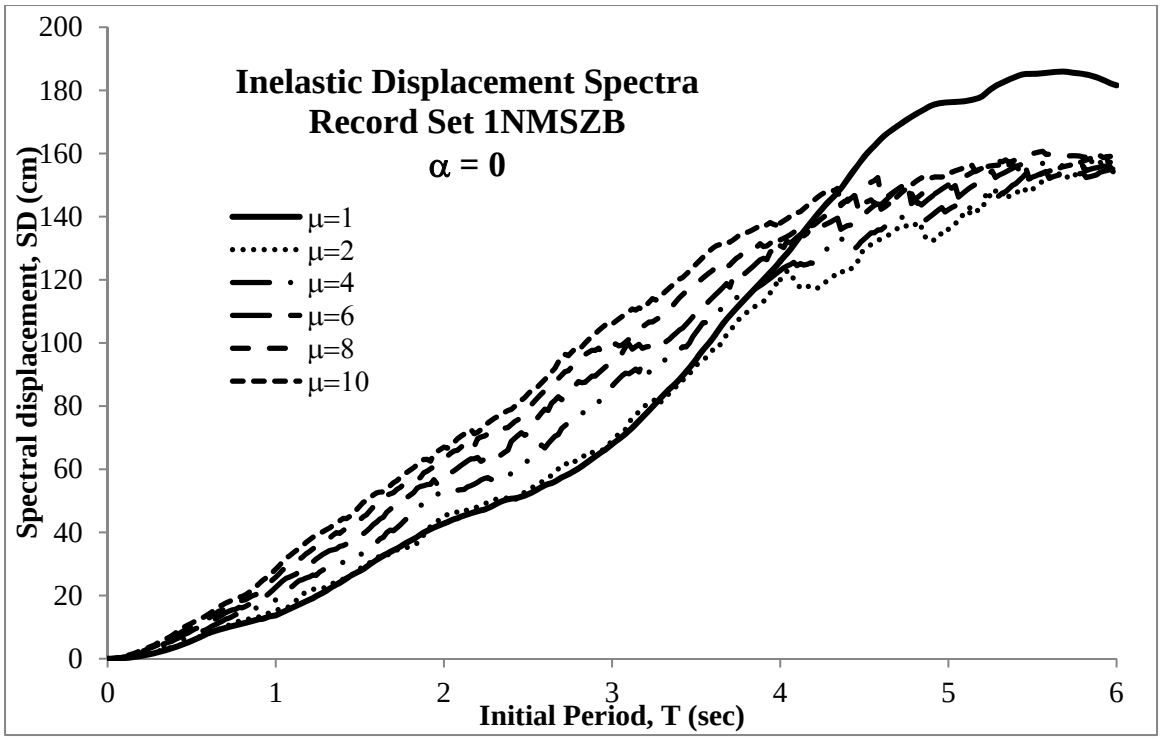

Figure F-17. Inelastic Displacement Spectra - Record Set NMSZB (α = 0)

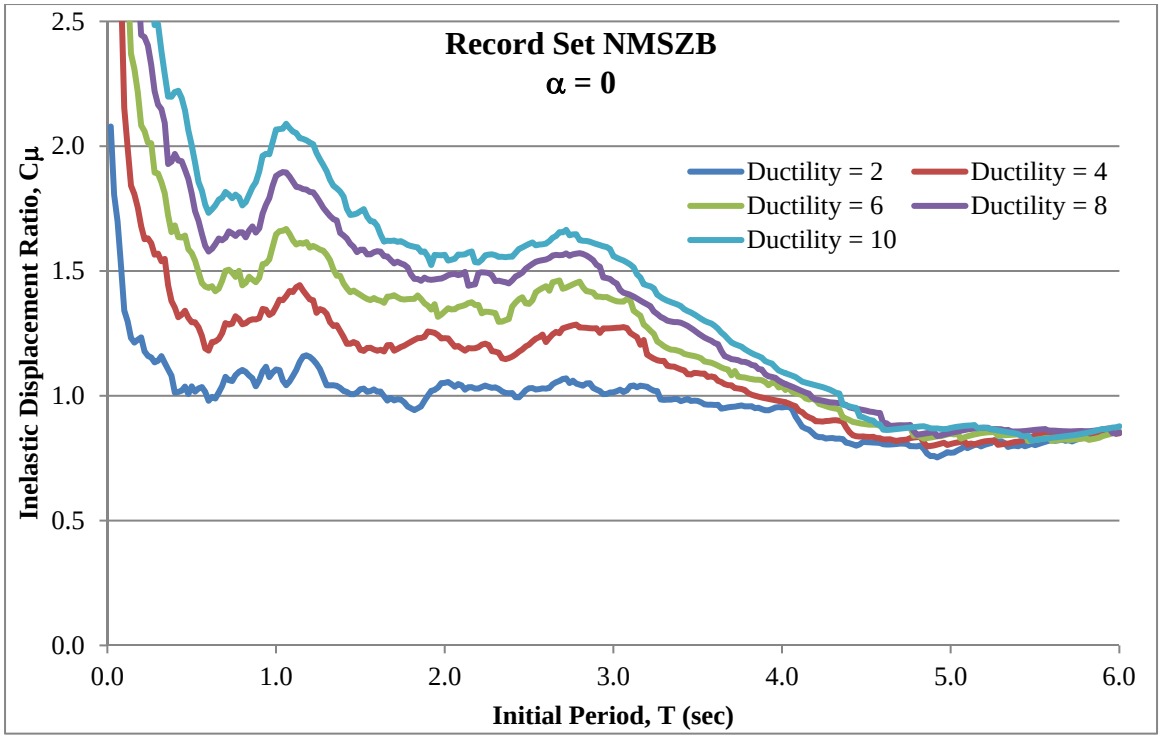

Figure F-18. Inelastic Displacement Ratio - Record Set NMSZB (α = 0)

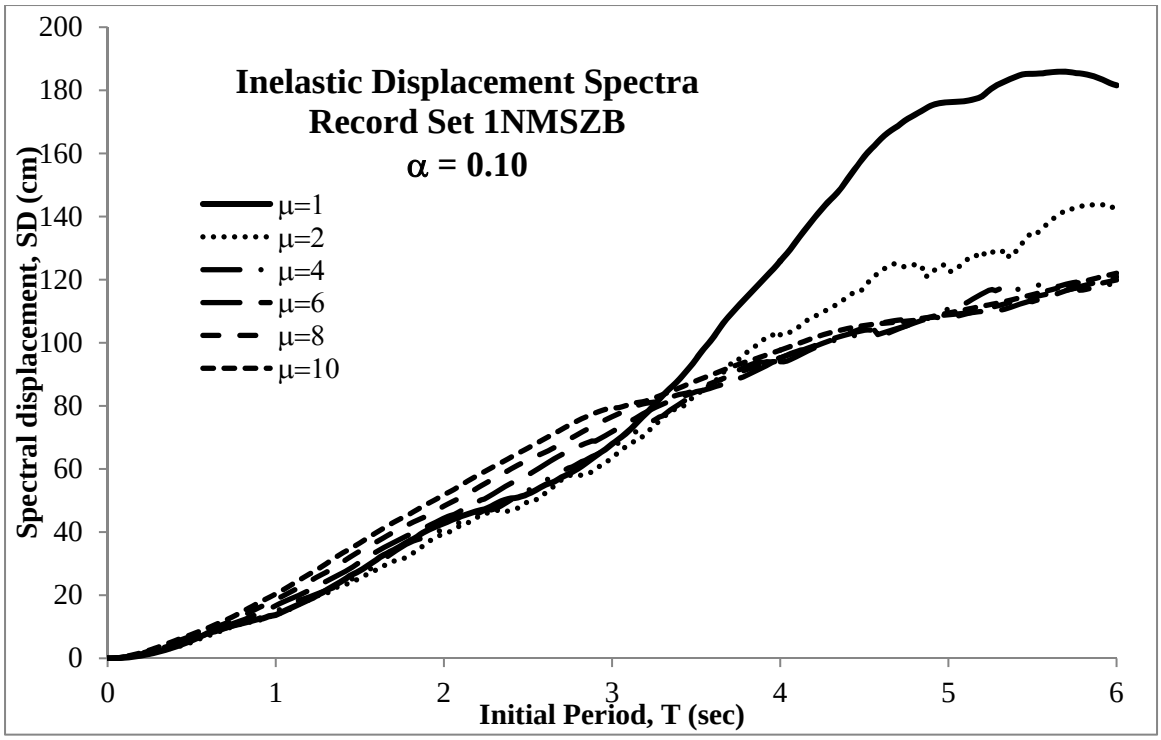

Figure F-19. Inelastic Displacement Spectra - Record Set NMSZB (α = 0.10)

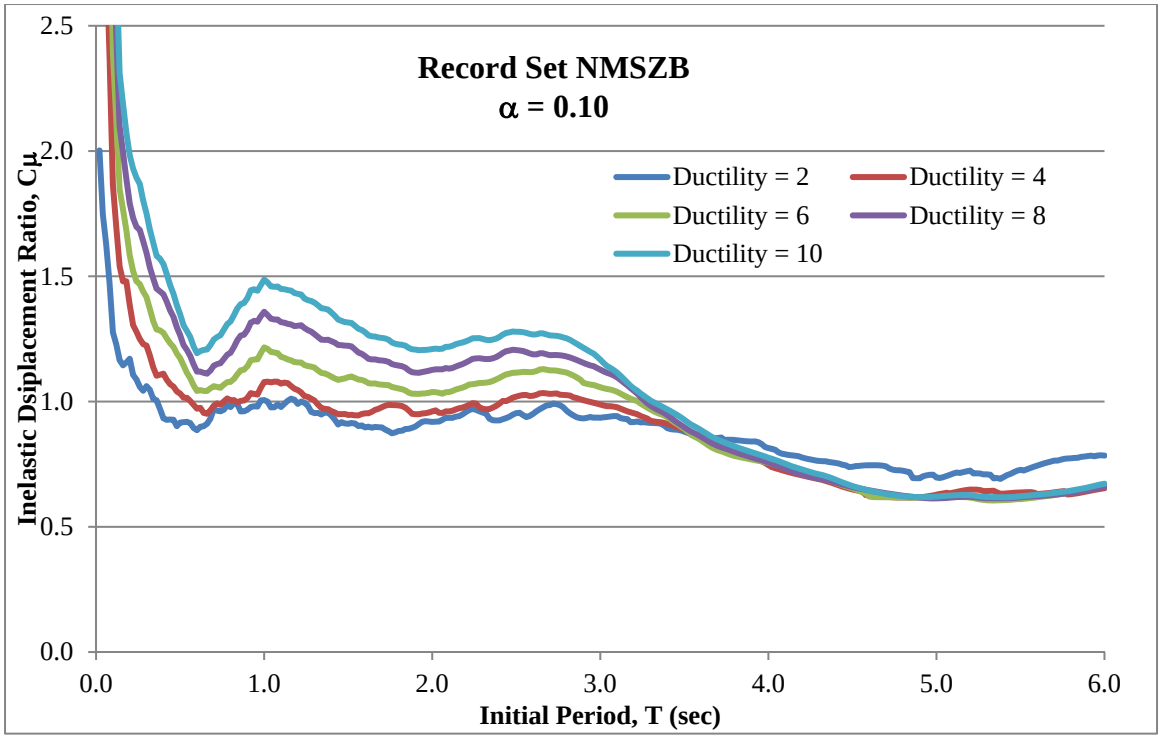

Figure F-20. Inelastic Displacement Ratio - Record Set NMSZB (α = 0.10)

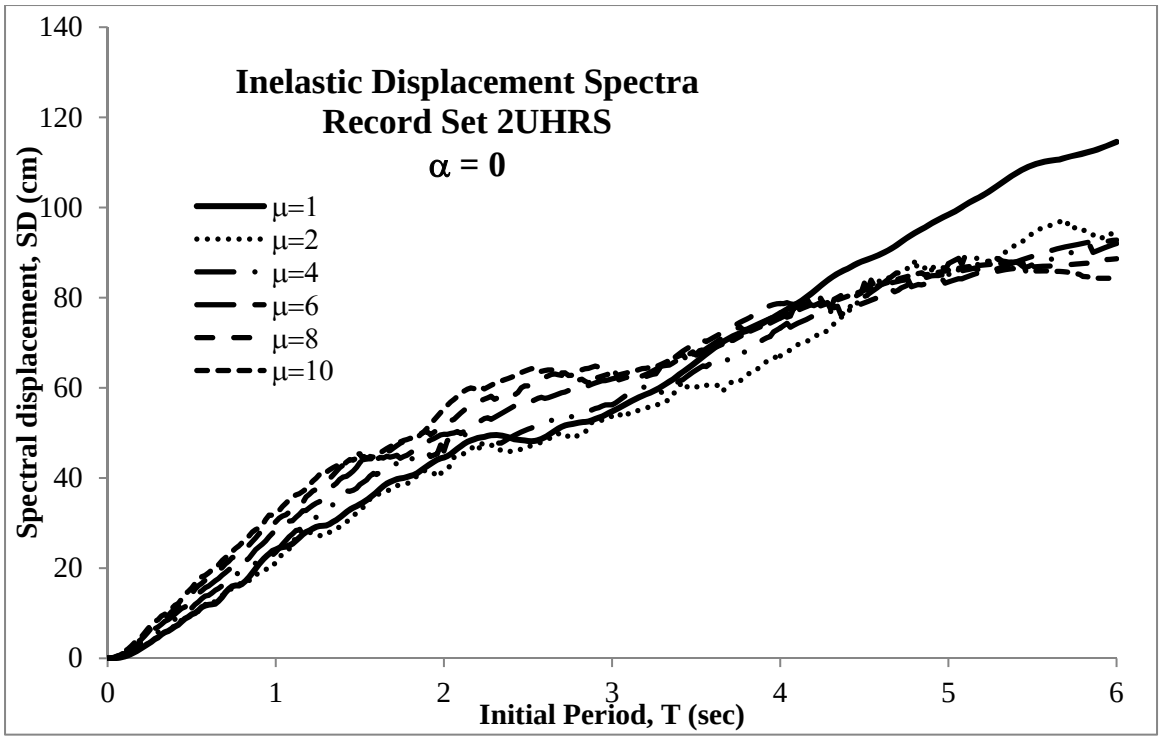

Figure F-21. Inelastic Displacement Spectra - Record Set 2UHRS (α = 0)

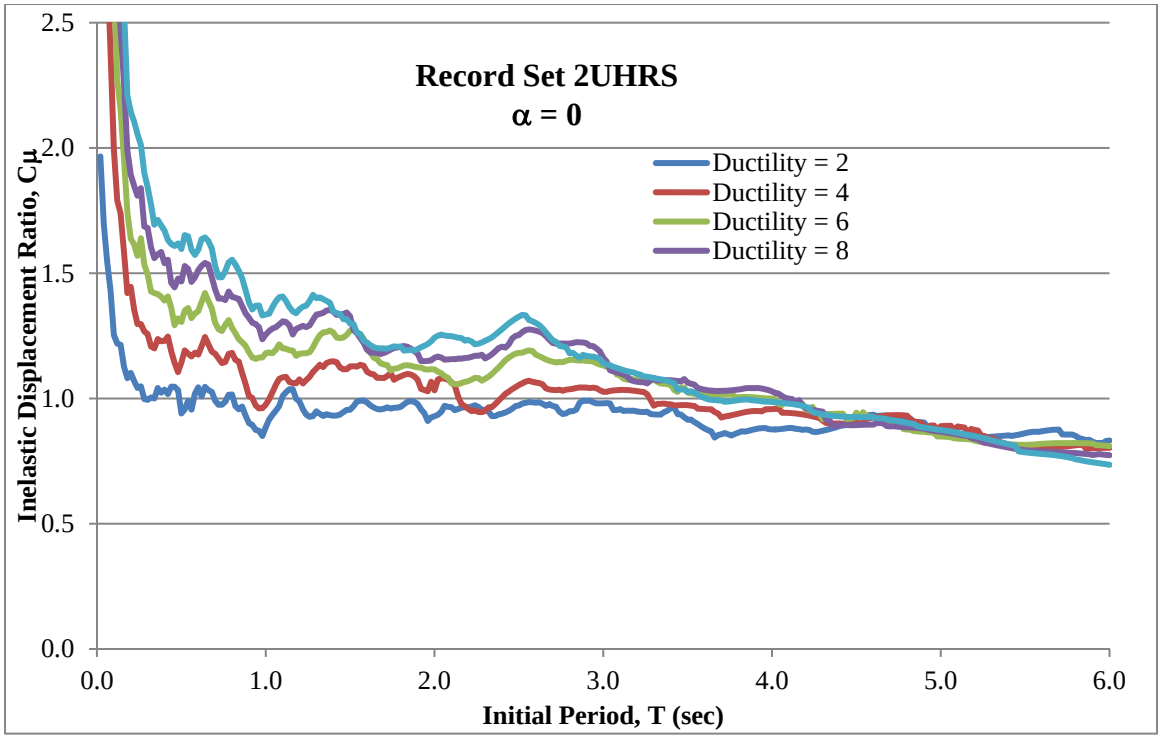

Figure F-22. Inelastic Displacement Ratio - Record Set 2UHRS (α = 0)

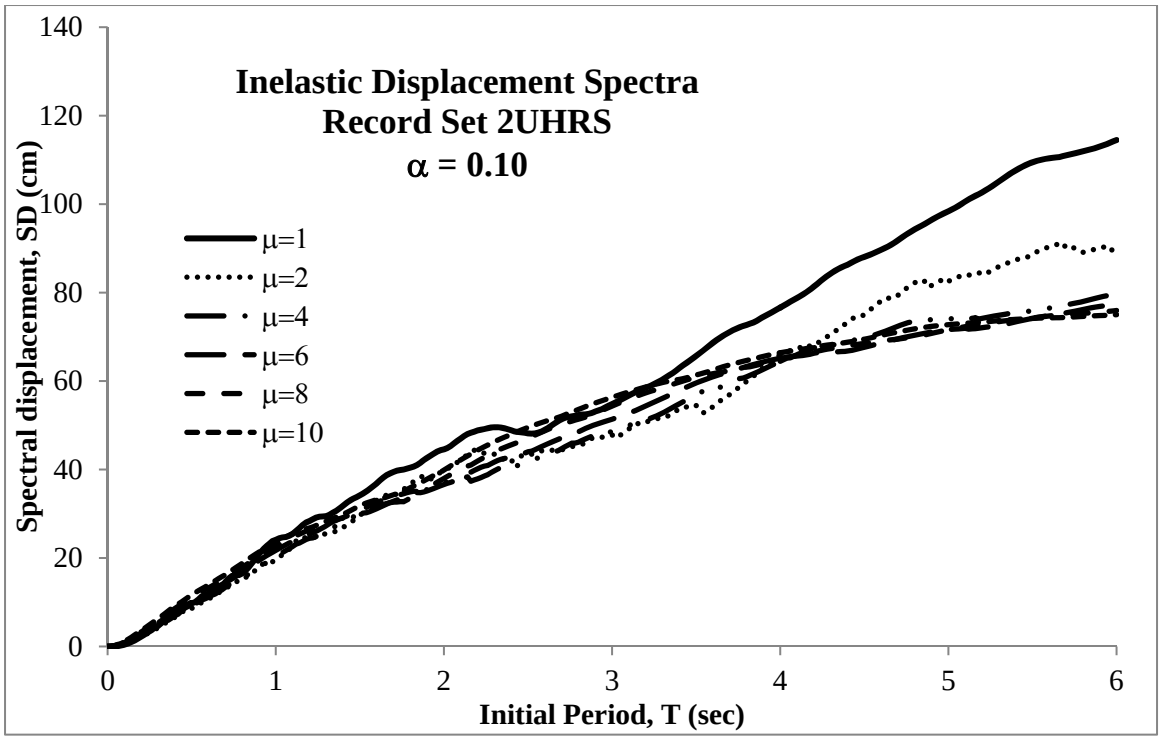

Figure F-23. Inelastic Displacement Spectra - Record Set 2UHRS (α = 0.10)

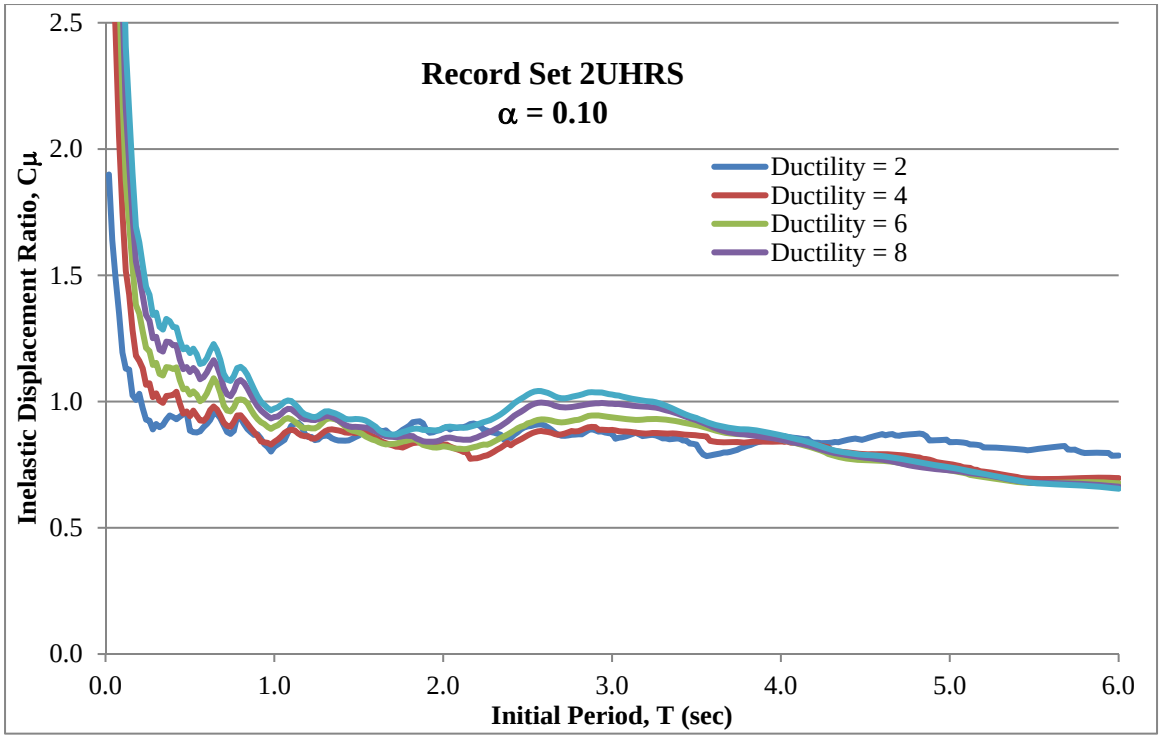

Figure F-24. Inelastic Displacement Ratio - Record Set 2UHRS (α = 0.10)

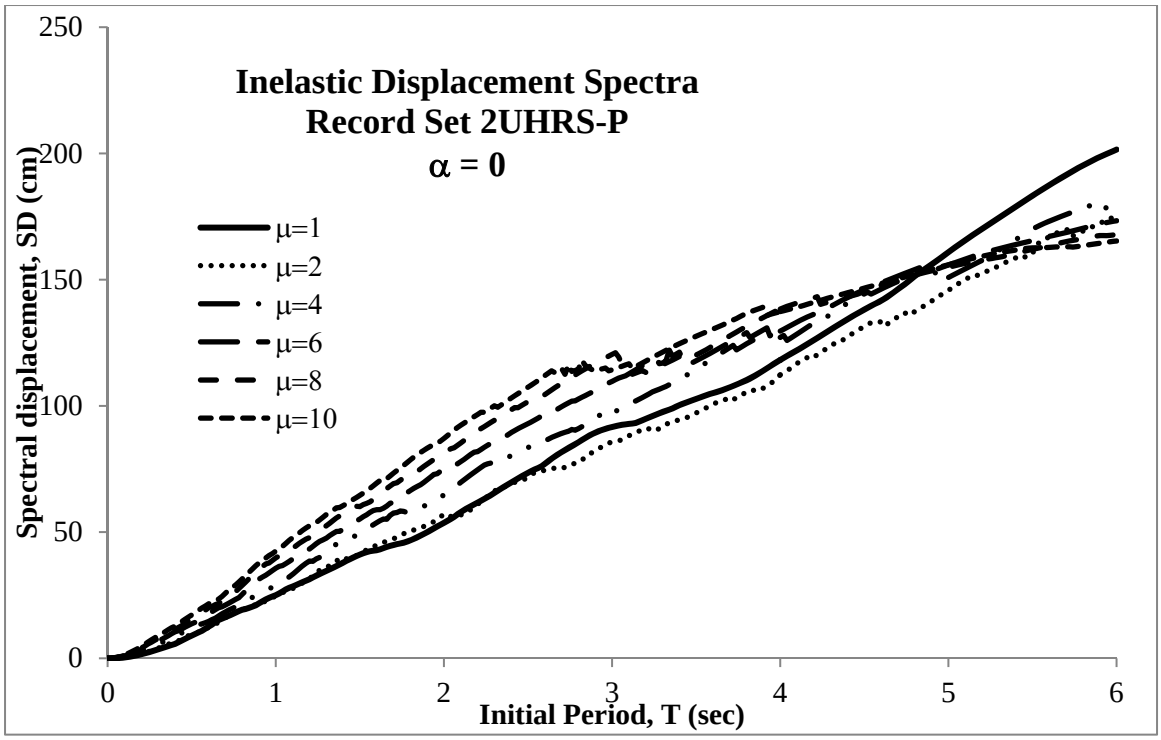

Figure F-25. Inelastic Displacement Spectra - Record Set 2UHRS-P (α = 0)

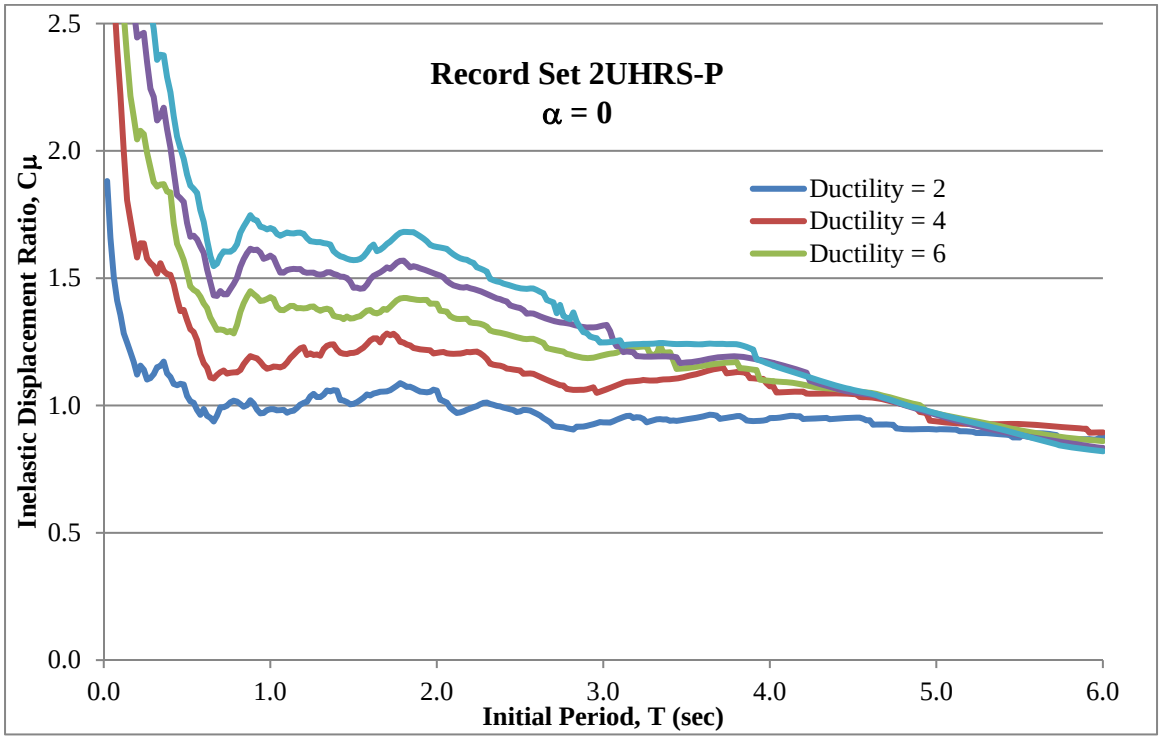

Figure F-26. Inelastic Displacement Ratio - Record Set 2UHRS-P (α = 0)

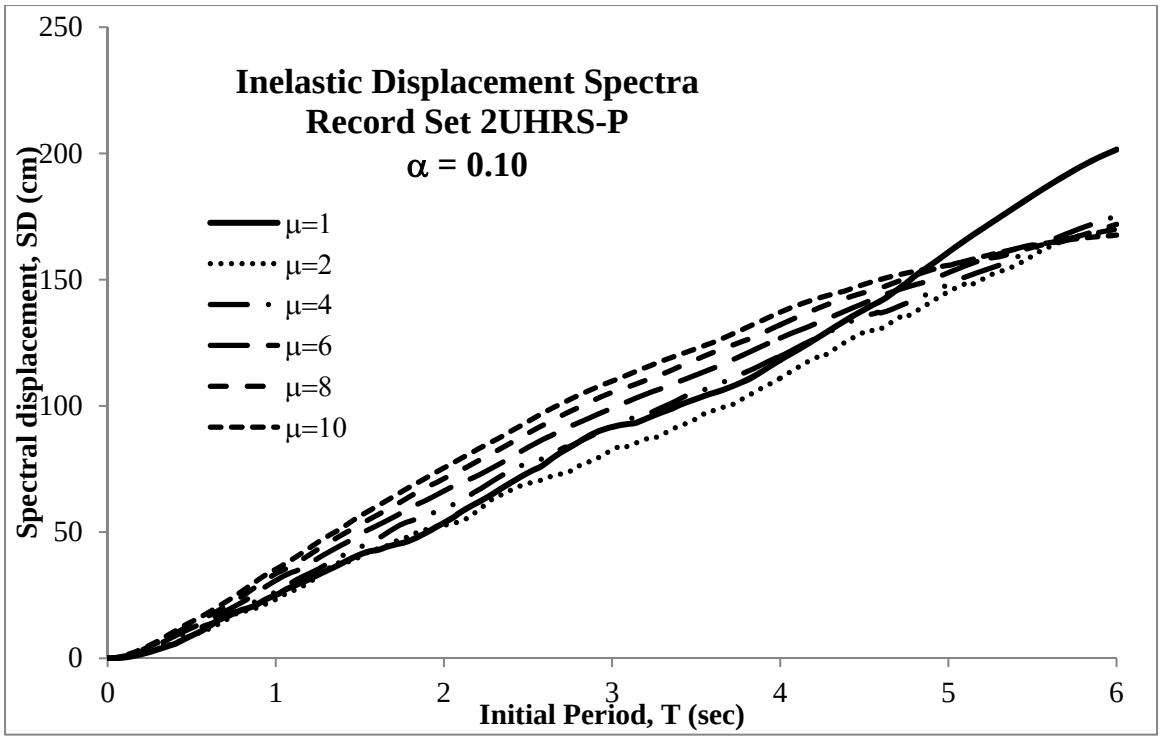

Figure F-27. Inelastic Displacement Spectra - Record Set 2UHRS-P (α = 0.10)

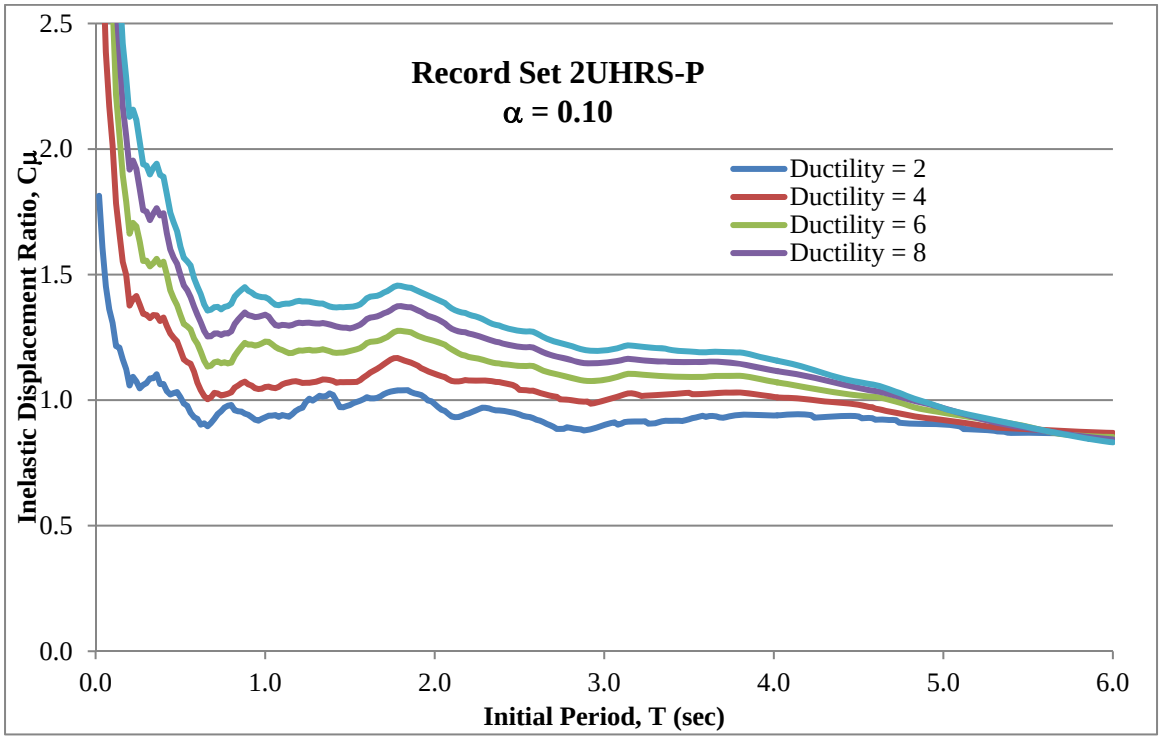

Figure F-28. Inelastic Displacement Ratio - Record Set 2UHRS-P (α = 0.10)

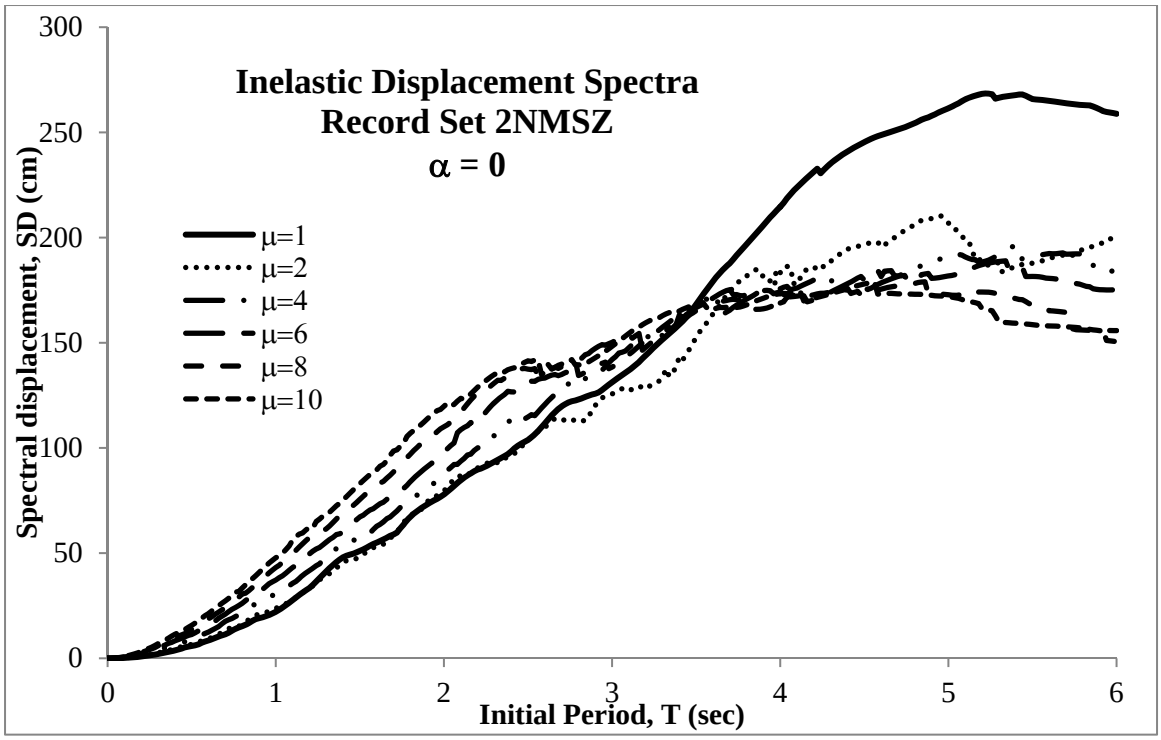

Figure F-29. Inelastic Displacement Spectra - Record Set 2NMSZ (α = 0)

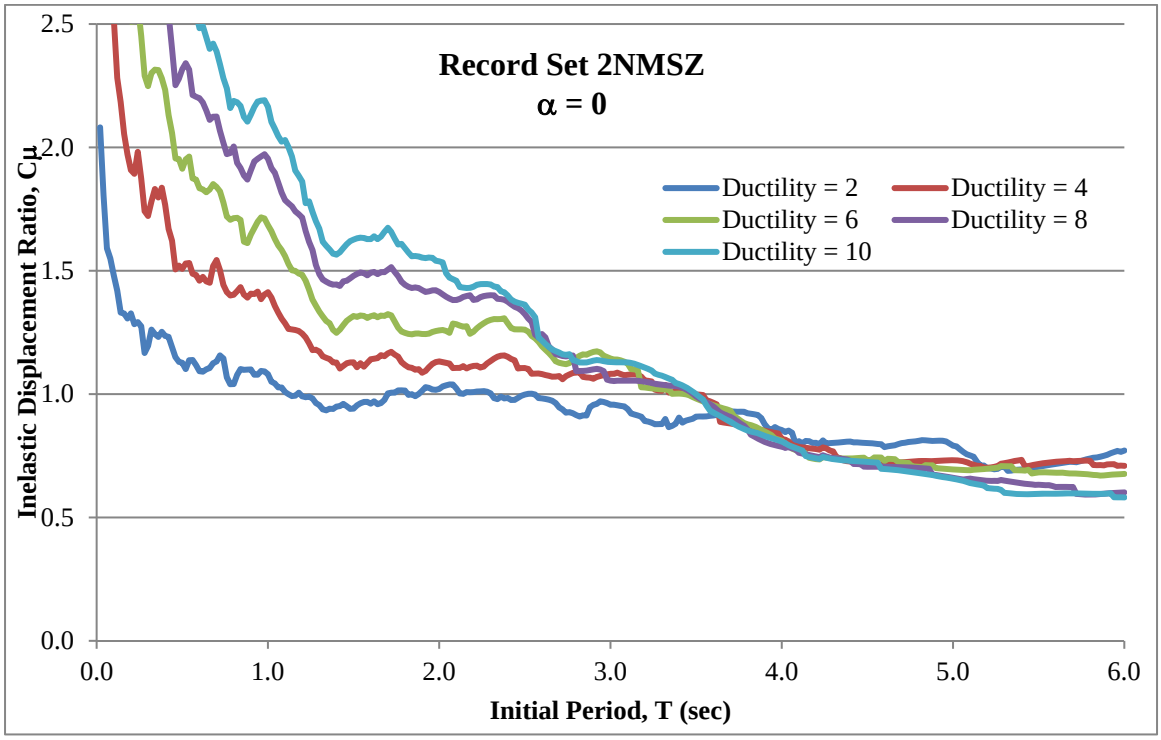

Figure F-30. Inelastic Displacement Ratio - Record Set 2NMSZ (α = 0)

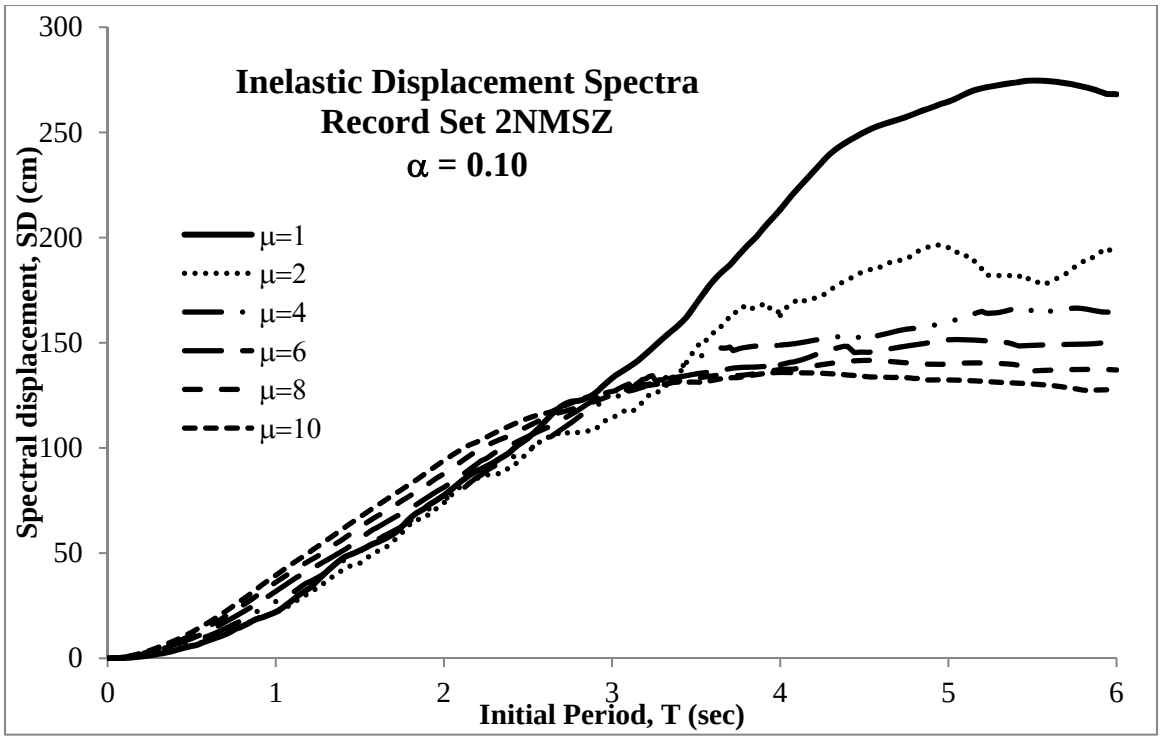

Figure F-31. Inelastic Displacement Spectra - Record Set 2NMSZ (α = 0.10)

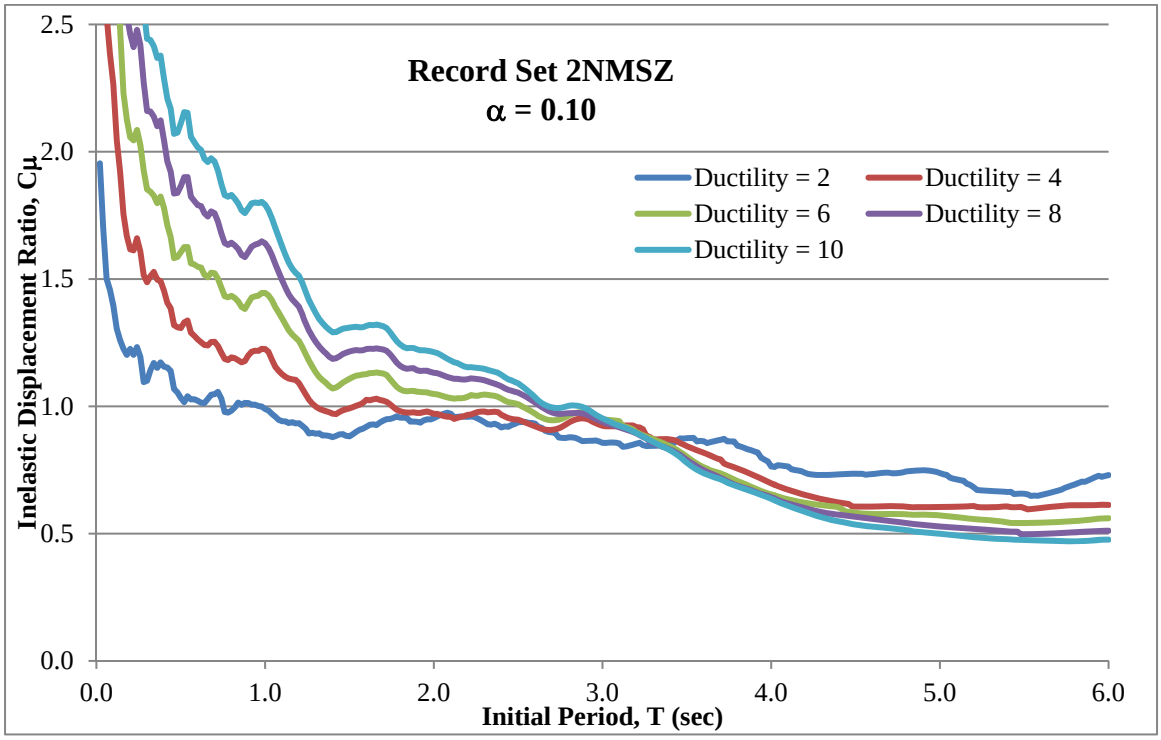

Figure F-32. Inelastic Displacement Ratio - Record Set 2NMSZ (α = 0.10)

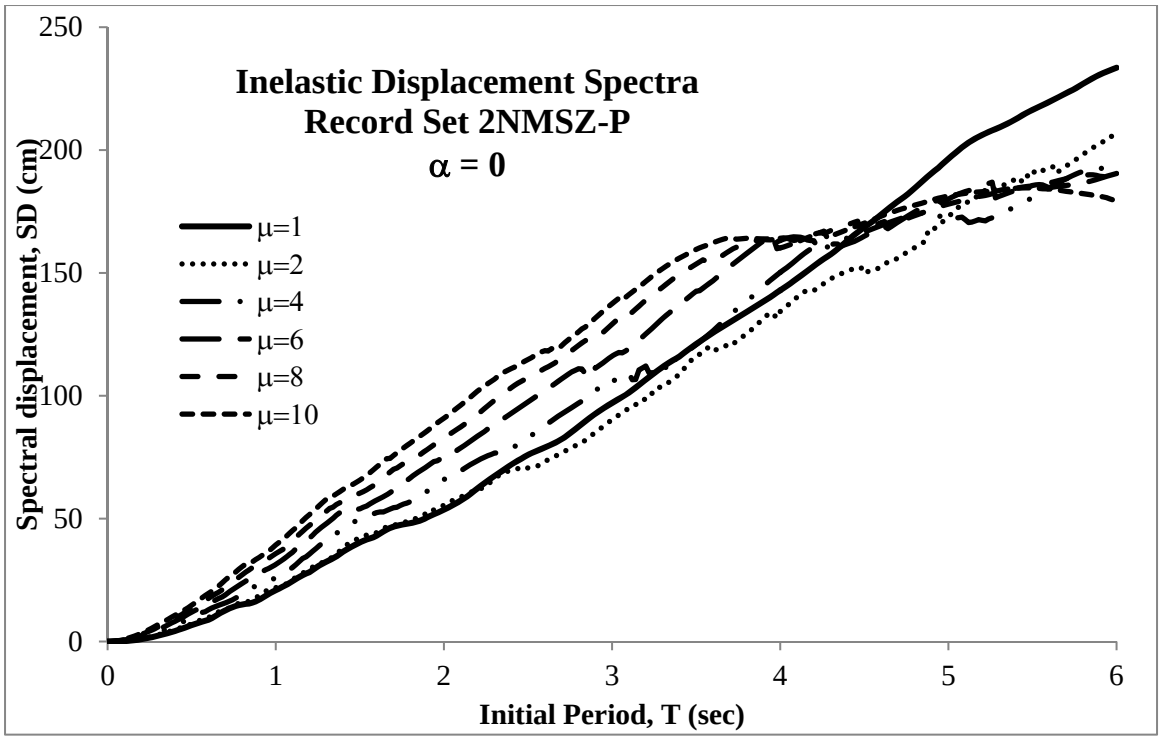

Figure F-33. Inelastic Displacement Spectra - Record Set 2NMSZ-P (α = 0)

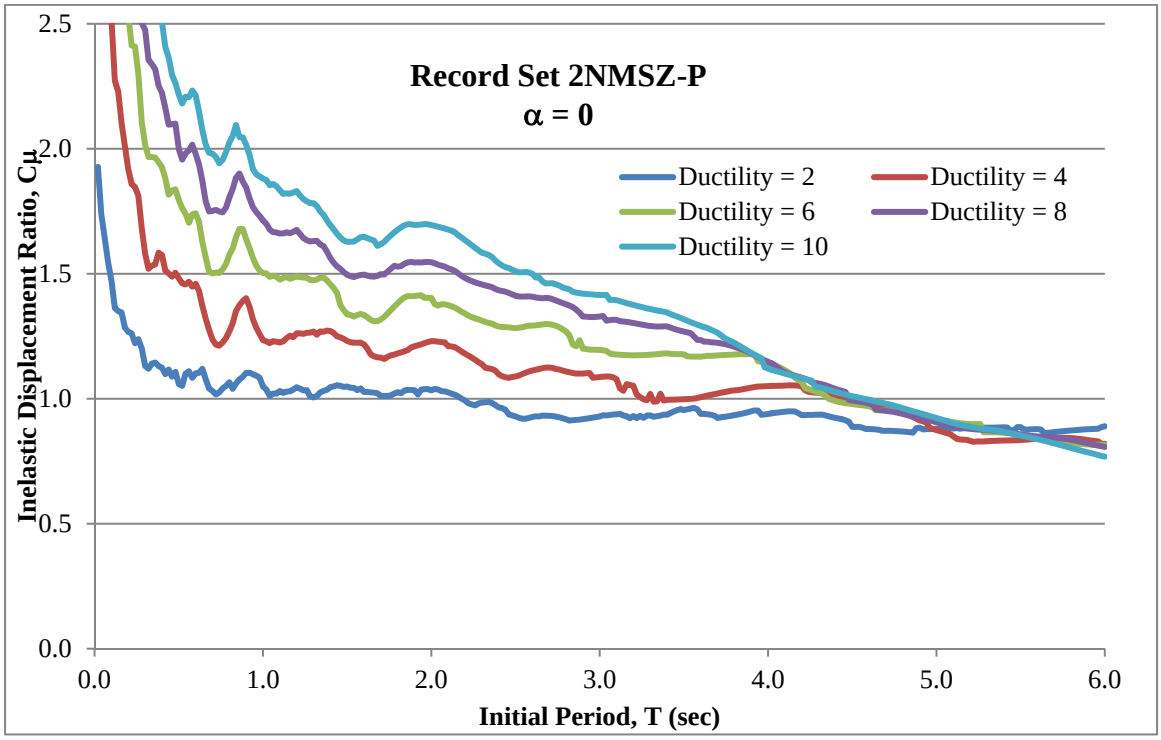

Figure F-34. Inelastic Displacement Ratio - Record Set 2NMSZ-P (α = 0)

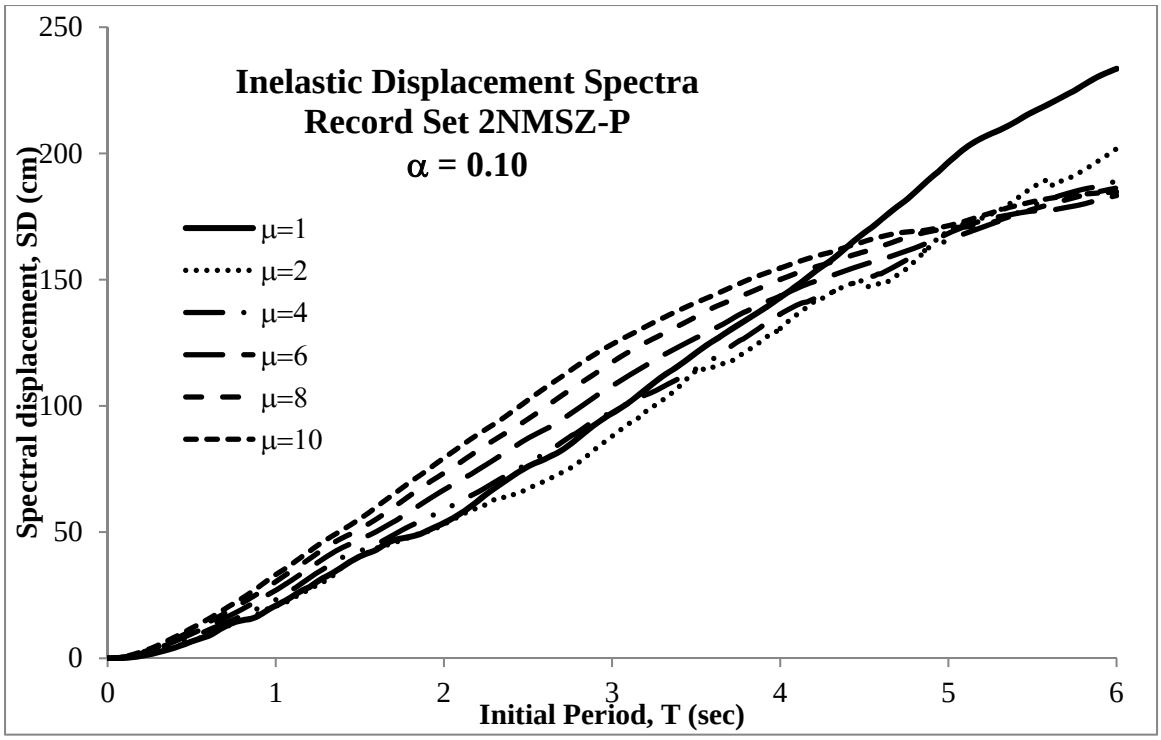

Figure F-35. Inelastic Displacement Spectra - Record Set 2NMSZ-P (α = 0.10)

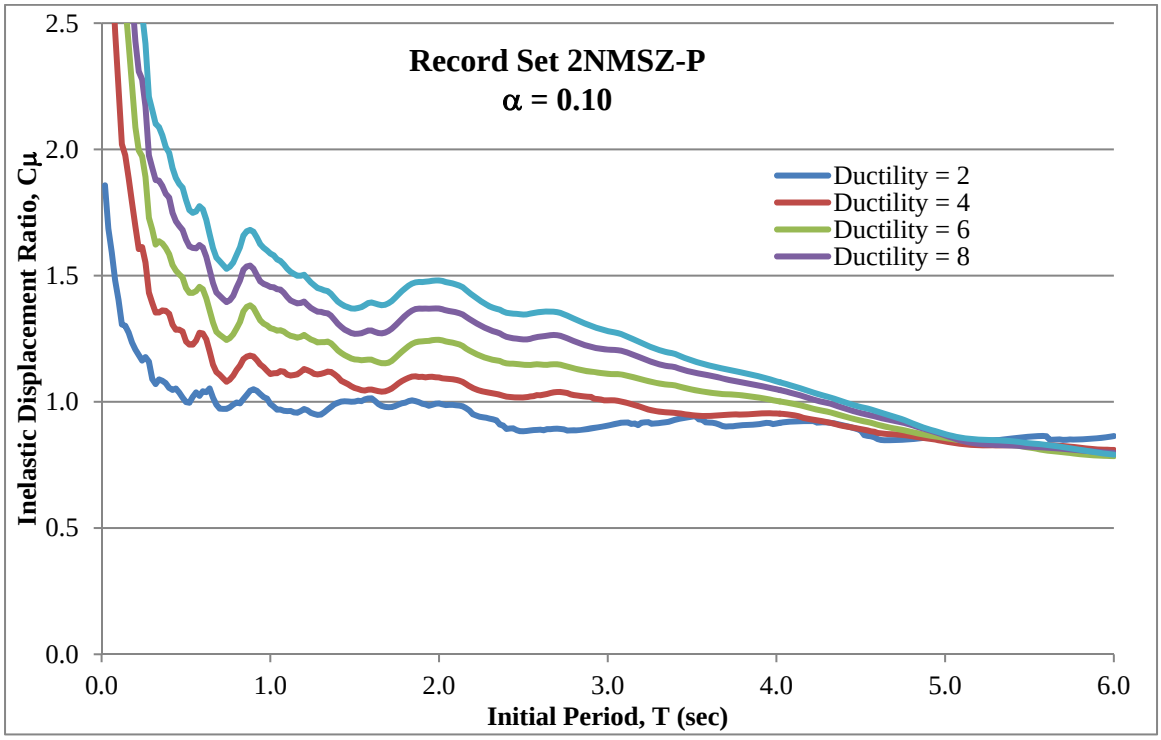

Figure F-36. Inelastic Displacement Ratio - Record Set 2NMSZ-P (α = 0.10)

APPENDIX G1 - CHAPTER 1 SUPPORTING FIGURES

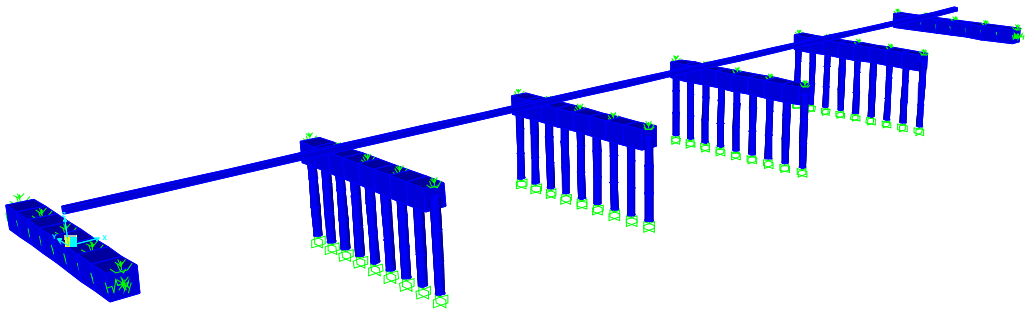

Figure G1.4-1. Bridge No. 1

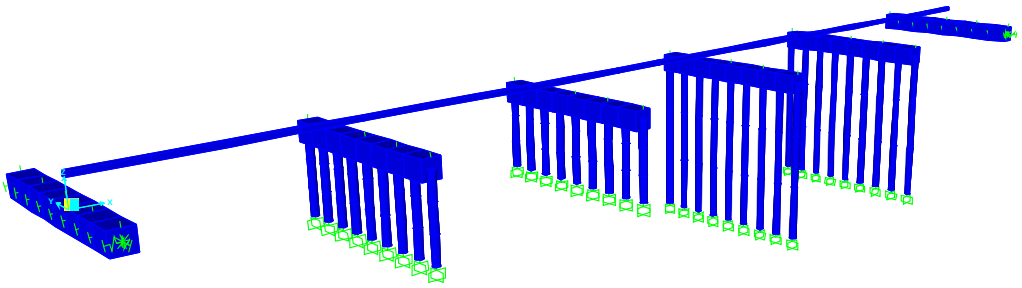

Figure G1.4-2. Bridge No. 2

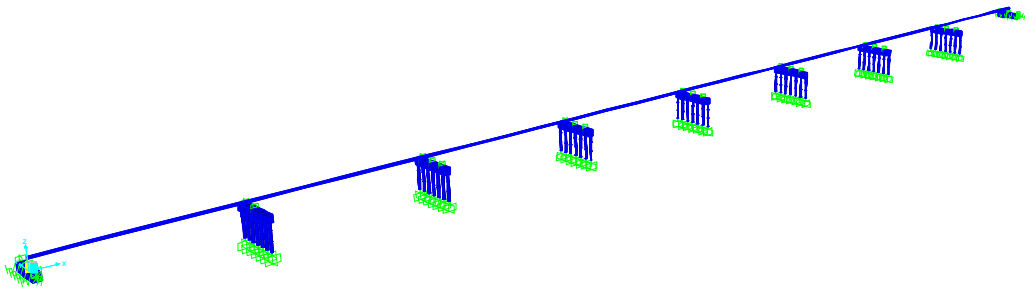

Figure G1.4-3. Bridge No. 3

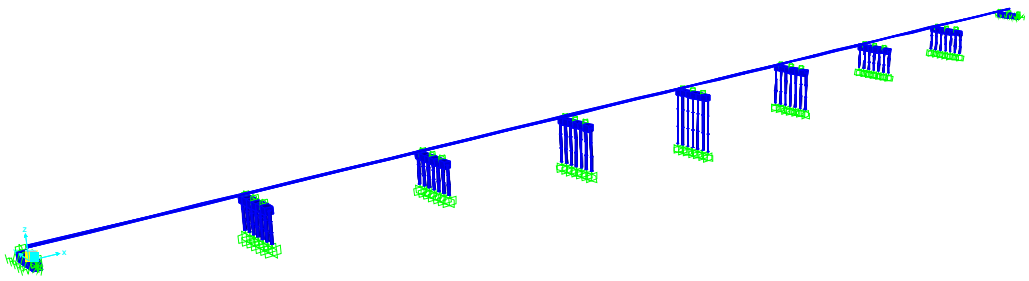

Figure G1.4-4. Bridge No. 4

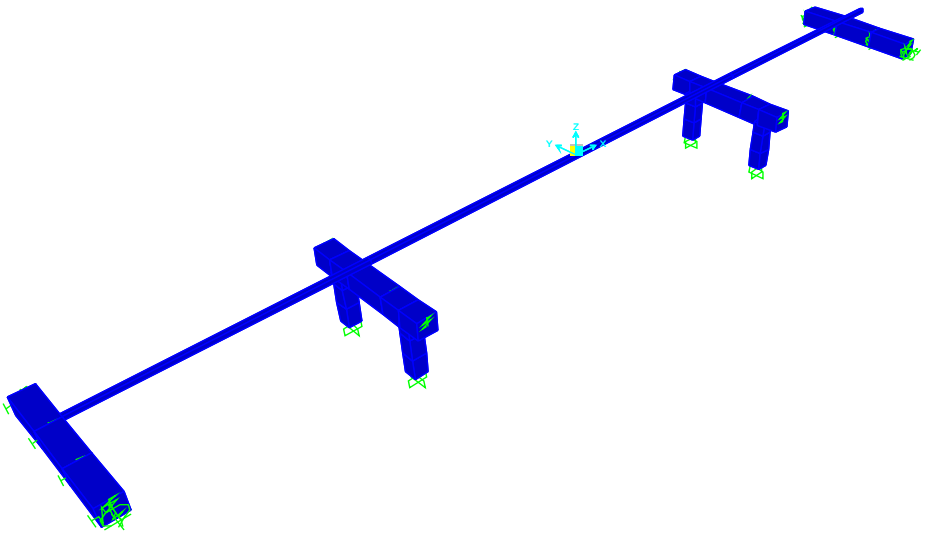

Figure G1.4-5. Bridge No. 5

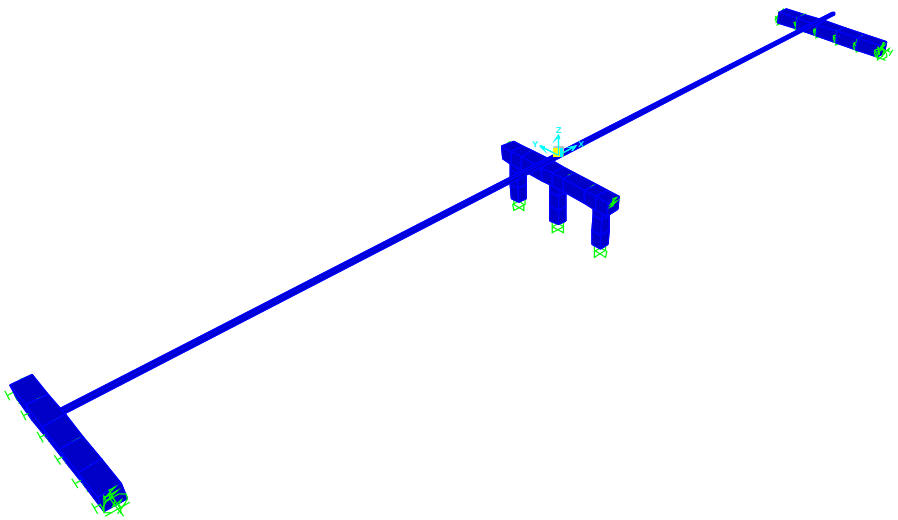

Figure G1.4-6. Bridge No. 6

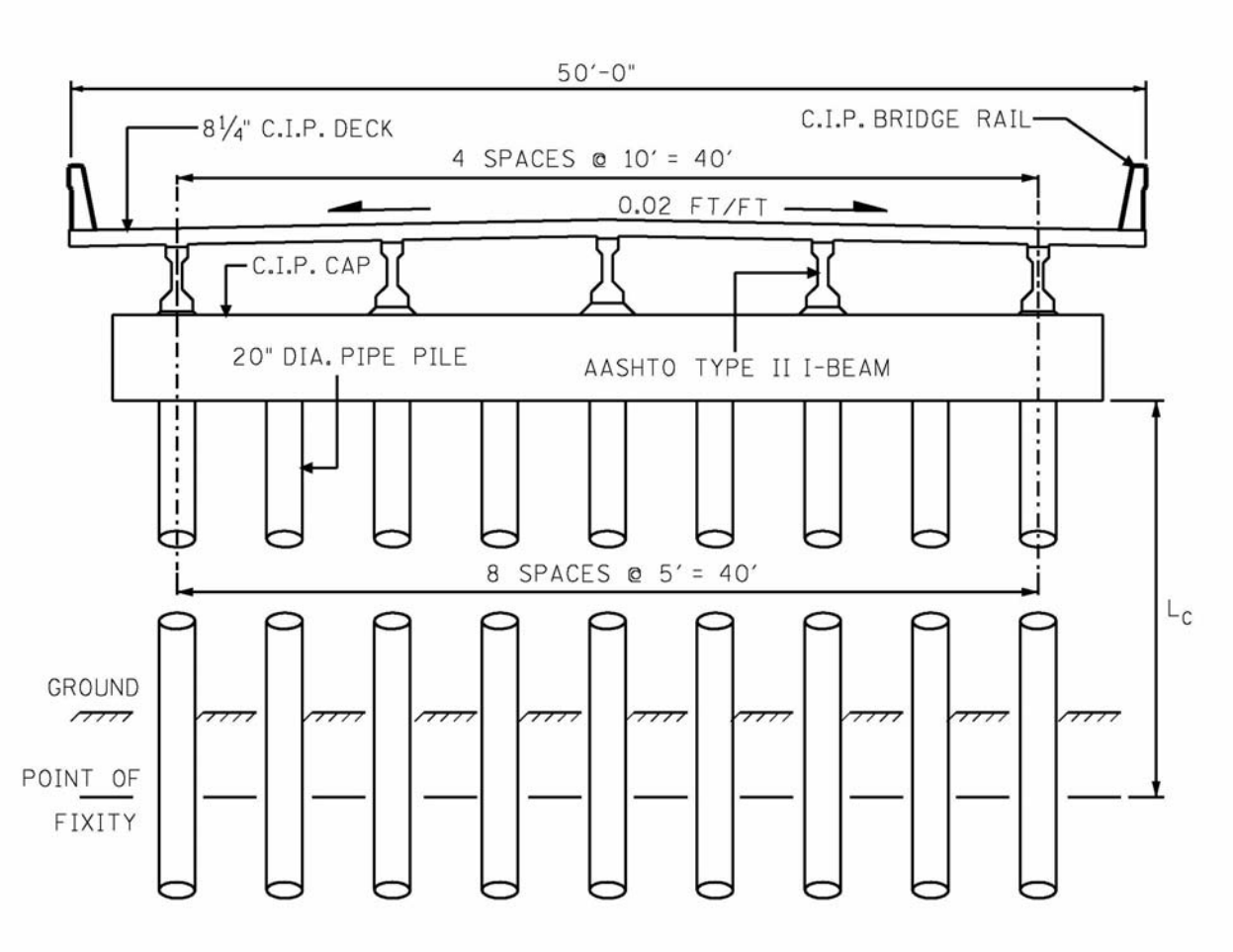

Figure G1.4-7. Cross-Section - Bridge Nos. 1 and 2

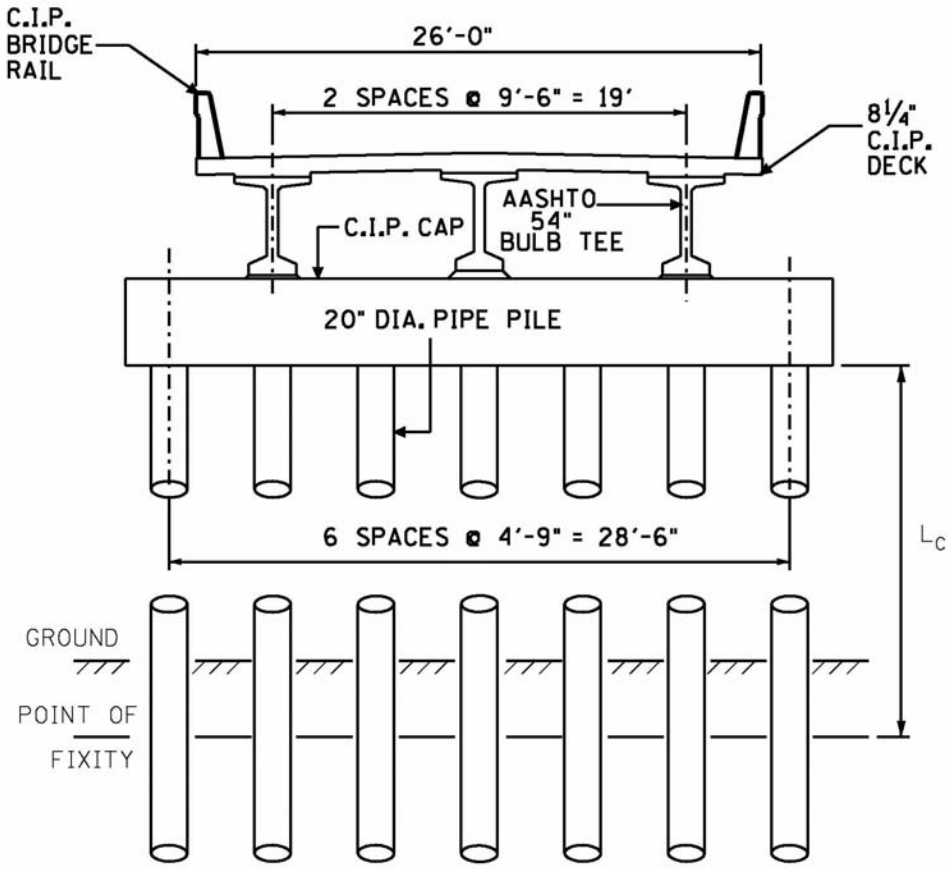

Figure G1.4-8. Cross-Section - Bridge Nos. 3 and 4

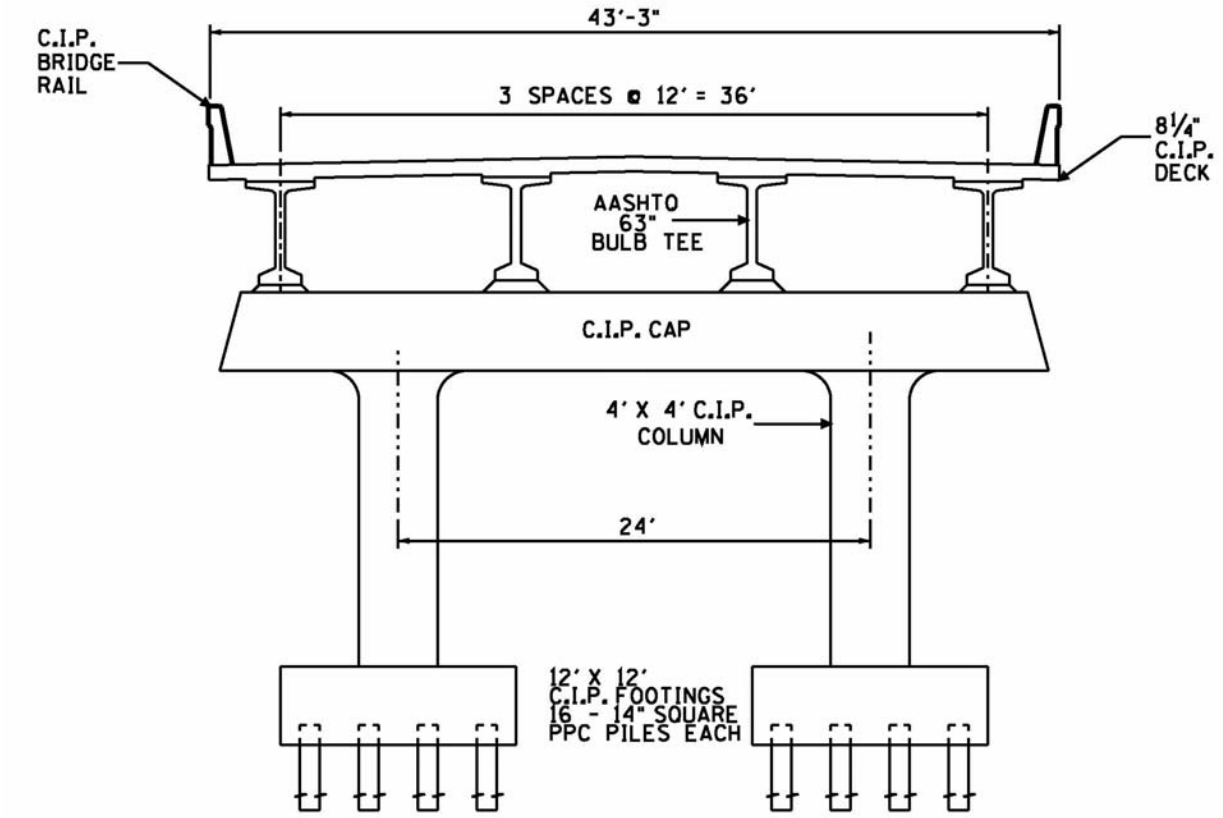

Figure G1.4-9. Cross-Section - Bridge No. 5

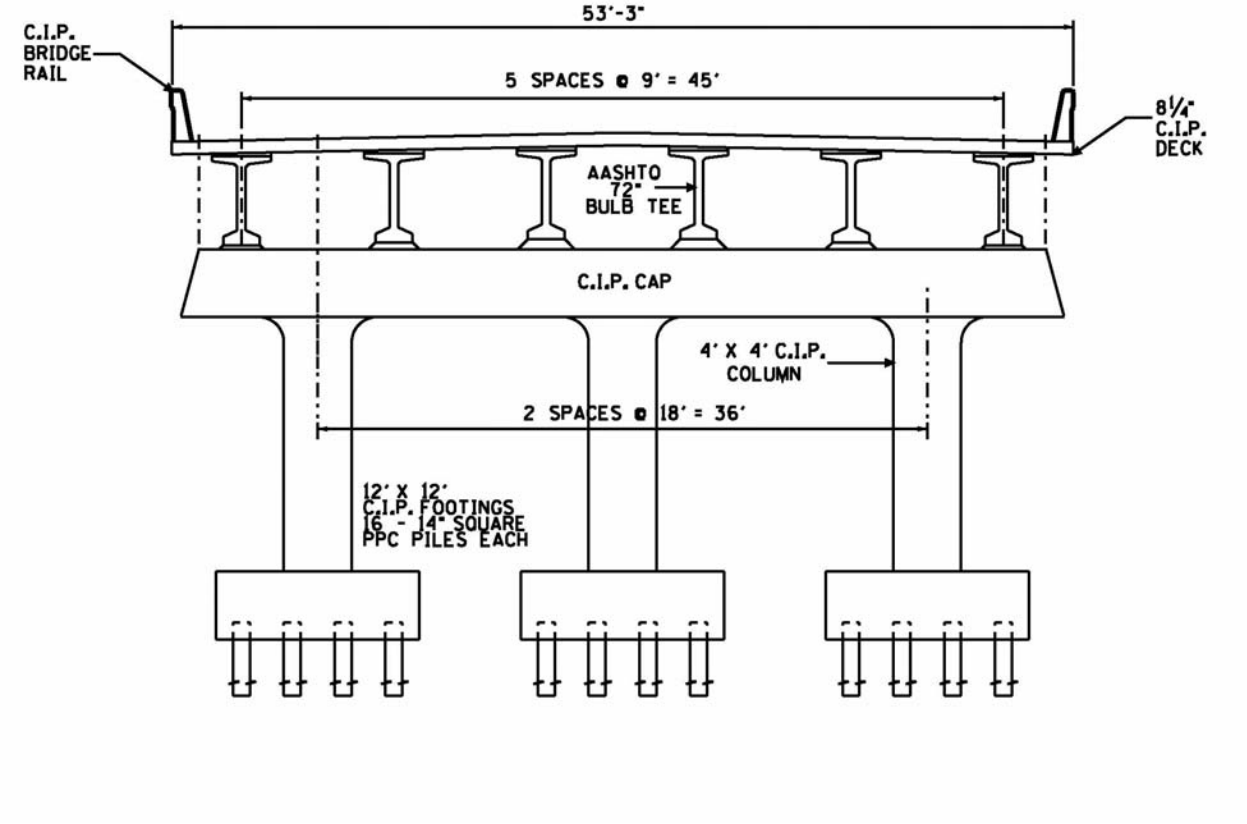

Figure G1.4-10. Cross-Section - Bridge No. 6

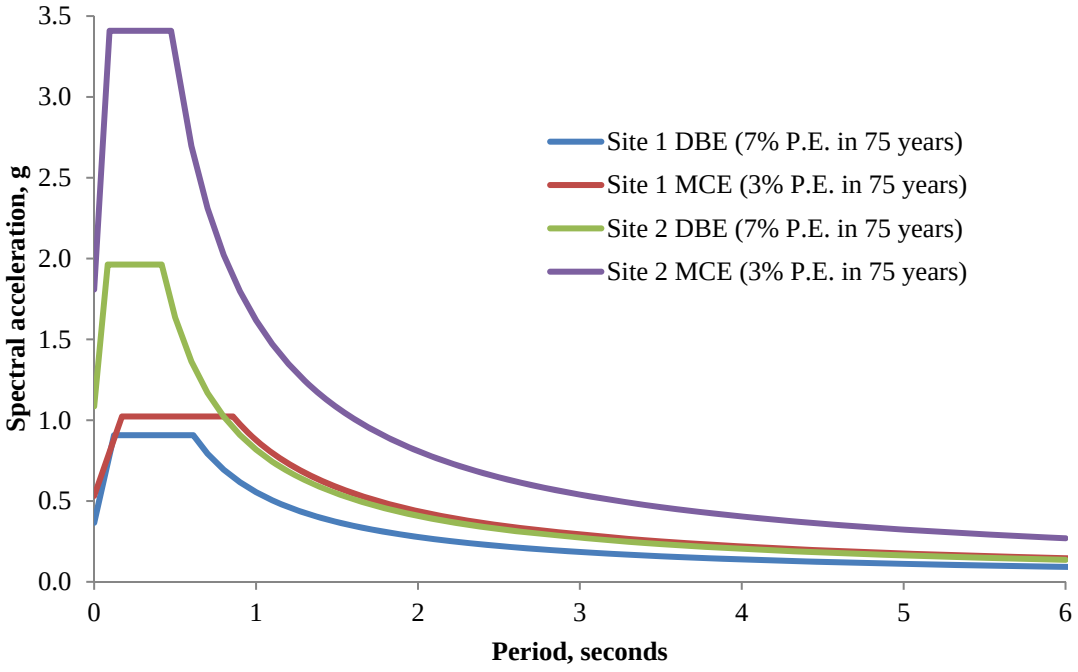

Figure G1.5.1-1. Uniform Hazard Response Spectra

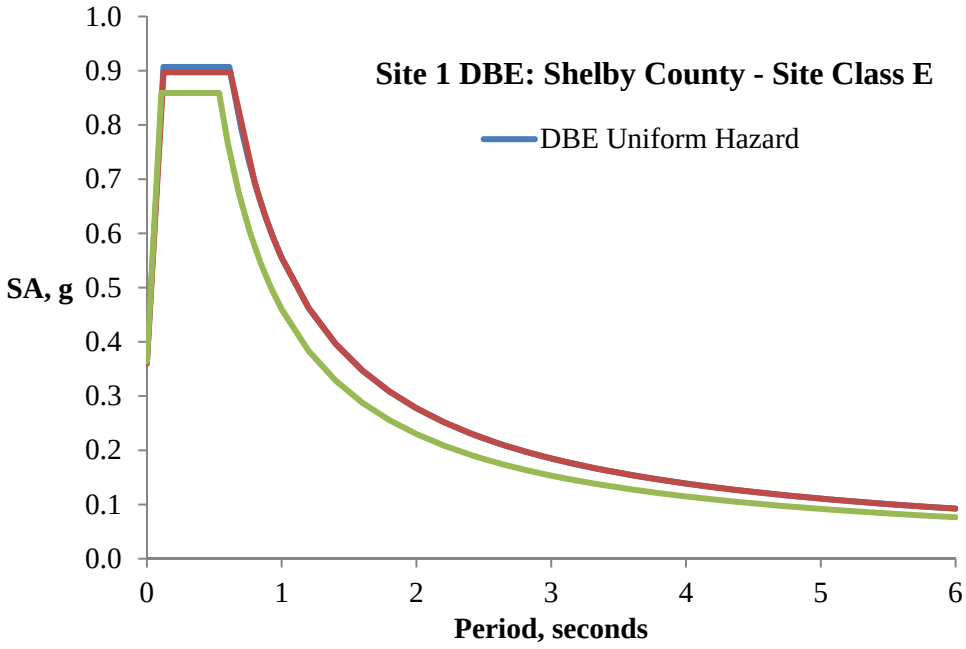

Figure G1.5.4-1. Site 1 DBE Spectra

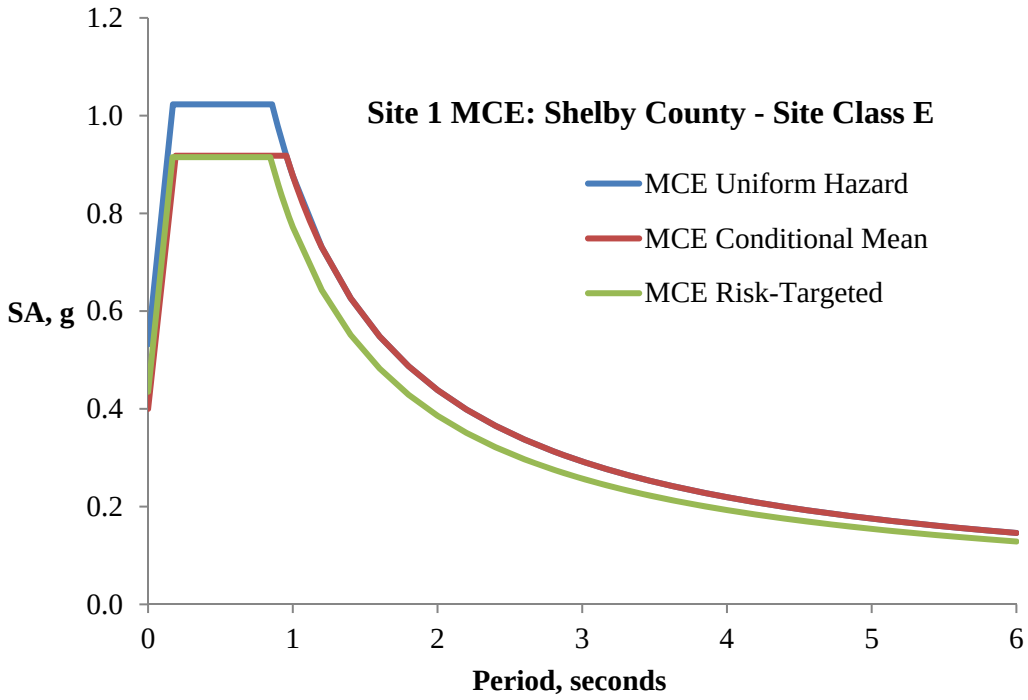

Figure G1.5.4-2. Site 1 MCE Spectra

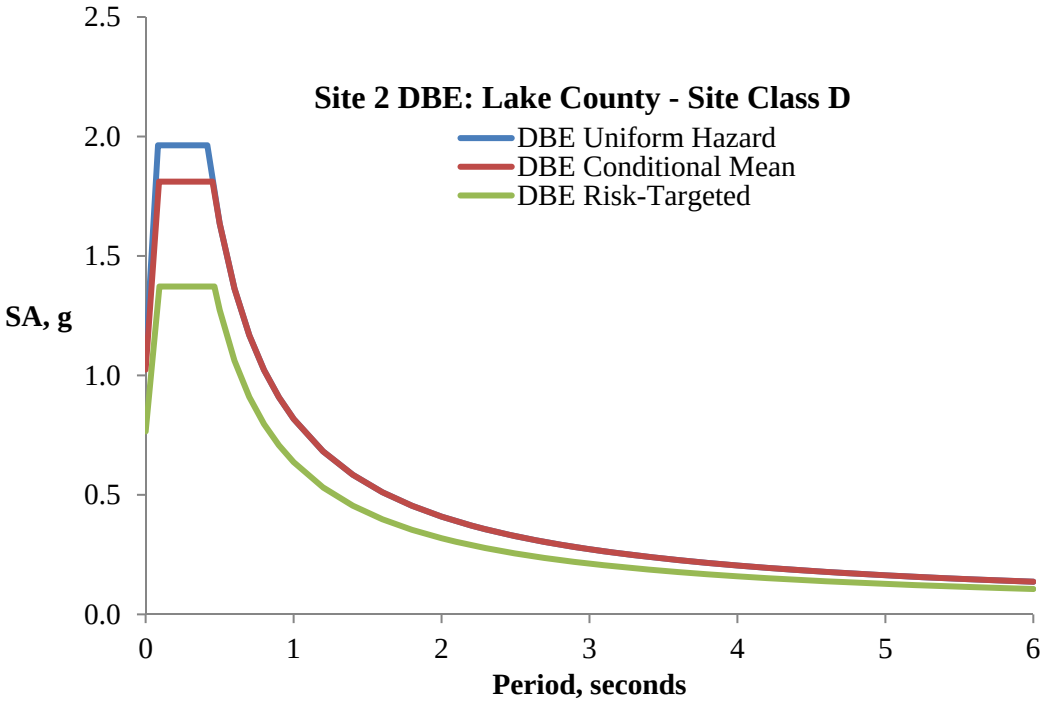

Figure G1.5.4-3. Site 2 DBE Spectra

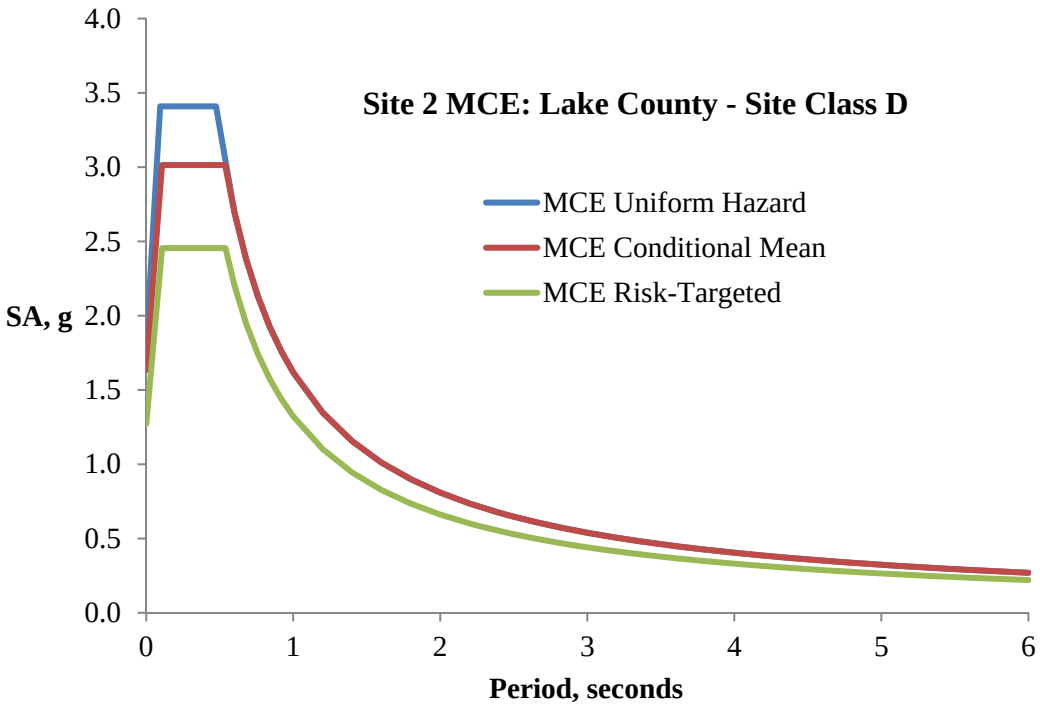

Figure G1.5.4-4. Site 2 MCE Spectra

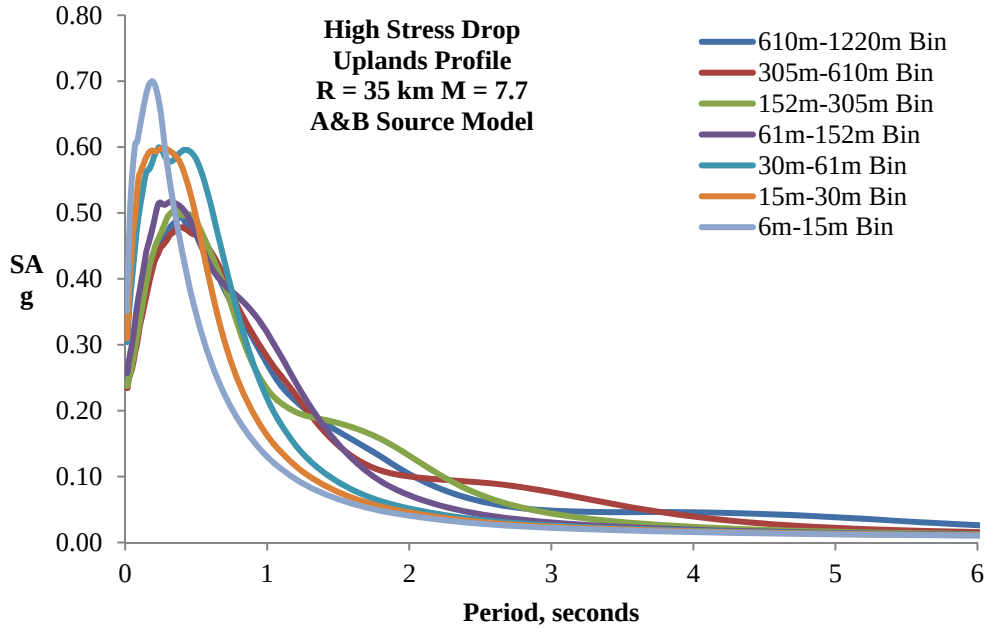

Figure G1.5.5-1. Acc-Spectra: High Stress Drop, Uplands, A&B

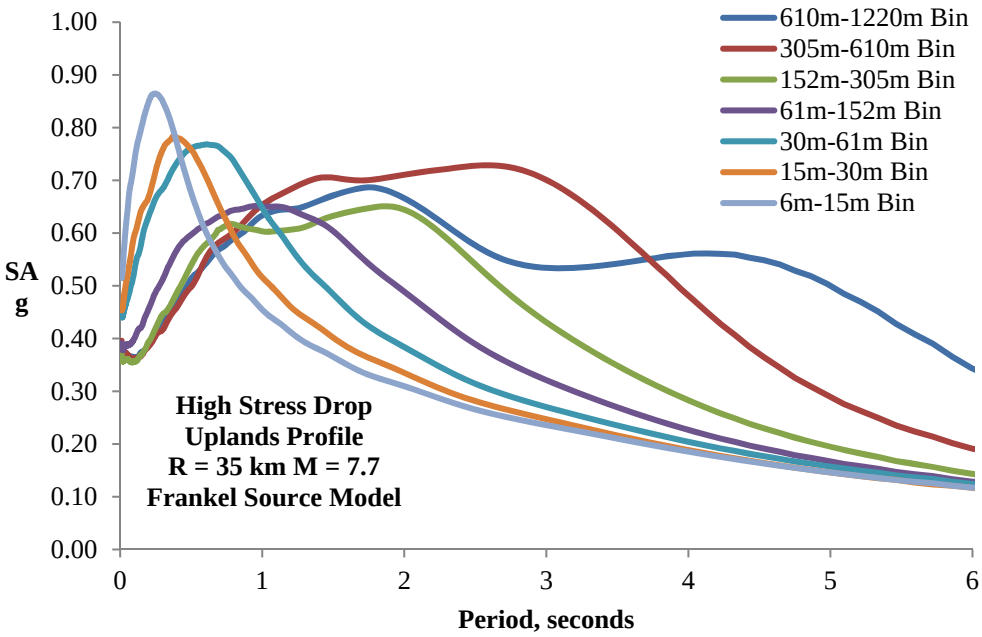

Figure G1.5.5-2. Acc-Spectra: High Stress Drop, Uplands, Frankel

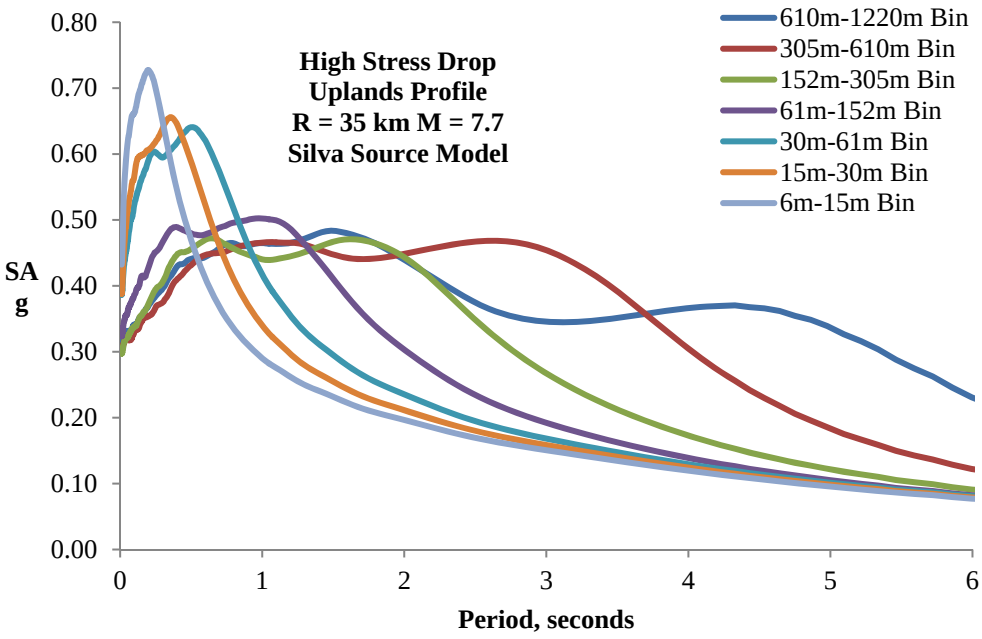

Figure G1.5.5-3. Acc-Spectra: High Stress Drop, Uplands, Silva

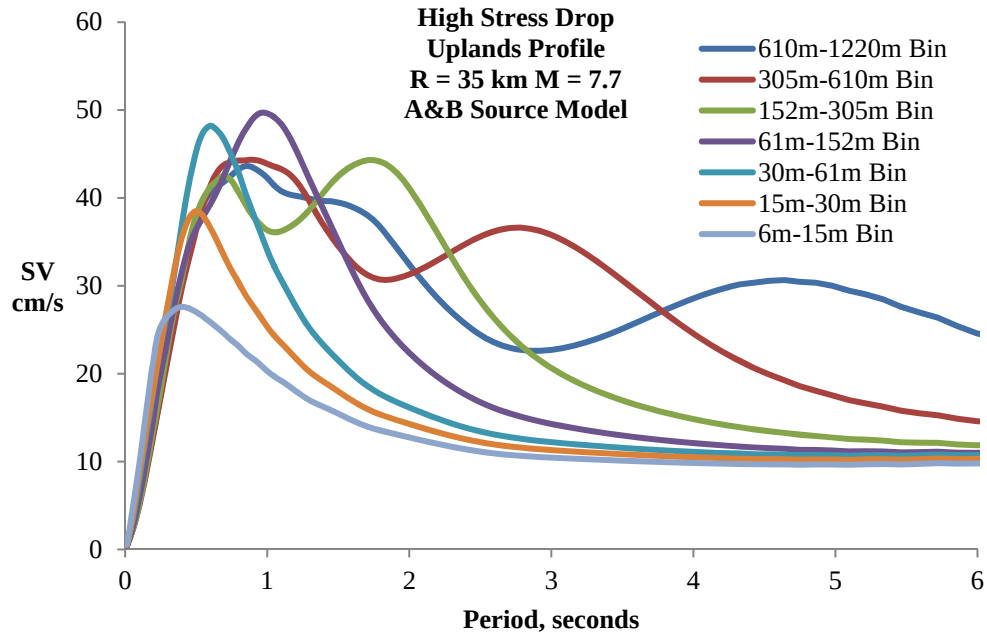

Figure G1.5.5-4. Velocity-Spectra: High Stress Drop, Uplands, A&B

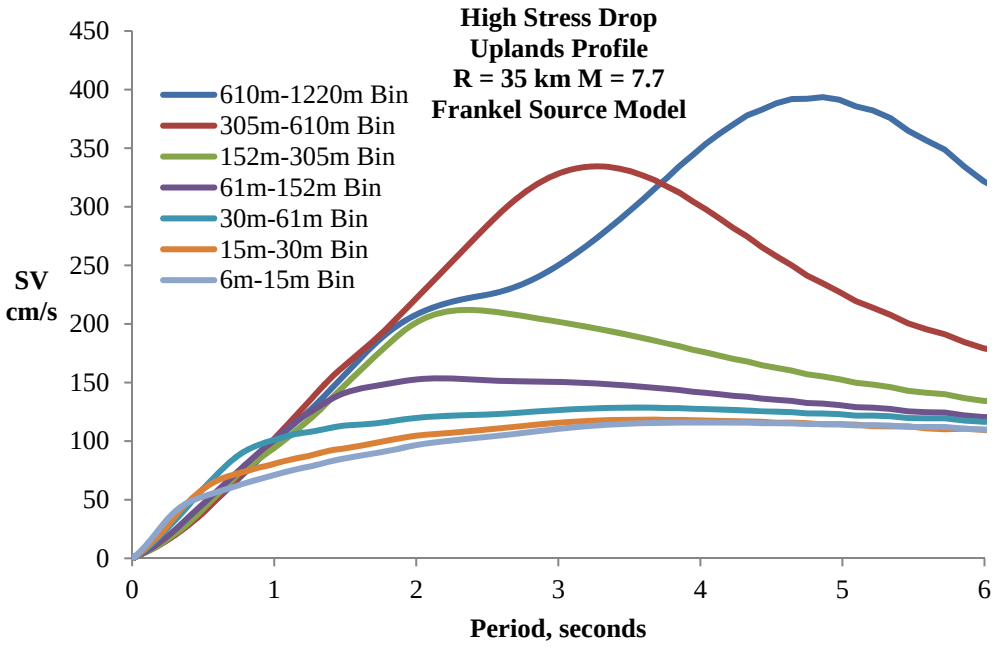

Figure G1.5.5-5. Velocity-Spectra: High Stress Drop, Uplands, Frankel

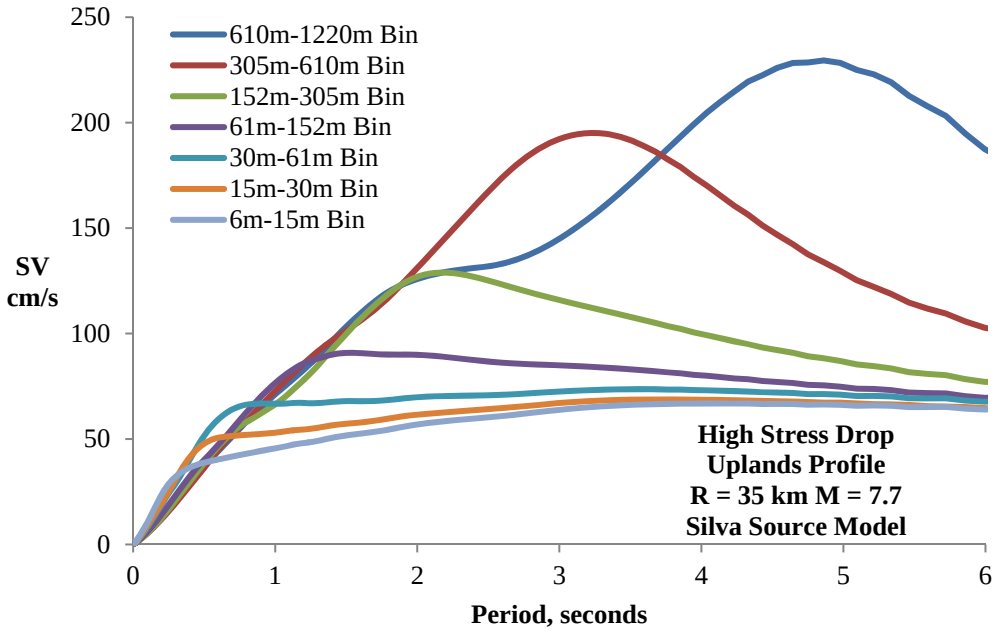

Figure G1.5.5-6. Velocity-Spectra: High Stress Drop, Uplands, Silva

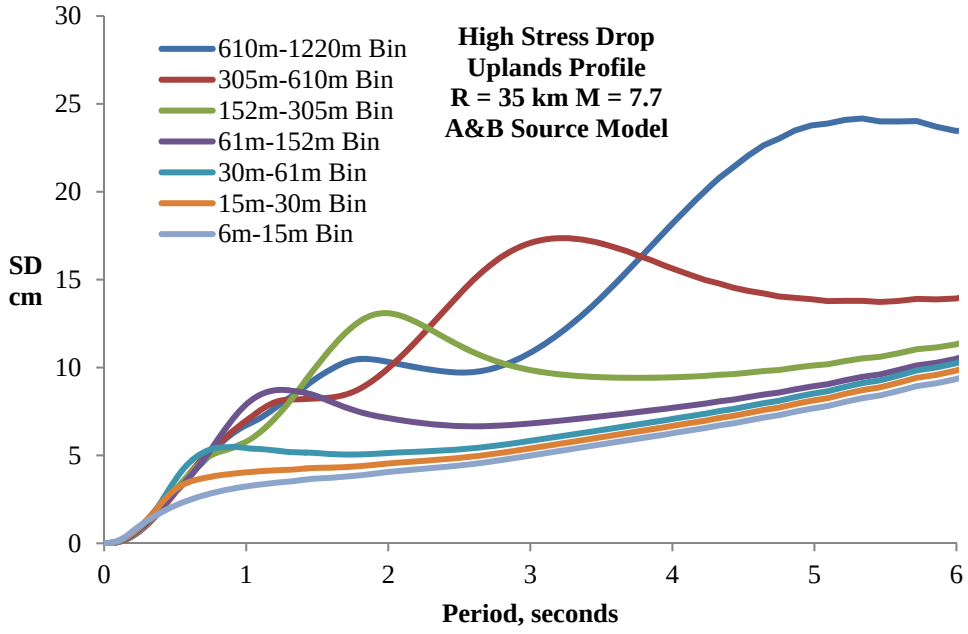

Figure G1.5.5-7. Displacement-Spectra: High Stress Drop, Uplands, A&B

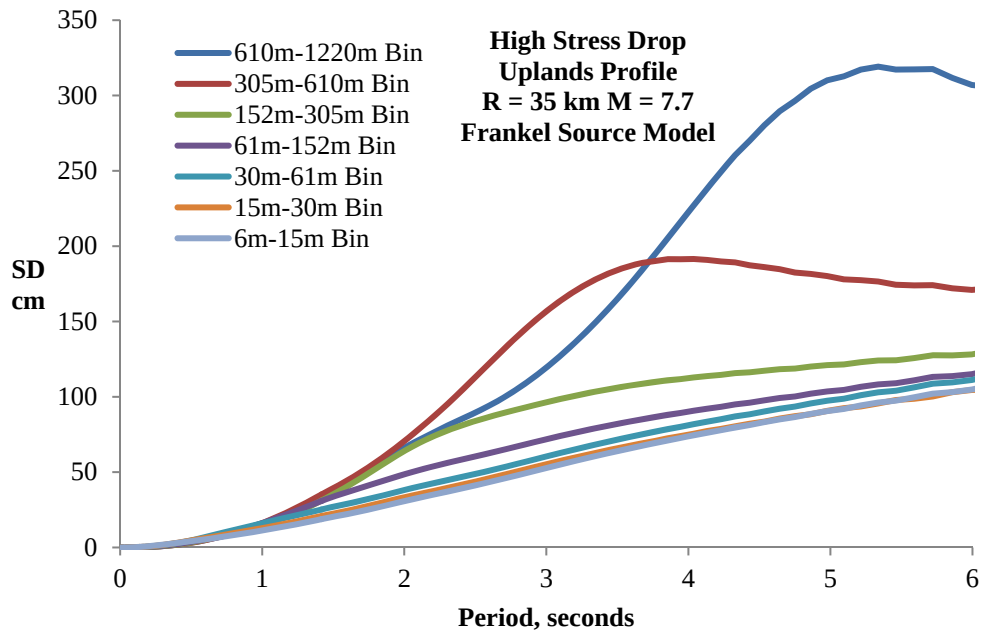

Figure G1.5.5-8. Displacement-Spectra: High Stress Drop, Uplands, Frankel

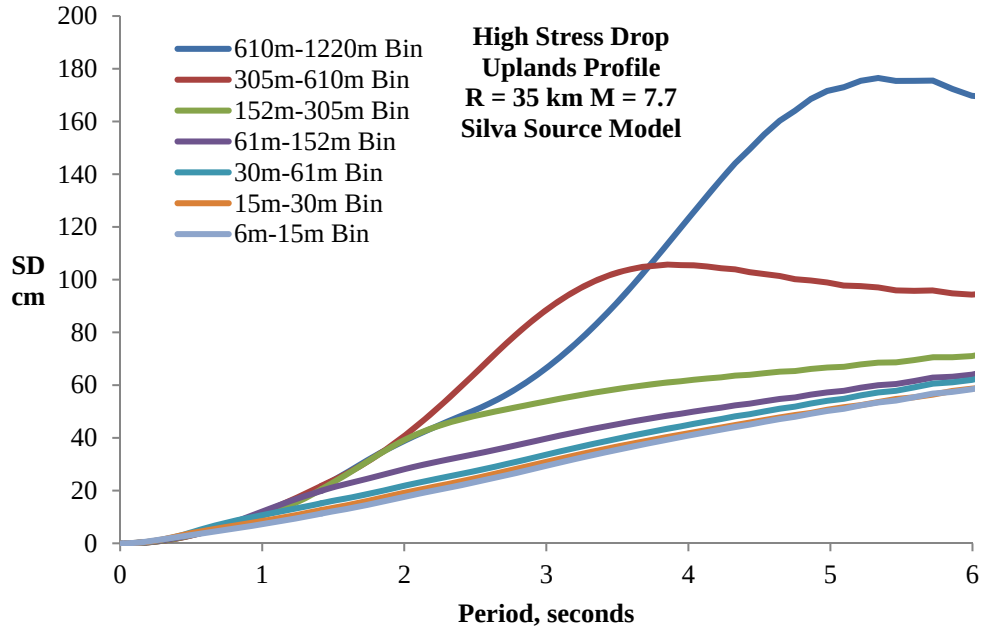

Figure G1.5.5-9. Displacement-Spectra: High Stress Drop, Uplands, Silva

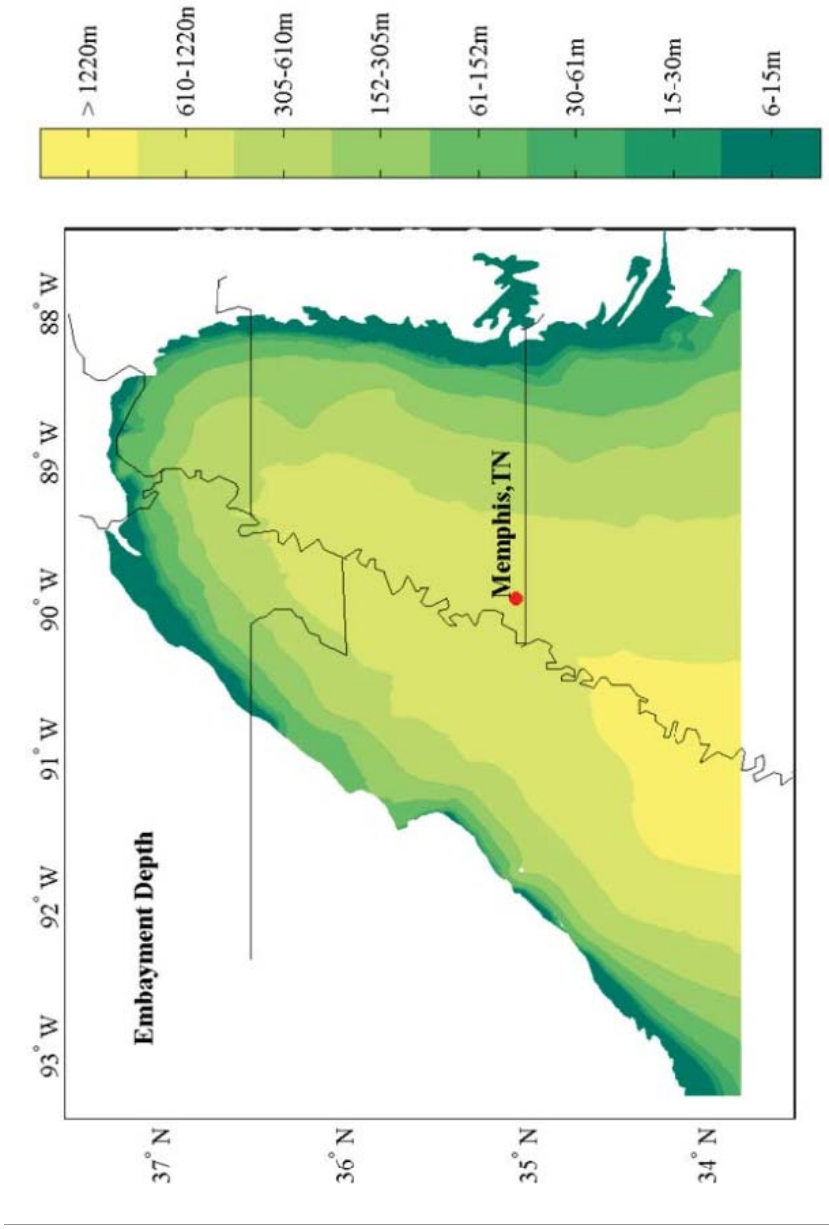

Figure G1.5.5-10. Mississippi Embayment Depth (From Fernandez, 2007)

APPENDIX G2 - CHAPTER 2 SUPPORTING FIGURES

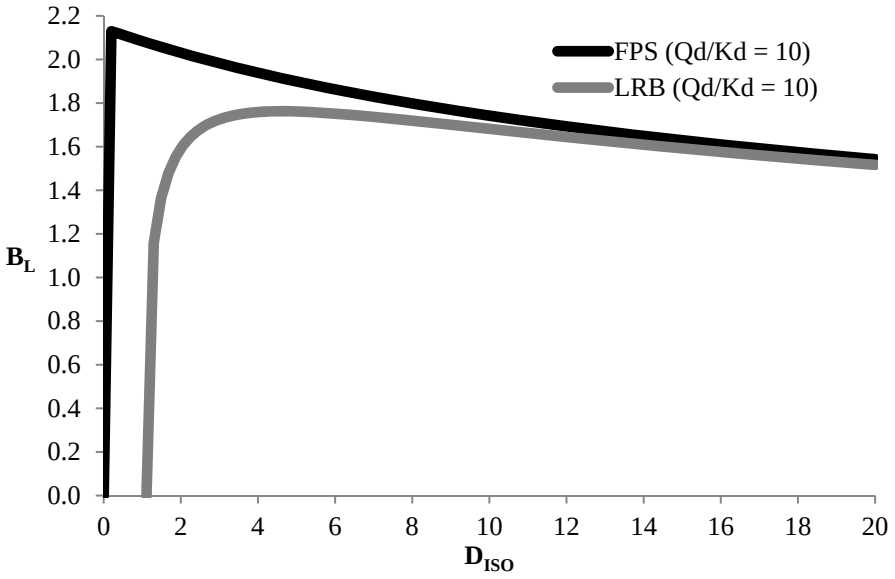

Figure G2.2-2. B_L vs. D_{ISO} - Q_d/K_d = 10

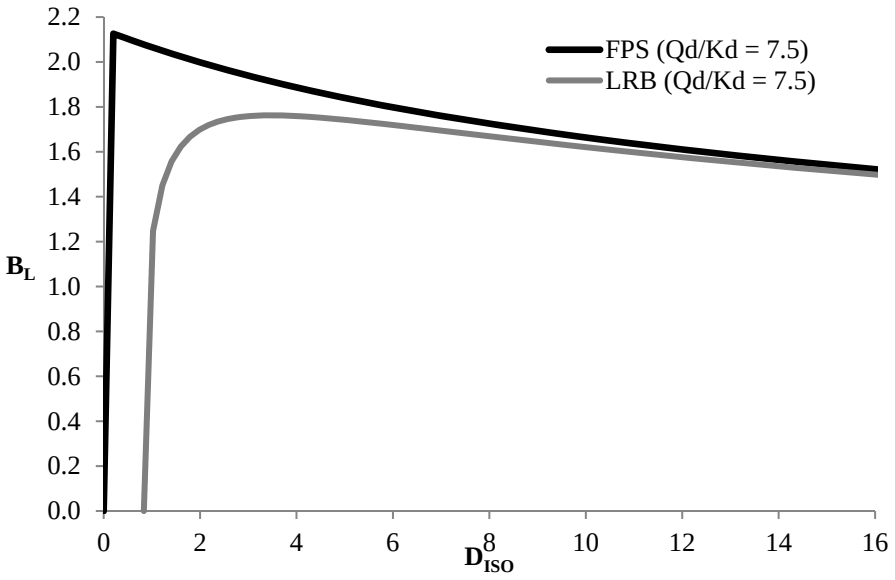

Figure G2.2-3. B_L vs. D_{ISO} - Q_d/K_d = 7.5

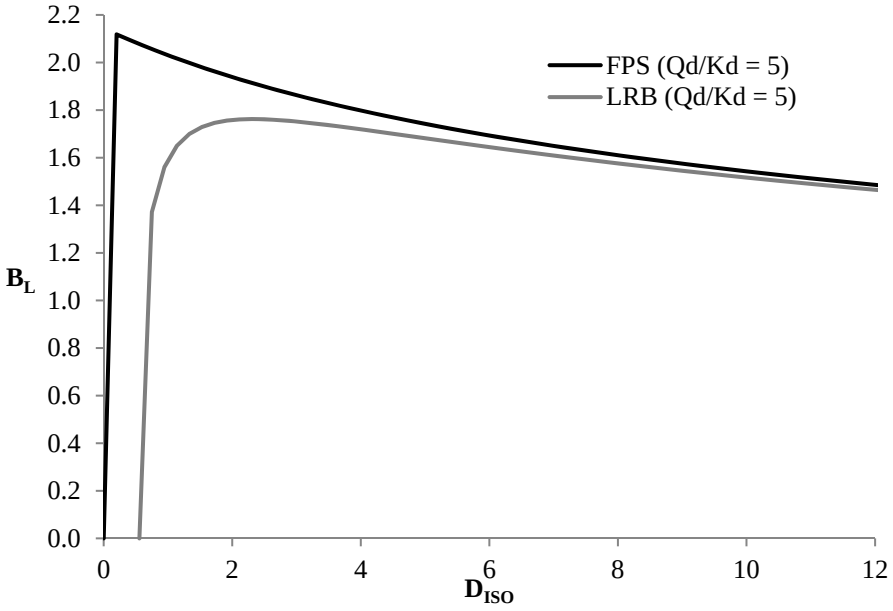

Figure G2.2-4. B_L vs. D_{ISO} - Q_d/K_d = 5

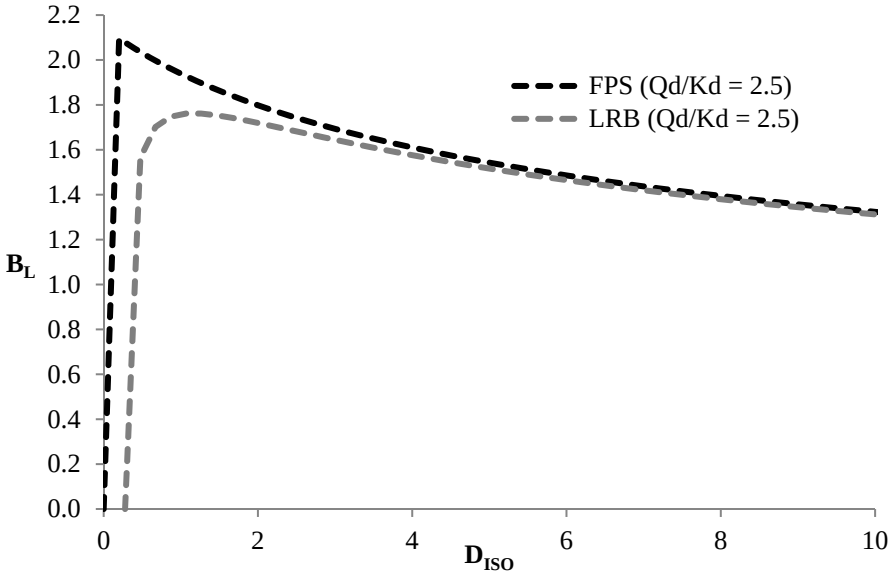

Figure G2.2-5. B_L vs. D_{ISO} - Q_d/K_d = 2.5

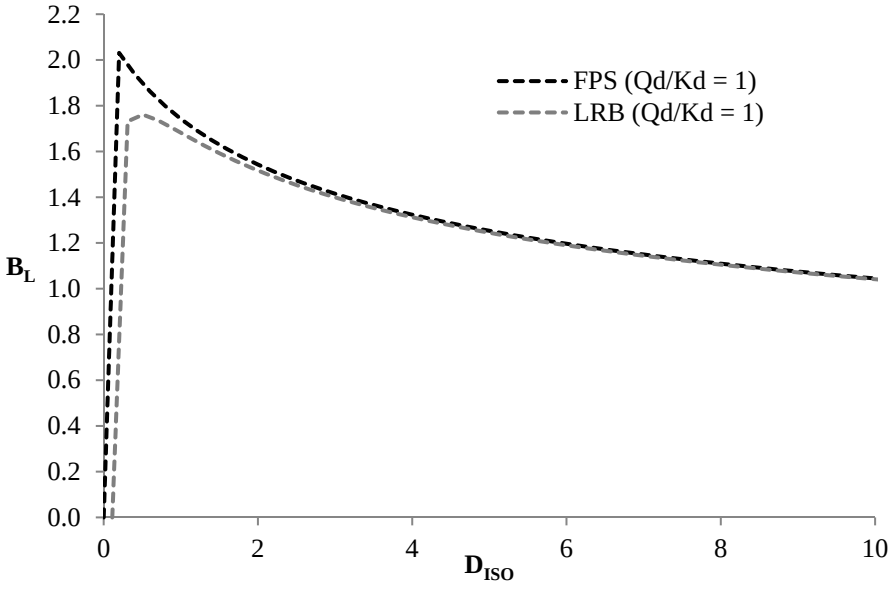

Figure G2.2-6. B_L vs. D_{ISO} - $Q_d/K_d = 1$

APPENDIX G3 - CHAPTER 3 SUPPORTING FIGURES

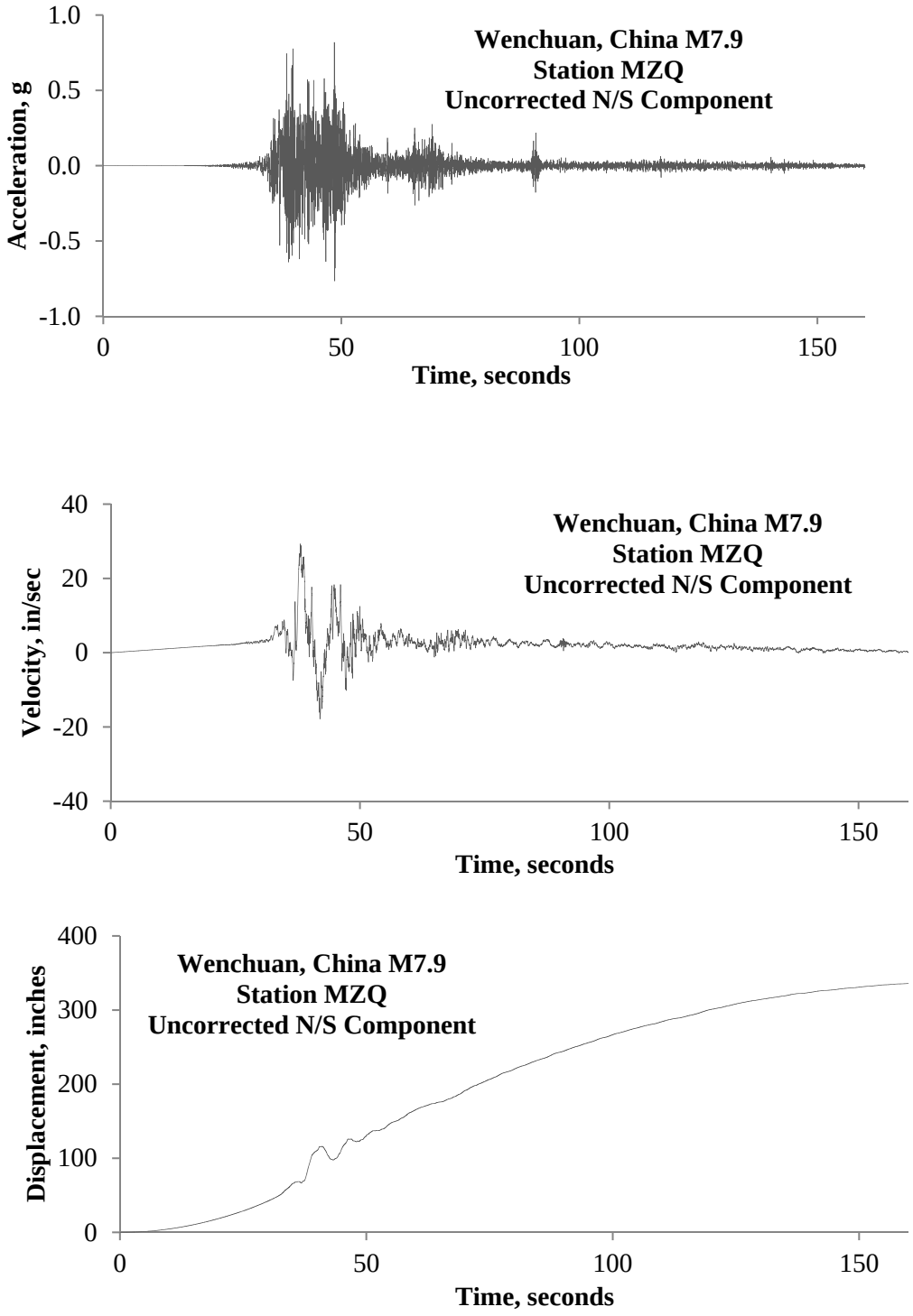

Figure G3.1.2-1. Uncorrected A,V,D: MZQ N/S component

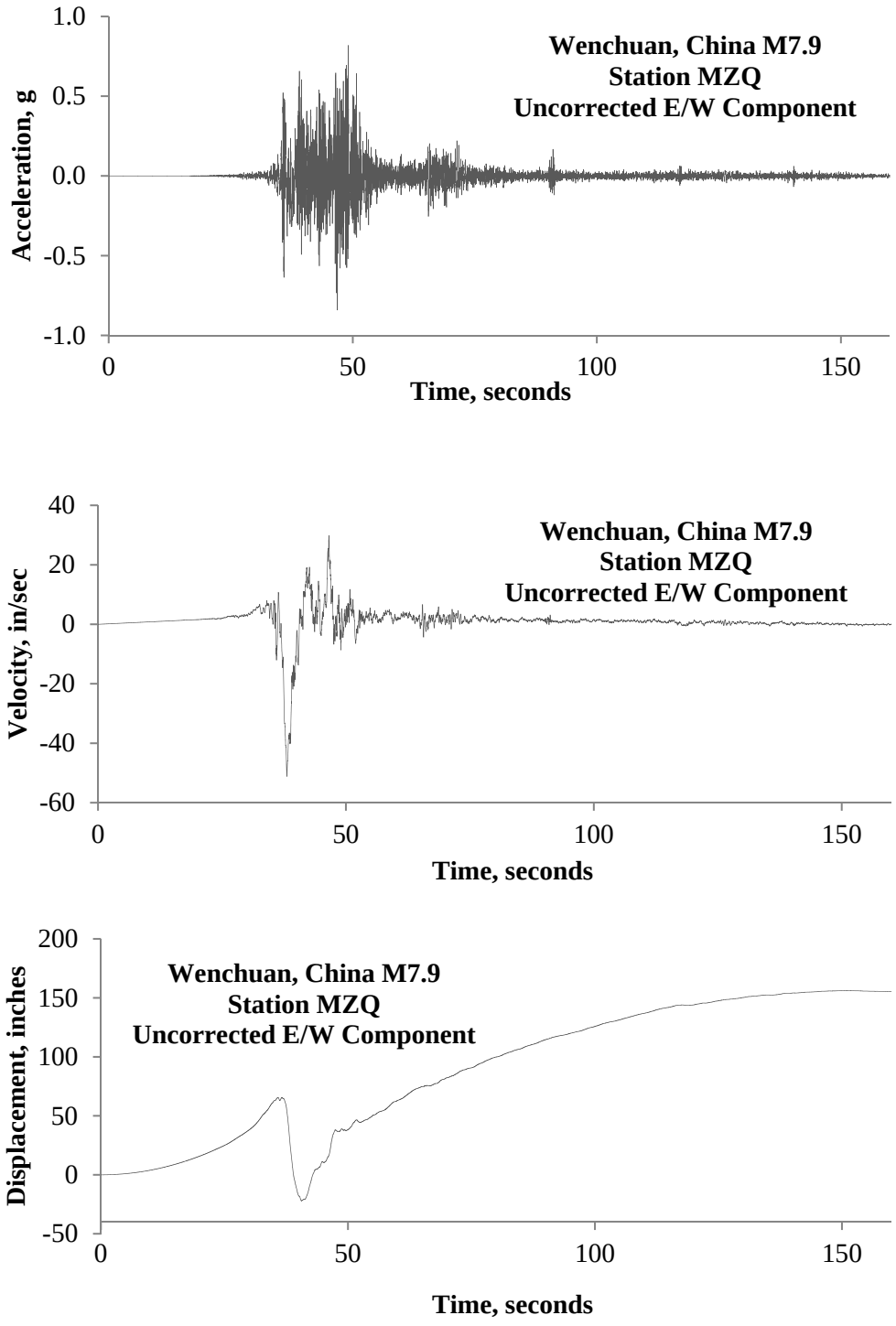

Figure G3.1.2-2. Uncorrected A,V,D: MZQ E/W component

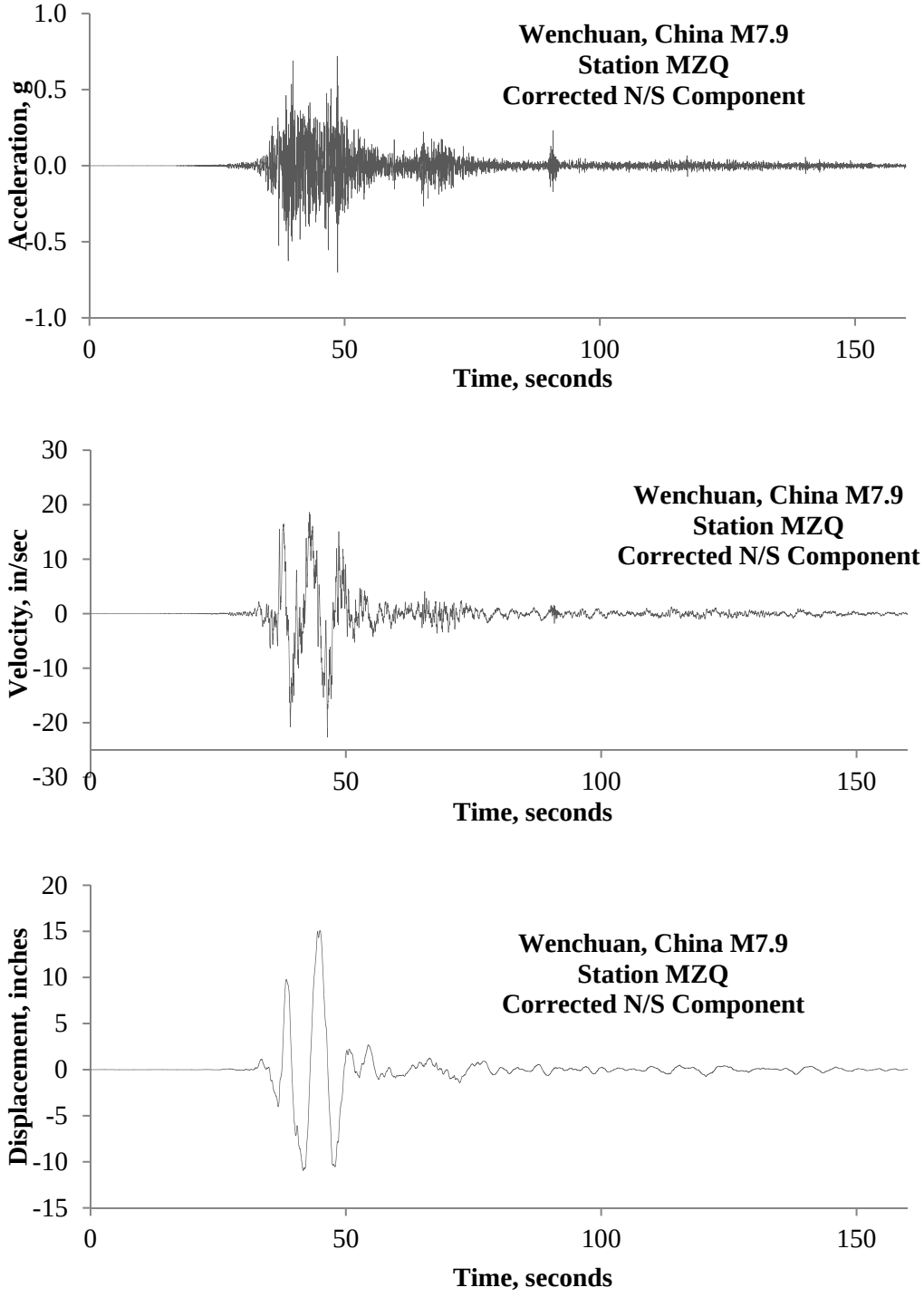

Figure G3.1.2-3. Corrected A,V,D: MZQ N/S component

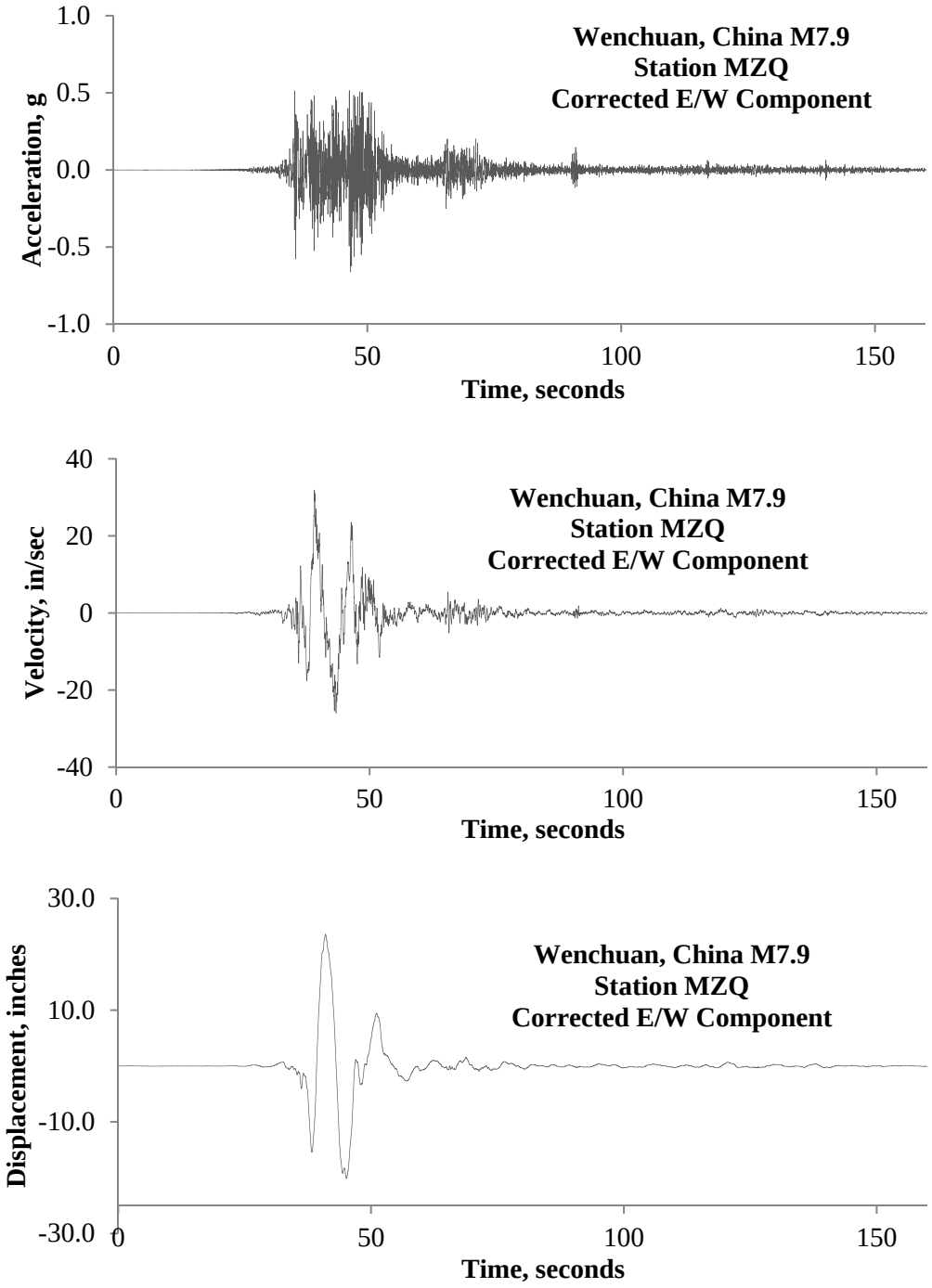

Figure G3.1.2-4. Corrected A,V,D: MZQ E/W component

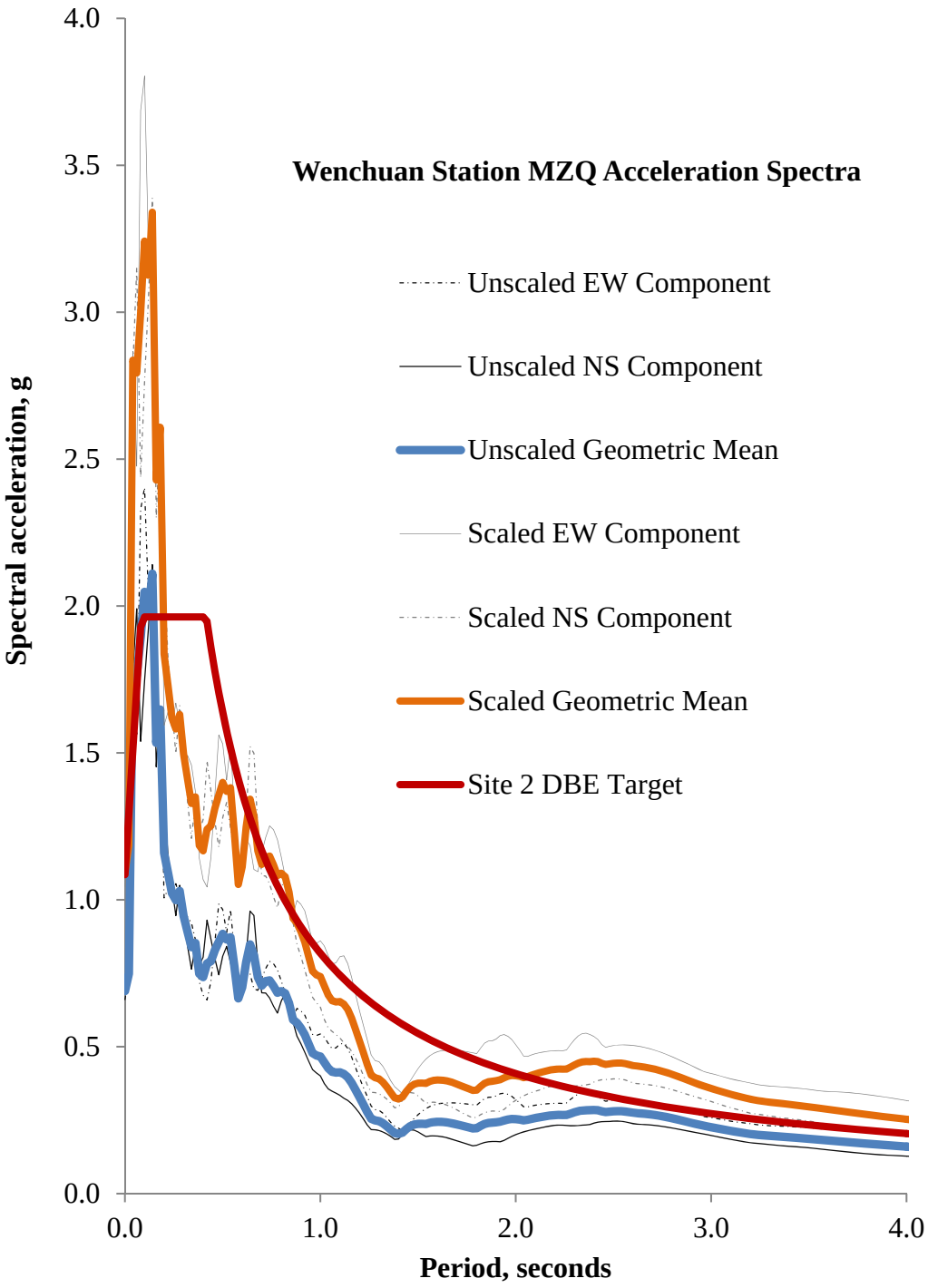

Figure G3.1.2-5. Wenchuan Station MZQ Spectra

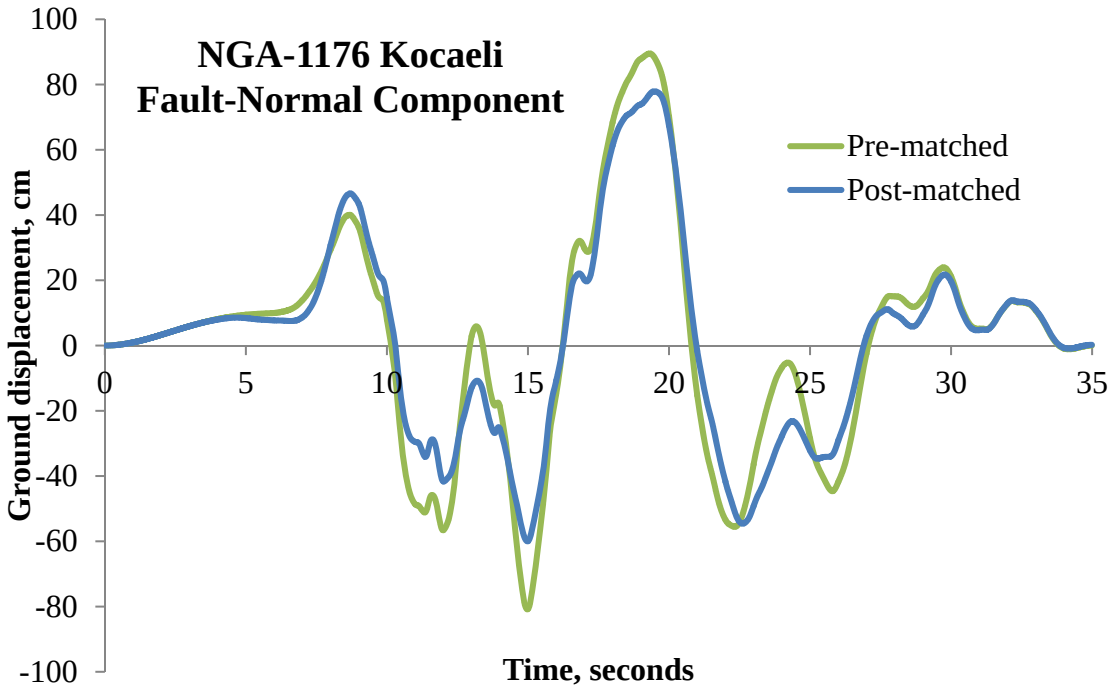

Figure G3.1.4-1. 1176 Kocaeli FN Matched to Site 2 UHRS

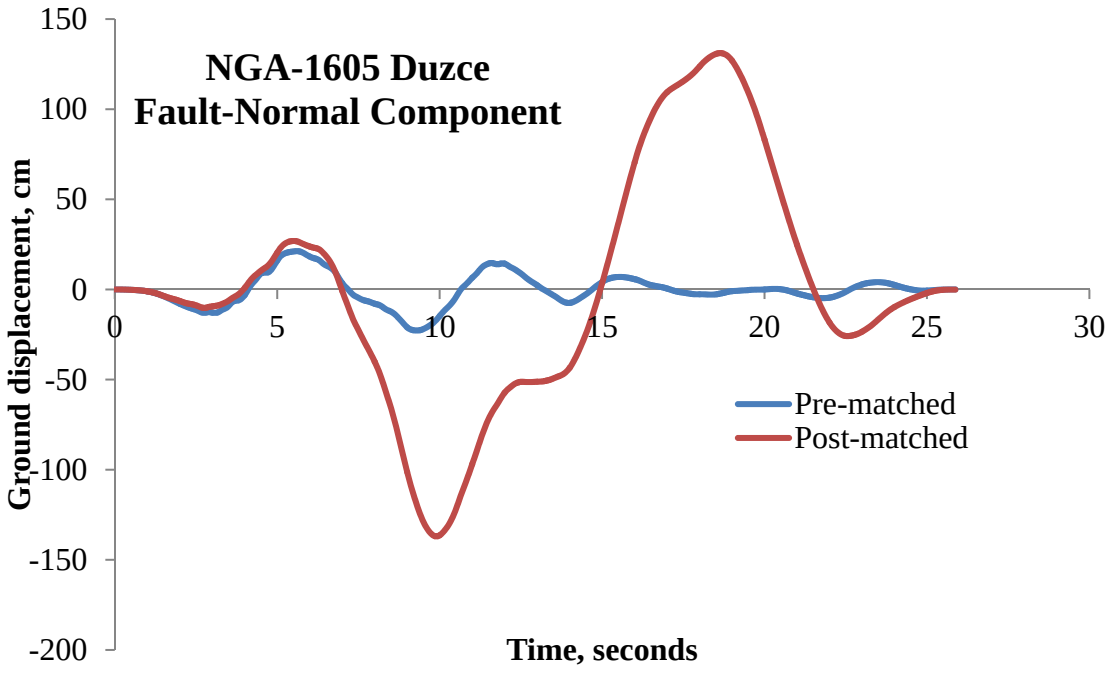

Figure G3.1.4-2. 1605 Duzce FN Matched to Site 2 NMSZ Spectrum

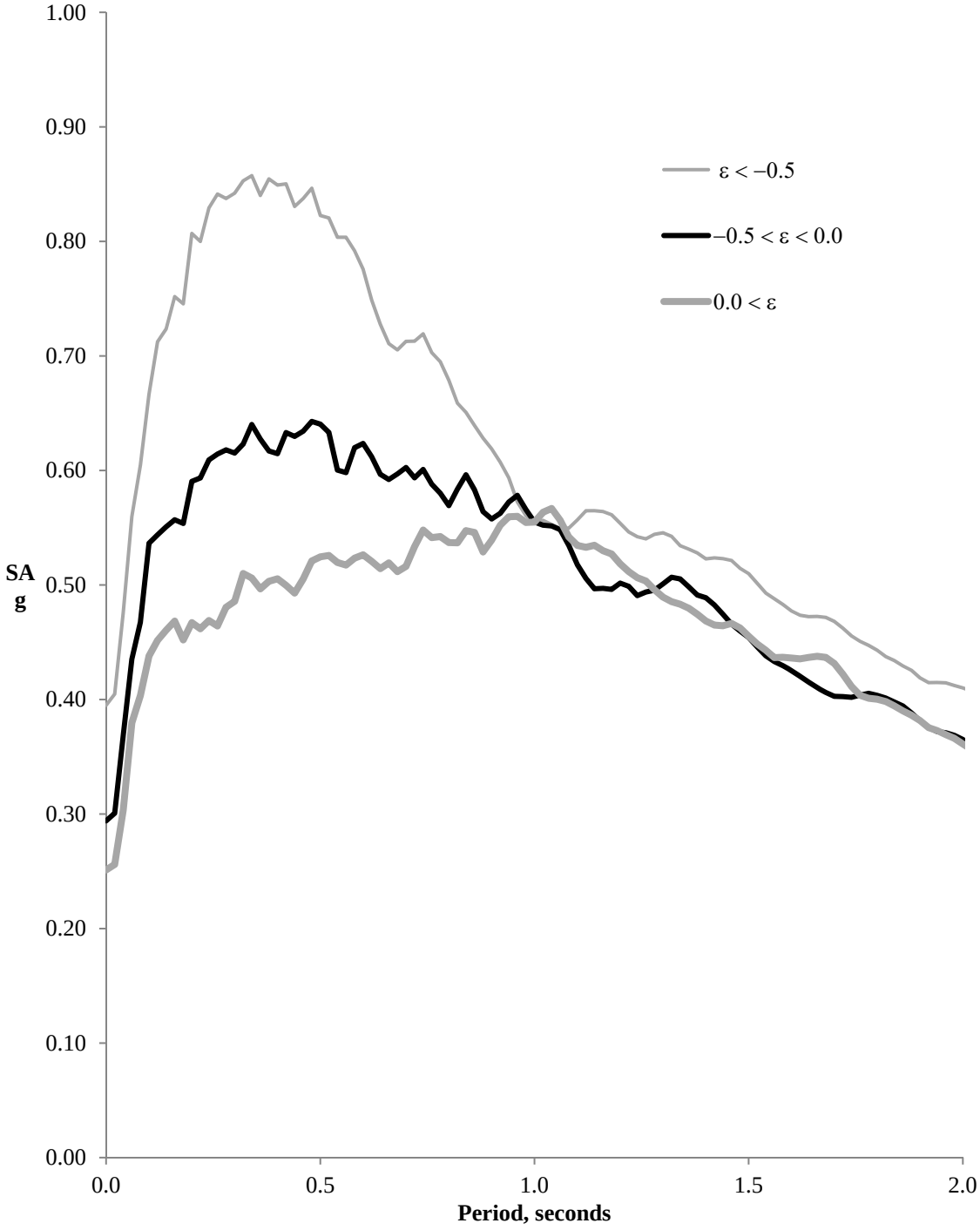

Figure G3.5.3-1. Effect of Epsilon on Spectral Shape

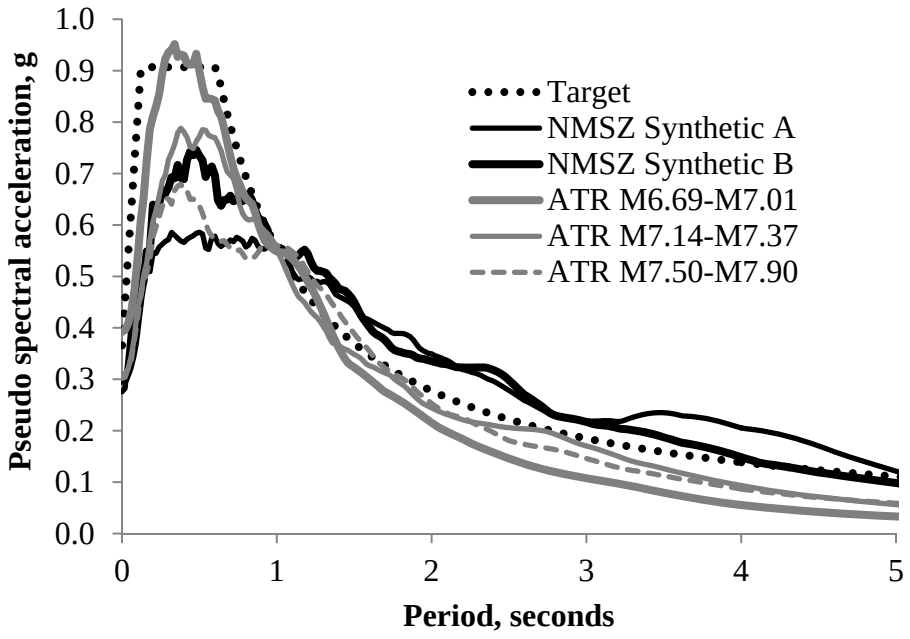

Figure G3.6-1. Site 1 NMSZ Spectra vs. ATR Spectra - Acceleration

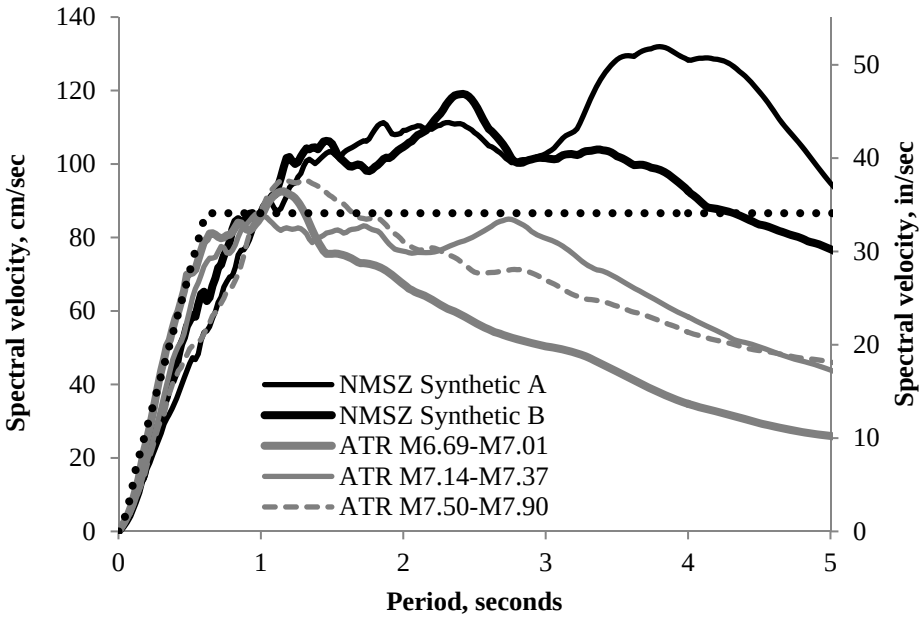

Figure G3.6-2. Site 1 NMSZ Spectra vs. ATR Spectra - Velocity

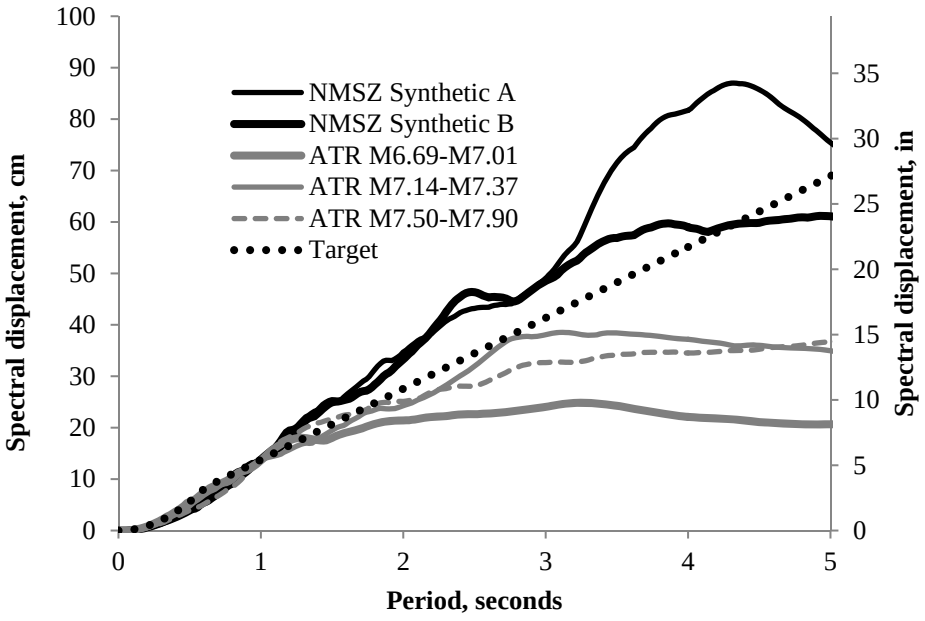

Figure G3.6-3. Site 1 NMSZ Spectra vs. ATR Spectra - Displacement

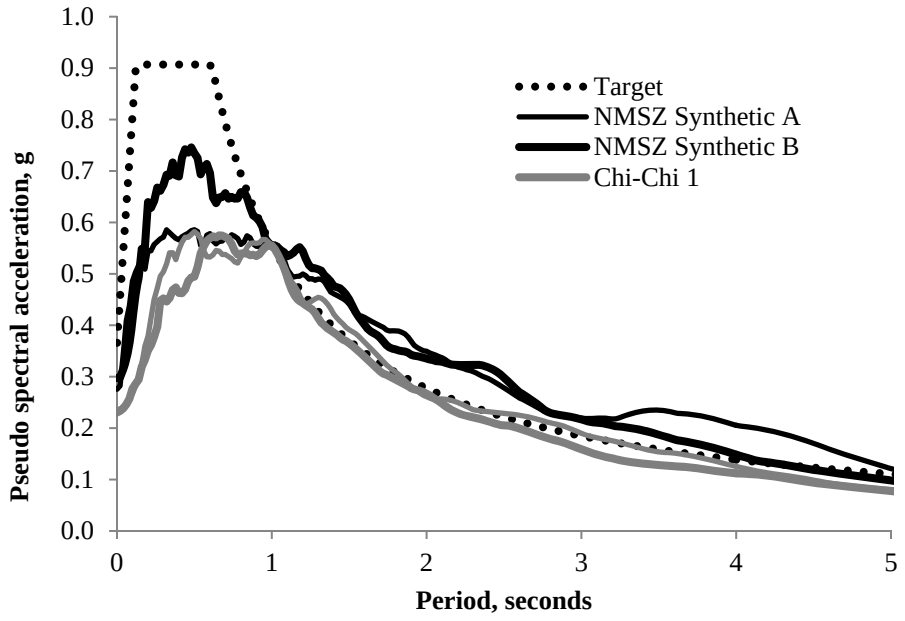

Figure G3.6-4. Site 1 NMSZ Spectra vs. Chi-Chi Spectra - Acceleration

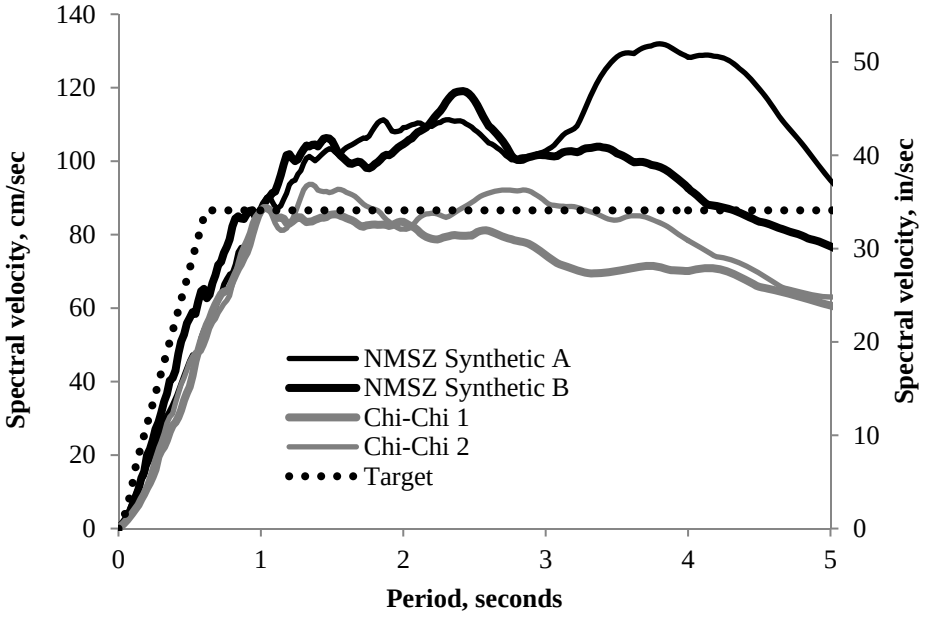

Figure G3.6-5. Site 1 NMSZ Spectra vs. Chi-Chi Spectra - Velocity

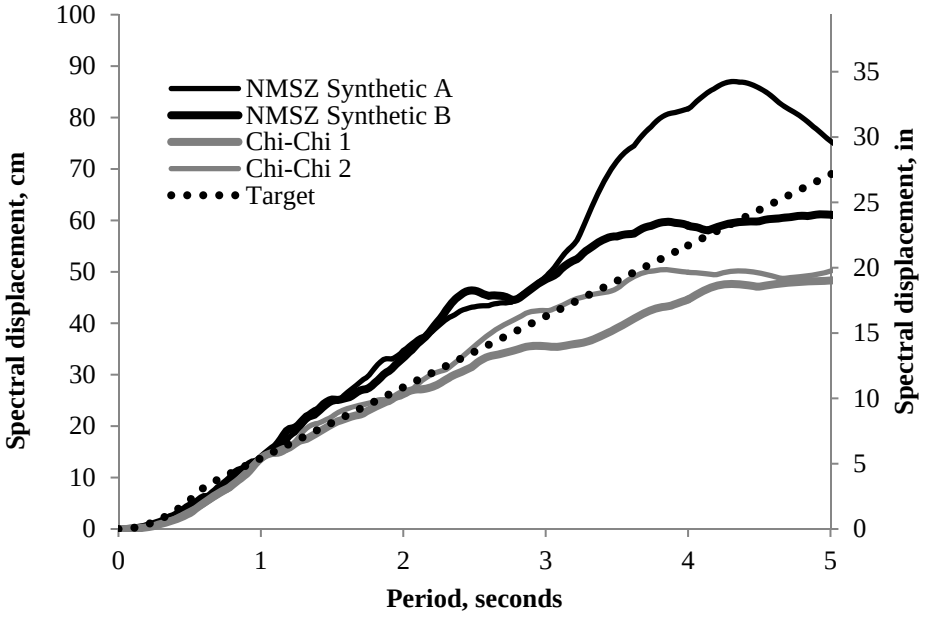

Figure G3.6-6. Site 1 NMSZ Spectra vs. ATR Spectra - Displacement

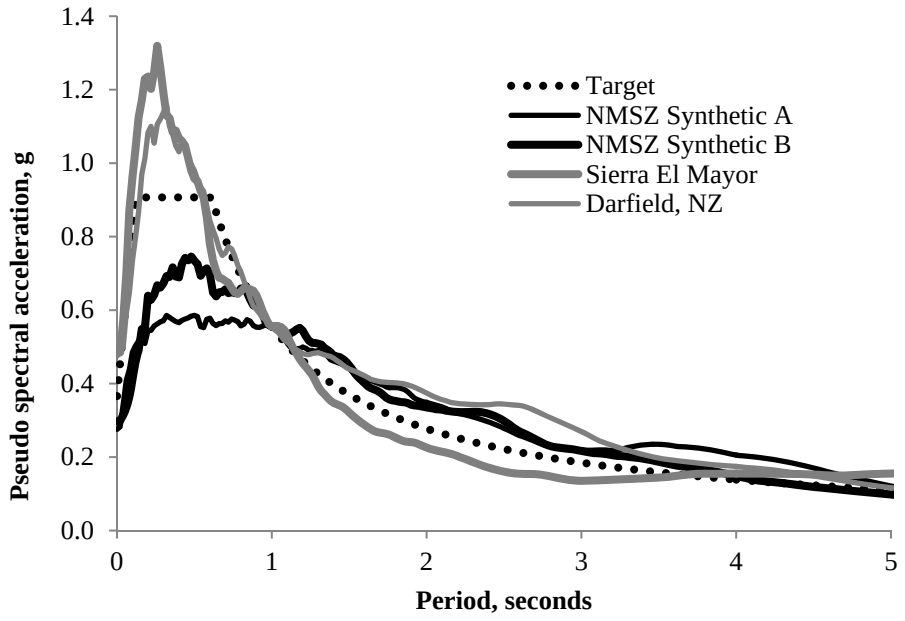

Figure G3.6-7. Site 1 NMSZ Spectra vs. Darfield Spectra - Acceleration

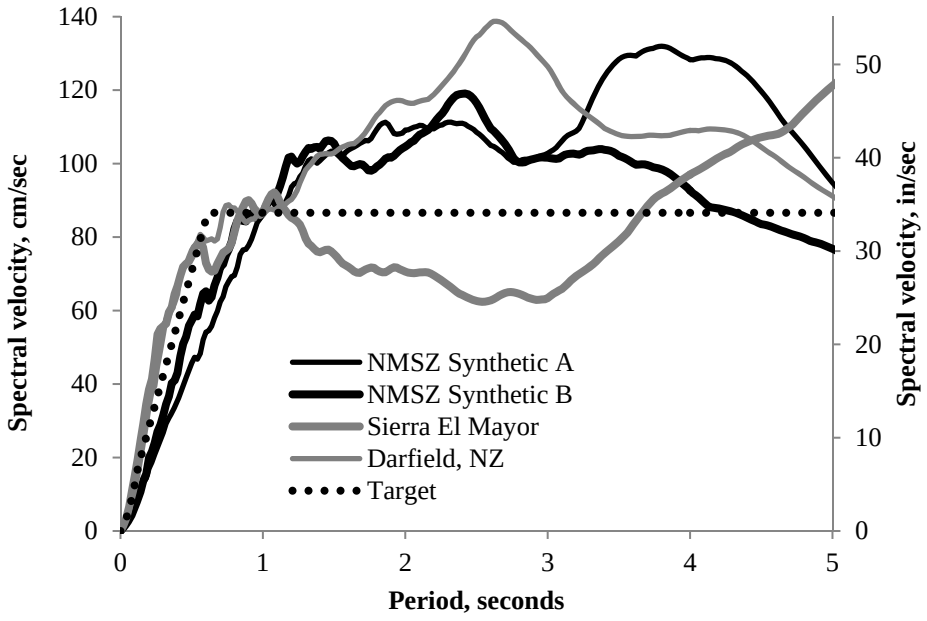

Figure G3.6-8. Site 1 NMSZ Spectra vs. Darfield Spectra - Velocity

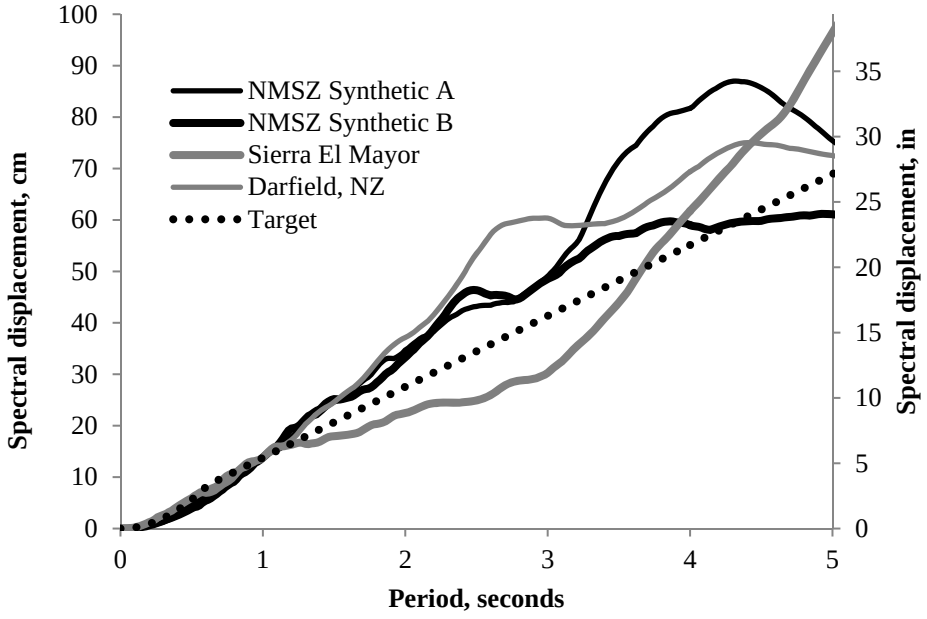

Figure G3.6-9. Site 1 NMSZ Spectra vs. Darfield Spectra - Displacement

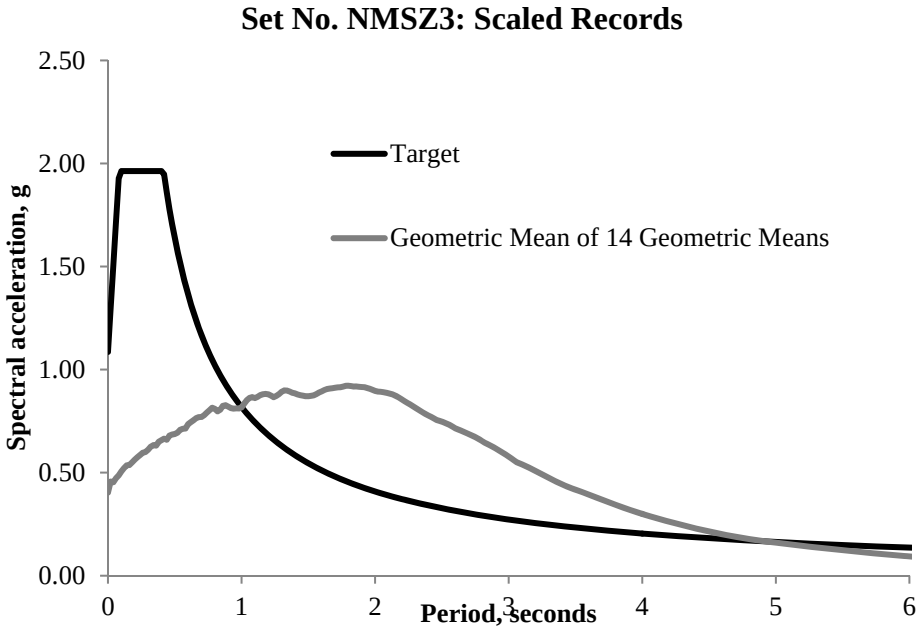

Figure G3.6-10. Acceleration Spectra - Set NMSZ-3

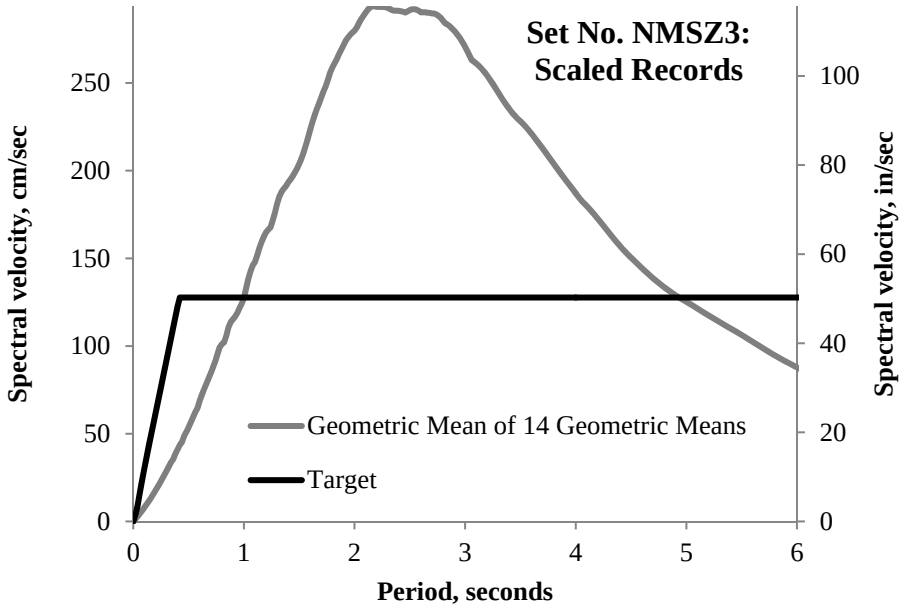

Figure G3.6-11. Velocity Spectra - Set NMSZ-3

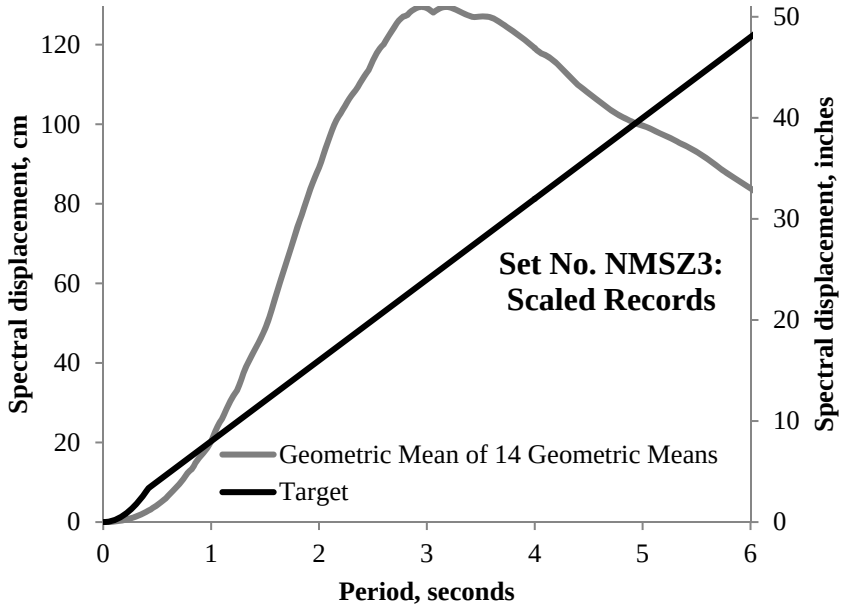

Figure G3.6-12. Displacement Spectra - Set NMSZ-3

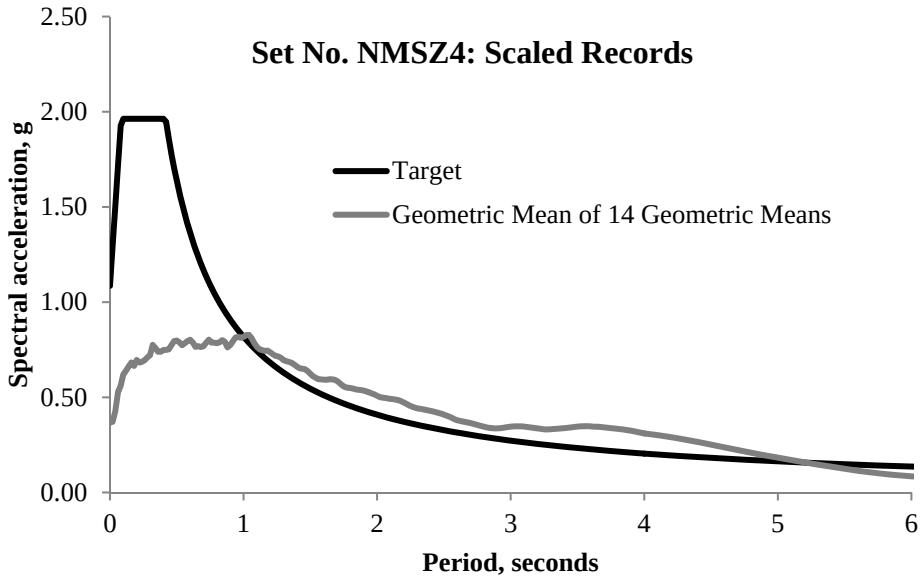

Figure G3.6-13. Acceleration Spectra - Set NMSZ-4

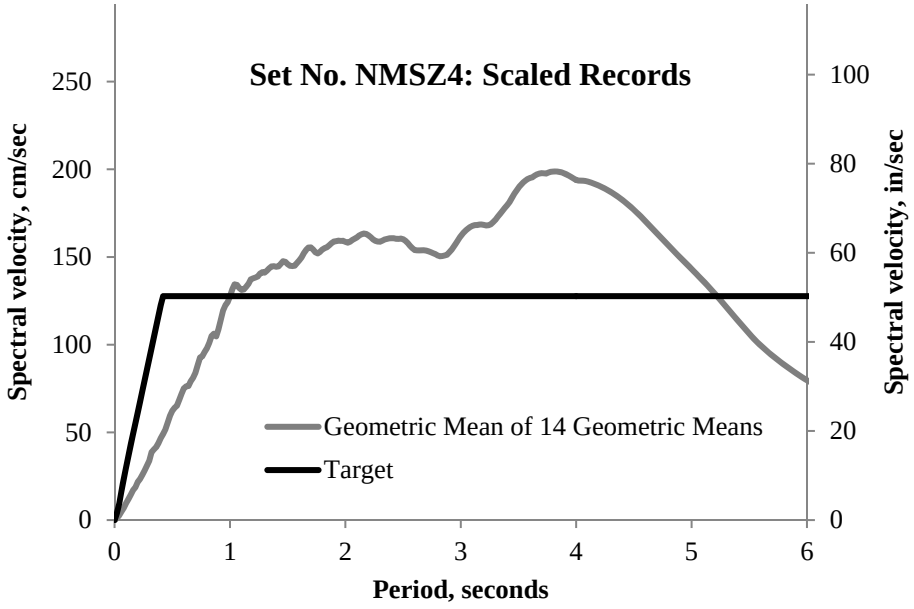

Figure G3.6-14. Velocity Spectra - Set NMSZ-4

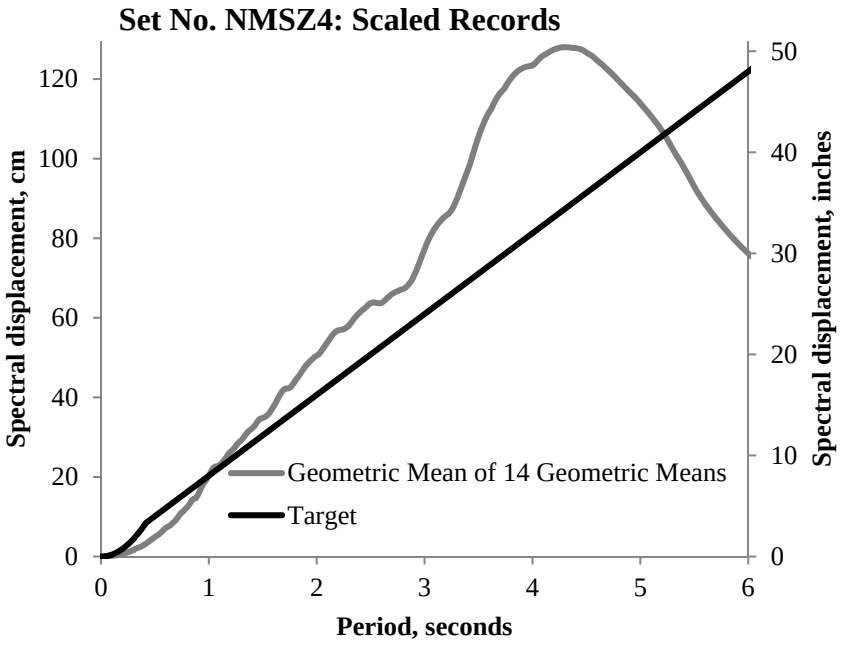

Figure G3.6-15. Displacement Spectra - Set NMSZ-4

APPENDIX G4 - CHAPTER 4 SUPPORTING FIGURES

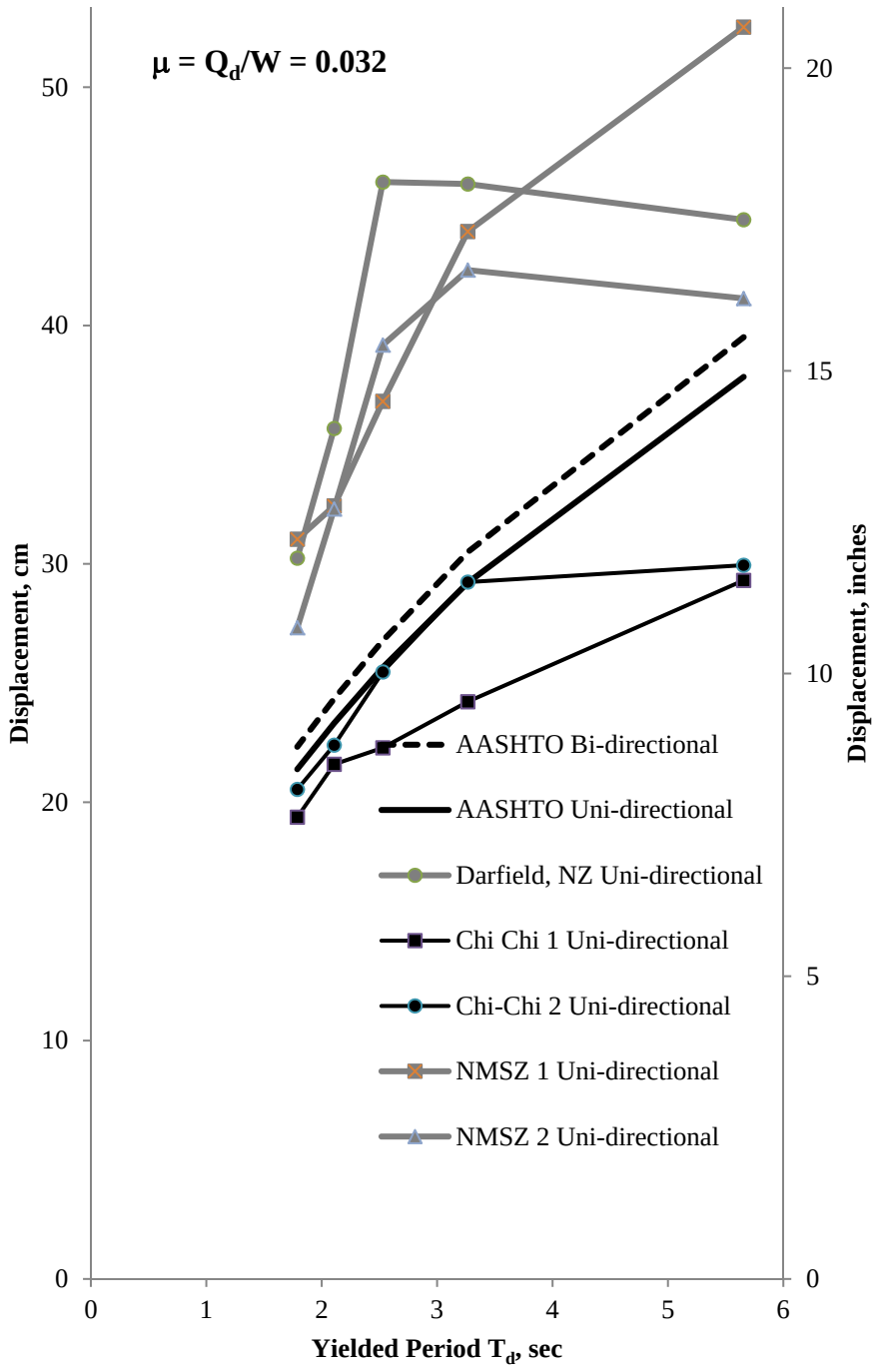

Figure G4.1-1. Uni-directional Response - NMSZ vs. Other: μ = 0.032 (LRB)

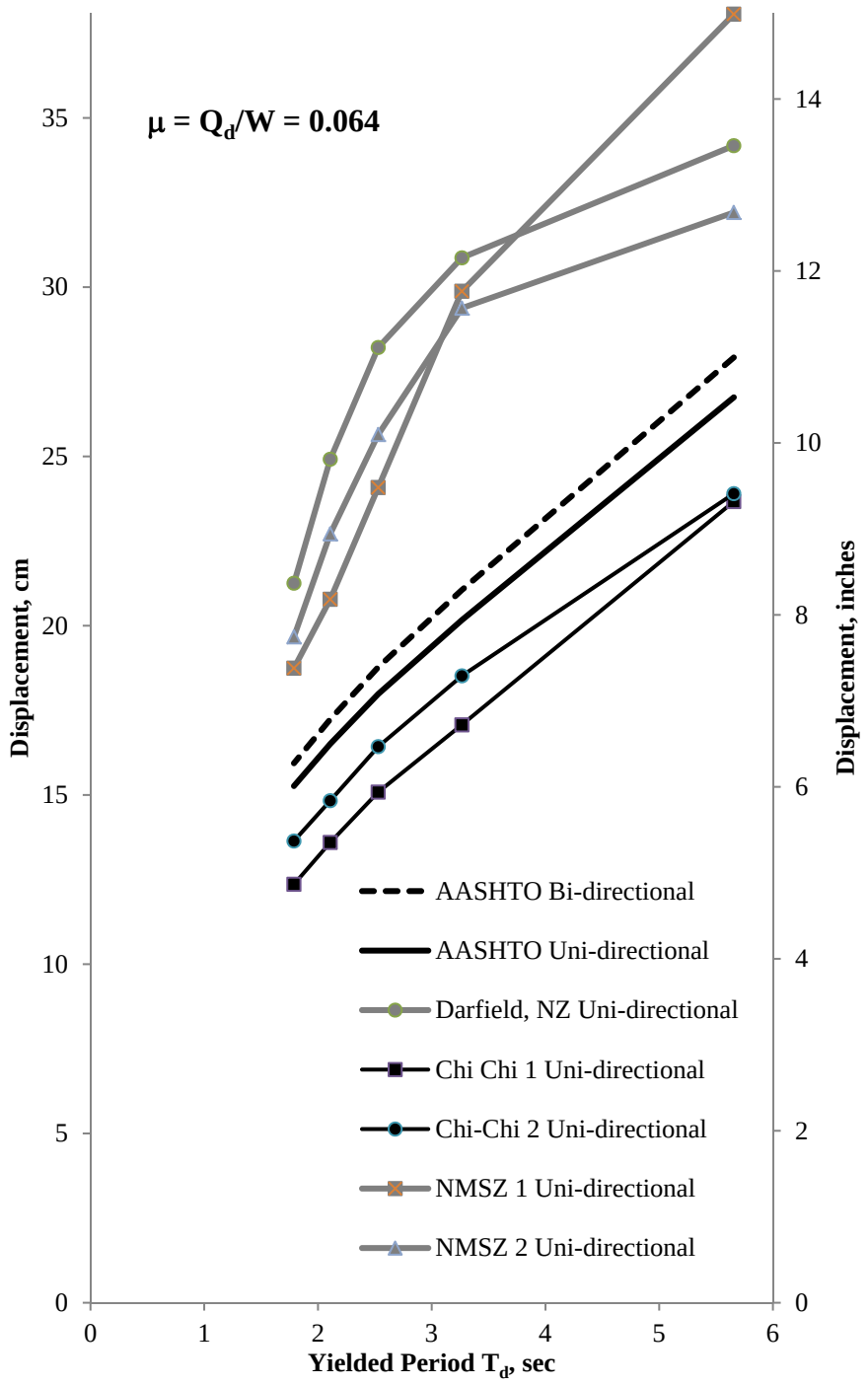

Figure G4.1-2. Uni-directional Response - NMSZ vs. Other: μ = 0.064 (LRB)

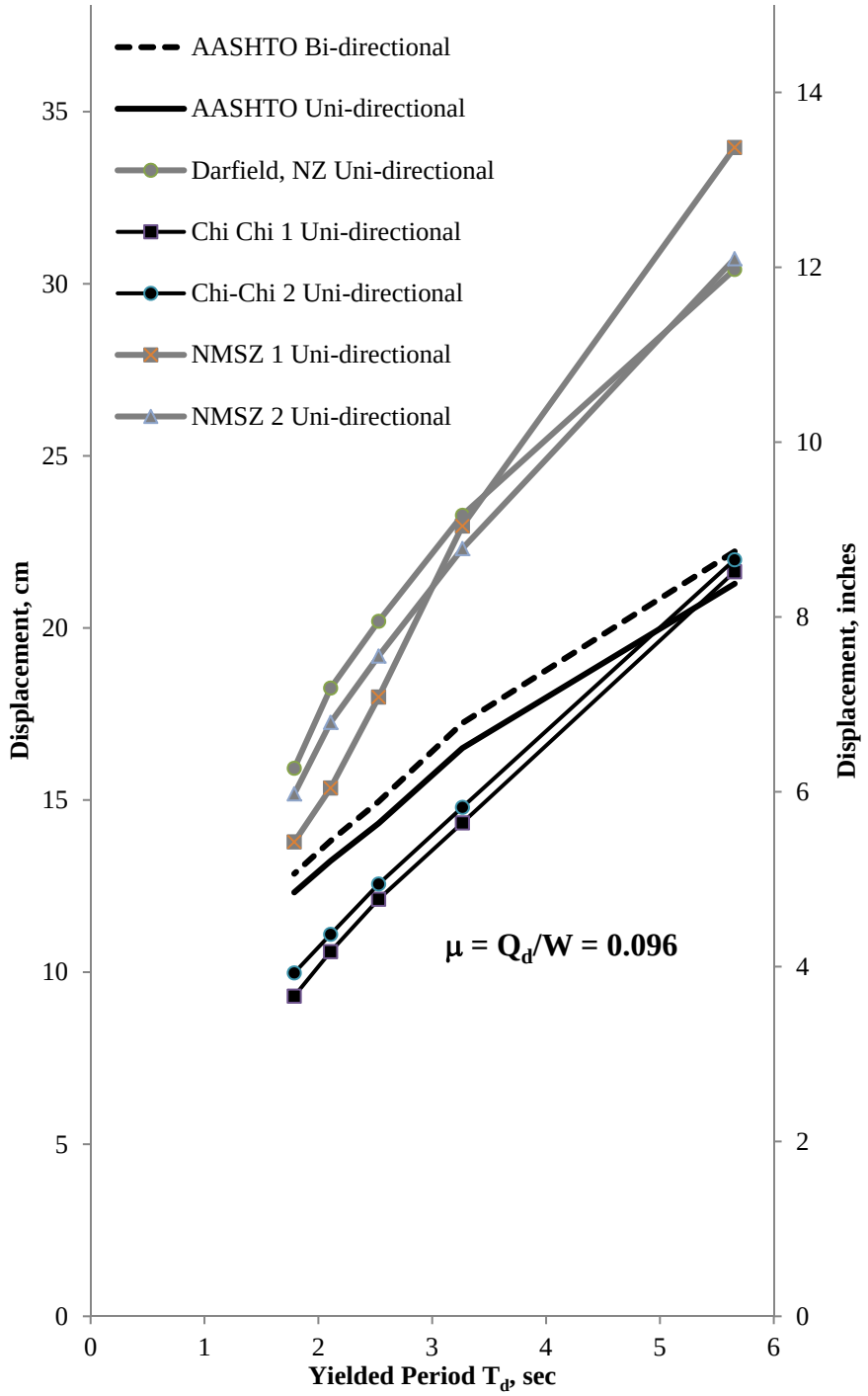

Figure G4.1-3. Uni-directional Response - NMSZ vs. Other: μ = 0.096 (LRB)

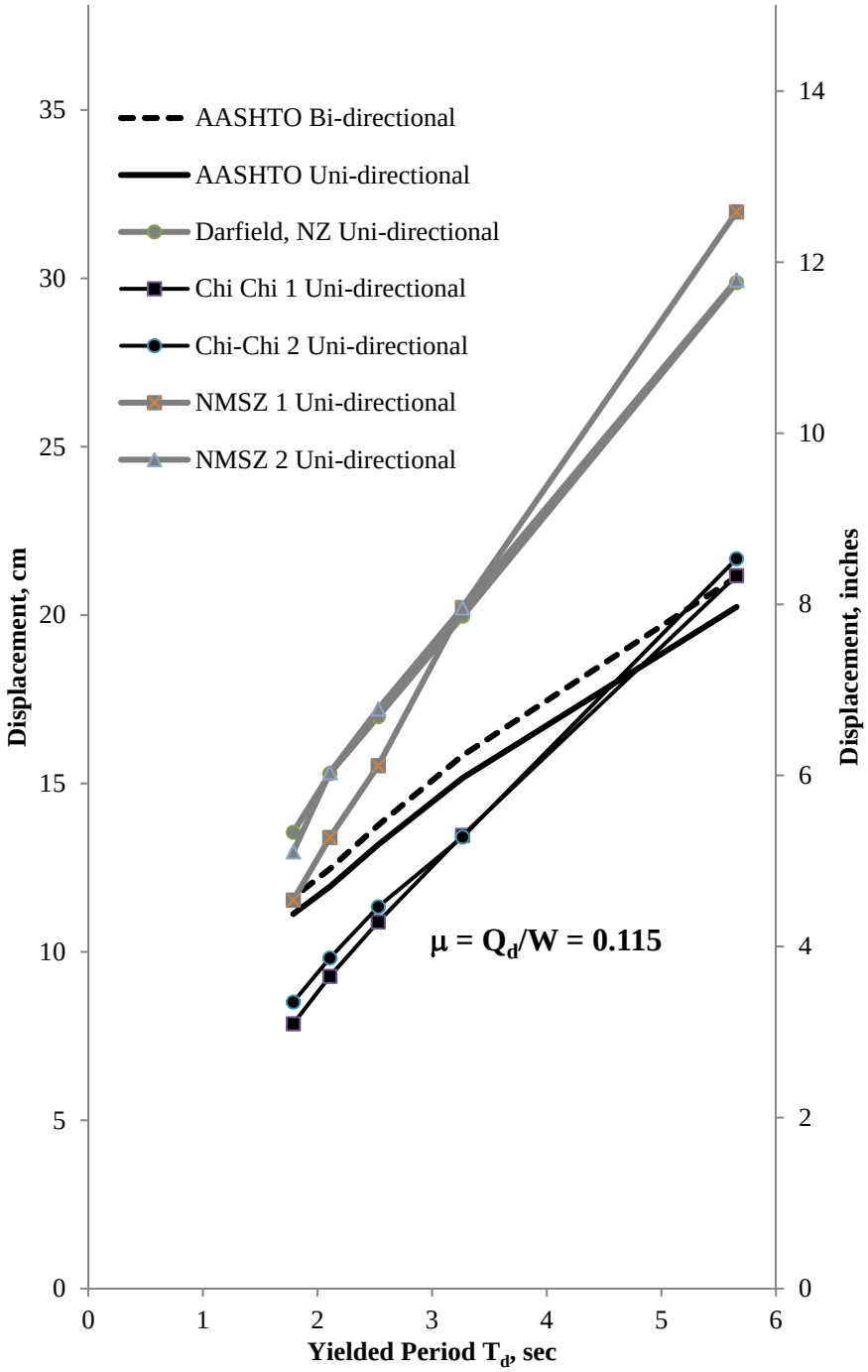

Figure G4.1-4. Uni-directional Response - NMSZ vs. Other: μ = 0.115 (LRB)

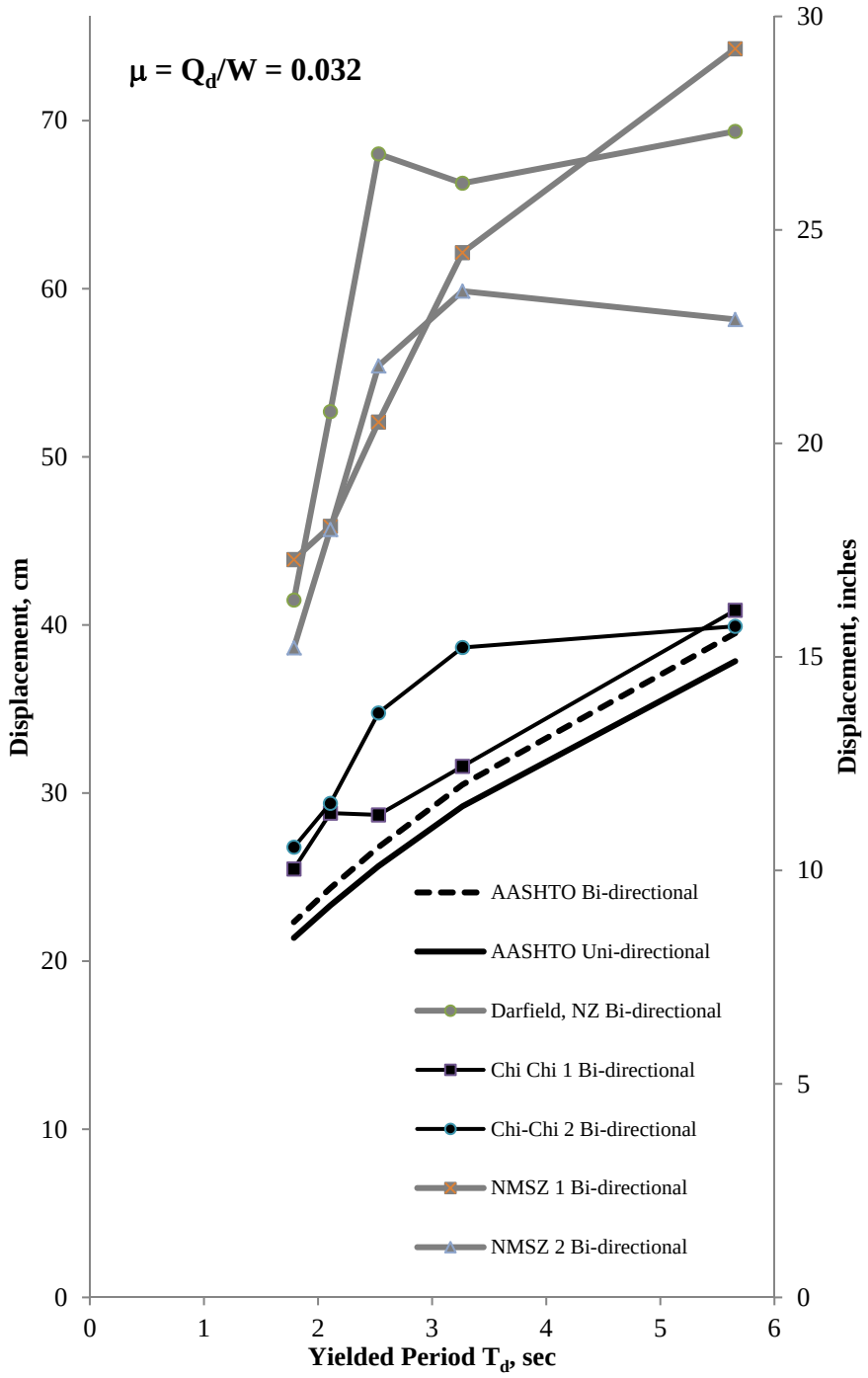

Figure G4.1-5. Bi-directional Response - NMSZ vs. Other: μ = 0.032 (LRB)

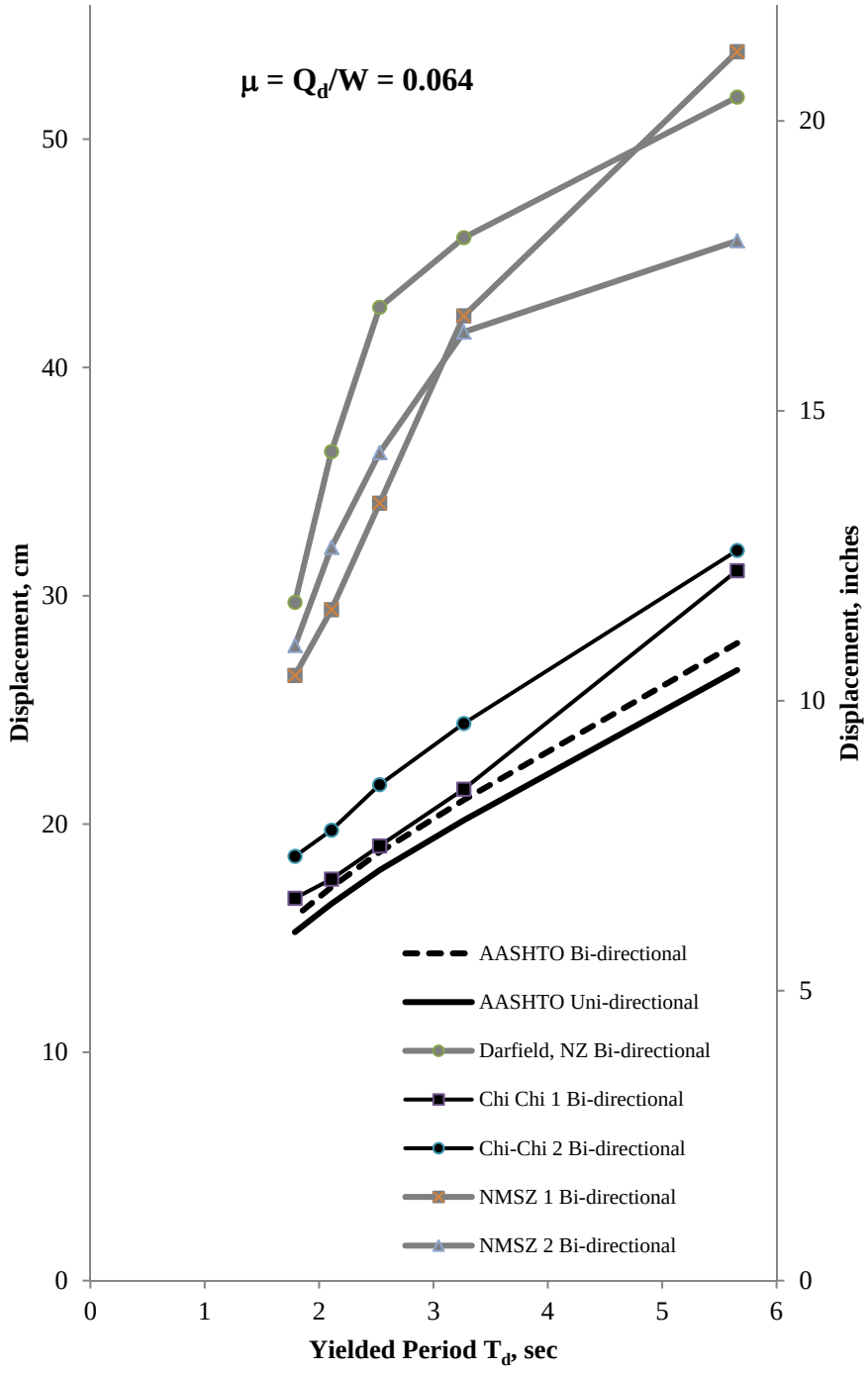

Figure G4.1-6. Bi-directional Response - NMSZ vs. Other: μ = 0.064 (LRB)

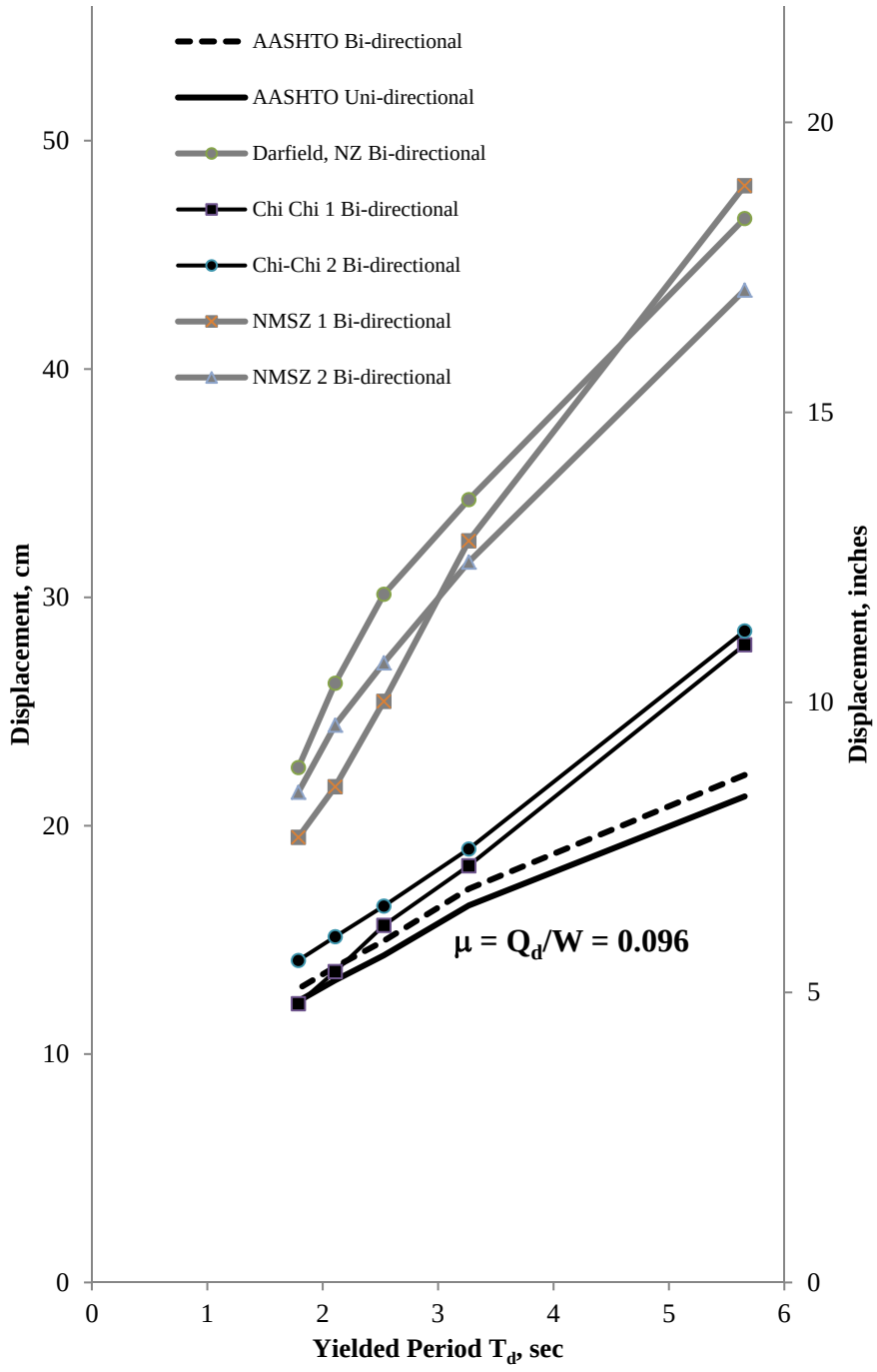

Figure G4.1-7. Bi-directional Response - NMSZ vs. Other: μ = 0.096 (LRB)

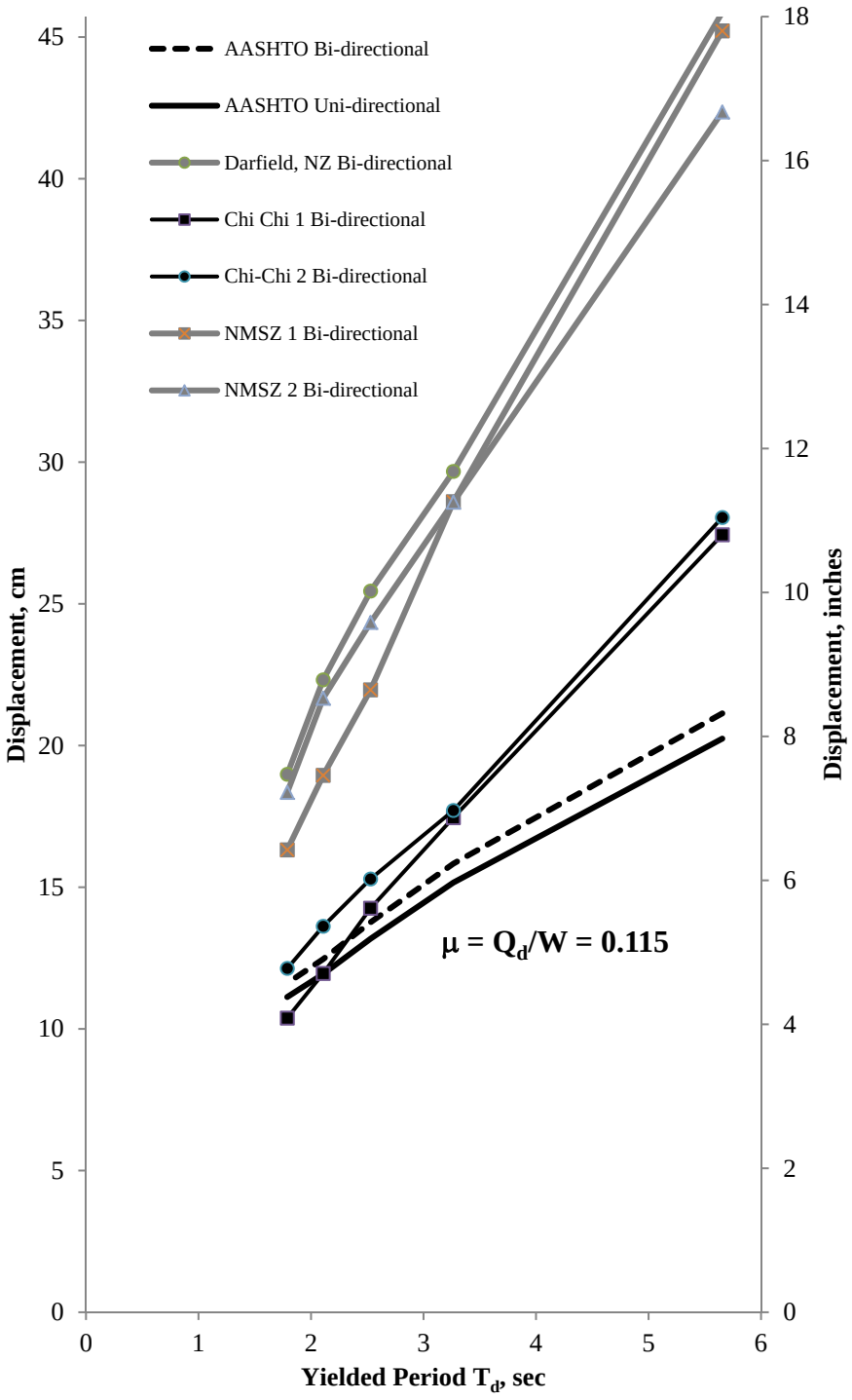

Figure G4.1-8. Bi-directional Response - NMSZ vs. Other: μ = 0.115 (LRB)

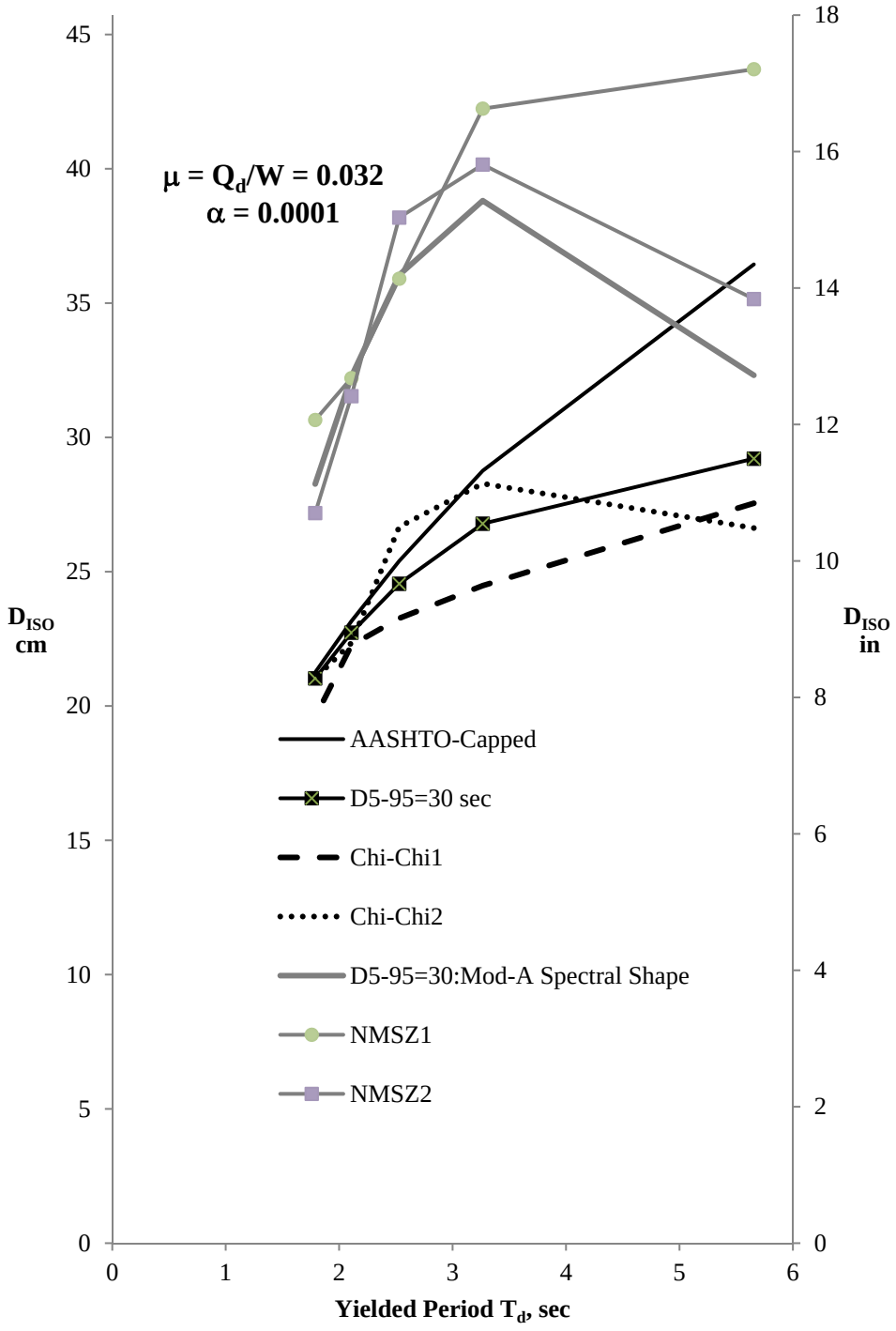

Figure G4.3-2. Proposed FPS Modifications: $\mu = Q_d/W = 0.032$

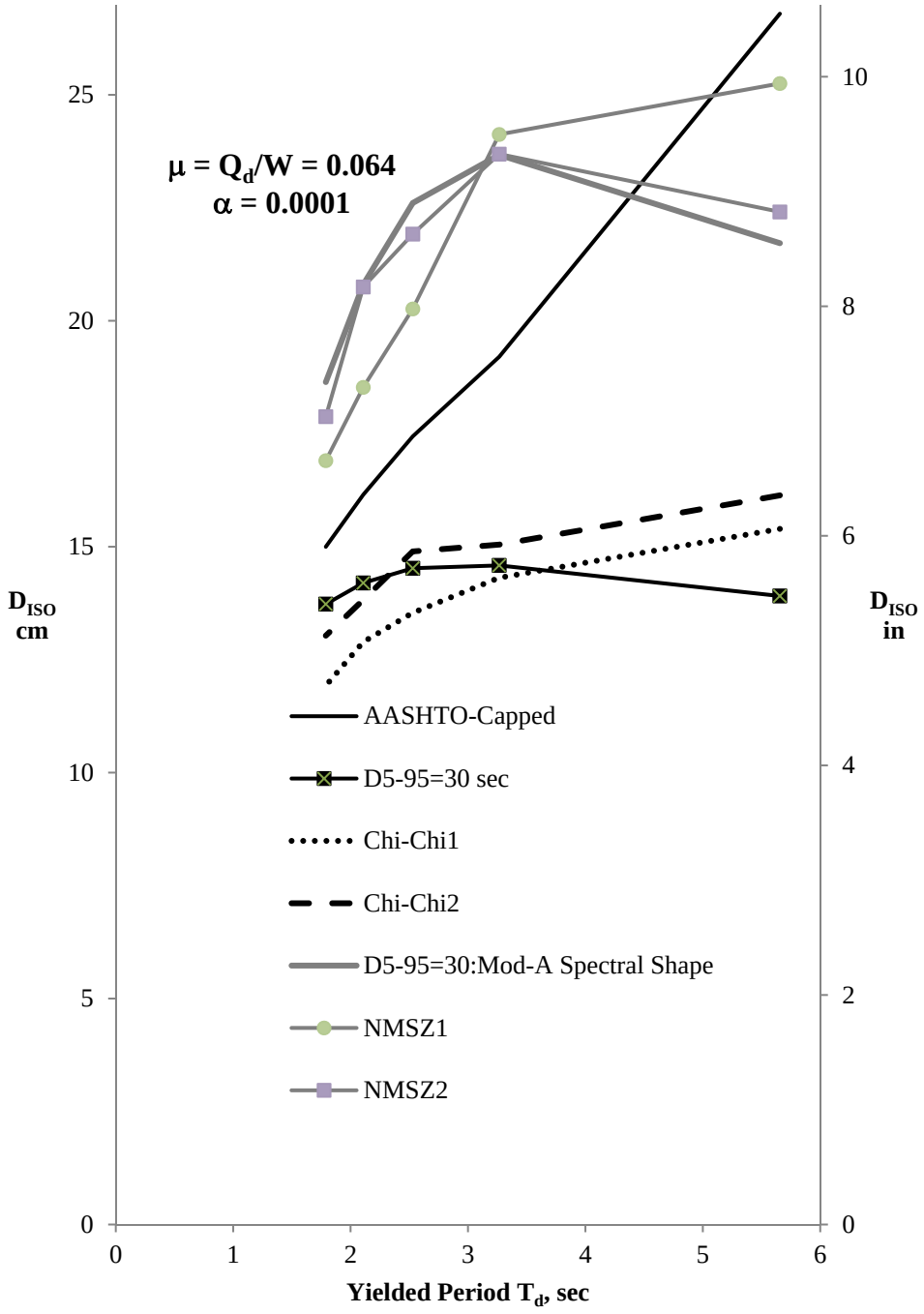

Figure G4.3-3. Proposed FPS Modifications: μ = Q_d/W = 0.064

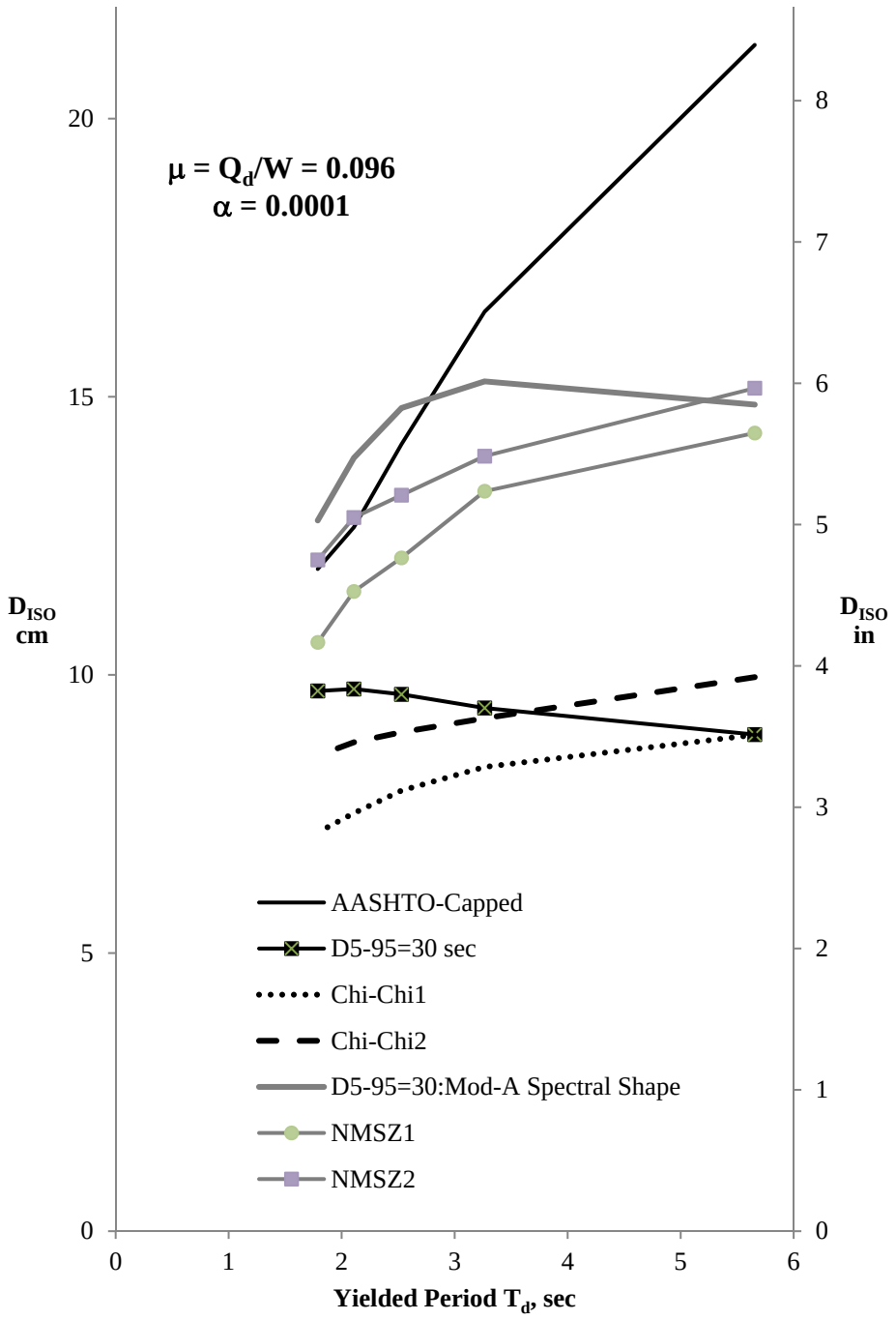

Figure G4.3-4. Proposed FPS Modifications: μ = Q_d/W = 0.096

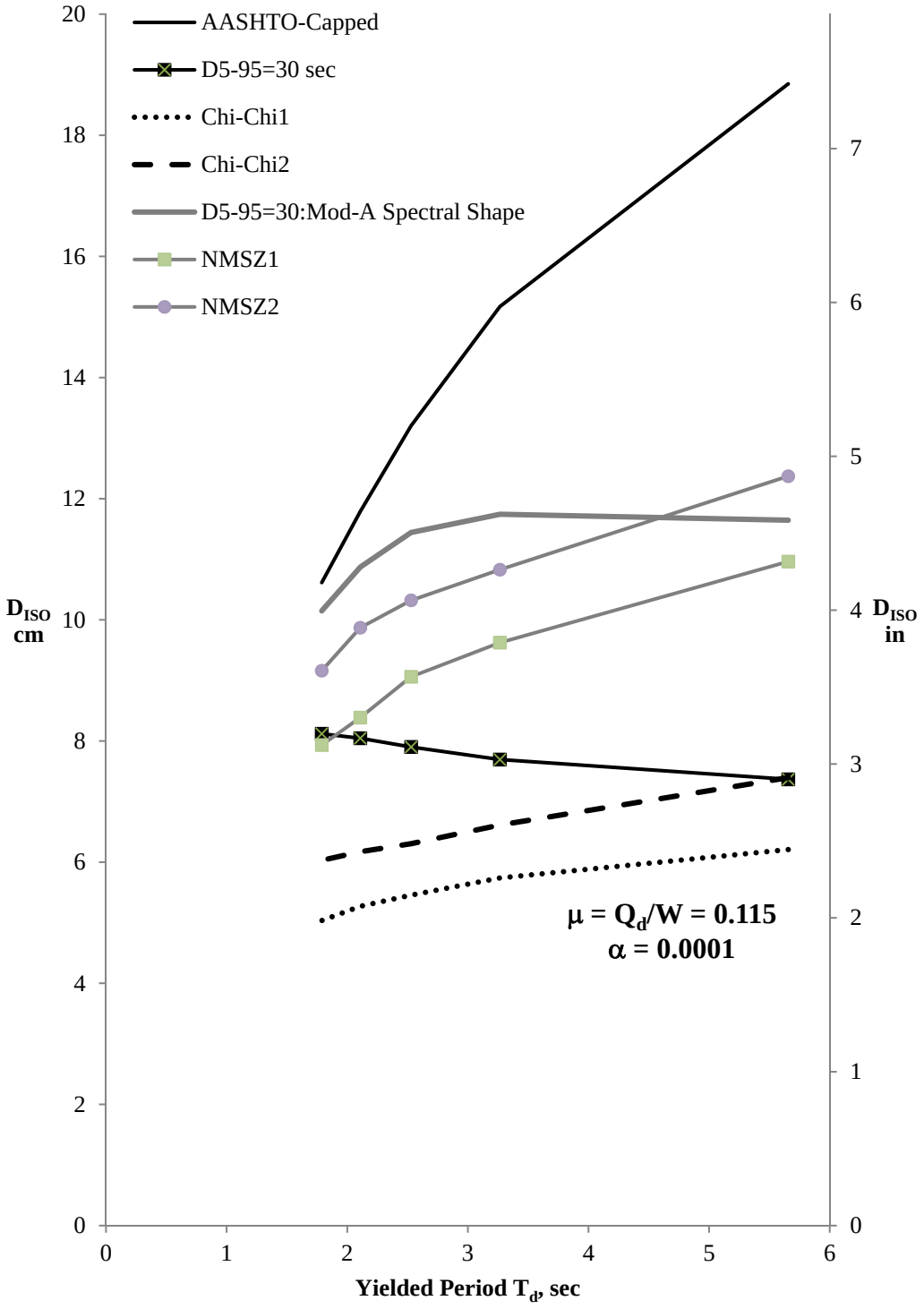

Figure G4.3-5. Proposed FPS Modifications: $\mu = Q_d/W = 0.115$

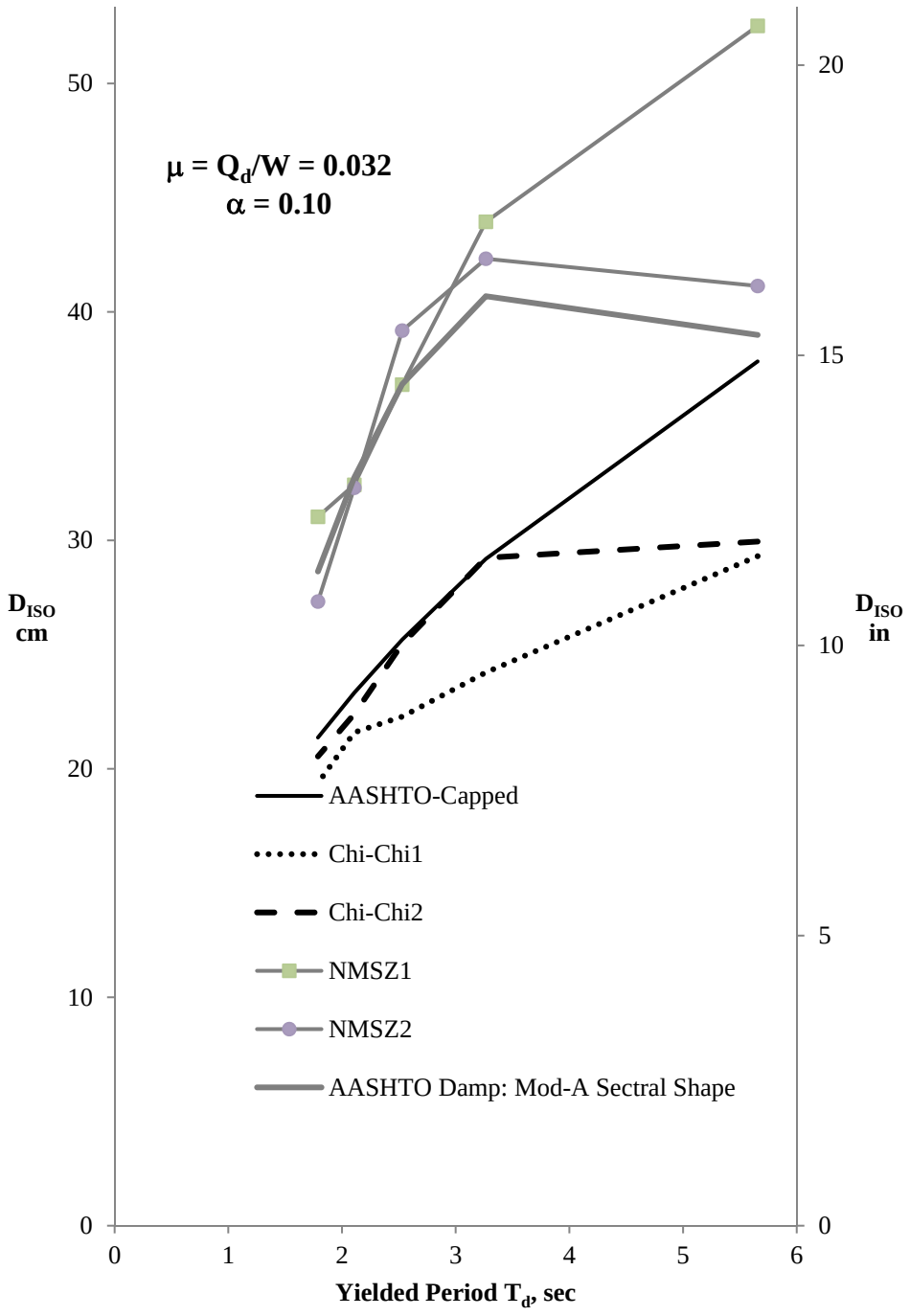

Figure G4.3-6. Proposed LRB Modifications: μ = Q_d/W = 0.032

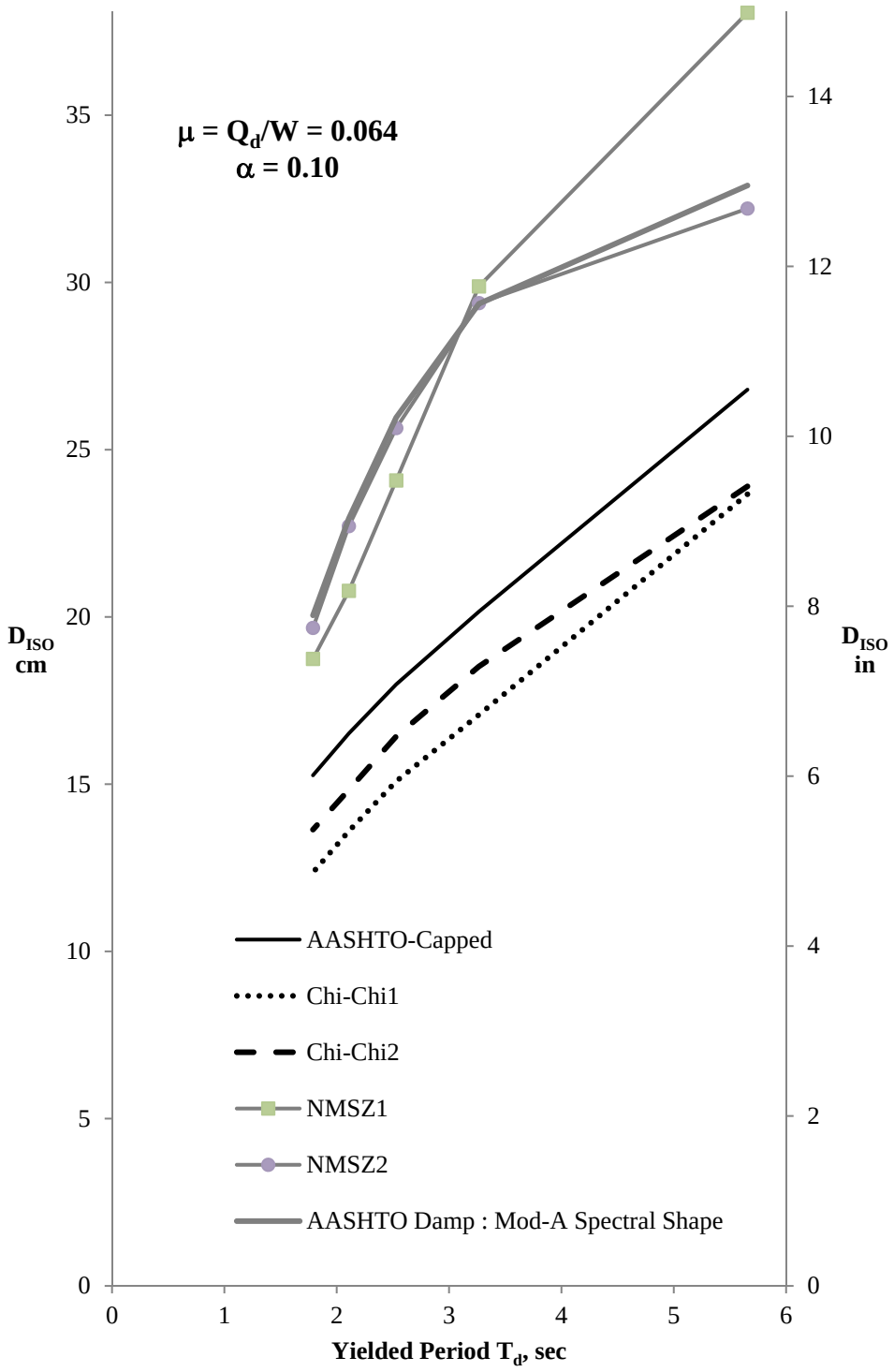

Figure G4.3-7. Proposed LRB Modifications: μ = Q_d/W = 0.064

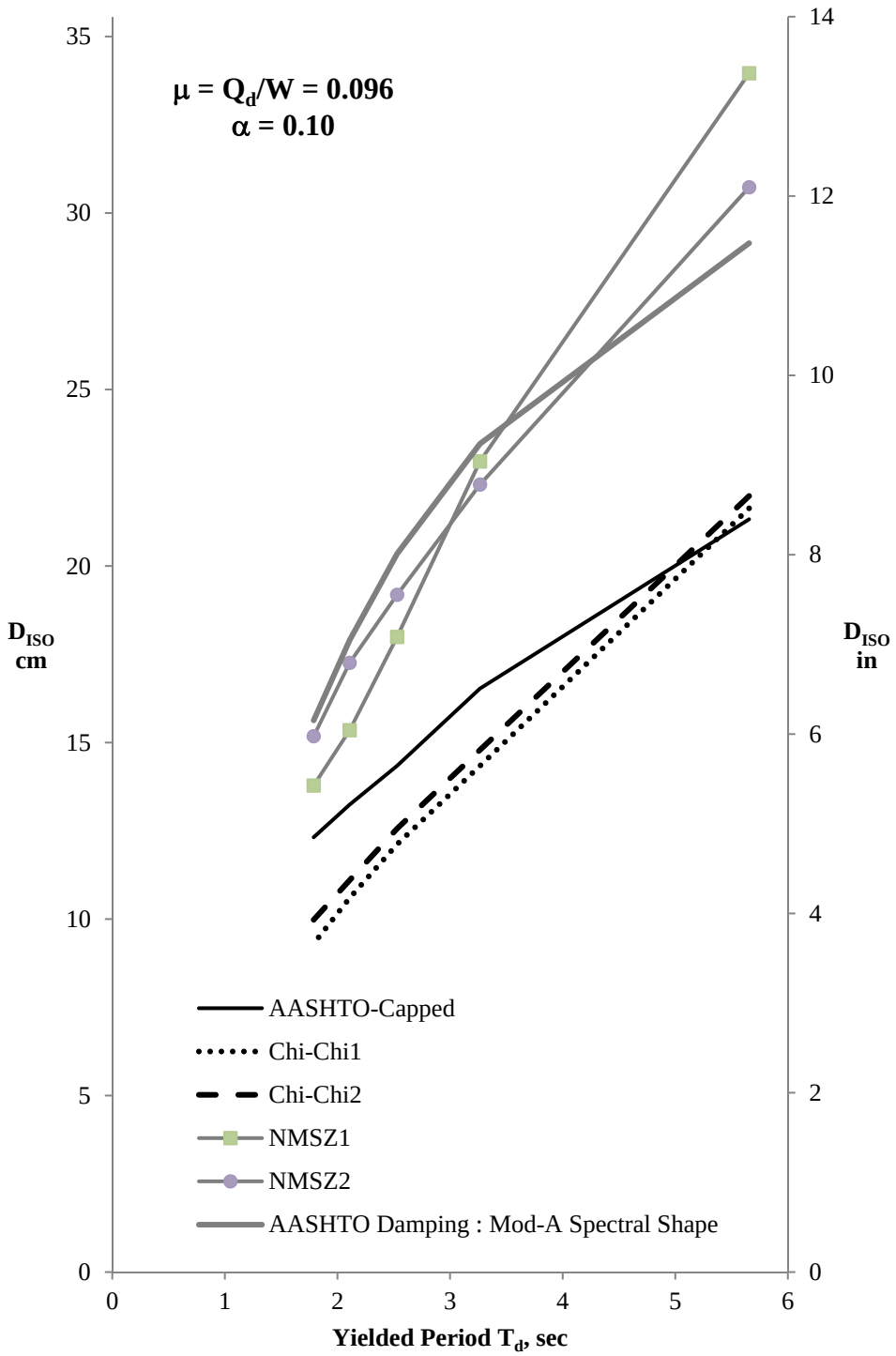

Figure G4.3-8. Proposed LRB Modifications: μ = Q_d/W = 0.096

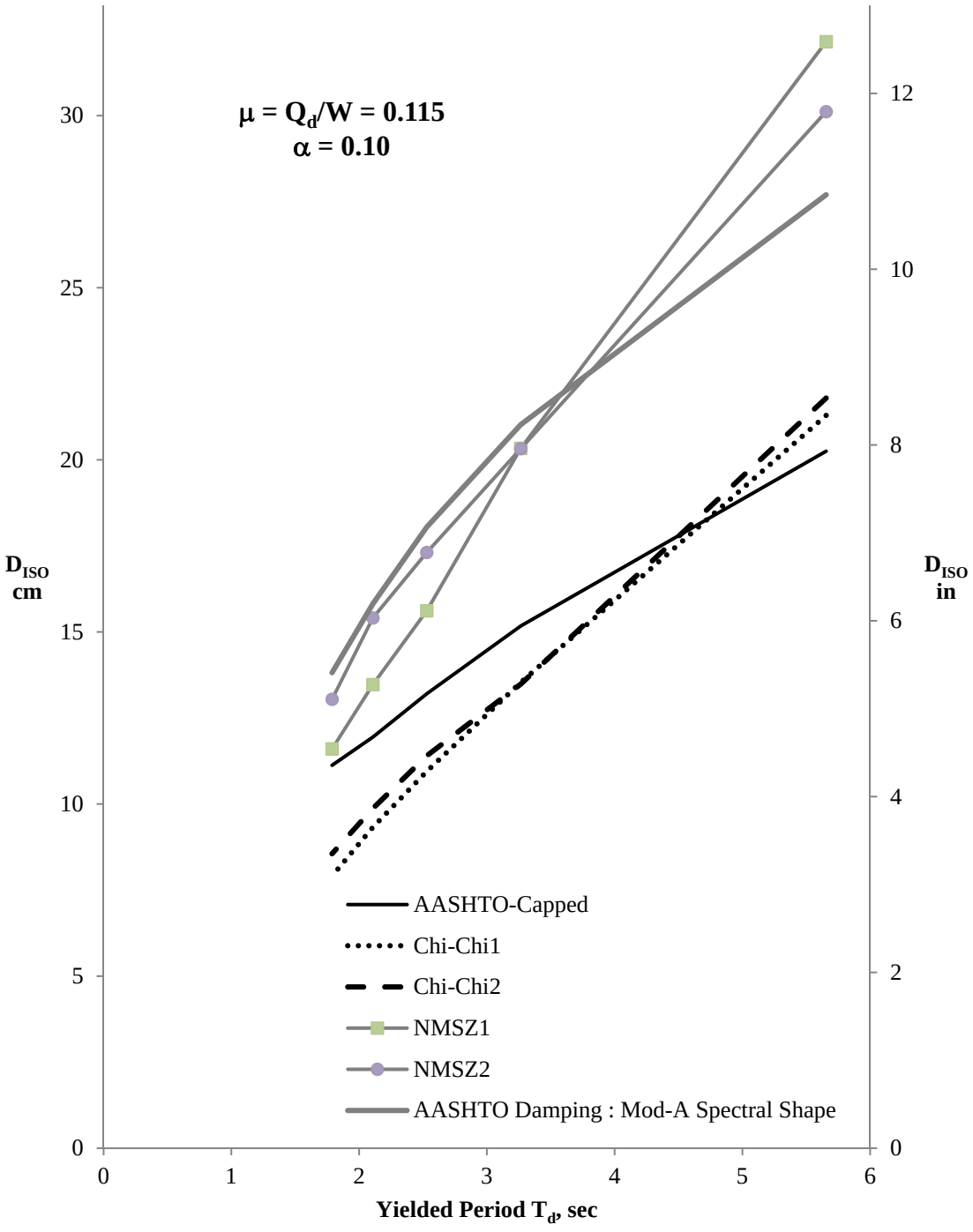

Figure G4.3-9. Proposed LRB Modifications: μ = Q_d/W = 0.115

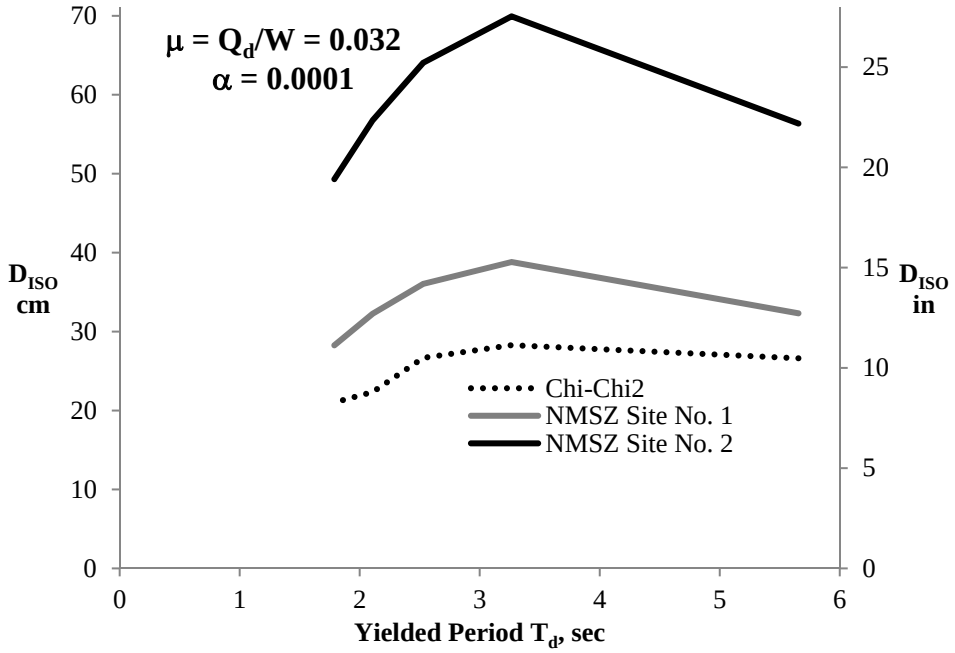

Figure G4.3-10. Chi-Chi vs. NMSZ FPS Isolator Demands: μ = Q_d/W = 0.032

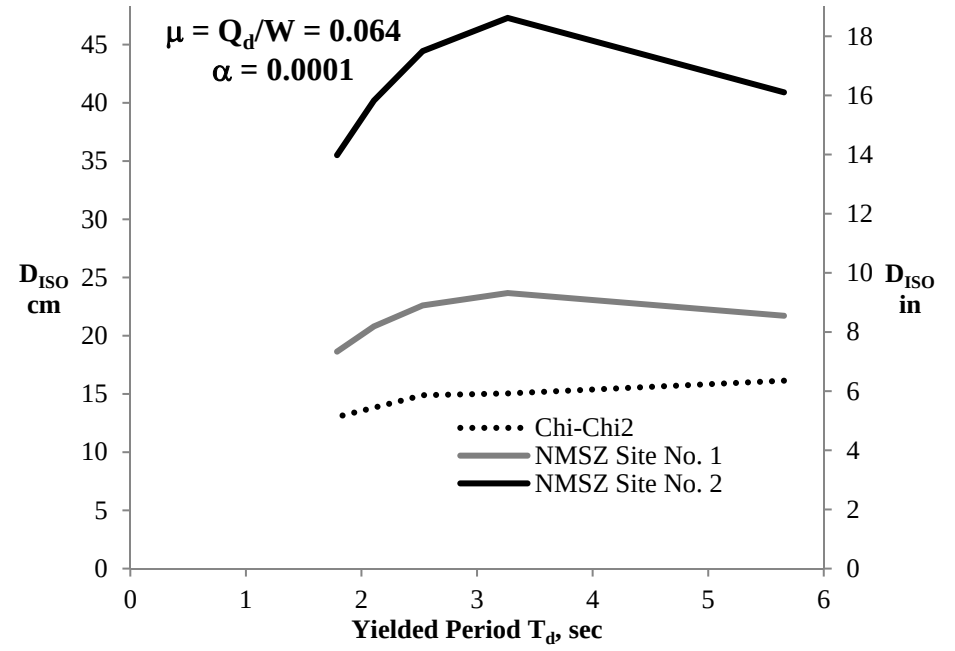

Figure G4.3-11. Chi-Chi vs. NMSZ FPS Isolator Demands: μ = Q_d/W = 0.064

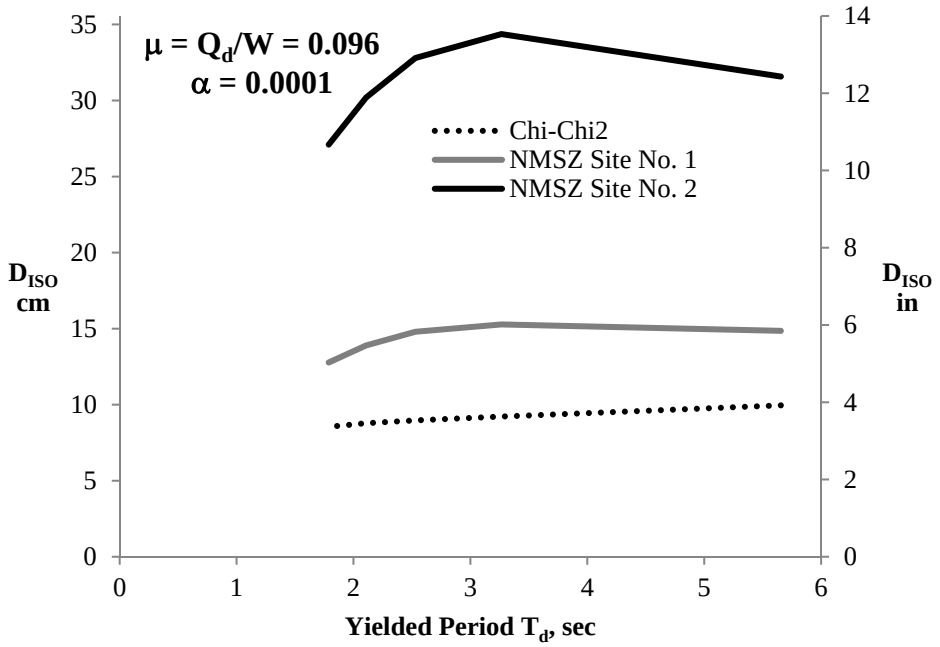

Figure G4.3-12. Chi-Chi vs. NMSZ FPS Isolator Demands: μ = Q_d/W = 0.096

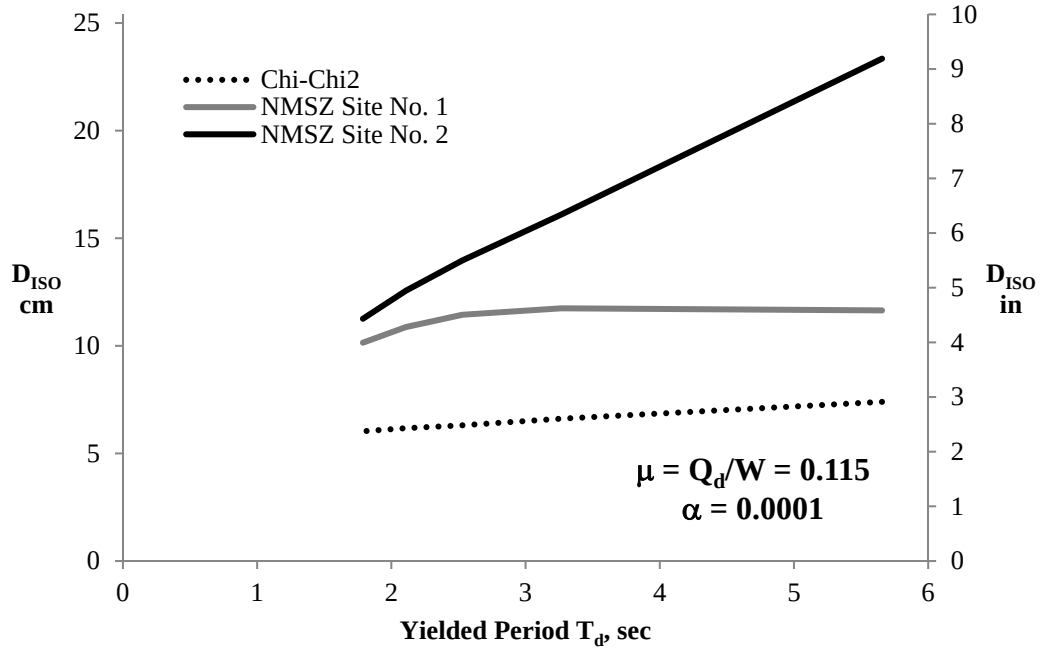

Figure G4.3-13. Chi-Chi vs. NMSZ FPS Isolator Demands: μ = Q_d/W = 0.115

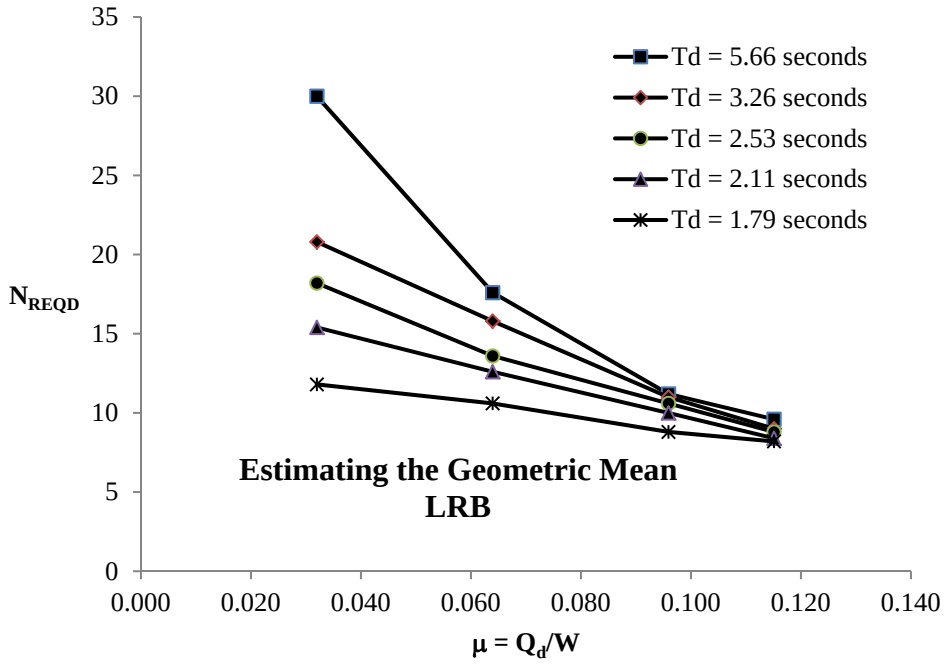

Figure G4.4-1. Sample Size - LRB Isolators - 20% Accuracy with 90% CL

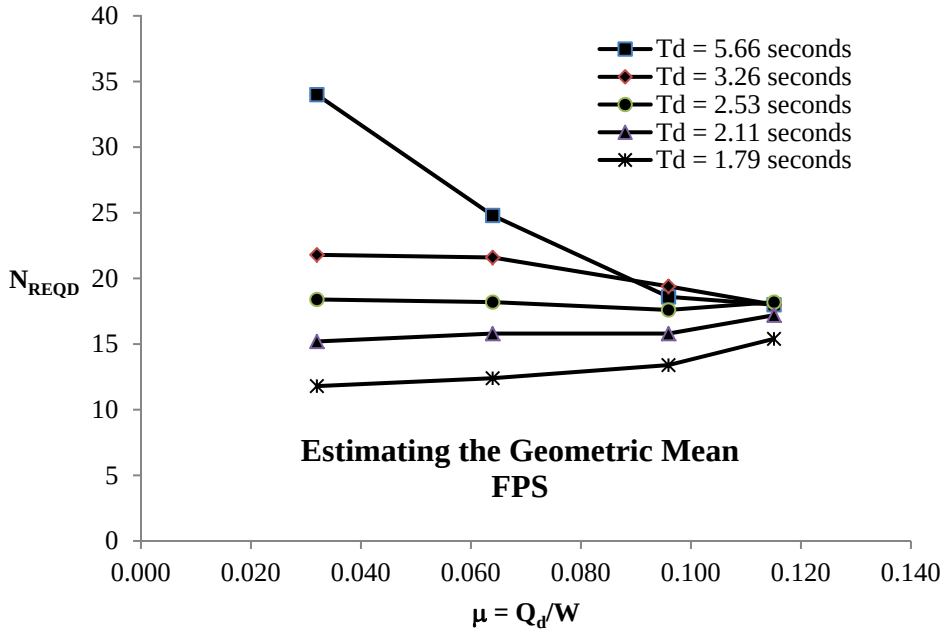

Figure G4.4-2. Sample Size - FPS Isolators - 20% Accuracy with 90% CL

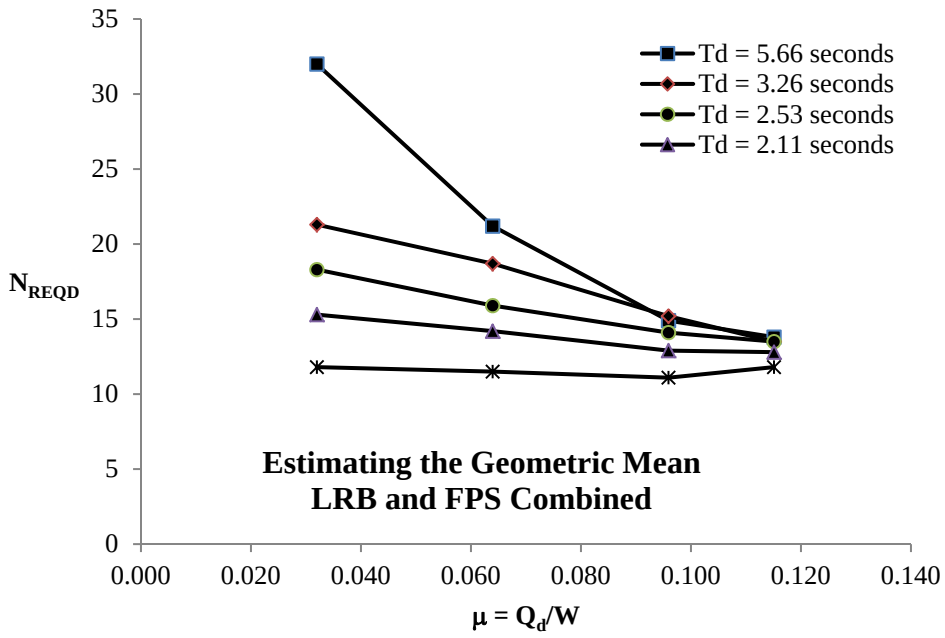

Figure G4.4-3. Sample Size - All Isolators - 20% Accuracy with 90% CL

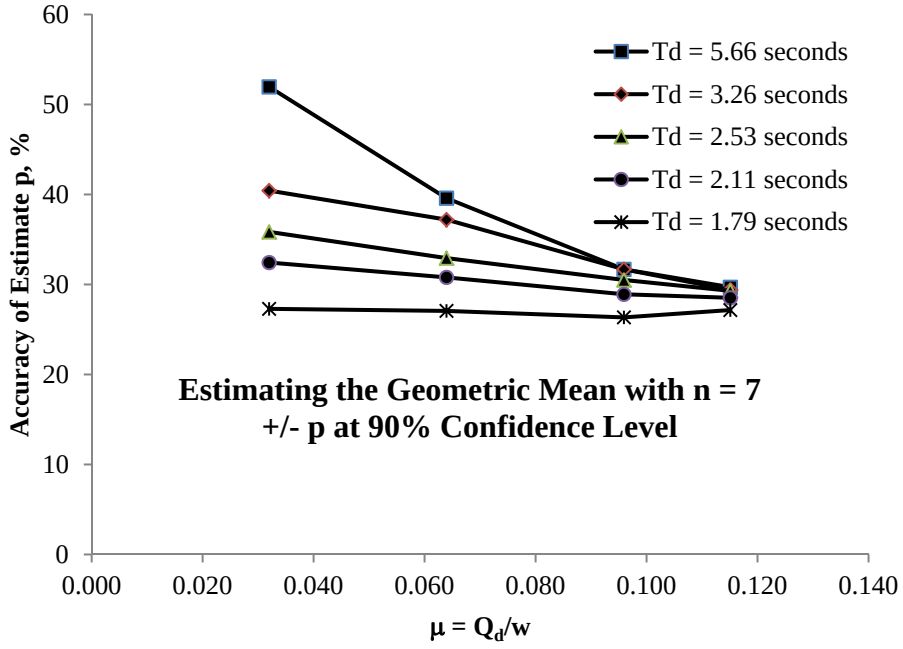

Figure G4.4-4. Accuracy of Estimate with 90% CL - n = 7

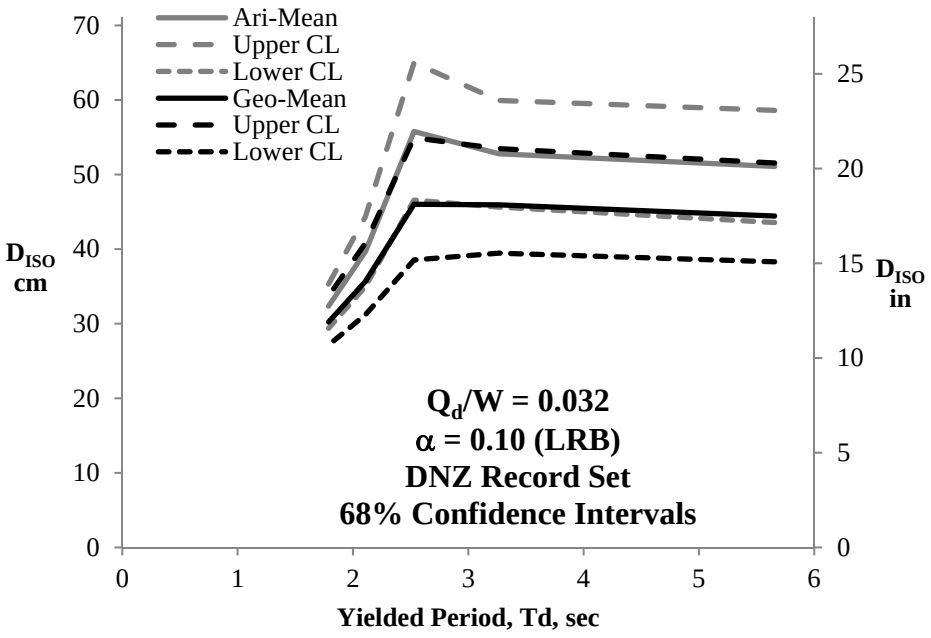

Figure G4.4-5. Geom. vs. Arith. Mean - DNZ Records - $\mu = 0.032$ - LRB

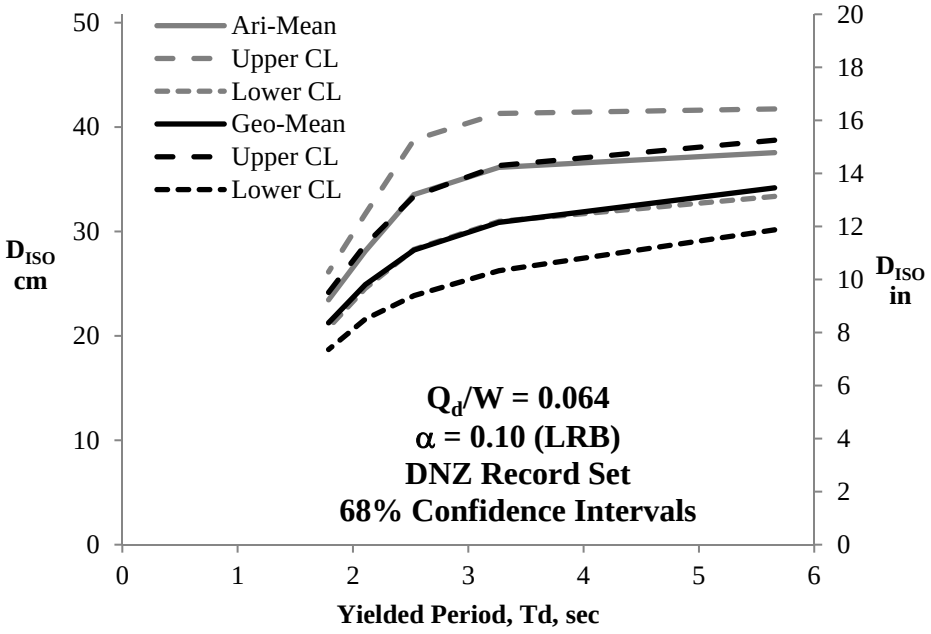

Figure G4.4-6. Geom. vs. Arith. Mean - DNZ Records - $\mu = 0.064$ - LRB

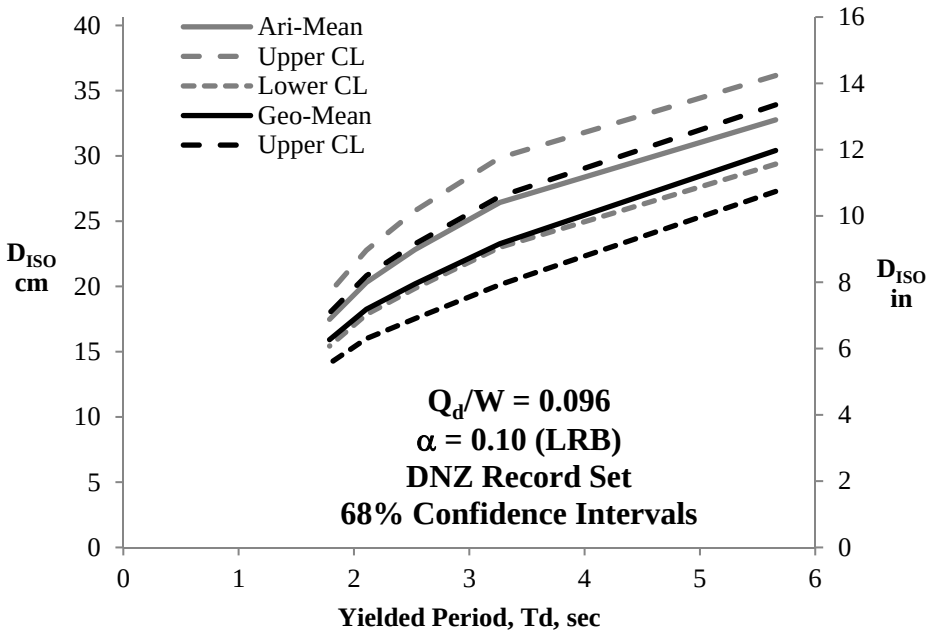

Figure G4.4-7. Geom. vs. Arith. Mean - DNZ Records - μ = 0.096 - LRB

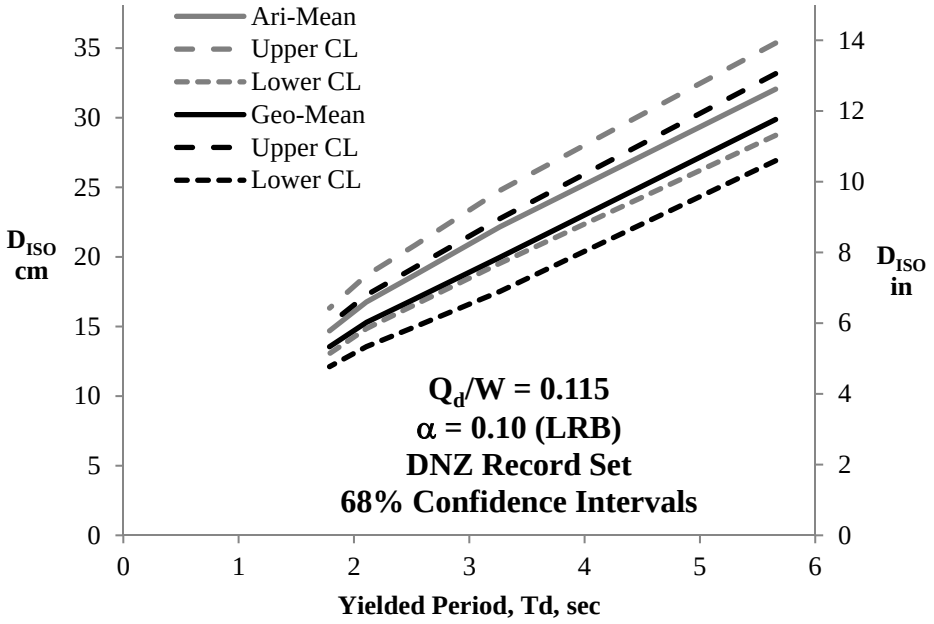

Figure G4.4-8. Geom. vs. Arith. Mean - DNZ Records - μ = 0.096 - LRB

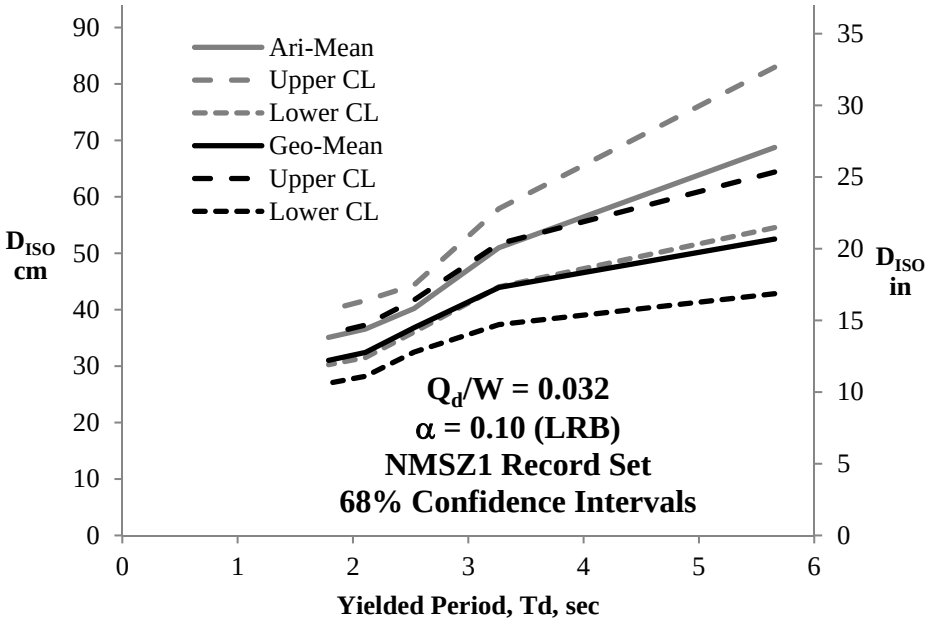

Figure G4.4-9. Geom. vs. Arith. Mean - NMSZ1 Records - μ = 0.032 - LRB

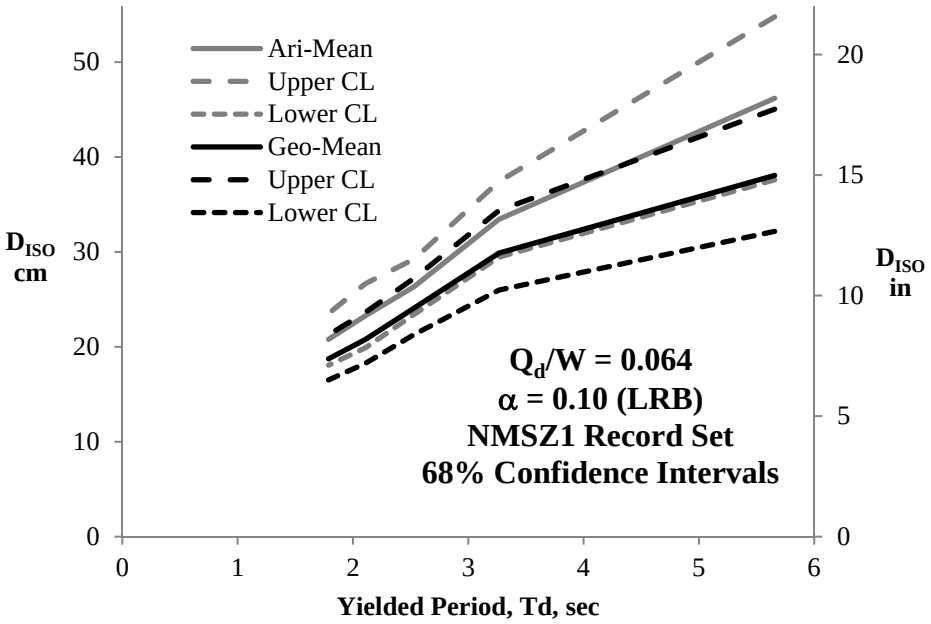

Figure G4.4-10. Geom. vs. Arith. Mean - NMSZ1 Records - μ = 0.064 - LRB

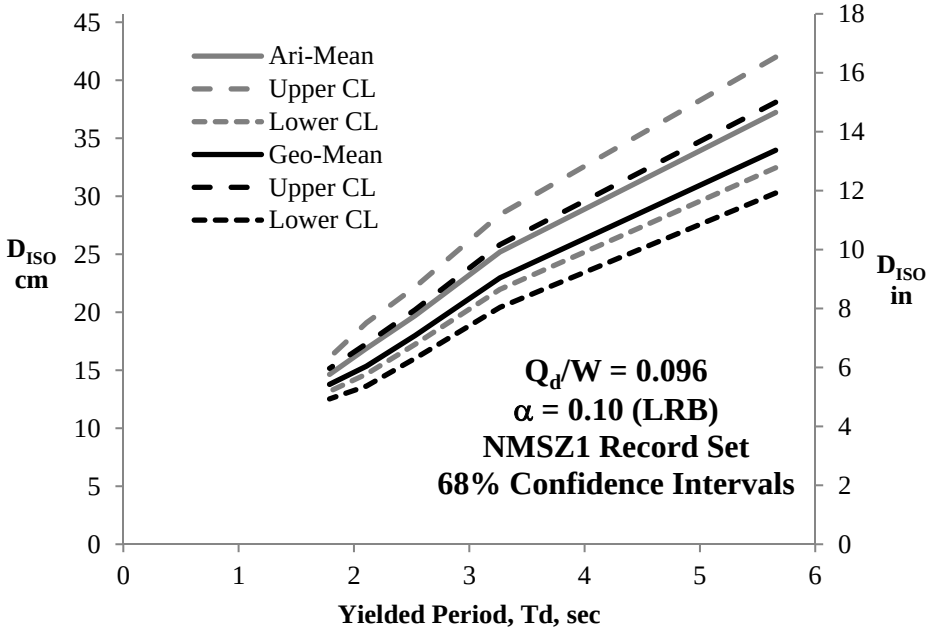

Figure G4.4-11. Geom. vs. Arith. Mean - NMSZ1 Records - $\mu = 0.096$ - LRB

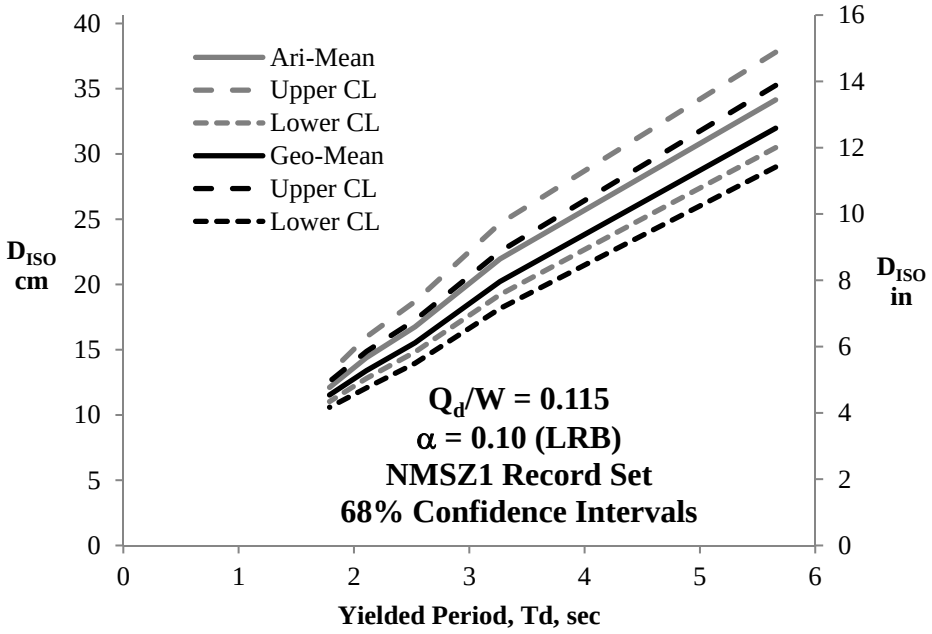

Figure G4.4-12. Geom. vs. Arith. Mean - NMSZ1 Records - $\mu = 0.115$ - LRB

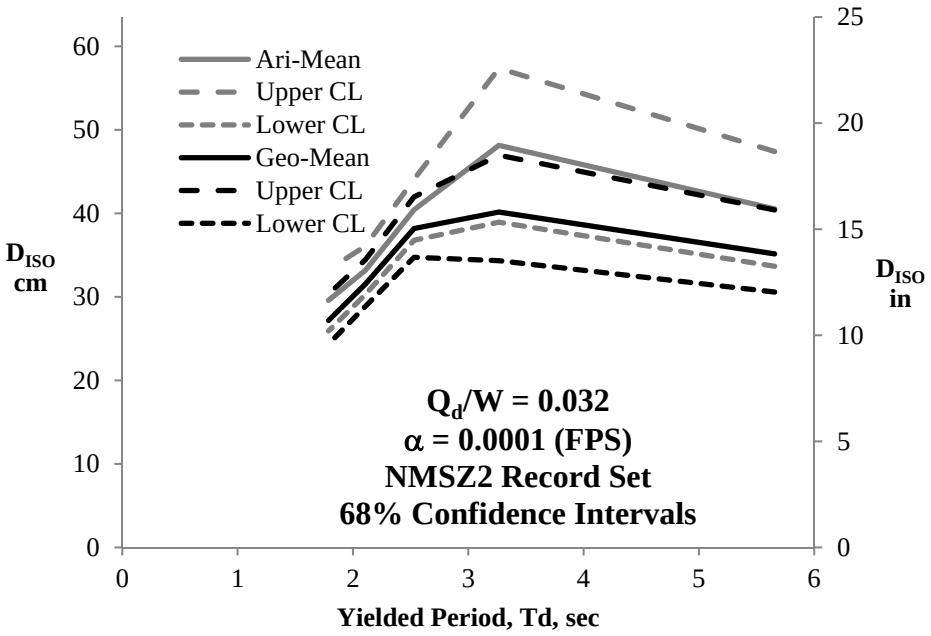

Figure G4.4-13. Geom. vs. Arith. Mean - NMSZ2 Records - μ = 0.032 - FPS

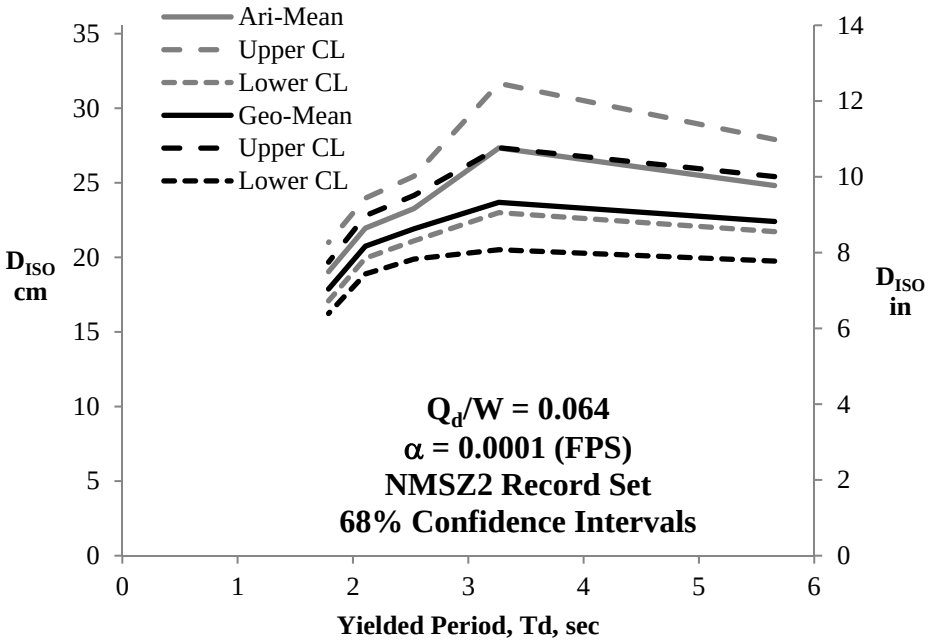

Figure G4.4-14. Geom. vs. Arith. Mean - NMSZ2 Records - μ = 0.064 - FPS

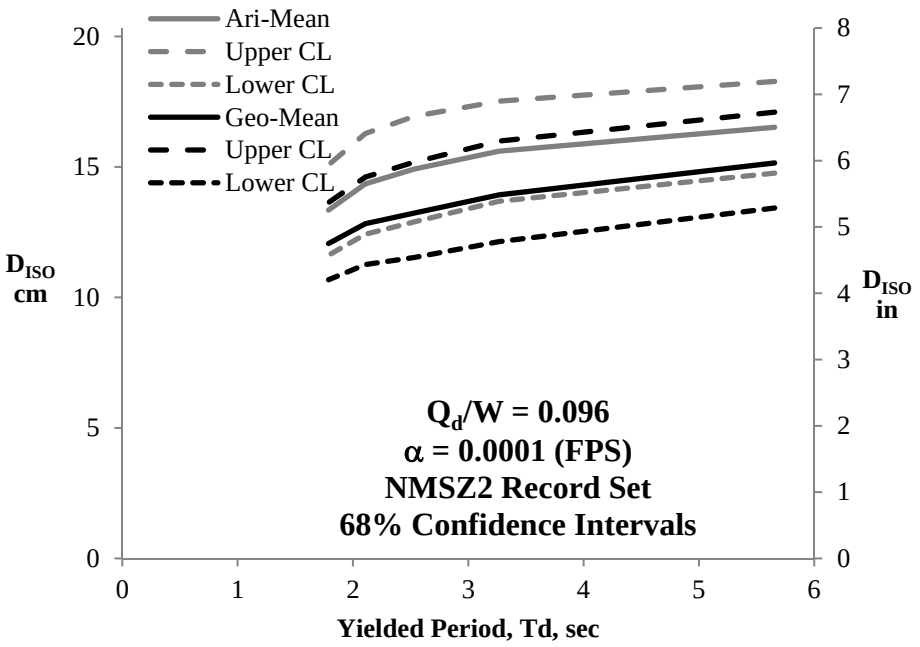

Figure G4.4-15. Geom. vs. Arith. Mean - NMSZ2 Records - μ = 0.096 - FPS

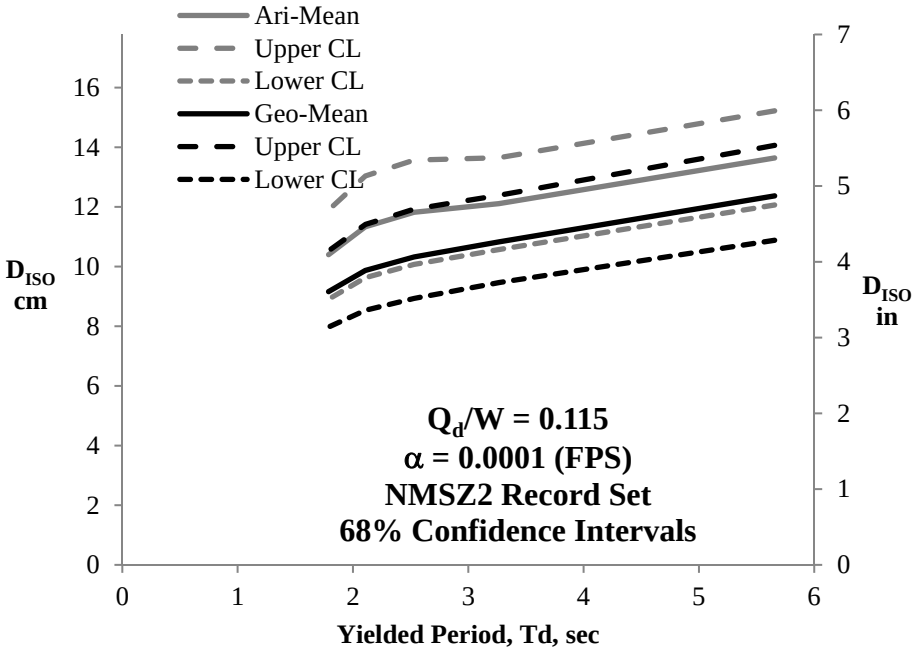

Figure G4.4-16. Geom. vs. Arith. Mean - NMSZ2 Records - μ = 0.115 - FPS

APPENDIX G5 - CHAPTER 5 SUPPORTING FIGURES

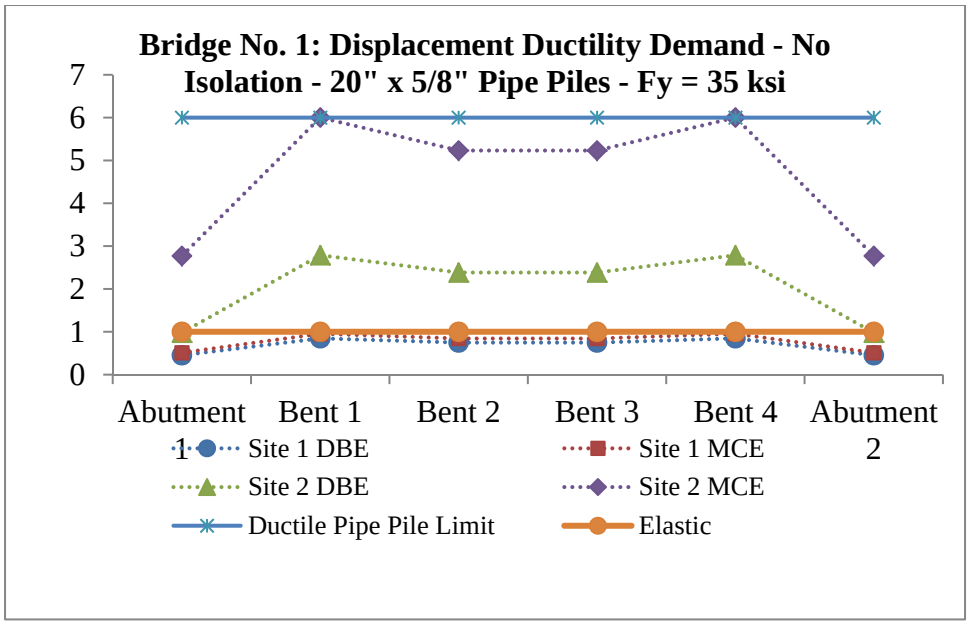

Figure G5.3-1. Non-isolated Bridge No. 1: Ductility Demand – Ductile Pipe Piles

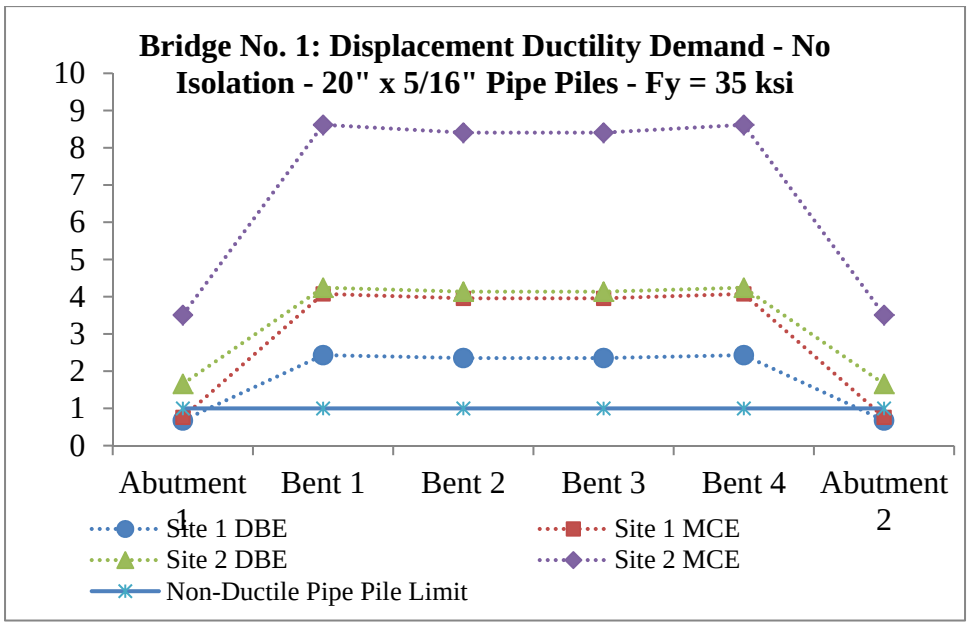

Figure G5.3-2. Non-isolated Bridge No. 1: Ductility Demand Non-ductile Pipe Piles

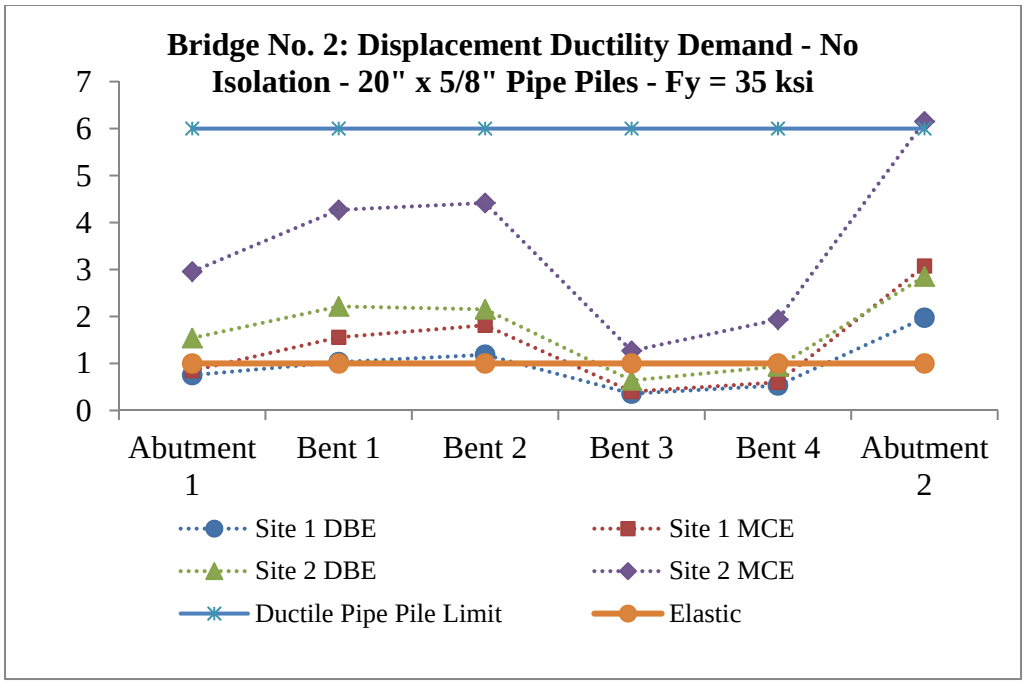

Figure G5.3-3. Non-isolated Bridge No. 2: Ductility Demand - Ductile Pipe Piles

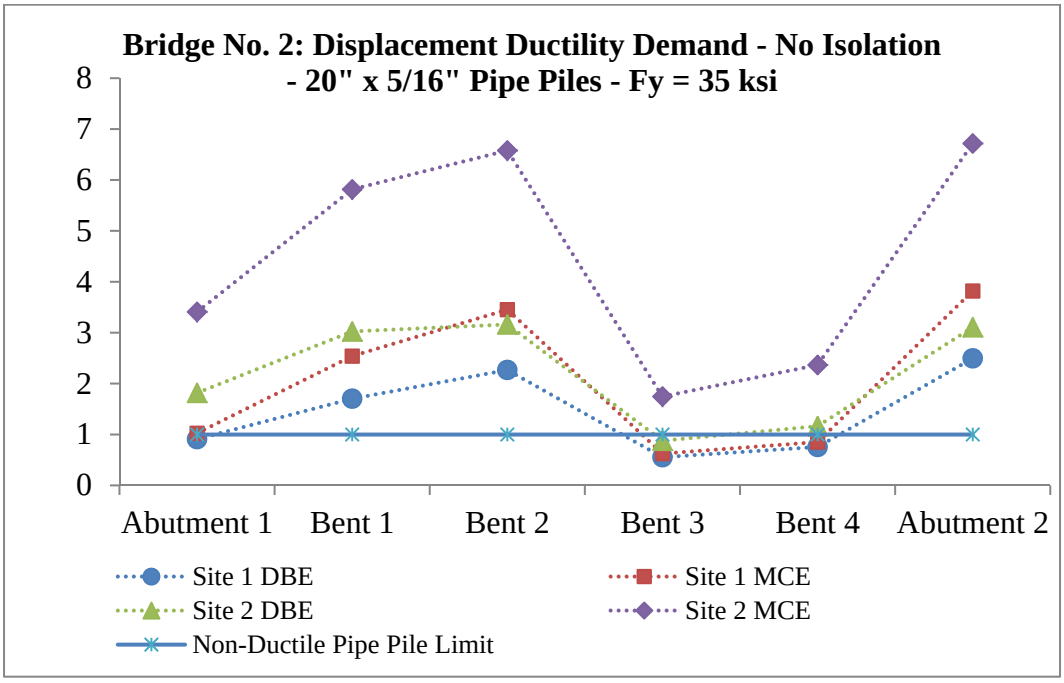

Figure G5.3-4. Non-isolated Bridge No. 2: Ductility Demand – Non-ductile Pipe Piles

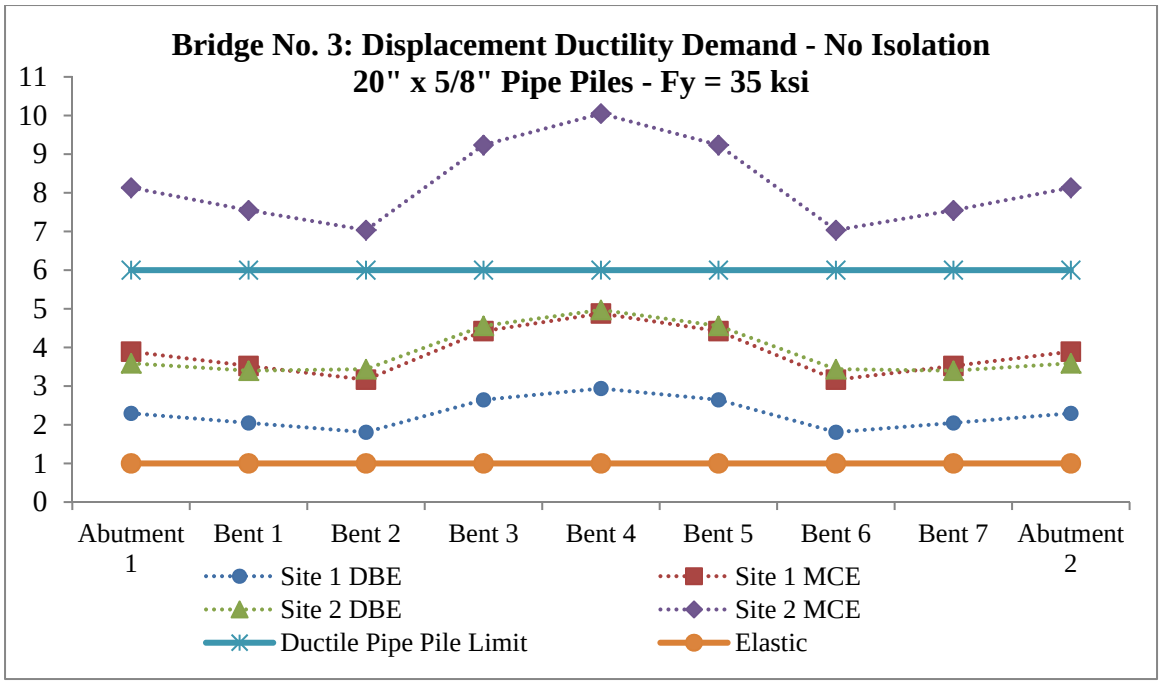

Figure G5.3-5. Non-isolated Bridge No. 3: Ductility Demand – Ductile Pipe Piles

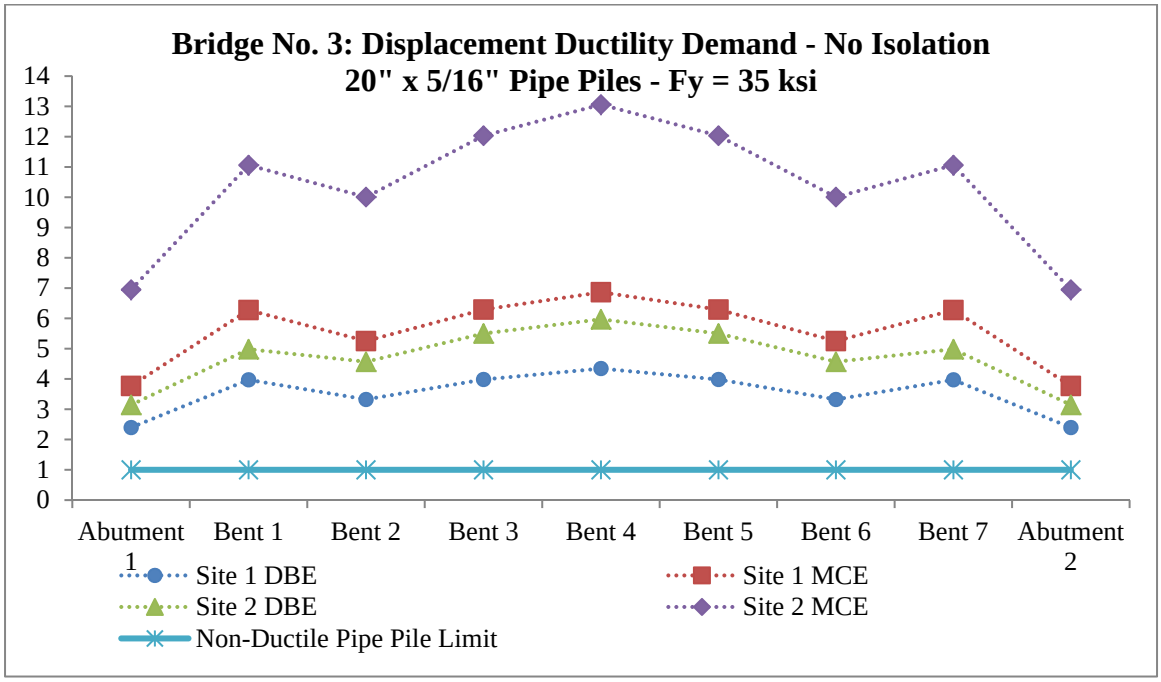

Figure G5.3-6. Non-isolated Bridge No. 3: Ductility Demand – Non-ductile Pipe Piles

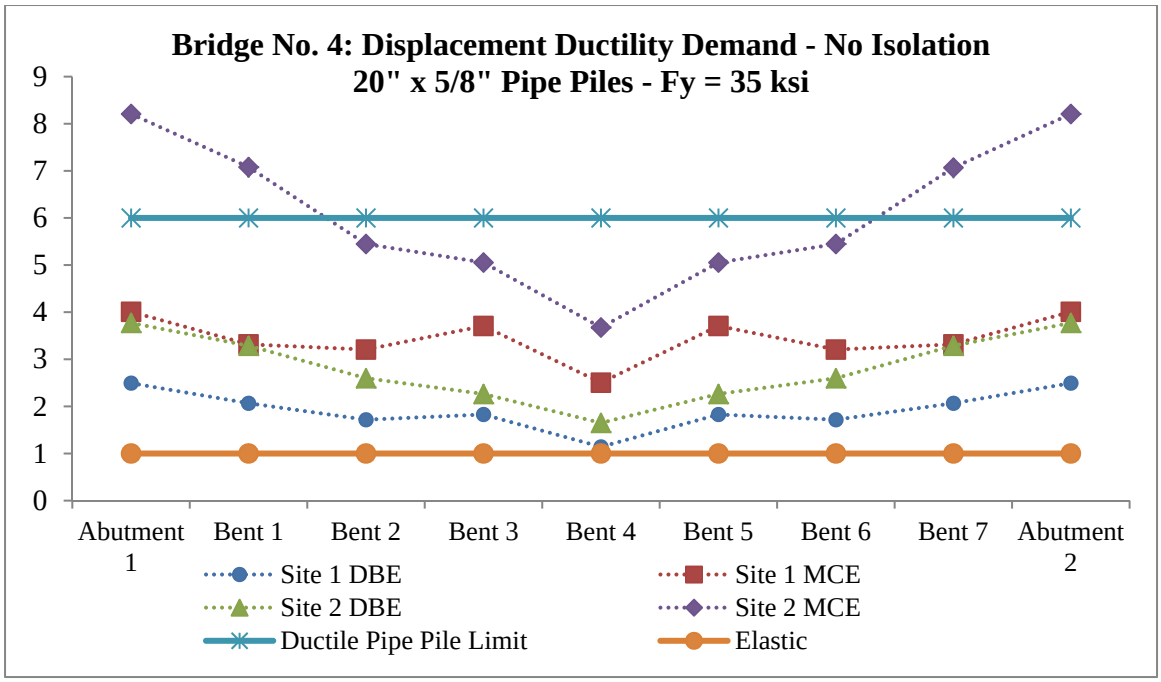

Figure G5.3-7. Non-isolated Bridge No. 4: Ductility Demand – Ductile Pipe Piles

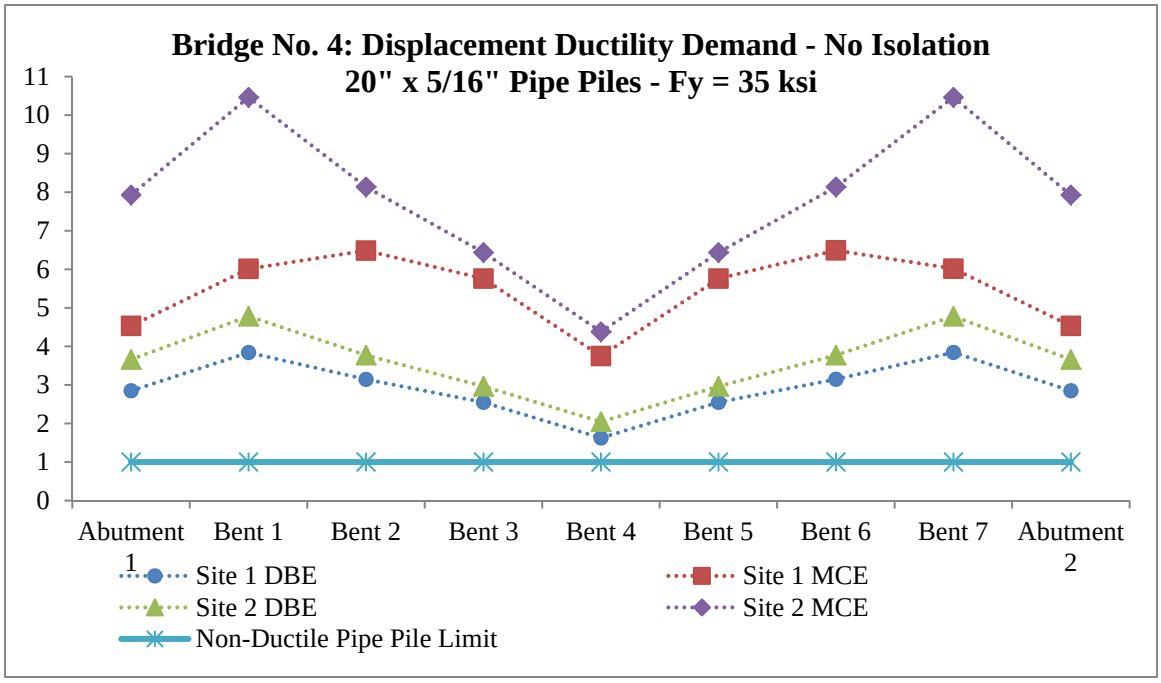

Figure G5.3-8. Non-isolated Bridge No. 4: Ductility Demand – Non-ductile Pipe Piles

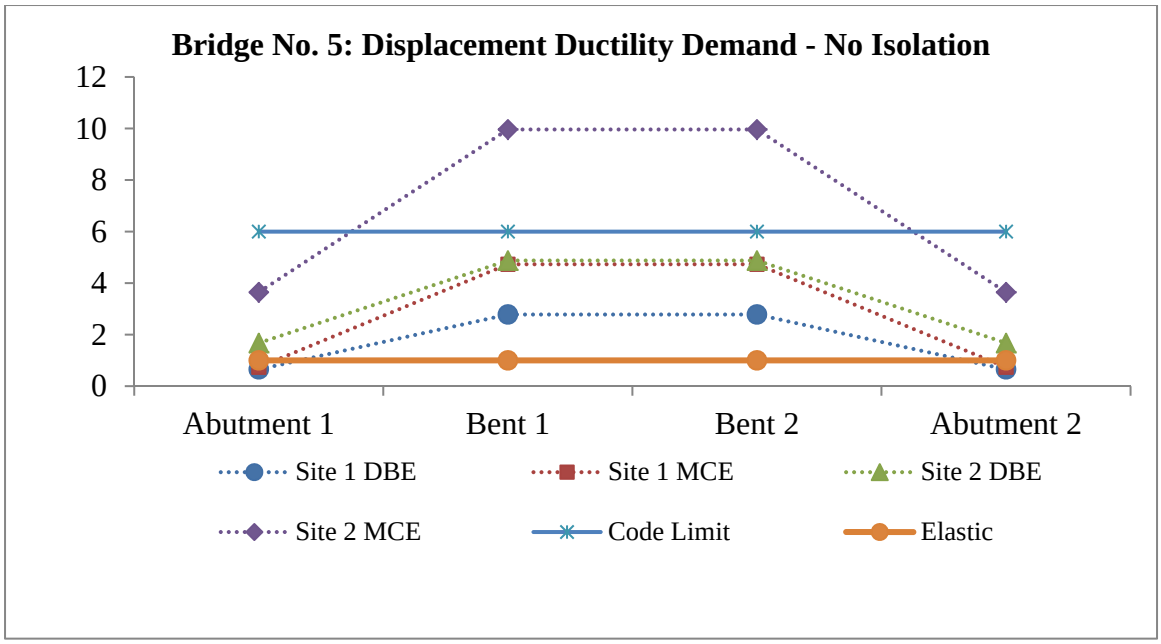

Figure G5.3-9. Non-isolated Bridge No. 5: Ductility Demand

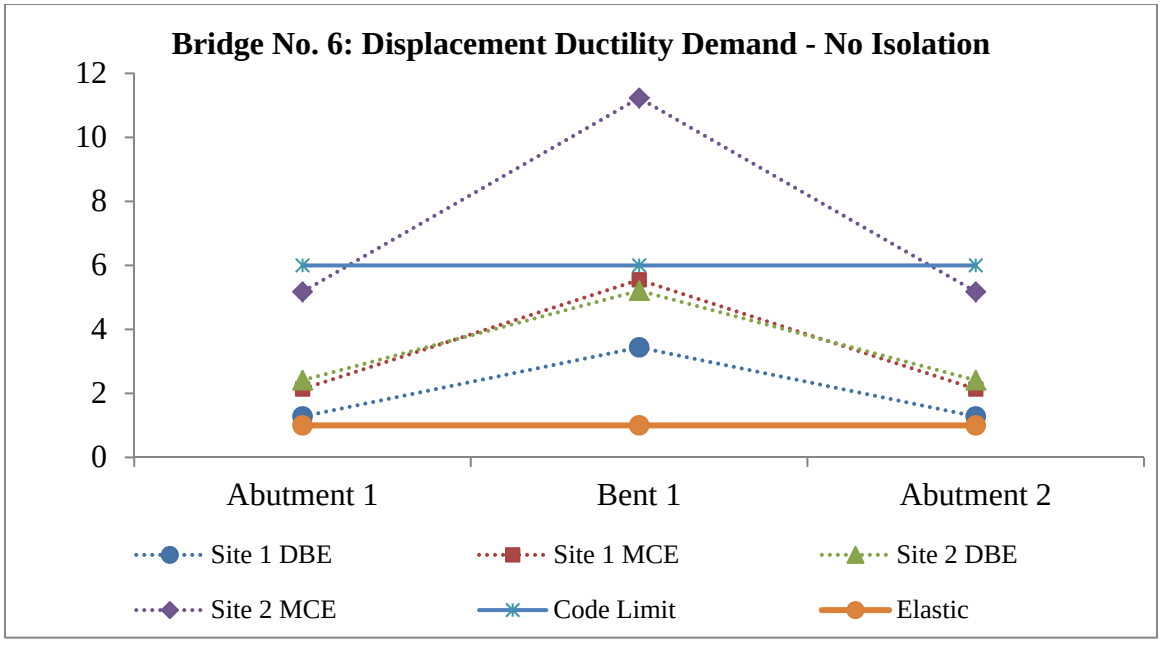

Figure G5.3-10. Non-isolated Bridge No. 6: Ductility Demand

APPENDIX G7 - CHAPTER 7 SUPPORTING FIGURES

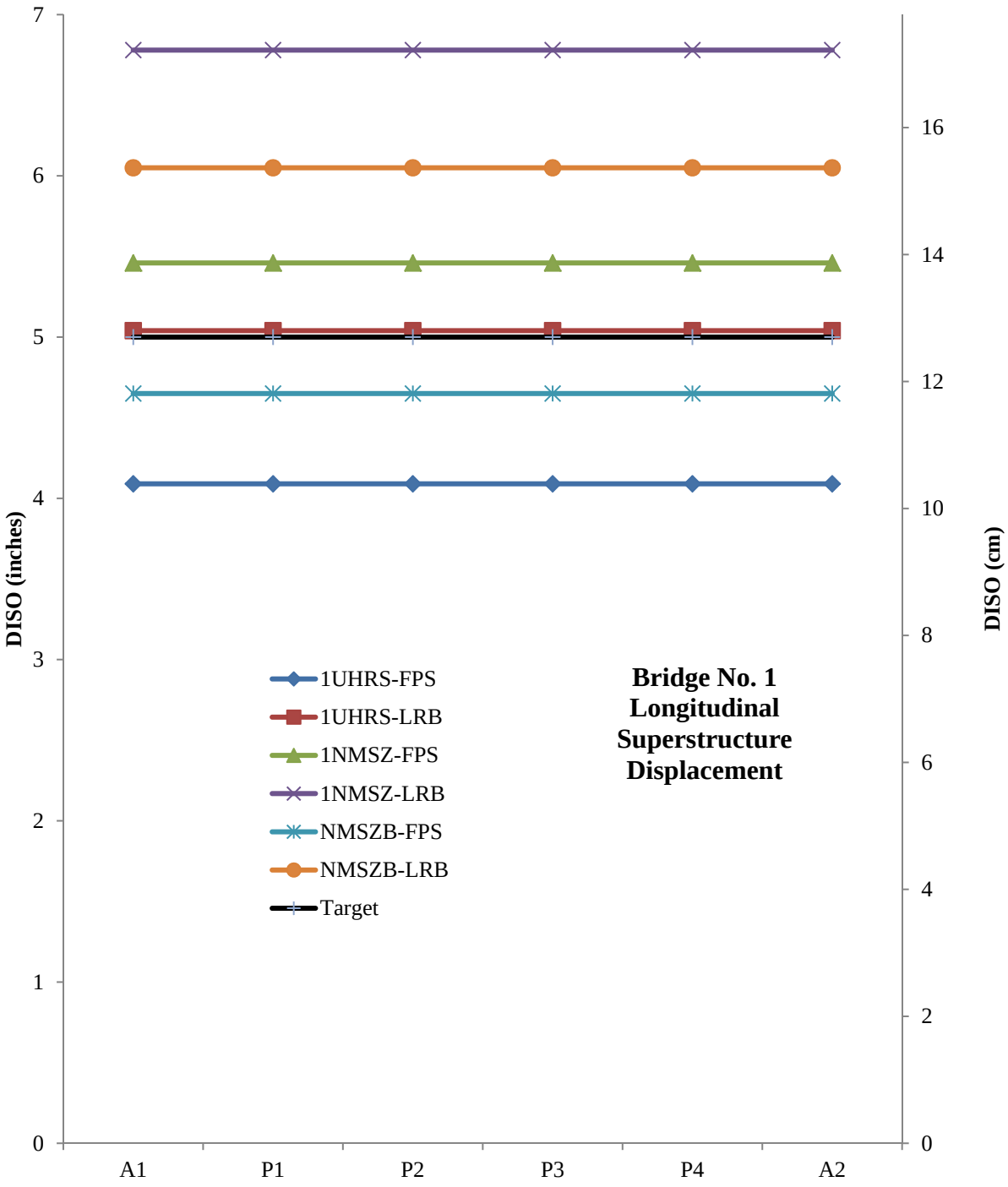

Figure G7.2.1-1. Superstructure Displacements - Bridge No. 1 (Longitudinal)

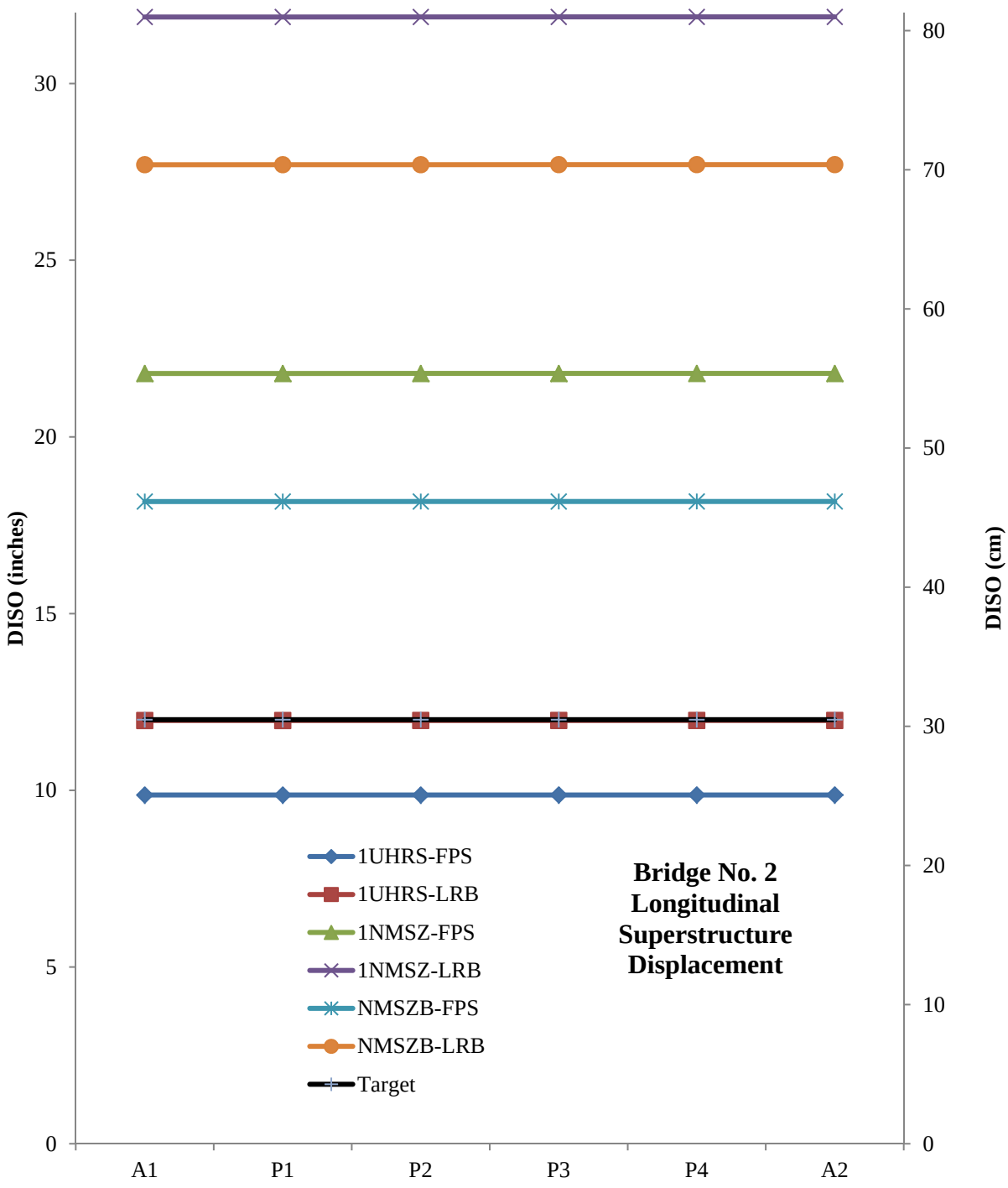

Figure G7.2.1-2. Superstructure Displacements - Bridge No. 2 (Longitudinal)

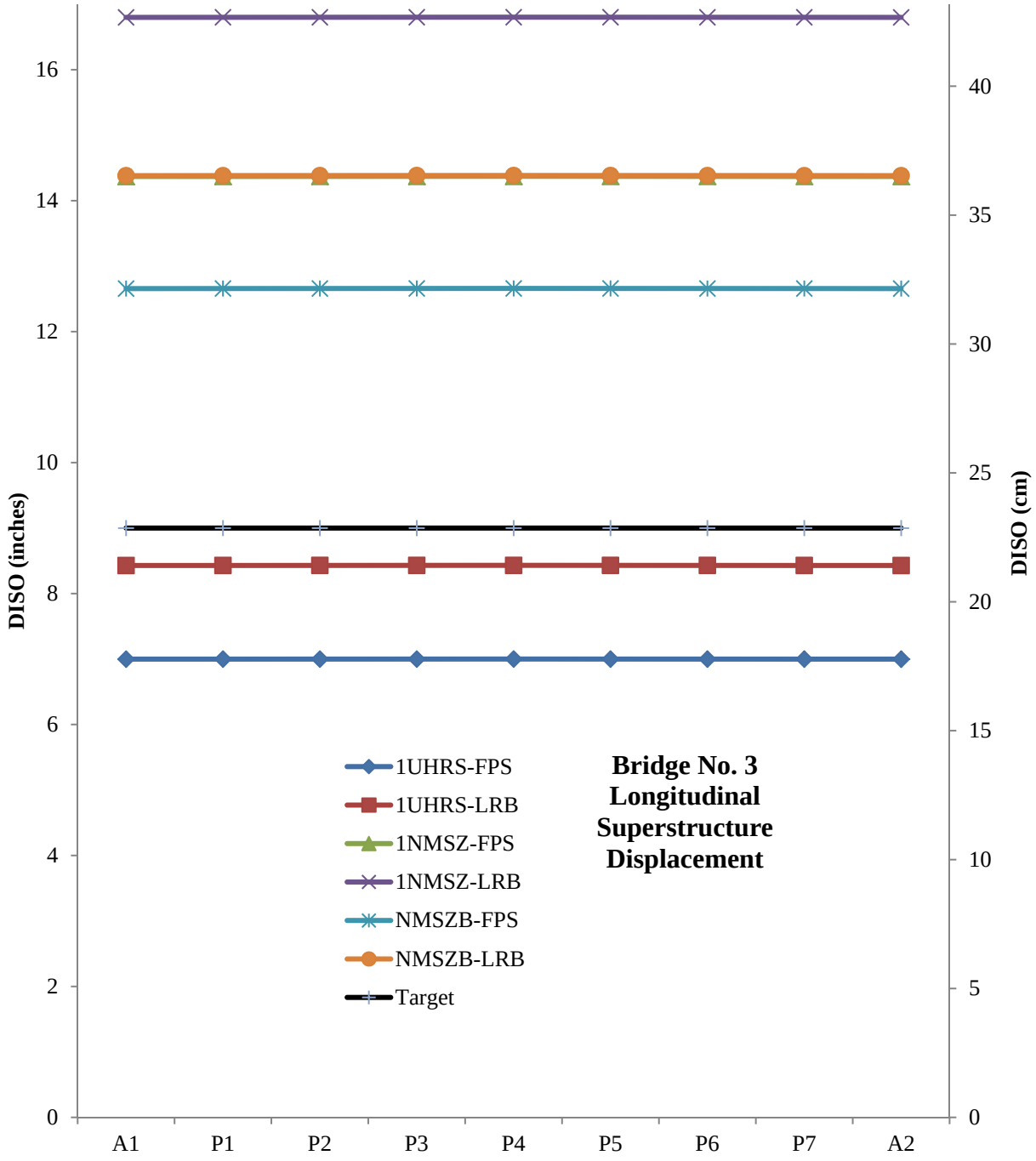

Figure G7.2.1-3. Superstructure Displacements - Bridge No. 3 (Longitudinal)

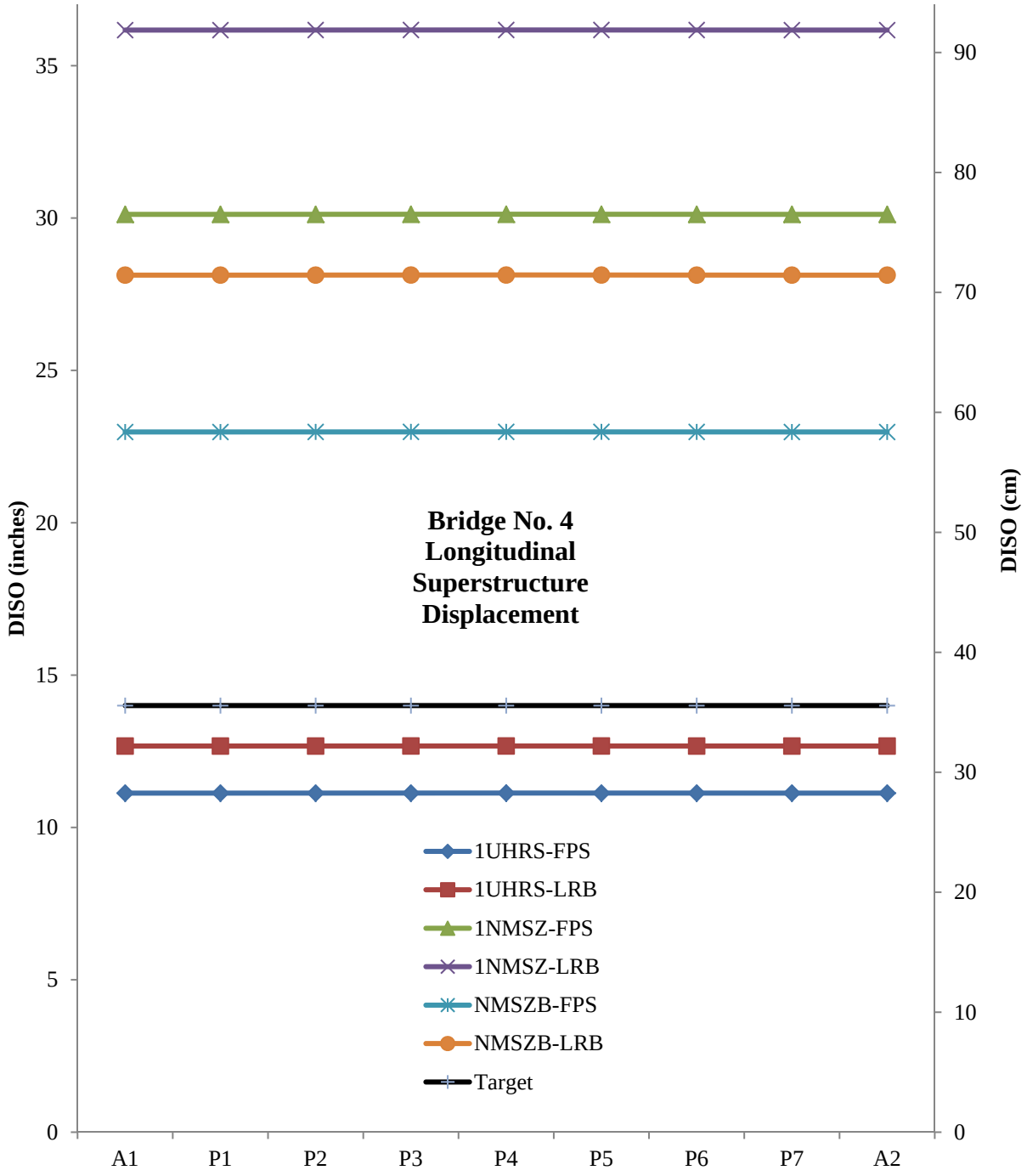

Figure G7.2.1-4. Superstructure Displacements - Bridge No. 4 (Longitudinal)

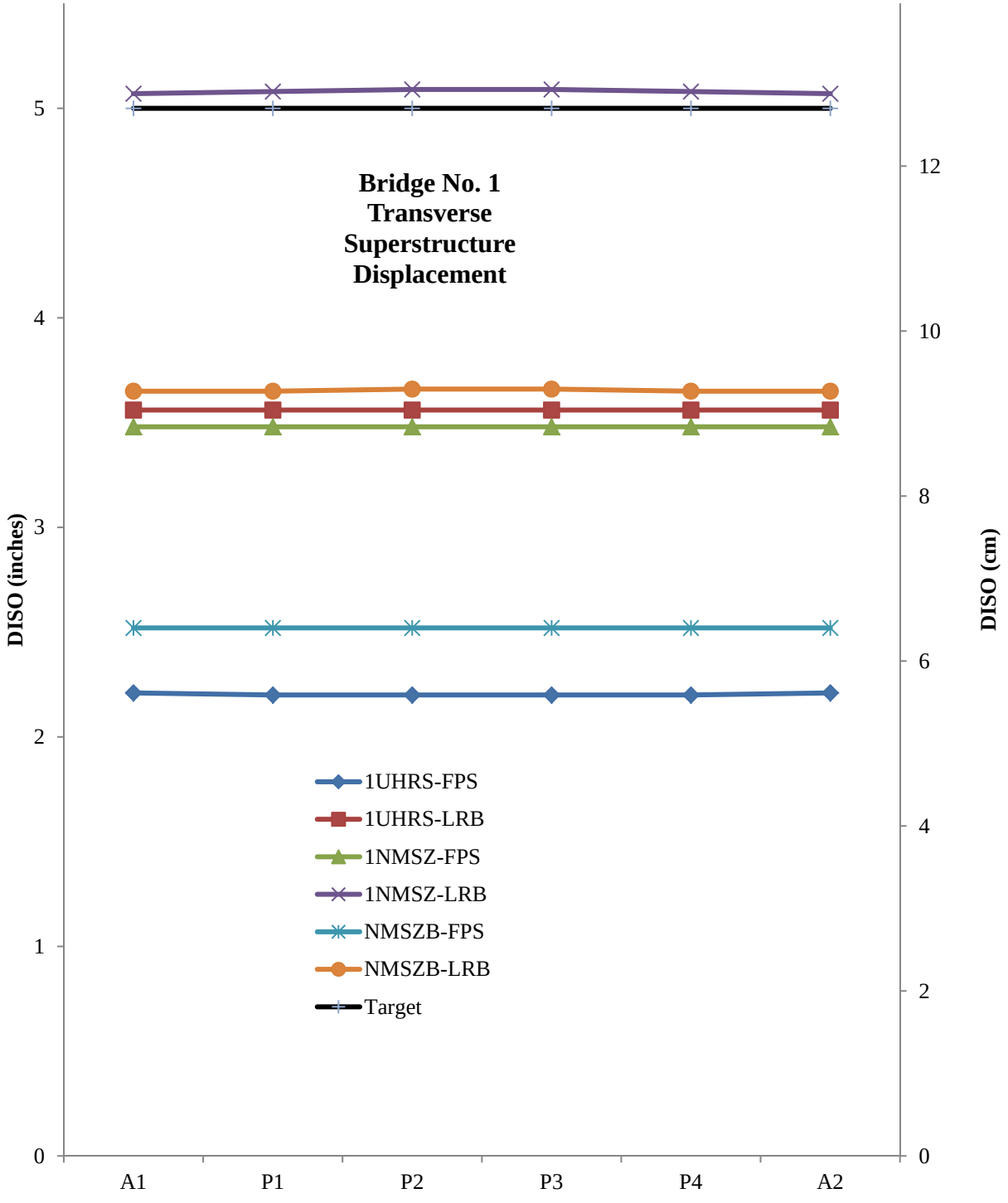

Figure G7.2.1-5. Superstructure Displacements - Bridge No. 1 (Transverse)

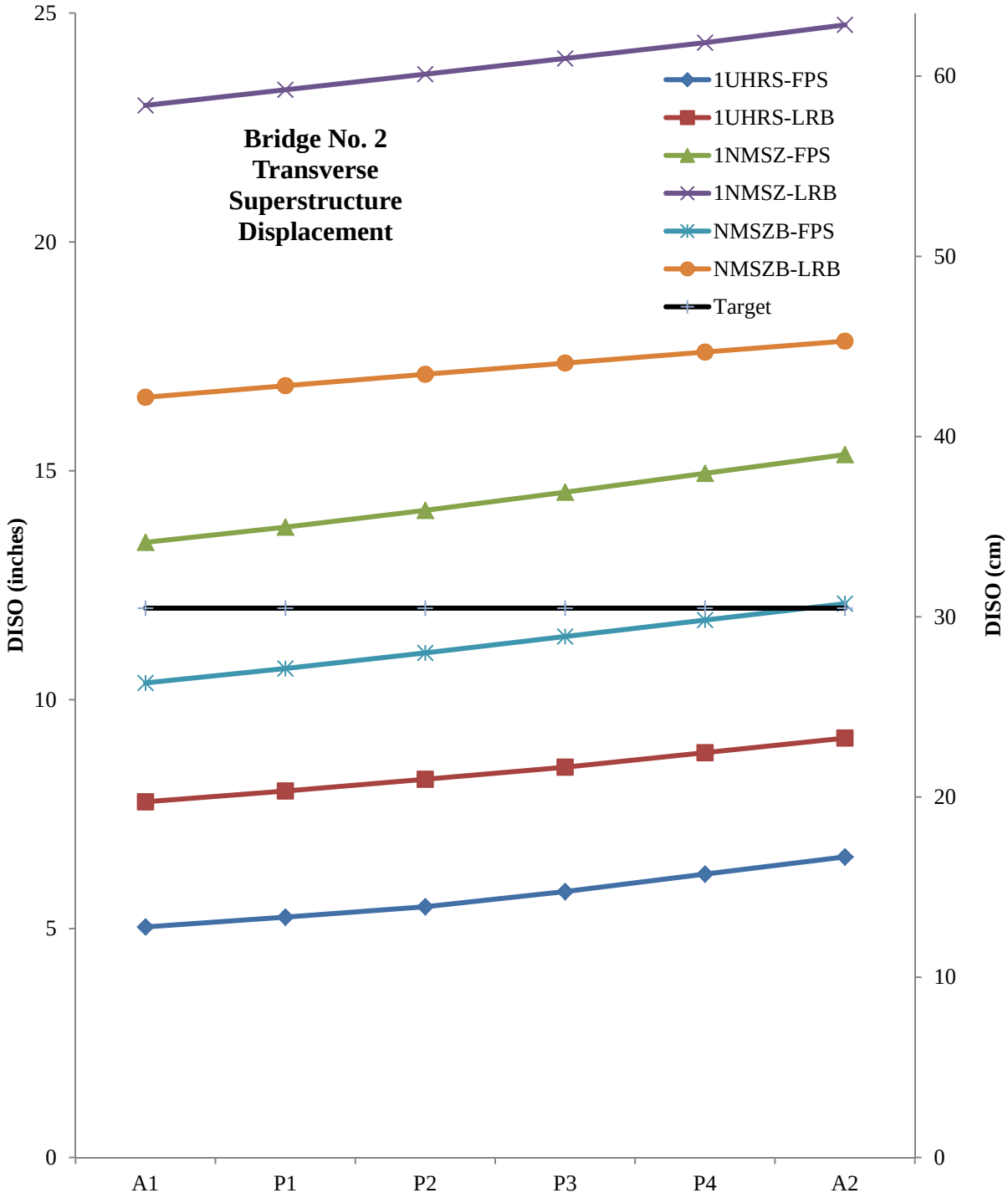

Figure G7.2.1-6. Superstructure Displacements - Bridge No. 2 (Transverse)

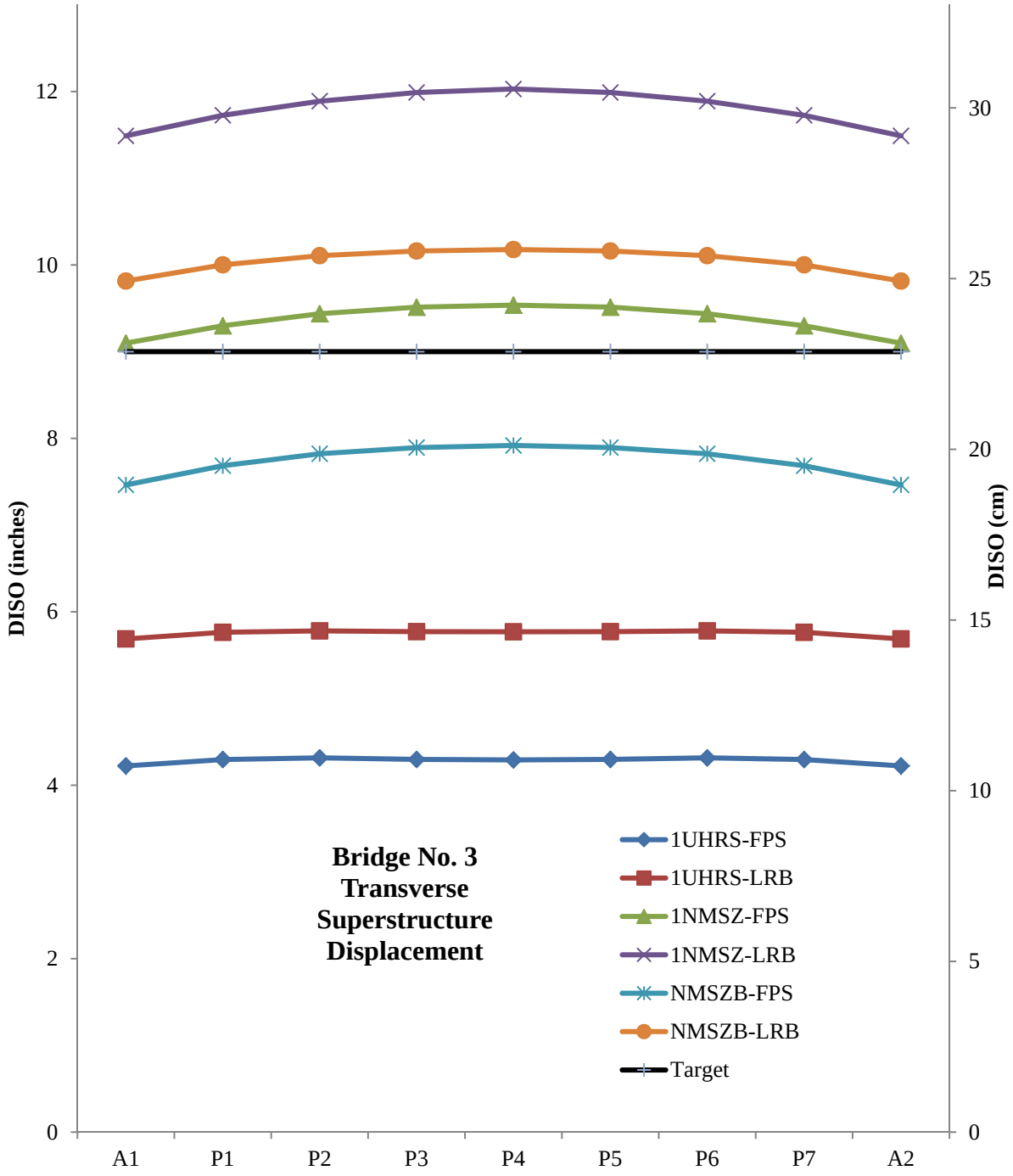

Figure G7.2.1-7. Superstructure Displacements - Bridge No. 3 (Transverse)

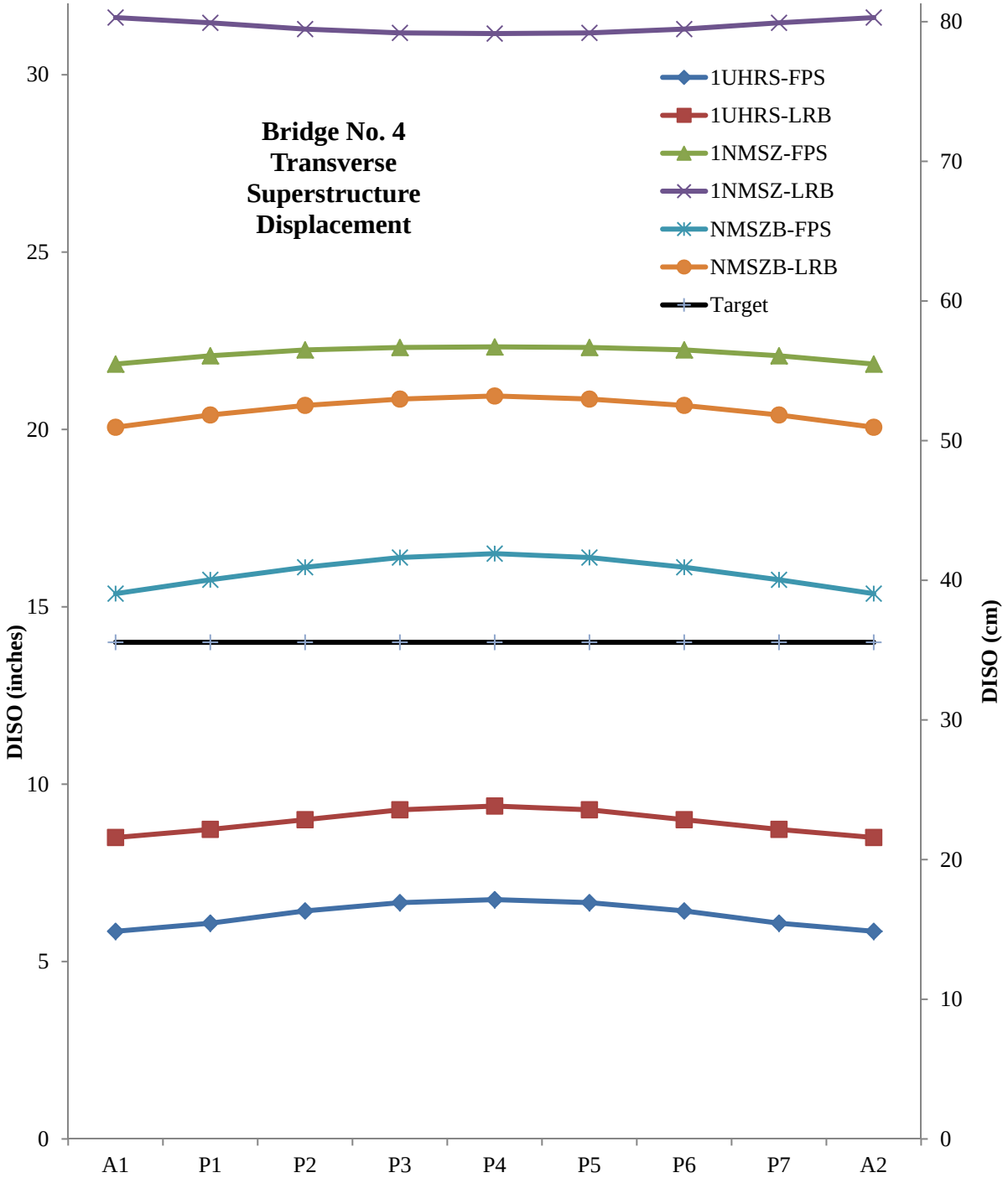

Figure G7.2.1-8. Superstructure Displacements - Bridge No. 4 (Transverse)

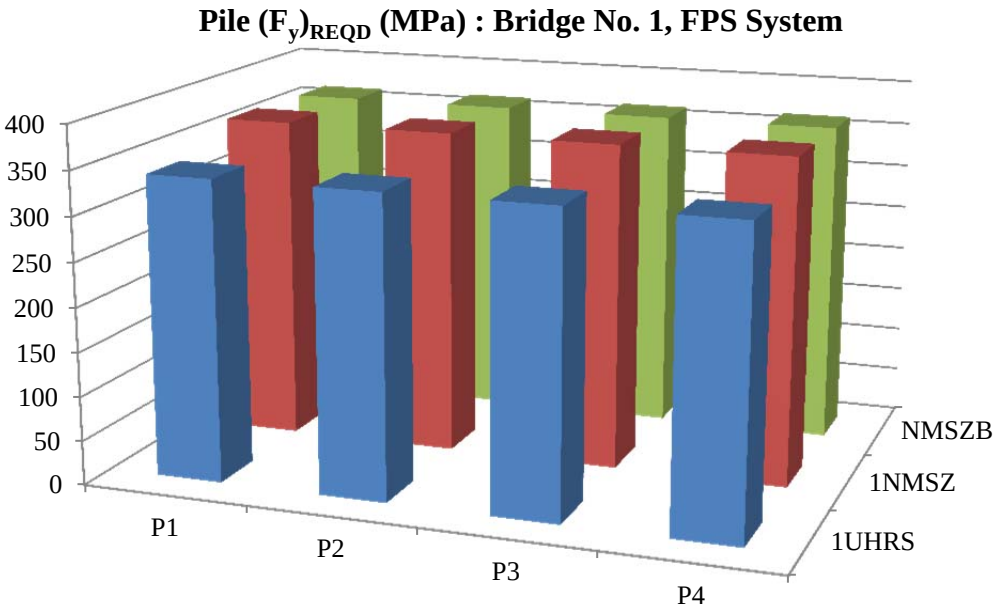

Figure G7.2.2-1. Pile Strength Requirements - Bridge No. 1 FPS (SI units)

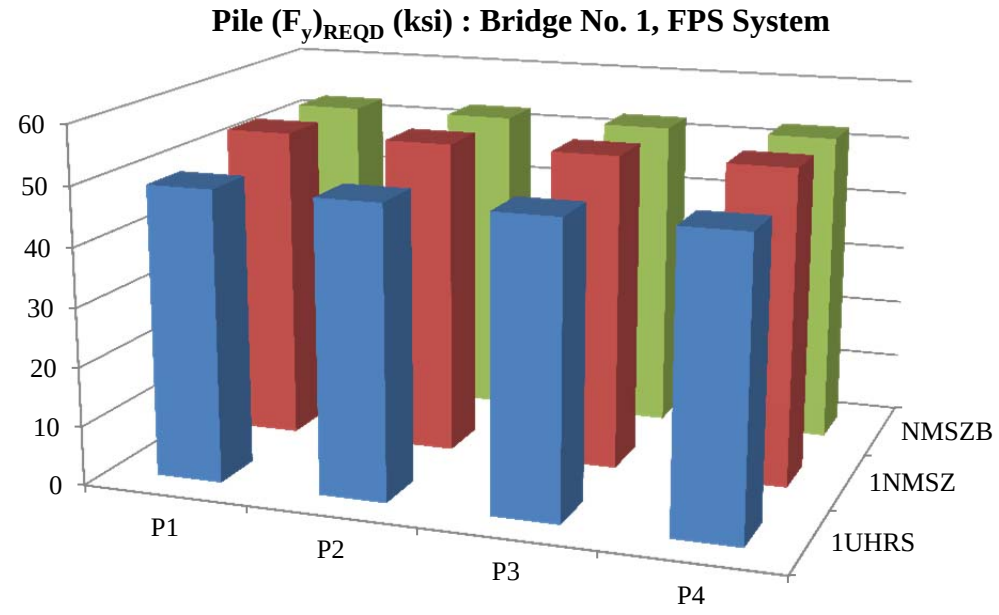

Figure G7.2.2-2. Pile Strength Requirements - Bridge No. 1 FPS (English units)

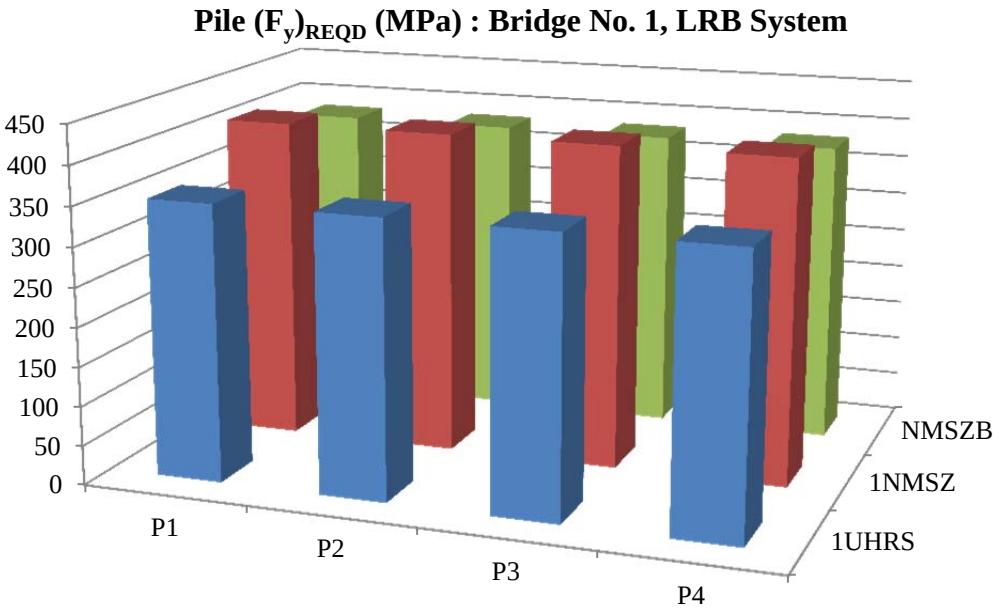

Figure G7.2.2-3. Pile Strength Requirements - Bridge No. 1 LRB (SI units)

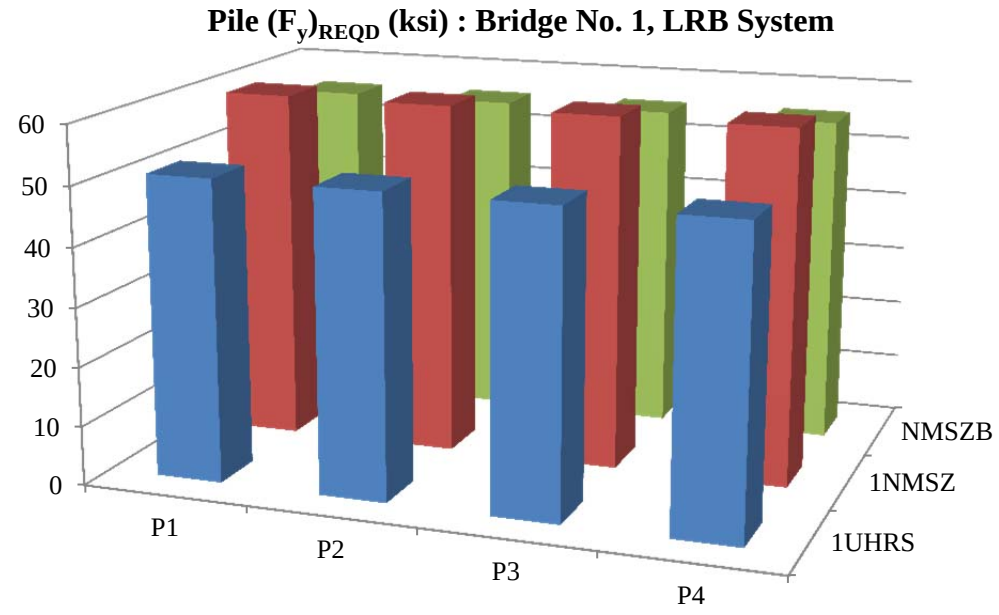

Figure G7.2.2-4. Pile Strength Requirements - Bridge No. 1 LRB (English units)

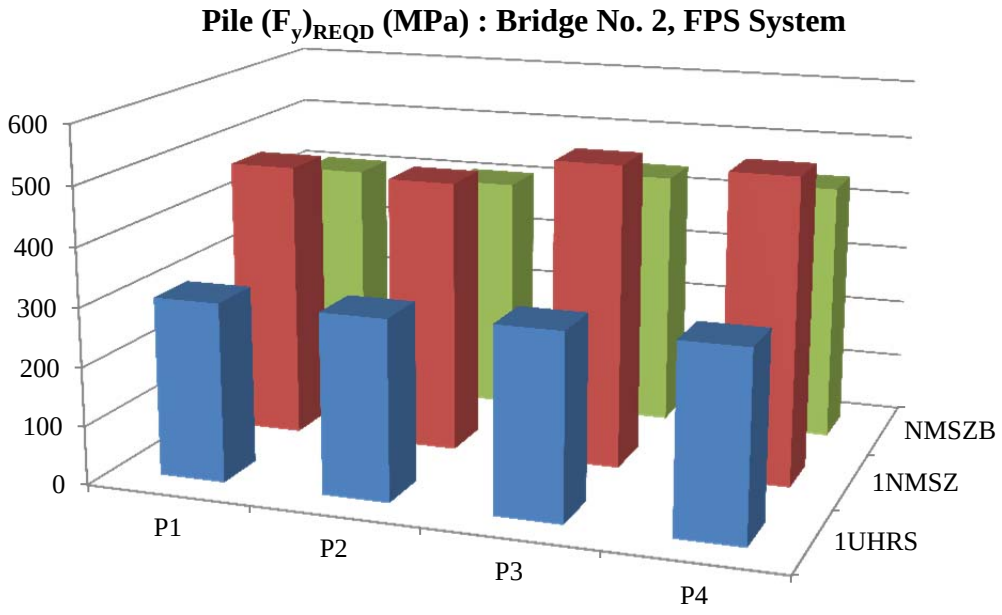

Figure G7.2.2-5. Pile Strength Requirements - Bridge No. 2 FPS (SI units)

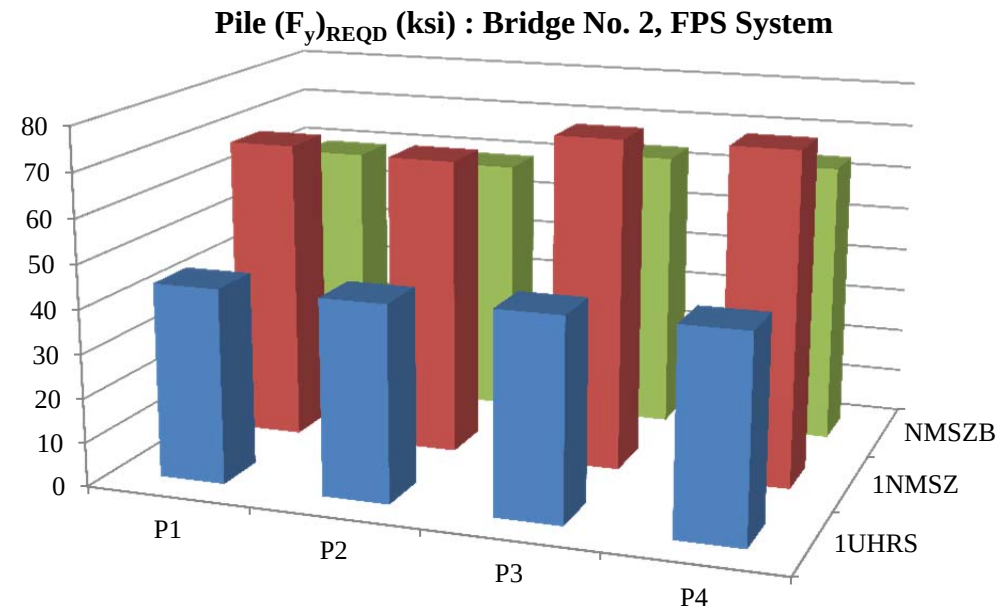

Figure G7.2.2-6. Pile Strength Requirements - Bridge No. 2 FPS (English units)

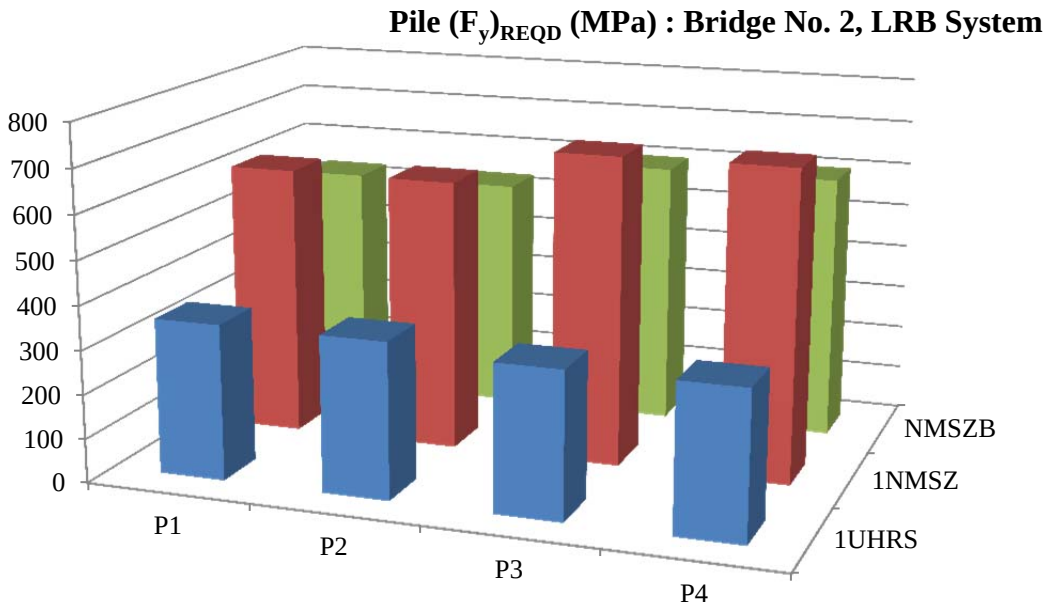

Figure G7.2.2-7. Pile Strength Requirements - Bridge No. 2 LRB (SI units)

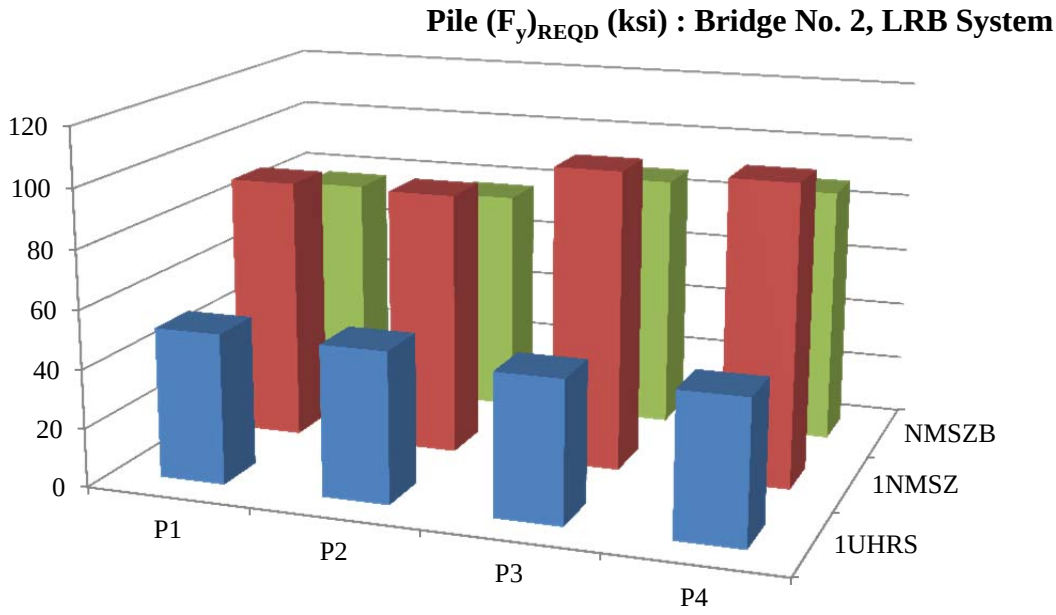

Figure G7.2.2-8. Pile Strength Requirements - Bridge No. 2 LRB (English units)

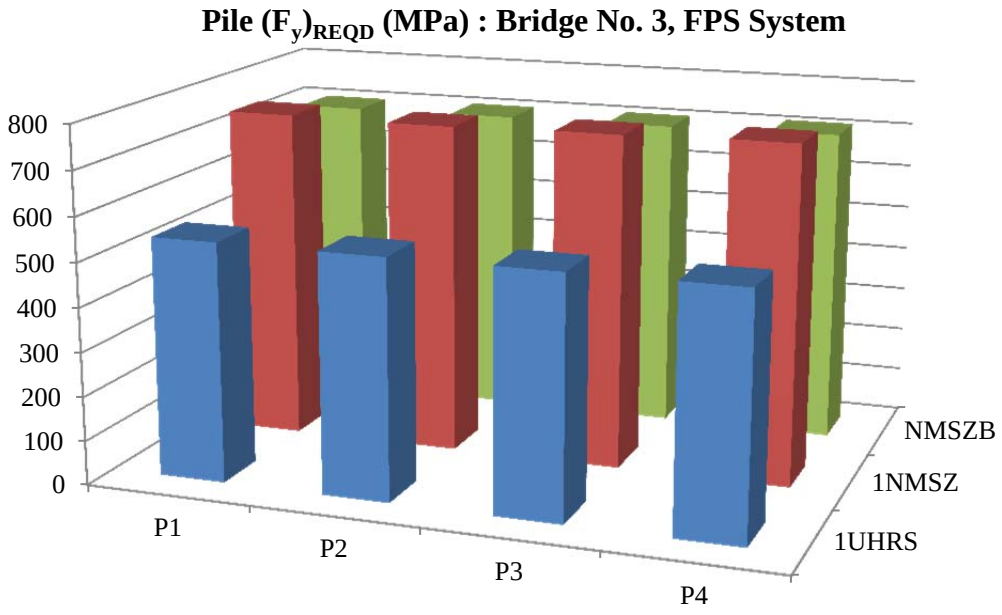

Figure G7.2.2-9. Pile Strength Requirements - Bridge No. 3 FPS (SI units)

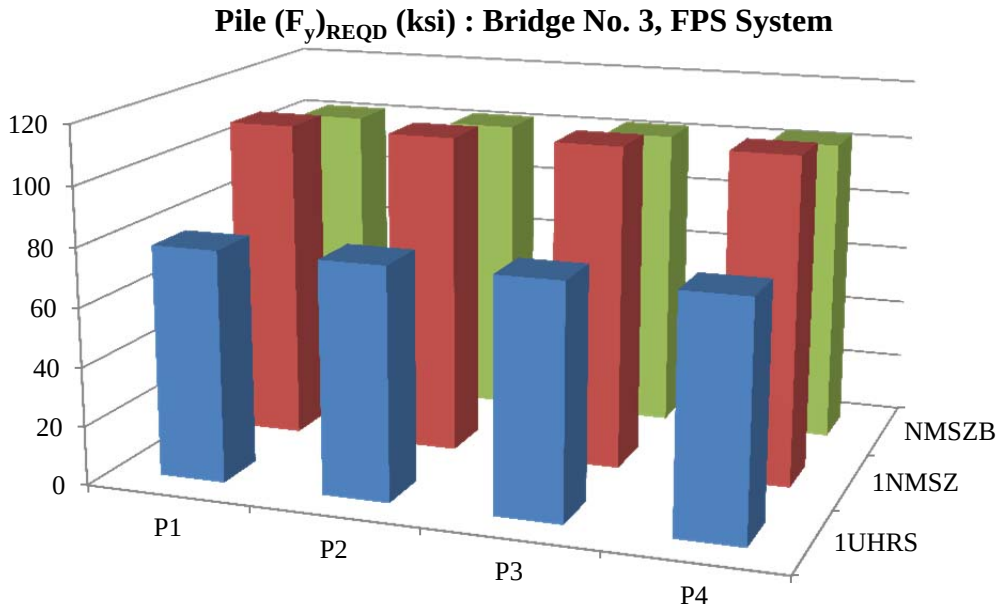

Figure G7.2.2-10. Pile Strength Requirements - Bridge No. 3 FPS (English units)

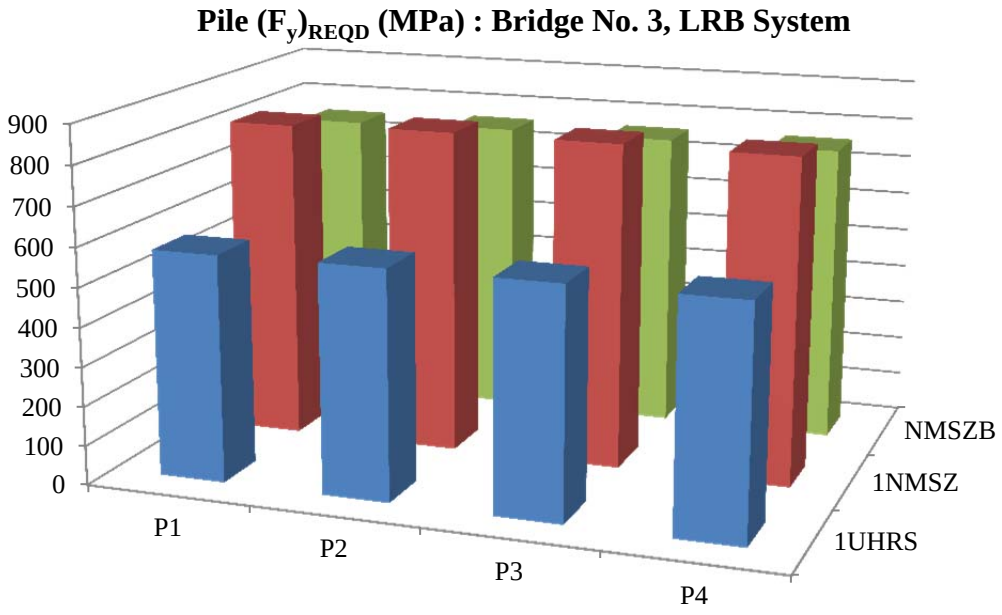

Figure G7.2.2-11. Pile Strength Requirements - Bridge No. 3 LRB (SI units)

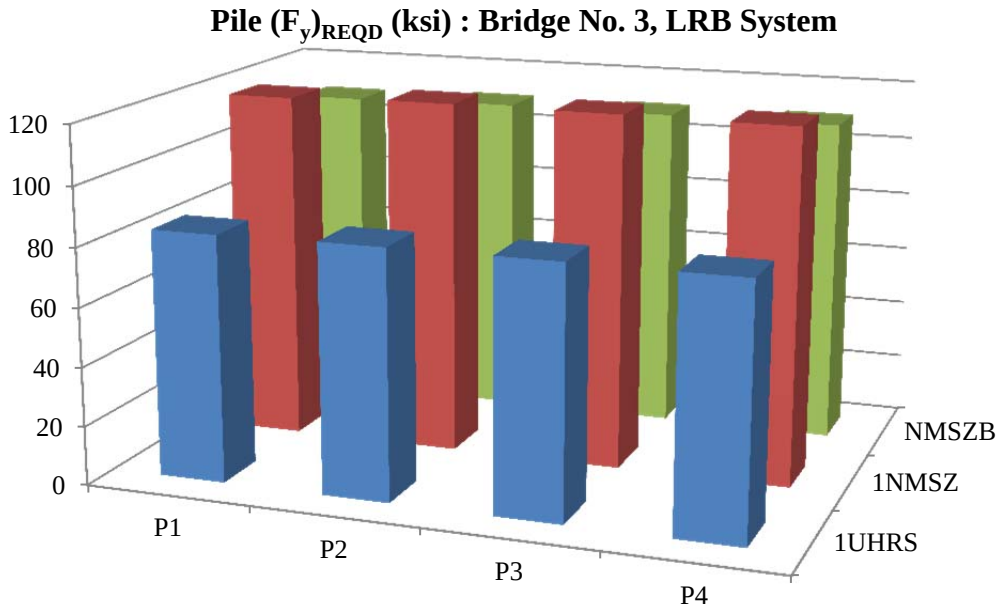

Figure G7.2.2-12. Pile Strength Requirements - Bridge No. 3 LRB (English units)

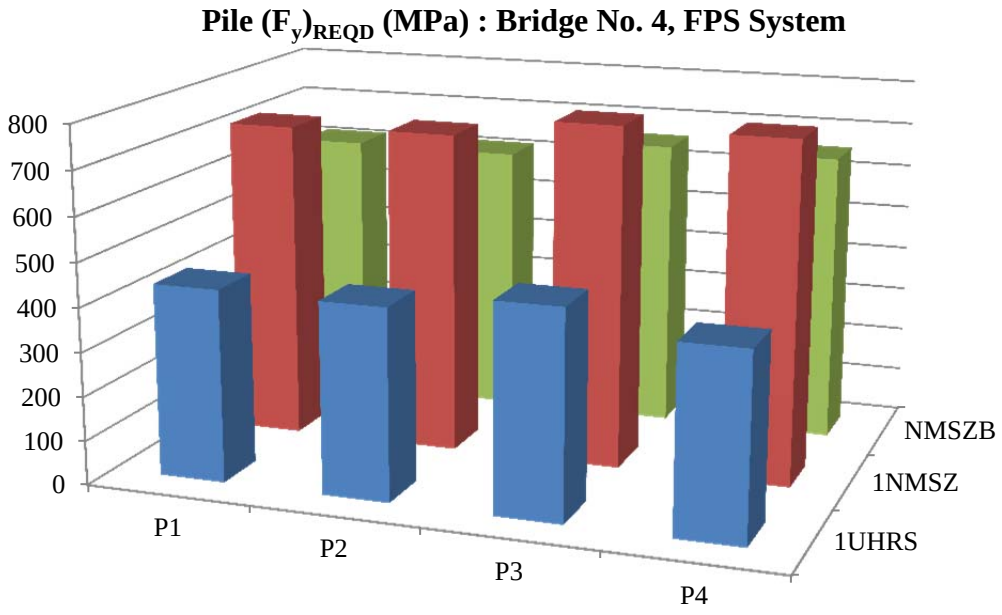

Figure G7.2.2-13. Pile Strength Requirements - Bridge No. 4 FPS (SI units)

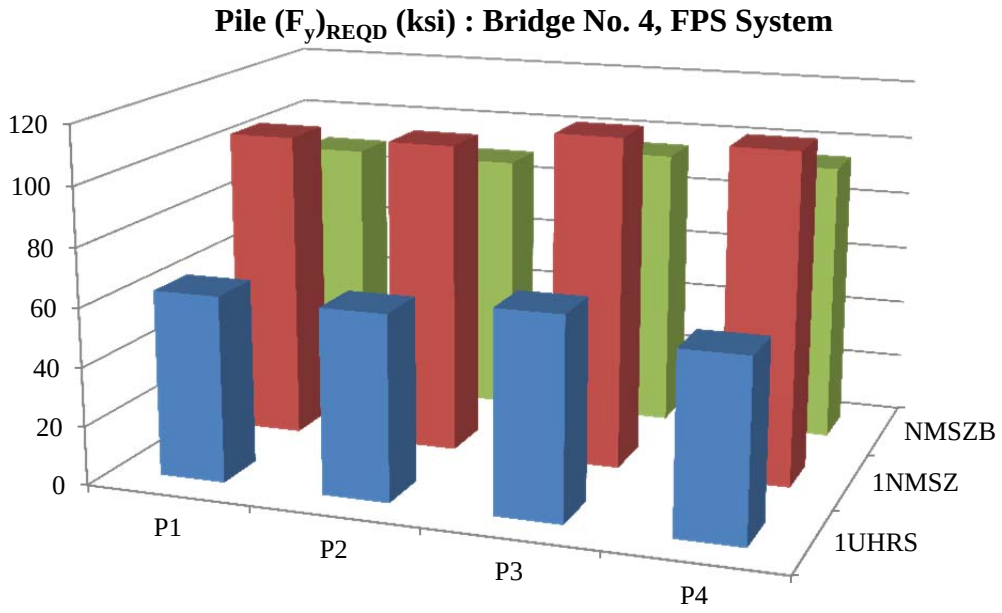

Figure G7.2.2-14. Pile Strength Requirements - Bridge No. 4 FPS (English units)

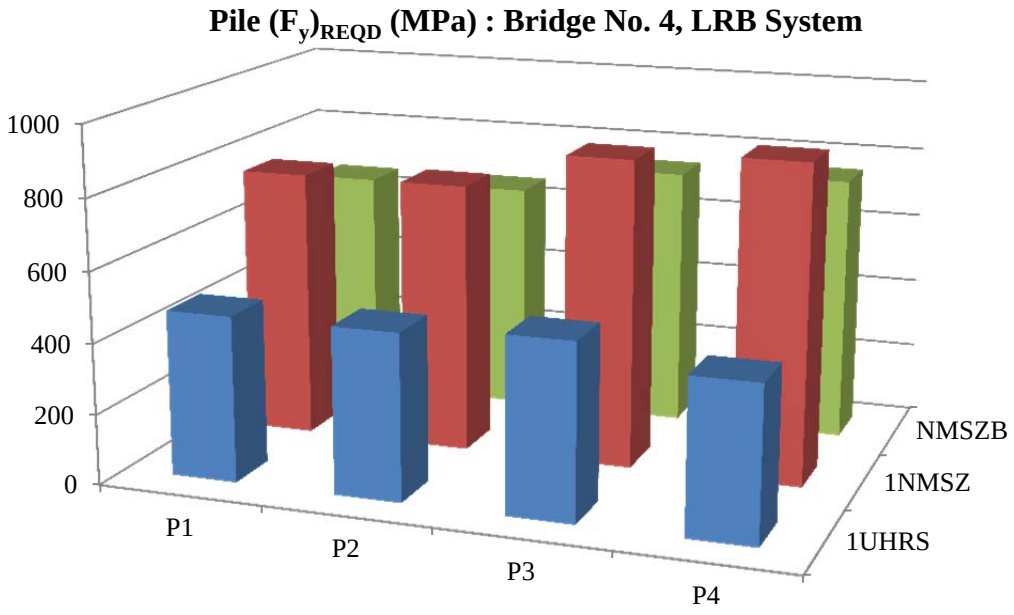

Figure G7.2.2-15. Pile Strength Requirements - Bridge No. 4 LRB (SI units)

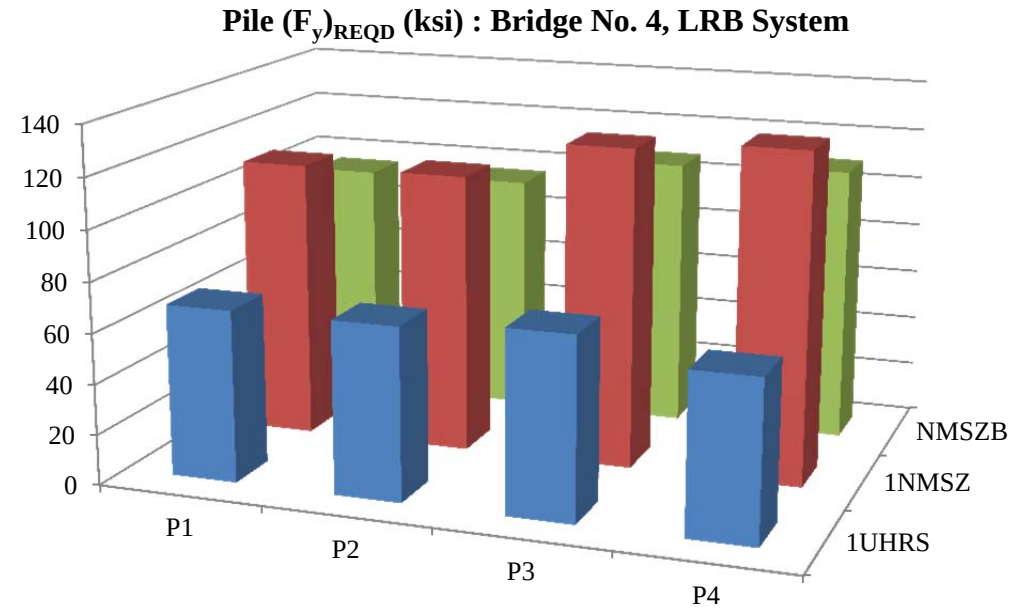

Figure G7.2.2-16. Pile Strength Requirements - Bridge No. 4 LRB (English units)

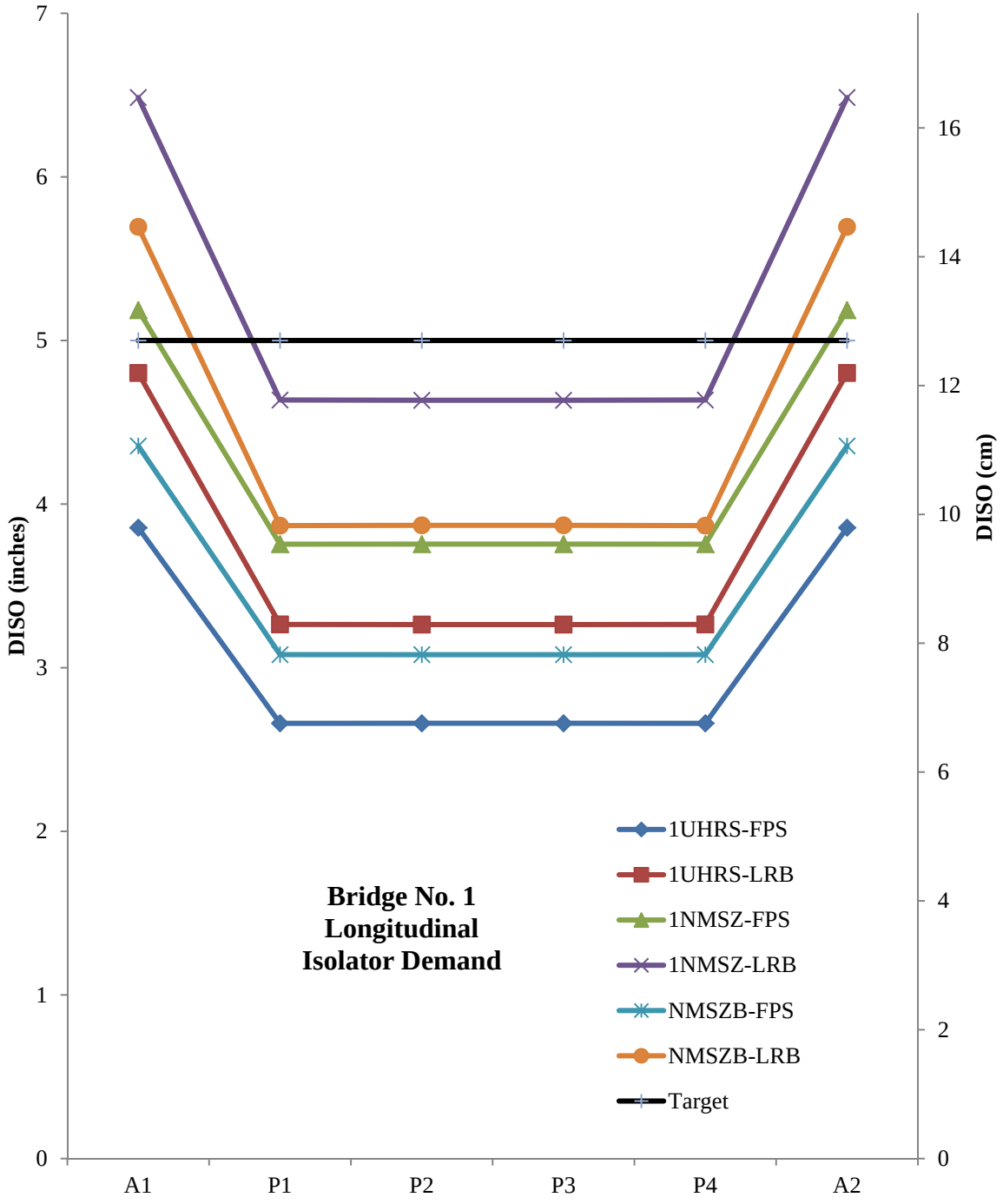

Figure G7.2.5-1. Isolator Demand - Bridge No. 1 (Longitudinal)

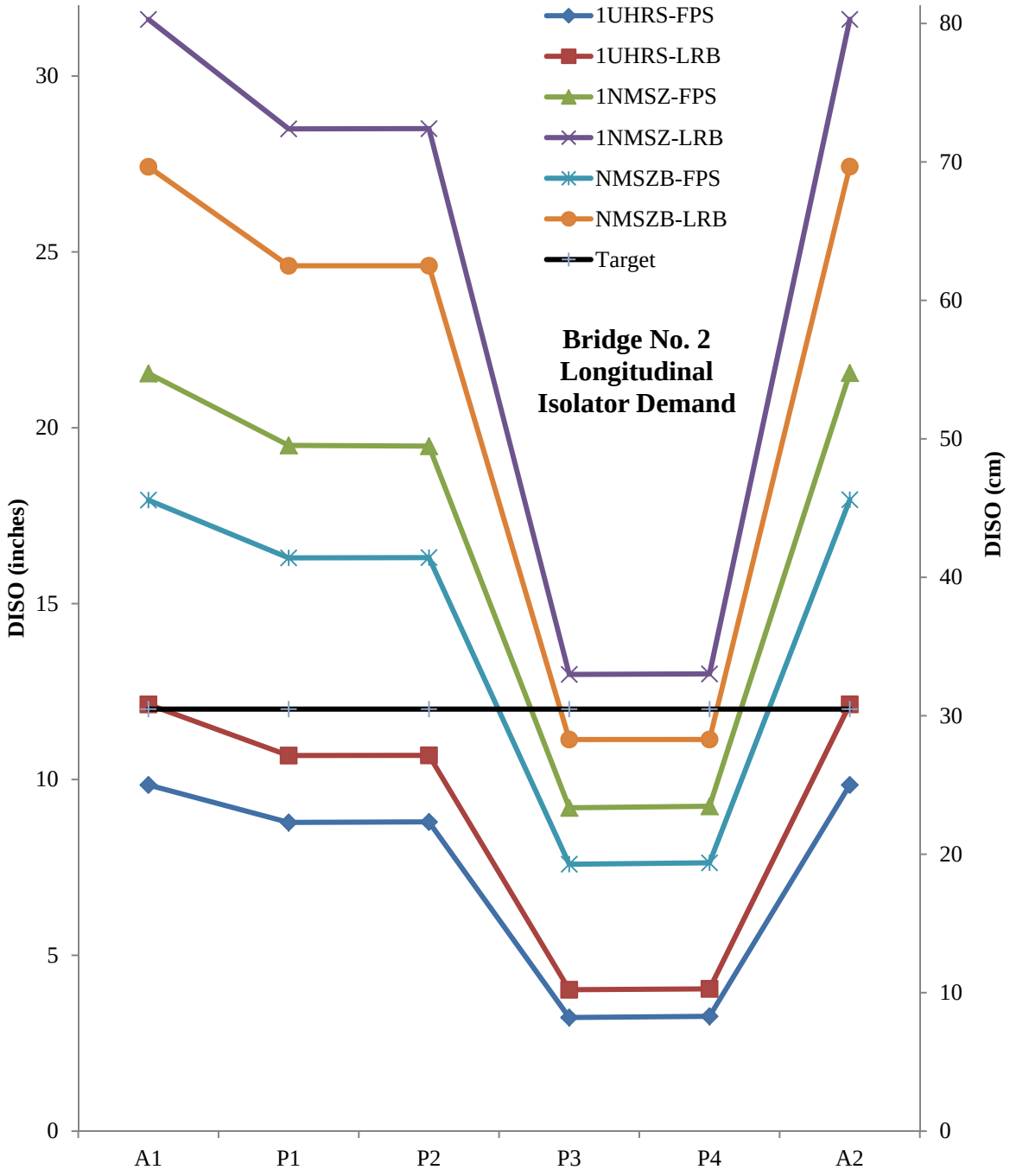

Figure G7.2.5-2. Isolator Demand - Bridge No. 2 (Longitudinal)

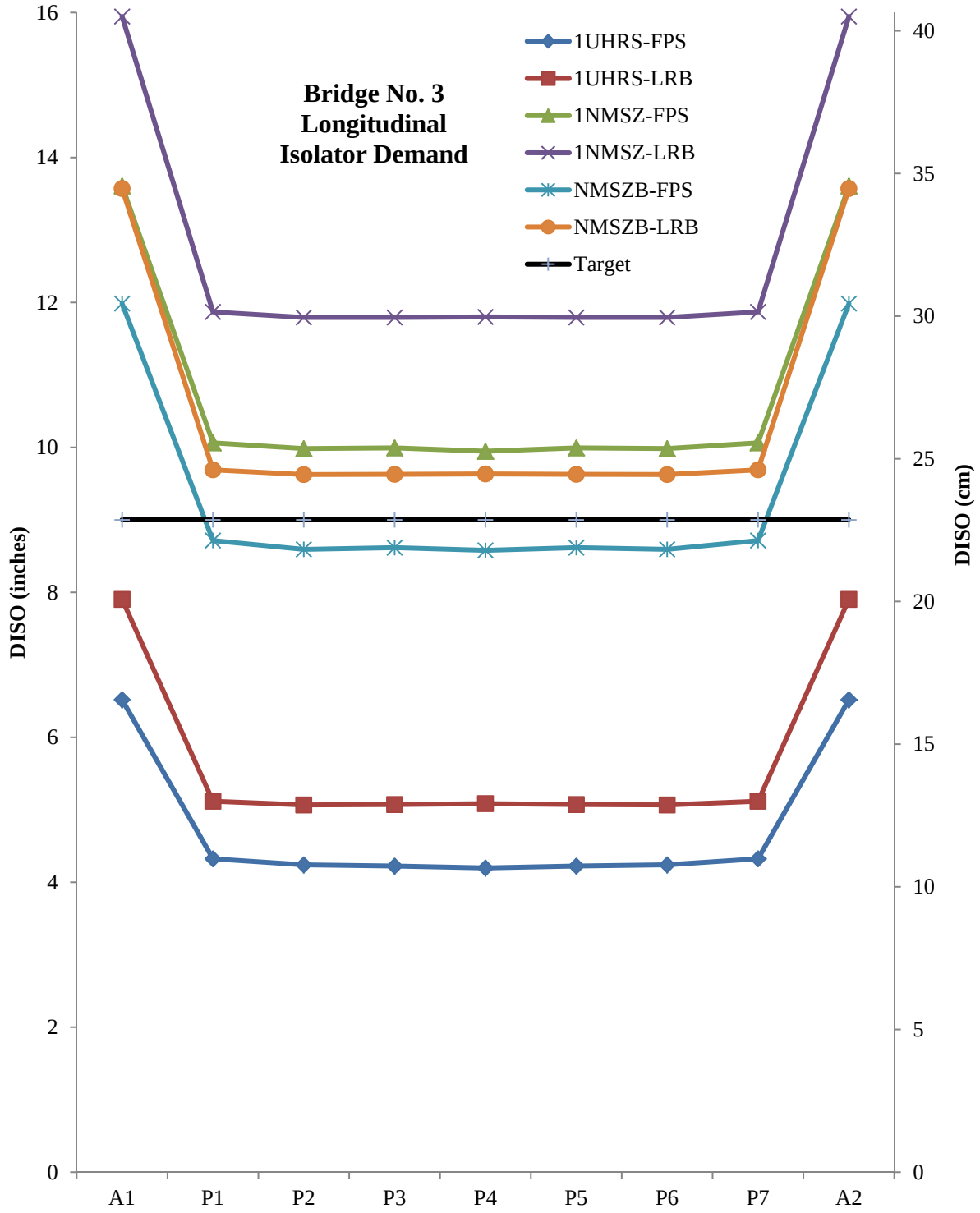

Figure G7.2.5-3. Isolator Demand - Bridge No. 3 (Longitudinal)

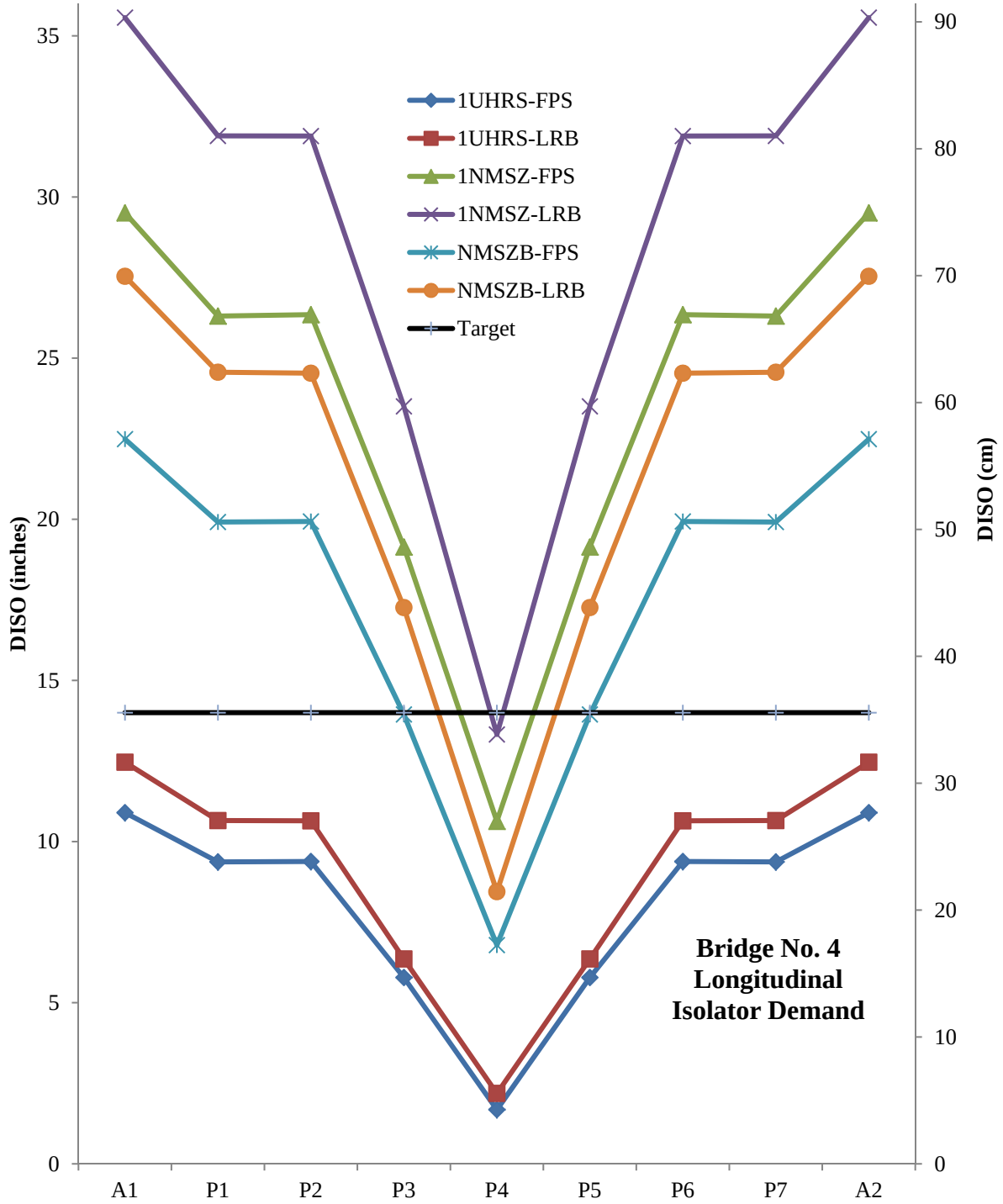

Figure G7.2.5-4. Isolator Demand - Bridge No. 4 (Longitudinal)

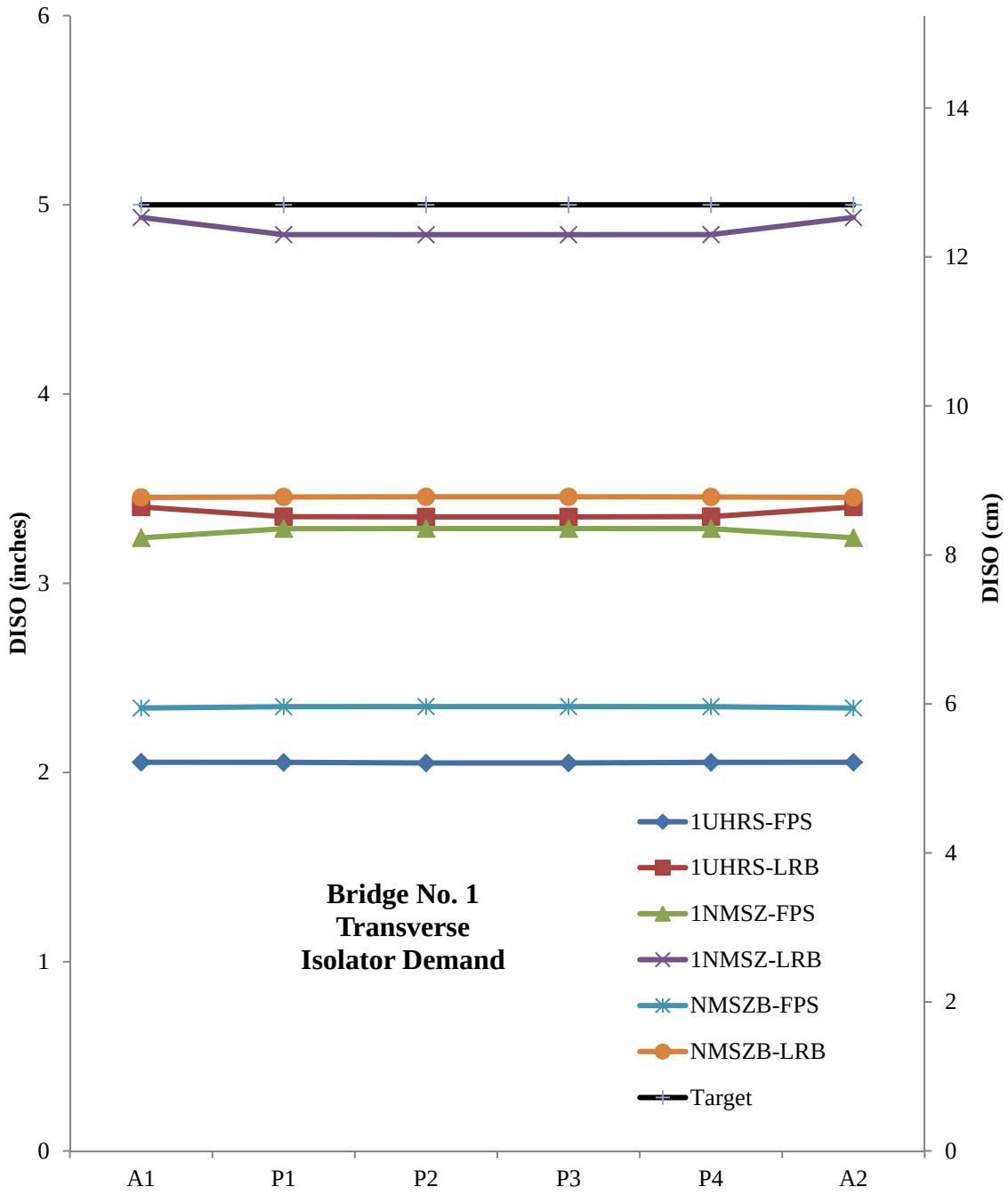

Figure G7.2.5-5. Isolator Demand - Bridge No. 1 (Transverse)

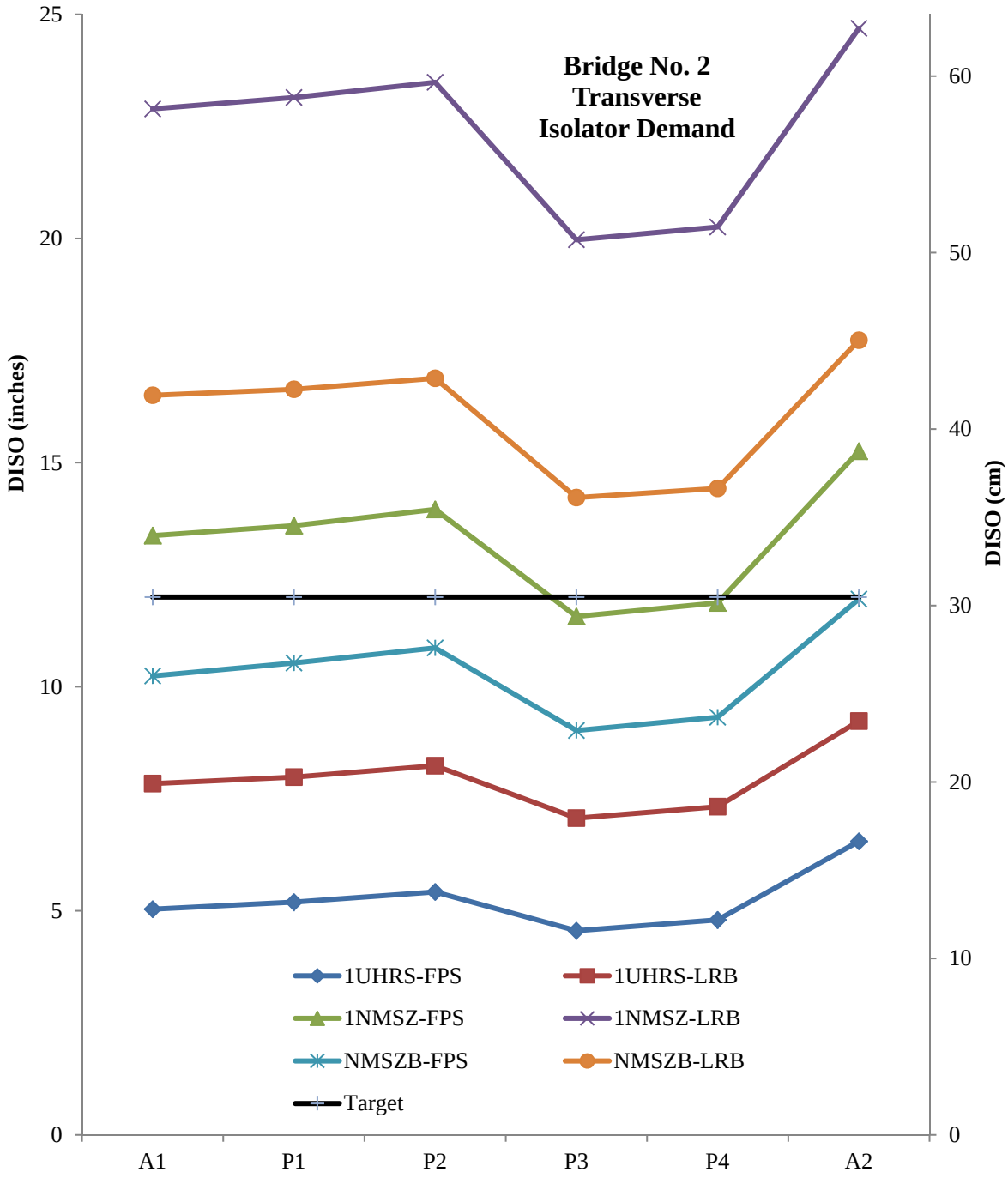

Figure G7.2.5-6. Isolator Demand - Bridge No. 2 (Transverse)

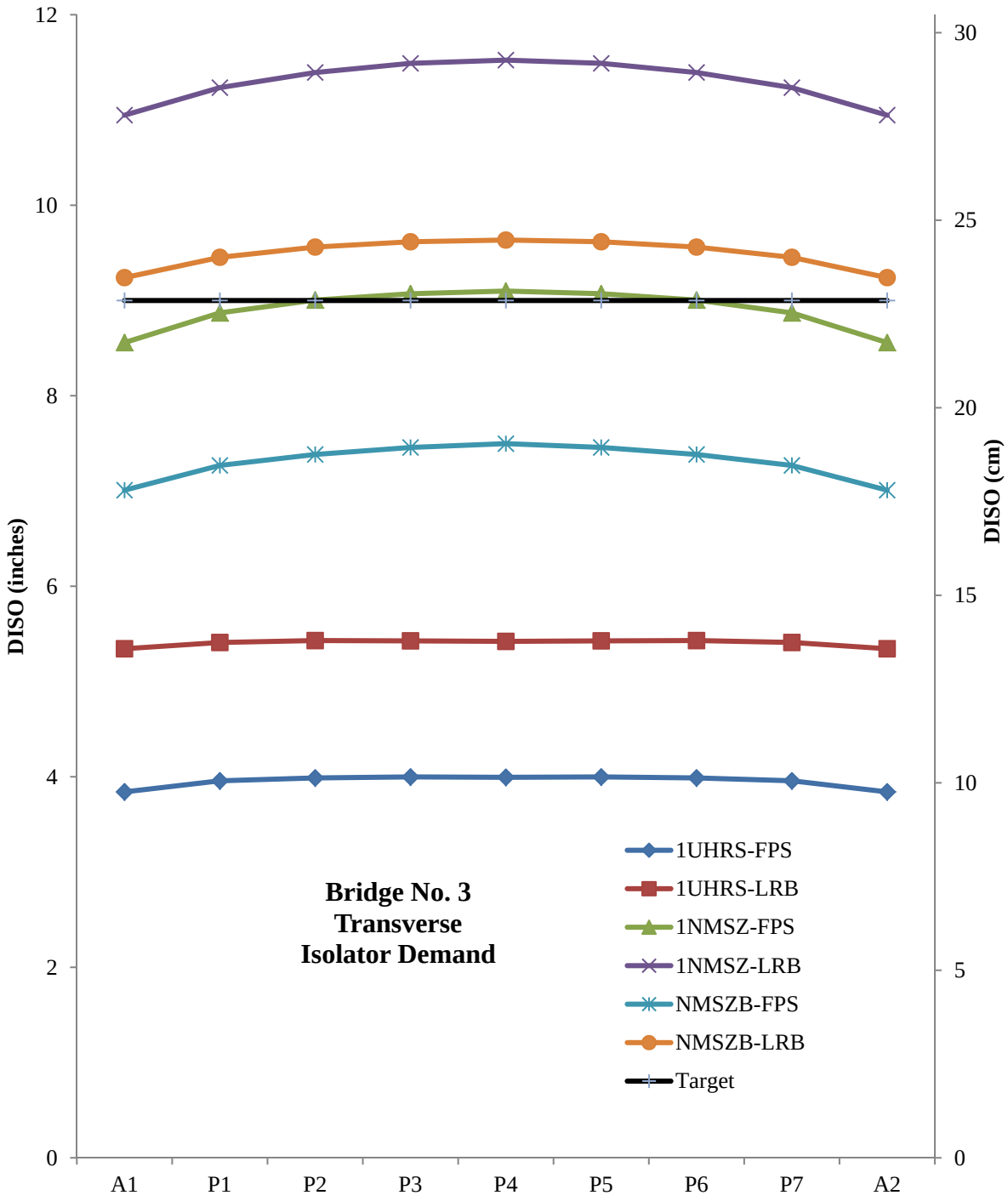

Figure G7.2.5-7. Isolator Demand - Bridge No. 3 (Transverse)

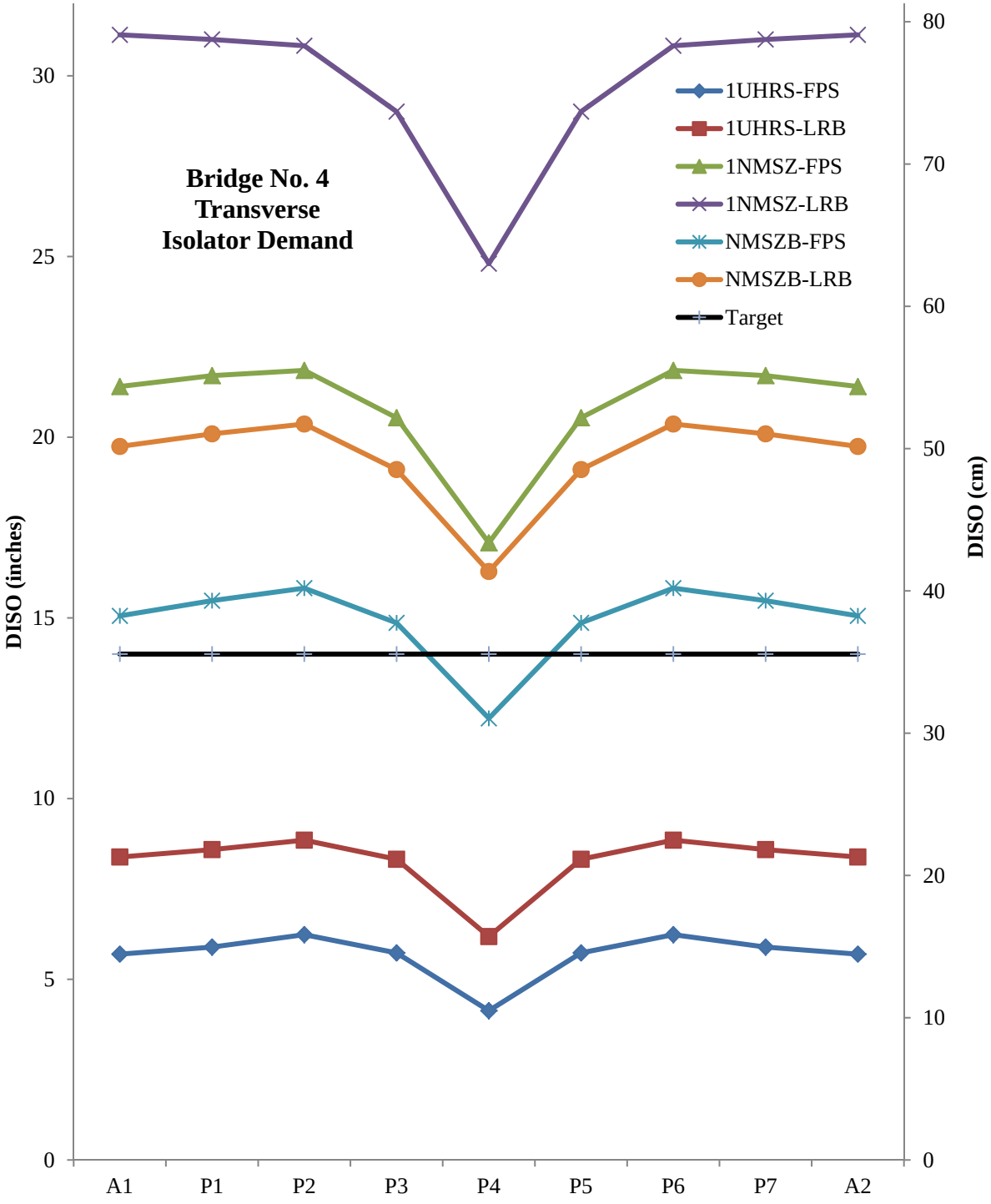

Figure G7.2.5-8. Isolator Demand - Bridge No. 4 (Transverse)

VITA

Tim Huff is the second son of William Cyril and Marva Sue Story Huff. He is the brother of Troy, the eldest, and Holli, the youngest. Tim graduated third in his class at Livingston Academy in 1980 and proceeded to major in Civil Engineering at Tennessee Tech University, completing a Master of Science degree in 1985. After working for the Tennessee Department of Transportation and Lockheed-Martin Energy Systems for 12 years, he took a year to travel abroad and engage in volunteer engineering work in the Philippines and India. Tim continued this type of work during subsequent trips to Haiti, Brazil, and Ethiopia. In 2001, he returned to the Tennessee Department of Transportation working in bridge design. He completed a Master's degree in Mathematics while working for TDOT and continues his education with the work presented here towards a Ph.D. in Engineering.